REGIOSELECTIVE AND ENANTIOSELECTIVE PD(II)- AND RU(II)-CATALYZED SP^2 AND SP^3 C-H BONDS INTRAMOLECULAR AND INTERMOLECULAR AMIDATION REACTIONS

LING CHO HON

PhD

The Hong Kong Polytechnic University

2021

The Hong Kong Polytechnic University

Department of Applied Biology and Chemical Technology

Regioselective and Enantioselective Pd(II)- and Ru(II)-Catalyzed sp^2 and sp^3 C-H Bonds Intramolecular and Intermolecular Amidation Reactions

LING Cho Hon

A thesis submitted in partial fulfillment of the requirements for the degree of Doctor of Philosophy

January 2020

CERTIFICATION OF ORIGINALITY

I hereby declare that this thesis is my own work and that, to the best of my knowledge and belief, it reproduces no material previously published or written, nor material that has been accepted for the award of any other degree or diploma, except where due acknowledgement has been made in the text.

_____

LING Cho Hon

ABSTRACT

Abstract of the thesis entitled

Regioselective and Enantioselective Pd(II)- and Ru(II)-Catalyzed sp^2 and sp^3 C-H Bonds Intramolecular and Intermolecular Amidation Reactions

Submitted by LING Cho Hon

for the degree of Doctor of Philosophy

at The Hong Kong Polytechnic University in January 2020

N-Aryl amides are very important because it can be found in many pharmaceutical compounds. Regioselective amidation reactions of simple arenes is very challenging as the selectivity of the reaction depends on electronic properties of the substituents. Recently, the *ortho*-selective transition metals catalyzed (e.g. Pd(II), Rh(III), Ru(II) and Cu(II) etc.) amidation reactions are well established. The functional groups (e.g. pyridyls, ketos, amides and carboxylic acids etc.) act as directing groups for coordination of catalysts and then perform C-H activation to form cyclometallated complexes. The chelation strategy achieves high regioselective at *ortho*-position of arenes. The Pd(II)-catalyzed regioselective amidation reaction with non-chelation strategy necessities the use of pre-functionalized arenes.

Our group was investigated Pd(II)-catalyzed regioselective amidation reaction of simple arenes to afford *N*-arylphthalimides. The steric repulsion offered

by the bulky *N*-heterocyclic carbene ligand controls regioselective C-H bond activation to form aryl-palladium intermediate for the further functionalization. In this work, employing the phthalimide (0.1 mmol) with [(IPr)Pd(OAc)$_2$(OH$_2$)] (10 mol %) (IPr = 1,3-bis(2,6-diisopropylphenyl)-2,3-dihydro-1*H*-imidazole) as a catalyst and PhI(OAc)$_2$ (10 equiv, 1 mmol) as an oxidant in neat arenes at 100 ^{o}C gave 50 – 70 % isolated yields of desired *N*-arylphthalimides formation. The amidation product of electron-deficiency arenes such as α,α,α-trifluorotoluene is *meta*-isomer in dominant (*o:m:p* = 1:16:5). For the electron-rich arenes such as toluene, the amidation product is *meta*- and *para*-isomers in mixture (*o:m:p* = 1:22:29). To explore the mechanism of the reaction, the kinetic studies on the catalytic reaction of phthalimide, benzene-d_6, PhI(OAc)$_2$ and [(IPr)Pd(OAc)$_2$(OH$_2$)] were conducted in ^{1}H NMR spectroscopic analysis. A rate law = k[PhI(OAc)$_2$][(IPr)Pd(OAc)$_2$(OH$_2$)][phthalimide]$^{0.3}$ was obtained. It is the first order of reaction with respect to PhI(OAc)$_2$ indicating that the resting state is Pd(IV) intermediate before the C-H bond activation step.

While, the enantioselective Ru(II)-catalyzed intramolecular C(sp^2)-H bond amidation reaction of 3-(2,2-diphenylethyl)-1,4,2-dioxazol-5-one (***1i***) examined. By employing ***1i*** (0.1 mmol) with catalytic amounts of [Ru(*p*-cymene)(L-proline)Cl] (**[Ru4]**, 10 mol %) and AgSbF$_6$ (10 mol %) in TFE (1 mL) at 50 ^{o}C to afford 4-phenyl-3,4-dihydroquinolin-2(1*H*)-one (***2i***) in 76 % yield with 30 % *ee*. Based on the HPLC analysis of product mixture obtained from Ru(II)-catalyzed reaction of ***1i***, (*S*)-4-phenyl-3,4-dihydroquinolin-2(1*H*)-one (peak at retention time = 21.4 mins) was found to be the major enantiomer. At the same time, the regioselectivity of the amidation reaction between C(sp^2)-H bond and C(sp^3)-H bond was studied.

Employing the 3-(2,3-diphenylpropyl)-1,4,2-dioxazol-5-one (***1a***) with Ru(II) catalysts (**[Ru1]** – **[Ru5]**, 10 mol %) and $AgSbF_6$ (10 mol %) in dry solvent (either DCE or TFE, 1 mL) at 50 ^{o}C, L-proline (**[Ru4]**) gave 4-benzyl-3,4-dihydroquinolin-2(1*H*)-one ***2a*** (sp^2 amidation product) in 78 % and trace amount of (5*R*)-4,5-diphenylpyrrolidin-2-one ***2a'*** (sp^3 amidation product) formation in TFE as a solvent. Several products formation in substrate scope studies demonstrated the mechanism of the reaction goes through spirocyclization followed by C-C migration rather than electrophilic aromatic substitution (S_EAr).

Enantioselective intramolcular Ru(II)-catalyzed nitrenoid insertion of arenes established the chiral ligand produces enantio-pure amidation products. The enantioselective intermolecular Ru(II)-catalyzed nitrenoid insertion of unactivated terminal alkenes was investigated. Treatment of terminal alkenes (0.2 mmol) with 1,4,2-dioxazol-5-ones (0.1 mmol) in the presence of $[Ru(p\text{-cymene})Cl_2]_2$ (10 mol %), $AgSbF_6$ (15 mol %), LiOAc (20 mol %) and HOAc (0.1 mmol) in distillated DCE (0.5 mL) at 35 ^{o}C to afford desired allylamides formation in 11 – 61 % isolated yields. By designing a chiral cymene ligand, the chiral cymene is a 10-membered ring structure with the axial chirality. After the coordination of the Ru(II) metal center, the chiral [**Ru2**] was characterized by ^{1}H NMR, ^{13}C NMR and X-ray crystalline spectrometers. By repeating the amidation reaction of terminal alkene, it gave 60 % isolated yield of the desired allylamide product but the enantiomeric excess of the product is 10 % *ee*.

PUBLICATIONS AND CONFRENECES

CONFRENECES

C.-H. Ling; W.-Y. Yu, "Regioselective Controlled Pd(II)-Catalyzed Non-Chelation Assisted C-H Bond Amidation of Arenes Enhanced by *N*-heterocyclic Carbene Ligand", The EuCheMS International Organometallic Conference XXII, Amsterdam, Netherlands, 9-13 July, 2017.

SYMPOSIUMS

Ling, C.-H.; Li, C.-K.; Yu, W.-Y. "Ligand-Enabled Pd-Catalyzed Site-Selective Non-Chelation-Assisted Direct Amidation of Simple Arenes", The 25th Symposium on Chemistry Postgraduate Research in Hong Kong, 28 April 2018.

Ling, C.-H.; Yu, W.-Y. "Regioselective Controlled Pd(II)-Catalyzed Non-Chelation Assisted C-H Bond Amidation of Arenes Enhanced by *N*-heterocyclic Carbene Ligand", The 23rd Symposium on Chemistry Postgraduate Research in Hong Kong, 23 April 2016.

ACKNOWLEDGEMENTS

I would like to have an opportunity to thank the people that have helped me in PhD program and writing the thesis.

First of all, I would like to thank my supervisor Prof. Wing-Yiu Yu, Michael for giving me a chance to be a PhD graduate. In these four years, he taught me how to become an independent researcher and also improve my writing skills and oral presentation skills during the discussion of research projects.

Second, I would like to thank the research members of Yu's group including Dr. Yuk-Tai Tsoi, Dr. Wai-Wing Chan, Dr. Ka-Ho Ng, Dr. Chun-Wo Chan, Dr. Hon-Wah Lam, Dr. Yan-Fung Lau, Dr. Qing Xi, Dr. Wenlong Sun, Miss Pui-Yiu Lee, Mr. Chun-Kit Li, Mr. Andy Ka-Yu Sin, Mr. Ka-Ho Chow, Mr. Chung-Pang Li, Mr. Leong-Hung Cheung and Mr. Jason Tak-Shing Ngan for their invaluable supports on academic area and technical skills. We build up a precious friendship in this group so that I have worked and explored the chemistry research with a happiness period.

In this moment, I would like to give my appreciation to my senior fellow apprentice, Dr. Fo-Ning Ng. He spent many time on my technical skills training so that I can perform all experiments and instrumental analysis independently. Moreover, He taught me how to perform literature reviews for development of my own research projects and research lines. He always challenges me after I set up the hypothesis so I can think more deeply and consider all possibilities before the experiment. Apart from the research, he always gives me a very useful recommendation in planning of my life in the future. After his graduation, he always comes back and discusses with me about the progress of my research and goal of my

life. When I feel upset and lose, he gave me comments and guidelines in order to solve and overcome my mental obstruction. He is a good demonstration of the senior researcher and I learn from him to do the same things on my junior researchers in our group. Thank you very much.

After that, I appreciate all technical supports from the staffs of Department of Applied Biology and Chemical Technology. I would like to thank Dr. Kenneth Yan in NMR spectroscopic analysis. His comments and suggestions allow me to finish the characterization of the complicated complexes and investigatation in the kinetic studies successfully. Also, Dr. Wesley Chan shared his experience in X-ray crystallographic studies with me so that I can design and modify the ligand for enantioselective cross-coupling reactions easily.

Last but not least, the most important, I thank my dad and mom for their unlimited encouragement and support in my research. After I finish my work and go back home, they provide a warm environment for me to take a rest so that I can continue my research everyday. The parent's love is my energy to keep going in my research. All my friends arranged the gathering dinners in these four years are highly appreciated because all of you listened my difficulties and gave me mentally supports so I will not give up the research.

TABLE OF CONTENTS

ABBREVIATIONS AND SYMBOLS

abbreviations and symbols	name
AAs	Anthranilic acids
AcOH	Acetic acid
acac	Acetylacetonate
BDE	Bond dissociation energy
bipy	2,2'-Bipyridine
BINAP	2,2'-Bis-1,1'-binaphthalene
BQ	1,4-Benzoquinone
Boc	*tert*-Butyloxycarbonyl group
Bz	Benzoyl group
Cbz	Carboxybenzyl group
CCD	Charge-coupled device
CCDC	The Cambridge Crystallographic Data Centre
CDC	Cross-dehydrogenative coupling
CO_2	Carbon dioxide
cod	1,5-Cyclooctadiene
Cp*	1,2,3,4,5-Pentamethylcyclopentadienyl
dba	Dibenzylidenacetone

CDI	Carbonyldiimidazole
DCE	1,2-Dichloroethane
DCM	Dichloromethane
THF	Tetrahydrofuran
DMA	*N,N*-Dimethylacetamide
DMF	*N,N*-Dimethylformamide
DMSO	Dimethyl sulfoxide
HFIP	1,1,1,3,3,3-Hexafluoro-2-propanol
TFE	2,2,2-Trifluoroethanol
o-DCB	1,2-Dichlorobenzene
DOSP	*N*-(Dodecylbenzenesulfonyl)prolinate
DTBP	2,6-Di-*tert*-butyl-4-methylpyridine
PPA	Polyphosphoric acid
ESI	Electrospray ionization
FT-ICR	Fourier transform ion cyclotron resonance
GC	Gas chromatography
GC-FID	Gas chromatography – flame ionization detector
GC-MS	Gas chromatography – mass spectroscopy
HRMS	High resolution mass spectra
IR	Infrared spectroscopy
KIE	Kinetic isotope effect
LUMO	Lowest unoccupied molecular orbital
OAc	Acetate group

Piv	Pivaloyl group
OTf	Trifluoromethanesulfonate group
MesO	1,3,5-trimethylbenzenesulfonate group
MO	Molecular orbital
MS	Mass spectroscopy
MTBE	Methyl *tert*-butyl ether
n.d.	Not determined
NBS	*N*-Bromosuccinimide
NCP	*N*-Chlorophthalimide
NCS	*N*-Chlorosuccinimide
NFSI	*N*-Fluorobenzenesulfonimide
NEt_3	Triethylamine
NIS	*N*-Iodosuccinimide
NMR	Nuclear magnetic resonance
Ns	*p*-Nitrobenzenesulfonyl group
phen	1,10-Phenanthroline
PhBPin	Phenylboronic acid pinacol ester
pybox	2,2-Bis(2-oxazolin-2-yl)pyridine
rt	Room temperature
*t*Bu	*tert*-Butyl group
Bn	Benzyl group
Tf	Trifluoromethylsulfonyl group
TLC	Thin layer chromatography

TMSCl	Trimethylsilyl chloride
TMEDA	Tetramethylethylenediamine
BMIM PF_6	1-Butyl- 3-methylimidazolium hexafluorophosphate
dppb	1,4-bis- (Diphenylphosphino)butane
Ts	*p*-Toluenesulfonyl group
p-TsOH	*p*-Toluenesulfonic acid
TTP	Meso-tetrakis(tolyl)porphyrinato
TFA	Trifluoroacetic acid
Xphos	2-Dicyclohexylphosphino-2',4',6'-triisopropylbiphenyl ligand
Å	Angstrom
s	Singlet
d	Doublet
t	Triplet
q	Quartet
m	Multiplet
m/z	Mass to charge ratio
η	Hapticity
δ	Chemical shift in NMR
J	Coupling constant
κ	Denticity
k	Rate constant
ν	IR absorption
ρ	Hammett rho value

μ	Bridging ligand
R^2	Coefficient of determination
R_f	Retention Value

LIST OF FIGURES

LIST OF SCHEMES

LIST OF TABLES

Chapter 1

Introduction

1.1 Transition Metal-Catalyzed Cross Coupling Reactions

Arylamines are very important motifs in many pharmaceutical compounds and natural products. Conventionally, anilines are synthesized by sequential nitration-reduction reactions of arenes. The regioselectivity of the nitration reaction being strongly dependent upon the electronic properties of the arenes remain an inherent drawback of this classical route. For instance, arenes with electron-donating substituents produced dominantly *ortho*- and *para*- region-isomers, whereas those bearing electron-withdrawing substituents produced mainly *meta*-isomer. Hartwig-Buchwald Amination[1] and Ullmann Coupling Reactions[2] (Scheme 1.1) are currently widely accepted approaches for regioselective C(aryl)-N bonds formation. Yet, pre-functionalized arenes are pre-requisite for effective transformation. Apparently, direct amidation or amination of unactivated C-H bonds of hydrocarbons (e.g. arenes) constitutes atom-economical and step-efficient route to C(sp^2/sp^3)-N bonds formation.

Scheme 1.1. Scheme of Hartwig-Buchwald Amination and Ullmann Coupling Reaction

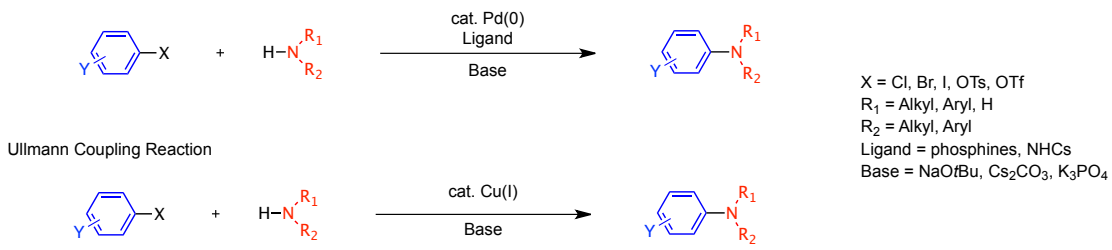

1.1.1 Pd-Catalyzed *ortho*-C-H Bond Intermolecular Aminations and Amidations of Arenes

Intermolecular direct aminations and amidations enable direct functionalization of simple arenes. Present of directing groups (chelation-assistance) on the arene substrates effect *ortho*-selective Pd-catalyzed intermolecular arene C-H bond aminations and amidations (Scheme 1.2).[3,4] The high degree of regiocontrol is brought about by pre-coordination of the donor groups (e.g. pyridyls, amides, ketones and carboxyls) to the Pd(II) catalyst; the C-H bond clevage step is mediated by the formation of five or six-membered cyclopalladated complexes. Subsequent functionalization of the aryl-metal bond with electrophilic amines through the nitrene insertion or Pd(II)/(IV) manifold furnished the arylamines.

Scheme 1.2. Pd-Catalyzed *ortho*-C-H Aminations and Amidations of Arenes

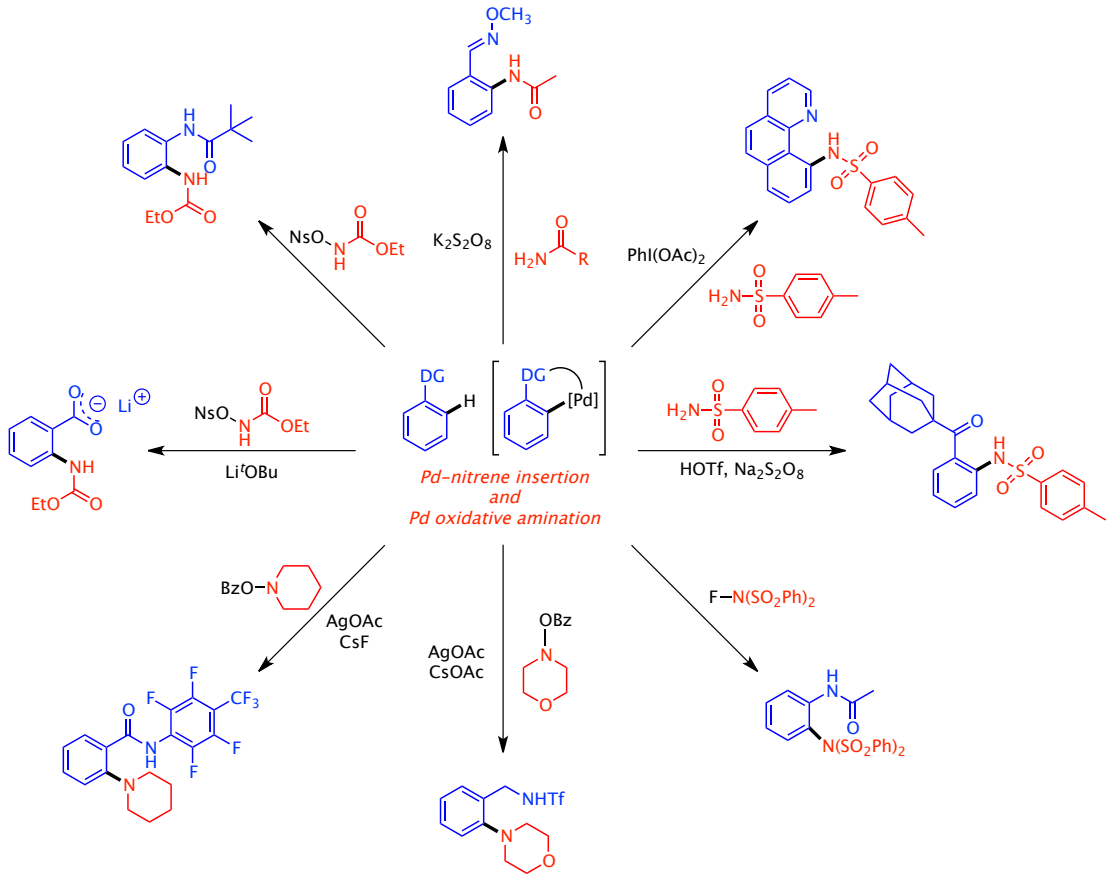

Che and co-workers[5] reported the first example of Pd(II)-catalyzed intermolecular *ortho*-C-H bond amidation reaction of aromatic oximes with various amides such as carbamates, acetamides, sulfonamides and cinnamides (Scheme 1.3). Treatment of the *O*-methyl oximes with $Pd(OAc)_2$ catalyst (10 mol %), amides (1.2 equiv) and $K_2S_2O_8$ (2.0 equiv) as oxidant in DCE at 80 ^{o}C gave excellent yield of *orhto*-amidation products. The proposed mechanism of the reaction involved formation of a five-membered palladacycle. It was proposed that nitrene insertion on the Pd-C bond produced the amidation products (Scheme 1.4).

Scheme 1.3. Pd-Catalyzed Direct *ortho*-C-H Amidation of Aromatic Oximes

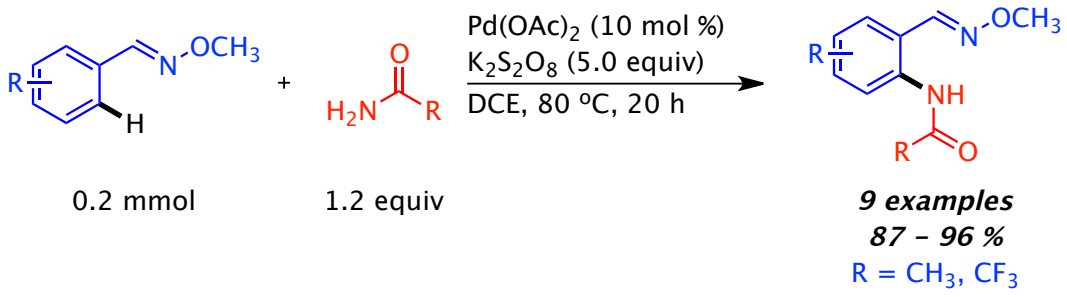

Selected Substrate Scope

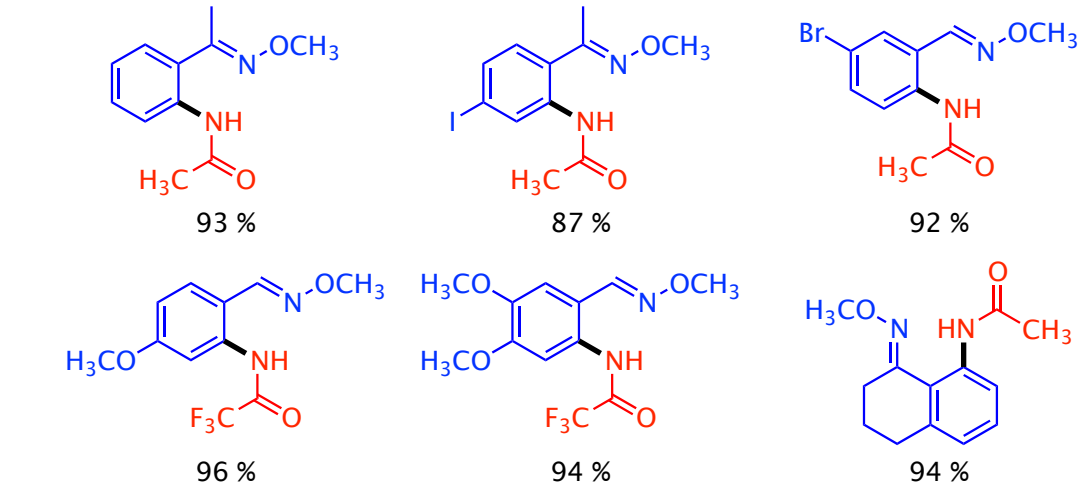

Scheme 1.4. Proposed Mechanism of *ortho*-C-H Amidation of Aromatic Oximes

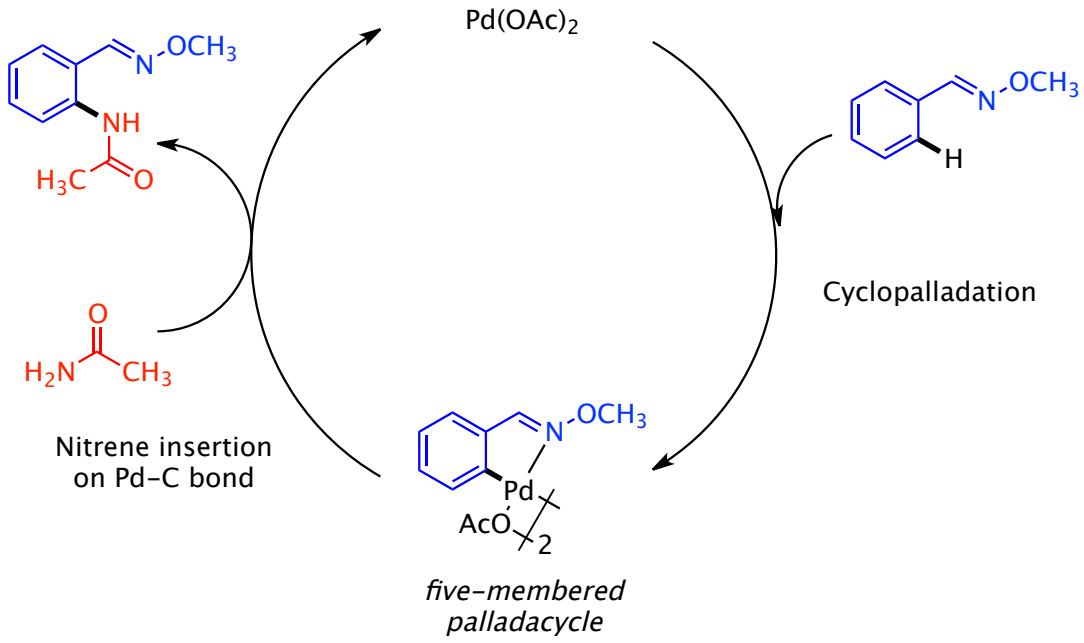

Yu and co-workers[4t] reported another intermolecular *ortho*-C-H bond amidation reaction of Pd catalyst and *N*-nosyloxycarbamates employing anilides as substrates (Scheme 1.5). In this reaction, the *N*-nosyloxycarbamates serve as nitrene source and any external oxidants are not required. Interestingly, the reaction demonstrated the differences in C-H bond activation of substrates bearing electron-donating substituents and electron-withdrawing substituents. The amidation is more efficient in the arene substrates bearing electon-withdrawing substituents (e.g. F, Br and $OCHF_2$). In addition, the pivalanilides containing vinyl and ester groups showed the selective C-N bond formation only at *ortho*-position to anilide directing group.

Scheme 1.5. Pd-Catalyzed *ortho*-C-H Amidation of Anilides by *N*-nosyloxycarbamates

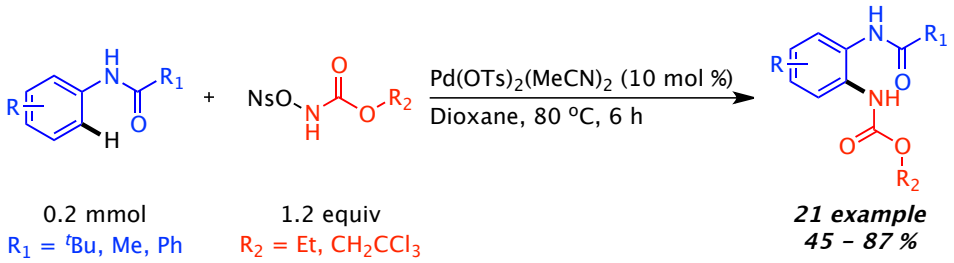

Selected Substrate Scope

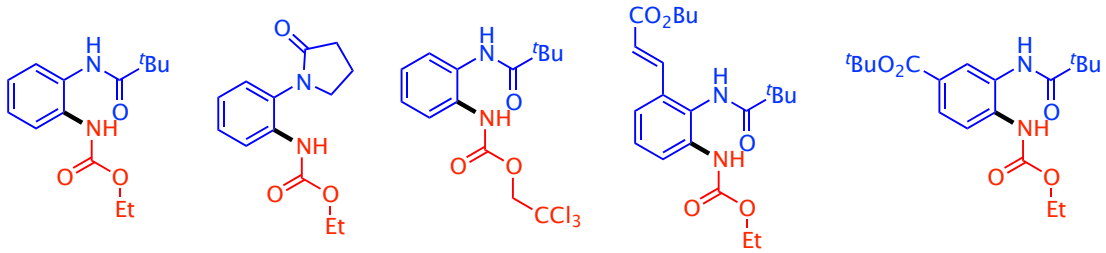

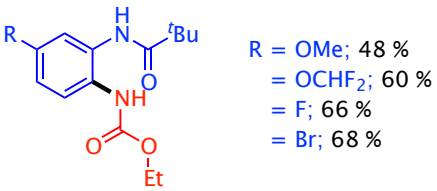

With regard to mechanism, the cyclopalladated anilide complex was isolated and characterized by X-ray crystallography (Scheme 1.6). After the *ortho*-C-H bond

clevage, the six-membered palladacycle intermediate was formed. The Pd-nitrene intermediate was formed by reacting with the *N*-nosyloxycarbamate, followed by the nitrene insertion on Pd-C bond to afford the desired C-N bond.

Scheme 1.6. Proposed Mechanism of *ortho*-C-H Amidation of Anilides by *N*-nosyloxycarbamates

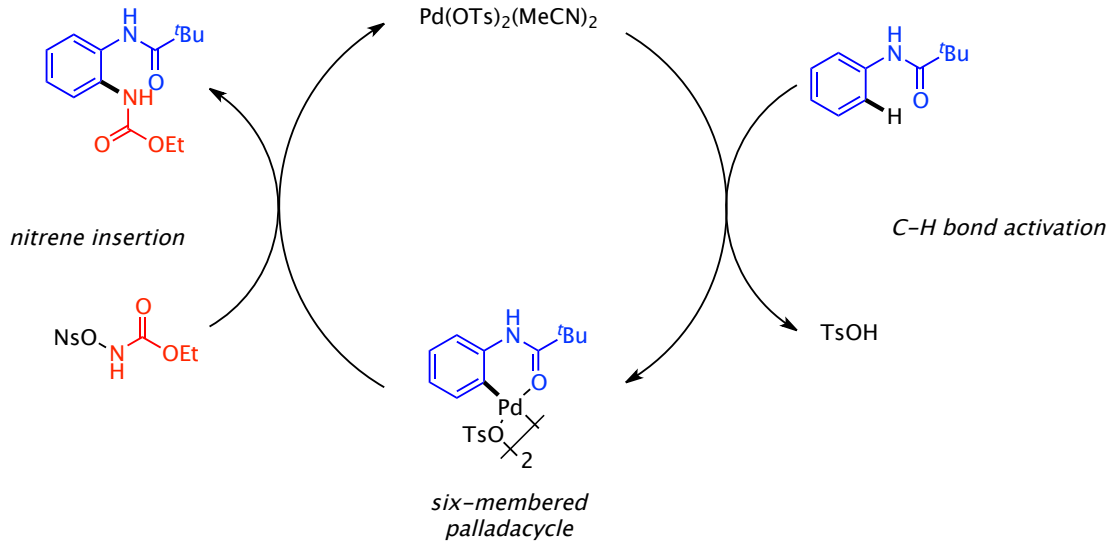

Pd(II)/(IV) oxidative aminations and amidations are another strategy for direct *ortho*-C-N bond formation on aromatic rings. JQ Yu's group[4q] reported the Pd-catalyzed oxidative *ortho*-C-H bond aminations employing trifyl-protected benzamides with *O*-benzyl hydroxylamines (Scheme 1.7). CsF was used as a base to deprotonate the benzamides for cyclopalladation. The aryl group of the benzamides is highly electrophilic so the N-H bond of benzamides is very acidic (pKa is very low). The N-H bond of benzamides was deprotonated by CsF easily. It was found that AgOAc is the best oxidant in this reaction. The silver ion should remove the OBz^- ion from the Pd catalyst for turnovers.

Scheme 1.7. Pd-Catalyzed Amination of *N*-Aryl Benzamides with *O*-benzyl Hydroxylamines

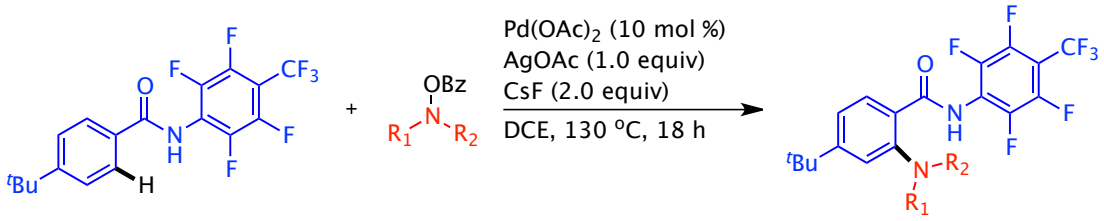

Selected Substrate Scope

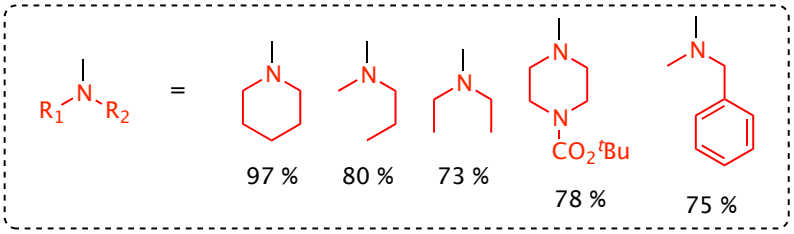

It was proposed that depronation of the benzamides by CsF should form a cesium salt, in which the carbonyl group be ketolized to afford an imine group. The imine group should coordinate to the Pd(II) catalyst for cyclopalladation of the arene ring (Scheme 1.8). Plausibly, the *O*-benzyl hydroxylamines underwent oxidative addition on the palladcycle complex to form a Pd(IV) complex. The amination products were produced by reductive elimination of the Pd(IV)-aryl-amido complex. The Pd(IV) intermediate would be stabilized by strong σ-donor ligands such as pyridines, quinolones and *N*-heterocyclic carbenes.

Scheme 1.8. Proposed Mechanism of Amination of *N*-Aryl Benzamides with *O*-benzyl Hydroxylamines

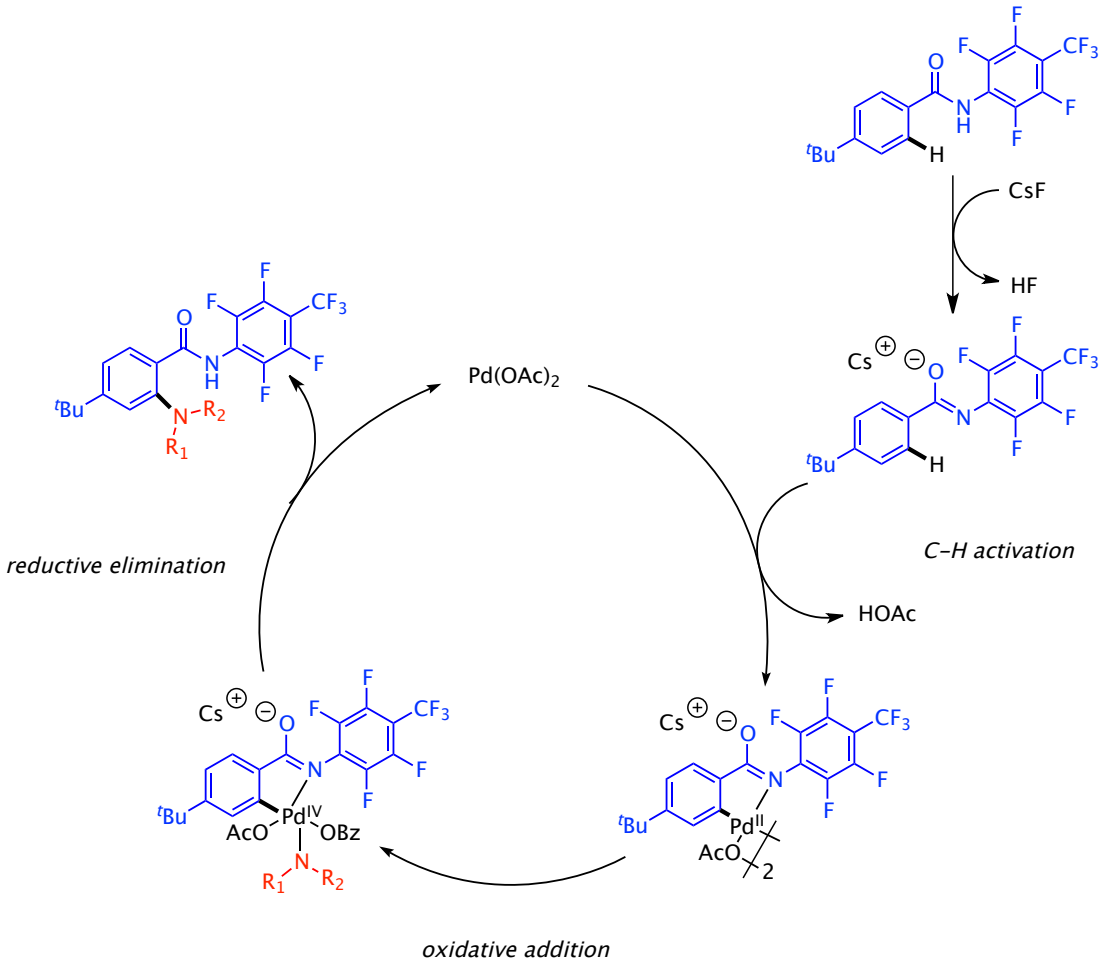

Liu and co-workers[4f] demonstrated another example of Pd(II)-catalyzed oxidative amidation of aromatic ketones (Scheme 1.9). Employing the aromatic ketones with catalytic amount of $Pd(OAc)_2$ (10 mol %), sulfonamides (2.0 equiv) as amidating reagent, HOTf (0.5 equiv) and $Na_2S_2O_8$ (2-4 equiv) as an oxidant in DCE at 80 ^oC gave moderate to good yield of amidation products. The combination of $Pd(OAc)_2$ and HOTf *in-situ* generated the electron-deficient $Pd(OTf)_2$ in the reaction. The sulfonamides bearing the electron-withdrawing group enhanced the amidation reaction.

Scheme 1.9. Pd-Catalyzed Oxidative Amidation of Aromatic Ketones

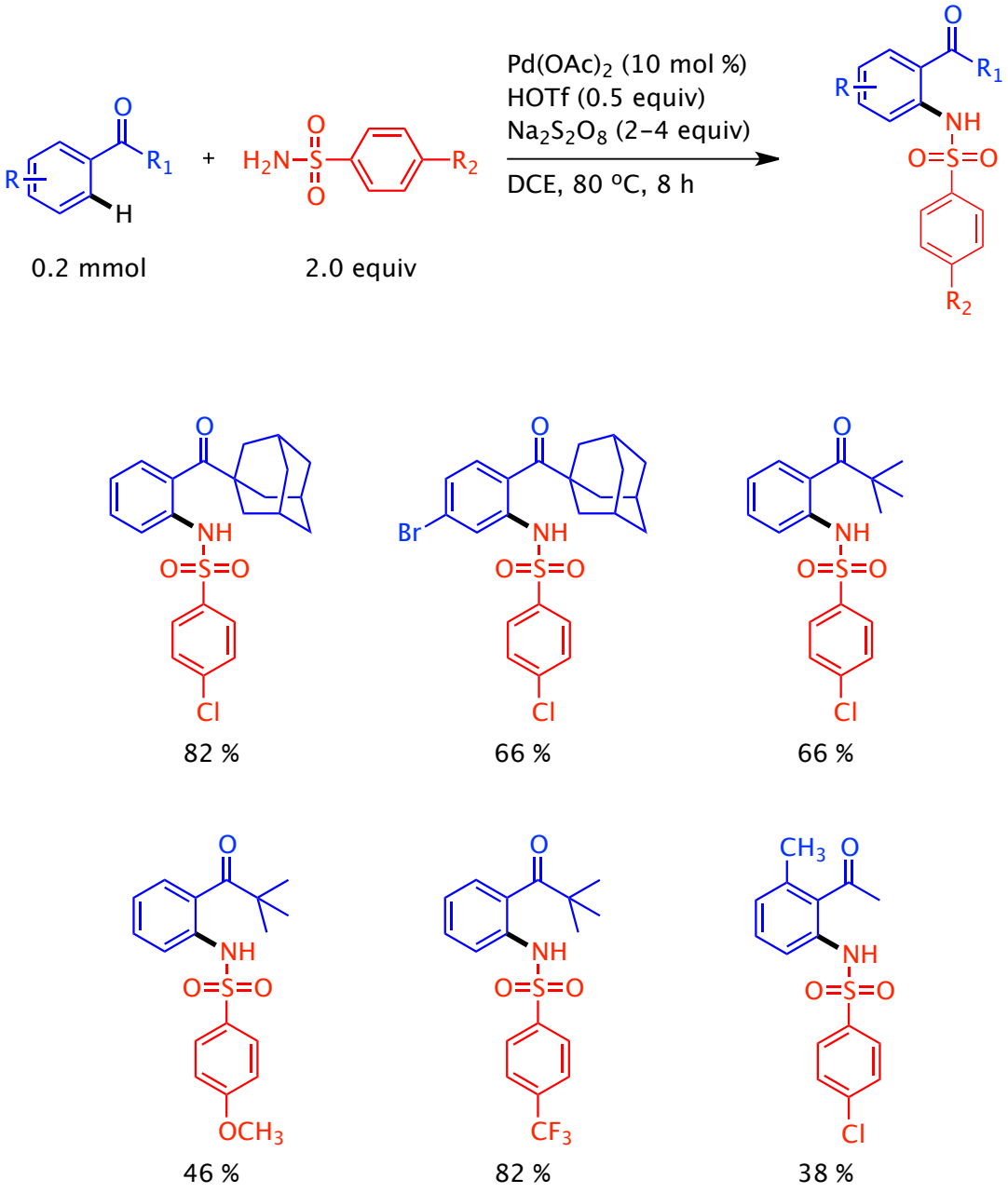

Scheme 1.10 shows the proposed mechanism. According to Liu's report, the intermediate II has been isolated by reacting ketones with $Pd(OAc)_2$ and HOTf. Then, the intermediate III was obtained by reacting intermediate II with sulfonamide. Intermediate III has been characterized by X-ray crystallography. By reacting intermediate III with an oxidant, the desired C-N bond formation was obtained. It is concluded that the amidation involved (1) cyclopalladation of ketones and $Pd(OTf)_2$

(2) Pd-aryl-amido complex formation (3) oxidation of Pd(II) to Pd(IV) (4) reductive elimination of Pd(IV) intermediate to give desired products.

Scheme 1.10. Proposed Mechanism of Oxidative Amidation of Aromatic Ketones

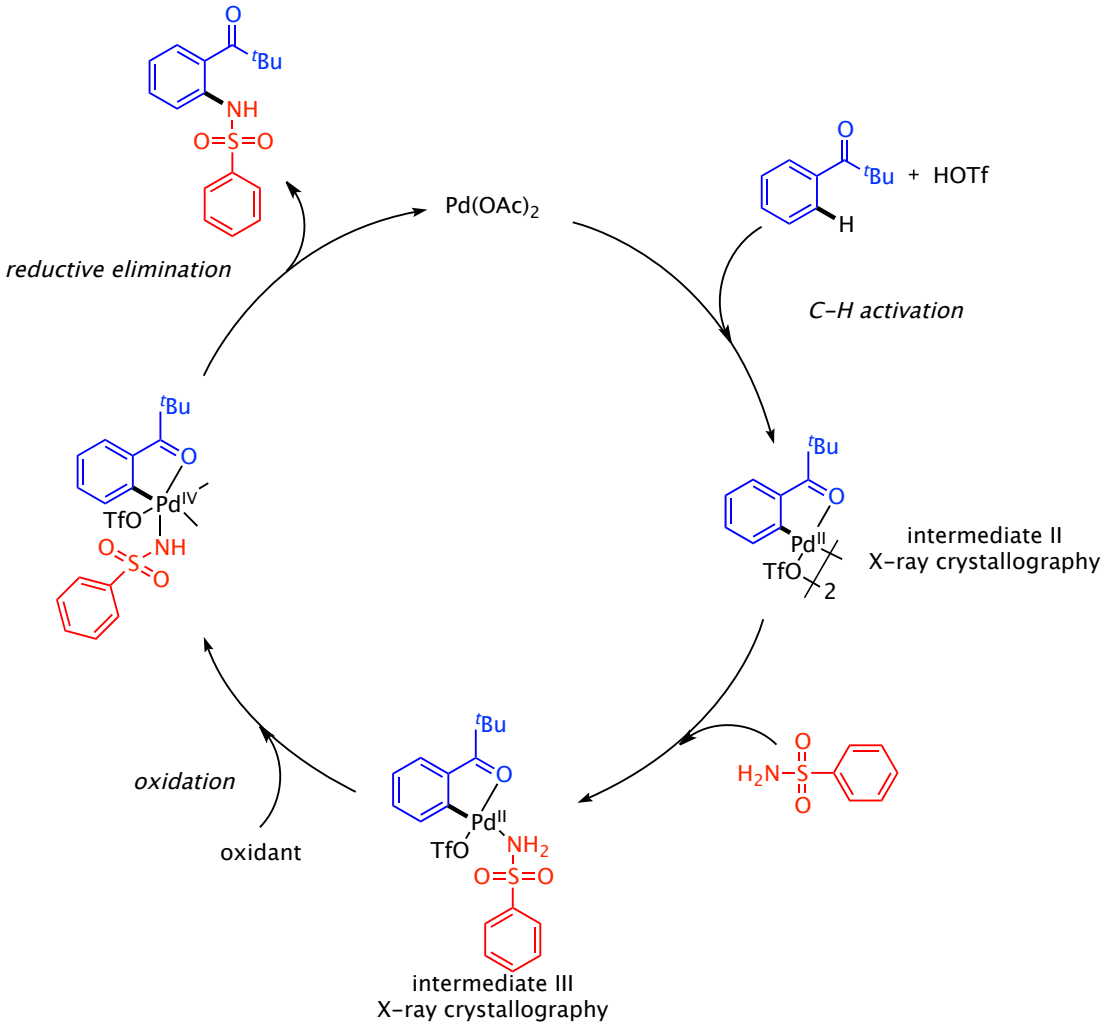

1.1.2 Pd-Catalyzed *meta*- and *para*-C-H Bonds Intermolecular Acetoxylations of Arenes

A majority of the literature examples of *ortho*-C-H bond aminations and amidations involved the cyclopalladation with five-membered or six-membered ring structures. Structural templates that cater for higher-membered metallocycles where may enable C-H activation at more distal positions (e.g. *meta*- or *para*- C-H bond). The

research groups of JQ Yu's group[6] and Maiti's group[7] indepentantly reported the design of U-shaped template for *meta*- and *para*-selective arene functionalizations. In their designs, the U-shaped template directing groups with weakly coordinating group (e.g. nitrile) and strongly coordinating groups (e.g. pyridyl) achieved the *meta*-selective and also the *para*-selective functionalization of arenes (Scheme 1.11). Molecular modelling studies for the *meta*-selective functionalization systems suggested that a 12-membered cycloplane structure is a key conformation to mediate *meta*-selective C-H palladation. Yet, a 16-membered cycloplane structure is the most likely conformation of the *para*-C-H palladation.

Scheme 1.11. Examples of U-Shaped Template for Non-*ortho*-Selective C-H Functionalization

JQ Yu

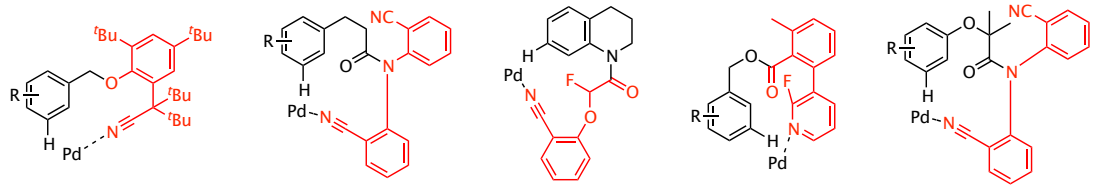

Maiti

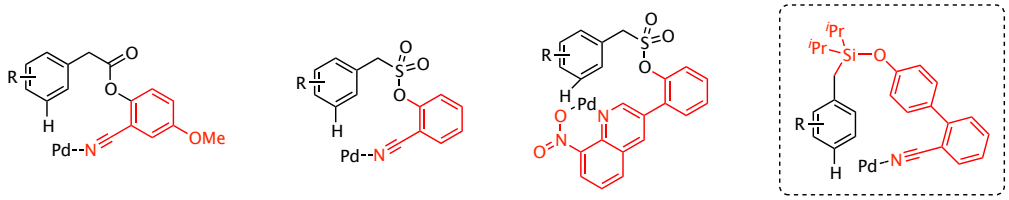

One of the successful examples for the *meta*-C-H bond acetoxylation is shown in Scheme 1.12.[7k] Treatment of the substrates containing 8-nitro-quinoline directing group with $Pd(OAc)_2$ (10 mol %), *N*-acetyl glycine (20 mol %) as a ligand, $PhI(OAc)_2$ (4.0 equiv) as an oxidant and acetoxylation reagent in mixture of HFIP and acetic anhydride at 80 ^{o}C gave moderate to good yield in acetoxylation products. *N*-acetyl glycine plays important rules in conversion of trimeric $Pd(OAc)_2$ into monomeric Pd catalyst and C-H bond activation step of the reaction.

Scheme 1.12. Pd-Catalyzed *meta*-C-H Acetoxylations of Arenes

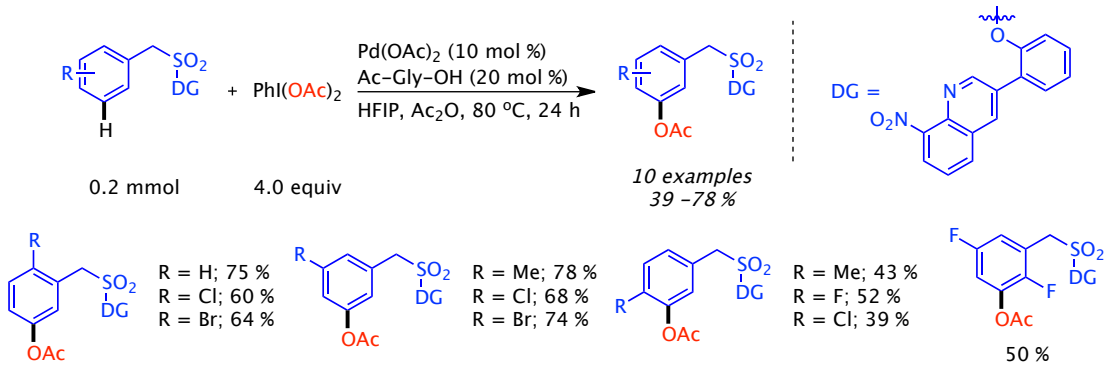

By ESI-MS analysis (m/z = 566), the 12-membered cycloplane conformation plausibly mediates the cyclopalladation at the *meta*-C-H position. After the ligand exchange reaction between acetate ions and *N*-acetyl glycine, the monomeric Pd catalyst was chelated by 8-nitro-quinoline directing group and then underwent the C-H bond activation forming the 12-membered palladacycle. The 12-membered palladacycle was oxidized by $PhI(OAc)_2$ to form the Pd(IV) intermediate and the aectoxylation products were produced by reductive elimination (Scheme 1.13). The 8-nitro-quinoline is good σ-donor with bidentate chelation to Pd center.

Scheme 1.13. Proposed Mechanism of *meta*-C-H Acetoxylation

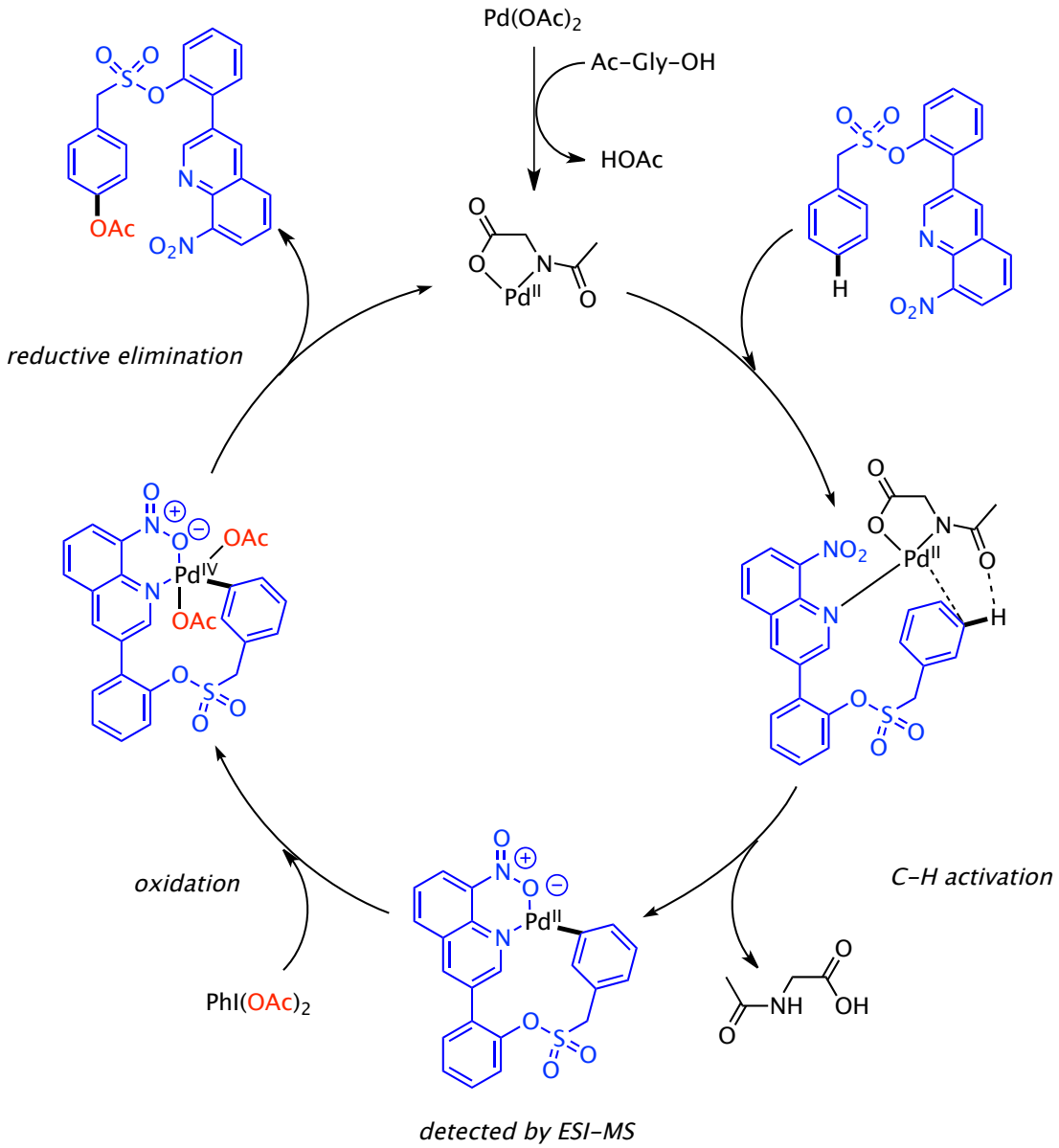

With C-H acetoxylation as a model, Maiti's group[7c] also designed the silylbiphenyl-based directing group for the C-O bond formation at the *para*-position (Scheme 1.14). It was proposed that the cyclopalladation might proceed through a 16-membered cycloplane liked transition-state. The silicon atom of the substrates should increase the flexibility of the directing group to favor the *para*-C-H bond acetoxylation.

Scheme 1.14. Pd-Catalyzed *para*-C-H Acetoxylation of Arenes

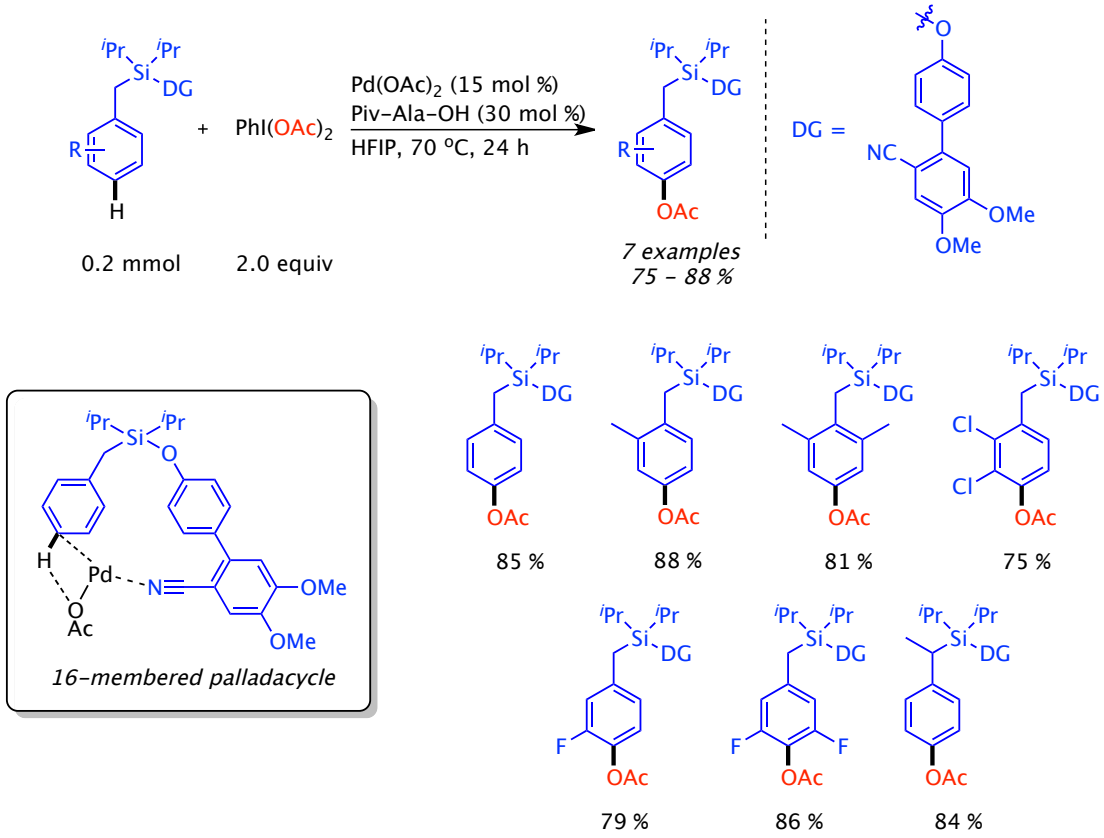

1.1.3 Directing Group Free Pd(II)- and Au(I)-Catalyzed Oxidative Amidations of Simple Arenes

In 2013, Hartwig and co-workers[8] reported the first example of directing group free Pd(II)-catalyzed amidation reaction of arenes (Scheme 1.15). Employing phthalimide as coupling partner with $Pd(OAc)_2$ (10 mol %) as catalyst, tri-*tert*-butyl phosphine (20 mol %) as a ligand, $PhI(OAc)_2$ (6.0 equiv) as an oxidant in neat arenes (1 mL) at 100 °C for 33 h produced the desired *N*-arylphthalimides in good to excellent yields. The regioselectivity of the reaction depends on the steric properties of the bulky tri-*tert*-butyl phosphine ligand. Also, the electronic properties of the substituents on the

arenes affect the regioselectivity of the reaction. For the arenes bearing electron-donating groups (e.g. Me, and OMe), the *para*-isomer is dominant. The arenes bearing electron-withdrawing groups such as CF_3 gave *meta*-isomer as a major product. The disubstitited and trisubstituted arenes, the C-N bond formation occurred at the less hindered position (i.e. β-position). According to Hartwig's report, dehalogenation of the arene substrates is not observed.

Scheme 1.15. Directing Group Free Pd(II)-Catalyzed Oxidative Amidation of Arenes

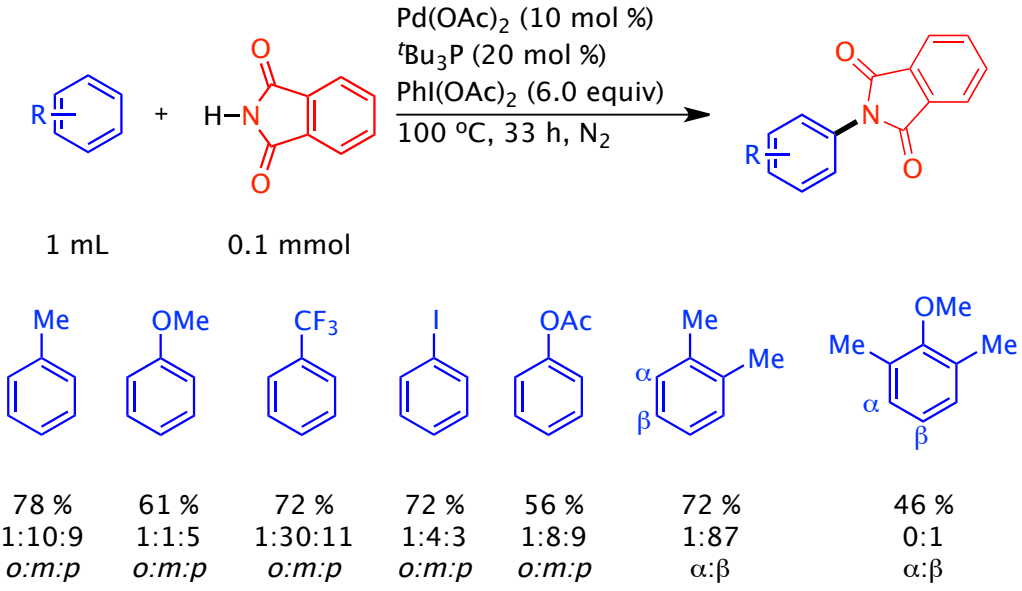

DeBoef and co-workers[9] also demonstrated a similar reaction using [Cy_3PAuCl] as a catalyst (Scheme 1.16). According to the report, only those arenes bearing electron-donating substituents favor the transformation. The fluorobenzene, chlorobenzene and 1,2-dichlorobenzene gave poor results, whereas toluene and anisole gave good yields in the desired product formation. The regioselectivity of the reaction mainly occurred at *para*-position or the less hindered position.

Scheme 1.16. Directing Group Free Au(I)-Catalyzed Amidation of Arenes

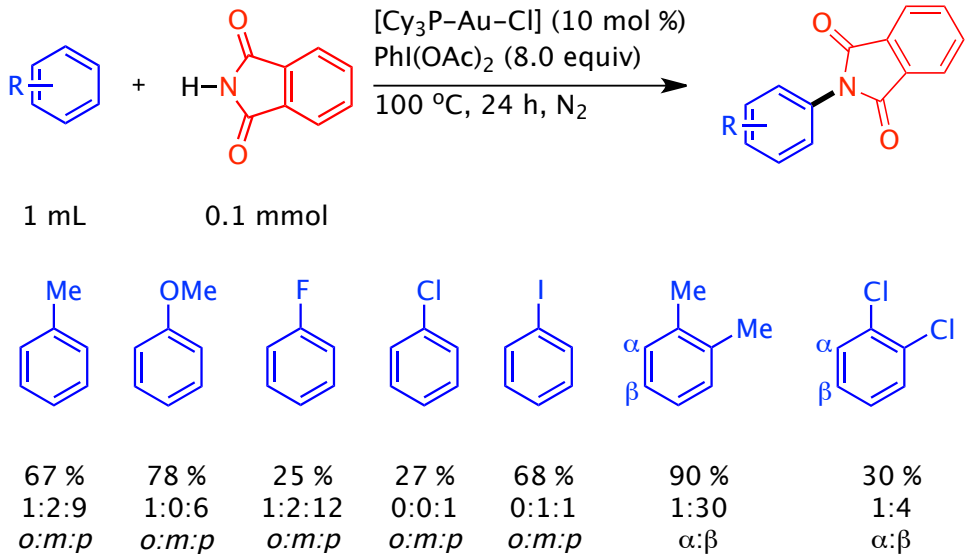

For the mechanism, they proposed the first step is oxidation of Au(I) catalyst to Au(III) catalyst with $PhI(OAc)_2$ oxidant. After the oxidation, the C-H activation of electron-rich arenes formed Au-C bond. The Au-C bond formation occurred at *para*-position because Au(III) ion is highly electrophilic. The partial negative charge is developed at the *para*-position due to the π-conjugation with the electron-donating groups. The $PhI(OAc)_2$ reacted with phthalimide to form [PhI(OAc)(NPhth)] which underwent transmetallation of Au(III)-aryl complex generating the Au(III)-aryl-amido complex. The fast reductive elimination produced the desired amidation products. A large amount of $PhI(OAc)_2$ is required to substain the oxidation of Au(I) to Au(III) and generation of [PhI(OAc)(NPhth)] species *in-situ* for transmetallation.

Scheme 1.17. Proposed Mechanism of Directing Group Free Au(I)-Catalyzed Amidation of Arenes

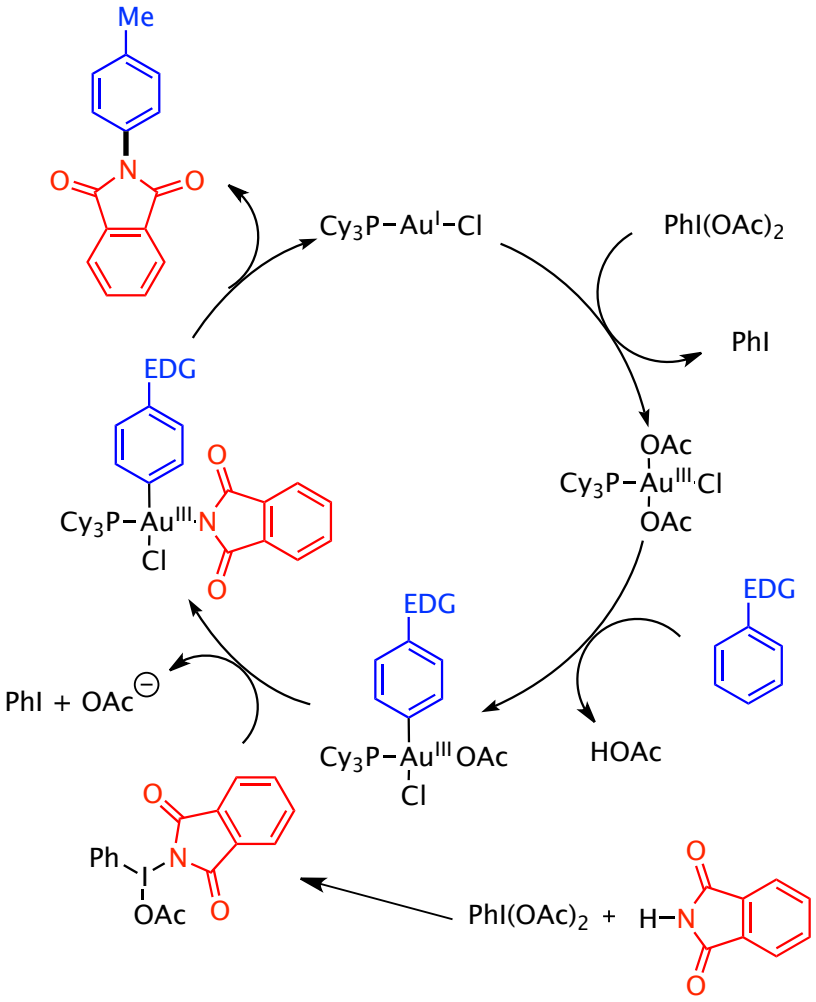

1.1.4 Directing Group Free Pd(II)- and Fe(II)-Catalyzed Electrophilic Amidations of Simple Arenes Through Single Electron Transfer System

Two examples demonstrated that phthalimide is a nucleophilic amidating reagent and the regioselectivity can be controlled by steric factors of the bulky ligands and substrates. However, two reactions required largely excess amount of both arenes and $PhI(OAc)_2$. Ritter's group[10a,b] reported a directing group-free arenes imidation reaction using a defined monomeric palladium complex to give a *para*-isomer as a major isomer (Scheme 1.18). In their reaction, arenes are limiting reagents and no extra oxidant was required. The regioselectivity of the reaction is controlled by

electronic properties of the substituents. The C-N bond formation on the arenes bearing the electron-donating substituents is more preferable.

Scheme 1.18. Directing Group Free Pd(II)-Catalyzed Imidation of Arenes

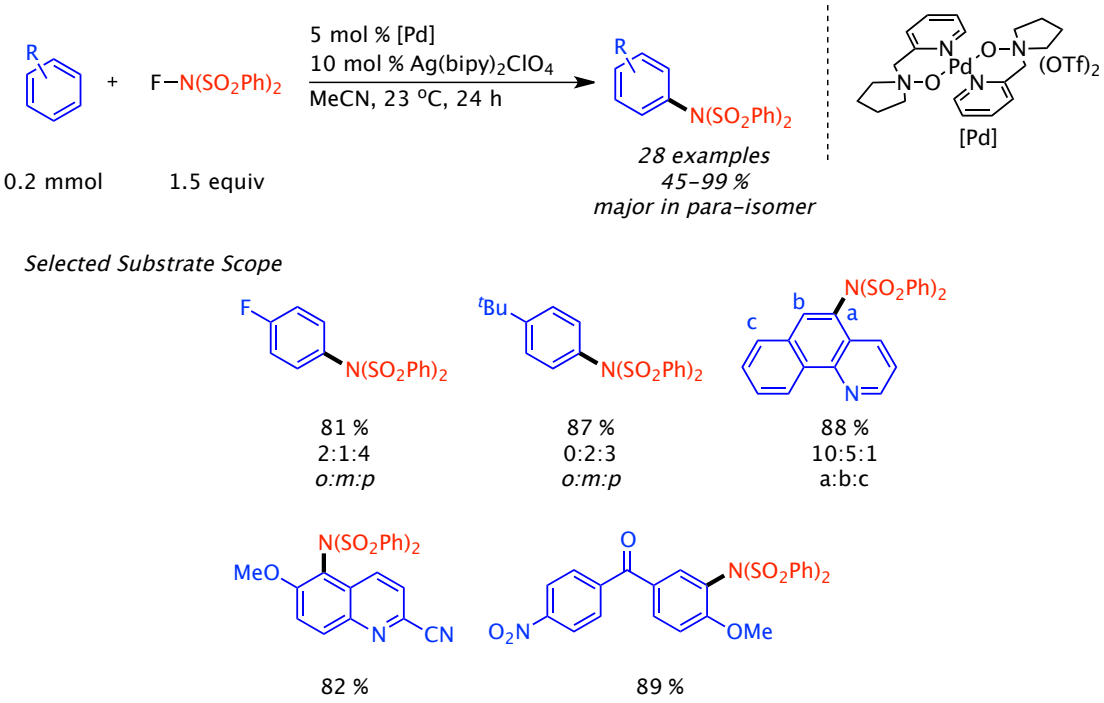

According to Ritter's report, the turnover limiting step of the reaction is the oxidation of Pd(II) to Pd(IV) intermediate. The monomeric Pd(II) complex is oxidized by NFSI to form Pd(IV) intermediate. The Pd(IV) intermediate is reduced immediately by $Ag^{I}(bipy)_2ClO_4$ to form Pd(III) intermediate which transfers sulfonimidyl radical to arenes. The radical species of arenes undergoes hydrogen radical abstraction by [Ag^{II}] species to form the imidation product (Scheme 1.19). The *para*-isomer is dominant because the electron-donating groups stabilize the radical generated at *para*-position of the arenes.

Scheme 1.19. Proposed Mechanism of Pd(II)-Catalyzed Imidation of Arenes

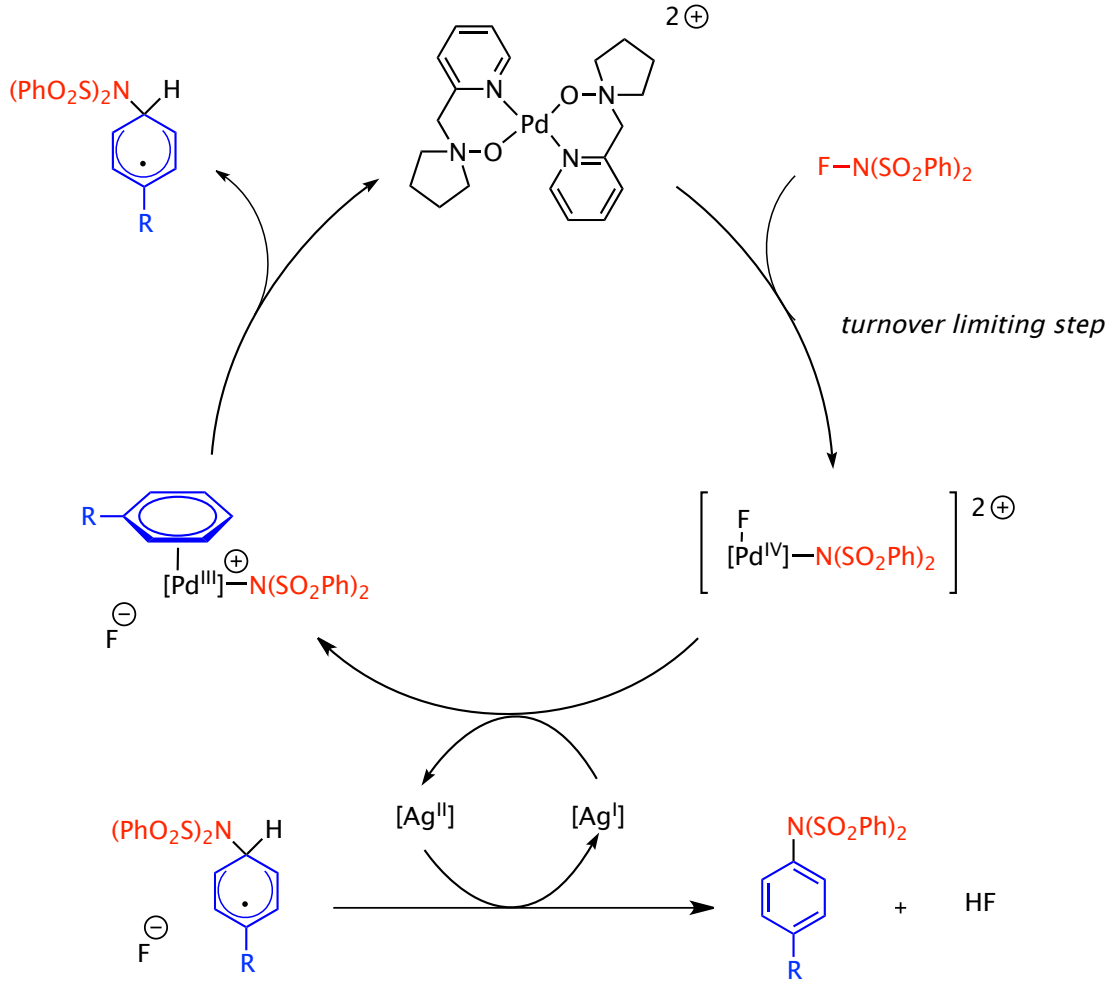

Apart from Pd(II) catalyst, Ritter's group also reported Fe(II)-catalyzed amination reaction of simple arenes[10c] (Scheme 1.20). The cationic $[MsO\text{-}NH_3]^+OTf^-$ acts as electrophilic aminating reagent and it undergoes N-O bond cleavage at 60 °C. Thec function of the Fe(II) catalyst is to abstract one electron from arenes to form Fe(III) and ammoniumyl radical. The ammoniumyl radical is then oxidized by Fe(III) complex to form corresponding aniline as a product. For this reaction, electron-deficient arenes and heterocyclic arenes are also applicable for the amination. The regioselectivity of Ritter's reaction strongly depends on the electronic properties of the substituent. *meta*-Isomer is dominant for the electron-deficient arenes.

Scheme 1.20. Directing Group Free Fe(II)-Catalyzed Amination of Arenes

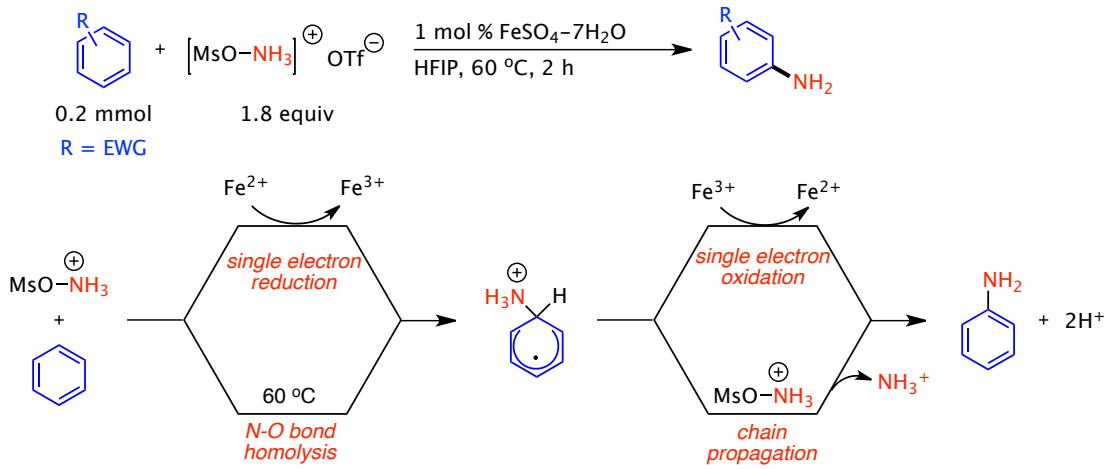

1.1.5 Directing Group Free Pd(II)- and Cu(I)-Catalyzed Electrophilic Amidations of Arenes Through Two Electrons Transfer System

As shown by Ritter's examples, direct C-H amidation or imidation can proceed by single electron transfer mechanism. Some examples demonstrated that the electrophilic amidations of arenes through two-electron mechanism. Emmert and co-workers[11] showed that treating *N*-acetylamides (0.1 mmol) with a catalytic amount of $Pd(OAc)_2$ (15 mol %), 2,2,6,6-tetramethyl-1,2,3,5,6,7-hexahydrodicyclopenta[*b*,*e*]pyridine (18 mol %) and AgOAc (5 mol %) in benzene (1 mL) at 100 ^{o}C gave the corresponding anilides in moderate yields (Scheme 1.21). Thermal decomposition of the *N*-acetylamides at 100 ^{o}C, however, limited the performance of Emmert's reaction.

Scheme 1.21. Eletrophilic Amidation of Arenes Reported by Emmert's Group

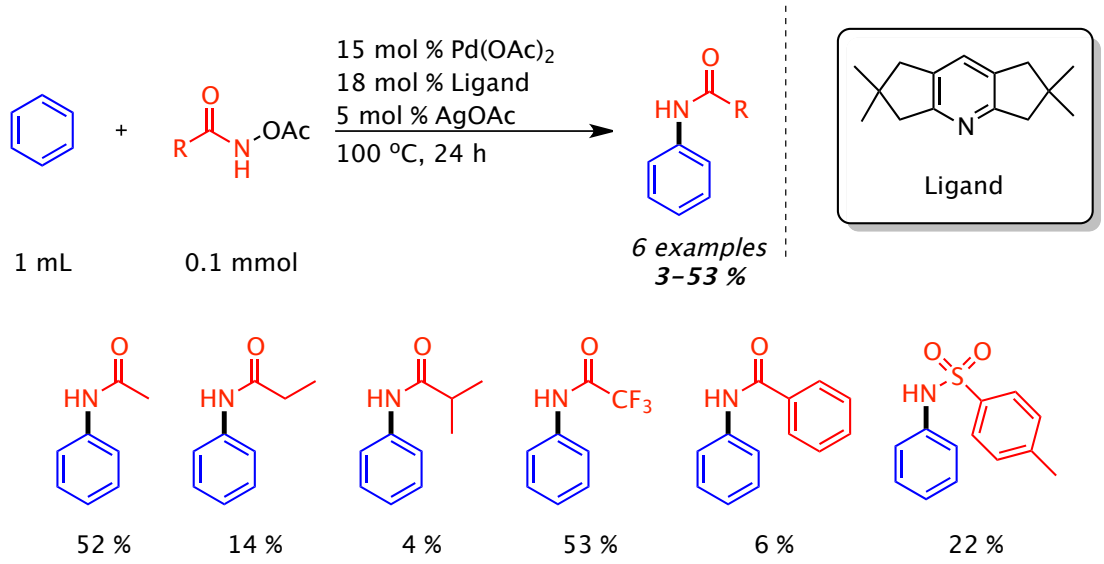

According to the mechanism postulated by Emmert (Scheme 1.22), the 2,2,6,6-tetramethyl-1,2,3,5,6,7-hexahydrodicyclopenta[*b*,*e*]pyridine is a strong σ donor ligand to dissociate the trimeric form of $Pd(OAc)_2$ into active monomeric $Pd(OAc)_2$. The first step is the formation of Pd(II)-aryl complex. In this step, the π-orbital of benzene coordinated with Pd(II) center. The π coordination to the Pd(II) center would allow C-H activation of the benzene through concerted-metallation-deprotonation (CMD) mechanism. Then, the *N*-acetylamides underwent oxidative addition to Pd(II)-aryl complex to form Pd(IV)-aryl-amido intermediate. The pyridine type ligand 2,2,6,6-tetramethyl-1,2,3,5,6,7-hexahydrodicyclopenta[*b*,*e*]pyridine helps to stabilize the highly electrophilic Pd(IV) intermediate. Finally, the Pd(IV)-aryl-amido intermediate was reductive eliminated to form a new C-N bond on benzene.

Scheme 1.22. Postulated Mechanism of Emmert's Amidation

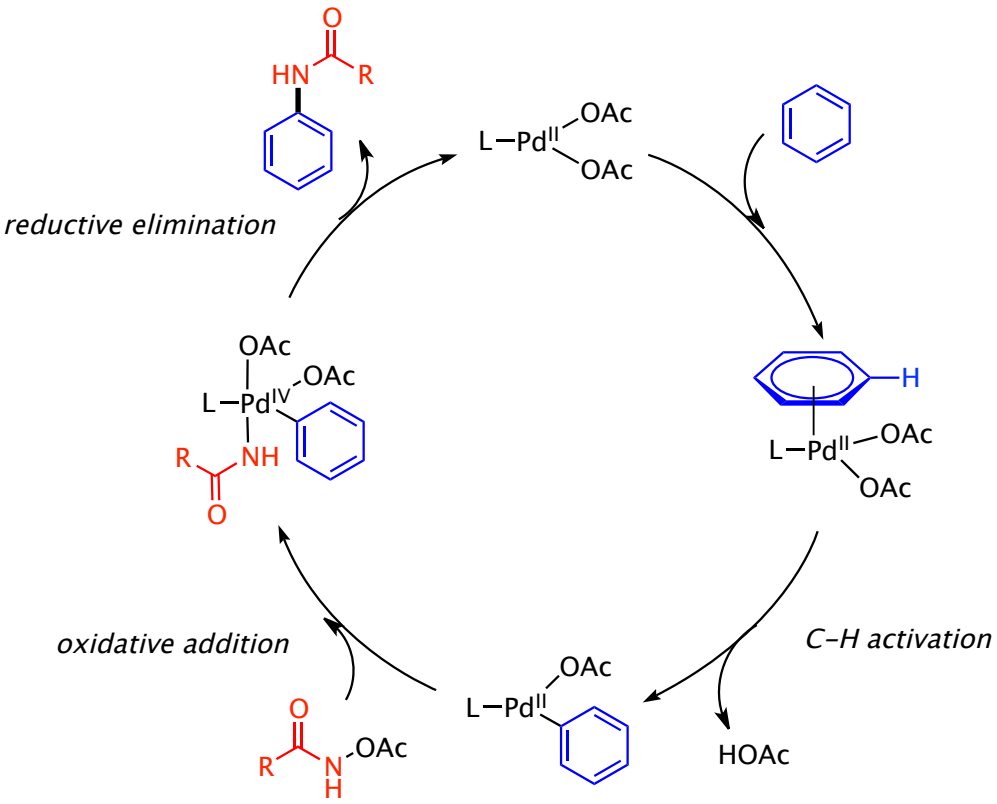

Another notable example is Cu(I)-catalyzed imidation reaction of heterocyclic arenes, fused arenes, porphyrins and natural products was also reported in the literature.[12] In the reaction, treatment of limiting amount of arenes (0.2 mmol) with NFSI (1.3 equiv) as a coupling partner and oxidant in the presence of CuBr (10 mol %) and 6,6'-dimethylbipyridine (15 mol %) in DCE (1 mL) at 70 ^{o}C gave good yield of the *ortho*-imidation products (Scheme 1.23). The mechanism of the reaction probably is going through Cu(I)/Cu(III) system as the NFSI underwent oxidative addition on Cu(I) catalyst to form Cu(III) complex followed by reductive elimination to form corresponding imidation products.

Scheme 1.23. Cu(I)-Catalyzed Imidation of Simple Arenes

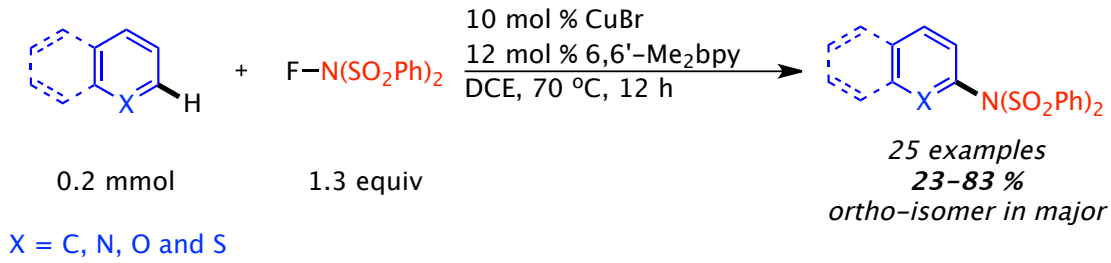

1.2 Transition Metal-Free Non-Chelation-Assisted C-H Bond Amidations of Simple Arenes

Transition metal-free C-H amidations and aminations have been reported for the synthesis of *N*-arylamides (Scheme 1.24). Chang[13] and DeBoef[14] reported the amidation reaction of simple arenes using phthalimide as nucleophile and $PhI(OAc)_2$ as oxidant at 140 ^{o}C in neat arene solvent. The results showed that the regioselectivity of the amidation depends on the electronic properties of the arenes analogous to Friedel-Craft-type reactions. It is likely that the key intermediate is hypervalent iodine(III) species [PhI(OAc)(NPhth)] according to ESI-MS analysis. The hypervalent iodine(III) intermediate abstracts one electron from the arenes to form a radical species. By classical Friedel-Craft model, the radical developed at the *ortho*-position should be more stabilized by electron-donating substituents (e.g. Me, OMe and OAc etc.). The transition state for the *ortho*-amidation product is more stable resulting in preferential *ortho*-amidation. The electron-withdrawing substituents (e.g. CF_3, CN and NO_2) probably destabilize the transition state resulting in less favored amidation for electron-deficient arenes. Antonchick and co-workers[15] used aminopyridines as coupling partners in HFIP solvent at room temperature. The

regioselectivity of the reaction is also *ortho*-isomer is dominant. It is because the key intermediate of Antonchick's reaction is also a hypervalent iodine(III) intermediate [PhI(OAc)(NHR)]. The mechanism of Antonchick's reaction is also going through electrophilic aromatic substitution in single electron transfer system (or radical substitution). As a result, the regioselectivity of the reaction is analogus to Friedel-Craft-type reactions, which is similar to the Chang's and DeBoef's reactions.

Scheme 1.24. Transition Metal Free Amidation and Amination of Arenes

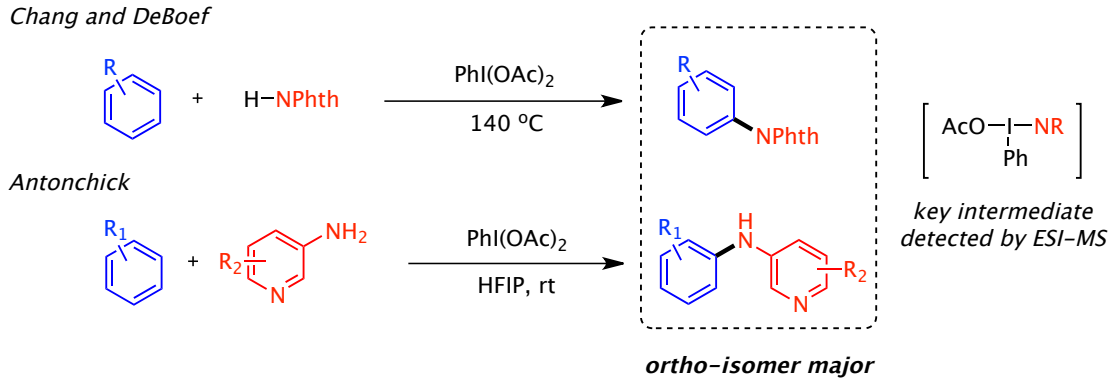

1.3 Asymmetric Transition Metal-Catalyzed Functionalization of C(sp^2)-H and C(sp^3)-H Controlled by Chiral Ligands

Asymmetric catalysis is of paramount importance for synthesis of enantioenriched molecules, which have found widespread application in drug development. Asymmetric catalysis employs non-covalent interactions such as steric repulsion, electrostatic, hydrogen bonding etc between the ligands and the substrates to effect enantiofacial differentiation. A notiable example is chiral phosphine ligands such as *(R)*-BINAP for asymmetric hydrogenation of dehydroamino acids to produce the enantio-pure amino acids. According to current understanding, the chiral *(R)*-BINAP provides steric differentiation on the substrate binding so that one of the

diastereomeric transition states would be destabilized. As a result, only one enantiomer of the product is dominant. For non-covalent interaction strategy, Corey and co-workers developed a chiral boronic acid as an organo-catalyst for the asymmetric Diels-Alder reaction. The chiral boronic acid ligand forms the Lewis-acid-base interaction with the functional group of the dienes. Therefore, the dienes overlap with dienophiles in only one specific direction. Inspired by two selected examples, many classes of ligands were modified and applied in several types of cross-coupling reactions.

1.3.1 Steric-Controlled Pd(II)-Catalyzed Desymmetrization of Arenes

JQ Yu and co-workers reported the asymmetric Pd(II)-catalyzed iodination reaction of trifluorosulfonic amides.[16] In this reaction, the symmetric trifluorosulfonic amide with pro-chiral center was functionalized by $Pd(OAc)_2$ as a catalyst and chiral *N*-benzylisoleucine as a ligand (Scheme 1.25). In the transition state model, the enantioselectivity-determining step is the C-H activation step. During the C-H activation, two intermediates, (*R*)- and (*S*)-intermediates were proposed. For the (*S*)-intermediate, the chiral isoleucine should experience steric repulsion between the side chain group and the arene ring of the substrates. This steric repulsion destabilizes the transition state of the (*S*)-intermediate. For the (*R*)-intermediate, on the other hands, the arene ring is located far away from the side chain of isoleucine ligand resulting in less steric repulsion. Thus, the (*R*)-intermediate is more stable and the arene ring (blue in color) of trifluorosulfonic amides was more activated for C-H functionalization

.

Scheme 1.25. Pd(II)-Catalyzed Desymmetrization of Trifluorosulfonic Amide

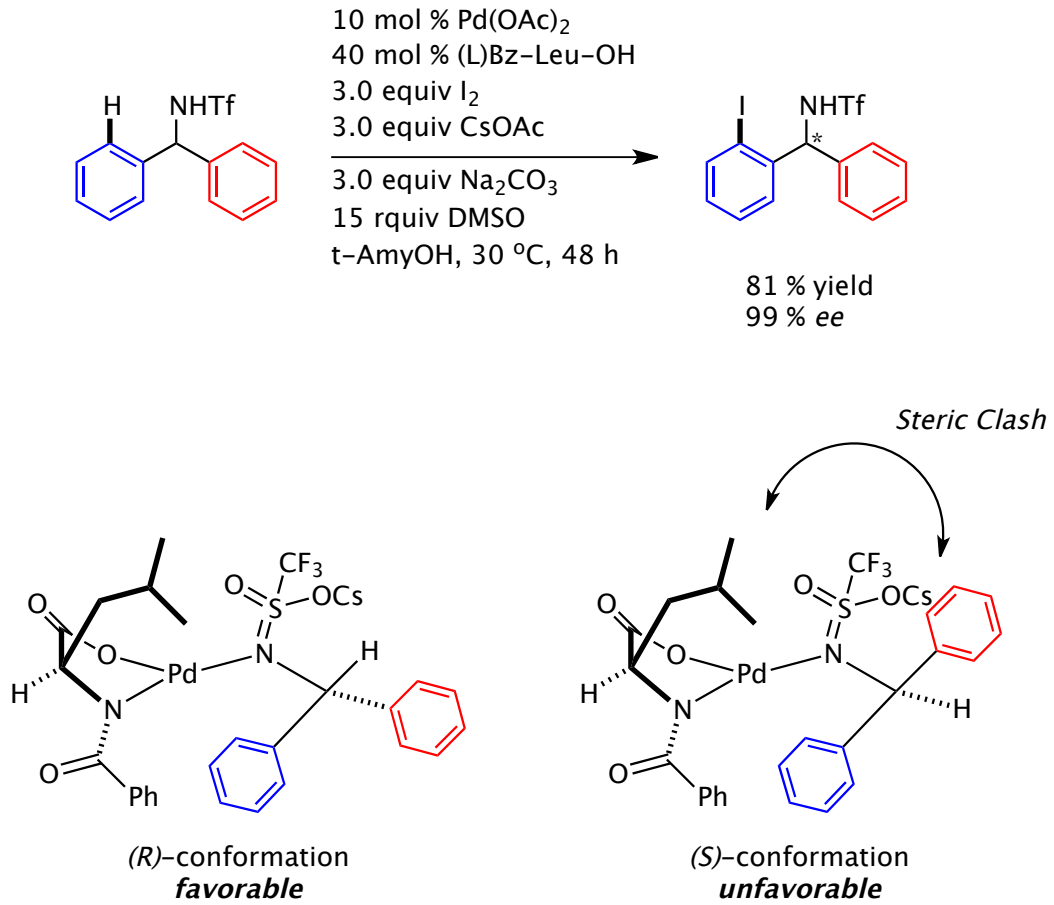

1.3.2 Steric-Controlled Asymmetric CpM(III)-Catalyzed Carbenoid Insertion on Arenes (M = Ir, Rh and Co)

Cramer and co-workers designed a chiral cyclopentadiene (Cp) ligand for the asymmetric d^6 metal-catalyzed carbenoid insertion on arene (Scheme 1.26).[17] In the reaction, the chiral center with absolute enantioselectivity was formed. In their hypothesis, the enantioselective-determining step is carbenoid insertion step (Scheme 1.27). After the Rh-carbenoid formation step, two intermediates (F and G) are formed with equilibrium position. When the carbenoid insertion occurs, the transition-state I is less stable. It is because the larger substituent of the carbenoid

has steric clash with the chiral Cp ligand, which destabilizes the transition-state I. Therefore, the formation of the (*S*)-isomer is unfavorable. For the transition-state H, the larger substituent of the carbenoid is far away from the chiral Cp ligand so that it has less steric repulsion leading (*R*)-isomer is more favorable. By thermodynamic consideration, the equilibrium should be shifted from intermediate G into intermediate F, and carbenoid insertion should produce the (*R*)-isomeric product.

Scheme 1.26. Asymmetric d[6] Metal-Catalyzed Carbenoid Insertion of Arenes

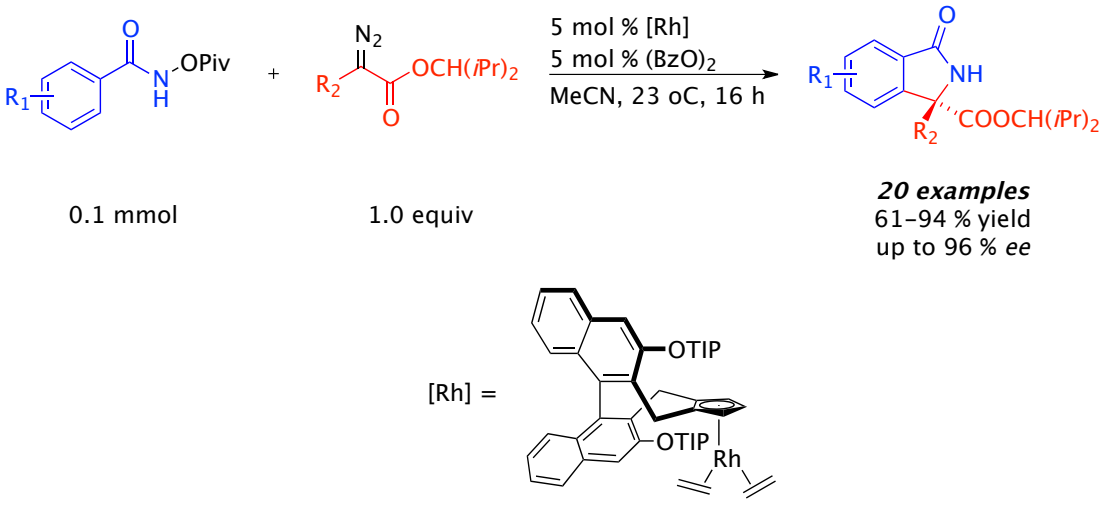

Scheme 1.27. Transition State Model of Enantioselective-Determining Step

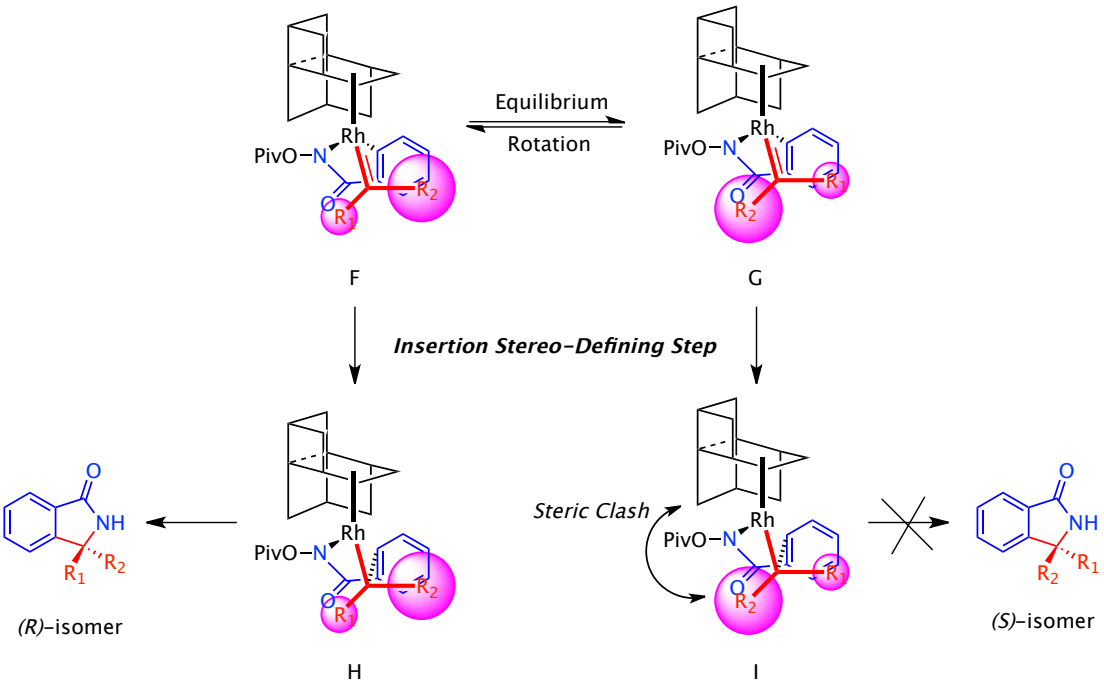

1.3.3 Enantioselective Ir(III)- and Ru(II)-Catalyzed γ-Lactam Formation Controlled by Steric Repulsion and Non-Covalent Interactions

By combining both steric factor and non-covalent interaction, it is very effective in controlling the enantioselectivity of the reaction. Chang and co-workers demonstrated Ir(III)-catalyzed asymmetric intramolecular nitrene C(sp^3)-H insertion fo γ-lactam formation.[18] Yu and co-workers also reported a related chiral Ru(II)-catalyzed reaction to achieve highly enantioselective γ-lactam formation (Scheme 1.28).[19a] Two examples showed that the chiral *N*-(quinolin-8-yl)amide and *R*,*R*-DPEN ligands in the Ir(III) and Ru(II) catalysts respectively achieve high enantioselective γ-lactam formation by exploiting both steric and non-covalent interactions. In the Ir(III)-catalyzed reaction, the phthalimide group of the *N*-(quinolin-8-yl)amide ligand exerted steric clash with the carbonyl group of the nitrenoid in the nitrenoid insertion step (Scheme 1.29a). Therefore, the transition state for the (*R*)-enantiomer formation is disfavored. On the other hands, the transition state for the (*S*)-enantiomer formation is more favored as no steric repulsion between the phthalimide group and the carbonyl group of the nitreniod. Moreover, the π-π stacking interaction between the aromatic quinoline of ligand and phenyl ring of nitrenoid stabilizes the transition state for the (*S*)-enantiomer formation. As a result, more favorable pro-(*S*)-γ-C(sp^3)-H bond should react preferentially the metal-nitrenoid from the opposite side of phthalimide group of the ligand to produce the (*S*)-enantiomeric γ-lactam.

Scheme 1.28. Asymmetric Intramolecular Nitrene C(sp^3)-H Insertion to Form Chiral γ-Lactams

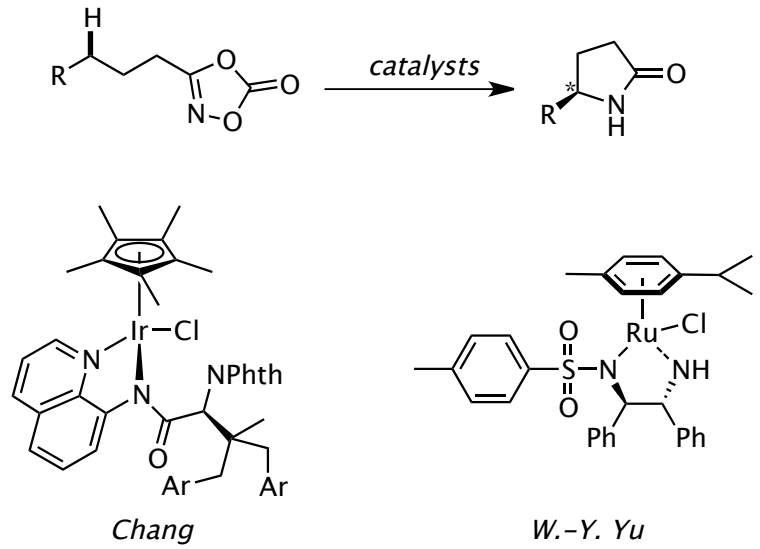

For the Ru(II)-catalyzed reaction, the enantioselectivity was analyzed by Newman projection model. The phenyl group adjacent to the amino group of the ligand is directing out of the plane. This conformation helps to provide steric repulsion with the nitrenoid (Scheme 1.29b). For **TS1-B**, the substituent R-group (e.g., Ph, Et, *t*Bu and Ad etc.) of the nitrenoid is closed to the phenyl ring of the ligand. This conformation has steric repulsion between the phenyl ring of the ligand and the substituent of the nitrenoid resulting in destabilization of **TS1-B**. For **TS1-A**, the conformation is characterized by that the substituent R-group of the nitrenoid is far away from the phenyl ring of the ligand. **TS1-A** should be more stable due to absence of steric repulsion. Moreover, the hydrogen bonding is formed between the amino group of the ligand and carbonyl group of nitreniod. This hydrogen bonding helps to stabilize **TS1-A** further for the nitreniod insertion. Therefore, the γ-C(sp^3)-H bond was approached the metal-nitrenoid through the more stable **TS1-A** to form γ-lactam with high enantiomeric excess.

Scheme 1.29. Transition State Model for Enantioselective Nitrenoid Insertion

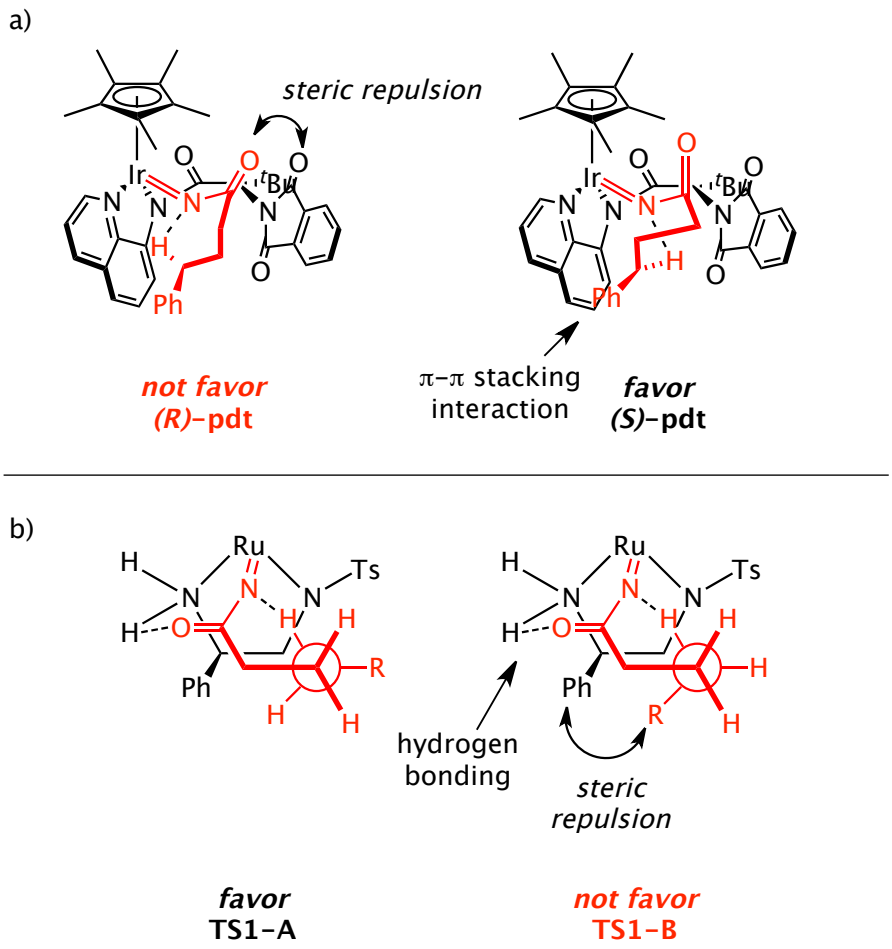

1.4 Conclusion

In non-chelation assistant strategy of C-H bond functionalization of arenes, the regioselectivity is affected by electronic properties of the substituents and steric repulsion of the ligands. In most cases, the effects of electronic properties of substituents on arenes are more influential to the outcomes. This is examplified by Ritter's amidation reaction with *para*-selective amidation for electron-rich arenes being more favored. No bulky ligands were applied in Ritter's amidation reactions. The rationale for dominant electronic effect for Ritter's amidation is that the radical

intermediate formed after C-N bond formation at *para*-position is stabilized by electron-donating substituents. Also, the nitrogen cation radical produced by SET should seek the most dominant HOMO on the arene for electrophilic attack. Based on the results of Emmert's amidation reaction, the regioselectivity is likely to be influenced by steric and electronic factors. In enantioselective catalysis, steric factor and non-covalent interactions are proved to be effective control elements. Steric repulsion between the ligand and the substrate differentiate diastereomeric transition states while non-covalent interactions between the ligand and the substrate would reinforce the stability of the favored transition state.

Chapter 2

Directing Group-Free Regioselective Pd(II)-Catalyzed Oxidative Amidation of Simple Arenes

2.1 Introduction

Arylamins are very important motifs many in pharmaceutical compounds. Notable examples include Imatinib (kinase inhibitor)[20] and Linezolid (antibiotic)[21] (Figure 2.1).

Figure 2.1. Chemical Structures of Imatinib and Linezolid

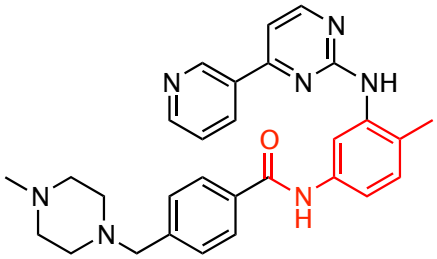

Imatinib
Kinase Inhibitor

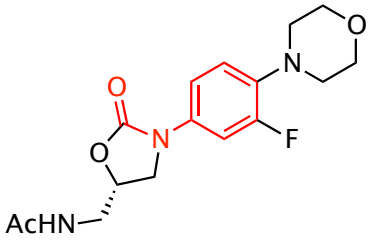

Linezolid
Anitbiotic for Treating Antibiotic–Resistant Bacteria

Directing group-free Pd-catalyzed functionalization of simple arenes is challenging. Recently, Yu (JQ) and co-workers reported the first example of directing group-free Pd-catalyzed vinylation reaction of simple arenes[22] using 2,6-bis(2-ethylhexyl)pyridine as a donor ligand, trimeric form $Pd(OAc)_2$ was converted to a more active monomeric form. The bulky 2,6-bis(2-ethylhexyl)pyridine disfavors coordination of a second 2,6-bis(2-ethylhexyl)pyridine ligand by steric repulsion, thereby forming a low-coordinating catalytically active Pd(II) complex as the resting state (Scheme 2.1).

Scheme 2.1. Directing Group-Free Pd-Catalyzed Vinylation of Arenes

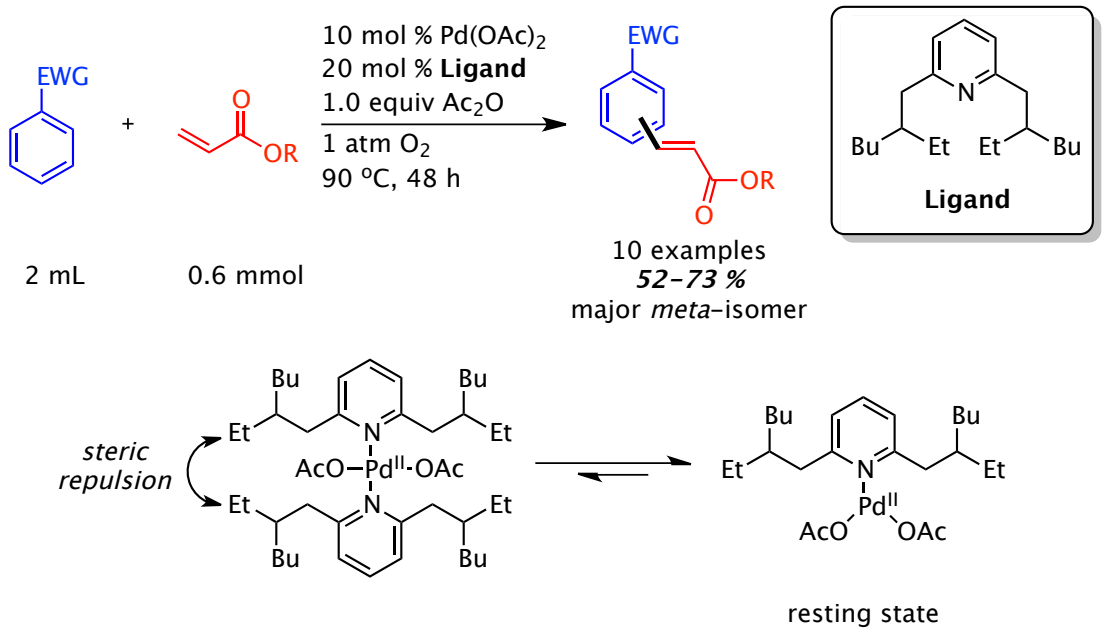

Recently, Hartwig and co-workers reported the directing group-free Pd(II)-catalyzed oxidative amidation reaction of simple arenes.[8] Bulky tri-*t*-butyl phosphine ligand was behaved to exert similar effect to bring about low-coordinate Pd complex as active catalyst. According to the literatures, 2,6-diisopropylphenyl-substituted *N*-heterocyclic carbene ligand exhibits analogous properties to bulky phosphine ligands in Heck reactions, Suzuki coupling reactions, oxidation of alcohols and Hartwig-Buchwald aminations.[23] *N*-Heterocyclic carbene ligands such as IPr and Mes are strong σ-donors and exhibit comparable steric properties as bulky phosphines. It is anticipated that the strong σ-donating bulky *N*-heterocyclic carbene ligands would stabilize the Pd complexes at some high oxidation states.

2.2 Results and Discussion

2.2.1 Preliminary Results

Here we describe regioselective Pd(II)-catalyzed oxidative amidation of simple arenes catalyzed by [(IPr)Pd(OAc)$_2$(OH$_2$)] complex (IPr = 1,3-bis(2,6-diisopropylphenyl)-2,3-dihydro-1*H*-imidazol-2-yl). For catalyst preparation, [Pd(allyl)Cl]$_2$ complex was treated with IPr-HCl and K^{t}OBu in THF at room temperature for 12 h. Then, the [(IPr)Pd(allyl)Cl] was reacted with hydrogen chloride gas at room temperature for 45 min to give [(IPr)PdCl$_2$]$_2$ complex. All the chloride ions of [(IPr)PdCl$_2$]$_2$ were then removed by AgOAc metathesis in DCM solvent to produce [(IPr)Pd(OAc)$_2$(OH$_2$)] (Scheme 2.2).

Scheme 2.2. Preparation of [(IPr)Pd(OAc)$_2$(OH$_2$)]

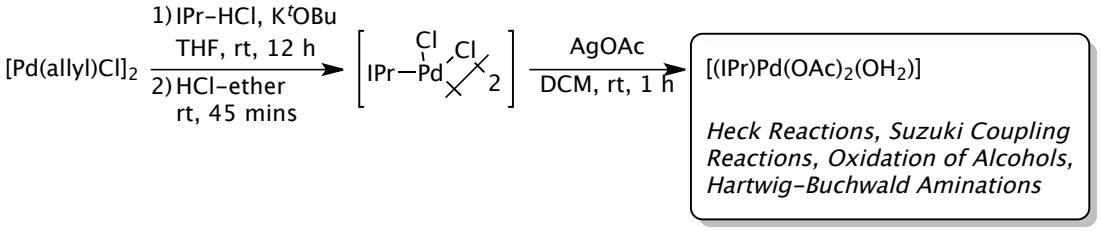

Treatment of [(IPr)Pd(OAc)$_2$(OH$_2$)] (10 mol %) with phthalimide (0.1 mmol), PhI(OAc)$_2$ (3 x 2.0 equiv / 9 h) and α, α, α- trifluorotoluene (1 mL) at 100 ^{o}C for 33 h afforded regioisomer *N*-arylphthalimides in 37 % combined yield [regioselectivity *ortho(o)* : *meta(m)* : *para(p)* ratio is 1:16:5] (Scheme 2.3).

Scheme 2.3. Preliminary Results

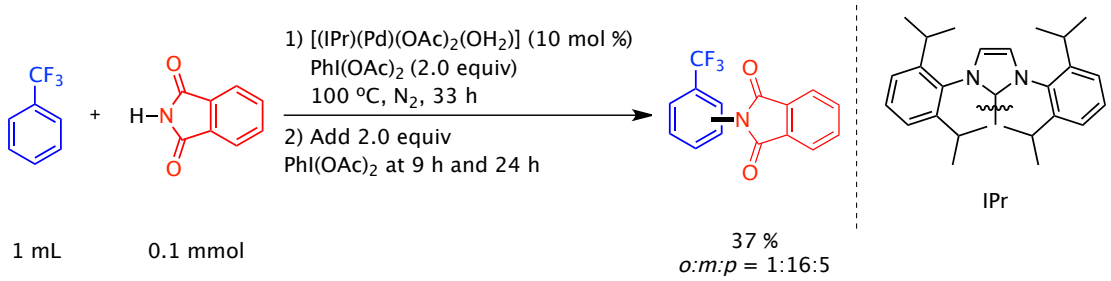

2.2.2 Optimization Results

For reaction optimization, the effect of the amount of $PhI(OAc)_2$ were studied first. Employing α, α, α- trifluorotoluene as substrate, $PhI(OAc)_2$ (3.0 equiv) was used to obtain in 17 % of amidation product (Table 2.1, entry 2). When 10.0 equiv of $PhI(OAc)_2$ were used, the amidation product was obtained in 50 % yield (entries 3 and 4). Employing more than 10.0 equiv of the $PhI(OAc)_2$ did not give better results (entry 5).

Second, more bulky monodentate *N*-heterocyclic carbene ligands gave higher yields of amidation product (**L1** – **L4**, entries 4 and 6 – 8). The bidentate ligands such as bis(3-methyl-2,3-dihydro-1*H*-imidazol-1-yl)methane (**L5**, entry 9), 2-((3-mesityl-2,3-dihydro-1*H*-imidazol-1-yl)methyl)pyridine (**L6**, entry 10) and 1,10-phenanthroline (**L7**, entry 11) are not effective ligand for the amidation reaction, and no amidation products were obtained in all cases comparing to the result of $Pd(OAc)_2$ as catalyst (entry 12).

Table 2.1. Optimization Studies

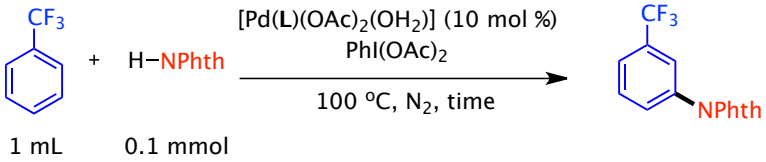

entry	time intervals of addition of $PhI(OAc)_2$	total amount of $PhI(OAc)_2$ used (equiv)	L	time (h)	yield (%)[a]	*o:m:p*[b]
1	2.0 equiv / 9 h	6.0	**L1**	33	37	1:16:5
2	1.0 equiv / 9 h	3.0	**L1**	33	17	1:16:5
3	2.0 equiv / 9 h	10.0	**L1**	57	50	1:16:5
4	2.0 equiv / 2 h	10.0	**L1**	24	50	1:16:5
5	2.0 equiv / 2 h	12.0	**L1**	24	53	1:16:5
6	2.0 equiv / 2 h	10.0	**L2**	24	40	1:16:5
7	2.0 equiv / 2 h	10.0	**L3**	24	30	1:16:5
8	2.0 equiv / 2 h	10.0	**L4**	24	30	1:16:5
9	2.0 equiv / 2 h	10.0	**L5**	24	9	1:16:5
10	2.0 equiv / 2 h	10.0	**L6**	24	9	1:16:5
11	2.0 equiv / 2 h	10.0	**L7**	24	4	1:16:5
12	2.0 equiv / 2 h	10.0	none	24	17	1:16:5

[a]Isolated yield. [b]Regioselectivity was determined by GC–MS with dodecane as an internal standard.

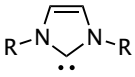

R = 2,6-diisopropylphenyl (**L1**)
R = 1,3,5-trimethylphenyl (**L2**)
R = *tert*-butyl (**L3**)
R = isopropyl (**L4**)

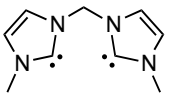

L5

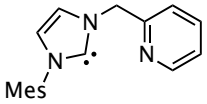

L6

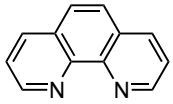

L7

The reaction temperature and different types of oxidants were examined. As shown in Table 2.2, the yields of the *N*-arylphthalimides formation reduced dramatically at 80 °C and 120 °C (entries 2 and 3). Other oxidants which are known to oxidize Pd(II) to Pd(IV) such as oxone, $Na_2S_2O_8$, $PhI(TFA)_2$, NFSI, TBHP and 1-fluoro-2,4,6-trimethylpyridin-1-ium tetrafluoroborate gave poor results (entries 4 – 12). Only $PhI(OAc)_2$ gave the desired amides in moderate yield.

Table 2.2. Temperature and Oxidants Screening

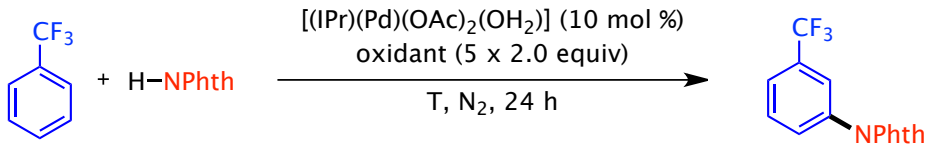

entry	temp	oxidant	yield (%)[a]
1	100 °C	$PhI(OAc)_2$	50
2	80 °C	$PhI(OAc)_2$	10
3	120 °C	$PhI(OAc)_2$	35
4	100 °C	$PhI(TFA)_2$	2
5	100 °C	TBHP	< 2
6	100 °C	$Na_2S_2O_8$	< 2
7	100 °C	oxone	< 2
8	100 °C	$Cu(OAc)_2$	not detected
9	100 °C	O_2	not detected
10	100 °C	1-fluoro-2,4,6-trimethylpyridin-1-ium tetrafluoroborate	< 2
11	100 °C	benzoyl peroxide	< 2
12	100 °C	NFSI	< 2
13	100 °C	none	not detected

[a]Isolated yield.

Moreover, extending the scope of the nitrogen nucleophiles was proved to be challenging. With α,α,α-trifluorotoluene as substrate, nucleophiles other than phthalimide such as succinimide (entry 2), tosylamide (entry 3) and trifluoromethanesulfonamide (entry 4) failed to effect significant arene amidation. For all unsuccessful cases, formation of acetoxylation products was not observed. Additionally, there is no acetoxylation product formation in the absence of the phthalimide (entry 5).

Table 2.3. Coupling Partners Screening

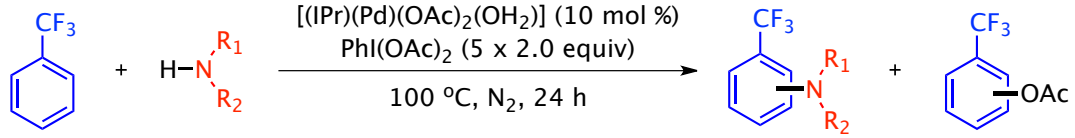

entry	amide (pK_a)	yield of amidation product (%)[a]	acetoxylation product formation[b]
1	 (8.93)	50 %	yes *C–N:C–O = 4:14*
2	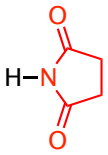 (14.3)	trace amount	trace amount
3	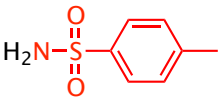 (10.9)	not detected	not detected
4	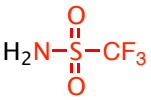 (6.93)	not detected	not detected
5	no amide	not applicable	not detected

[a]Isolated yield. [b]Acetoxylation product observed in GC–MS chromatograph.

2.2.3 Substrate Scope Studies

Table 2.4 depicts the results of substrate scope studies. For the amidation of monosubstituted arenes, substrates bearing electron-releasing (entries 2 – 4, 6 and 7) and –withdrawing (entries 5 – 9) groups furnished the corresponding monoamidation products. In all cases, the amidation preferentially occurred at the less hindered sites (i.e., the *meta*- and *para*- positions). For arenes with electron-withdrawing groups (CF_3, CO_2Et and Ph), *meta*-amidation is especially favored. Amidation at the *para*-position became more dominant for arenes with the electron-releasing OMe group. The amidation of di- and tri-substituted arenes afforded the

regioisomeric *N*-arylphthalimides in good yields with the amide group being located *meta* to the substituents. Notably, arenes containing carbon-halogen bonds (entries 6, 10, 11 and 14) were effectively transformed to their amides without any proto-dehalogenation or carbon-halogen bond amidation. Apparently, in all cases, the reactions were selective for the less hindered *meta*- and *para*- isomers. With naphthalene as substrate (entry 12), amidation at the C1 position is more dominant (α:β = 20:1).

Table 2.4. Substrate Scope Studies

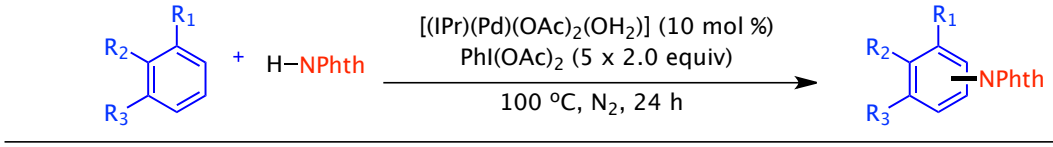

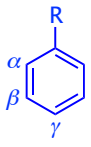

(**1**) R = H; 48 %
(2) R = Me; 63 % (*1:22:29*)
(3) R = OMe; 60 % (*1:2:19*)
(4) R = ^{i}Pr; 66 % (*1:43:34*)
(5) R = CF_3; 50 % (*1:16:5*)
(6) R = I; 63 % (*1:5:6*)
(7) R = OAc; 61 % (*1:19:30*)
(8) R = CO_2Et; 40 % (*1:22:3*)
(9) R = Ph; 47 % (*1:49:36*)

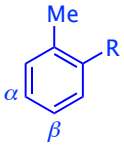

(10) R = Br; 65 % (*3:5*)[b]
(11) R = I; 67 % (*3:5*)[b]

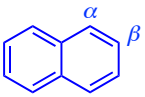

(12)
53 % (*20:1*)

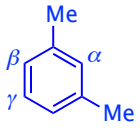

(13)
51 % (*1:5:14*)

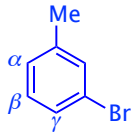

(14)
57 % (*4:16:1*)

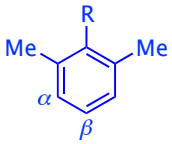

(15) R = OMe; 60 % (*1:94*)

[a]Reaction conditions: arene (1 mL), phthalimide (0.1 mmol), [(IPr)(Pd)(OAc)$_2$(OH$_2$)] (10 mol %), PhI(OAc)$_2$ (5 x 2.0 equiv), 100 °C, 24 h under N$_2$; isolated yield and regioisomers ratio *α:β:γ* shown in parathesis. [b]Regioselectivity was determined by ^{1}H NMR with dibromomethane as an internal standard.

Comparing to the results obtained by a transition-metal-free protocol reported by Chang's group (Table 2.5), the arenes with electron-withdrawing substituents (CF_3, CO_2Et and Ph) did not give the desired amide products. For monosubstituted arenes bearing electron-donating groups, formation of the *ortho*-isomer is dominant in all

cases. Reaction of naphthalene via the metal-free pathway afford predominant C2-amidation product (α:β = 1:11). For 2,6-dimethylanisole (entry 15), the amidation at α position be more favored.

Table 2.5. Substrate Scope Studies in Transition-Metal-Free Pathway

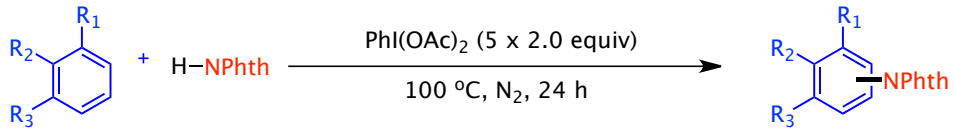

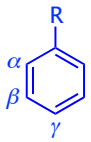

(**1**) R = H; trace amount
(2) R = Me; 36 % (*3:1:2*)
(3) R = OMe; 34 % (*14:4:1*)
(4) R = ^{i}Pr; trace amount
(5) R = CF_3; trace amount
(6) R = I; 15 % (*3:1:1*)
(7) R = OAc; 5 % (*5:1:2*)
(8) R = CO_2Et; trace amount
(9) R = Ph; trace amount

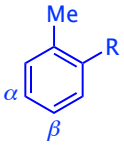

(10) R = Br; trace amount
(11) R = I; trace amount

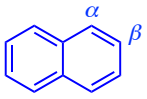

(12)
30 % (*1:11*)

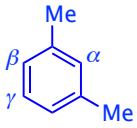

(13)
17 % (*1:1:3*)

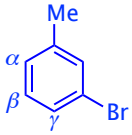

(14)
15 % (*2:1:9*)

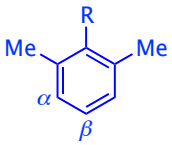

(15) R = OMe; 10 % (*2:1*)

[a]Reaction conditions: arene (1 mL), phthalimide (0.1 mmol), $PhI(OAc)_2$ (5 x 2.0 equiv), 100 °C, 24 h under N_2; isolated yield and regioselectivity ratio $\alpha:\beta:\gamma$ shown in parathesis.
[b]Regioselectivity was determined by ^{1}H NMR with dibromomethane as an internal standard.

2.3 Mechanistic Investigations

To verify the acceleration effect of the IPr (IPr = 1,3-bis(2,6-diisopropylphenyl)-2,3-dihydro-1*H*-imidazol-2-yl) ligand, a time course analysis of the catalytic amidation of benzene was performed. Samples were drawn at a regular interval (60 min) from a reaction mixture containing benzene (1 mL), $[(IPr)(Pd)(OAc)_2(OH_2)]$ (10 mol %), phthalimde (0.1 mmol) and $PhI(OAc)_2$ (2 equiv) at 100 °C, and the aliquots were analyzed by GC-MS with dodecane as internal standard. As depicted in Figure 2.2,

the [(IPr)(Pd)$(OAc)_2(OH_2)$]-catalyzed reaction displayed significant product formation during the first 1 h. Notably, *with Pd(OAc)$_2$ alone* as catalyst (i.e., without IPr ligand), a latent period of about 4 h prior to product formation was observed. The occurrence of the latent period may imply derivatization of the $Pd(OAc)_2$ to some *active* forms for effective product formation.[24] Based on the time course analysis, we concluded that the IPr ligand would promote the Pd-catalyzed direct arene amidation.

Figure 2.2. Reaction Profile

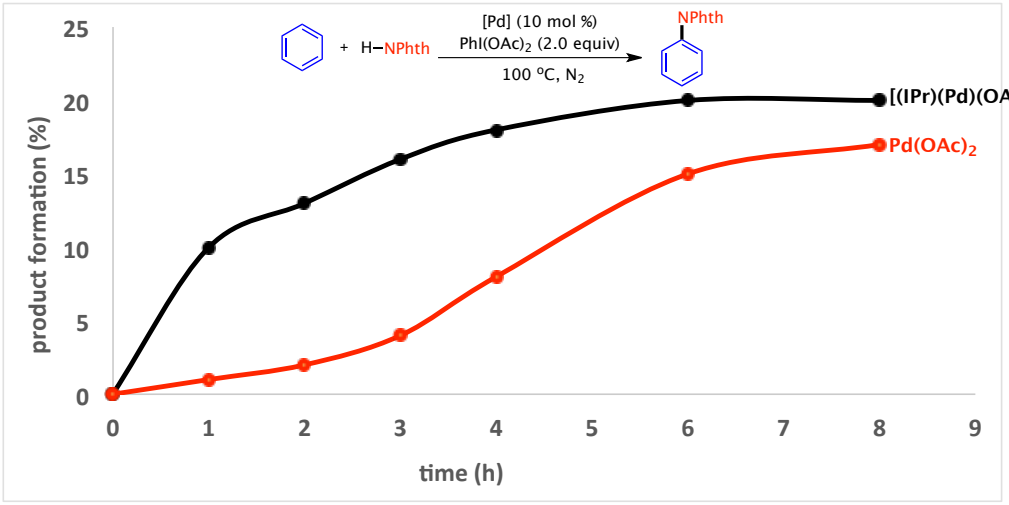

The primary kinetic H-D isotope effect has been examined. In this study, phthalimide (0.1 mmol, 14.7 mg), [(IPr)(Pd)$(OAc)_2(OH_2)$] (0.01 mmol, 6.3 mg), and 2.0 equiv. $PhI(OAc)_2$ (0.2 mmol, 64.4 mg) were added into a mixture of benzene (0.5 mL) and deuterated benzene (0.5 mL) in a 10 mL-Schlenk tube. The reaction was performed in 100 ^{o}C for 2 h under N_2 atmosphere. The result shown in Table 2.6, the average k_H/k_D = 3.32 indicating that the rate-determining step involves substantial the C-H bond clevage of the arenes.

Table 2.6. Kinetic Isotope Studies

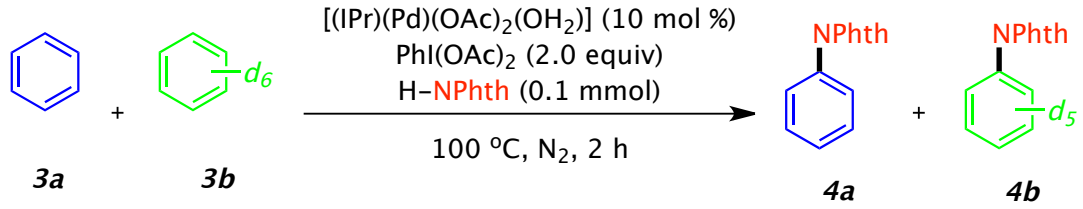

trial	***4a : 4b***
1	3.67 : 1
2	2.88 : 1
3	3.41 : 1
average	3.32 : 1

Two possible pathways were proposed (Figure 2.3). For pathway A (blue in color), after the formation of intermediate A by ligand exchange reaction of phthalimide with acetate ligand, it goes through the C-H activation of the arenes to form [(IPr)(Pd)(NPhth)Ar] complex. Then, the complex is oxidized by $PhI(OAc)_2$ to form Pd(IV) intermediate and finally the *N*-arylphthalimide is formed by reductive elimination. For pathway B (red in color), the intermediate A is oxidized by $PhI(OAc)_2$ first to form Pd(IV) intermediate B. Then, the C-H bond of arenes is activated by Pd(IV) intermediate B[25] and the *N*-arylphthalimide is formed by reductive elimination.

Figure 2.3. Hypothetical Catalytic Pathways

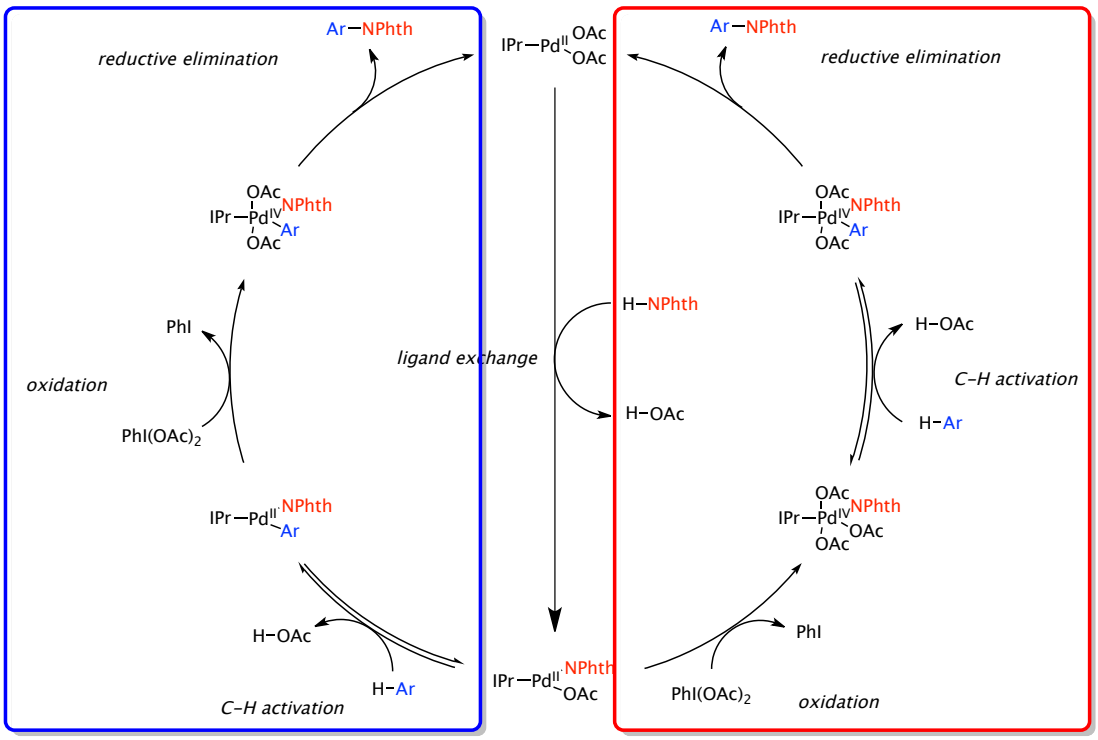

To differentiate the two hypothetical pathways, respective reaction orders of each component (rate = $k[PhI(OAc)_2]^a\{[(IPr)Pd(OAc)_2(OH_2)]\}^b[HNPhth]^c$) have been determined. The calibration curve was prepared by real-time ^1H NMR spectrometry (Figure 2.4). Various concentrations of the *N*-phenylphthalimide were prepared (10 mol %, 15 mol %, 20 mol %, 25 mol %, 30 mol %, 35 mol % and 40 mol % in 1 mL $CDCl_3$) and the quantity of the *N*-phenylphthalimide was determined based on the integration ratios for the proton signals δ_H = 7.91 ppm (*N*-phenylphthalimide), and δ_H = 4.90 ppm (dibromomethane as internal standard). The graph was plotted on the basis of the integration of the NMR signal against percentage of product and the equation is y = 0.0172x with R^2 is 0.98555.

Figure 2.4. Calibration Curve

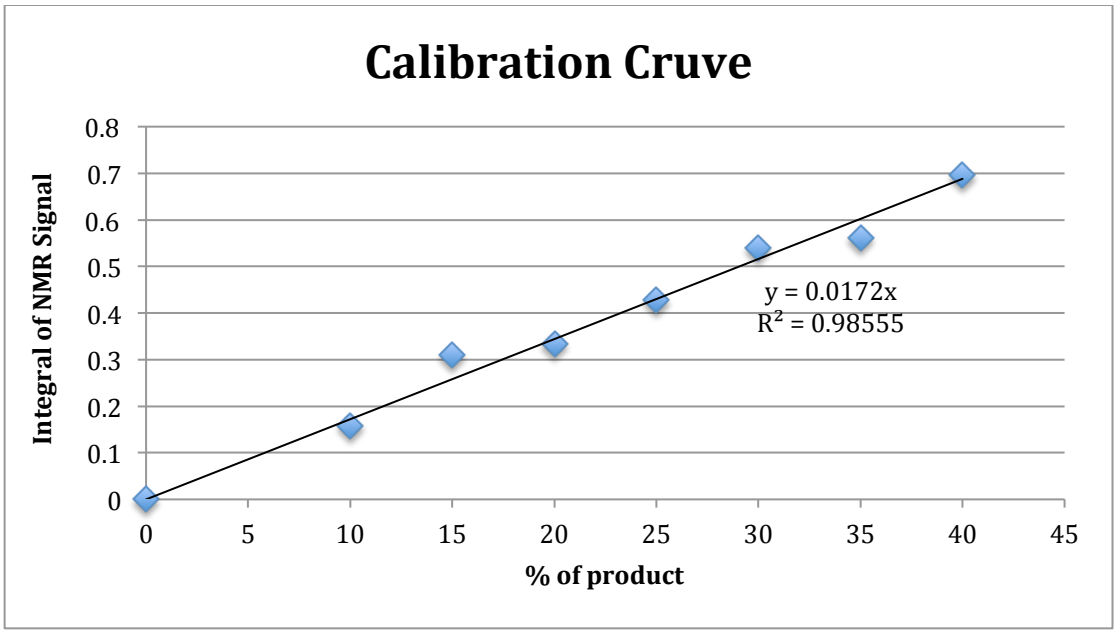

2.3.1 Reaction Order With Respect To $PhI(OAc)_2$

Firstly, the rate order of $PhI(OAc)_2$ was acquired by performing the amidation at various concentrations of $PhI(OAc)_2$ (50 mM to 200 mM) [reaction conditions: phthalimide (100 mM) and $[(IPr)Pd(OAc)_2(OH_2)]$ (10 mM) in d_6-benzene (1 mL) at 100 ^{o}C]. At every 30 min interval, aliquot (0.1 mL) was drawn from the crude mixture and diluted with $CDCl_3$ (0.9 mL with 3.49 µL of dibromomethane as an internal standard) for ^{1}H NMR analysis. The initial rate method was employed to determine the reaction rate at each $[PhI(OAc)_2]$, and a plot of initial rate (d[product]/dt) versus $[PhI(OAc)_2]$ revealed that the reaction rate is directly proportional to $[PhI(OAc)_2]$ (Figure 2.5). The order of reaction with respect to $[PhI(OAc)_2]$ was further verified by plotting log(d[product]/dt) against log($[PhI(OAc)_2]$) (Figure 2.6). The linear curve was obtained (slope = +0.8358 and R^2 = 0.9944) indicating that it is a first order of reaction with respect to $PhI(OAc)_2$ (a = 1).

Figure 2.5. Plot of Initial Rate d[product]/dt versus [PhI(OAc)$_2$]

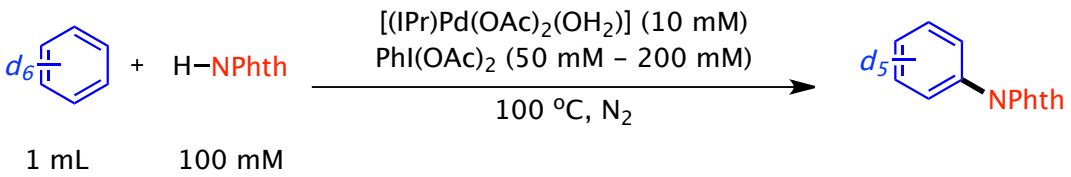

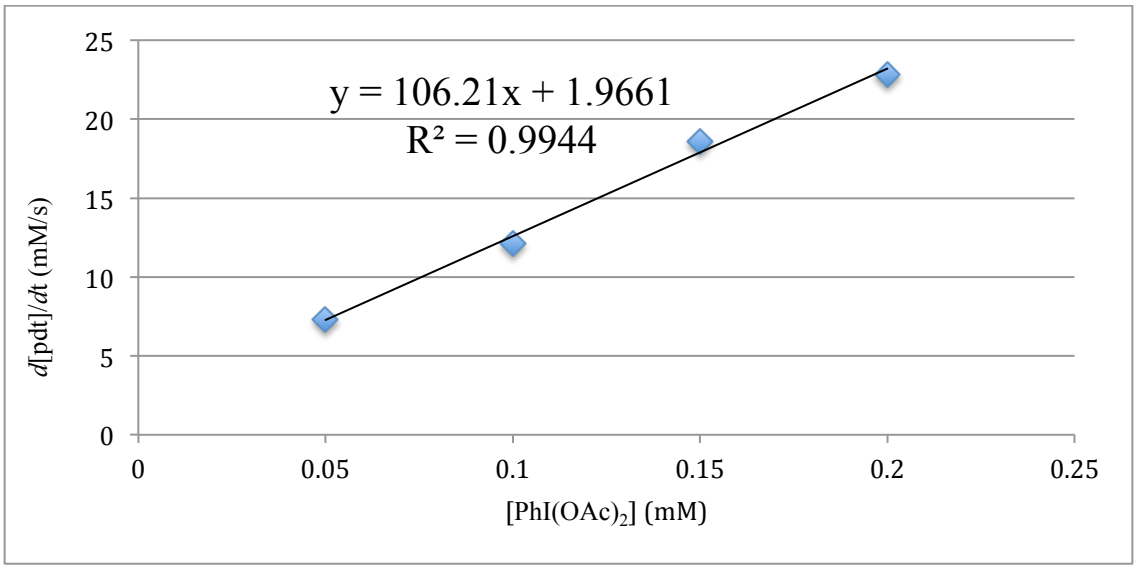

Figure 2.6. Plot of log(d[product]/dt) versus log[PhI(OAc)$_2$]

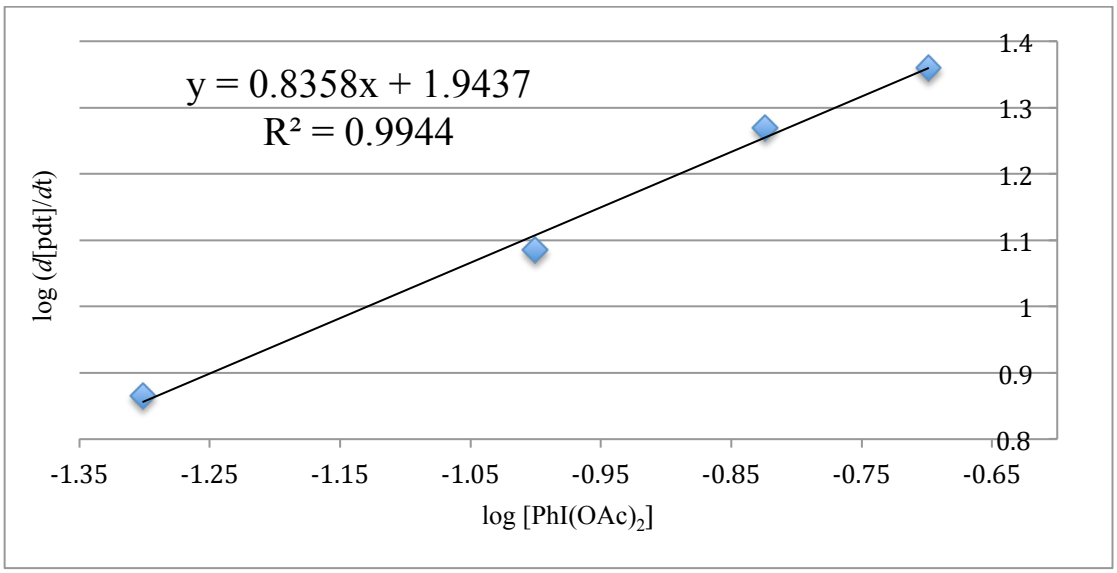

2.3.2 Reaction Order With Respect To [(IPr)Pd(OAc)$_2$(OH$_2$)]

Next, the order of reaction with respect to [(IPr)(Pd)(OAc)$_2$(OH$_2$)] was [concentration of [(IPr)Pd(OAc)$_2$(OH$_2$)] (1 mM – 10 mM); reaction conditions: phthalimide (100 mM) and PhI(OAc)$_2$ (200 mM) in d_6-benzene (1 mL) at 100 ^{o}C]. At every 30 min interval, aliquot (0.1 mL) was drawn from the crude mixture and diluted with $CDCl_3$ (0.9 mL with 3.49 µL of dibromomethane as an internal standard) for ^{1}H NMR analysis. The initial rate method was employed to determine the reaction rate at each [(IPr)Pd(OAc)$_2$(OH$_2$)], and a plot of initial rate (d[product]/dt) versus [(IPr)Pd(OAc)$_2$(OH$_2$)] revealed that the reaction rate is directly proportional to [(IPr)Pd(OAc)$_2$(OH$_2$)] (Figure 2.7). The order of reaction with respect to [(IPr)Pd(OAc)$_2$(OH$_2$)] was further verified by plotting log(d[product]/dt) against log[(IPr)Pd(OAc)$_2$(OH$_2$)]) (Figure 2.8). The linear curve was obtained (slope = +0.7593 and R^2 = 0.8657) indicating that it is a first order of reaction with respect to [(IPr)Pd(OAc)$_2$(OH$_2$)] (b = 1).

Figure 2.7. Plot of Initial Rate d[product]/dt versus [(IPr)Pd(OAc)$_2$(OH$_2$)]

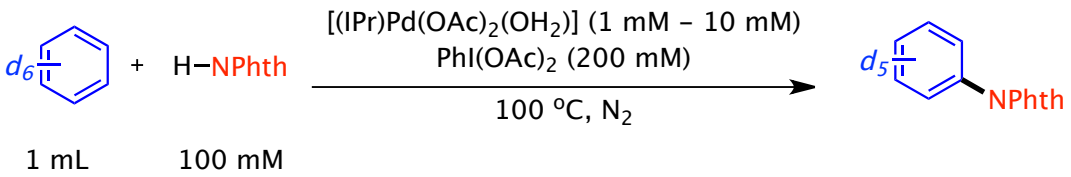

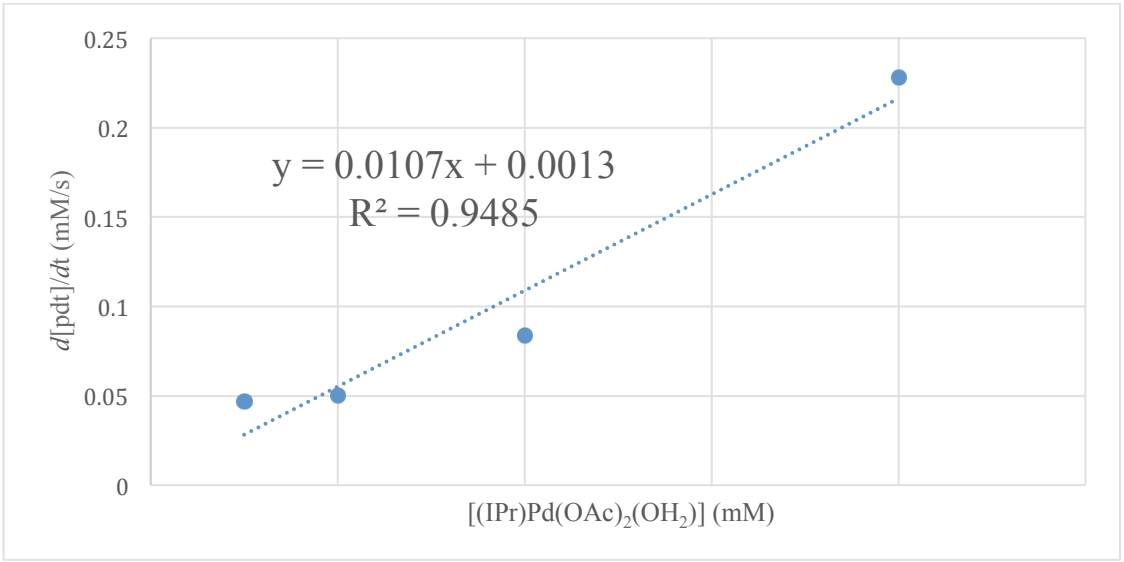

Figure 2.8. Plot of log(d[product]/dt) versus log[(IPr)Pd(OAc)$_2$(OH$_2$)]

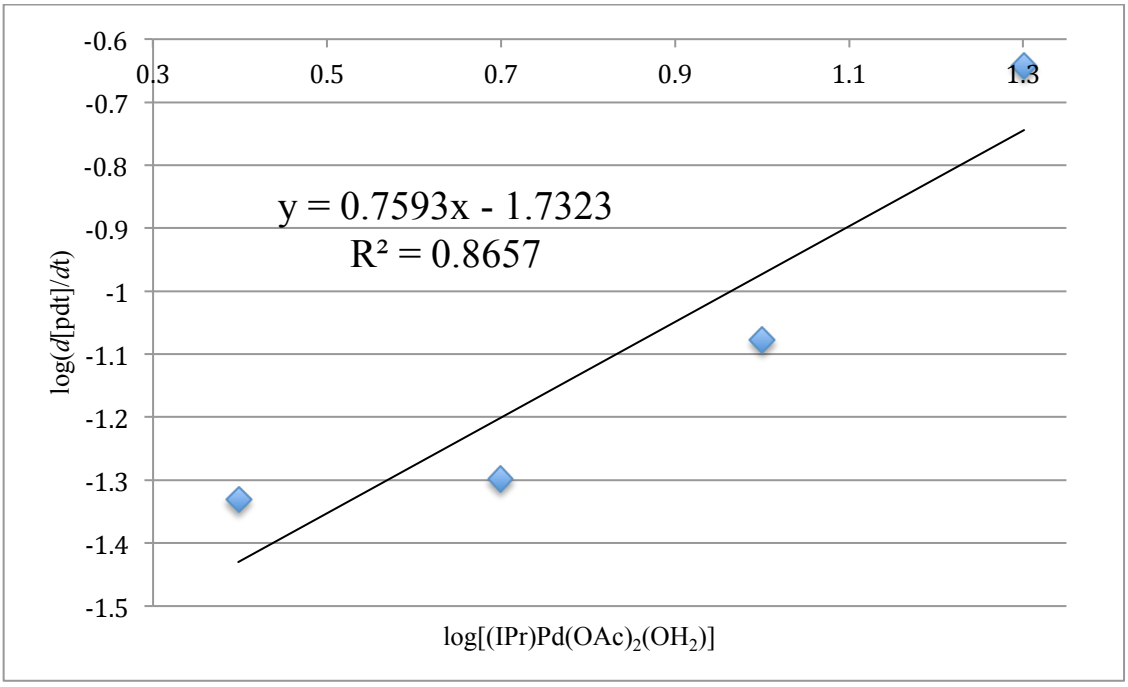

2.3.3 Reaction Order With Respect To Phthalimide

Finally, similar experiments were conducted for the determination of the order of reaction with respect to phthalimide. The concentration of phthalimide was varied (10 mM to 100 mM) in the amidation [reaction conditions: [(IPr)Pd$(OAc)_2(OH_2)$] (10 mM) and $PhI(OAc)_2$ (200 mM) in d_6-benzene (1 mL) at 100 ^oC]. At every 30 min interval, aliquot (0.1 mL) was drawn from the crude mixture and diluted with $CDCl_3$ (0.9 mL with 3.49 µL of dibromomethane as an internal standard) for ^1H NMR analysis. The initial rate method was employed to determine the reaction rate at each [Phthalimide], and a plot of initial rate (d[product]/dt) versus [Phthalimide] revealed that the reaction rate is directly proportional to [Phthalimide] (Figure 2.9). The order of reaction with respect to [Phthalimide] was further verified by plotting log(d[product]/dt) against log[Phthalimide] (Figure 2.10). The linear curve was obtained (slope = +0.2783 and R^2 = 0.89604) indicating that it is 1/3 order of reaction with respect to [(IPr)Pd$(OAc)_2(OH_2)$] (c = 0.3). Probably, it involved a trimeric form Pd-amido complex.

Figure 2.9. Plot of Initial Rate d[product]/dt versus [Phthalimide]

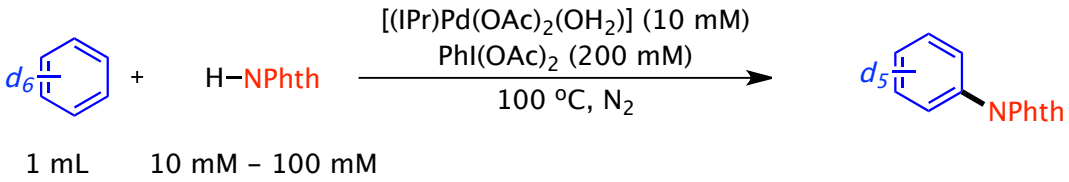

1 mL 10 mM – 100 mM

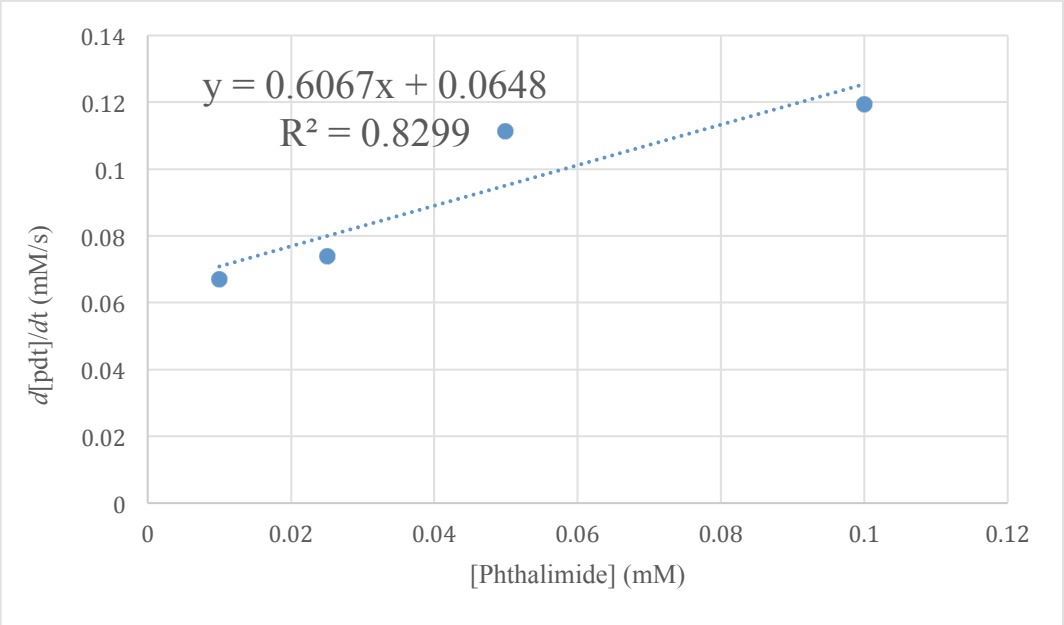

Figure 2.10. Plot of log(d[product]/dt) versus log [Phthalimide]

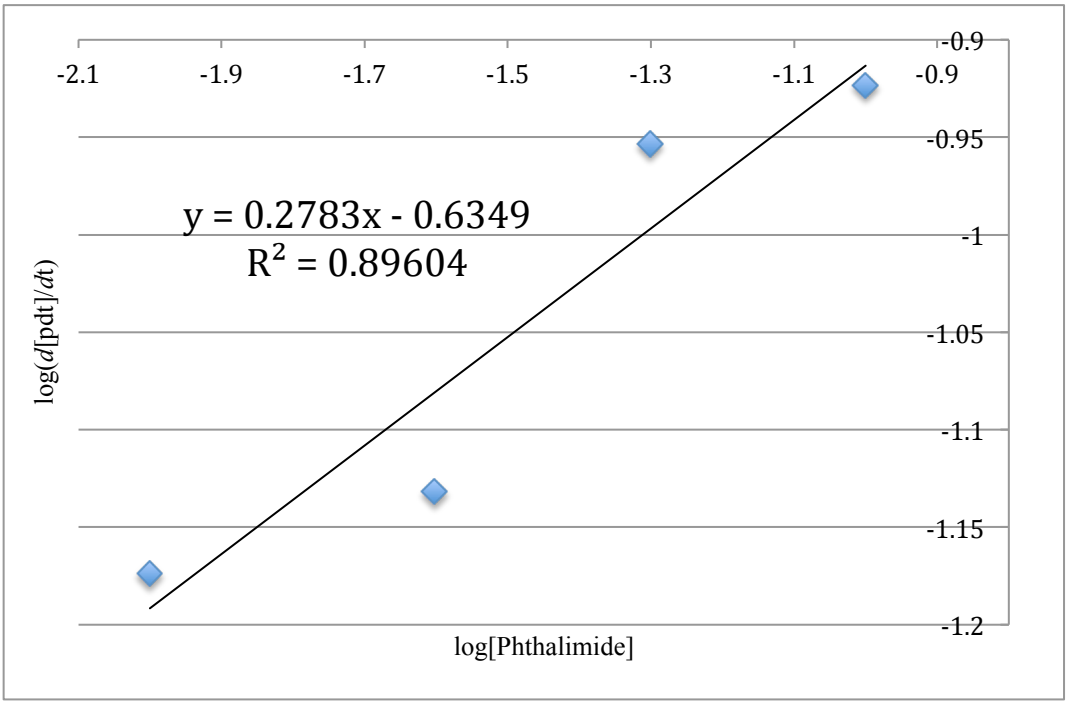

As a result, the rate equation of the reaction is rate = $k[PhI(OAc)_2][(IPr)Pd(OAc)_2(OH_2)][HNPhth]^{0.3}$. Since the order of reaction with respect to $PhI(OAc)_2$ is 1, the oxidation of Pd(II) to Pd(IV) is likely to take place before the C-H activation step (Figure 2.3). Therefore, pathway B appears to be a more plausible mechanism.

To examinate further, a sub-stoichiometric reaction was performed by reacting phthalimide (0.1 mmol, 14.7 mg), $[(IPr)(Pd)(OAc)_2(OH_2)]$ (0.03 mmol, 18.9 mg) and α, α, α- trifluorotoluene (1.0 mL) without addition of $PhI(OAc)_2$ as oxidant at 100 ^{o}C for 24 h under N_2 atmosphere. The result showed that no amidation product was found in the reaction crude (Scheme 2.4). The result is inconsistent to the mechanism involving Pd(II)-mediated C-H activation and the putative aryl (phthalimide) Pd(II) complex was probably not generated.

At the same time, the homo-coupling of the arenes was not detected in the reaction crude. This finding is consistent with the notion that the reaction system should not go through Pd(II)-mediated C-H activation. Furthermore, heating d_6-benzene (1 mL) with $[(IPr)Pd(OAc)_2(OH_2)]$ (10 mol %) and acetic acid (0.1 mL) did not result in any H-D exchange in the benzene. Based on these findings, we conclude that the observed C-H arene activation is unlikely to be mediated by a Pd(II) center. Indeed, preliminary kinetic analysis found that the rate of the catalytic amidation is first-order with respect to $[PhI(OAc)_2]$. This finding is compatible with the mechanism involving oxidation of Pd(II) to Pd(IV) prior to the arene C-H activation step.

Scheme 2.4. Reaction Scheme of Sub-stoichiometric Reactions

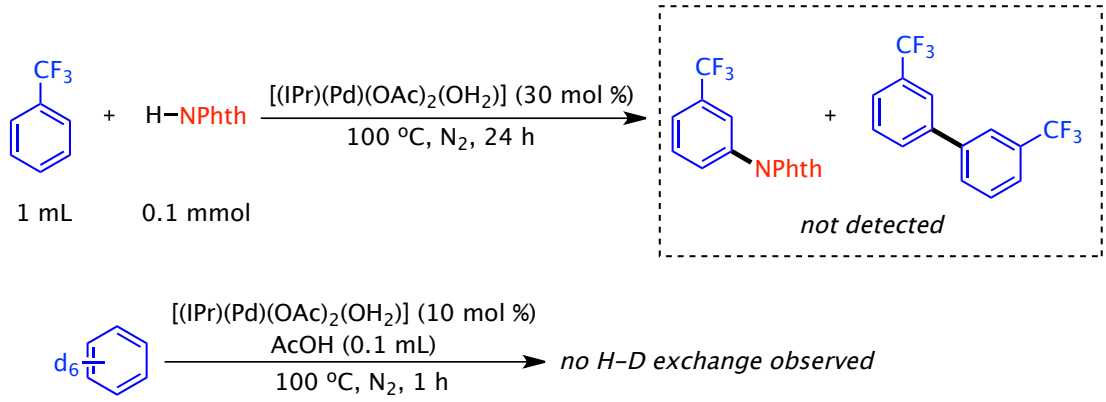

The amidation reaction was further examined by ESI-MS analysis. In this work, phthalimide (1.0 equiv) was treated with $[(IPr)(Pd)(OAc)_2(OH_2)]$ (10 mol %) and $PhI(OAc)_2$ (2.0 equiv) as oxidant in dry DCE (1 mL) at 100 °C for 2 h. After cooling down to room temperature, pyridine (30 mol %) was added to the mixture. After stirring for 10 min, 50 µL of the reaction mixture was withdrawn and was diluted with methanol (0.5 mL) for ESI-MS analysis. In the ESI-MS spectrum (Figure 2.11), the prominent cluster peaks at *m/z* 777 and *m/z* 798 were observed. The peaks are assigned to $[(IPr)(Pd)(NPhth)(OAc)_2(OH_2)]^+$ (*m/z* 777) and $[(IPr)(Pd)(NPhth)(py)OAc(OH_2)]$ (*m/z* 798) complexes in agreement with the mass values and the simulated isotopic patterns. However, when $[(IPr)(Pd)(OAc)_2(OH_2)]$ (10 mol %) was treated with phthalimide (1.0 equiv) in dry DCE (1 mL) at 100 °C *without $PhI(OAc)_2$ oxidant*, the signal at *m/z* 387 corresponding to the free IPr ligand was observed. This indicates decomposition of the complex in the absence of the $PhI(OAc)_2$ oxidant. The ESI-MS resutl seems to suggest that some reactive Pd(IV)-phthalimide complexes were probably involved in the arene amidation reaction.

Figure 2.11. High Resolution of ESI-MS Analysis

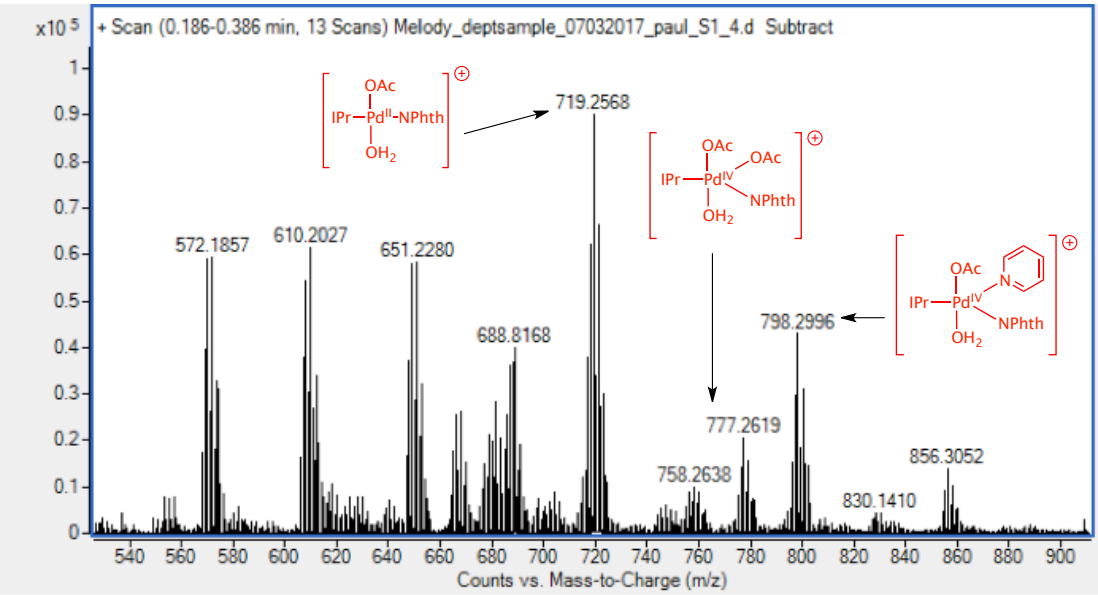

Figure 2.12. Isotopic Simulation of Pd(IV) Complex 1

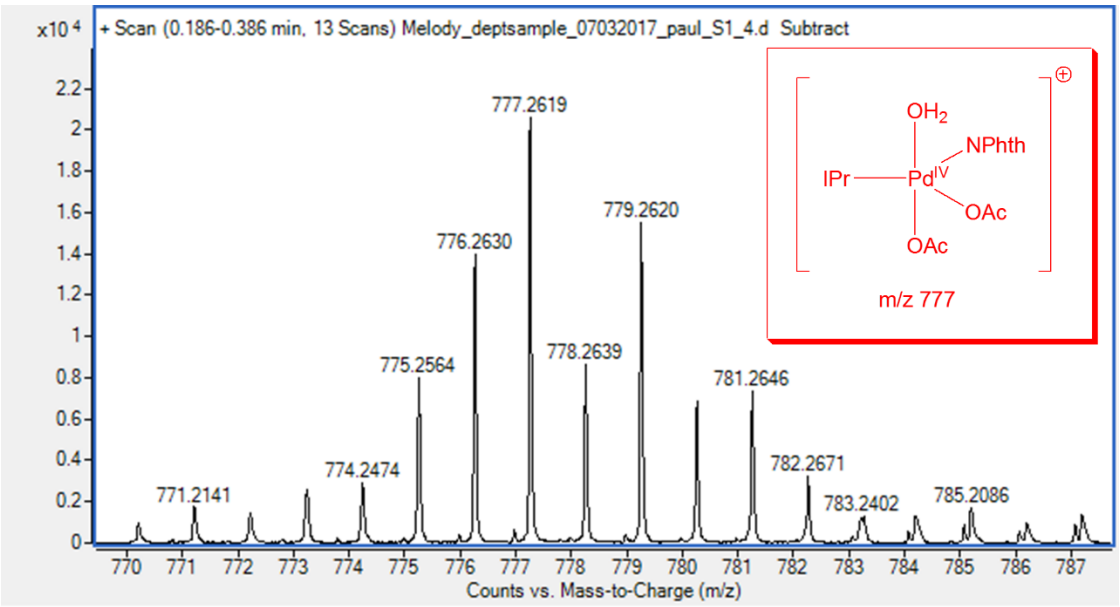

Figure 2.13. Isotopic Simulation of Pd(IV) Complex 2

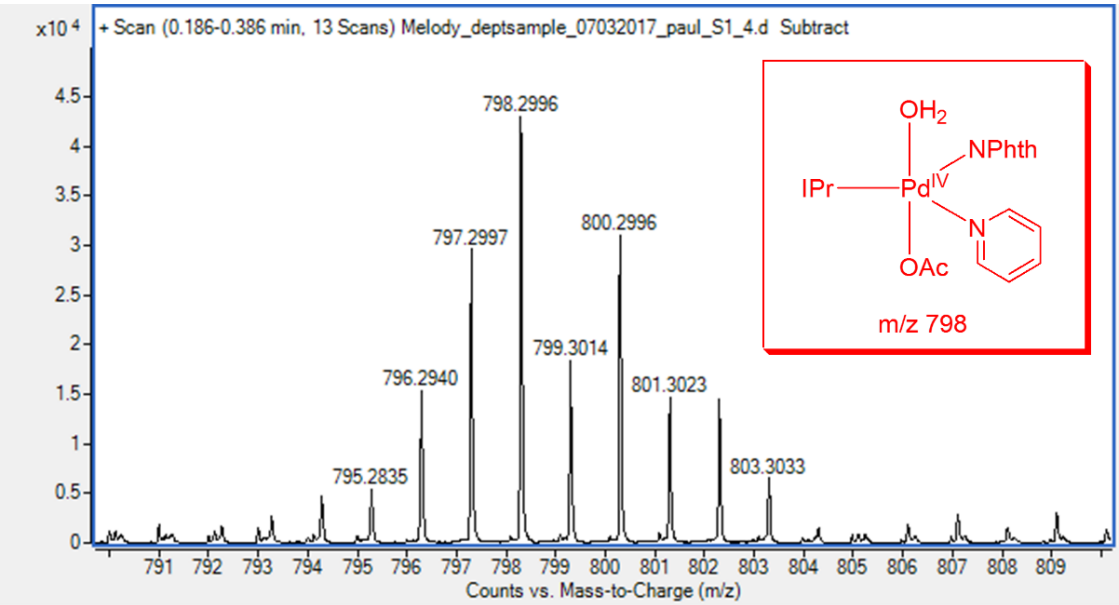

Finally, the chemoselectivity of the [(IPr)(Pd)$(OAc)_2(OH_2)$]-catalyzed amidation was studied by subjecting a 1:1 mixture of α,α,α-trifluorotoluene and some electron-rich arenes[26] (including benzene, toluene, 1,3-xylene and naphthalene) to the standard reaction conditions with phthalimide (0.1 mmol) and $PhI(OAc)_2$ (0.2 mmol). In all cases, the amidation occurred more selectively to the more electron-rich arenes with a product ratio of 3:1 (toluene, xylene, naphthalene) to 4:1 (benzene). However, the observed chemoselectivity does not correlate well with the nucleophilicity of the arenes (Table 2.6). This finding suggests that the chemoselectivity-determining step may not proceed via the classical electrophilic aromatic substitution pathway.

Table 2.7. Chemoselectivity Studies

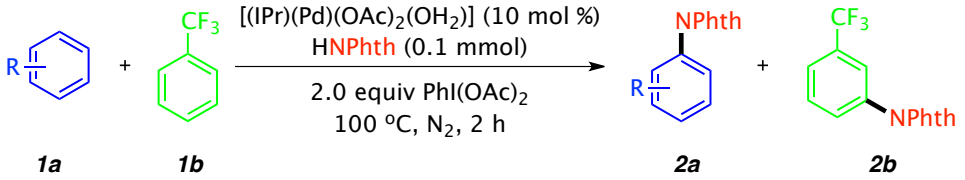

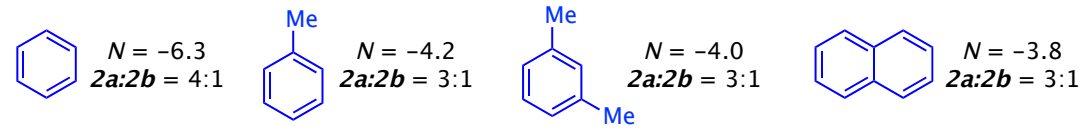

[a]*N* is nucleophilicity. Reaction conditions: ***1a*** (40 equiv), trifluorotoluene (40 equiv), phthalimide (0.1 mmol), [(IPr)(Pd)(OAc)$_2$(H$_2$O)] (10 mol %), PhI(OAc)$_2$ (2.0 equiv), 100 °C, 2 h under N$_2$; ratio ***2a:2b*** was determined by GC–MS using dodecane as an internal standard.

2.4 Proposed Mechanism

Scheme 2.5 depicts a postulated mechanism consistent with our observation. The catalytic amidation involves (i) generation of the phthalimide-palladium(II) complex by ligand exchange reaction, (ii) oxidation by PhI(OAc)$_2$ to afford the Pd(IV) complex, (iii) arene C-H palladation to form arylpalladium(IV) phthalimide complex, and (iv) C-N bond forming reductive elimination to release the *N*-arylphthalimide product. Consistent with this mechanism, competitive C-O bond reductive elimination was observed. Both the acetoxylation and amidation exhibit identical regioselectivity, and this indicates that the regioselectivity step (probably the C-H palladation) occurs prior to the reductive elimination steps.

Scheme 2.5. Postulated Catalytic Cycle

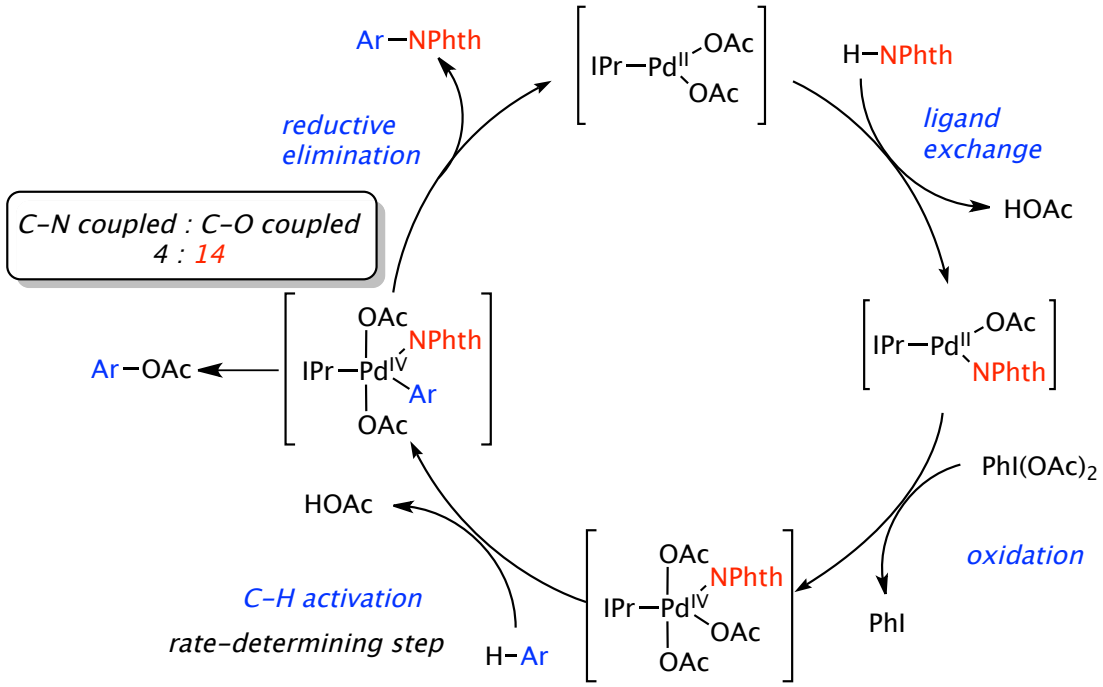

2.5 Conclusion

In conclusion, the NHC ligand-enabled Pd-catalyzed regioselective nondirected amidation of unactivated arenes was developed. The amidation is directed to the less hindered positions of the arenes. Preliminary mechanistic study suggested a Pd(II)/Pd(IV) reaction manifold involving arene C-H activation by Pd(IV), and this is followed by C-N bond forming reductive elimination. This work demonstrates that it is plausible to manipulate the reactivity and selectivity of organopalladium(IV) species by ligand modification. We are currently applying a similar strategy to develop other catalyst-controlled cross coupling reactions of arenes.

2.6 Experimental Section

Methods

Thin layer chromatography was performed on silica gel plates. Flash column chromatography was performed on a silica gel (Merck, 230-400 mesh) column. ^{1}H and ^{13}C NMR spectra were recorded on a Brüker DPX-400 MHz spectrometer. The chemical shift (δ) values given in ppm and are referenced to residual solvent peaks; carbon multiplicities were determined by DEPT-135 experiments. Coupling constants (J) were reported in hertz (Hz).

Gas Chromatography/Mass Spectrometry: GC/MS analyses were performed on Agilent Technologies 6890N equipped with an HP-5MS (Crosslinked 5% PH ME Siloxane) column Model 19091S-433 from Agilent (30 m x 0.25 mm x 0.25 µm) with a Mass Selective Detector and helium as the carrier gas. The analysis method used in all cases was 1 µL injection sample, injector temperature of 300 ^{o}C, and 10:1 split ratio. The initial pressure was 10 psi, but varied as the column flow was held constant at 1.3 mL/min for the duration of the run. The interface temperature was held at 300 ^{o}C, and the electron impact (EI, 30 eV) ion source was at 300 ^{o}C. The initial oven temperature was held at 45 ^{o}C for 2.25 min with the detector off, followed by a temperature ramp to 300 ^{o}C at 15 ^{o}C/min with the detector turned on at 3.75 min. The final temperature was held at 300 ^{o}C for 3 min. The total run time was 22.5 min. Data are reported in the form of m/z (intensity relative to the base peak = 100, ion).

General Experimental Section

(A) Preparation of [(NHC)(Pd)$(OAc)_2(OH_2)$] Complexes

[(IMes)(Pd)$(OAc)_2(OH_2)$] and [(IPr)(Pd)$(OAc)_2(OH_2)$] were prepared according to the procedures reported by Sigma and co-workers. 2,2'-Bis(2-adamantylamino)biphenyl palladium diacetate was prepared with the same procedure as [(IMes)(Pd)$(OAc)_2(OH_2)$] and [(IPr)(Pd)$(OAc)_2(OH_2)$]. All amidation products of arenes were prepared and characterized independently from the corresponding anilines and phthalic anhydride according to the synthetic method reported by *Hartwig et al*.[8]

(B) Identification of retention time of corresponding amidation products of arenes

The regioisomeric ratios of the products in GC/MS chromatogram were verified in the following methods. The retention time of each authentic product was identified by analysis of the mixture containing same equivalent (0.02 mmol) of three isomers that synthesized independently by Hartwig's method. After the first analysis, additional 0.02 mmol of *meta*-isomers was added to the mixture and performed the GC/MS analysis again. The significantly increase of the intensity at particular retention time corresponded to *meta*-isomer. After that, additional 0.02 mmol of *para*-isomer was added to the mixture to obtain the significantly increase of the signal in order to identify the retention time corresponding to *para*-isomer.

(C) Relative error of the GC/MS analysis method

1.0 equiv of *N*-(o-tolyl)phthalimide, 1.0 equiv of *N*-(m-tolyl)phthalimide and 1.0 equiv *N*-(p-tolyl)phthalimide were added to a GC vial and diluted with 1 mL dichloromethane. The mixture was analyzed by GC/MS for three times.

Trials	ratio		
	o	*m*	*p*
1	1.1	1.0	1.4
2	1.1	1.0	1.4
3	1.0	1.0	1.3
Average value	1.067 ± 0.003	1.0 ± 0	1.367 ± 0.003
Relative error	0.28 %	0 %	0.22 %

2.0 equiv of *N*-(o-tolyl)phthalimide, 1.0 equiv. of *N*-(m-tolyl)phthalimide and 1.0 equiv *N*-(p-tolyl)phthalimide were added to GC vial and diluted with 1 mL dichloromethane. The mixture was analyzed by GC/MS three times.

Trials	ratio		
	o	*m*	*p*
1	2.8	1.0	1.4
2	2.8	1.0	1.4
3	2.9	1.0	1.3
Average value	2.833 ± 0.003	1.0 ± 0	1.367 ± 0.003
Relative error	0.11 %	0 %	0.22 %

Experimental Procedures and Physical Characterizations

Preparation of *N*-arylphthalimides[8]

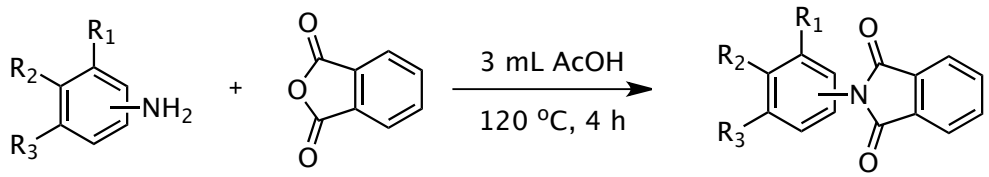

0.5 mmol 0.5 mmol

The arylamines (0.5 mmol) and phthalic anhydride (74.0 mg, 0.5 mmol) were dissolved in AcOH (3 mL). The reaction mixture was stirred at 120 °C for 4 h. After the completion of the reaction, the crude mixture was cooled to room temperature. The cold water (10 mL) was added to the crude mixture causing the precipitation of *N*-arylphthamides. The resultant precipitate was filtered and washed with cold water (10 mL) and hexane (30 mL), and then dried in air. The characterization data of *N*-arylphthamides are consistent to Hartwig's group reported.

Procedure for the Pd(II)-Catalyzed Intermolecular Oxidative Amidation of Arenes

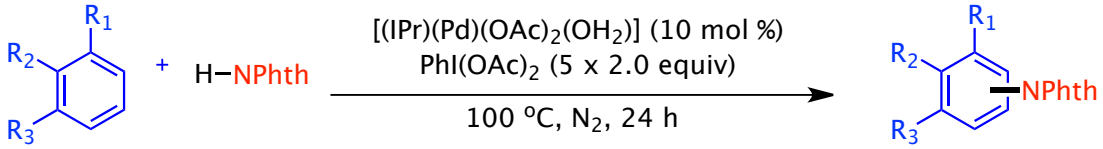

Phthalimide (0.1 mmol, 14.7 mg), [(IPr)(Pd)$(OAc)_2(OH_2)$] (0.01 mmol, 6.3 mg), $PhI(OAc)_2$ (0.2 mmol, 64.4 mg) and arenes (1 mL) were added to a 10 mL-Schlenk tube, and the reaction tube was evacuated and back-filled with N_2 for three times. The reaction was allowed to react at 100 °C oil bath. At 2, 4, 6 and 8 h, the reaction was cooled to room temperature, and evacuated and back-filled with N_2 for three imes. Four portions of additional 2.0 equiv of $PhI(OAc)_2$ were added to the crude

mixture. After 24 h, the reaction mixture was treated with silica gel. 100 mL of n-hexane was used to remove all arenes and then 100 mL of ethyl acetate was used to extract the products from the silica gel. The solvent was removed by vacuum and the crude mixture was diluted with dichloromethane (2 mL) and dodecane (5 µL) was added as an internal standard for GC-MS analysis. 1 mL of sample was withdrawn and analyzed by GC-MS for determination of regioselectivity ratio of the amidation products. The amidation products were purified by flash chromatography with n-hexane/EtOAc (8:2) as eluent. The products were collected as a mixture of regioisomeric products, and isolated yields were registered.[8]

Amidation of Benzene (1)

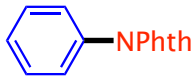

Isolated yield: 48 %; off-white solid

TLC: R_f 0.33 (n-hexane:EtOAc = 8:2)

Retention time: 14.0 min

Amidation of Toluene (2)

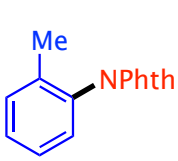

2a

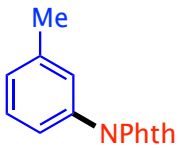

2b

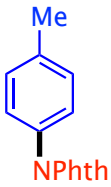

2c

Isolated yield: 63 %; off-white solid

Regioselectivity ratio (**2a:2b:2c**): *1:22:29*

TLC: R_f 0.43 (n-hexane:EtOAc = 8:2)

Retention time: **2a** = 15.0 min, **2b** = 15.6 min, **2c** = 15.8 min

Amidation of Anisole (3)

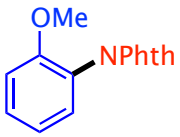

3a

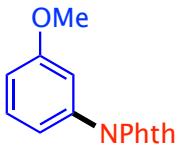

3b

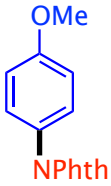

3c

Isolated yield: 60 %; off-white solid

Regioselectivity ratio (**3a**:**3b**:**3c**): *1:2:19*

TLC: R_f 0.27 (n-hexane:EtOAc = 8:2)

Retention time: **3a** = 19.8 min, **3b** = 20.1 min, **3c** = 20.6 min

Amidation of Isopropylbenzene (4)

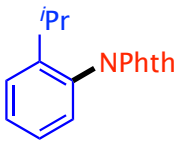

4a

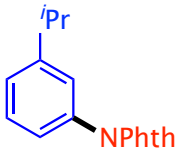

4b

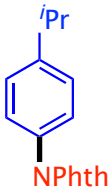

4c

Isolated yield: 66 %; off-white solid

Regioselectivity ratio (**4a**:**4b**:**4c**): *1:43:34*

TLC: R_f 0.47 (n-hexane:EtOAc = 8:2)

Retention time: **4a** = 16.7 min, **4b** = 17.2 min, **4c** = 17.8 min

Amidation of α,α,α-Trifluorotoluene (5)

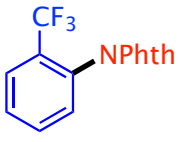

5a

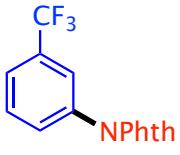

5b

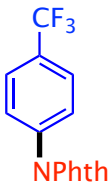

5c

Isolated yield: 50 %; off-white solid

Regioselectivity ratio (**5a**:**5b**:**5c**): *1:16:5*

TLC: R_f 0.43 (n-hexane:EtOAc = 8:2)

Retention time: **5a** = 14.0 min, **5b** = 14.7 min, **5c** = 15.1 min

Amidation of Iodobenzene (6)

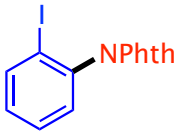

6a

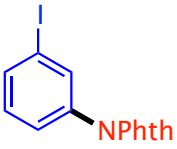

6b

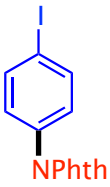

6c

Isolated yield: 61 %; off-white solid

Regioselectivity ratio (**6a**:**6b**:**6c**): *1:22:29*

TLC: R_f 0.4 (n-hexane:EtOAc = 8:2)

Retention time: **6a** = 20.0 min, **6b** = 20.8 min, **6c** = 21.4 min

Amidation of Phenylacetate (7)

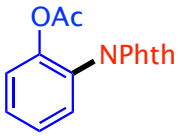

7a

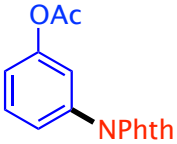

7b

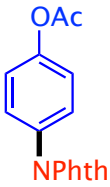

7c

Isolated yield: 61 %; off-white solid

Regioselectivity ratio (**7a**:**7b**:**7c**): *1:19:30*

TLC: R_f 0.47 (n-hexane:EtOAc = 8:2)

Retention time: **7a** = 16.0 min, **7b** = 16.5 min, **7c** = 16.8 min

Amidation of Ethyl Benzoate (8)

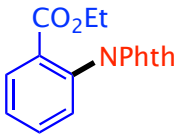

8a

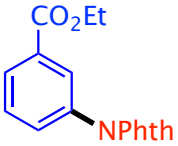

8b

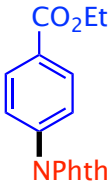

8c

Isolated yield: 40 %; off-white solid

Regioselectivity ratio (**8a**:**8b**:**8c**): *1:22:3*

TLC: R_f 0.3 (n-hexane:EtOAc = 8:2)

Retention time: **8a** = 14.1 min, **8b** = 14.8 min, **8c** = 15.0 min

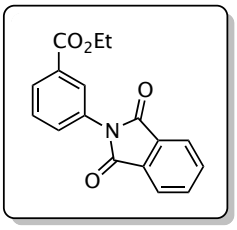

^{1}H NMR (400 MHz, $CDCl_3$): δ 8.13 (s, 1 H), 8.09 (d, *J* = 8 Hz, 1 H), 7.96 (m, 2 H), 7.80 (m, 2 H), 7.65 (d, *J* = 1.6 Hz, 1 H), 7.58 (t, *J* = 7.8 Hz, 1 H), 4.39 (q, *J* = 7.2 Hz, 2 H), 1.39 (t, *J* = 7.2 Hz, 3 H). ^{13}C NMR (100 MHz, $CDCl_3$): δ 167.1, 165.8, 134.7, 132.1, 131.8, 131.7, 130.9, 129.3, 127.8, 124.0, 61.4, 14.4.

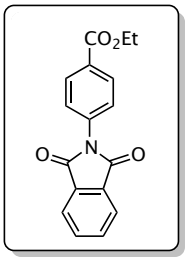

^{1}H NMR (400 MHz, $CDCl_3$): δ 8.16 (d, *J* = 8.4 Hz, 2 H), 7.94 (m, 2 H), 7.79 (m, 2 H), 7.58 (d, *J* = 8.8 Hz, 2 H), 4.39 (q, *J* = 6.8 Hz, 2 H), 1.40 (t, *J* = 7.2 Hz, 3 H). ^{13}C NMR (100 MHz, $CDCl_3$): δ 166.9, 165.9, 135.9, 134.8, 131.7, 130.5, 129.8, 126.0, 124.1, 61.3, 14.4.

Amidation of Biphenyl (9)

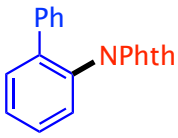

9a

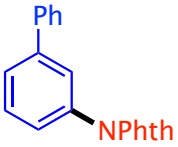

9b

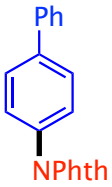

9c

Isolated yield: 47 %; off-white solid

Regioselectivity ratio (**9a:9b:9c**): *1:49:36*

TLC: R_f 0.3 (n-hexane:EtOAc = 8:2)

Retention time: **9a** = 14.9 min, **9b** = 15.3 min, **9c** = 16.7 min

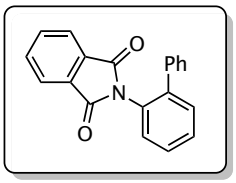

^{1}H NMR (400 MHz, $CDCl_3$): δ 7.80 (m, 2 H), 7.68 (m, 2H), 7.50 (m, 3 H), 7.31 (m, 1 H), 7.22 (m, 5 H). ^{13}C NMR (100 MHz, $CDCl_3$): δ 167.6, 141.8, 139.0, 134.2, 131.9, 131.1, 129.8, 129.5, 128.6, 128.4, 128.2, 127.6, 123.8.

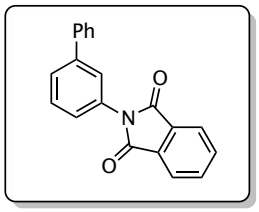

^{1}H NMR (400 MHz, $CDCl_3$): δ 7.96 (m, 2 H), 7.80 (m, 2 H), 7.62 (m, 5 H), 7.43 (m, 3 H), 7.34 (m, 1 H). ^{13}C NMR (100 MHz, $CDCl_3$): δ 167.4, 142.6, 140.4, 134.6, 132.3, 131.9, 129.6, 128.9, 127.8, 127.4, 127.0, 125.6, 125.4, 123.9.

Amidation of 2-Bromotoluene (10)

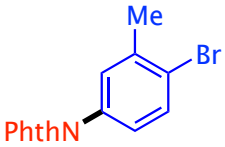

10a

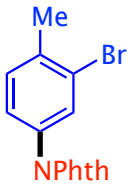

10b

Isolated yield: 65 %; off-white solid

Regioselectivity ratio (**10a**:**10b**): *3:5*

TLC: R_f 0.47 (n-hexane:EtOAc = 8:2)

Retention time: **10a** = 16.8 min, **10b** = 16.9 min

Amidation of 2-Iodotoluene (11)

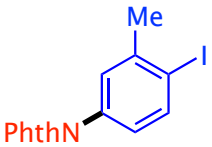

11a

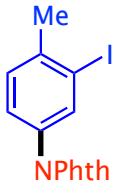

11b

Isolated yield: 67 %; off-white solid

Regioselectivity ratio (**8a**:**8b**): *3:5*

TLC: R_f 0.47 (n-hexane:EtOAc = 8:2)

Retention time: **11a** = 17.9 min, **11b** = 18.0 min

Amidation of Naphthalene (12)

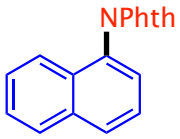

12a

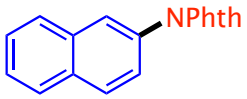

12b

Isolated yield: 40 %; off-white solid

Regioselectivity ratio (**12a**:**12b**): *20:1*

TLC: R_f 0.4 (n-hexane:EtOAc = 8:2)

Retention time: **12a** = 14.9 min, **12b** = 15.2 min

Amidation of *m*-Xylene (13)

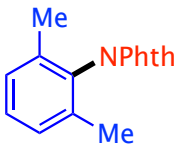

13a

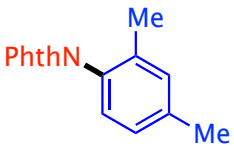

13b

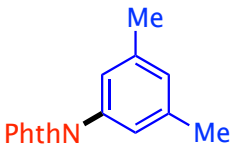

13c

Isolated yield: 51 %; yellow liquid

Regioselectivity ratio (**13a**:**13b**:**13c**): *1:5:14*

TLC: R_f 0.47 (n-hexane:EtOAc = 8:2)

Retention time: **13a** = 17.1 min, **13b** = 17.5 min, **13c** = 17.9 min

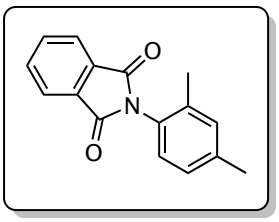

^{1}H NMR (400 MHz, d_6-acetone): δ 7.93 (m, 4 H), 7.21 (m, 2 H), 7.15 (d, *J* = 8 Hz, 1 H), 2.37 (s, 3 H), 2.15 (s, 3 H). ^{13}C NMR (100 MHz, d_6-acetone): δ 167.1, 165.8, 134.7, 132.1, 131.8, 131.7, 130.9, 129.3, 127.8, 124.0, 61.4, 14.4.

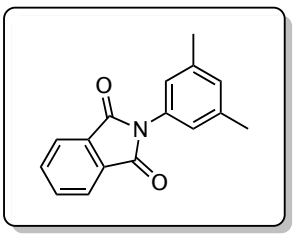

^{1}H NMR (400 MHz, d_6-acetone): δ 7.91 (m, 4 H), 7.08 (d, *J* = 5.6 Hz, 3 H), 2.35 (s, 6 H). ^{13}C NMR (100 MHz, d_6-acetone): δ 167.1, 138.5, 134.6, 132.4, 132.2, 129.5, 125.0, 123.3, 20.5.

Amidation of 3-Bromotoluene (14)

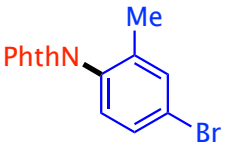

14a

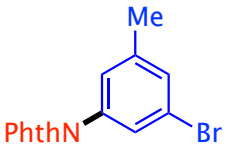

14b

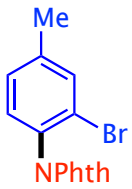

14c

Isolated yield: 57 %; white solid

Regioselectivity ratio (**14a**:**14b**:**14c**): *4:16:1*

TLC: R_f 0.47 (n-hexane:EtOAc = 8:2)

Retention time: **14a** = 16.9 min, **14b** = 17.4 min, **14c** = 17.8 min

Amidation of 2,6-Dimethylanisole (15)

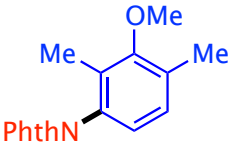

15a

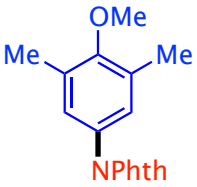

15b

Isolated yield: 60 %; off-white solid

Regioselectivity ratio (**15a**:**15b**): *1:94*

TLC: R_f 0.3 (n-hexane:EtOAc = 8:2)

Retention time: **15a** = 18.9 min, **15b** = 20.6 min

Figure S2.1 ^{1}H NMR Spectrum of **(8b)**

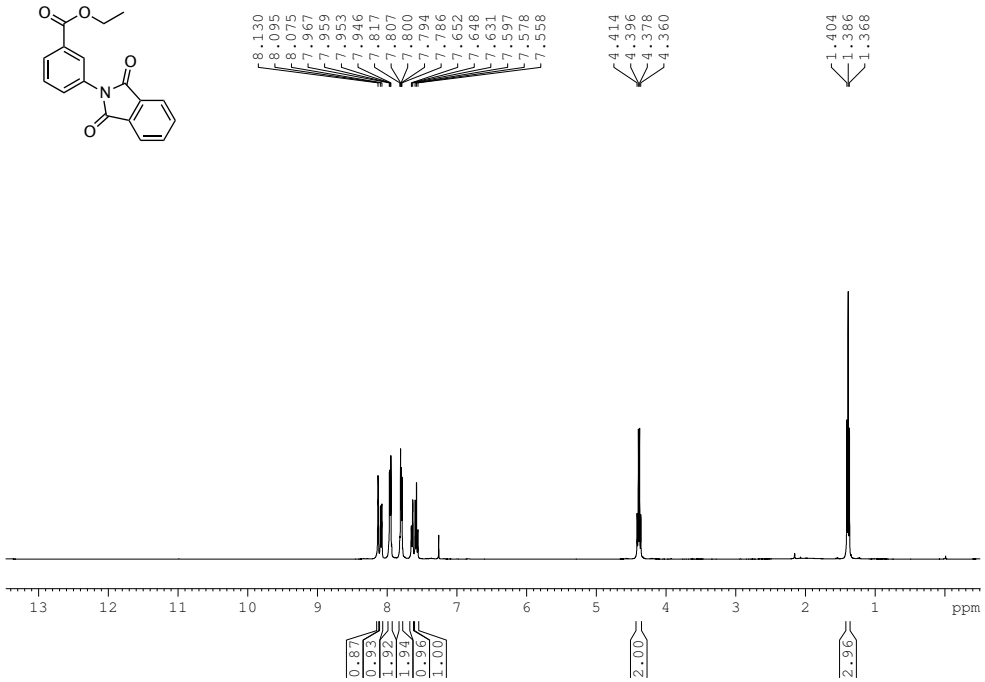

Figure S2.2 ^{13}C NMR Spectrum of **(8b)**

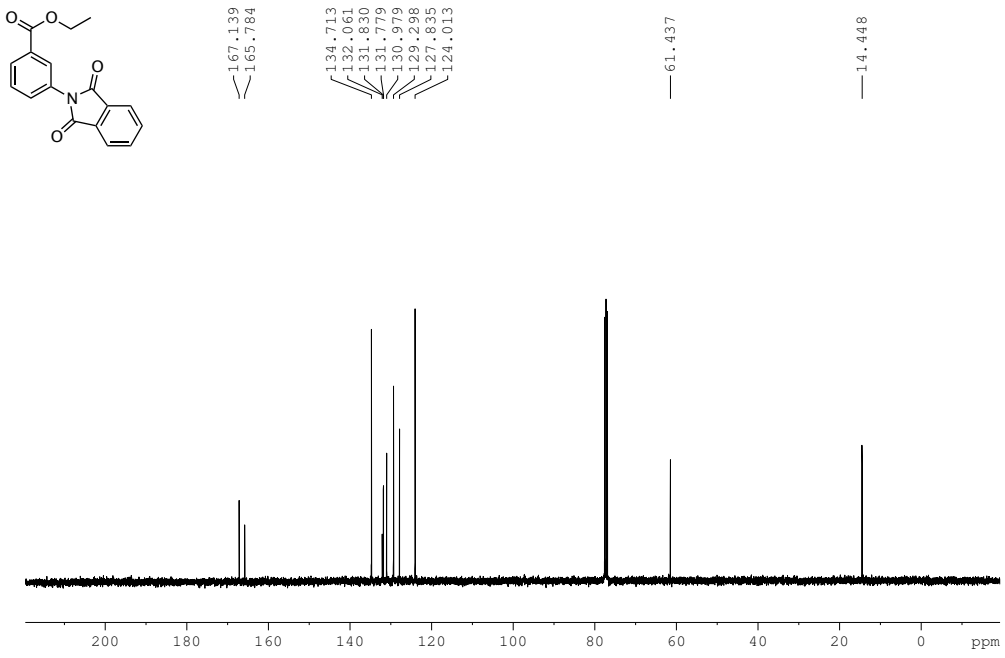

Figure S2.3 DEMT135 NMR Spectrum of **(8b)**

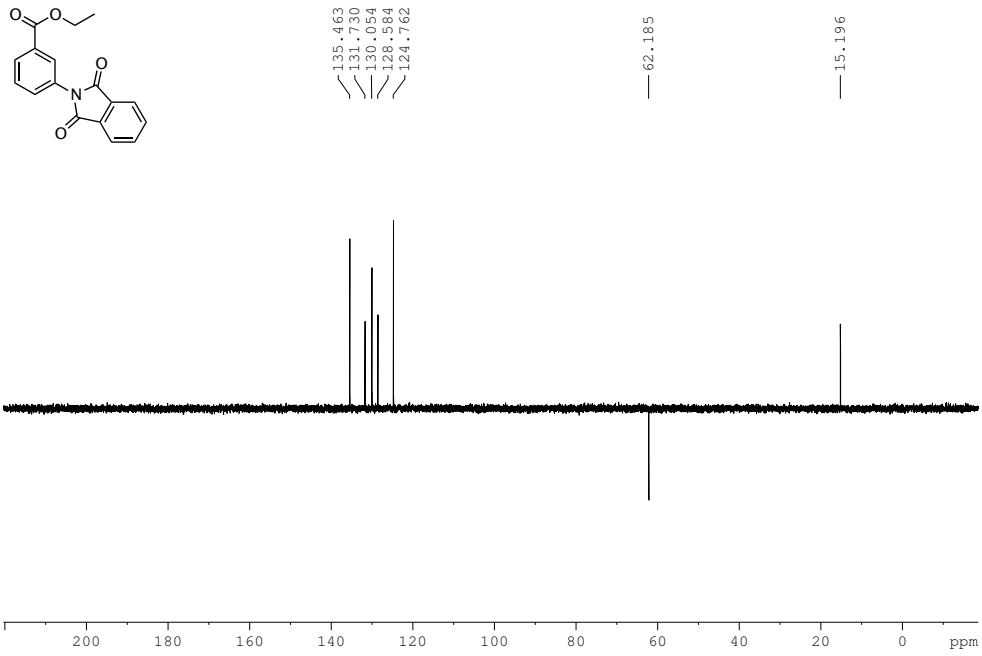

Figure S2.4 ^{1}H NMR Spectrum of **(8c)**

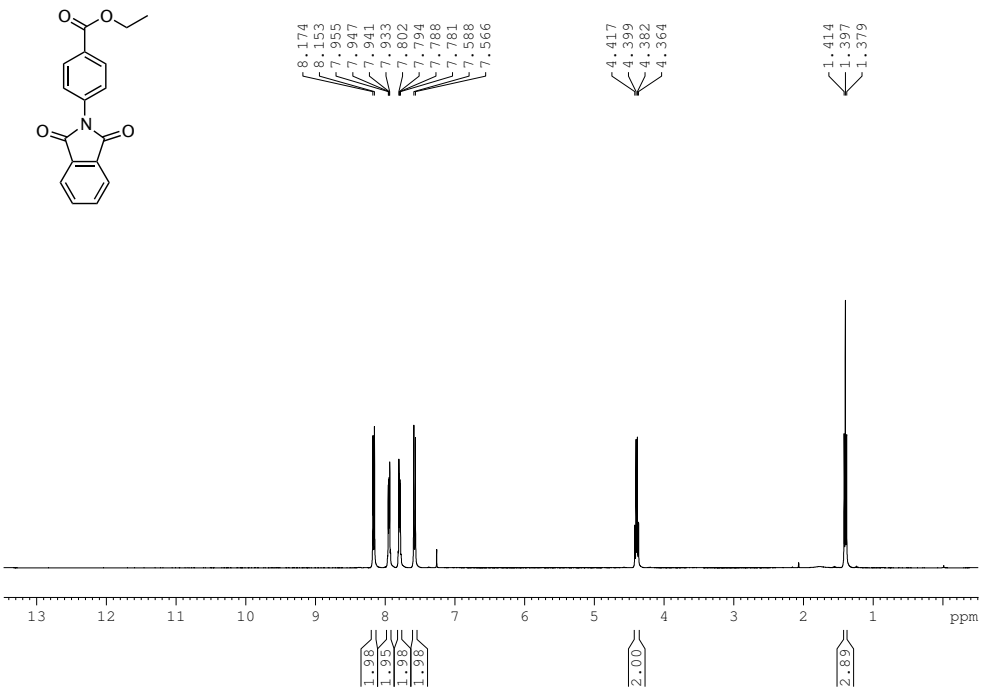

Figure S2.5 ^{13}C NMR Spectrum of **(8c)**

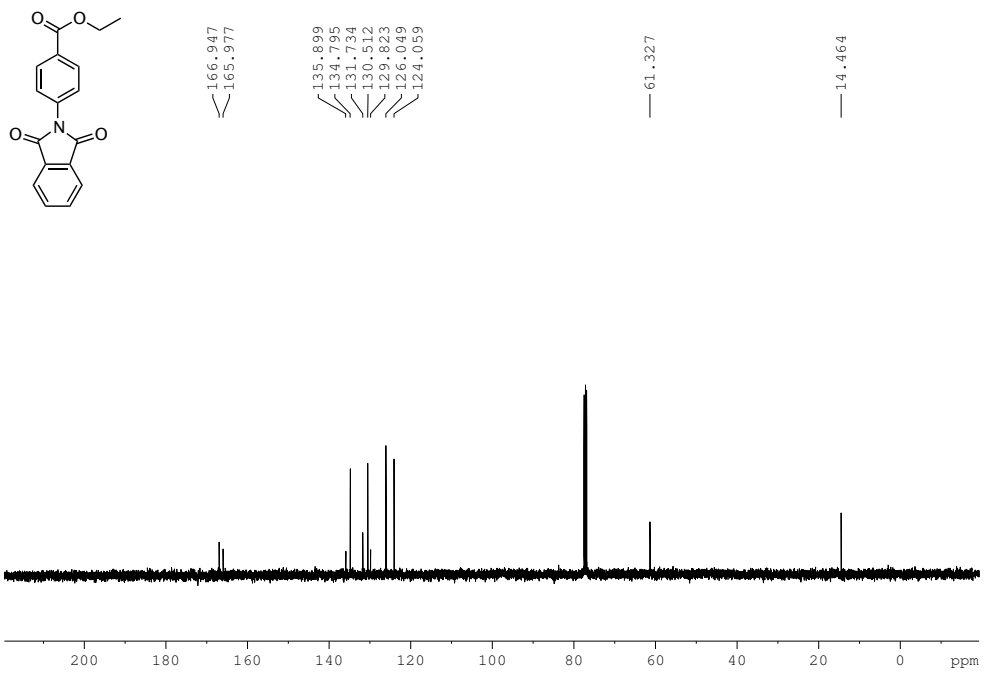

Figure S2.6 DEMT135 NMR Spectrum of **(8c)**

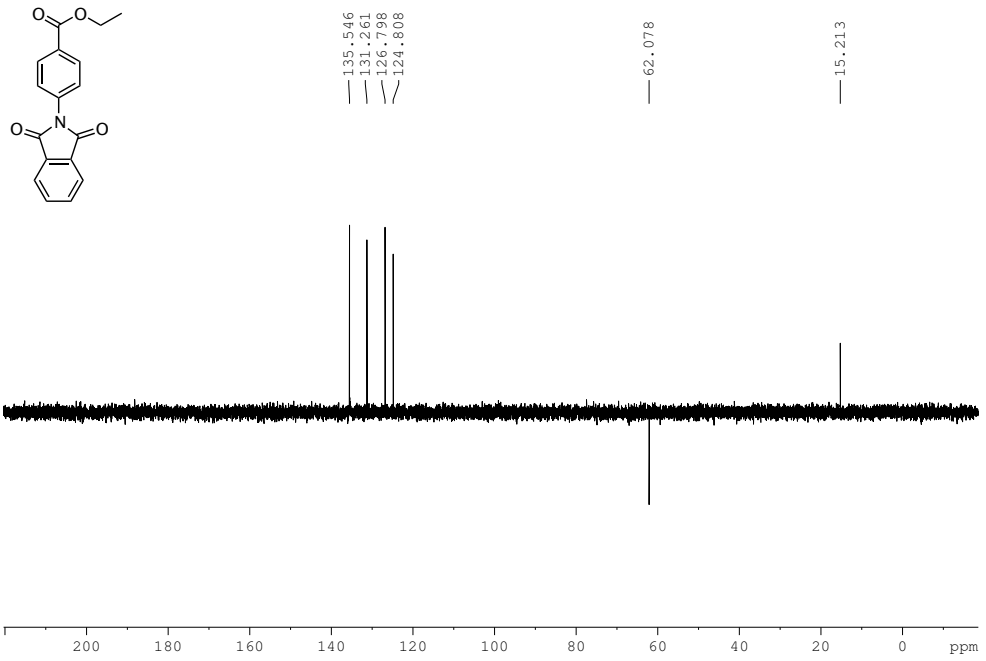

Figure S2.7 ^{1}H NMR Spectrum of **(9a)**

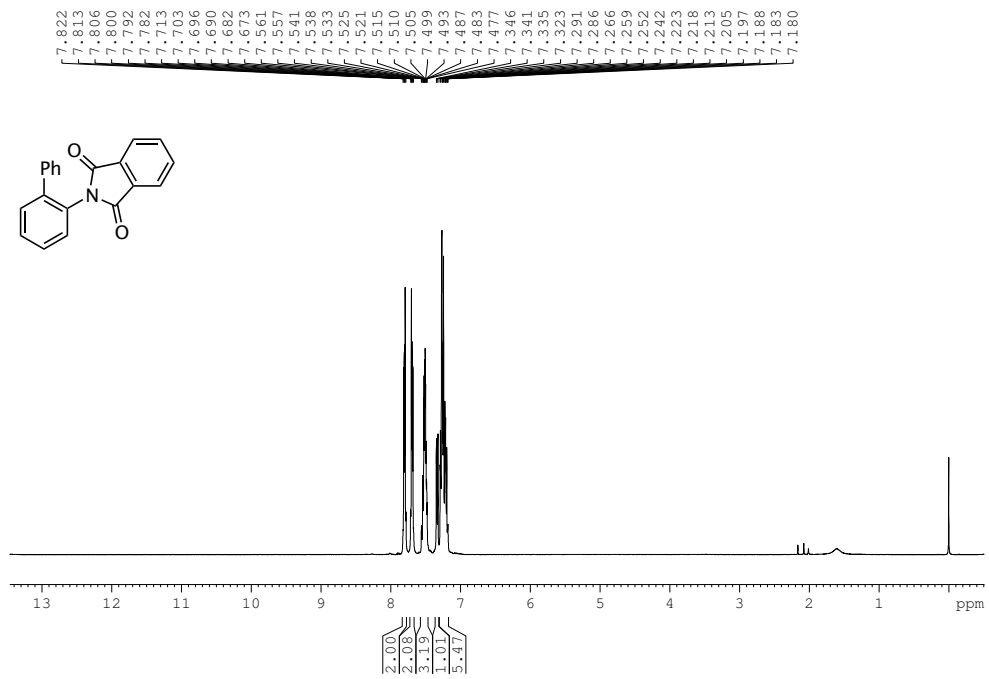

Figure S2.8 ^{13}C NMR Spectrum of **(9a)**

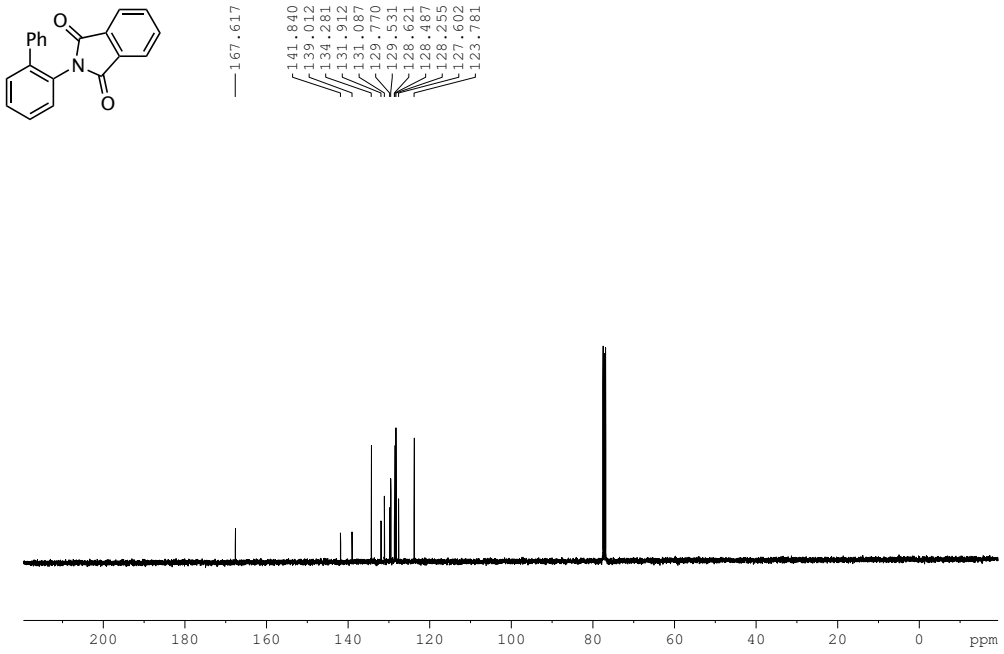

Figure S2.9 DEMT135 NMR Spectrum of **(9a)**

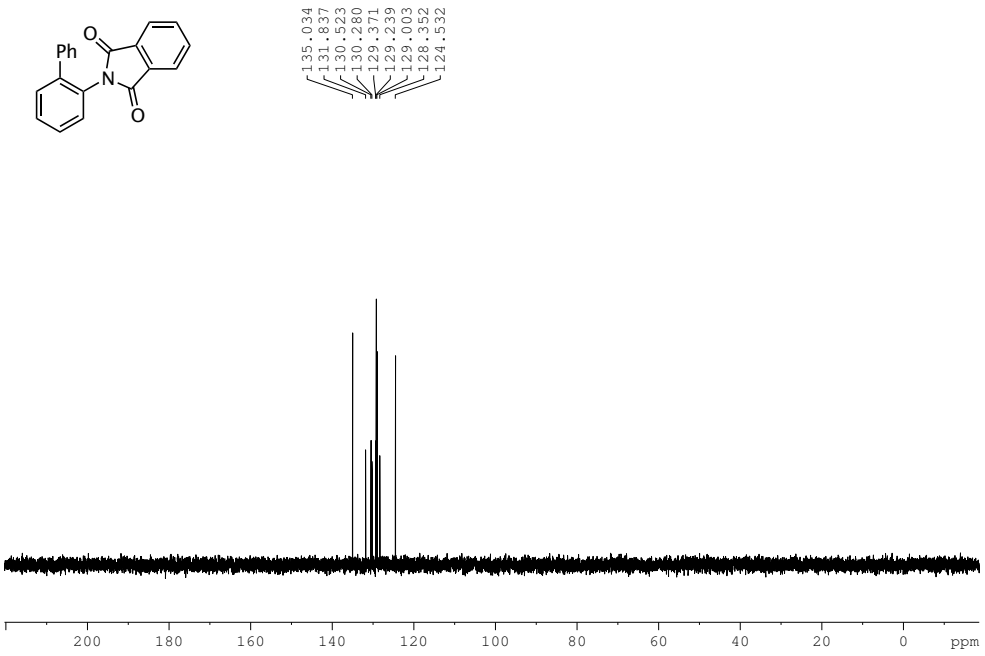

Figure S2.10 ^{1}H NMR Spectrum of **(9b)**

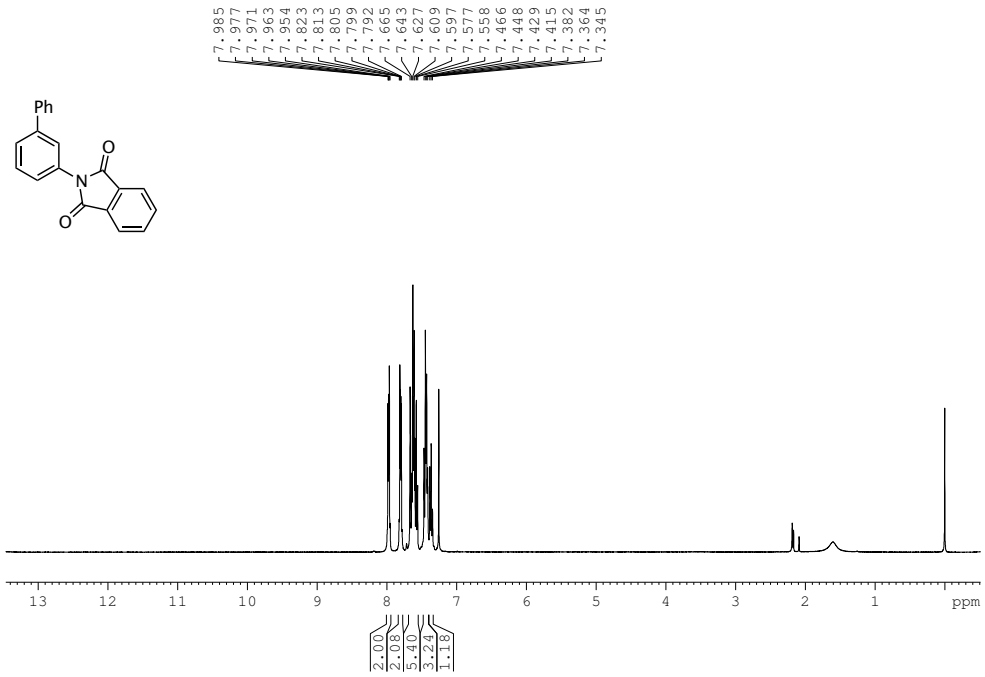

Figure S2.11 ^{13}C NMR Spectrum of **(9b)**

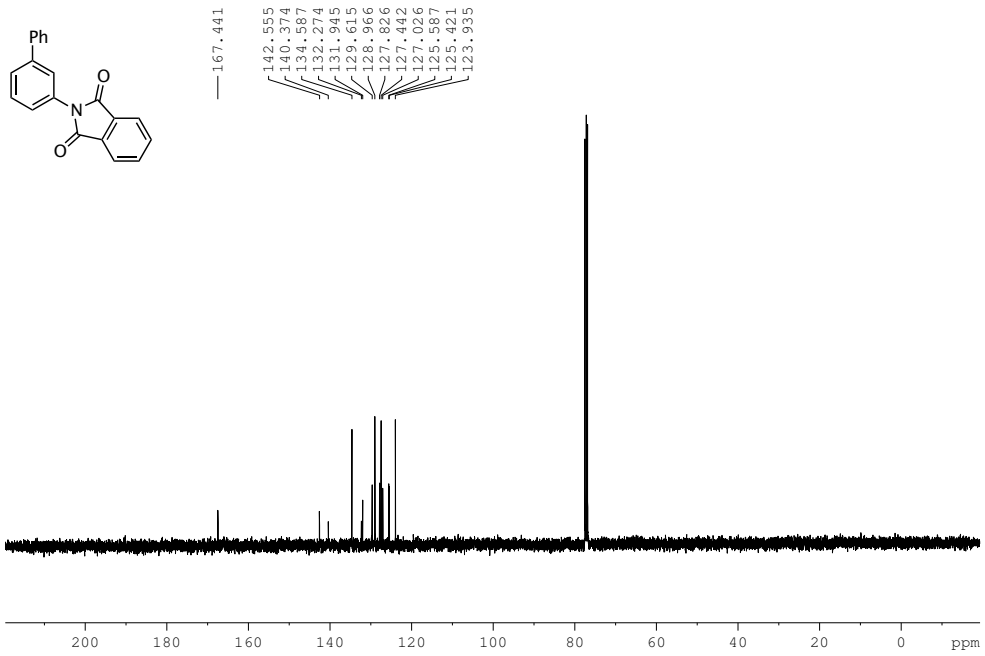

Figure S2.12 DEMT135 Spectrum of **(9b)**

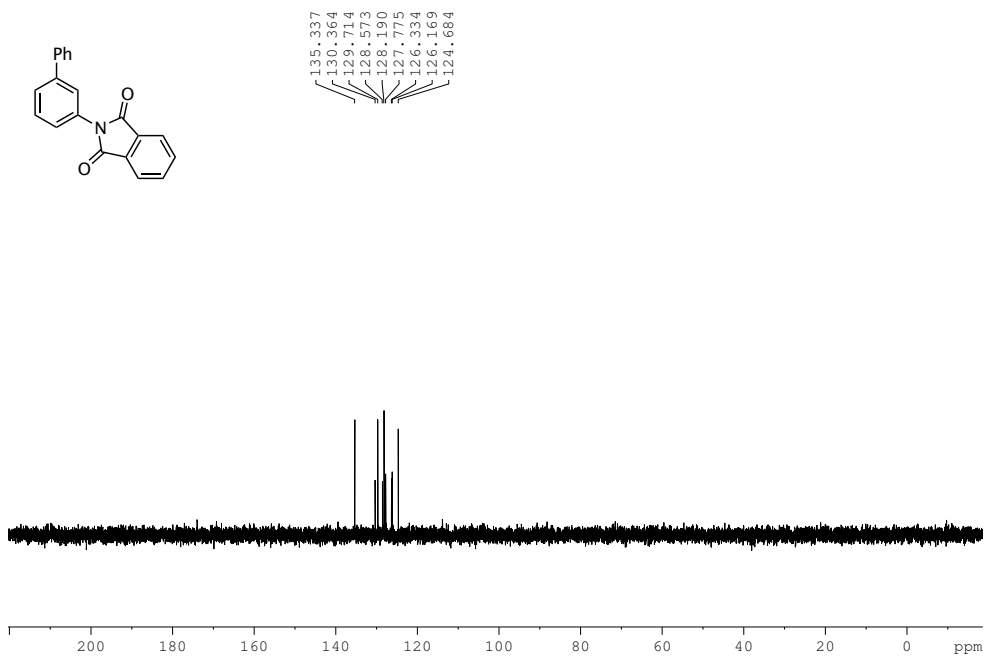

Figure S2.13 ^{1}H NMR Spectrum of **(13b)**

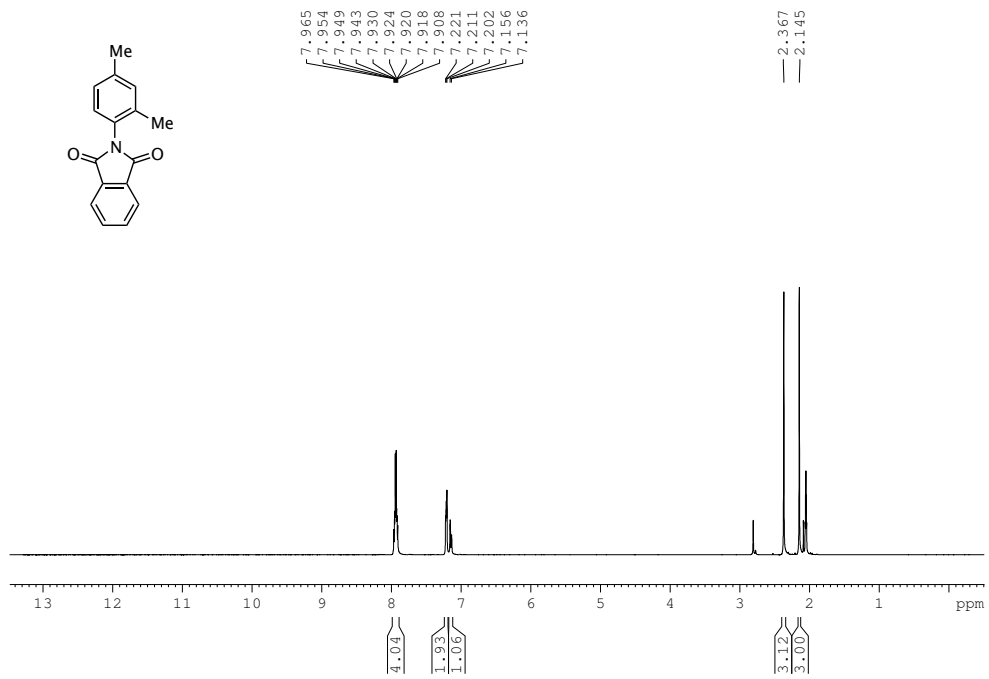

Figure S2.14 ^{13}C NMR Spectrum of **(13b)**

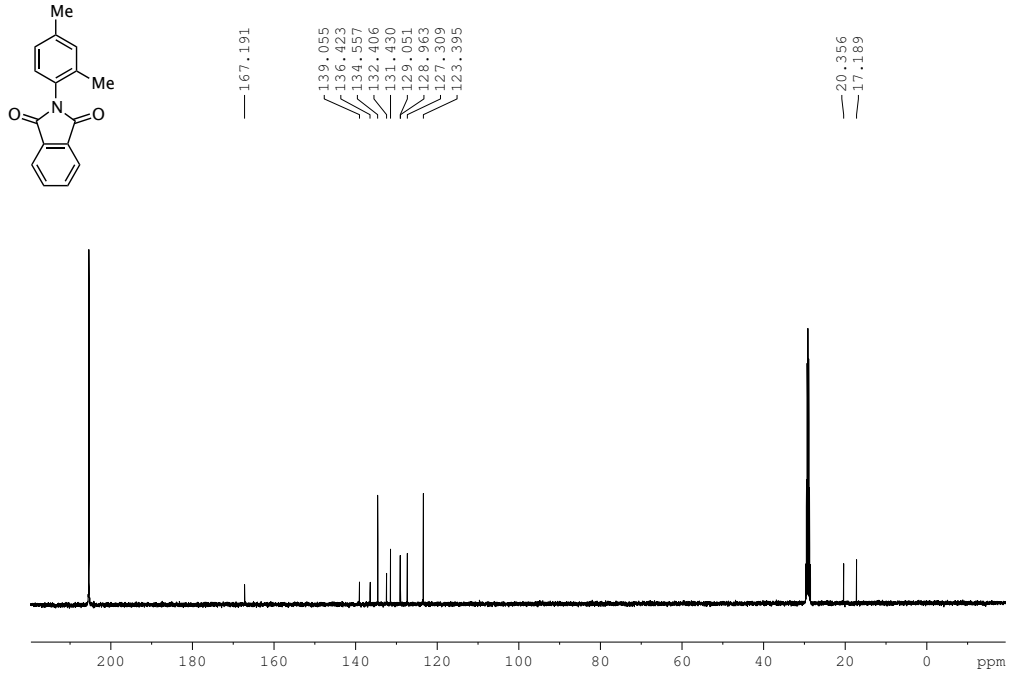

Figure S2.15 DEMT135 NMR Spectrum of **(13b)**

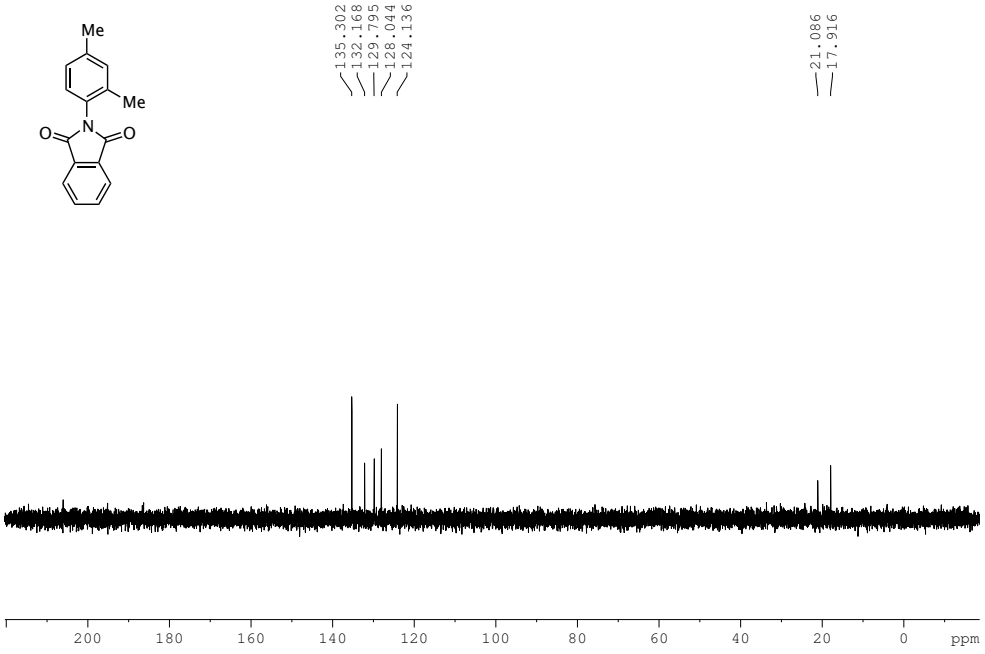

Figure S2.16 ^{1}H NMR Spectrum of **(13c)**

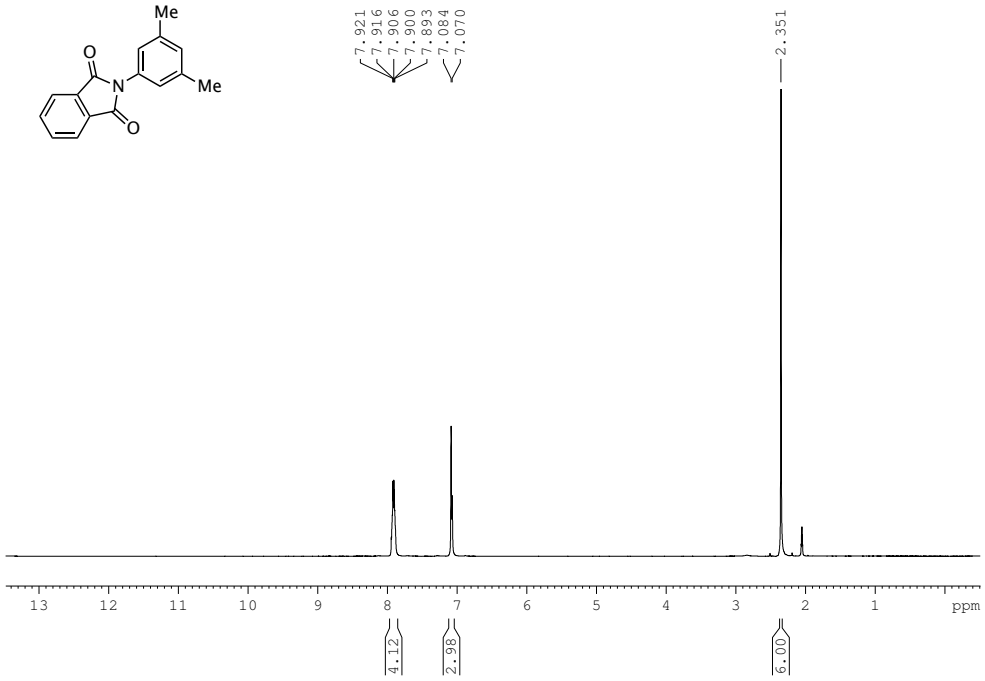

Figure S2.17 ^{13}C NMR Spectrum of **(13c)**

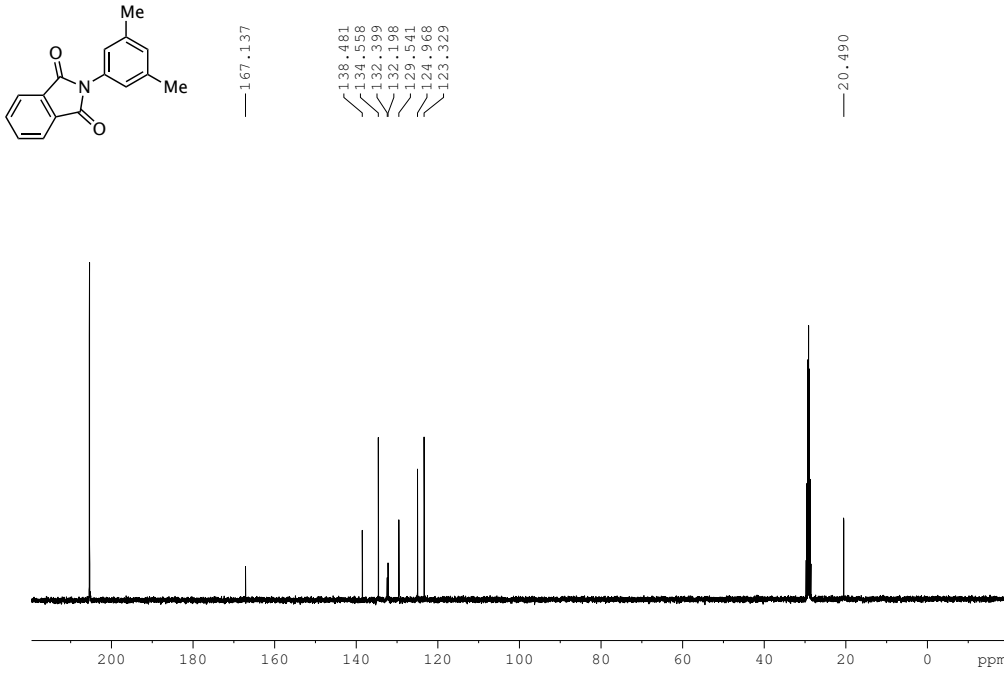

Figure S2.18 DEMT135 NMR Spectrum of **(13c)**

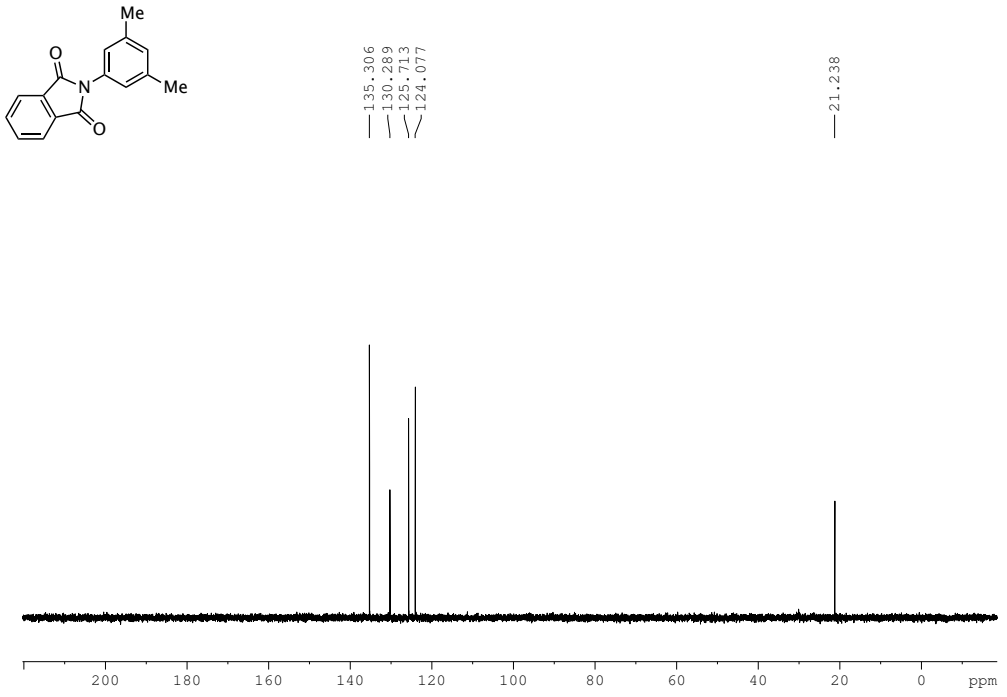

Figure S2.19 ^{1}H NMR Spectrum of [(IPr)Pd(OAc)$_2$(OH$_2$)]

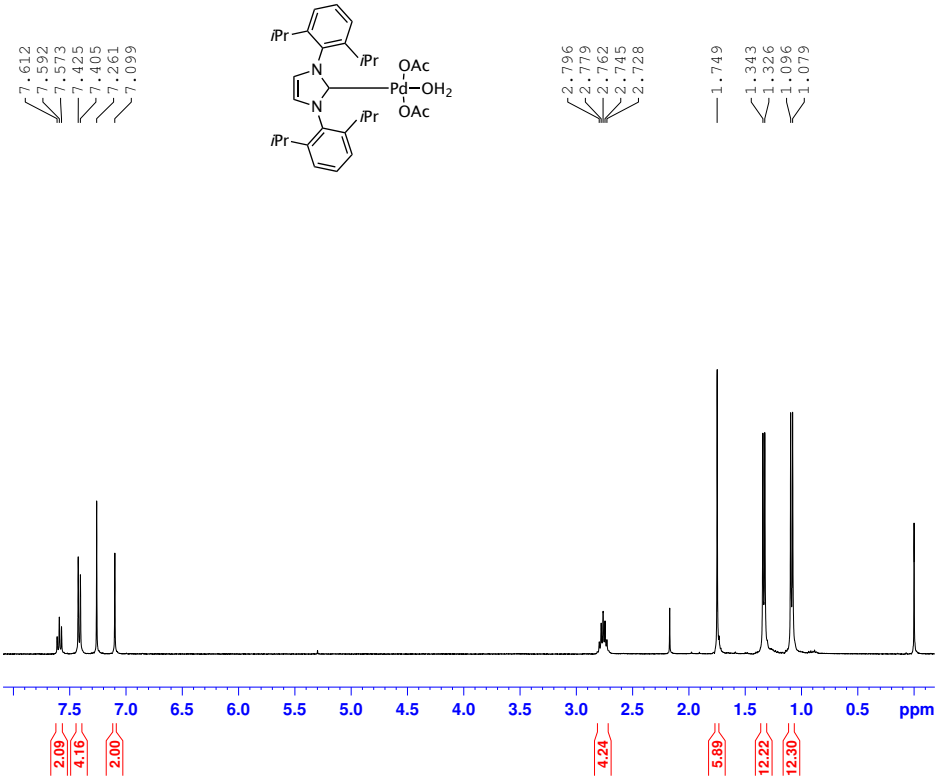

Chapter 3

Enantioselective and Regioselective Synthesis of Dihydroxyquinolin-2-ones by Ru(II)-Catalyzed Intramolecular C(sp^2)-H Amidation of 1,4,2-Dioxazol-5-ones

3.1 Introduction

Dihydroquinolin-2-one and its derivatives are found in many natural products and pharmaceutical compounds.[27] Figure 3.1 shows three representative dihydroquinolin-2-one alkaloids, namely 22-*O*-(*N*-methyl-valyl)aflaquinolone B, Yaequinolone A1 and Penigequinolone A isolated from natural sources.

Figure 3.1. Representative Natural Products Examples Containing Dihydroquinolin-2-one Motifs

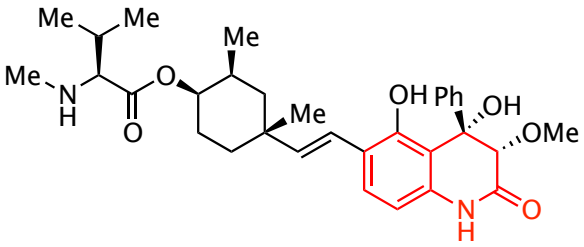

22-*O*-(*N*-Methyl-L-valyl)aflaquinolone B

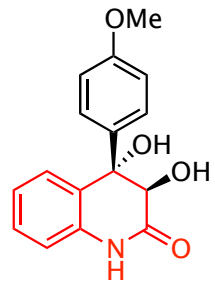

Yaequinolone A1

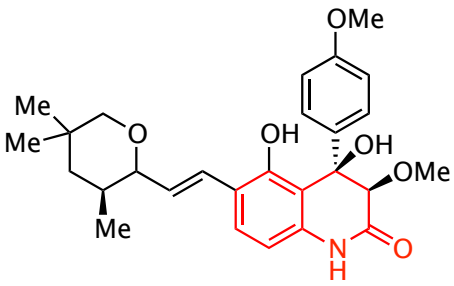

Penigequinolone A

Conventionally, dihydroquinolin-2-ones are synthesized by Friedel-Craft reactions (Scheme 3.1). For example, treating anilines with (*E*)-but-2-enoyl chloride with triethylamine in THF would produce *N*-phenylbut-2-enamides, which would react by Friedel-Craft reaction with $AlCl_3$[28] or polyphosphoric acid[29] as catalyst.

Scheme 3.1. Conventional Organic Synthesis of Dihydroquinolin-2-ones

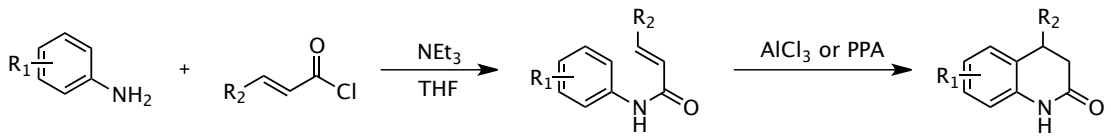

Transition metals-catalyzed approaches are known to produce dihydroquinolin-2-ones (Scheme 3.2). Alper and co-workers reported the Pd(II)-catalyzed cyclocarbonylation of 2-aminostyrenes in an ionic liquid medium to afford dihydroquinolin-2-ones in excellent yields.[30] The amino group of the 2-aminostyrene coordinates to the Pd(II) metal center. The π-bonding of the terminal alkene coordinates with Pd metal center would forge a new Pd-C σ bond by olefin insertion. Carbonylation of palladacycle and then reductive elimination on the amino group and the carbonyl group afford a new C-N bond. In 2010, Youn and co-workers reported the Rh(I)-catalzyed domino conjugated addition-cyclization reaction of α,β-unsaturated esters bearing *N*-benzyl amino group at the *ortho*-position of the arene with organoboroxines.[31] In this reaction, the olefin act as electrophile and the protected amino group should be highly nucleophilic for the reaction. Rh(I) catalyst undergoes the transmetalation with organoboroxine to form Rh(I)-aryl complex. The Rh(I)-aryl complex performs the conjugate addition on the C=C bond to form the oxa-π-allyl Rh(I) intermediate. The final step of the reaction is the cyclization of the nucleophilic amino group attacking on carbonyl carbon with the elimination of methoxide group of the ester in the form of [(COD)Rh(I)OMe] as a resting state.

Chang and co-workers also demonstrated the Ru-catalyzed olefin hydrocarbamoylation of *N*-(2-vinylphenyl)-formamides to form dihydroquinolin-2-ones.[32] Based on the mechanistic studies by Chang and co-workers, the N-H bond of the amido group of *N*-(2-vinylphenyl)-formamides is cleavage by Ru(II) complex and then undergoes the hydride insertion on the C=C bond. β-Hydride abstraction from the formyl C-H bond occurs to form isocyanates. The insertion of alkylruthenium intermediate on isocyanate forms a cyclic imidate and then undergoes tautomerization to form corresponding products. The reaction, however, has an unsatisfactory selectivity between five and six-membered benzo-fused lactams formation. The substrates bearing an electron-rich substituent (e.g. Me and OMe) favors six-membered benzo-fused lactams formation. The substrates bearing an electron-deficient substituent (e.g. CF_3, CN and CO_2Me) favors five-membered benzo-fused lactams formation.

Scheme 3.2. Catalytic Approaches of Dihydroquinolin-2-ones Formation

Howard Alper

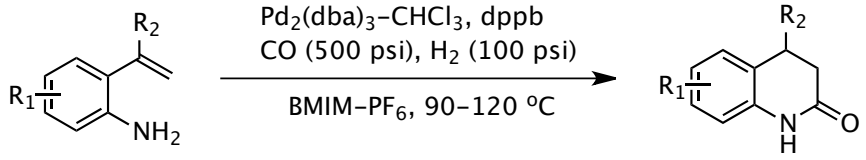

$R_1 = R_2 = H$, Me

60–95 %
30 examples

So Won Youn

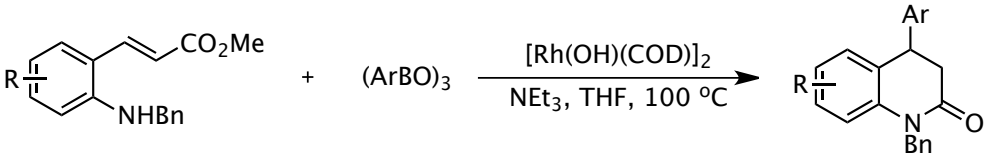

R = H, Me, OMe, CF_3, NO_2

53–88 %
17 examples

Sukbok Chang

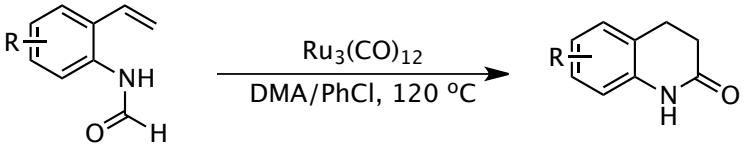

R = H, Me, OMe, CF_3, Cl, Br, CO_2Me, OPh, CN

63–91 %
16 examples

The electrophilic amidation reactions are known to be versatile approaches for C-N bond formation via highly reactive metal-nitrenoid intermediate.[33] Several nitrene precursors such as organic azides,[34] hydroxylamines[35] and dioxazolones[36] have been examined for electrophilic amidation reactions. The intramolecular amidation reaction involving carbonyl nitrene intermediate is very challenging because of the competitive formation of isocyanates from the metal-nitrenoid intermediate by Curtius-typed rearrangement.[37] Employing 3-(4-methoxyphenethyl)-1,4,2-dioxazol-5-one, Chang and co-workers demonstrated that some Cp*-Ir(III) complexes can effect catalytic intramolecular C(sp^2)-H bond amidation[38] and C(sp^3)-H bond amidation reactions[18] without competitive isocyanate formation. Our group also demonstrated

the [Ru(*p*-cymene)(*R*,*R*-DPEN)Cl] catalyst (*R*,*R*-DPEN = *N*-((1*R*,2*R*)-2-amino-1,2-diphenylethyl)-4-methylbenzenesulfonamide) achieved the highly enantioselective intramolecular C(sp^3)-H bond amidation of 1,4,2-dioxazol-5-one to form Y-lactam in 98 % *ee* without competitive isocyanate formation.[19]

Scheme 3.3. Ir(III)-Catalyzed Intramolecular C(sp^2)-H Bond Amidation

Sukbok Chang

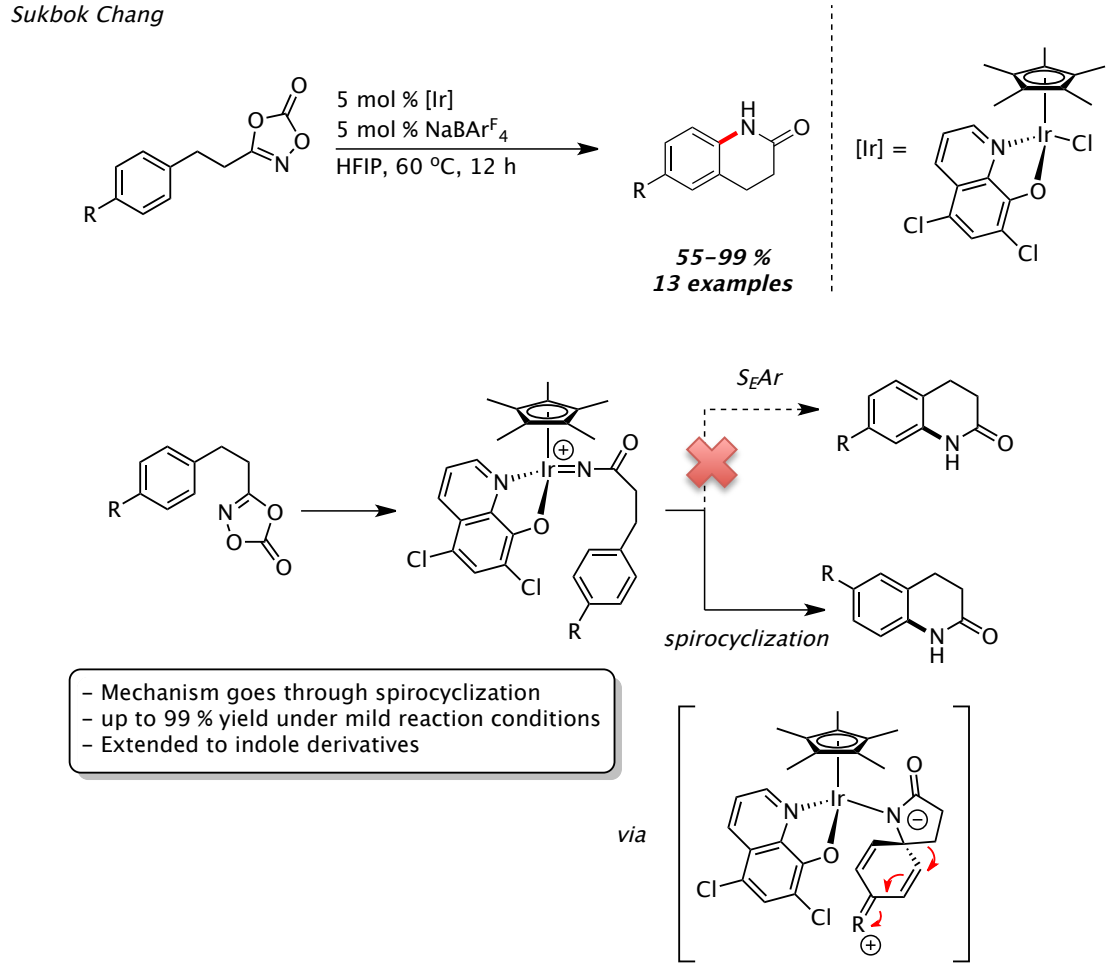

Prompted by this study, we would like to investigate the Ru(II)-catalyzed enantioselective intramolecular C(sp^2)-H bond amidation reaction. In addition, the regioselective between C(sp^2)-H bond and C(sp^3)-H bond amidation reaction is also investigated in different reaction conditions and different types of ligands.

3.2 Results and Discussion

3.2.1 Preliminary Results

Initially, 3-(2,2-diphenylethyl)-1,4,2-dioxazol-5-one ***1a*** was prepared for the investigation of Ru(II)-catalyzed intramolecular amidation forming the dihydroxquinolin-2-one. For substrate preparation, 3,3-diphenylpropanoic acid was reacted with oxalyl chloride and then underwent the amide bond formation with hydroxylamine hydrogen chloride to form *N*-hydroxy-3,3-diphenylpropanamide. The *N*-hydroxy-3,3-diphenylpropanamide reacted with 1,1'-carbonyldiimidazole in DCM at room temperature for 30 mins to give 3-(2,2-diphenylethyl)-1,4,2-dioxazol-5-one in 90 % isolated yield. By employing the ***1a*** (0.1 mmol) with a catalytic amount of [Ru(*p*-cymene)(L-proline)Cl] (10 mol %, **[Ru2]**) and $AgSbF_6$ (10 mol %) in dry DCE (1 mL) at 50 ^{o}C gave 4-phenyl-3,4-dihydroquinolin-2(1*H*)-one (***2a***) in 9 % isolated yield with 53 % *ee* (Scheme 3.4).

Scheme 3.4. Preliminary Results

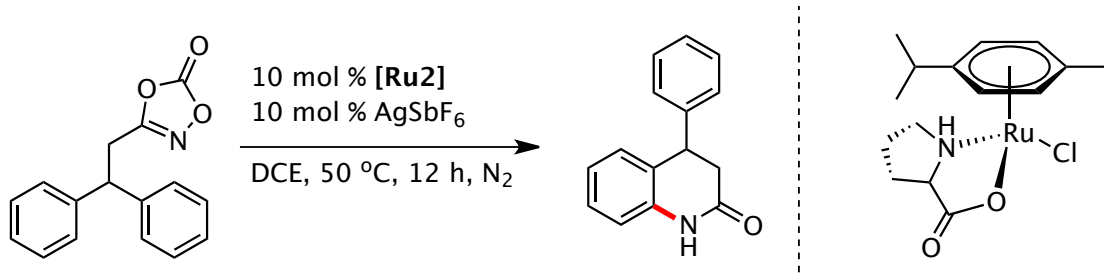

Two enantiomers, (*R*)-4-phenyl-3,4-dihydroquinolin-2(1*H*)-one and (*S*)-4-phenyl-3,4-dihydroquinolin-2(1*H*)-one were prepared according to literature report.[51] Racemic dihydroquinolin-2-one ***2a*** was injected into HPLC equipped with a Chiralcel® OD-H

column (0.46 φ x 25 cm) with UV detection at 280 nm. The flow rate was set at 0.7 mL/min and the eluent solvent system is n-hexane/isopropyl alcohol = 9:1. Two signals were detected at 21.4 mins and 24.8 mins. Then, a sample of (*S*)-4-phenyl-3,4-dihydroquinolin-2(1*H*)-one was added into the racemic mixture, and the combined mixture was subjected to chiral HPLC analysis. The peak at retention time = 21.4 mins was enhanced in intersity; therefore, the peak was assigned to (*S*)-4-phenyl-3,4-dihydroquinolin-2(1*H*)-one. The peak at 24.8 mins was assigned to (*R*)-4-phenyl-3,4-dihydroquinolin-2(1*H*)-one. Based on the HPLC analysis of product mixture obtained from the Ru-catalyzed reaction of ***1a***, (*S*)-4-phenyl-3,4-dihydroquinolin-2(1*H*)-one was found to be the major enantiomer.

Figure 3.2. HPLC Chromatogram of Enatiomers of ***2a***

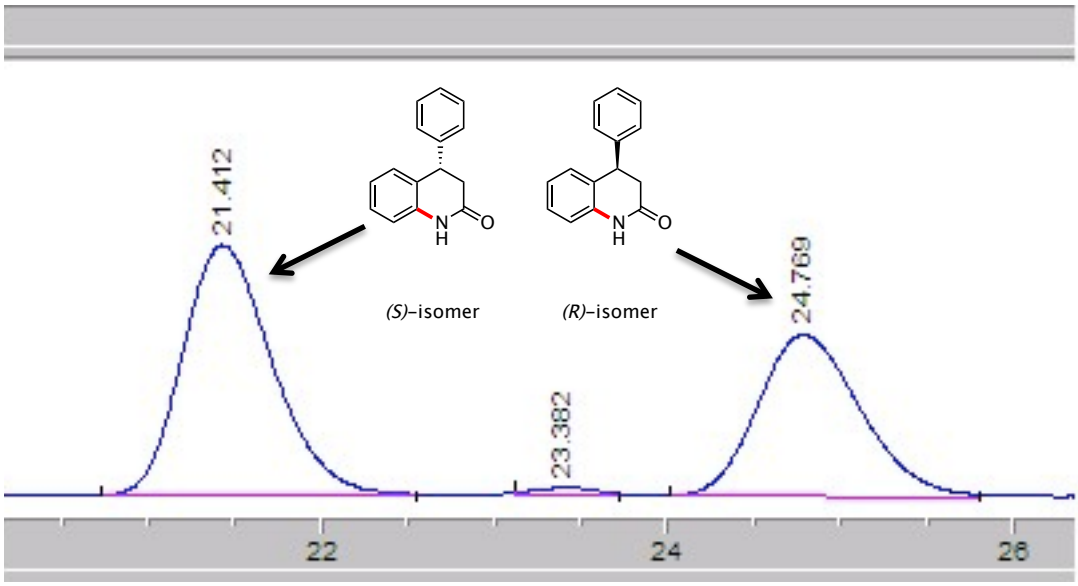

Several chiral amino acids such as L-*tert*-leucine, L-leucine, L-phenylalanine, D-phenylglycine, L-serine, L-glutamic acid, L-isoleucine and L-valine were tested for the amidation and the results showed that only L-proline gave the most satistfactory result in terms of enantiomeric excess (Table 3.1). Therefore, L-proline (**[Ru2]**) was chosen for the optimization of reaction conditions.

Table 3.1. Ligand Scope Studies in Enantioselectivity Amidation

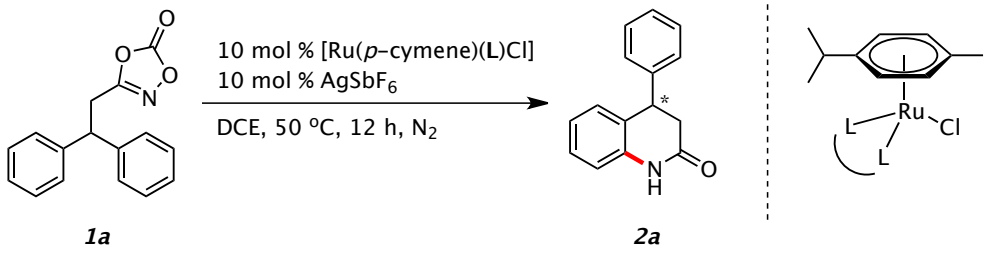

1a *2a*

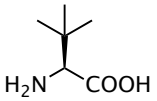	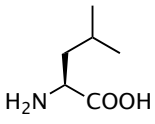	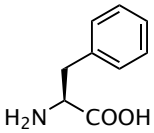	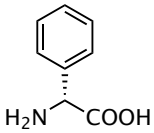	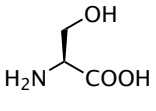
30 % 9 % *ee*	13 % 23 % *ee*	17 % 9 % *ee*	13 % 3 % *ee*	n.r.
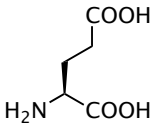	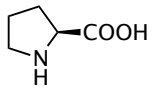	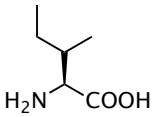	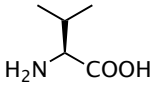	
9 % 11 % *ee*	9 % 53 % *ee*	4 % 17 % *ee*	9 % 11 % *ee*	

[a]Reaction conditions: ***1a*** (0.1 mmol), [Ru(*p*-cymene)(**L**)Cl] (10 mol %), $AgSbF_6$ (10 mol %) in DCE (1 mL) at 50 °C for 12 h under N_2; Isolated yield; *ee* is determined by HPLC with chiral column; (*S*)-isomer is dominant.

3.2.2 Optimization Results

Encouraged by the preliminary results, we optimized the reaction conditions for improving the performance of the amidation reaction and the enantioselectivity of the dihyroxquinolin-2-one formation (Table 3.2). Employing polar aprotic solvents (entries 1-8), only DCE (entry 1) and acetone (entry 7) gave 53 % *ee* and 63 % *ee* of dihyroxquinolin-2-one formation respectively but the yield of desired product was far from satisfactory. Using polar protic solvents (entries 10 – 15), MeOH (entry 10) and EtOH (entry 11) did not improve both the product yield and enantioselectivity. The reaction in HFIP (entry 14) and TFE (entry 15) produced dihydroxquiolin-2-one in 65 % and 76 % isolated yield respectively but the enaniomeric excess dropped to 30

%*ee*. Therefore, the mixture of solvents with various proportions (DCE and HFIP) was for any improvement in enantioselectivity (entries 16 – 17), examined no significant improvement in *ee* was observed. Higher reaction temperature (entry 20) did not bring about further improvement in both isolated yield and enantiomeric excess of dihydroxquiolin-2-one formation. Yet, temperature below 50 ^{o}C (entries 18 – 19) would sluggish amidation reaction. As a result, the most optimized reaction condition is employing 3-(2,2-diphenylethyl)-1,4,2-dioxazol-5-one (***1a***, 0.1 mmol) with **[Ru2]** (10 mol %) and $AgSbF_6$ (10 mol %) in TFE (1 mL) at 50 ^{o}C.

Table 3.2. Optimization of Reaction Conditions

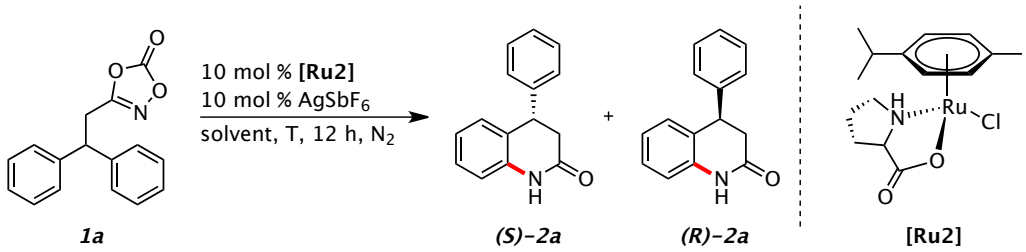

entry	solvent	T (^{o}C)	yield (%)[a]	*ee* (%)[b]
1	DCE	50	9	53
2	$CHCl_3$	50	>2	n.d.
3	$PhCF_3$	50	>2	n.d.
4	EtOAc	50	>2	n.d.
5	THF	50	>2	n.d.
6	MeCN	50	>2	n.d.
7	Acetone	50	21	63
8	DMA	50	>2	n.d.
9	Toluene	50	>2	n.d.
10	MeOH	50	13	52
11	EtOH	50	21	53
12	^{i}PrOH	50	>2	n.d.
13	$MeO(CH_2)_2OH$	50	28	53
14	HFIP	50	65	15
15	TFE	50	76	30
16	DCE/HFIP (4:1)	50	48	30
17	DCE/HFIP (9:1)	50	27	31
18	TFE	rt	38	29
19	TFE	40	48	32
20	TFE	60	78	29

[a]Reaction conditions: ***1a*** (0.1 mmol), **[Ru2]** (10 mol %), $AgSbF_6$ (10 mol %), solvent (1 mL) at T ^{o}C for 12 h under N_2; Isolated yield. [b]*ee* is determined by HPLC with chiral column; ***(S)-2i*** is major.

3.2.3 Regioselectivity Studies between C(sp^2)-H and C(sp^3)-H Amidations

Noted that the current, C(sp^2)-H amidation system is favored in polar protic solvent (i.e TFE), whereas the analogous intramolecular C(sp^3)-H amidation is favored in polar aprotic solvent (i.e. DCE).[19] Chang and co-workers also demonstrated the selectivities toward C(sp^2)-H versus C(sp^3)-H amidations could be influenced by ligand effects.[18] For instance, pyridine carboxylate ligands seem to favor C(sp^2)-H amidation while pyridine amide ligands would favor C(sp^3)-H amidation. Apparently, the Ru(II)-catalyzed amidations of C(sp^2)-H and C(sp^3)-H bonds would be influenced by solvent and ligand effects. In this work, several Ru(II) complexes were tested for this reaction, and the results are shown in Table 3.3. Employing the ***1a*** (0.1 mmol) with a catalytic amount of [Ru(*p*-cymene)(**L**)Cl] (10 mol %) and $AgSbF_6$ (10 mol %) in dry solvent [either DCE or TFE, (1 mL)] at 50 ^oC for 12 h afford either 4-phenyl-3,4-dihydroquinolin-2(1*H*)-one (***2a***) or no products. As shown in Table 3.3, all *R,R*-DPEN ligands (**L1** – **L4**) did not effec any ***2a*** formation in either DCE or TFE. With the 8-hydroxyquinoline (**L5**) as a ligand, ***2a*** was obtained in 78 % isolated yield in TFE solvent; the product was obtained in 56 % yield when DCE as solvent. Similar results were obtained with *t*-butyl quinolin-8-ylcarbamate (**L6**) as a ligand. Notably, while the amidation was unfavorable in DCE solvent when the ligand is L-proline (**L8**), an excellent product yield (76 %) was obtained in TFE as solvent. The (*E*)-2-((phenylimino)methyl)phenol (**L7**) did not effect any conversion of the 3-(2,2-diphenylethyl)-1,4,2-dioxazol-5-one (***1a***) in both DCE and TFE solvents.

Table 3.3. Ligands and Solvents Screening in Intramolecular C(sp^2)-H Amidation

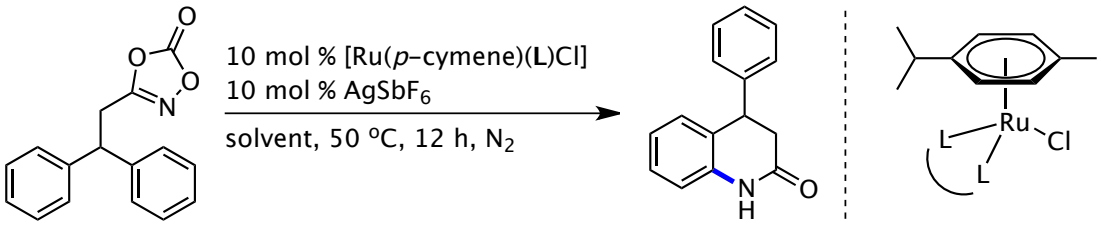

1a ***2a***

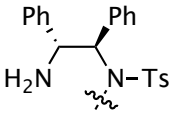	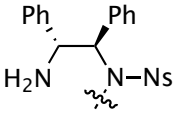	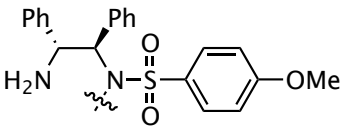
DCE: n.r. TFE: n.r. **L1**	DCE: n.r. TFE: n.r. **L2**	DCE: n.r. TFE: n.r. **L3**
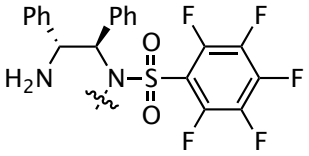	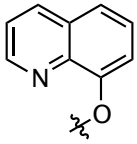	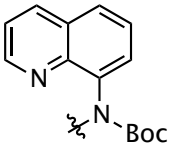
DCE: n.r. TFE: n.r. **L4**	DCE: 56 % TFE: 78 % **L5**	DCE: 45 % TFE: 63 % **L6**
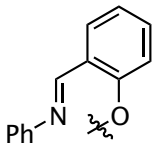	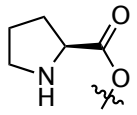	No Ligand
DCE: n.r. TFE: n.r. **L7**	DCE: 9 % TFE: 76 % **L8**	DCE: n.r. TFE: n.r.

Reaction conditions: ***1a*** (0.1 mmol), [Ru(*p*–cymene)(**L**)Cl] (10 mol %) and $AgSbF_6$ (10 mol %) in solvent (1 mL) at 50 °C for 12 h under N_2 protection; Isolated yield.

Those Ru complexes which are catalytically inactive for the C(sp^2)-H amidation are still active for the analogous C(sp^3)-H amidation reaction. Ru complexes with the *R,R*-DPEN systems gave an excellent yield in intramolecular C(sp^3)-H bond amidation using 3-(3-phenylpropyl)-1,4,2-dioxazol-5-one in DCE. For instance, no product formation was in TFE as solvent (Table 3.4, **L1** – **L4**). Similar findings were observed with 8-hydroxyquinoline (**L5**) and *t*-butyl quinolin-8-ylcarbamate (**L6**) as ligands.

Interestingly, Ru complexes bearing (*E*)-2-((phenylimino)methyl)phenol (**L7**) and L-proline (**L8**) showed better results in TFE rather than DCE. By combining two data sets, the selectivity between C(sp^2)-H amidation (dihydroxyquinolin-2-one formation) appears to be influenced by the ligands. Apparently, the polar protic solvent TFE favors the C(sp^2)-H amidation (dihyroxyquinolin-2-one formation), whereas the polar aprotic solvent DCE favors the C(sp^3)-H amidation (γ-lactam formation). For the case of ligand influence, the DPENs and pyridine amides favor C(sp^3)-H amidation (γ-lactam formation) while amino carboxylates and pyridine carboxylates favor C(sp^2)-H amidation (dihyroxyquinolin-2-one formation).

Table 3.4. Ligands and Solvents Screening in Intramolecular C(sp^3)-H Amidation

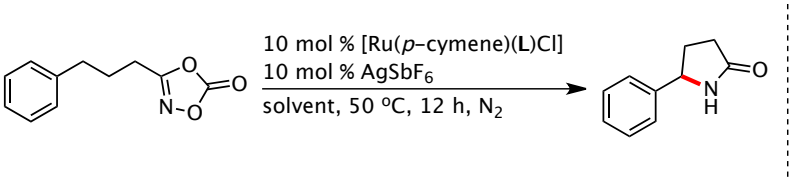

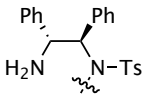	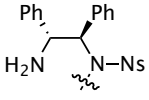	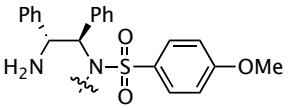
DCE: 92 % TFE: n.r. **L1**	DCE: 99 % TFE: n.r. **L2**	DCE: 76 % TFE: n.r. **L3**
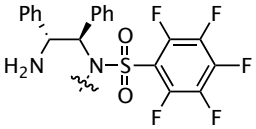	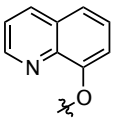	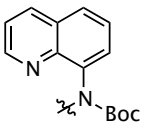
DCE: 99 % TFE: n.r. **L4**	DCE: 82 % TFE: < 2 % **L5**	DCE: 45 % TFE: < 2 % **L6**
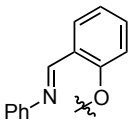	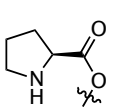	No Ligand
DCE: 18 % TFE: 37 % **L7**	DCE: 20 % TFE: 44 % **L8**	DCE: n.r. TFE: n.r.

Reaction conditions: dioxazolone (0.1 mmol), [Ru(*p*–cymene)(**L**)Cl] (10 mol %) and $AgSbF_6$ (10 mol %) in solvent (1 mL) at 50 °C for 12 h under N_2 protection; Isolated yield.

To further examine the regioselectivity of the C(sp^2)-H and C(sp^3)-H amidations, 3-(2,3-diphenylpropyl)-1,4,2-dioxazol-5-one (***1s***) was synthesized using the same synthetic route as 3-(2,2-diphenylethyl)-1,4,2-dioxazol-5-one (***1a***).[39] 3-(2,3-diphenylpropyl)-1,4,2-dioxazol-5-one (***1s***) is a good model substrate to investigate the regioselective amidations between C(sp^2)-H bond and C(sp^3)-H bond because ***1s*** contains benzylic C-H bond for Y-lactam formation and aromatic C-H bond for dihydroxyquinolin-2-one formation. Treatment of ***1s*** (0.1 mmol) with Ru(II) catalysts (**[Ru1] – [Ru5]**, 10 mol %) and $AgSbF_6$ (10 mol %) in dry solvent (either DCE or TFE, 1 mL) at 50 ^oC gave either 4-benzyl-3,4-dihydroquinolin-2(1*H*)-one (***2s***) or (5*R*)-4,5-diphenylpyrrolidin-2-one (***2s'***). After the purification by preparative thin-layer chromatography, the yields of 4-benzyl-3,4-dihydroquinolin-2(1*H*)-one (***2s***) and (5*R*)-4,5-diphenylpyrrolidin-2-one (***2s'***) were calculated by ^1H NMR separately. As shown in Table 3.5, Ru complexes bearing either *R,R*-DPEN (**[Ru4]**) or *t*-butyl quinolin-8-ylcarbamate (**[Ru3]**) failed to give any desired 4-benzyl-3,4-dihydroquinolin-2(1*H*)-one (***2s***) and (5*R*)-4,5-diphenylpyrrolidin-2-one (***2s'***) in either TFE or DCE solvent. 8-Hydroxyquinoline (**[Ru1]**) and L-proline (**[Ru2]**) gave product ***2s*** in 44 % and 78 % isolated yield respectively. While, **[Ru1]** and **[Ru2]** gave a trace amount of product ***2s'*** formation in TFE. The (*E*)-2-((phenylimino)methyl)phenol (**[Ru5]**) failed to give any amidation products in this reaction conditions. Interestingly, for the cases with DCE as solvent gave product ***2s*** was obtained in 13 % isolated yield when 8-hydroxyquinoline be the ligand. Complexes bearing other ligands did not give any C(sp^2)-H and C(sp^3)-H amidation products. With TFE as solvent, catalysts bearing 8-hydroxyquinoline (**[Ru1]**) and L-proline (**[Ru2]**) showed an outstanding regioselectivity in C(sp^2)-H amidation reaction. The ligands favorable in C(sp^3)-H

amidation reaction, *R,R*-DPEN (**[Ru4]**) and *t*-butyl quinolin-8-ylcarbamate (**[Ru3]**) did not give C(sp^3)-H amidation product in our reaction conditions presumably due to the intrinsic steric hinderance for the nitrenoid insertion.

Table 3.5. Regioselectivity between C(sp^2)-H and C(sp^3)-H Bonds Amidations

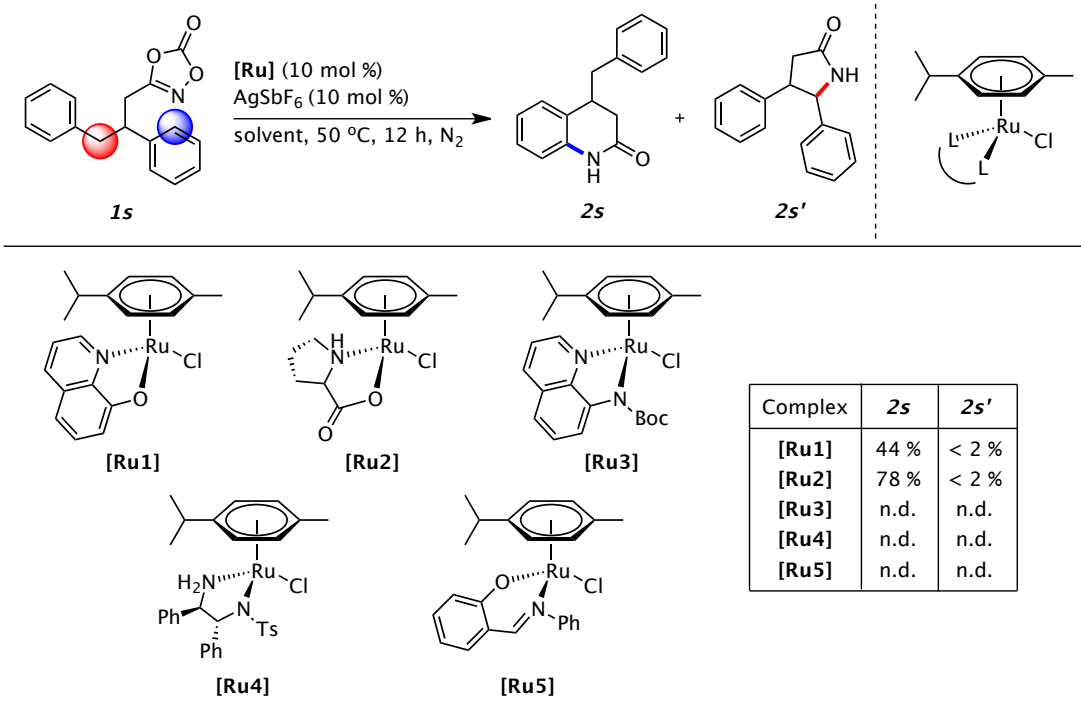

Complex	*2s*	*2s'*
[Ru1]	44 %	< 2 %
[Ru2]	78 %	< 2 %
[Ru3]	n.d.	n.d.
[Ru4]	n.d.	n.d.
[Ru5]	n.d.	n.d.

Reaction conditions: ***1s*** (0.1 mmol), **[Ru]** (10 mol %) and $AgSbF_6$ (10 mol %) in solvent (1 mL) at 50 °C for 12 h under N_2 protection; The ratio of ***2s*** to ***2s'*** was obtained by ^1H NMR; Isolated yield.

It was found that the pKa of pyridine amide ligands is inversely correlated to the C(sp^2)-H amidation (Table 3.6). The most basic ligand, *t*-butyl quinolin-8-ylcarbamate (pKa = 12.11), gave 63 % isolated yield of the desired product. When the pKa of pyridine amide ligands is lower than 12, (*R*)-*tert*-butyl 2-(quinolin-8-ylcarbamoyl)pyrrolidine-1-carboxylate (pKa = 11.78), 4-methyl-*N*-(quinolin-8-yl)benzenesulfonamide (pKa = 7.58) and 4-nitro-*N*-(quinolin-8-yl)benzenesulfonamide (pKa = 6.70), the isolated yield of the 4-phenyl-3,4-dihydroquinolin-2(1*H*)-one (***2a***) is dropped dramatically (13 – 20 %). The most acidic 1,1,1-trifluoro-*N*-(quinolin-8-yl)methanesulfonamide (pKa = -0.22) did not have any

amidation product formation. 8-Hydroxyquinoline (pKa = 9.90) gave a better result than *t*-butyl quinolin-8-ylcarbamate even though it is more acidic. L-Proline (pKa = 1.99) and D-α-phenylglycine (pKa = 1.94) are more acidic than 8-hydroxyquinoline but they gave a similar result in the formation of 4-phenyl-3,4-dihydroquinolin-2(1*H*)-one (***2a***). Apparently, there is no clear relationship be established between the pKa of the ligands and the catalytic activity.

Table 3.6. The Effect of the pKa of Ligands

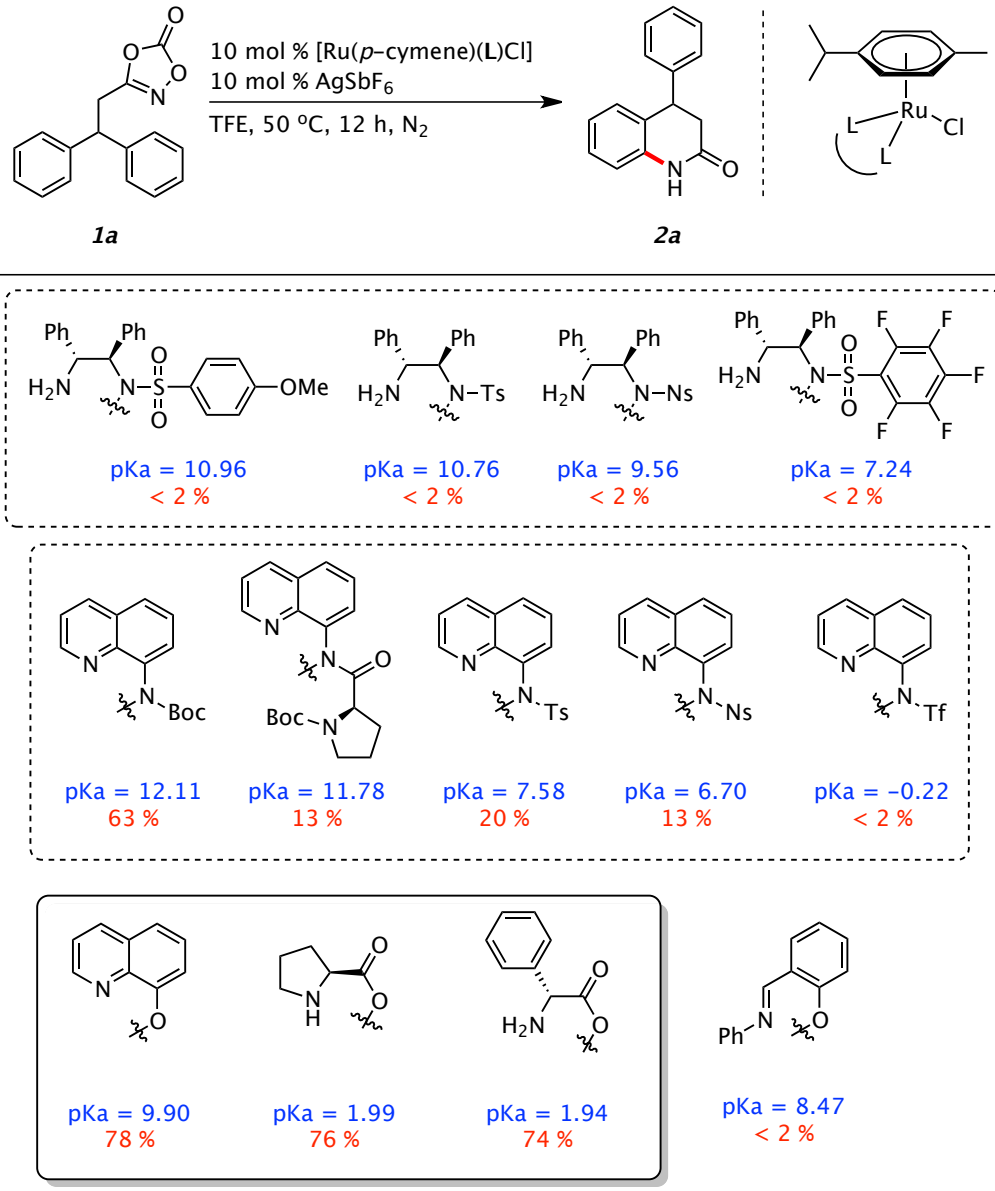

Reaction conditions: ***1a*** (0.1 mmol), [Ru(*p*-cymene)(**L**)Cl] (10 mol %) and $AgSbF_6$ (10 mol %) in TFE (1 mL) at 50 °C for 12 h under N_2 protection; Isolated yield.

3.2.4 Substrate Scope Studies for Ru(II)-Catalyzed C(sp^2)-H Amidation

In the substrate scope studies (Table 3.7), substrates bearing electron-donating groups (Me and OMe) and halogens (F, Cl and Br) gave the dihydroquinolin-2-one products in up to 90 % compared to 3-(2,2-diphenylethyl)-1,4,2-dioxazol-5-one (***2a*** – ***2f***). Substrates bearing electron-withdrawing substituent (CF_3) are poor substrate and less than 5 % yield ***2g*** being obtained. 3-(2-(4-methoxyphenyl)-2-phenylethyl)-1,4,2-dioxazol-5-one (***1h***) showed preference for the C-N bond being formed at methoxy-substituted arene (82 %; ***2h***). In addition, all *para*-substituted dioxazolones (***1a*** – ***1k***) may afford two possible products: the spirocyclization product and electrophilic aromatic substitution (S_EAr) product. If the reaction goes through the electrophilic aromatic substitution, the C-N bond would be formed at C3-position to the substituents. If reaction goes through the spirocyclization followed by skeletal rearrangement (C-C migration), the C-N bond should be formed at C4-position to the substituents. In this work, products having the C-N bond being formed at C4-position to substituents (i.e. spirocyclization product) were obtained with moderate to excellent yield (44 – 91 %; ***2a*** – ***2k***). Apparently, the electrophilic aromatic substitution products were not formed in this Ru-catalyzed condition.

For *ortho*-substituted dioxazolones, 3-(2-methylphenethyl)-1,4,2-dioxazol-5-one (***1l***), 3-(2-methoxyphenethyl)-1,4,2-dioxazol-5-one (***1m***) and 3-(2-bromophenethyl)-1,4,2-dioxazol-5-one (***1n***), the electrophilic aromatic substitution products were characterized by C-N bond being formed at C3-position to the substituents while those having C-N bond formation at C2-position to the substituents characterize the spirocyclization products. Again, it was found that ***2l*** and ***2n*** were exclusion products

obtained in ~60 % yields. No electrophilic aromatic substitution product was detected between two substrates. However, 3-(2-methoxyphenethyl)-1,4,2-dioxazol-5-one (***1m***) did not give the desired amidation product in the reaction condition. All results are comparable to Chang's findings on the Ir(III)-catalyzed C(sp^2)-H amidation.[38]

Table 3.7. Substrate Scope Studies for Dihydroxquinolin-2-ones Formation

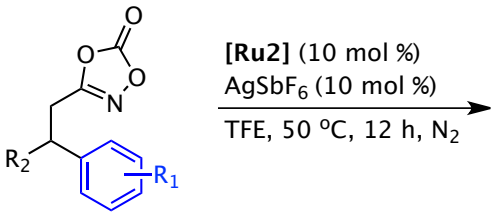

1a – 1n | *2a – 2n* | **[Ru2]**

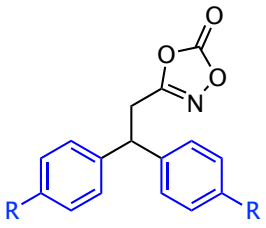 *1a – 1g*	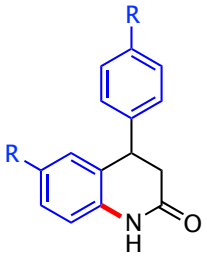 *major product* + 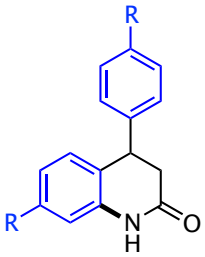 S_EAr product ***not detected***	R = H: 76 %, ***2a*** = Me: 84 %, ***2b*** = OMe: 86 %, ***2c*** = F: 87 %, ***2d*** = Cl: 91 %, ***2e*** = Br: 90 %, ***2f*** = CF_3: <5 %, ***2g***
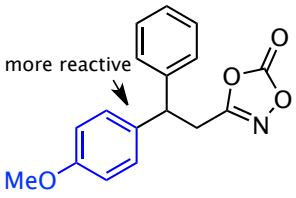 ***1h***	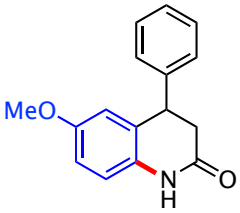 ***2h*** 82 % + 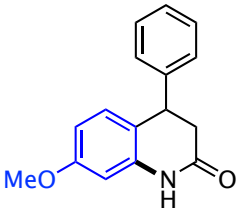 S_EAr product ***not detected***	
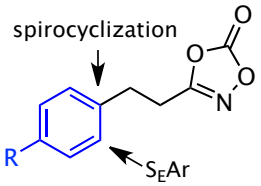 ***1i – 1k***	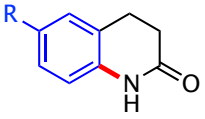 R = Me: 78 %, ***2i*** = OMe: 80 %, ***2j*** = Br: 44 %, ***2k*** + 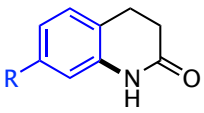 S_EAr product ***not detected***	
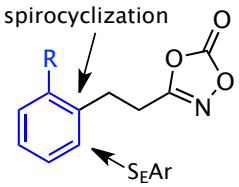 ***1l – 1n***	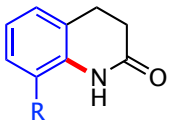 R = Me: 60 %, ***2l*** = OMe: < 2 %, ***2m*** = Br: 59 %, ***2n*** + 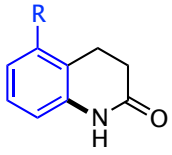 S_EAr product ***not detected***	

Reaction conditions: dioxazolones ***1*** (0.1 mmol), **[Ru2]** (10 mol %) and $AgSbF_6$ (10 mol %) in TFE (1 mL) at 50 °C for 12 h under N_2 protection; Isolated yield.

To further verify the operation of the spirocyclization pathway, the *para*-hydroxyl-substituted and *ortho*-substituted dioxazolones were used as substrates under the reaction condition (Table 3.8). It is because they would form the spiro-ɣ-lactam if the mechanism is going through spirocyclization. If the reaction is going through electrophilic aromatic substitution, the hydroxyl-substituted quinolin-2-ones were produced instead. As a result, 3-(4-hydroxyphenethyl)-1,4,2-dioxazol-5-one (***4a***) produced 1-azaspiro[4.5]deca-6,9-diene-2,8-dione (***5a***) in 95 % isolated yield. The phenol-based dioxazolone bearing the OMe group at *ortho*-position (***4b***) and *meta*-position (***4c***) underwent the dearomative spirocyclization reaction smoothly in excellent yield (***5b***; 88 % and ***5c***; 83 %). The dioxazolones bearing two electron-donating groups (***4d*** – ***4e***), the dearomative spirocyclization reaction was improved over 90 % (***5d*** – ***5e***). The results demonstrated that the reaction mechanism is going through spirocyclization but not electrophilic aromatic substitution. Adding the electron-donating substituents on the phenyl ring enhanced the spirocyclization. For 2-hydroxyl-substituted dioxazolones, the dearomative spirocyclization reaction depends strongly on the electronic properties of the substituents. For 3-(2-hydroxyphenethyl)-1,4,2-dioxazol-5-one (***4f***), it cannot be converted into (*S*)-1-azaspiro[4.5]deca-7,9-diene-2,6-dione (***6f***). Increasing the nucleophilicity of the arene with OMe group at C4 position (***4g***), the dearomative spirocyclization of 2-hydroxy-substituted dioxazolone is more favorable. The production of (*S*)-8-methoxy-1-azaspiro[4.5]deca-7,9-diene-2,6-dione (***6g***) was obtained in 56 %. Therefore, the electron-donating substituents gave the better performance in dearomative spirocyclization reaction.

Table 3.8. Scope of Dearomative Spirocyclization Reaction

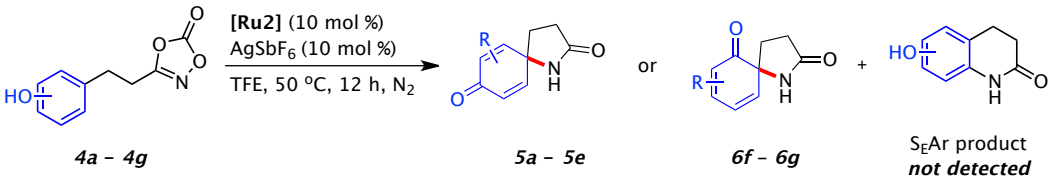

4a – 4g | *5a – 5e* | *6f – 6g*

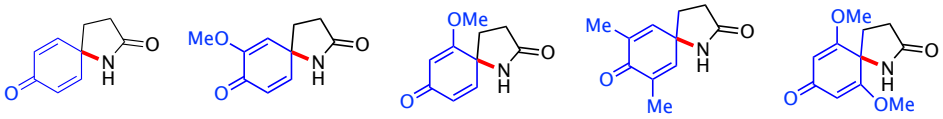

5a, 95 % | ***5b***, 88 % | ***5c***, 83 % | ***5d***, 91 % | ***5e***, 92 %

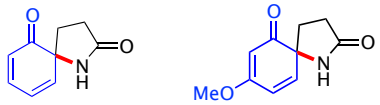

6f, n.r. | ***6g***, 56 %

Reaction conditions: dioxazolones ***4*** (0.1 mmol), **[Ru2]** (10 mol %) and $AgSbF_6$ (10 mol %) in TFE (1 mL) at 50 °C for 12 h under N_2 protection; Isolated yield.

Based on the dearomative spirocyclization reaction, the C-N bond formation in *ortho*-substituted and *para*-substituted dioxazolones should go through spirocyclization, followed by skeletal rearrangement (C-C migration) to afford the six-membered ring structure dihydroquinolin-2-ones. Yet, the *meta*-substituted dioxazolones were converted to the corresponding dihydroquinolin-2-ones probably without skeletal rearrangement. Table 3.9 shows that 3-(3-methylphenethyl)-1,4,2-dioxazol-5-one (***1o***), 3-(3-methoxyphenethyl)-1,4,2-dioxazol-5-one (***1p***) and 3-(3-bromophenethyl)-1,4,2-dioxazol-5-one (***1q***) formed C-N bond at C4-position to the substituents. In these entries, the rearrangement products were not obtained. For 3-(3,4-dimethoxyphenethyl)-1,4,2-dioxazol-5-one (***1r***) bearing two electron-donating substituents on the phenyl ring, product ***2r*** was formed in 83 % yield. Apparently more electron-rich arenes favor the amidation reaction.

Table 3.9. The Dihydroxquinolin-2-ones Formation of 3-Substituted Dioxazolones

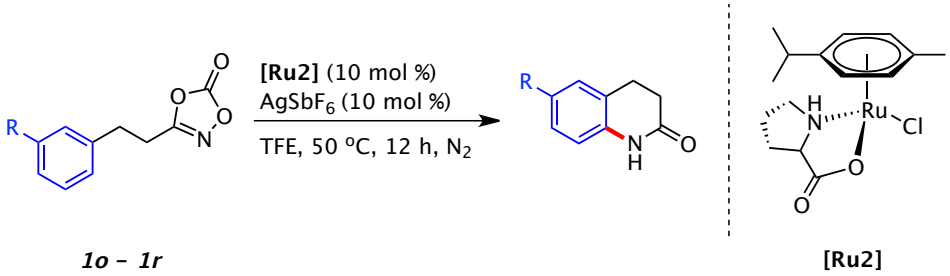

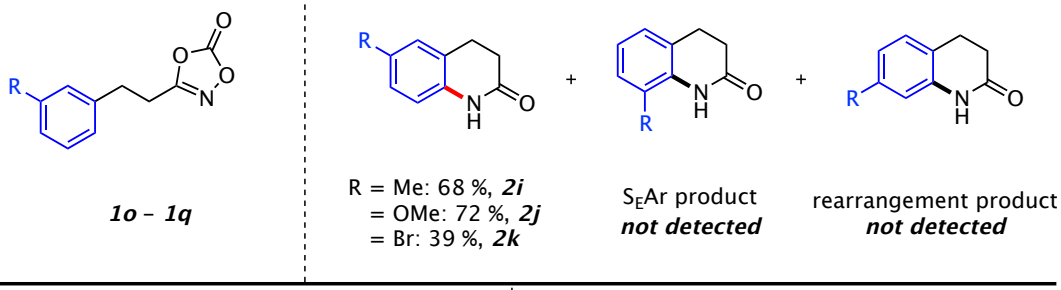

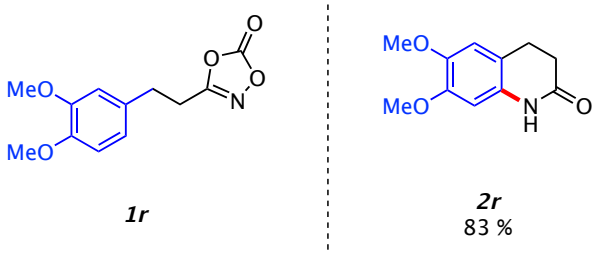

Reaction conditions: dioxazolones ***1*** (0.1 mmol), **[Ru2]** (10 mol %) and $AgSbF_6$ (10 mol %) in TFE (1 mL) at 50 °C for 12 h under N_2 protection; Isolated yield.

Three different types of C(sp^3)-H bonds (benzylic C-H, 2^0 C-H and 3^0 C-H) are active towards the Ir(III)-catalyzed[38] and Ru(II)-catalyzed[19] intramolecular amidations. In Table 3.10, the reaction showed a highly regioselective on C(sp^2)-H bond amidation rather than benzylic C(sp^3)-H bond, 2^0 C(sp^3)-H bond and 3^0 C(sp^3)-H bond amidation with an excellent yield in desired amidation products (78 – 83 %; ***2s*** – ***2u***). Interestingly, the electronic properties of the substituents did not have a significant effect on the amidation (***2v*** – ***2z***).

Table 3.10. Site-selective Substrate Scope Studies

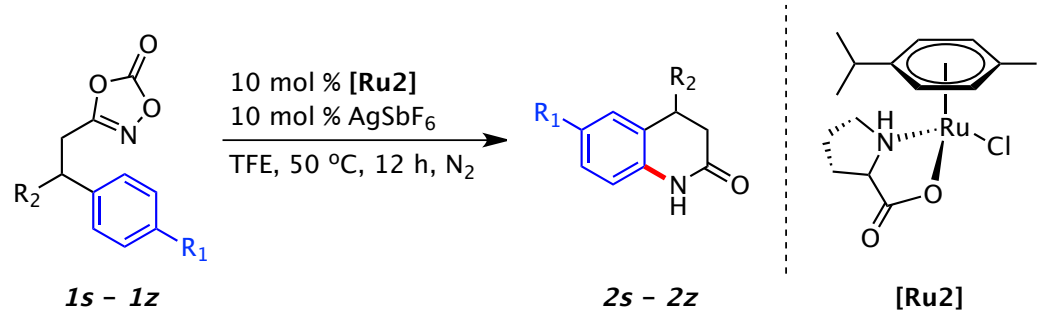

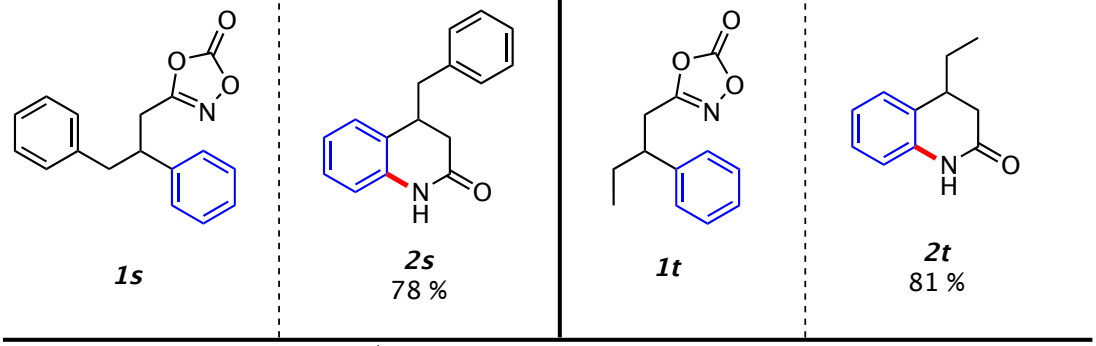

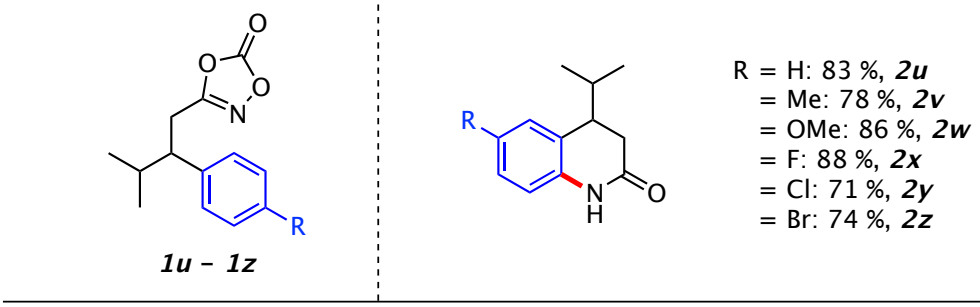

Reaction conditions: dioxazolones ***1*** (0.1 mmol), **[Ru2]** (10 mol %) and $AgSbF_6$ (10 mol %) in TFE (1 mL) at 50 °C for 12 h under N_2 protection; Isolated yield.

Based on the results, the regioselectivity of the C-N bond formation was controlled by the position of the substituents. For substituents at *ortho*- and *para*-positions, the C2 and C4 carbons to the substituents are the most nucleophilic respectively to attack the Ru-nitrenoid due to π-conjugation of lone pair electrons of the substituents (Figure 3.3). After the C-N bond formation, it underwent the C-C migration (or skeletal rearrangement) forming the desired hydroxquinolin-2-one products. For the substituents at *meta*-position, the C-N bond was formed at C4 carbon to the substituents. In this case, the six-membered ring structure was

produced so the C-C migration (or skeletal rearrangement) did not involved in the mechanism.

Figure 3.3. The Mechanism of Intramolecular Amidation

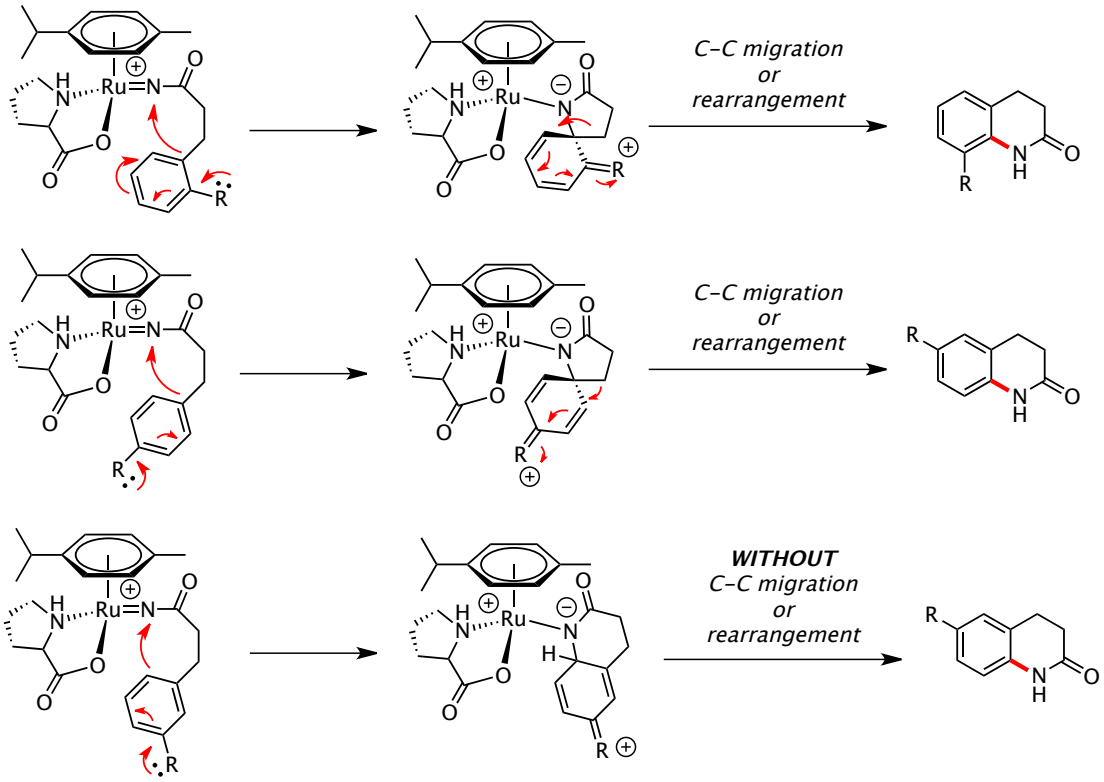

3.2.5 Hammett Correlation Study for the Amidation of *para*-Substituted 1,4,2-Dioxazol-5-ones

The reactions of *para*-substituted 3-phenethyl-1,4,2-dioxazol-5-ones (1-Y) were examined. In the study, the *para*-substituted 3-phenethyl-1,4,2-dioxazol-5-ones (0.1 mmol) were treated with **[Ru2]** (10 mol %) and $AgSbF_6$ (10 mol %) in TFE (1 mL) at 50 ^{o}C for 1 h. The reactions were quenched by filtration of a short pad of silica gel eluted with 50 mL of n-hexane/EtOAc (8:2) first to remove the unreacted *para*-substituted 3-phenethyl-1,4,2-dioxazol-5-ones and then eluted with EtOAc (50 mL) to extract the products from silica gel. After the removal of solvent under rotatory

evaporator, the crude mixtures were dissolved in $CDCl_3$ for ^1H NMR analysis. A parallel reaction using unsubstituted 3-phenethyl-1,4,2-dioxazol-5-one (1-H) as substrate was also performed in the same manner. The reactions were run in triplicate. The initial rates of the amidation were determined by measuring the product formation (integration of the triplet signal at 2.61 – 2.62 ppm) using ^1H NMR Spectroscopy with dibromomethane (0.1 mmol, 6.98 μL) as an internal standard. Plot the graph $\log(k_Y/k_H)$ against Hammett σ_{para} constants, a straight line (R^2 = 0.94) with ρ = -1.52 was obtained (Figure 3.4). The negative value of ρ suggests that the build-up of a partial positively charged during the nitrene insertion step. Based on the results, the electron-donating substituents (e.g. OMe and Me groups) accelerated the amidation reaction. The electron-withdrawing substituents (e.g. F and Cl groups) would decelerate the amidation reaction.

Figure 3.4. Hammett Correlation Study for Ru(II)-Catalyzed Intramolecular Amidation of *para*-Substituted 3-Phenethyl-1,4,2-dioxazol-5-ones

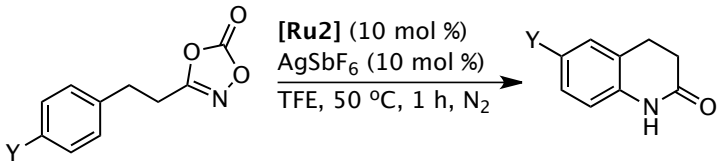

1–Y (0.1 mmol) **2–Y**

Y	k_Y/k_H	σ_{para}
OMe	1.48	–0.27
Me	1.32	–0.17
H	1.00	0
F	0.84	0.06
Cl	0.78	0.23

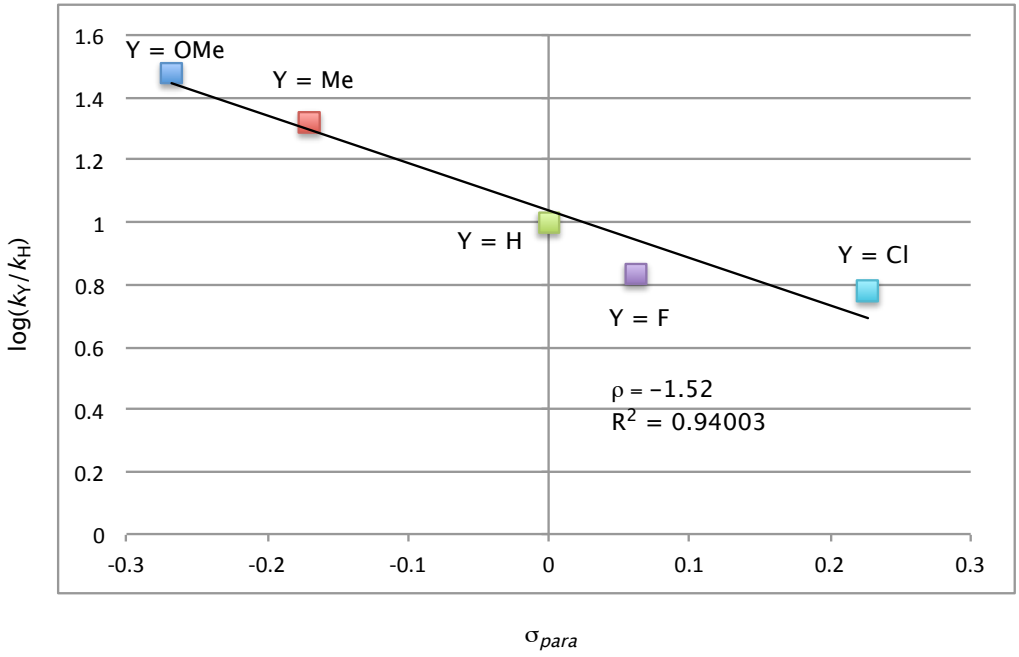

3.2.6 Ligand Screening for Enantioselective Amidation

At the outset of this investigation, we observed the formation of enantioenriched dihydroquinolin-2-one ***2a*** when subjecting ***1a*** to the Ru-catalyzed conditions using L-proline as ligand in DCE. Encouraged by this finding and the remarkable regiocontrolled C(sp^2)-H amidation, we turned our attention to develop enantioselective dihydroquinolin-2-one formation.

In this study, several chiral ligands were examined for their activities toward enantioselective C(sp^2)-H amidation. As shown in Table 3.11, different proline derivatives obtained from commercial resources (**L9** – **L11**) did not give any improvement in enantioselectivity. The *(S)*-piperidine-2-carboxylic acid (**L11**) and (*R*)-α-phenylglycine (**L12**) did not show the kinetic resolution in the enantio-determining step due to the 3D structure of two ligands did not fit into the hypothesized transition state model. Also, all amide ligands (**L13** – **L16**) reported from literatures[18,41] gave the similar enantiomeric excess (30 – 39 % *ee*) to L-proline (**L8**, 30 % *ee*), yet the product yield remains low for most of the amide ligands being tested.

Table 3.11. Ligand Scope Studies for Enantioselective Amidation

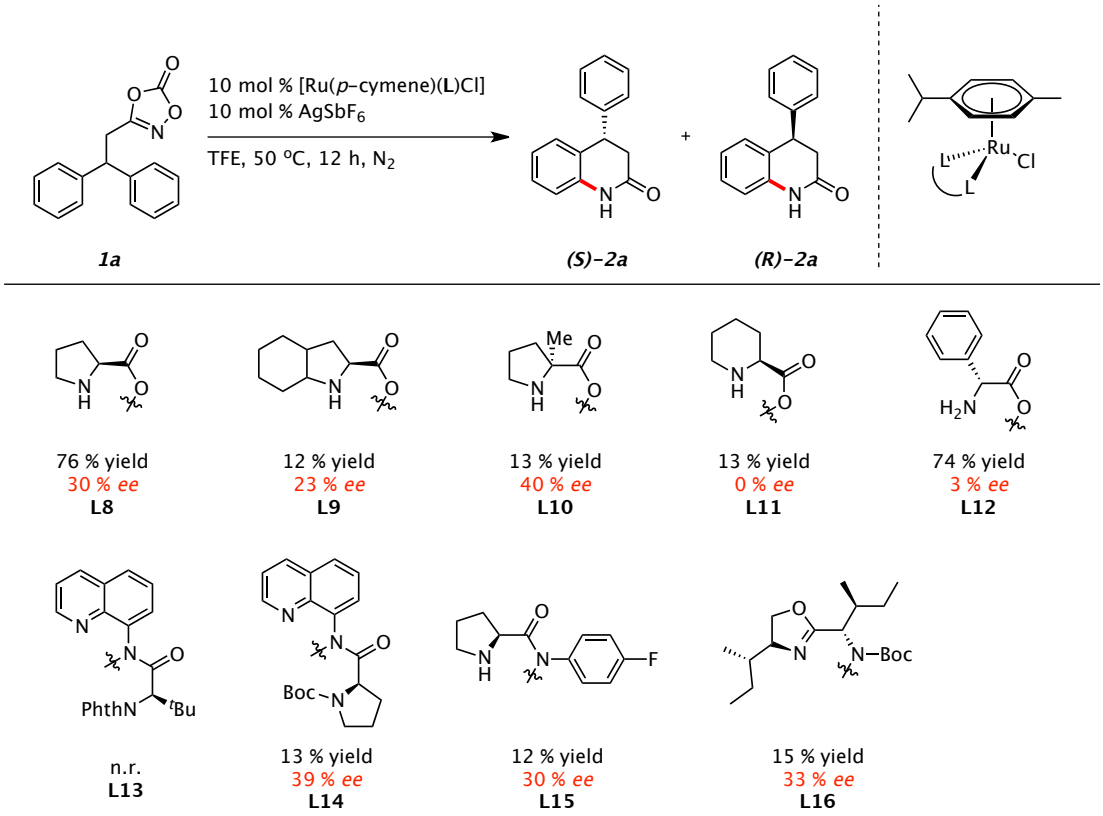

[a]Reaction conditions: ***1a*** (0.1 mmol), [Ru(*p*-cymene)(**L**)Cl] (10 mol %), $AgSbF_6$ (10 mol %), solvent (1 mL) at 50 °C for 12 h under N_2; Isolated yield. [b]*ee* is determined by HPLC with chiral column; ***(S)-2a*** is major.

3.2.7 Substrate Scope Studies for Enantioselective Amidation

With L-proline as chiral ligand, we pursued the substrate scope study for the enantioselective C(sp^2)-H amidation. As depicted in Table 3.12, all symmetric dioxazolones bearing a substituent on the phenyl ring gave comparable enantioselectivity. When one of the phenyl rings changes into isopropyl group, the enantioselectivity lowed presumably due to weaker steric differentiation of the isopropyl group versus phenyl ring. The high enantioselective amidation should be achieved by developing the chiral cymene ligand rather chiral amino-carboxylic acid ligands. It is because chiral Cp ligands achieved high enantioselectivity in Ru(II)-catalyzed intramolecular carbenoid insertion.[17] With the reference to the design of chiral Cp ligands, chiral cymene ligand is the alternative type of ligand for the enantioselective intramolecular cross-coupling reactions. In addition, cyemene ligands have rigid chemical structure and will not be detach from Ru(II) center easily so that the chirality of the Ru(II) complexes will not be lost in reaction conditions.

Table 3.12. Substrate Scope Studies for Enantioselective Amidation

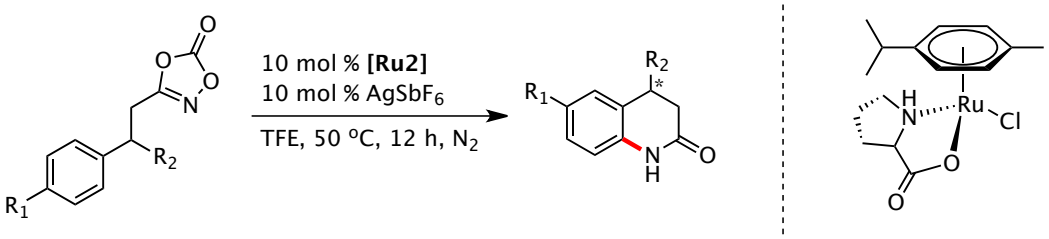

1 **2** **[Ru2]**

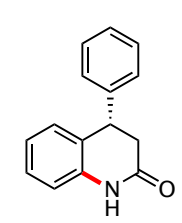

76 %
30 % *ee*

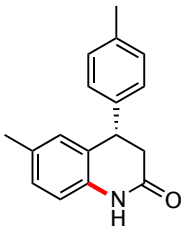

84 %
30 % *ee*

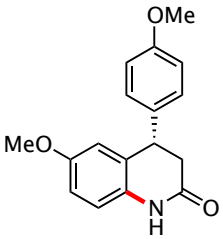

89 %
45 % *ee*

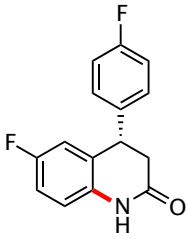

87 %
23 % *ee*

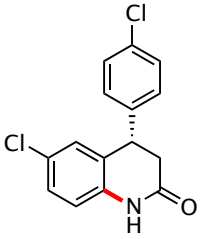

91 %
14 % *ee*

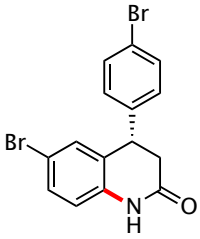

90 %
47 % *ee*

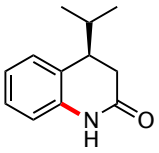

83 %
14 % *ee*

[a]Reaction conditions: ***1*** (0.1 mmol), **[Ru2]** (10 mol %), $AgSbF_6$ (10 mol %), TFE (1 mL) at 50 °C for 12 h under N_2; Isolated yield. [b]*ee* is determined by HPLC with chiral column.

The large-scale of Ru(II)-catalyzed intramolecular amidation was conducted (Scheme 3.5). By employing 2 mmol of substrate ***1a*** (0.534 g) with 10 mol % of **[Ru2]** and 10 mol % of $AgSbF_6$ in TFE at 50 °C for 12 h gave ***2a*** in 61 % isolated yield. The experiment showed that our catalytic protocol can be scaled-up to gram-scale quanity.

Scheme 3.5. Large-Scale of Dihydroquinolin-2-one Formation

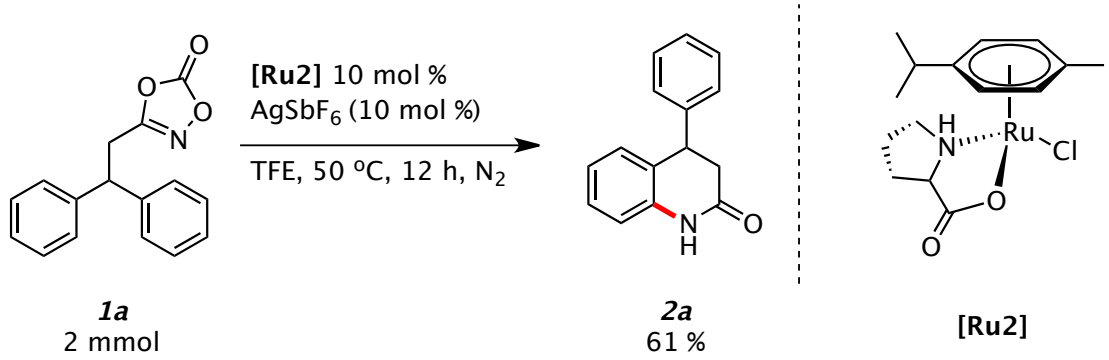

1a
2 mmol

2a
61 %

[Ru2]

6-Bromo-3,4-dihydroquinolin-2(1*H*)-one (***2k***) is a useful precursor for synthesis of pharmaceutical compounds (Scheme 6). By Buchwald-Hartwig Amination, 6-bromo-3,4-dihydroquinolin-2(1*H*)-one (***2k***) could be coupled with methyl 4-aminobenzoate to form methyl 4-((2-oxo-1,2,3,4-tetrahydroquinolin-6-yl)amino)benzoate, which is an anticancer agent.[51a] On the other hands, 6-(1'-isopropyl-6'-oxo-1',6'-dihydro-[3,3'-bipyridin]-5-yl)-1-methyl-3,4-dihydroquinolin-2(1*H*)-one (Alk-2 inhibitor) could be synthesized by Suzuki Coupling Reaction of 6-bromo-3,4-dihydroquinolin-2(1*H*)-one (***2k***).[51b] According to the literature reports, 6-bromo-3,4-dihydroquinolin-2(1*H*)-one (***2k***) was synthesized by two steps. First the 3-phenylpropanamide undergoes the oxidative amidation reaction mediated by *N*-iodosuccinimde (NIS) to form 3,4-dihydroquinolin-2(1*H*)-one in 33 % yield.[52] Then, 6-bromo-3,4-dihydroquinolin-2(1*H*)-one (***2k***) was synthesized using the traditional bromination reaction of 3,4-dihydroquinolin-2(1*H*)-one with *N*-bromosuccinimde (NBS).[53] The overall yield of ***2k*** formation in these approaches is 28 %. In our reaction condition, the product ***2k*** could be produced in single step catalysis in 44 % yield, which is a one-pot synthesis with two-fold higher in product yield. Alternatively, 6-methoxy-3,4-dihydroquinolin-2(1*H*)-one (***2j***) is another precursor of the methyl 4-((2-oxo-1,2,3,4-

tetrahydroquinolin-6-yl)amino)benzoate synthesis. In our reaction condition, 80 % yield of ***2j*** was obtained. Then, the OMe group could be converted into OTf group involving the demethylation of ***2j*** with $AlCl_3$ followed by treatment of CF_3SO_2Cl.[54] By Buchwald-Hartwig Amination, methyl 4-((2-oxo-1,2,3,4-tetrahydroquinolin-6-yl)amino)benzoate can be synthesized in this route.

Scheme 3.6. Late Stage Functionalization of Dihydroquinolin-2-ones

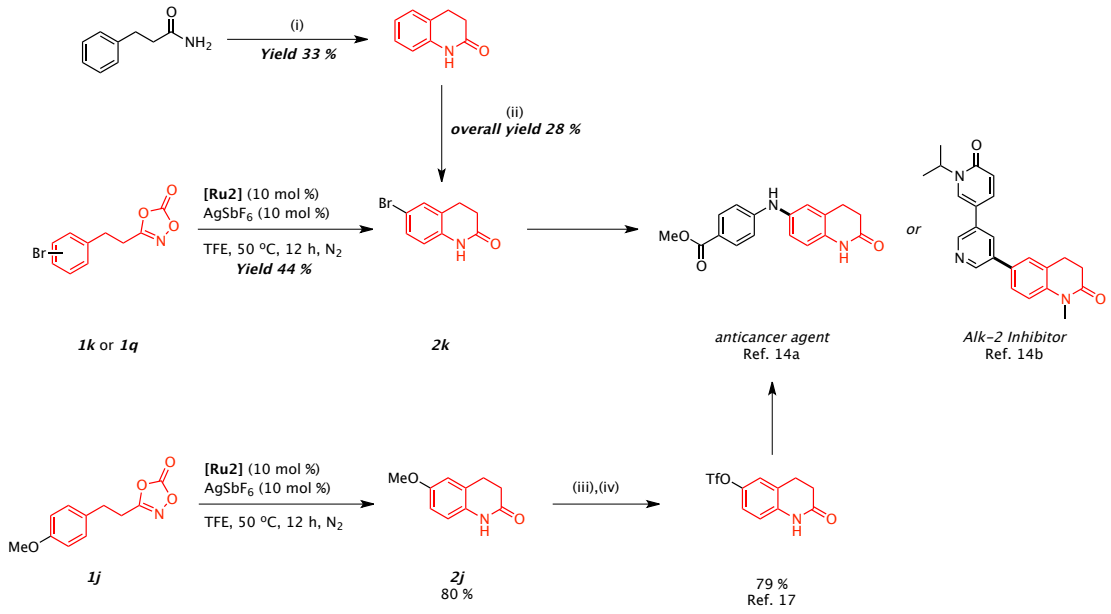

Reagent and conditions: (i) NIS, DCE, 110 °C, 10 h; (ii) NBS, DMF, 0 °C, 2 h; (iii) $AlCl_3$, DCE, reflux; (iv) CF_3SO_2Cl, Et_3N, DMF.

3.2.8 Mechanistic Studies in Enantioselectivity Amidation

Based on the results of optimization of reaction conditions, it was found that the *ee* of the reaction is good in polar aprotic solvents such as DCE and acetone (53 – 63 % *ee*). In polar protic solvents (e.g. HFIP and TFE), the *ee* of the reaction was dropped to 30 %. We would like to investigate the reason behind the phenomenia. In the ESI-MS study, employing **[Ru2]** (0.01 mmol) with $AgSbF_6$ (1.0 equiv) in TFE (0.5 mL) at 50 °C for 5 min was subjected to ESI-MS analysis. From the ESI-MS spectrum (Figure 3.5), signal m/z = 565 is assigned to [Ru(*p*-cymene)(L-proline)$(CF_3CH_2OH)_2$] in agreement

with formula mass value and the simulated isotopic pattern. It is likely that, the amino group of the L-proline was detached from the Ru center, which the chirality of the complex was lost. This reduces the kinetic resolution of the dihydroxyquinolin-2-ones formation during the enantio-determining step.

Figure 3.5. ESI-MS Analysis of **[Ru2]** in TFE

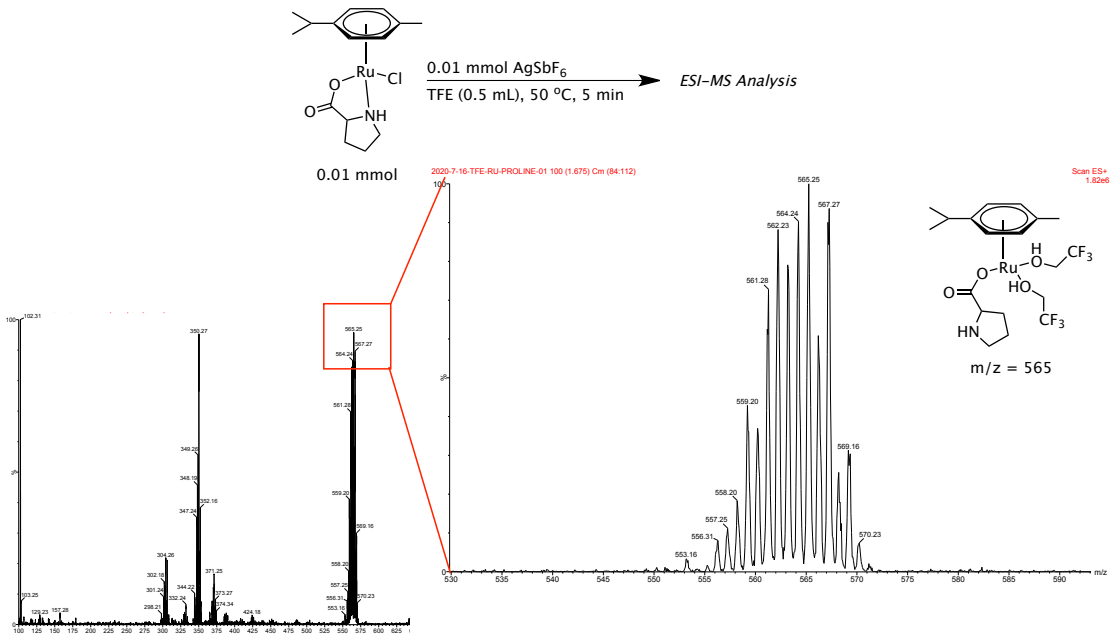

For the weak polar DCE solvents, the ^{1}H NMR analysis was employed to study **[Ru2]** in halogenated solvent since the complex cannot be detected in ESI-MS when DCE as solvent. For NMR study, the reaction was performed in CD_2Cl_2 instead of TFE. The shifting of the NH signal of catalyst was monitored by ^{1}H NMR spectroscopy at every 15 min time intervals (Figure 3.6). The NH signal was assigned by adding one to two drops of D_2O. The signal δ_H 4.05 ppm in the ^{1}H NMR spectrum disappeared after adding the D_2O into the reaction mixture so that this signal was then assigned as the NH signal of the catalyst. As revealed by the ^{1}H NMR study, the shifting of the NH signal was not changed after 30 min. If the amino group of L-proline was detached

from the Ru center, the NH signal should become more upfield. However, the expected upfileld shifting of the NH signal was not observed. Therefore, the amino group of the L-proline is likely to remain coordinated to the Ru center.

Figure 3.6. ^{1}H NMR Analysis of **[Ru2]** in CD_2Cl_2

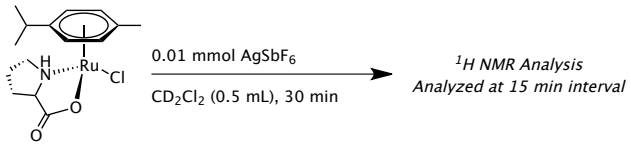

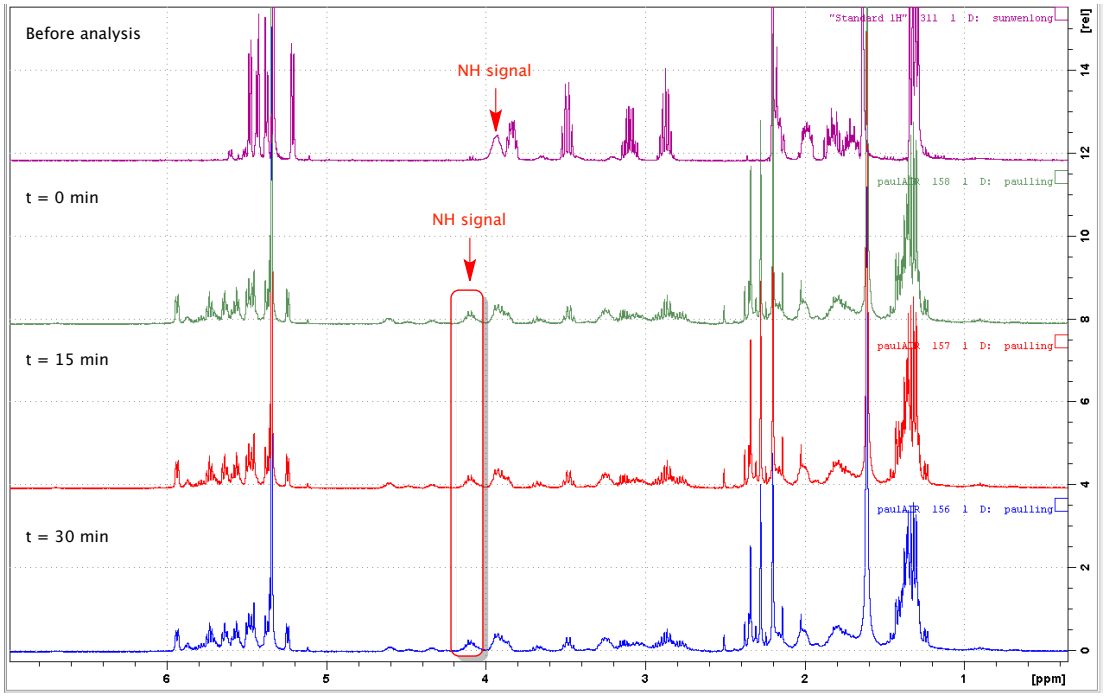

Reaction Condition: **[Ru2]** (0.01 mmol), $AgSbF_6$ (0.01 mmol) in CD_2Cl_2 at room temperature. The reaction was occurred in NMR tube and analyzed with ^{1}H NMR Spectroscopy (400 MHz) at 15 mins time intervals; (a) **[Ru2]**, (b) t = 0 min, (c) t = 15 mins, (d) t= 30 mins

3.3 Conclusion

The Ru-catalyzed cyclization of 1,4,2-dioxazol-5-ones to form dihydroquinolin-2-ones was achieved in remarkable regioselectivity; the reaction involves formal C(sp^2)-H bond functionalization. By studying the regioselectivity profile of *ortho*-, *meta*- and *para*-substituted dioxazolones, the reaction may proceed by spirocyclization

followed by C-C migration (skeletal rearranegement) depending on the substitution patterns of the arene ring. Hammett correlation study revealed a reaction constant ρ = -1.52, indicative of a partial positive charge build-up at transition state.

3.4 Experimental Section

Methods

Thin layer chromatography was performed on silica gel plates. Flash column chromatography was performed on a silica gel (Merck, 230-400 mesh) column. ^{1}H and ^{13}C NMR spectra were recorded on a Brüker DPX-400 MHz spectrometer. The chemical shift (δ) values are given in ppm and are referenced to residual solvent peaks; carbon multiplicities were determined by DEPT-135 experiments. Coupling constants (J) were reported in hertz (Hz).

High Performance Liquid Chromatography/UV-Visible Detector: High performance liquid chromatography analyses were performed on an Agilent 1100 series HPLC equipped with a Chiralcel® OD-H column (0.46 cm φ x 25 cm) with UV detection at 280 nm. The flow rate of HPLC was set at 0.7 mL/min and the pressure was kept at 30 bar. The eluent solvent system is n-hexane/isopropyl alcohol = 9:1. The total running time for the analysis is 50 min.

General Experimental Section

All *R,R*-DPEN ligands (**L1** – **L4**) were prepared and characterized according to literature report.[19] *tert*-Butyl quinolin-8-ylcarbamate (**L6**) was prepared by Boc protection with 8-aminoquinoloine. 8-Hydroxyquinoline (**L5**) and all chiral amino acids (**L8** – **L12**) were obtained from commercial sources (Sigma Aldrich and TCI as available) and used as received. (*R*)-2-(1,3-dioxoisoindolin-2-yl)-3,3-dimethyl-*N*-(quinolin-8-yl)butanamide (**L13**) and (*R*)-*tert*-butyl 2-(quinolin-8-ylcarbamoyl)pyrrolidine-1-carboxylate (**L14**) were prepared according to the procedures reported by Chang's group.[18] (*S*)-*N*-(4-fluorophenyl)pyrrolidine-2-

carboxamide (**L15**) was synthesized by amide bond formation with L-proline and 4-fluoroaniline. *tert*-butyl ((1*S*,2*S*)-1-((*R*)-4-((*S*)-*sec*-butyl)-4,5-dihydrooxazol-2-yl)-2-methylbutyl)carbamate (**L16**) was prepared according to the procedures reported by JQ Yu's group.[41] All the [Ru(*p*-cymene)(**L**)Cl] complexes were prepared and characterized according to literature reports.[40]

Experimental Procedures and Physical Characterizations

Preparation of 3,3-diphenylpropanoic acids[4]

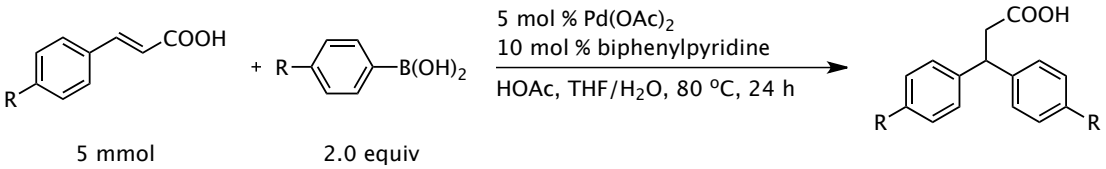

Cinnamic acids (5 mmol), arylboronic acids (2.0 equiv), $Pd(OAc)_2$ (5 mol %, 56.1 mg) and biphenylpyridine (10 mol %, 78.1 mg) were mixed in HOAc (5 mL), THF (10 mL) and H_2O (3 mL) and stirred at 80 ^oC for 24 h. THF and HOAc were removed under vacuum at 100 ^oC after the reaction. The reaction crude was cooled to 60 ^oC and then 5 mL of H_2O was added into reaction crude at 60 ^oC. After cool to room temperature, the aqueous layer was extracted by chloroform. The combined organic layer was dried with $MgSO_4$. After removal of solvent, the products were purified by flash chromatography (n-hexane/EtOAc = 7:3, R_f = 0.3) and the characterization spectra are consistent to literature report.[4]

Preparation of 3-(2,2-diphenylethyl)-1,4,2-dioxazol-5-ones

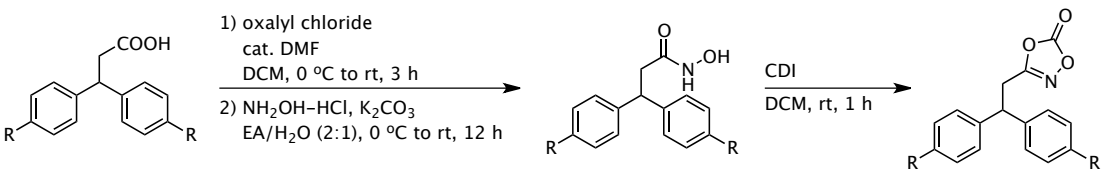

To a DCM (30 mL) solution of 3,3-diphenylpropanoic acids (2 mmol) was added oxalyl chloride (2.0 equiv, 0.34 mL) at 0 ^{o}C in a dropwise manner, and DMF (0.2 mL) was added to the mixture.. After stirring the mixture at room temperature for 3 h, the solvent and excess oxalyl chloride were removed by vacuum distillation. K_2CO_3 (2.0 equiv, 552.8 mg) was dissolved in EtOAc/H_2O = 2:1 (16 mL of EtOAc and 8 mL of H_2O) and then cooled to 0 ^{o}C. The hydroxylamine hydrogen chloride (1.2 equiv, 166.8 mg) was added into the K_2CO_3 solution. The corresponding 3,3-diphenylpropanoyl chlorides obtained were dissolved in DCM (5 mL) and was transferred to the reaction mixture. The reaction mixture was stirred at room temperature for overnight. To work-up, the distillated water (30 mL) was added into reaction mixture and the organic layer was separated. The aqueous phase was extracted with EtOAc (3 x 50 mL) and the combined organic extracts were dried with $MgSO_4$. The solvent was evaporated under rotatory evaporation to obtain the corresponding *N*-hydroxy-3,3-diphenylpropanamides without further purification.

The *N*-hydroxy-3,3-diphenylpropanamides (2 mmol) and CDI (1.1 equiv, 356.8 mg) were dissolved in DCM (20 mL) and stirred at room temperature for 30 min. Then, 1M HCl (3 mL) was added into reaction mixture and stirred at room temperature for another 1 h. After that, the organic layer was separated and the aqueous phase was extracted with DCM (3 x 20 mL). The combined organic extracts were dried by $MgSO_4$ and concentrated under rotatory evaporation. The crude mixture was purified by flash chromatography (n-hexane/EtOAc = 9:1) to obtain 3-(2,2-diphenylethyl)-1,4,2-dioxazol-5-ones (***1a*** – ***1h***).

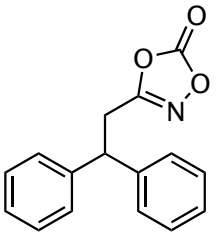

3-(2,2-diphenylethyl)-1,4,2-dioxazol-5-one (***1a***)

Yield: 90 %, colorless liquid

R_f = 0.4 (n-hexane/EtOAc = 9:1)

^{1}H NMR (400 MHz, CD_2Cl_2): δ 7.37-7.34 (m, 4H), 7.30-7.25 (m, 6H), 4.51 (t, *J* = 8.2 Hz, 1H), 3.42 (d, *J* = 8.2 Hz, 2H).

^{13}C NMR (100 MHz, CD_2Cl_2): δ 165.3, 153.9, 141.6, 128.9, 127.4, 127.3, 46.7, 31.0.

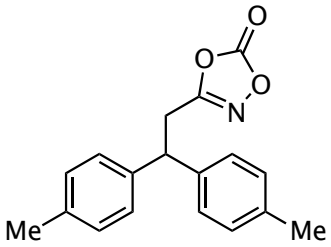

3-(2,2-di-*p*-tolylethyl)-1,4,2-dioxazol-5-one (***1b***)

Yield: 80 %, white solid

R_f = 0.4 (n-hexane/EtOAc = 9:1)

^{1}H NMR (400 MHz, $CDCl_3$): δ 7.13 (s, 8H), 4.41 (t, *J* = 8.4 Hz, 1H), 3.33 (d, *J* = 8.4 Hz, 2H), 2.32 (s, 6H).

^{13}C NMR (100 MHz, $CDCl_3$): δ 165.3, 154.0, 138.6, 137.1, 129.8, 127.4, 46.1, 31.4, 21.1.

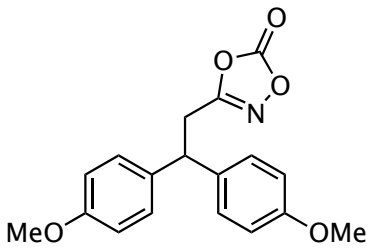

3-(2,2-bis(4-methoxyphenyl)ethyl)-1,4,2-dioxazol-5-one (***1c***)

Yield: 88 %, white solid

R_f = 0.4 (n-hexane/EtOAc = 9:1)

^{1}H NMR (400 MHz, $CDCl_3$): δ 7.16 (d, *J* = 8.8 Hz, 4H), 6.87 (d, *J* = 8.8 Hz, 4H), 4.40 (t, *J* = 8.4 Hz, 1H), 3.78 (s, 6H), 3.29 (d, *J* = 8.0 Hz, 2H).

^{13}C NMR (100 MHz, $CDCl_3$): δ 165.4, 158.8, 154.1, 133.9, 128.5, 114.5, 55.4, 45.3, 31.6.

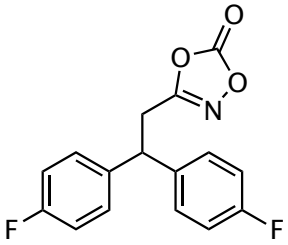

3-(2,2-bis(4-fluorophenyl)ethyl)-1,4,2-dioxazol-5-one (***1d***)

Yield: 60 %, white solid

R_f = 0.4 (n-hexane/EtOAc = 9:1)

^{1}H NMR (400 MHz, $CDCl_3$): δ 7.23-7.19 (m, 4H), 7.06-7.01 (m, 4H), 4.48 (t, *J* = 8.4 Hz, 1H), 3.34 (d, *J* = 8.0 Hz, 2H).

^{13}C NMR (100 MHz, $CDCl_3$): δ 164.9, 163.3, 160.9, 153.9, 137.0 (splitting), 129.1 (splitting), 116.2 (splitting), 45.3, 31.5.

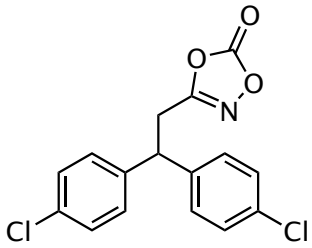

3-(2,2-bis(4-chlorophenyl)ethyl)-1,4,2-dioxazol-5-one (***1e***)

Yield: 53 %, pale yellow solid

R_f = 0.4 (n-hexane/EtOAc = 9:1)

^{1}H NMR (400 MHz, $CDCl_3$): δ 7.32 (d, *J* = 8.0 Hz, 4H), 7.16 (d, *J* = 8.0 Hz, 4H), 4.45 (t, *J* = 8.4 Hz, 1H), 3.33 (d, *J* = 8.0 Hz, 2H).

^{13}C NMR (100 MHz, $CDCl_3$): δ 164.7, 153.7, 139.4, 133.7, 129.5, 128.9, 45.5, 31.1.

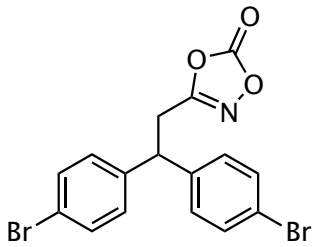

3-(2,2-bis(4-bromophenyl)ethyl)-1,4,2-dioxazol-5-one (***1f***)

Yield: 56 %, yellow solid

R_f = 0.4 (n-hexane/EtOAc = 9:1)

^{1}H NMR (400 MHz, $CDCl_3$): δ 7.47 (d, *J* = 8.4 Hz, 4H), 7.09 (d, *J* = 8.4 Hz, 4H), 4.41 (t, *J* = 8.4 Hz, 1H), 3.32 (d, *J* = 8.4 Hz, 2H).

^{13}C NMR (100 MHz, $CDCl_3$): δ 164.6, 153.7, 139.8, 132.4, 129.2, 121.8, 45.7, 31.0.

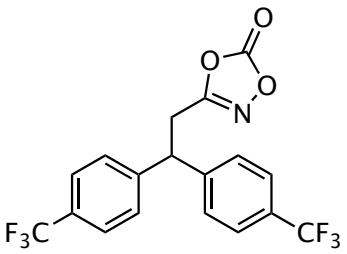

3-(2,2-bis(4-(trifluoromethyl)phenyl)ethyl)-1,4,2-dioxazol-5-one (***1g***)

Yield: 25 %, white solid

R_f = 0.4 (n-hexane/EtOAc = 9:1)

^{1}H NMR (400 MHz, $CDCl_3$): δ 7.63 (d, *J* = 8.4 Hz, 4H), 7.38 (d, *J* = 8.0 Hz, 4H), 4.63 (t, *J* = 8.4 Hz, 1H), 3.43 (d, *J* = 8.0 Hz, 2H).

^{13}C NMR (100 MHz, $CDCl_3$): δ 164.3, 153.5, 144.3, 130.5, 127.9, 126.4, 126.3, 46.2, 30.8.

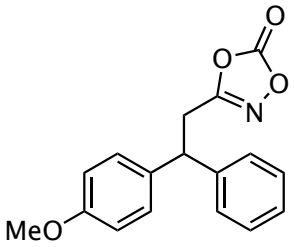

3-(2-(4-methoxyphenyl)-2-phenylethyl)-1,4,2-dioxazol-5-one (***1h***)

Yield: 60 %, white solid

R_f = 0.4 (n-hexane/EtOAc = 9:1)

^{1}H NMR (400 MHz, $CDCl_3$): δ 7.35-7.31 (m, 2H), 7.26-7.22 (m, 3H), 7.17-7.15 (m, 2H), 6.87-6.85 (m, 2H), 4.46-4.41 (t, *J* = 8.4 Hz, 1H), 3.78 (s, 3H), 3.34-3.32 (d, *J* = 8.4 Hz, 2H).

^{13}C NMR (100 MHz, $CDCl_3$): δ 165.1, 158.8, 153.9, 141.6, 133.2, 128.9, 128.5, 127.3, 114.4, 55.3, 45.9, 31.4.

Preparation of 3-phenethyl-1,4,2-dioxazol-5-ones

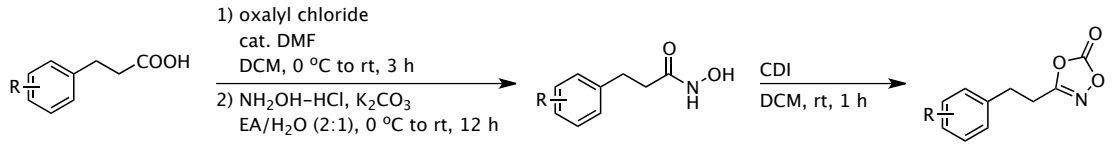

To a DCM (30 mL) solution of 3-phenylpropanoic acids (2 mmol) was added oxalyl chloride (2.0 equiv, 0.34 mL) at 0 ^{o}C in a dropwise manner, and DMF (0.2 mL) was added to the mixture.. After stirring the mixture at room temperature for 3 h, the solvent and excess oxalyl chloride were removed by vacuum distillation. K_2CO_3 (2.0 equiv, 552.8 mg) was dissolved in EtOAc/H_2O = 2:1 (16 mL of EtOAc and 8 mL of H_2O) and then cooled to 0 ^{o}C. The hydroxylamine hydrogen chloride (1.2 equiv, 166.8 mg) was added into the K_2CO_3 solution. The corresponding 3-phenylpropanoyl chlorides obtained were dissolved in DCM (5 mL) and was transferred to the reaction mixture. The reaction mixture was stirred at room temperature for overnight. To work-up, the distillated water (30 mL) was added into reaction mixture and the organic layer was separated. The aqueous phase was extracted with EtOAc (3 x 50 mL) and the combined organic extracts were dried with $MgSO_4$. The solvent was evaporated under rotatory evaporation to obtain the corresponding *N*-hydroxy-3-phenylpropanamides without further purification.

The *N*-hydroxy-3-phenylpropanamides (2 mmol) and CDI (1.1 equiv, 356.8 mg) were dissolved in DCM (20 mL) and stirred at room temperature for 30 min. Then, 1M HCl (3 mL) was added into reaction mixture and stirred at room temperature for another 1 h. After that, the organic layer was separated and the aqueous phase was extracted with DCM (3 x 20 mL). The combined organic extracts were dried by $MgSO_4$ and concentrated under rotatory evaporation. The crude mixture was

purified by flash chromatography to obtain 3-phenethyl-1,4,2-dioxazol-5-ones (***1i*** – ***1r***).

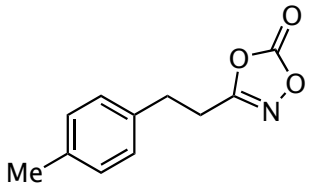

3-(4-methylphenethyl)-1,4,2-dioxazol-5-one (***1i***)

Yield: 80 %, white solid

R_f = 0.5 (n-hexane/EtOAc = 9:1)

^{1}H NMR (400 MHz, $CDCl_3$): δ 7.15-7.08 (m, 4H), 3.02-2.90 (m, 4H), 2.34 (s, 3H).

^{13}C NMR (100 MHz, $CDCl_3$): δ 165.9, 154.1, 136.8, 134.9, 129.6, 128.1, 30.1, 26.8, 21.0.

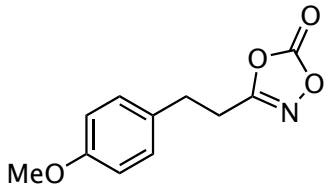

3-(4-methoxyphenethyl)-1,4,2-dioxazol-5-one (***1j***)

Yield: 83 %, white solid

R_f = 0.5 (n-hexane/EtOAc = 9:1)

^{1}H NMR (400 MHz, $CDCl_3$): δ 7.13-7.11 (d, *J* = 8.4 Hz, 2H), 6.87-6.85 (d, *J* = 8.4 Hz, 2H), 3.80 (s, 3H), 3.00-2.96 (m, 2H), 2.92-2.88 (m, 2H).

^{13}C NMR (100 MHz, $CDCl_3$): δ 165.9, 158.7, 154.0, 130.0, 129.2, 114.3, 55.3, 29.7, 27.0.

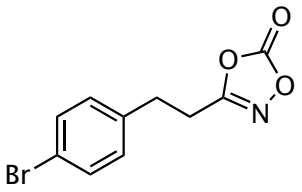

3-(4-bromophenethyl)-1,4,2-dioxazol-5-one (***1k***)

Yield: 76 %, white solid

R_f = 0.5 (n-hexane/EtOAc = 9:1)

^{1}H NMR (400 MHz, $CDCl_3$): δ 7.47-7.45 (d, *J* = 8.4 Hz, 2H), 7.10-7.08 (d, *J* = 8.4 Hz, 2H), 3.02-2.98 (m, 2H), 2.94-2.90 (m, 2H).

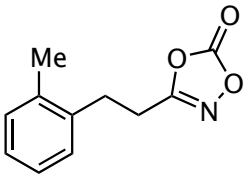

3-(2-methylphenethyl)-1,4,2-dioxazol-5-one (***1l***)

Yield: 90 %, white solid

R_f = 0.5 (n-hexane/EtOAc = 9:1)

^{1}H NMR (400 MHz, $CDCl_3$): δ 7.18-7.16 (m, 3H), 7.14-7.12 (m, 1H), 3.05-3.01 (m, 2H), 2.91-2.87 (m, 2H), 2.34 (s, 3H).

^{13}C NMR (100 MHz, $CDCl_3$): δ 166.0, 154.0, 136.2, 135.8, 130.8, 128.5, 127.3, 126.5, 28.0, 25.4, 19.1.

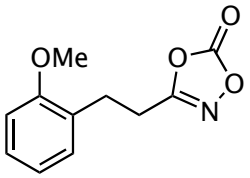

3-(2-methoxyphenethyl)-1,4,2-dioxazol-5-one (***1m***)

Yield: 85 %, white solid

R_f = 0.5 (n-hexane/EtOAc = 9:1)

^{1}H NMR (400 MHz, $CDCl_3$): δ 7.28-7.24 (m, 1H), 7.14-7.12 (m, 1H), 6.93-6.87 (m, 2H), 3.83 (s, 3H), 3.04-3.01 (m, 2H), 2.93-2.89 (m, 2H).

^{13}C NMR (100 MHz, $CDCl_3$): δ 166.4, 157.4, 154.3, 130.1, 128.6, 126.4, 120.8, 110.4, 55.2, 26.3, 25.1.

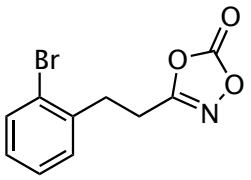

3-(2-bromophenethyl)-1,4,2-dioxazol-5-one (***1n***)

Yield: 79 %, white solid

R_f = 0.5 (n-hexane/EtOAc = 9:1)

^{1}H NMR (400 MHz, $CDCl_3$): δ 7.59-7.58 (m, 1H), 7.57-7.13 (m, 3H), 3.18-3.15 (m, 2H), 3.00-2,96 (m, 2H).

^{13}C NMR (100 MHz, $CDCl_3$): δ 165.6, 154.0, 137.4, 133.3, 130.5, 129.1, 128.0, 124.2, 31.2, 25.1.

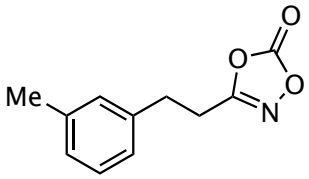

3-(3-methylphenethyl)-1,4,2-dioxazol-5-one (***1o***)

Yield: 92 %, white solid

R_f = 0.5 (n-hexane/EtOAc = 9:1)

^{1}H NMR (400 MHz, $CDCl_3$): δ 7.23-7.20 (m, 1H), 7.08-7.06 (d, *J* = 7.6 Hz, 1H), 7.01-6.98 (d, *J* = 11.2 Hz, 2H), 3.02-2.97 (m, 2H), 2.94-2.90 (m, 2H), 2.34 (s, 3H).

^{13}C NMR (100 MHz, $CDCl_3$): δ 165.9, 154.1, 138.6, 138.0, 129.0, 128.8, 127.9, 125.2, 55.2, 26.3, 25.1.

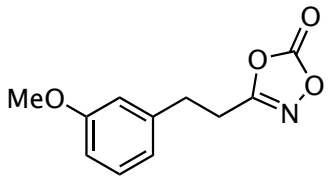

3-(3-methoxyphenethyl)-1,4,2-dioxazol-5-one (***1p***)

Yield: 78 %, white solid

R_f = 0.5 (n-hexane/EtOAc = 9:1)

^{1}H NMR (400 MHz, CD_2Cl_2): δ 7.28-7.24 (t, *J* = 8.0 Hz, 1H), 6.83-6.78 (m, 3H), 3.80 (s, 3H), 3.05-3.01 (m, 2H), 2.98-2.94 (m, 2H).

^{13}C NMR (100 MHz, CD_2Cl_2): δ 166.2, 160.0, 154.1, 139.9, 129.8, 120.4, 114.0, 112.2, 55.1, 30.3, 26.5.

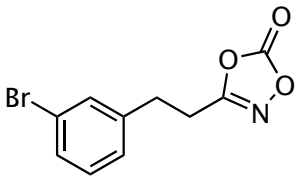

3-(3-bromophenethyl)-1,4,2-dioxazol-5-one (***1q***)

Yield: 71 %, white solid

R_f = 0.5 (n-hexane/EtOAc = 9:1)

^{1}H NMR (400 MHz, CD_2Cl_2): δ 7.44-7.42 (m, 2H), 7.26-7.18 (m, 2H), 3.06-3.02 (m, 2H), 2.98-2.94 (m, 2H).

^{13}C NMR (100 MHz, CD_2Cl_2): δ 165.8, 154.0, 140.7, 131.3, 130.4, 130.1, 127.0, 122.6, 29.8, 26.3.

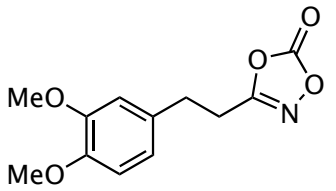

3-(3,4-dimethoxyphenethyl)-1,4,2-dioxazol-5-one (***1r***)

Yield: 84 %, white solid

R_f = 0.5 (n-hexane/EtOAc = 9:1)

^{1}H NMR (400 MHz, $CDCl_3$): δ 6.83-6.75 (m, 1H), 6.74-6.70 (m, 2H), 3.86 (s, 6H), 3.00-2.90 (m, 4H).

^{13}C NMR (100 MHz, $CDCl_3$): δ 165.9, 154.0, 149.2, 148.2, 130.5, 120.2, 111.5, 111.4, 56.0, 55.9, 30.2, 26.9.

Preparation of substituted 3-(4-hydroxyphenethyl)-1,4,2-dioxazol-5-ones

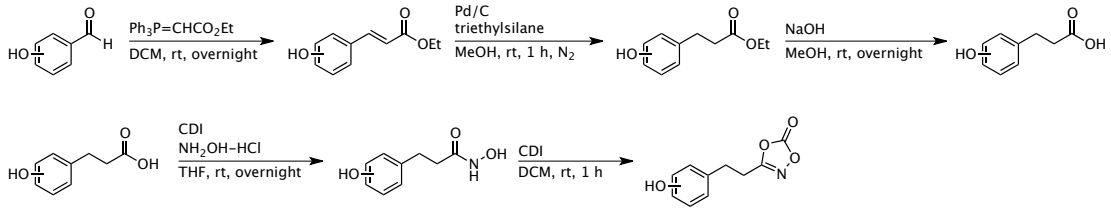

To a solution of aldehyde (10 mmol) in 50 mL DCM was added ethyl (triphenylphosphoranylidene) acetate (1.5 equiv, 5.015 g) at 0 ^{o}C in several portions. The reaction mixture was stirred at room temperature overnight. After the reaction, the solvent was evaporated under rotatory evaporator. The residue was purified by flash chromatography to obtain the desired ethyl cinnamate products.

To a suspension of ethyl cinnamates (1.2 mmol) and 10 % Pd/C (100 mg) in 5 mL MeOH was added triethylsilane (11.7 mmol, 1.8 mL) dropwise under N_2. After the addition, the reaction mixture was stirred at room temperature for 1 h. The reaction crude mixture was filtered through celite and concentrated under rotatory evaporator. The desired ethyl ester products were purified by short silica gel column chromatography, eluting with EtOAc.

The ethyl esters (2 mmol) and NaOH (5 mmol, 0.2 g) were dissolved in 20 mL MeOH and then stirred at room temperature overnight. After the reaction, the solvent was

evaporated under rotatory evaporator. Water was added into residue and then 1M HCl was added into mixture until pH = 1. The aqueous layer was extracted with EtOAc (3 x 50 mL) and the combined organic extracts were dried with $MgSO_4$. The solvent was evaporated under rotatory evaporation to give the corresponding 3-(hydroxyphenyl)propanoic acids, which can be used for next step without further purification.

To a solution of corresponding 3-(hydroxyphenyl)propanoic acids (2 mmol) in 15 mL dry THF was added CDI (1.5 equiv, 486.45 mg). The reaction mixture was stirred at room temperature for 1 h. After 1 h, hydroxylamine hydrochloride (4 mmol) was added into reaction mixture. The resulting mixture was stirred at room temperature overnight. The reaction was quenched by 5 % aq $KHSO_4$ (20 mL). The aqueous layer was extracted with EtOAc (3 x 50 mL). The combined organic extracts was washed with brine (20 mL) and dried with $MgSO_4$. The organic extract was filtered and concentrated under rotatory evaporator to obtain the corresponding *N*-hydroxy-3-phenylpropanamides without further purification.

The *N*-hydroxy-3-phenylpropanamides (2 mmol) and CDI (1.1 equiv, 356.8 mg) were dissolved in DCM (20 mL) and stirred at room temperature for 30 min. Then, 1M HCl (3 mL) was added into reaction mixture and stirred at room temperature for another 1 h. After that, the organic layer was separated and the aqueous phase was extracted with DCM (3 x 20 mL). The combined organic extracts were dried by $MgSO_4$ and concentrated under rotatory evaporation. The crude mixture was purified by flash chromatography (n-hexane/EtOAc = 1:9) to obtain 3-phenethyl-1,4,2-dioxazol-5-ones (***4c*** **–** ***4h***).

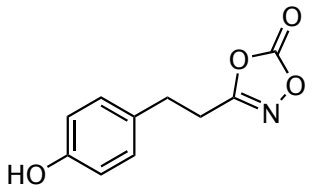

3-(4-hydroxyphenethyl)-1,4,2-dioxazol-5-one (***4a***)

Yield: 87 %, white solid

R_f = 0.5 (n-hexane/EtOAc = 1:20)

^{1}H NMR (400 MHz, $CDCl_3$): δ 7.07-7.05 (m, 2H), 6.81-6.78 (m, 2H), 5.02 (bs, 1H), 2.99-2.95 (m, 2H), 2.92-2.87 (m, 2H).

^{13}C NMR (100 MHz, $CDCl_3$): δ 165.9, 154.6, 154.1, 130.2, 129.4, 115.8, 29.7, 26.9.

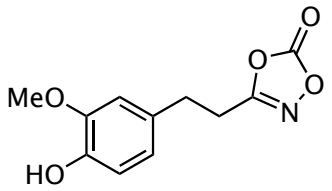

3-(4-hydroxy-3-methoxyphenethyl)-1,4,2-dioxazol-5-one (***4b***)

Yield: 80 %, white solid

R_f = 0.4 (n-hexane/EtOAc = 1:20)

^{1}H NMR (400 MHz, $CDCl_3$): δ 6.88-6.86 (d, *J* = 8.0 Hz, 1H), 6.71-6.68 (m, 2H), 5.56 (s, 1H), 3.88 (s, 3H), 2.99-2.95 (m, 2H), 2.93-2.89 (m, 2H).

^{13}C NMR (100 MHz, $CDCl_3$): δ 165.9, 154.0, 146.7, 144.7, 129.8, 120.9, 114.7, 110.7, 55.9, 30.3, 27.0.

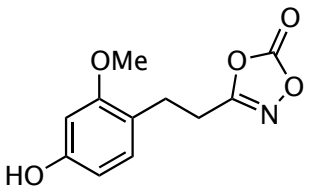

3-(4-hydroxy-2-methoxyphenethyl)-1,4,2-dioxazol-5-one (***4c***)

Yield: 53 %, white solid

R_f = 0.3 (n-hexane/EtOAc = 1:20)

^{1}H NMR (400 MHz, $CDCl_3$): δ 6.95-6.93 (d, *J* = 8.0 Hz, 1H), 6.41-6.33 (m, 2H), 5.03 (bs, 1H), 3.78 (s, 3H), 2.95-2.92 (m, 2H), 2.88-2.84 (m, 2H).

^{13}C NMR (100 MHz, $CDCl_3$): δ 166.7, 158.6, 156.4, 154.7, 130.8, 118.6, 107.1, 99.2, 55.4, 25.8, 25.5.

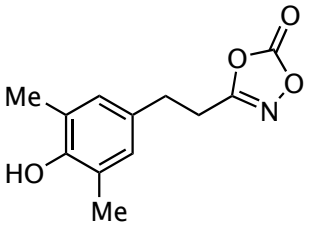

3-(4-hydroxy-3,5-dimethylphenethyl)-1,4,2-dioxazol-5-one (***4d***)

Yield: 65 %, white solid

R_f = 0.4 (n-hexane/EtOAc = 1:20)

^{1}H NMR (400 MHz, $CDCl_3$): δ 6.80 (s, 2H), 4.59 (bs, 1H), 2.89 (s, 4H), 2.23 (s, 3H).

^{13}C NMR (100 MHz, $CDCl_3$): δ 166.0, 154.1, 151.2, 129.6, 128.3, 123.5, 29.7, 27.0, 15.9.

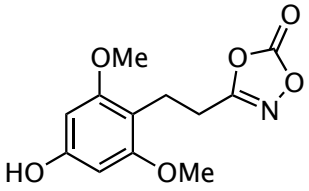

3-(4-hydroxy-2,6-dimethoxyphenethyl)-1,4,2-dioxazol-5-one (***4e***)

Yield: 56 %, white solid

R_f = 0.5 (n-hexane/EtOAc = 1:20)

^{1}H NMR (400 MHz, $CDCl_3$): δ 6.05 (s, 2H), 4.80 (bs, 1H), 3.76 (s, 6H), 2.99-2.95 (t, *J* = 7.2 Hz, 2H), 2.74-2.71 (t, *J* = 7.2 Hz, 2H).

^{13}C NMR (100 MHz, $CDCl_3$): δ 186.5, 179.1, 171.0, 100.8, 60.9, 56.4, 31.4, 29.9, 29.7.

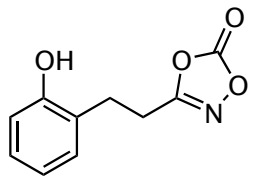

3-(2-hydroxyphenethyl)-1,4,2-dioxazol-5-one (***4f***)

Yield: 84 %, white solid

R_f = 0.5 (n-hexane/EtOAc = 1:20)

^{1}H NMR (400 MHz, $CDCl_3$): δ 7.16-7.11 (m, 2H), 6.91-6.88 (t, *J* = 7.6 Hz, 1H), 6.76-6.74 (d, *J* = 8.0 Hz, 1H), 5.13 (s, 1H), 3.07-3.03 (m, 2H), 2.99-2.95 (m, 2H).

^{13}C NMR (100 MHz, $CDCl_3$): δ 166.3, 154.3, 153.6, 130.6, 128.6, 124.7, 121.3, 115.5, 25.9, 25.1.

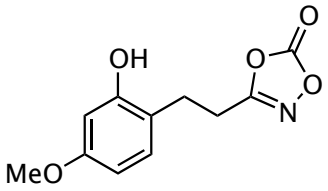

3-(2-hydroxy-4-methoxyphenethyl)-1,4,2-dioxazol-5-one (***4g***)

Yield: 39 %, white solid

R_f = 0.4 (n-hexane/EtOAc = 1:20)

^{1}H NMR (400 MHz, $CDCl_3$): δ 7.02-6.99 (d, *J* = 8.4 Hz, 1H), 6.45-6.42 (m, 1H), 6.33-6.32 (m, 1H), 5.43 (bs, 1H), 3.76 (s, 3H), 2.99-2.95 (m, 2H), 2.94-2.91 (m, 2H).

^{13}C NMR (100 MHz, $CDCl_3$): δ 166.5, 159.9, 154.5, 154.4, 131.1, 117.1, 106.0, 102.2, 55.4, 25.4, 25.3.

Preparation of 3-(2,3-diphenylpropyl)-1,4,2-dioxazol-5-ones According to Literature Report[2b]

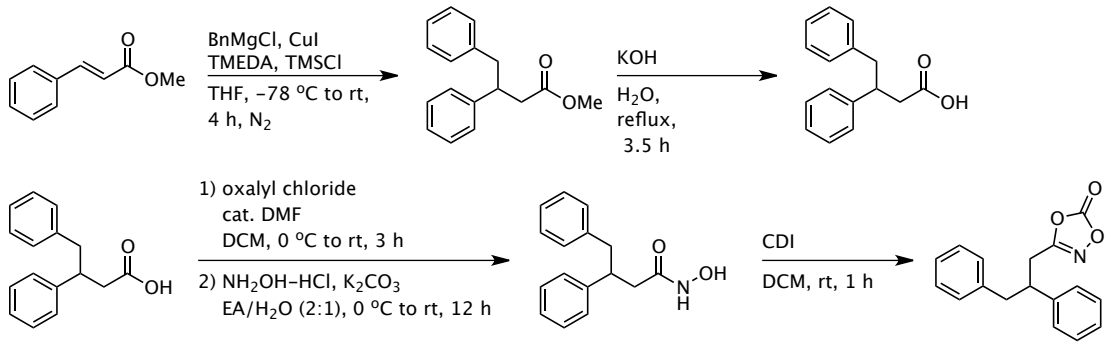

CuI (1.0 equiv, 380.9 mg) was added into a 25mL Schlenk flask, and the reaction flask was evacuated and back-filled with N_2 for three times. Dry THF (6 mL) was added into the flask through a syringe. TMEDA (1.1 equiv, 0.33 mL) was added into the THF solution, and the solution was stirred at room temperature for 15 min. Then, the reaction mixture was cooled to -78 ^{o}C, the BnMgCl (2.0 M in diethyl ether, 1 mL, 1.0 equiv) was added slowly. The reaction mixture was stirred at -78 ^{o}C for another 15 min. The methyl cinnamate (2 mmol) and TMSCl (2.5 equiv, 0.63 mL) were dissolved into dry THF (6 mL) in another vial. The "methyl cinnamate + TMSCl" mixture was added into reaction flask at -78 ^{o}C slowly. After the addition, the reaction was allowed to warm to room temperature and continued to stand for another 4 h. To work-up, the reaction was quenched by a saturated NH_4Cl solution. The aqueous phase was extracted with diethyl ether (3 x 30 mL), and the combined organic extracts were washed with water and brine and then dried with $MgSO_4$. The solvent was removed by the rotatory evaporation. The crude residue was filtered through a short pad silica gel column eluted with n-hexane/acetone 9:1 to remove any copper residue to obtain a yellow liquid, which was then used directly for the next step.

The methyl 3,4-diphenylbutanoate (2 mmol) and KOH (7.3 equiv, 819 mg) was dissolved in water (4 mL) and reflux for 3.5 h. After cooling to room temperature, the pH of reaction mixture was adjusted to 1 with 6M HCl and the aqueous phase was extracted with diethyl ether (2 x 10 mL). The combined organic extracts were dried with $MgSO_4$ and the solvent was evaporated by rotatory evaporation to obtain the 3,4-diphenylbutanoic acid in almost quantitative yield.

To a DCM (30 mL) solution of 3,4-diphenylbutanoic acid (2 mmol) was added oxalyl chloride (2.0 equiv, 0.34 mL) at 0 ^{o}C in a dropwise manner, and DMF (0.2 mL) was added to the mixture. After stirring the mixture at room temperature for 3 h, the solvent and excess oxalyl chloride were removed by vacuum distillation. K_2CO_3 (2.0 equiv, 552.8 mg) was dissolved in EtOAc/H_2O = 2:1 (16 mL of EtOAc and 8 mL of H_2O) and then cooled to 0 ^{o}C. The hydroxylamine hydrogen chloride (1.2 equiv, 166.8 mg) was added into the K_2CO_3 solution. The 3,4-diphenylbutanoyl chloride obtained was dissolved in DCM (5 mL) and was transferred to the reaction mixture. The reaction mixture was stirred at room temperature for overnight. To work-up, the distillated water (30 mL) was added into reaction mixture and the organic layer was separated. The aqueous phase was extracted with EtOAc (3 x 50 mL) and the combined organic extracts were dried with $MgSO_4$. The solvent was evaporated under rotatory evaporation to obtain the corresponding *N*-hydroxy-3,4-diphenylbutanamide without further purification.

The *N*-hydroxy-3,4-diphenylbutanamide (2 mmol) and CDI (1.1 equiv, 356.8 mg) were dissolved in DCM (20 mL) and stirred at room temperature for 30 min. Then, 1M HCl (3 mL) was added into reaction mixture and stirred at room temperature for another 1 h. After that, the organic layer was separated and the aqueous phase was

extracted with DCM (3 x 20 mL). The combined organic extracts were dried by $MgSO_4$ and concentrated under rotatory evaporation. The crude mixture was purified by flash chromatography (n-hexane/EtOAc = 9:1) to obtain 3-(2,3-diphenylpropyl)-1,4,2-dioxazol-5-one (***1a***). The ^{1}H and ^{13}C NMR spectra were consistent to the literature report.[2]

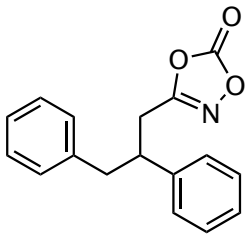

3-(2,3-diphenylpropyl)-1,4,2-dioxazol-5-one (***1s***)[2]

Yield: 60 %, yellow liquid

R_f = 0.5 (n-hexane/EtOAc = 9:1)

Preparation of 3-(2-phenylbutyl)-1,4,2-dioxazol-5-one According to Literature Report[2]

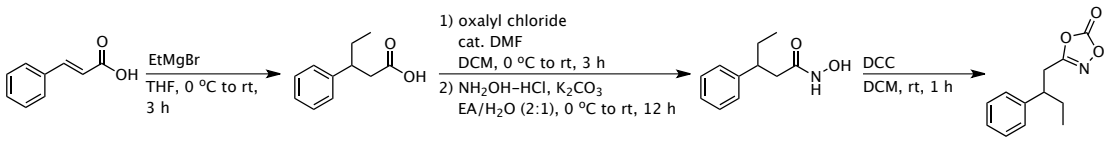

A solution of cinnamic acid (2 mmol) in dry THF (2 mL) was cooled to 0 ^{o}C. The EtMgBr (3.0 M in THF, 2 mL, 6 mmol) was added to the cinnamic acid solution at 0 ^{o}C in a dropwise manner. After that, the solution was allowed to warm to room temperature and stirred for another 3 h. 6M HCl (1.5 mL) was added to reaction mixture and the ice was added to reaction mixture until solution cooling down. The aqueous layer was extracted with diethyl ether (2 x 10 mL) and the combined

organic extracts were dried with $MgSO_4$. The solution was concentrated under rotatory evaporation and use to the next step with further purification.

To a DCM (30 mL) solution of 3-phenylpentanoic acid (2 mmol) was added oxalyl chloride (2.0 equiv, 0.34 mL) at 0 ^{o}C in a dropwise manner, and DMF (0.2 mL) was added to the mixture.. After stirring the mixture at room temperature for 3 h, the solvent and excess oxalyl chloride were removed by vacuum distillation. K_2CO_3 (2.0 equiv, 552.8 mg) was dissolved in EtOAc/H_2O = 2:1 (16 mL of EtOAc and 8 mL of H_2O) and then cooled to 0 ^{o}C. The hydroxylamine hydrogen chloride (1.2 equiv, 166.8 mg) was added into the K_2CO_3 solution. The 3-phenylpentanoyl chloride obtained was dissolved in DCM (5 mL) and was transferred to the reaction mixture. The reaction mixture was stirred at room temperature for overnight. To work-up, the distillated water (30 mL) was added into reaction mixture and the organic layer was separated. The aqueous phase was extracted with EtOAc (3 x 50 mL) and the combined organic extracts were dried with $MgSO_4$. The solvent was evaporated under rotatory evaporation to obtain the *N*-hydroxy-3-phenylpentanamide without further purification.

The *N*-hydroxy-3-phenylpentanamide (2 mmol) and CDI (1.1 equiv, 356.8 mg) were dissolved in DCM (20 mL) and stirred at room temperature for 30 min. Then, 1M HCl (3 mL) was added into reaction mixture and stirred at room temperature for another 1 h. After that, the organic layer was separated and the aqueous phase was extracted with DCM (3 x 20 mL). The combined organic layer was dried by $MgSO_4$ and concentrated under vacuum. The crude mixture was purified by flash chromatography (n-hexane/EtOAc = 9:1) to obtain 3-(2-phenylbutyl)-1,4,2-dioxazol-5-one (***1c***). The ^{1}H and ^{13}C NMR spectra were consistent to the literature report.[2]

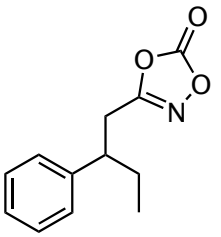

3-(2-phenylbutyl)-1,4,2-dioxazol-5-one (***1t***)[2]

Yield: 80 %, pale yellow liquid

R_f = 0.5 (n-hexane/EtOAc = 9:1)

Preparation of 3-(3-methyl-2-phenylbutyl)-1,4,2-dioxazol-5-ones

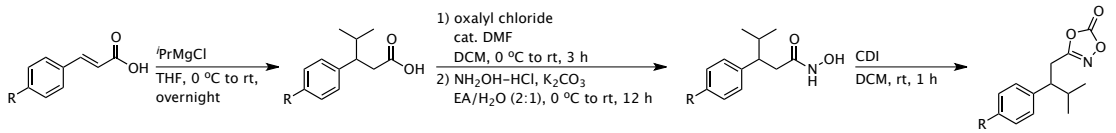

A solution of cinnamic acids (2 mmol) in dry THF (2 mL) was cooled to 0 ^{o}C. The ^{i}PrMgCl (2.0 M in THF, 3 mL, 6 mmol) was added to cinnamic acids solution at 0 ^{o}C in a dropwise manner. After that, the solution was allowed to warm to room temperature and stirred for another 12 h. 6M HCl (1.5 mL) was added to reaction mixture and the ice was added to reaction mixture until solution cooling down. The aqueous layer was extracted with diethyl ether (2 x 10 mL) and the combined organic extracts were dried with $MgSO_4$. The solution was concentrated by rotatory evaporation and use to the next step with further purification.

To a DCM (30 mL) solution of corresponding 4-methyl-3-phenylpentanoic acids (2 mmol) was added oxalyl chloride (2.0 equiv, 0.34 mL) at 0 ^{o}C in a dropwise manner, and DMF (0.2 mL) was added to the mixture.. After stirring the mixture at room temperature for 3 h, the solvent and excess oxalyl chloride were removed by vacuum distillation. K_2CO_3 (2.0 equiv, 552.8 mg) was dissolved in EtOAc/H_2O = 2:1

(16 mL of EtOAc and 8 mL of H_2O) and then cooled to 0 ^oC. The hydroxylamine hydrogen chloride (1.2 equiv, 166.8 mg) was added into the K_2CO_3 solution. The corresponding 4-methyl-3-phenylpentanoyl chlorides obtained were dissolved in DCM (5 mL) and was transferred to the reaction mixture. The reaction mixture was stirred at room temperature for overnight. To work-up, the distillated water (30 mL) was added into reaction mixture and the organic layer was separated. The aqueous phase was extracted with EtOAc (3 x 50 mL) and the combined organic extracts were dried with $MgSO_4$. The solvent was evaporated under rotatory evaporation to obtain the corresponding *N*-hydroxy-4-methyl-3-phenylpentanamides without further purification.

The corresponding *N*-hydroxy-4-methyl-3-phenylpentanamides (2 mmol) and CDI (1.1 equiv, 356.8 mg) were dissolved in DCM (20 mL) and stirred at room temperature for 30 mins. Then, 1M HCl (3 mL) was added into reaction mixture and stirred at room temperature for another 1 h. After that, the organic layer was separated and the aqueous phase was extracted with DCM (3 x 20 mL). The combined organic extracts were dried by $MgSO_4$ and concentrated under rotatory evaporation. The crude mixture was purified by flash chromatography (n-hexane/EtOAc = 9:1) to obtain corresponding 3-(3-methyl-2-phenylbutyl)-1,4,2-dioxazol-5-ones (***1b*** **–** ***1z***).

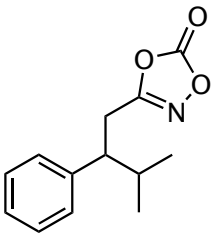

3-(3-methyl-2-phenylbutyl)-1,4,2-dioxazol-5-one (***1u***)

Yield: 75 %, yellow liquid

R_f = 0.5 (n-hexane/EtOAc = 9:1)

^{1}H NMR (400 MHz, CD_2Cl_2): δ 7.32-7.25 (m, 2H), 7.24-7.21 (m, 1H), 7.14-7.12 (m, 2H), 3.08 (dd, *J* = 15.1, 4.6 Hz, 1H) 2.90-2.77 (m, 2H), 2.00-1.89 (m, 1H), 1.00 (d, *J* = 6.7 Hz, 3H), 0.76 (d, *J* = 6.7 Hz, 3H).

^{13}C NMR (100 MHz, CD_2Cl_2): δ 166.2, 154.0, 140.5, 128.5, 128.1, 127.1, 48.8, 33.1, 29.0, 20.3, 19.9.

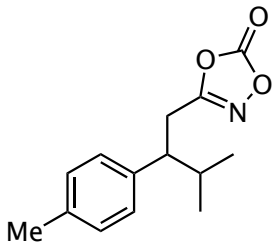

3-(3-methyl-2-(*p*-tolyl)butyl)-1,4,2-dioxazol-5-one (***1v***)

Yield: 80 %, yellow liquid

R_f = 0.5 (n-hexane/EtOAc = 9:1)

^{1}H NMR (400 MHz, $CDCl_3$): δ 7.10 (d, *J* = 7.8 Hz, 2H), 6.99 (d, *J* = 8.0 Hz, 2H), 3.05 (dd, *J* = 15.1, 4.8 Hz, 1H), 2.91-2.74 (m, 2H), 2.32 (s, 3H), 1.96-1.88 (m, 1H), 1.01 (d, *J* = 6.7 Hz, 3H), 0.79 (d, *J* = 6.7 Hz, 3H).

^{13}C NMR (100 MHz, $CDCl_3$): δ 165.9, 154.0, 137.0, 136.9, 129.3, 127.8, 48.4, 33.2, 29.1, 21.0, 20.6, 20.1.

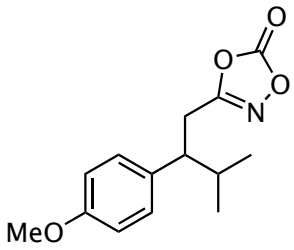

3-(2-(4-methoxyphenyl)-3-methylbutyl)-1,4,2-dioxazol-5-one (***1w***)

Yield: 75 %, yellow liquid

R_f = 0.5 (n-hexane/EtOAc = 9:1)

^{1}H NMR (400 MHz, $CDCl_3$): δ 7.03 (d, *J* = 8.6 Hz, 2H), 6.84 (d, *J* = 8.6 Hz, 2H), 3.79 (s, 3H), 3.07 (dd, *J* = 15.0, 4.7 Hz, 1H), 2.89-2.73 (m, 2H), 1.94-1.86 (m, 1H), 1.00 (d, *J* = 6.6 Hz, 3H), 0.78 (d, *J* = 8.0 Hz, 3H).

^{13}C NMR (100 MHz, $CDCl_3$): δ 166.0, 158.7, 154.0, 132.0, 128.9, 114.0, 55.2, 48.1, 33.3, 29.2, 20.6, 20.1.

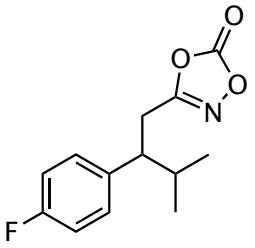

3-(2-(4-fluorophenyl)-3-methylbutyl)-1,4,2-dioxazol-5-one (***1x***)

Yield: 70 &, yellow liquid

R_f = 0.5 (n-hexane/EtOAc = 9:1)

^{1}H NMR (400 MHz, $CDCl_3$): δ 7.11-7.07 (m, 2H), 7.03-6.99 (m, 2H), 3.07 (dd, *J* = 10.4, 8.6 Hz, 1H), 2.89-2.78 (m, 2H), 1.96-1.87 (m, 1H), 1.02 (d, *J* = 6.6 Hz, 3H), 0.78 (d, J = 6.7 Hz, 3H).

^{13}C NMR (100 MHz, $CDCl_3$): δ 165.7, 163.1, 160.7, 135.8 (splitting), 129.4 (splitting), 115.6 (splitting), 48.1, 33.2, 29.1, 20.6, 20.0.

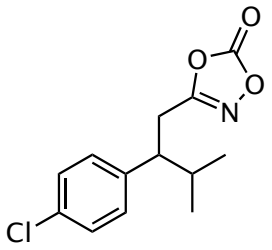

3-(2-(4-chlorophenyl)-3-methylbutyl)-1,4,2-dioxazol-5-one (***1y***)

Yield: 70 %, yellow liquid

R_f = 0.5 (n-hexane/EtOAc = 9:1)

^{1}H NMR (400 MHz, CD_2Cl_2): δ 7.29 (d, *J* = 8.4 Hz, 2H), 7.08 (d, *J* = 8.4 Hz, 2H), 3.07 (dd, *J* = 14.8, 4.1 Hz, 1H), 2.90-2.77 (m, 2H), 1.95-1.86 (m, 1H), 0.98 (d, *J* = 6.7 Hz, 3H), 0.76 (d, *J* = 6.7 Hz, 3H).

^{13}C NMR (100 MHz, CD_2Cl_2): δ 165.9, 153.9, 139.0, 132.8, 129.5, 128.7, 48.1, 33.2, 28.8, 20.2, 19.7.

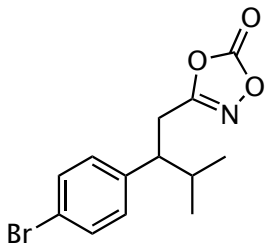

3-(2-(4-bromophenyl)-3-methylbutyl)-1,4,2-dioxazol-5-one (***1z***)

Yield: 60 %, orange liquid

R_f = 0.5 (n-hexane/EtOAc = 9:1)

^{1}H NMR (400 MHz, $CDCl_3$): δ 7.45 (d, *J* = 8.4 Hz, 2H), 7.00 (d, *J* = 8.4 Hz, 2H), 3.06 (dd, *J* = 14.8, 4.4 Hz, 1H), 2.90-2.77 (m, 2H), 1.96-1.88 (m, 1H), 1.01 (d, *J* = 6.8 Hz, 3H), 0.79 (d, *J* = 6.8 Hz, 3H).

^{13}C NMR (100 MHz, $CDCl_3$): δ 165.7, 154.0, 139.4, 131.9, 129.9, 121.3, 48.3, 33.2, 28.9, 20.7, 20.1.

Preparation of [Ru(*p*-cymene)(L-proline)Cl] (**[Ru2]**)[3]

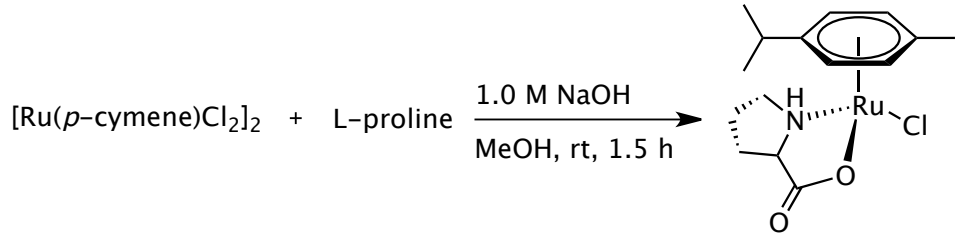

0.5 mmol 2.0 equiv 90 %

$[Ru(p\text{-cymene})Cl_2]_2$ (0.5 mmol, 321.23 mg) and L-proline (1.0 mmol, 115.13 mg) were dissolved in MeOH (5 mL). The reaction mixture was stirred at room temperature for 5 min. Then, 1.0 M NaOH (1 mL) was added into reaction mixture at room temperature. The reaction was allowed to react for 1.5 h. After 1.5 h, the reaction mixture was filtered through celite and concentrated under rotatory evaporator. The complex was recrystallized by DCM/diethyl ether to obtain [Ru(*p*-cymene)(L-proline)Cl] (**[Ru2]**) as orange crystal.

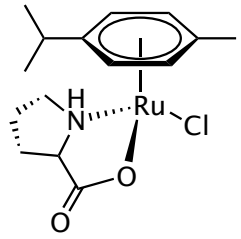

[Ru(*p*-cymene)(L-proline)Cl] (**[Ru2]**)

Yield: 90 %, orange solid

R_f = 0.2 (DCM/Acetone = 8:2)

^{1}H NMR (400 MHz, CD_2Cl_2): δ 5.44-5.40 (m, 1H), 5.39-5.35 (m, 2H), 5.19-5.18 (m, 1H), 3.95 (bs, 1H), 3.84-3.78 (m, 1H), 3.49-3.43 (q, *J* = 8.4 Hz, 1H), 3.09-3.03 (m, 1H), 2.87-2.81 (p, *J* = 7.2 Hz, 1H), 2.17 (s, 3H), 1.98-1.92 (m, 1H), 1.82-1.69 (m, 2H), 1.31-1.29 (d, *J* = 6.8 Hz, 3H), 1.27-1.25 (d, *J* = 7.2 Hz, 3H).

^{13}C NMR (100 MHz, CD_2Cl_2): δ 181.8, 101.1, 96.3, 83.6, 81.9, 79.4, 79.3, 62.0, 57.0, 31.0, 28.9, 27.3, 22.5, 22.0, 18.1.

Procedures for Regioselective Ru(II)-Catalyzed Intramolecular C(sp^2)-H Bond Amidation

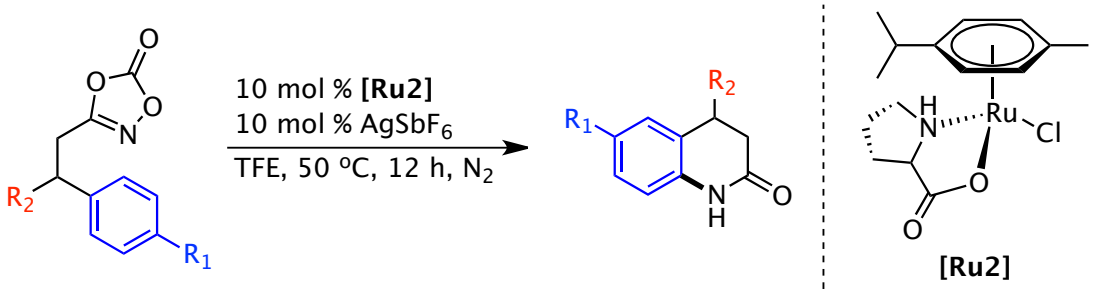

In a glove box, **[Ru4]** (10 mol %, 3.8 mg) and $AgSbF_6$ (10 mol %, 3.4 mg) were added into brown 8 mL vial A. The dry TFE (0.5 mL) was added into 8 mL vial. The reaction was stirred at room temperature for 5 min. The dioxazolones (0.1 mmol) was added into another 4 mL vial B and dissolved in dry TFE (0.5 mL). The dioxazolones solution was transferred from vial B to vial A. The reaction vial A was sealed and stirred at 50 °C for 12 h. After 12 h, the reaction crude mixture was passed through the celite eluted with EtOAc (15 mL). The solvent was evaporated under vacuum and the products ***2a*** – ***2z***, ***5a*** – ***5e*** and ***6g*** – ***6h*** were purified by preparative thin layer chromatography.

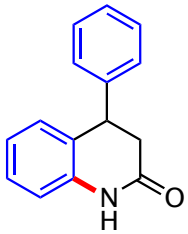

4-phenyl-3,4-dihydroquinolin-2(1*H*)-one (***2a***)

Yield: 76 %, white solid

R_f = 0.2 (n-hexane/EtOAc = 8:2)

^{1}H NMR (400 MHz, $CDCl_3$): δ 8.87 (bs, 1H), 7.35-7.32 (m, 2H), 7.29-7.25 (m, 1H), 7.23-7.20 (m, 3H), 6.99-6.87 (m, 3H), 4.32 (t, *J* = 7.2 Hz, 1H), 2.96-2.93 (m, 2H).

^{13}C NMR (100 MHz, $CDCl_3$): δ 171.1, 141.4, 136.8, 128.9, 128.4, 128.1, 127.8, 127.3, 126.7, 123.6, 115.8, 41.9, 38.3.

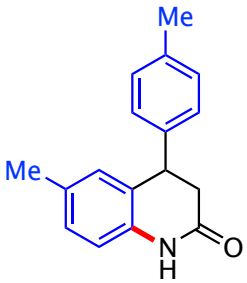

6-methyl-4-(*p*-tolyl)-3,4-dihydroquinolin-2(1*H*)-one (***2b***)

Yield: 84 %, white solid

R_f = 0.2 (n-hexane/EtOAc = 8:2)

^{1}H NMR (400 MHz, $CDCl_3$): δ 7.81 (bs, 1H), 7.14 (d, *J* = 8.0 Hz, 2H), 7.07 (d, *J* = 8.0 Hz, 2H), 7.00 (d, *J* = 7.2 Hz, 1H), 6.74 (s, 1H), 6.69 (d, *J* = 8.8 Hz, 1H), 4.21 (t, *J* = 7.2 Hz, 1H), 2.89-2.86 (m, 2H), 2.33 (s, 3H), 2.22 (s, 3H).

^{13}C NMR (100 MHz, $CDCl_3$): δ 170.9, 138.8, 136.9, 134.7, 133.1, 129.7, 129.0, 128.5, 127.8, 126.9, 115.7, 41.8, 38.7, 21.2, 20.9.

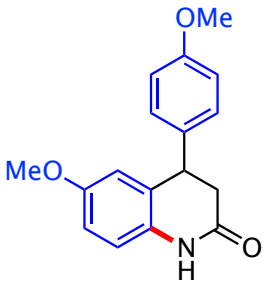

6-methoxy-4-(4-methoxyphenyl)-3,4-dihydroquinolin-2(1*H*)-one (***2c***)

Yield: 89 %, white solid

R_f = 0.2 (n-hexane/EtOAc = 8:2)

^{1}H NMR (400 MHz, $CDCl_3$): δ 9.13 (bs, 1H), 7.11 (d, *J* = 8.4 Hz, 2H), 6.87-6.81 (m, 3H), 6.73 (dd, *J* = 8.6, 2.8 Hz, 1H), 6.48 (d, *J* = 2.4 Hz, 1H), 4.20 (t, *J* = 7.6 Hz, 1H), 3.79 (s, 3H), 3.69 (s, 3H), 2.92-2.81 (m, 2H).

^{13}C NMR (100 MHz, $CDCl_3$): δ 171.0, 158.9, 155.9, 133.4, 130.8, 128.9, 128.7, 116.7, 114.4, 112.9, 55.7, 55.4, 41.7, 38.7.

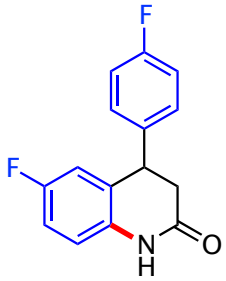

6-fluoro-4-(4-fluorophenyl)-3,4-dihydroquinolin-2(1*H*)-one (***2d***)

Yield: 87 %, white solid

R_f = 0.2 (n-hexane/EtOAc = 8:2)

^{1}H NMR (400 MHz, $CDCl_3$): δ 8.16 (bs, 1H), 7.11-7.07 (m, 2H), 7.01-6.96 (m, 2H), 6.88-6.83 (m, 1H), 6.74-6.71 (m, 1H), 6.54 (dd, *J* = 8.8, 2.4 Hz, 1H), 4.19 (t, *J* = 6.8 Hz, 1H), 2.87-2.75 (m, 2H).

^{13}C NMR (100 MHz, $CDCl_3$): δ 170.4, 129.5, 129.4, 117.0, 116.9, 116.3, 116.0, 115.5, 115.3, 115.1, 114.9, 41.6, 38.3.

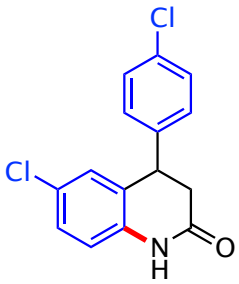

6-chloro-4-(4-chlorophenyl)-3,4-dihydroquinolin-2(1*H*)-one (***2e***)

Yield: 91 %, off-white solid

R_f = 0.2 (n-hexane/EtOAc = 8:2)

^{1}H NMR (400 MHz, $CDCl_3$): δ 8.07-8.04 (bs, 1H), 7.33 (d, *J* = 8.4 Hz, 2H), 7.20 (d, *J* = 2.4 Hz, 1H), 7.18 (d, *J* = 2.0 Hz, 2H), 6.87 (d, *J* = 2.0 Hz, 1H), 6.77 (d, *J* = 8.4 Hz, 1H), 4.24 (t, *J* = 7.6 Hz, 1H), 2.94-2.82 (m, 2H).

^{13}C NMR (100 MHz, $CDCl_3$): δ 170.1, 139.2, 135.7, 133.6, 129.5, 129.2, 128.7, 128.4, 128.0, 117.0, 41.5, 38.1.

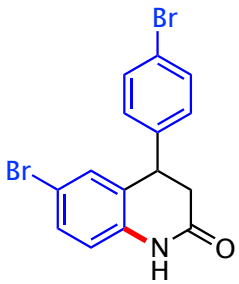

6-bromo-4-(4-bromophenyl)-3,4-dihydroquinolin-2(1*H*)-one (***2f***)

Yield: 90 %, off-white solid

R_f = 0.2 (n-hexane/EtOAc = 8:2)

^{1}H NMR (400 MHz, $CDCl_3$): δ 8.82 (bs, 1H), 7.48 (d, *J* = 8.4 Hz, 2H), 7.33 (dd, *J* = 8.4, 2.0 Hz, 1H), 7.07-7.03 (m, 3H), 6.76 (d, *J* = 8.4 Hz, 1H), 4.23 (t, *J* = 8.0 Hz, 1H), 2.94-2.81 (m, 2H).

^{13}C NMR (100 MHz, $CDCl_3$): δ 169.5, 139.5, 136.0, 132.3, 131.2, 131.1, 129.4, 128.2, 121.6, 117.1, 116.0, 41.4, 38.0.

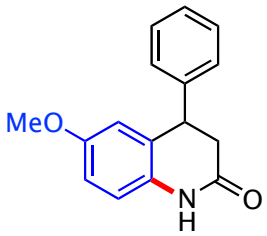

6-methoxy-4-phenyl-3,4-dihydroquinolin-2(1*H*)-one (***2h***)

Yield: 82 %, off-white solid

R_f = 0.2 (n-hexane/EtOAc = 8:2)

^{1}H NMR (400 MHz, $CDCl_3$): δ 9.13 (bs, 1H), 7.36-7.20 (m, 5H), 6.85-6.74 (m, 2H), 6.49 (s, 1H), 4.28-4.25 (t, *J* = 7.2 Hz, 1H), 3.70 (s, 3H), 2.93-2.90 (m, 2H).

^{13}C NMR (100 MHz, $CDCl_3$): δ 170.8, 155.9, 141.5, 130.8, 129.1, 128.2, 128.0, 127.4, 116.7, 114.5, 113.0, 55.7, 42.5, 38.5.

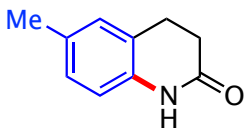

6-methyl-3,4-dihydroquinolin-2(1*H*)-one (***2i***)

Yield: 68 % (for ***1r***); 78 % (for ***1s***), white solid

R_f = 0.2 (n-hexane/EtOAc = 8:2)

^{1}H NMR (400 MHz, $CDCl_3$): δ 8.61 (bs, 1H), 6.97 (s, 2H), 6.71-6.69 (m, 1H), 2.93 (t, *J* = 8.0 Hz, 2H), 2.63 (t, *J* = 6.4 Hz, 2H), 2.29 (s, 3H).

^{13}C NMR (100 MHz, $CDCl_3$): δ 172.0, 134.9, 132.7, 128.7, 128.1, 123.7, 115.4, 30.9, 25.5, 20.9.

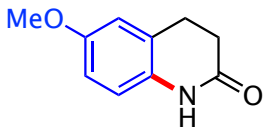

6-methoxy-3,4-dihydroquinolin-2(1*H*)-one (***2j***)

Yield: 72 % (for ***1u***); 80 % (for ***1v***), white solid

R_f = 0.1 (n-hexane/EtOAc = 8:2)

^{1}H NMR (400 MHz, $CDCl_3$): δ 8.76 (bs, 1H), 6.76-6.70 (m, 3H), 3.78 (s, 3H), 2.94 (t, *J* = 8.0 Hz, 2H), 2.62 (t, *J* = 7.2 Hz, 2H).

^{13}C NMR (100 MHz, $CDCl_3$): δ 171.8, 155.6, 130.9, 125.0, 116.3, 113.8, 112.4, 55.6, 30.6, 25.7.

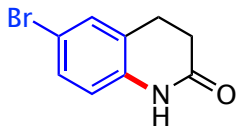

6-bromo-3,4-dihydroquinolin-2(1*H*)-one (***2k***)

Yield: 39 % (for ***1x***); 44 % (for ***1y***), white solid

R_f = 0.3 (n-hexane/EtOAc = 8:2)

^{1}H NMR (400 MHz, $CDCl_3$): δ 8.35 (bs, 1H), 7.30-7.38 (m, 2H), 6.67-6.65 (d, *J* = 8.0 Hz, 1H), 2.97-2.93 (t, *J* = 7.6 Hz, 2H), 2.65-2.61 (q, *J* = 8.0 Hz, 2H).

^{13}C NMR (100 MHz, $CDCl_3$): δ 171.3, 136.3, 130.9, 130.4, 125.7, 116.8, 115.5, 30.3, 25.2.

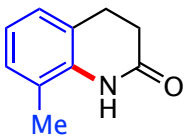

8-methyl-3,4-dihydroquinolin-2(1*H*)-one (***2l***)

Yield: 60 %, white solid

R_f = 0.2 (n-hexane/EtOAc = 8:2)

^{1}H NMR (400 MHz, $CDCl_3$): δ 8.64 (bs, 1H), 7.09-7.05 (t, *J* = 7.6 Hz, 1H), 6.87-6.85 (d, *J* = 7.6 Hz, 1H), 6.67-6.65 (d, *J* = 7.6 Hz, 1H), 2.93-2.90 (t, *J* = 7.6 Hz, 2H), 2.66-2.62 (t, *J* = 7.6 Hz, 2H), 2.29 (s, 3H).

^{13}C NMR (100 MHz, $CDCl_3$): δ 171.8, 137.4, 136.2, 127.2, 125.1, 122.1, 113.6, 30.5, 22.1, 19.5.

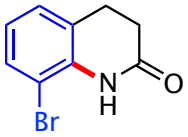

8-bromo-3,4-dihydroquinolin-2(1*H*)-one (***2n***)

Yield: 59 %, white solid

R_f = 0.3 (n-hexane/EtOAc = 8:2)

^{1}H NMR (400 MHz, $CDCl_3$): δ 7.80 (bs, 1H), 7.40 (d, *J* = 8.0 Hz, 1H), 7.12 (d, *J* = 7.6 Hz, 1H), 6.87 (t, *J* = 8.0 Hz, 1H), 3.00 (t, *J* = 7.6 Hz, 2H), 2.65 (t, *J* = 8.0 Hz, 2H).

^{13}C NMR (100 MHz, $CDCl_3$): δ 170.6, 135.2, 130.9, 127.2, 125.6, 123.8, 109.6, 30.6, 26.0.

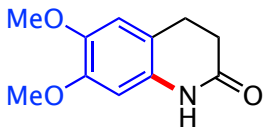

6,7-dimethoxy-3,4-dihydroquinolin-2(1*H*)-one (***2r***)

Yield: 83 %, white solid

R_f = 0.2 (n-hexane/EtOAc = 8:2)

^{1}H NMR (400 MHz, $CDCl_3$): δ 9.00 (bs, 1H), 6.68 (s, 1H), 6.41 (s, 1H), 3.85 (s, 6H), 2.91-2.87 (t, *J* = 7.6 Hz, 2H), 2.63-2.60 (t, *J* = 7.6 Hz, 2H).

^{13}C NMR (100 MHz, $CDCl_3$): δ 172.1, 148.6, 144.9, 130.9, 115.0, 111.8, 100.6, 56.5, 56.3, 31.1, 25.2.

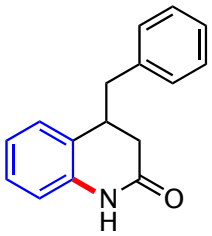

4-benzyl-3,4-dihydroquinolin-2(1*H*)-one (***2s***)

Yield: 78 %, white solid

R_f = 0.2 (n-hexane/EtOAc = 8:2)

^{1}H NMR (400 MHz, $CDCl_3$): δ 8.09 (bs, 1H), 7.29-7.17 (m, 4H), 7.08-7.07 (m, 2H), 7.00-6.93 (m, 2H), 6.79 (d, *J* = 7.6 Hz, 1H), 3.23-3.16 (m, 1H), 2.93 (dd, *J* = 13.4, 6.8 Hz, 1H), 2.79-2.65 (m, 2H), 2.55 (dd, *J* = 16.4, 3.6 Hz, 1H).

^{13}C NMR (100 MHz, $CDCl_3$): δ 170.7, 138.8, 136.5, 129.5, 128.6, 128.2, 127.9, 126.9, 126.6, 123.2, 115.7, 40.9, 38.8, 35.3.

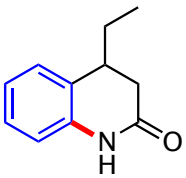

4-ethyl-3,4-dihydroquinolin-2(1*H*)-one (***2t***)

Yield: 81 %, white solid

R_f = 0.2 (n-hexane/EtOAc = 8:2)

^{1}H NMR (400 MHz, $CDCl_3$): δ 8.59 (bs, 1H), 7.20-7.15 (m, 2H), 7.02-6.99 (m, 1H), 6.81 (d, *J* = 7.6 Hz, 1H), 2.88-2.74 (m, 2H), 2.56 (dd, *J* = 16.0, 4.0 Hz, 1H), 1.70-1.56 (m, 2H), 0.94 (t, *J* = 7.6 Hz, 3H).

^{13}C NMR (100 MHz, $CDCl_3$): δ 171.5, 136.6, 128.1, 127.7, 127.6, 123.1, 115.8, 38.0, 36.0, 27.2, 11.5.

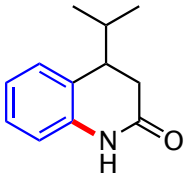

4-isopropyl-3,4-dihydroquinolin-2(1*H*)-one (***2u***)

Yield: 83 %, white solid

R_f = 0.2 (n-hexane/EtOAc = 8:2)

^{1}H NMR (400 MHz, $CDCl_3$): δ 8.92 (bs, 1H), 7.20-7.13 (m, 2H), 7.00 (t, *J* = 7.6 Hz, 1H), 6.83 (d, *J* = 8.0 Hz, 1H), 2.70 (s, 3H), 1.94-1.89 (m, 1H), 0.95 (d, *J* = 6.4 Hz, 3H), 0.89 (d, *J* = 6.8 Hz, 3H).

^{13}C NMR (100 MHz, $CDCl_3$): δ 172.1, 137.1, 129.2, 127.7, 126.5, 122.8, 115.9, 43.0, 33.6, 31.8, 20.7, 19.3.

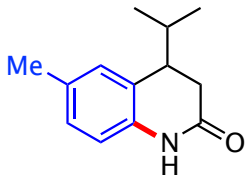

4-isopropyl-6-methyl-3,4-dihydroquinolin-2(1*H*)-one (***2v***)

Yield: 78 %, white solid

R_f = 0.2 (n-hexane/EtOAc = 8:2)

^{1}H NMR (400 MHz, $CDCl_3$): δ 8.69 (bs, 1H), 6.99-6.94 (m, 2H), 6.70 (d, *J* = 8.0 Hz, 1H), 2.67-2.65 (m, 3H), 2.30 (s, 3H), 1.92-1.86 (m, 1H), 0.94 (d, *J* = 6.8 Hz, 3H), 0.89 (d, *J* = 6.8 Hz, 3H).

^{13}C NMR (100 MHz, $CDCl_3$): δ 171.9, 134.6, 132.3, 129.8, 128.1, 126.4, 115.7, 43.0, 33.6, 31.9, 21.0, 20.7, 19.3.

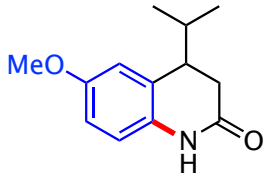

4-isopropyl-6-methoxy-3,4-dihydroquinolin-2(1*H*)-one (***2w***)

Yield: 86 %, white solid

R_f = 0.1 (n-hexane/EtOAc = 8:2)

^{1}H NMR (400 MHz, $CDCl_3$): δ 9.17 (bs, 1H), 6.80-6.69 (m, 3H), 3.79 (s, 3H), 2.67 (s, 3H), 1.94-1.88 (m, 1H), 0.96 (d, *J* = 6.8 Hz, 3H), 0.91 (d, *J* = 6.8 Hz, 3H).

^{13}C NMR (100 MHz, $CDCl_3$): δ 171.9, 155.4, 130.7, 128.0, 116.6, 115.1, 112.4, 55.7, 43.3, 33.4, 31.7, 20.7, 19.3.

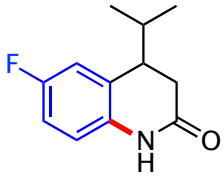

6-fluoro-4-isopropyl-3,4-dihydroquinolin-2(1*H*)-one (***2x***)

Yield: 88 %, white solid

R_f = 0.2 (n-hexane/EtOAc = 8:2)

^{1}H NMR (400 MHz, $CDCl_3$): δ 9.31 (bs, 1H), 6.91-6.79 (m, 3H), 2.68 (s, 3H), 1.96-1.88 (m, 1H), 0.96 (d, *J* = 6.8 Hz, 3H), 0.91 (d, *J* = 6.4 Hz, 3H).

^{13}C NMR (100 MHz, $CDCl_3$): δ 172.0, 159.8, 157.4, 133.3, 128.4 (splitting), 116.9 (splitting), 115.9 (splitting), 114.3 (splitting), 43.0, 33.1, 31.6, 20.6, 19.2.

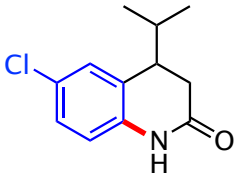

6-chloro-4-isopropyl-3,4-dihydroquinolin-2(1*H*)-one (***2y***)

Yield: 71 %, white solid

R_f = 0.2 (n-hexane/EtOAc = 8:2)

^{1}H NMR (400 MHz, $CDCl_3$): δ 9.17 (bs, 1H), 7.17-7.12 (m, 2H), 6.80-6.77 (m, 1H), 2.69-2.68 (m, 3H), 1.93-1.89 (m, 1H), 0.95 (d, *J* = 6.4 Hz, 3H), 0.92 (d, *J* = 6.8 Hz, 3H).

^{13}C NMR (100 MHz, $CDCl_3$): δ 171.9, 135.8, 129.0, 128.2, 127.9, 127.6, 117.0, 42.9, 33.1, 31.8, 20.6, 19.2.

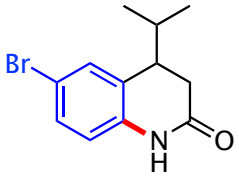

6-bromo-4-isopropyl-3,4-dihydroquinolin-2(1*H*)-one (***2z***)

Yield: 74 %, off-white solid

R_f = 0.2 (n-hexane/EtOAc = 8:2)

^{1}H NMR (400 MHz, $CDCl_3$): δ 8.27 (bs, 1H), 7.31-7.27 (m, 2H), 6.67 (d, *J* = 8.4 Hz, 1H), 2.71-2.66 (m, 3H), 1.94-1.86 (m, 1H), 0.95 (d, *J* = 6.4 Hz, 3H), 0.91 (d, *J* = 6.8 Hz, 3H).

^{13}C NMR (100 MHz, $CDCl_3$): δ 171.5, 136.2, 131.9, 130.6, 128.7, 117.3, 115.4, 42.9, 33.1, 31.8, 20.6, 19.1.

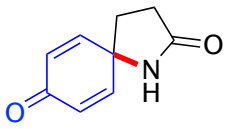

1-azaspiro[4.5]deca-6,9-diene-2,8-dione (***5a***)

Yield: 95 %, white solid

R_f = 0.3 (n-hexane/EtOAc = 1:20)

^{1}H NMR (400 MHz, $CDCl_3$): δ 6.85-6.81 (m, 2H), 6.61 (bs, 1H), 6.25-6.21 (m, 2H), 2.57-2.53 (m, 2H), 2.27-2.23 (m, 2H).

^{13}C NMR (100 MHz, $CDCl_3$): δ 184.4, 177.6, 149.3, 128.8, 57.5, 32.2, 29.4.

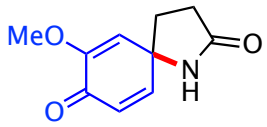

(*S*)-7-methoxy-1-azaspiro[4.5]deca-6,9-diene-2,8-dione (***5b***)

Yield: 88 %, white solid

R_f = 0.2 (n-hexane/EtOAc = 1:9)

^{1}H NMR (400 MHz, $CDCl_3$): δ 6.85-6.82 (m, 1H), 6.38 (bs, 1H), 6.24-6.21 (d, *J* = 10.0 Hz, 1H), 5.71-5.70 (d, *J* = 2.4 Hz, 1H), 3.68 (s, 3H), 2.59-2.54 (m, 2H), 2.32-2.26 (m, 2H).

^{13}C NMR (100 MHz, $CDCl_3$): δ 179.9, 177.3, 150.7, 149.8, 127.8, 116.5, 59.1, 55.1, 33.4, 29.7.

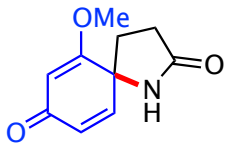

(*S*)-6-methoxy-1-azaspiro[4.5]deca-6,9-diene-2,8-dione (***5c***)

Yield: 83 %, white solid

R_f = 0.2 (n-hexane/EtOAc = 1:20)

^{1}H NMR (400 MHz, $CDCl_3$): δ 6.59-6.56 (d, *J* = 10.0 Hz, 1H), 6.19-6.16 (m, 1H), 5.86 (bs, 1H), 5.53 (s, 1H), 3.78 (s, 3H), 2.73-2.64 (m, 1H), 2.51-2.45 (m, 1H), 2.44-2.35 (m, 1H), 2.34-2.18 (m, 1H).

^{13}C NMR (100 MHz, $CDCl_3$): δ 186.6, 178.6, 174.7, 146.0, 128.4, 101.6, 58.9, 56.3, 32.3, 29.8.

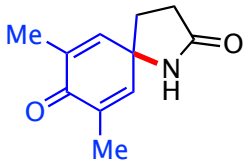

7,9-dimethyl-1-azaspiro[4.5]deca-6,9-diene-2,8-dione (***5d***)

Yield: %, white solid

R_f = 0.3 (n-hexane/EtOAc = 1:20)

^{1}H NMR (400 MHz, $CDCl_3$): δ 6.59 (s, 2H), 6.32 (bs, 1H), 2.55-2.51 (t, *J* = 8.0 Hz, 2H), 2.23-2.19 (t, *J* = 8.0 Hz, 2H), 1.90 (s, 6H).

^{13}C NMR (100 MHz, $CDCl_3$): δ 186.0, 177.6, 144.6, 135.3, 57.7, 32.7, 29.7, 16.0.

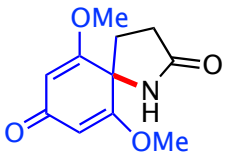

6,10-dimethoxy-1-azaspiro[4.5]deca-6,9-diene-2,8-dione (***5e***)

Yield: %, white solid

R_f = 0.3 (EtOAc/MeOH = 20:1)

^{1}H NMR (400 MHz, MeOD): δ 5.50 (s, 2H), 3.81 (s, 6H), 2.56-2.52 (m, 2H), 2.42-2.37 (m, 2H).

^{13}C NMR (100 MHz, MeOD): δ 188.2, 180.4, 173.0, 99.6, 61.6, 56.0, 31.2, 30.0.

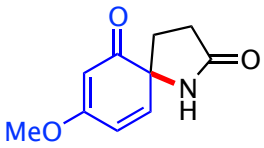

(*S*)-8-methoxy-1-azaspiro[4.5]deca-7,9-diene-2,6-dione (***6g***)

Yield: %, white solid

R_f = 0.2 (n-hexane/EtOAc = 1:20)

^{1}H NMR (400 MHz, $CDCl_3$): δ 6.41-6.38 (d, *J* = 10.0 Hz, 1H), 6.20-6.11 (m, 2H), 5.42 (bs, 1H), 3.80 (s, 3H), 2.72-2.63 (m, 1H), 2.39-2.24 (m, 2H), 2.06-1.99 (m, 1H).

^{13}C NMR (100 MHz, $CDCl_3$): δ 199.6, 179.5, 170.6, 143.5, 123.1, 97.9, 64.3, 56.3, 32.5, 28.5.

Procedures for Enantioselective Ru(II)-Catalyzed Intramolecular C(sp^2)-H Bond Amidation

In a glove box, **[Ru2]** (10 mol %, 3.8 mg) and $AgSbF_6$ (10 mol %, 3.4 mg) were added into brown 8 mL vial A. The dry TFE (0.5 mL) was added into 8 mL vial. The reaction was stirred at room temperature for 5 mins. The dioxazolones ***1*** (0.1 mmol) was added into another 4 mL vial B and dissolved in dry TFE (0.5 mL). The dioxazolones ***1*** solution was transferred from vial B to vial A. The reaction vial A was sealed and stirred at 50 ^{o}C for 12 h. After 12 h, the reaction crude mixture was passed through the celite eluted with EtOAc (15 mL). The solvent was evaporated under rotatory evaporation and the products ***2*** were purified by preparative thin layer chromatography (n-hexane/EtOAc = 8:2). After the purification, 4 mg of products ***2*** were dissolved in DCM (1 mL) and then injected into HPLC for enantioselectivity analysis.

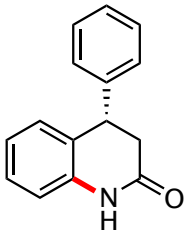

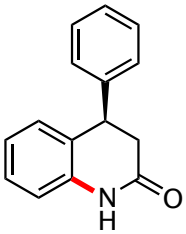

(S)–isomer *(R)*–isomer

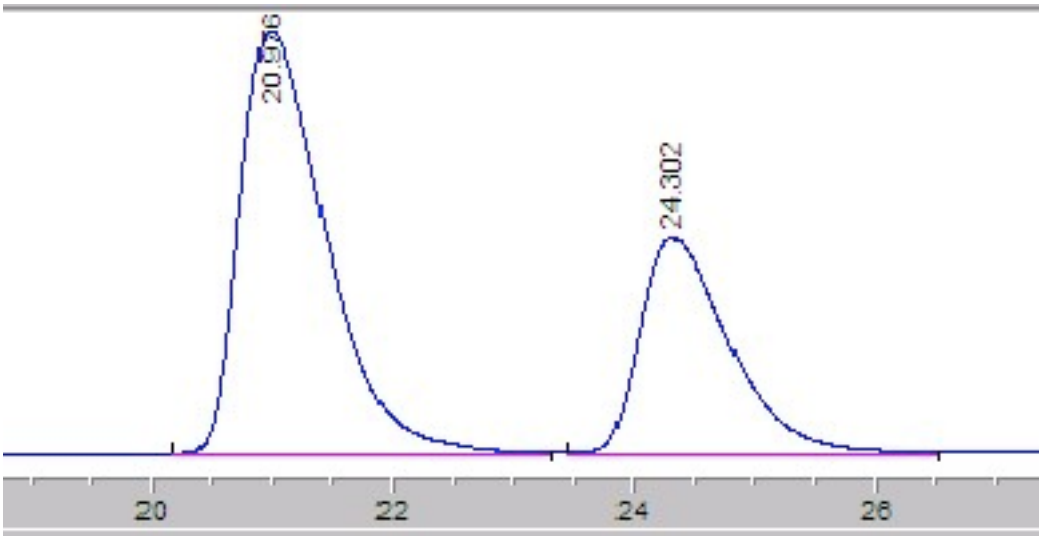

	retention time (mins)	peak area	*ee* (%)
(S)-isomer	20.976	34490.1	$\frac{(34490.1-18546.8)}{(34490.1+18546.8)} x\ 100\ \% = 30\ \%$
(R)-isomer	24.302	18546.8	

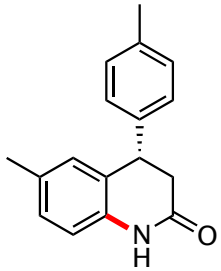

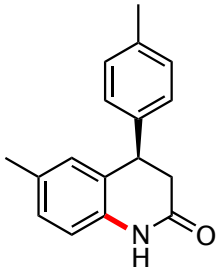

(S)–isomer *(R)*–isomer

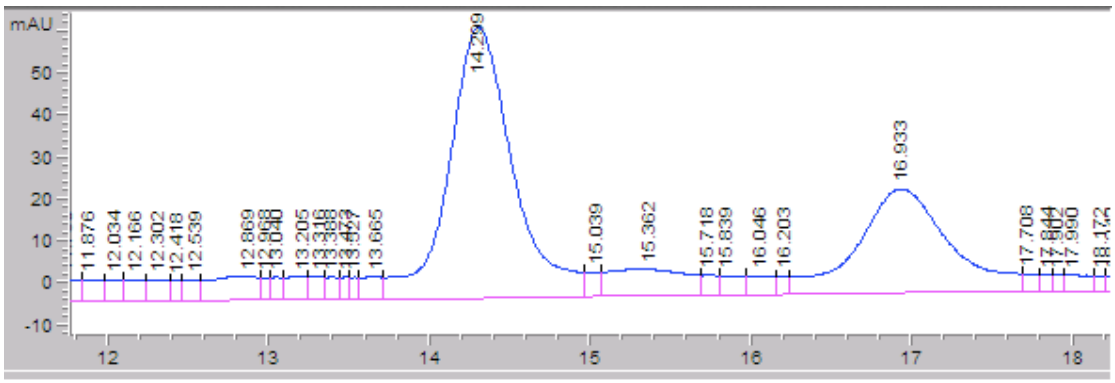

	retention time (mins)	peak area	*ee* (%)
(S)-isomer	14.299	1792.1	$\frac{(1792.1-1006.2)}{(1792.1+1006.2)} x\ 100\ \% = 30\ \%$
(R)-isomer	16.933	1006.2	

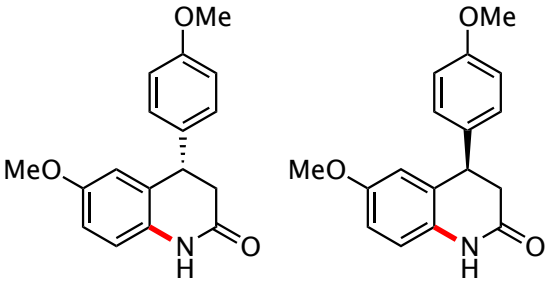

(S)–isomer *(R)*–isomer

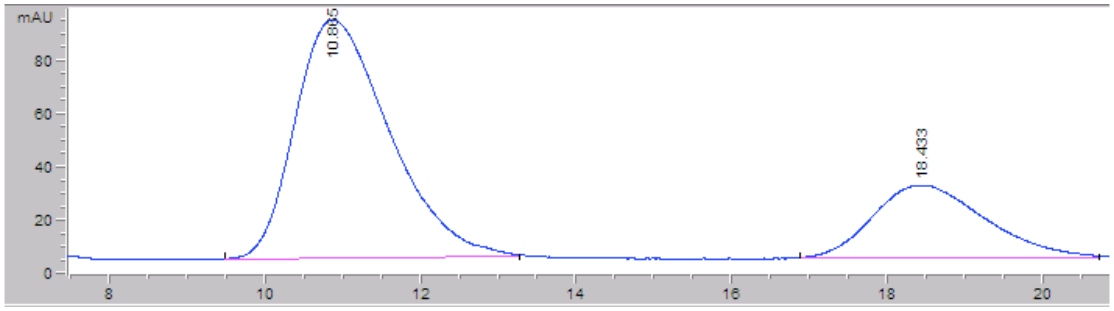

	retention time (mins)	peak area	*ee* (%)
(S)-isomer	10.866	7581.7	$\frac{(7581.7-2831.8)}{(7581.7+2831.8)} x\ 100\ \% = 45\ \%$
(R)-isomer	18.433	2831.8	

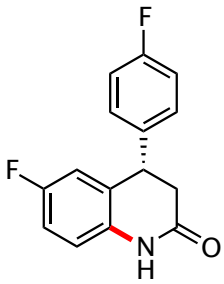

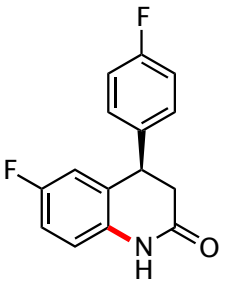

(S)–isomer *(R)*–isomer

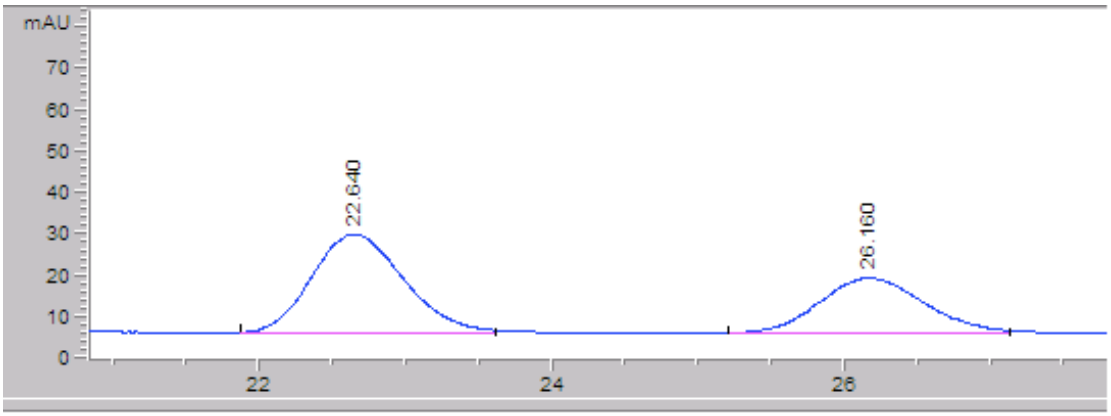

	retention time (mins)	peak area	*ee* (%)
(S)-isomer	22.640	1078.0	$\frac{(1078.0-682.9)}{(1078.0+682.9)} x\ 100\ \% = 23\ \%$
(R)-isomer	26.160	682.9	

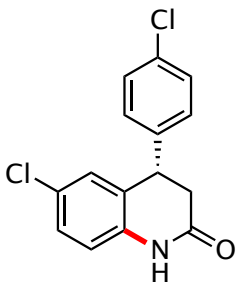

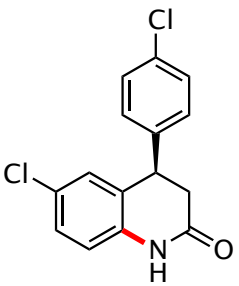

(S)–isomer *(R)*–isomer

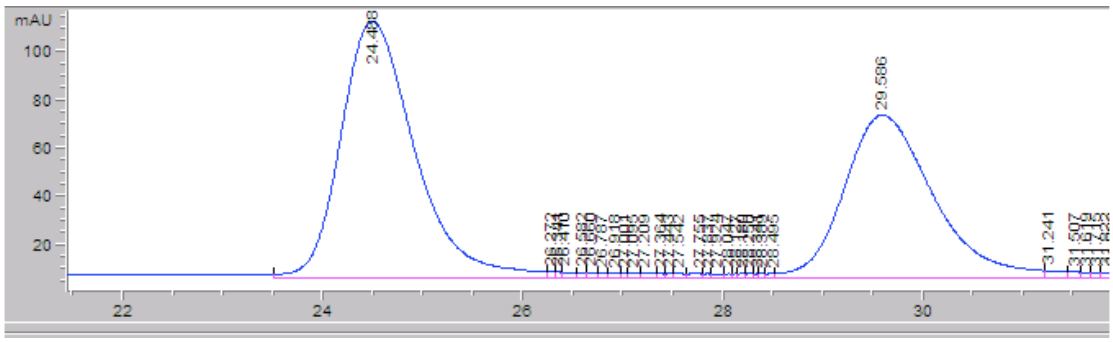

	retention time (mins)	peak area	*ee* (%)
(S)-isomer	24.488	5493.8	$\frac{(5493.8-4199.2)}{(5493.8+4199.2)} x\ 100\ \% = 14\ \%$
(R)-isomer	29.586	4199.2	

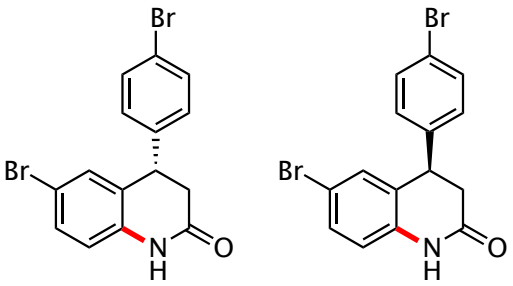

(S)–isomer *(R)*–isomer

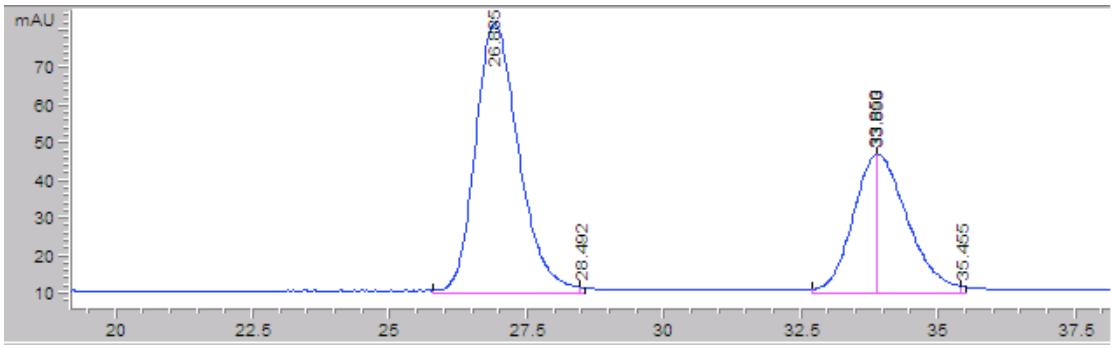

	Retention Time (mins)	Peak Area	*ee* (%)
(S)-isomer	26.886	3984.0	$\frac{(3984.0-1426.2)}{(3984.0+1426.2)} x\ 100\ \% = 47\ \%$
(R)-isomer	33.898	1426.2	

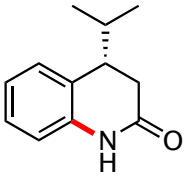

(S)–isomer

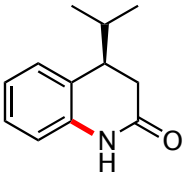

(R)–isomer

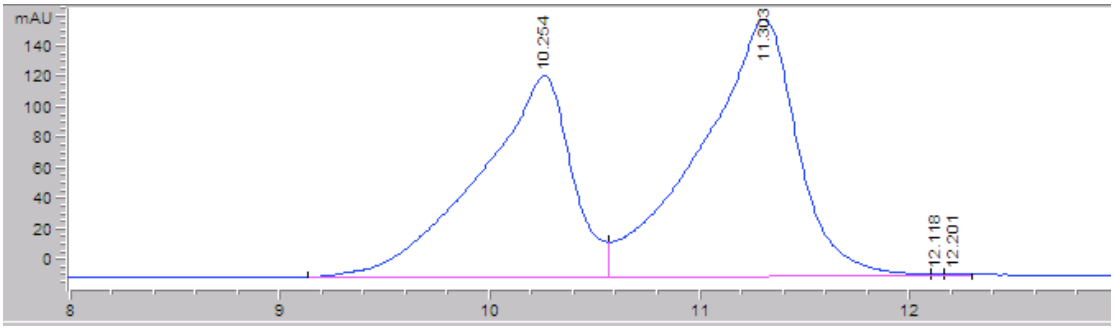

	retention time (mins)	peak area	*ee* (%)
(S)-isomer	10.254	4095.8	$\frac{(5481.0-4095.8)}{(5481.0+4095.8)} x\ 100\ \% = 14\ \%$
(R)-isomer	11.393	5481.0	

Figure S3.1 ^{1}H NMR Spectrum of 3-(2,2-diphenylethyl)-1,4,2-dioxazol-5-one (***1a***)

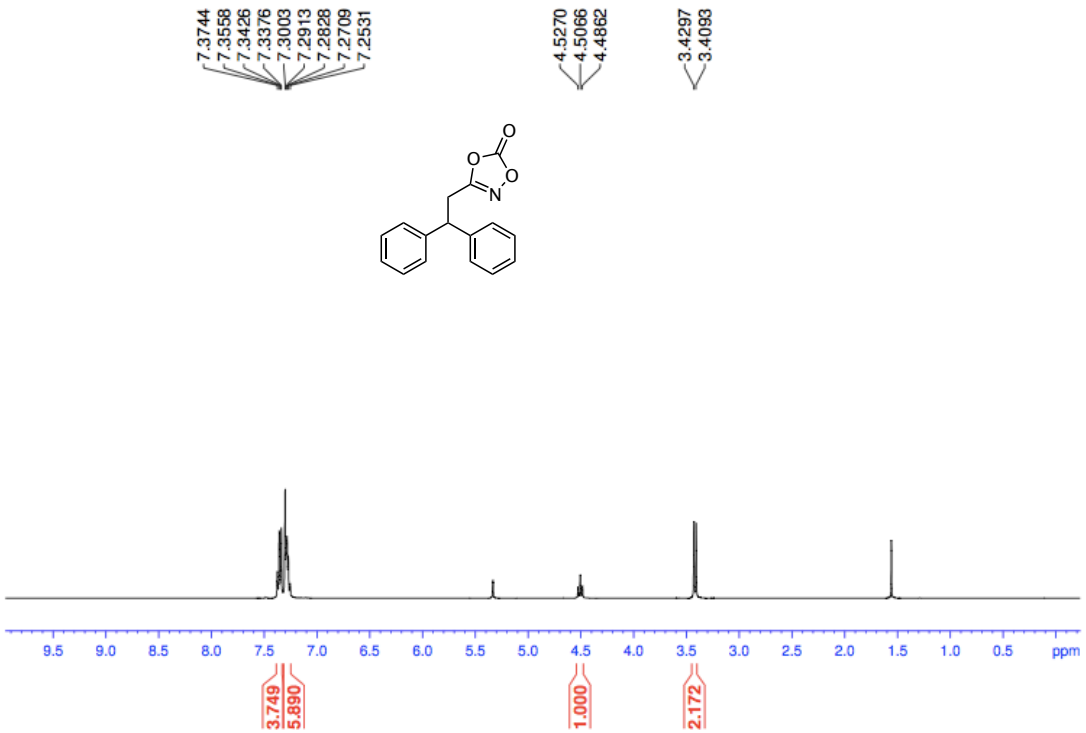

Figure S3.2 ^{13}C NMR Spectrum of 3-(2,2-diphenylethyl)-1,4,2-dioxazol-5-one (***1a***)

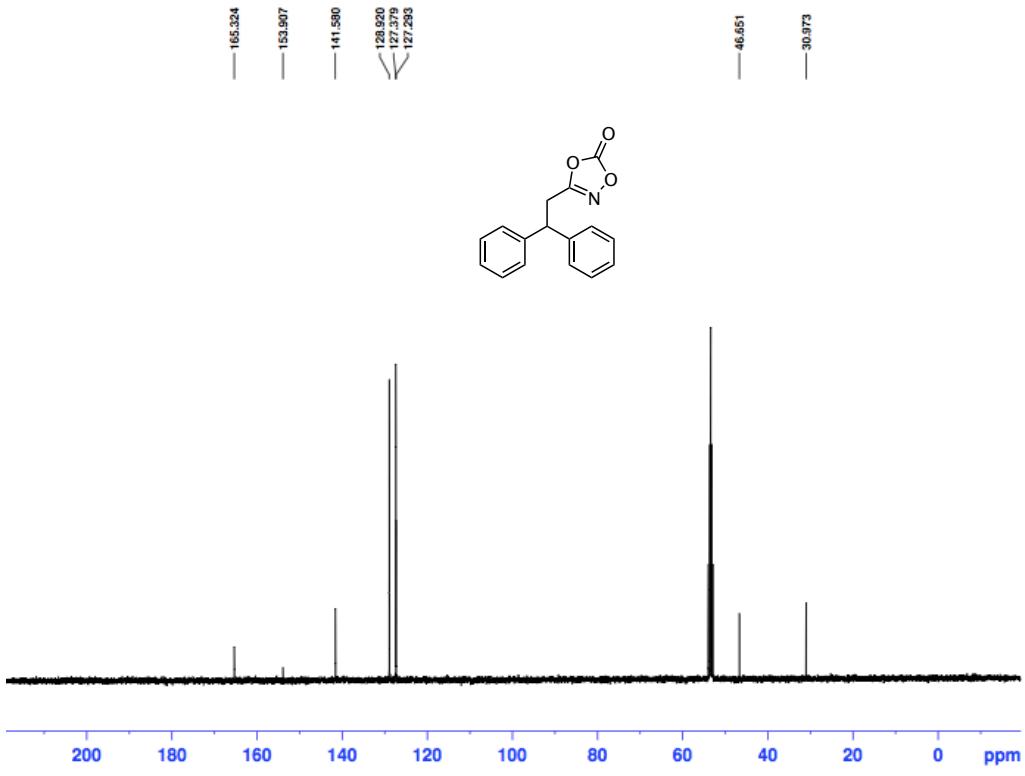

Figure S3.3 ^{1}H NMR Spectrum of 3-(2,2-di-*p*-tolylethyl)-1,4,2-dioxazol-5-one (***1b***)

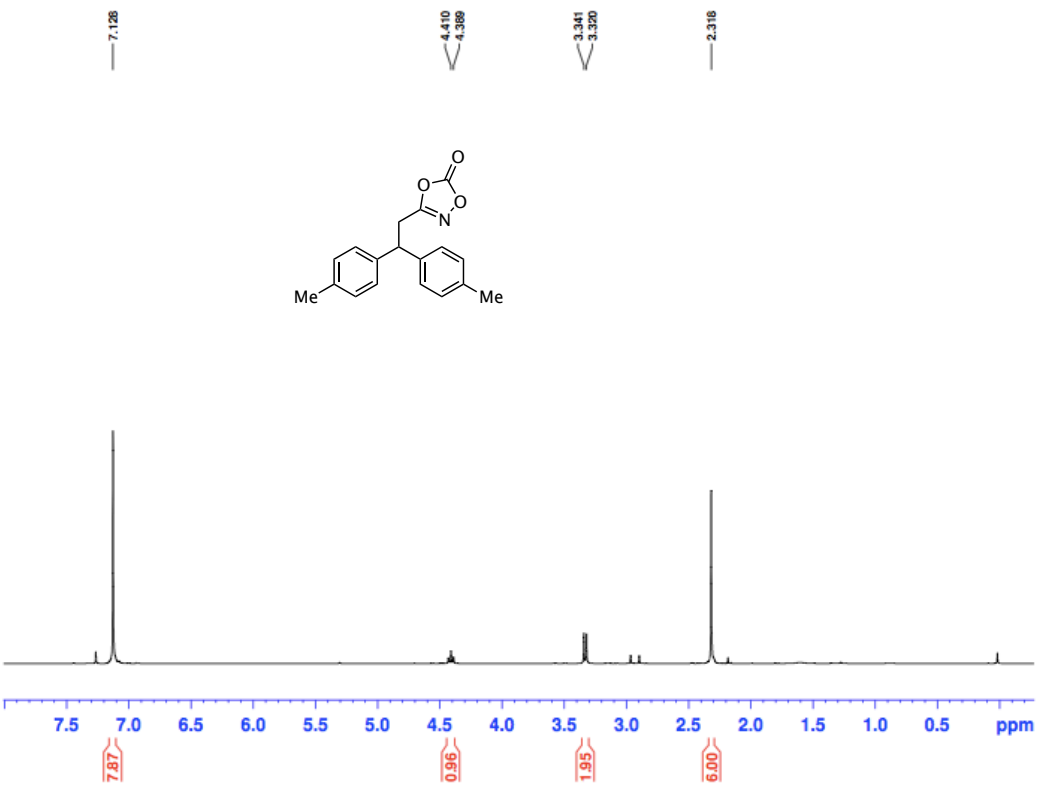

Figure S3.4 ^{13}C NMR Spectrum of 3-(2,2-di-*p*-tolylethyl)-1,4,2-dioxazol-5-one (***1b***)

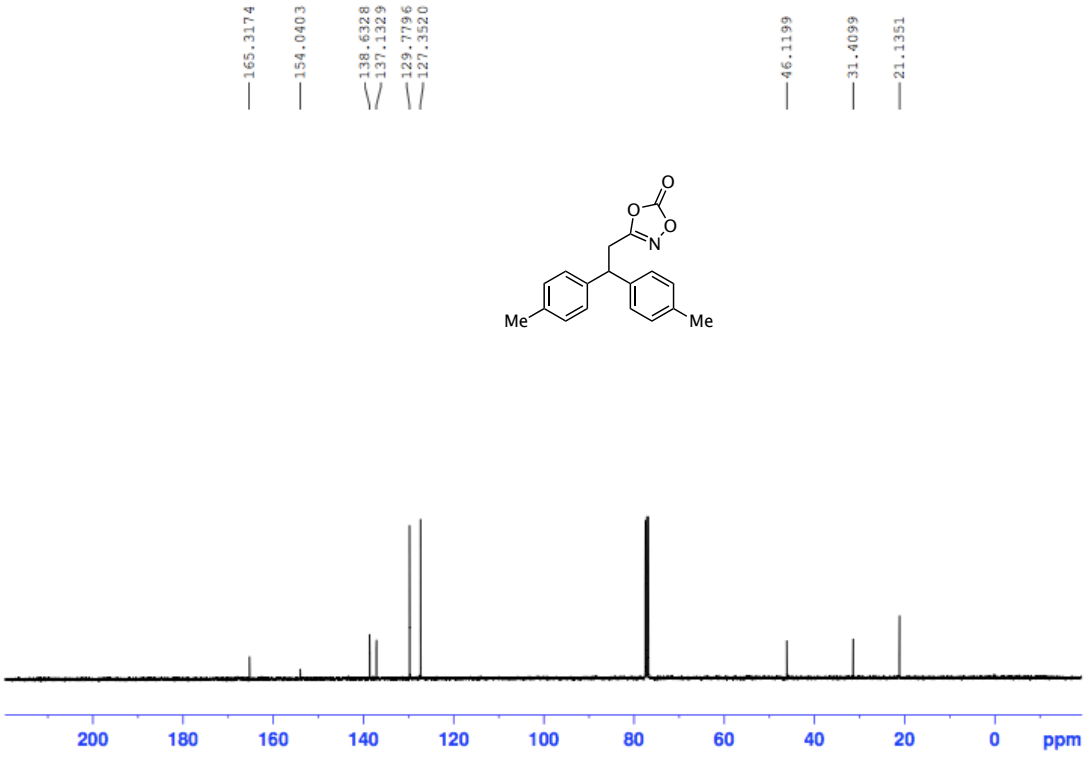

Figure S3.5 ^{1}H NMR Spectrum of 3-(2,2-bis(4-methoxyphenyl)ethyl)-1,4,2-dioxazol-5-one (***1c***)

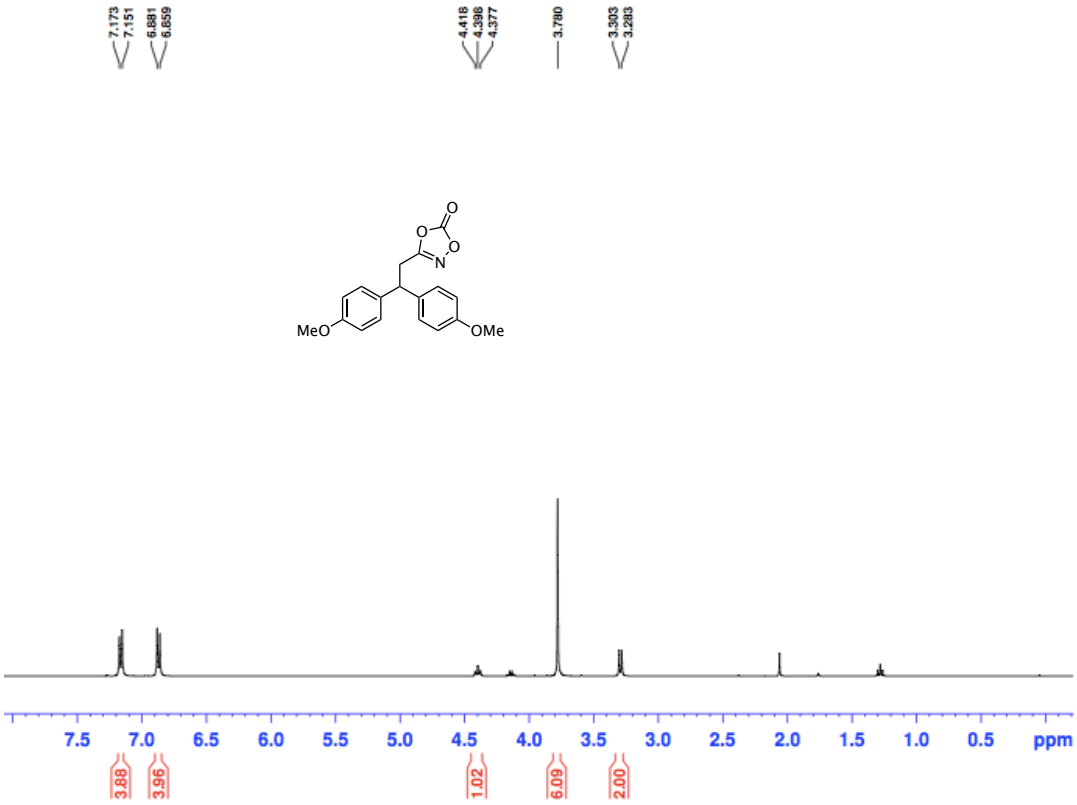

Figure S3.6 ^{13}C NMR Spectrum of 3-(2,2-bis(4-methoxyphenyl)ethyl)-1,4,2-dioxazol-5-one (***1c***)

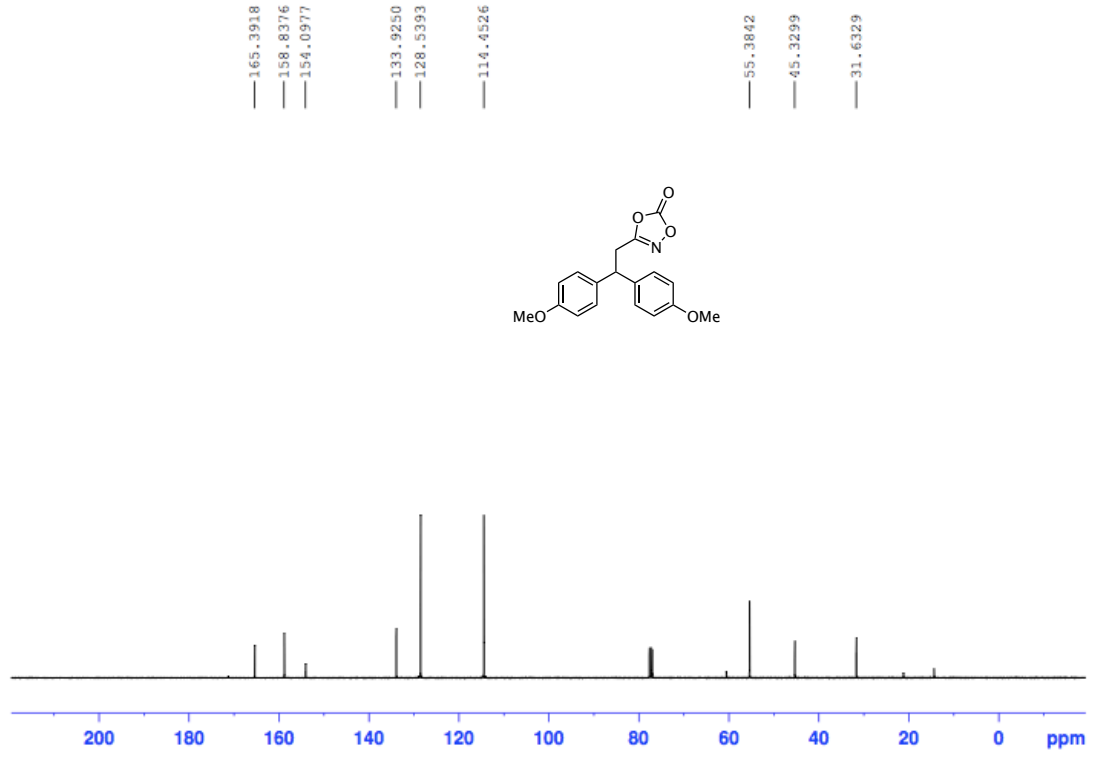

Figure S3.7 ^{1}H NMR Spectrum of 3-(2,2-bis(4-fluorophenyl)ethyl)-1,4,2-dioxazol-5-one (***1d***)

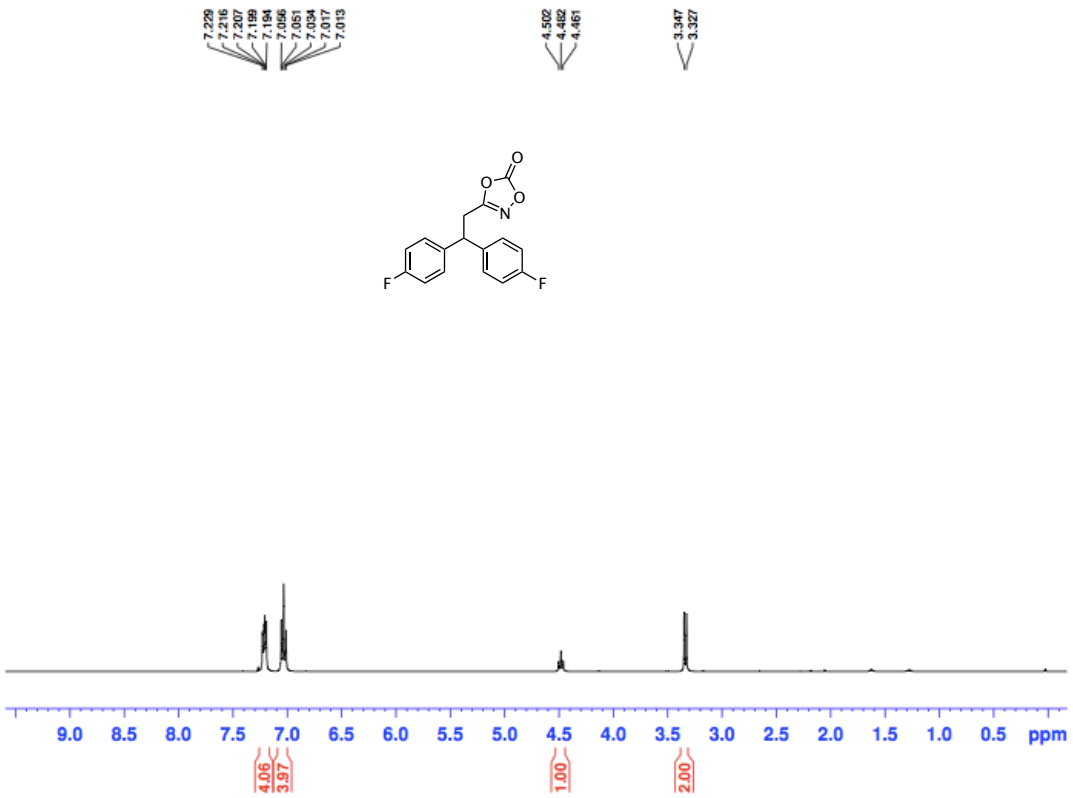

Figure S3.8 ^{13}C NMR Spectrum of 3-(2,2-bis(4-fluorophenyl)ethyl)-1,4,2-dioxazol-5-one (***1d***)

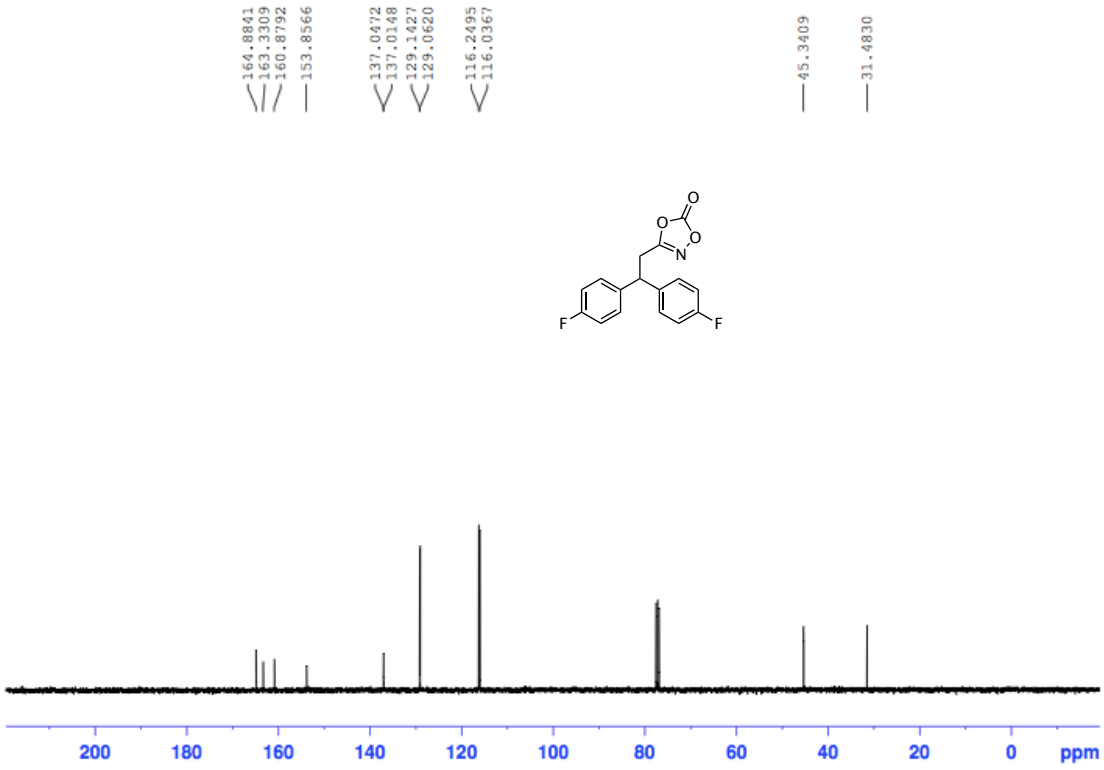

Figure S3.9 ^{1}H NMR Spectrum of 3-(2,2-bis(4-chlorophenyl)ethyl)-1,4,2-dioxazol-5-one (***1e***)

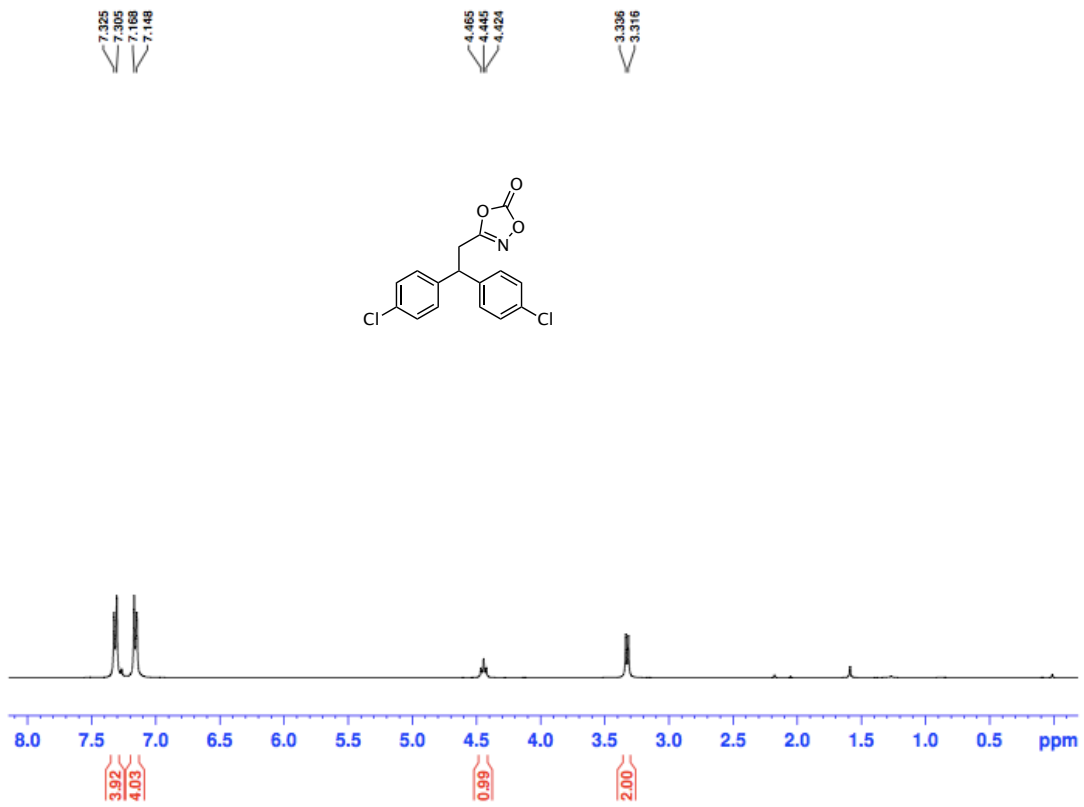

Figure S3.10 ^{13}C NMR Spectrum of 3-(2,2-bis(4-chlorophenyl)ethyl)-1,4,2-dioxazol-5-one (***1e***)

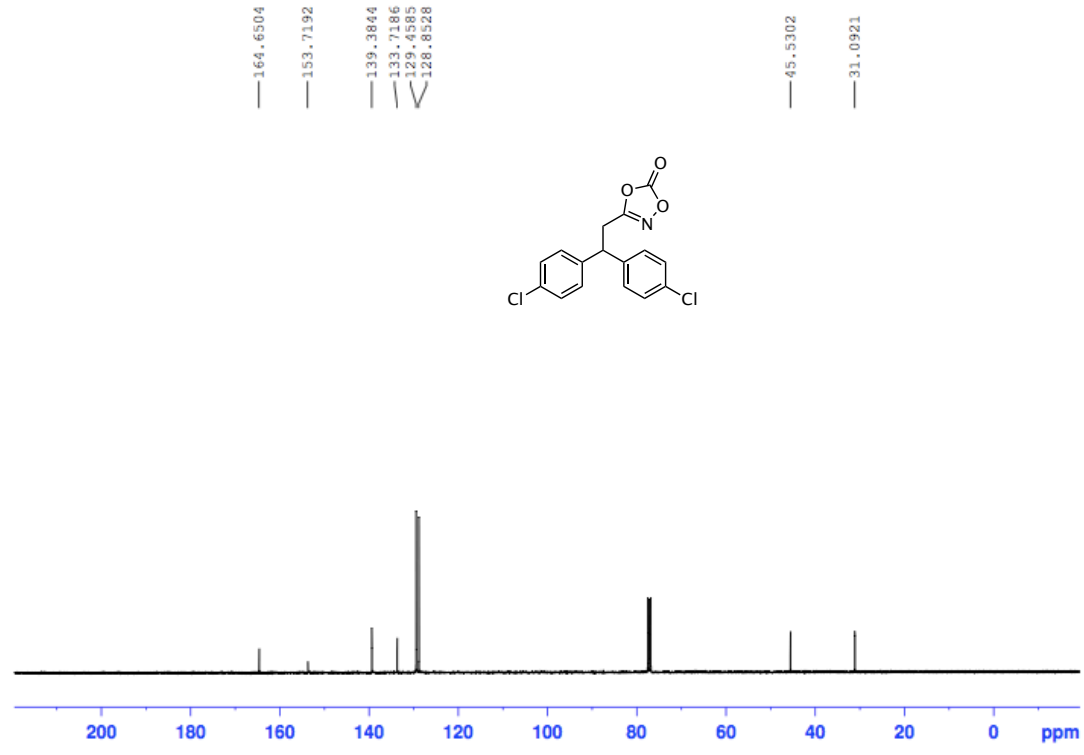

Figure S3.11 ^{1}H NMR Spectrum of 3-(2,2-bis(4-bromophenyl)ethyl)-1,4,2-dioxazol-5-one (***1f***)

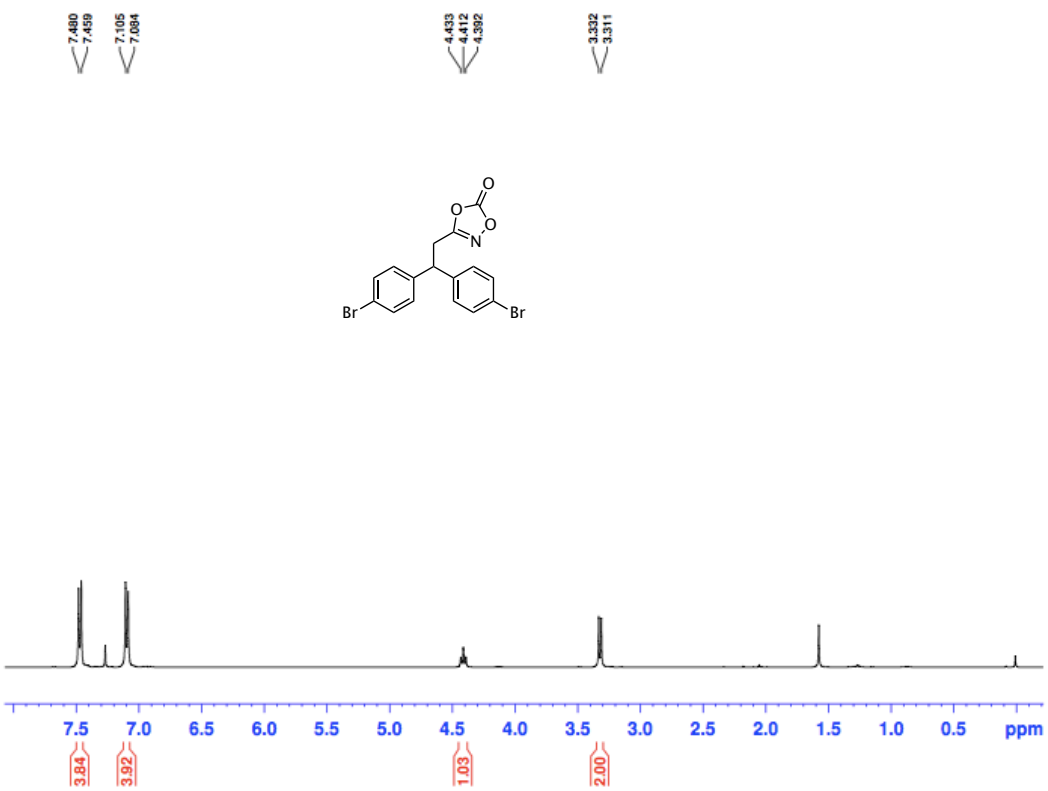

Figure S3.12 ^{13}C NMR Spectrum of 3-(2,2-bis(4-bromophenyl)ethyl)-1,4,2-dioxazol-5-one (***1f***)

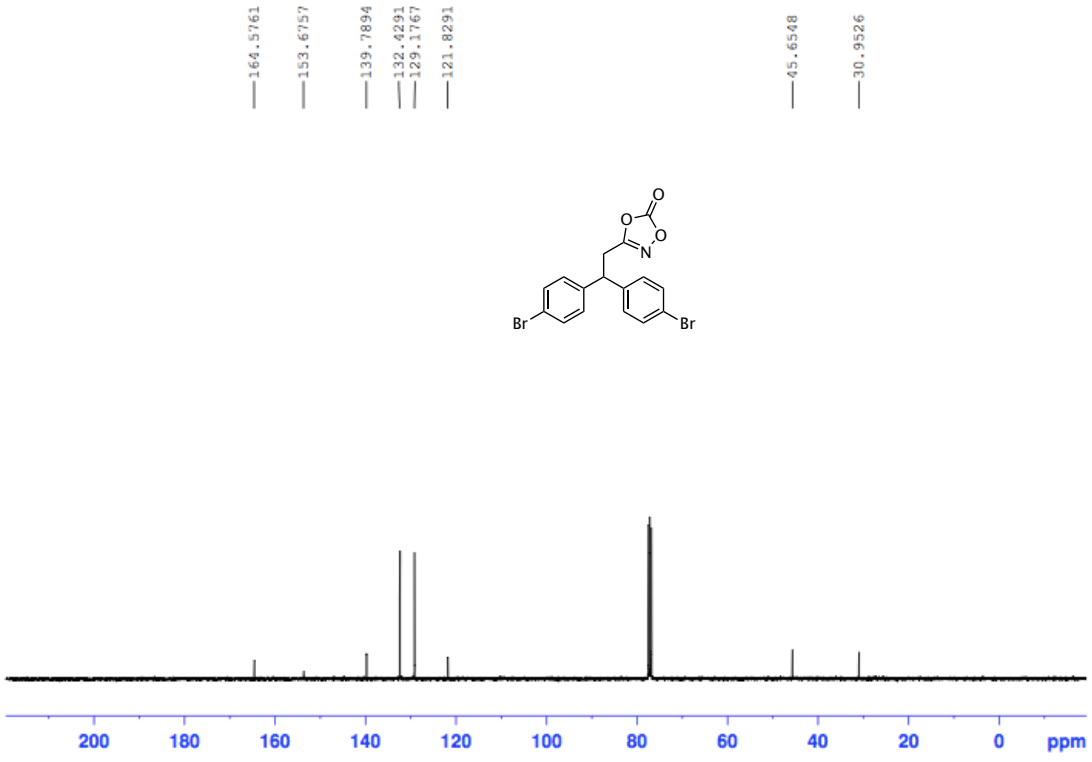

Figure S3.13 ^{1}H NMR Spectrum of 3-(2,2-bis(4-(trifluoromethyl)phenyl)ethyl)-1,4,2-dioxazol-5-one (***1g***)

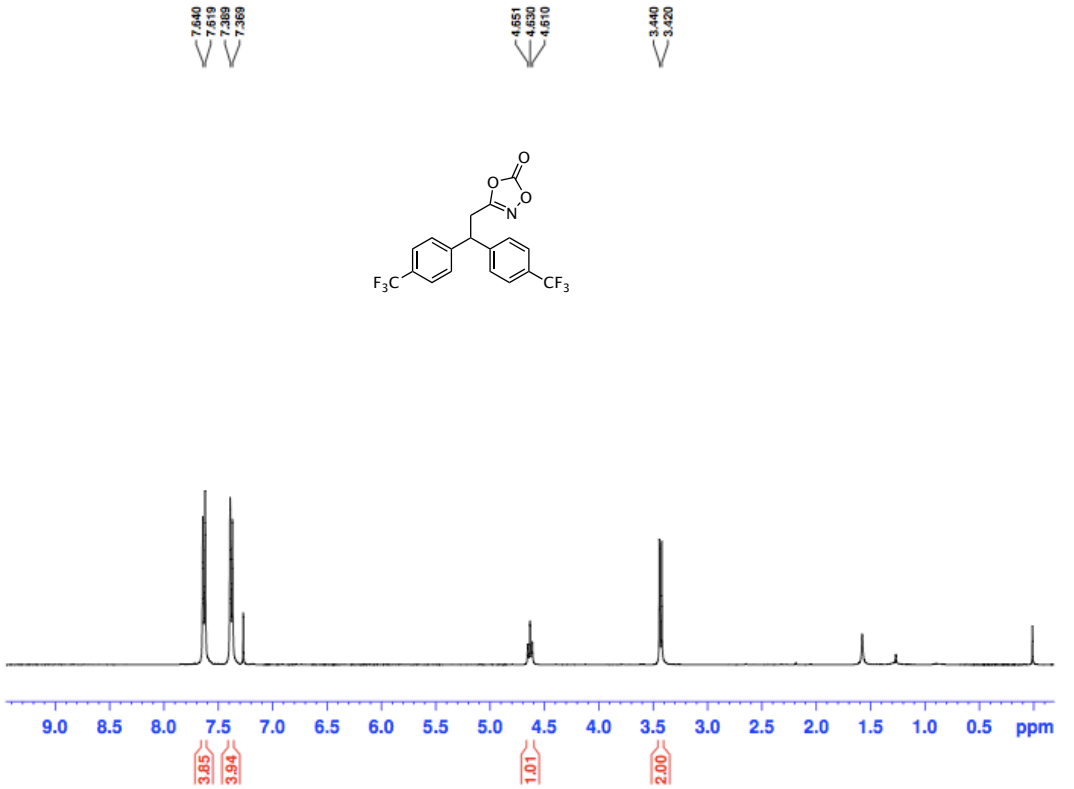

Figure S3.14 ^{13}C NMR Spectrum of 3-(2,2-bis(4-(trifluoromethyl)phenyl)ethyl)-1,4,2-dioxazol-5-one (***1g***)

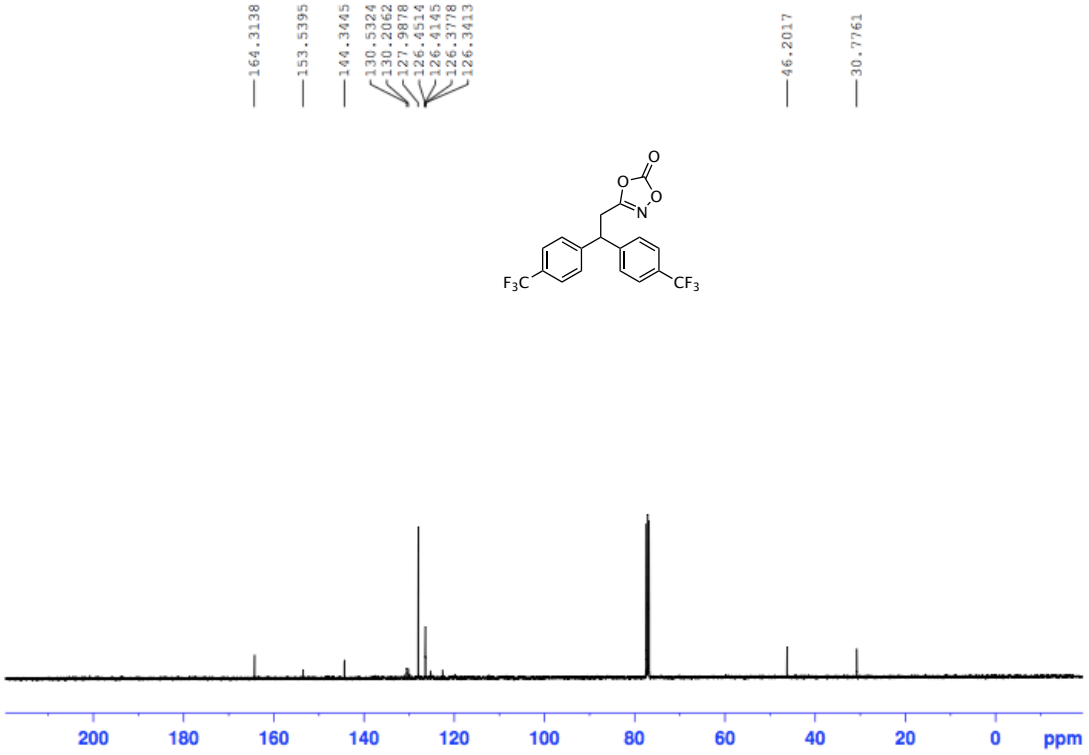

Figure S3.15 ^{1}H NMR Spectrum of 3-(2,2-bis(4-(trifluoromethyl)phenyl)ethyl)-1,4,2-dioxazol-5-one (***1h***)

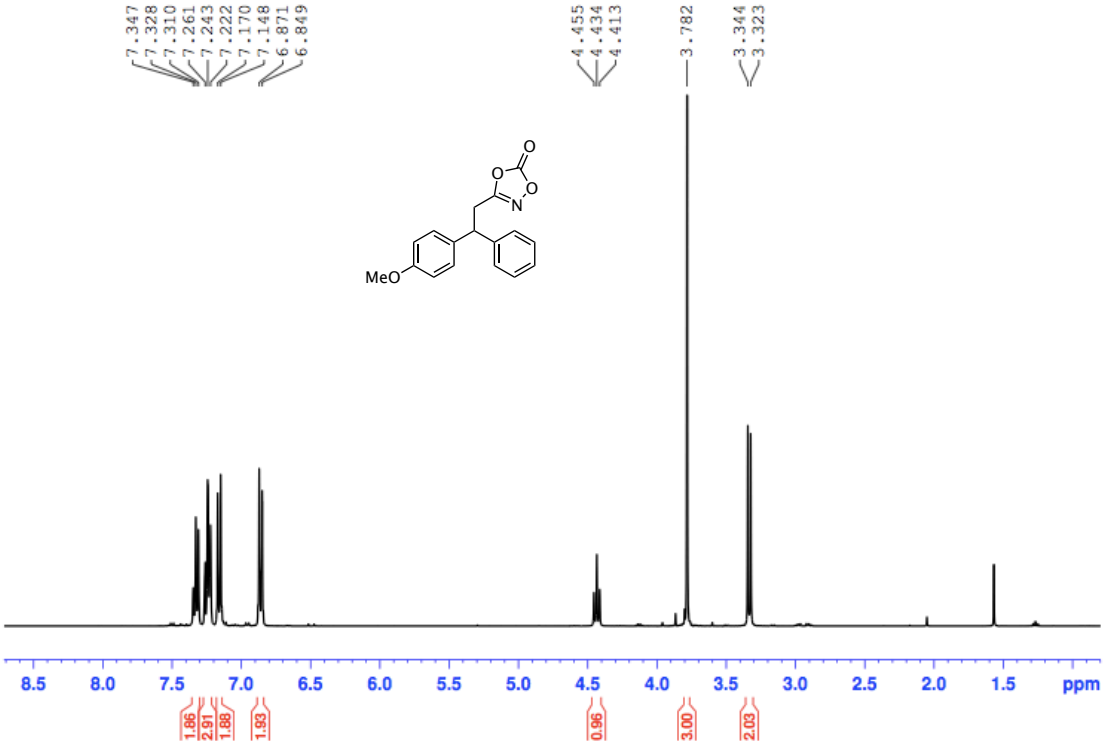

Figure S3.16 ^{13}C NMR Spectrum of 3-(2,2-bis(4-(trifluoromethyl)phenyl)ethyl)-1,4,2-dioxazol-5-one (***1h***)

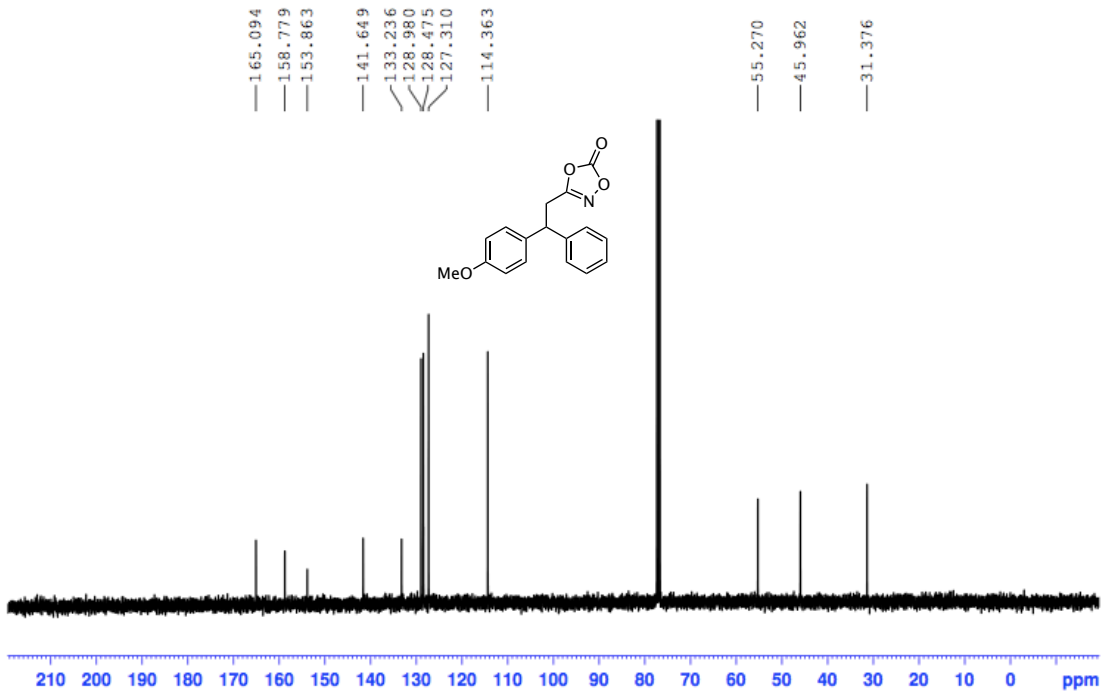

Figure S3.17 ^{1}H NMR Spectrum of 3-(4-methylphenethyl)-1,4,2-dioxazol-5-one (***1i***)

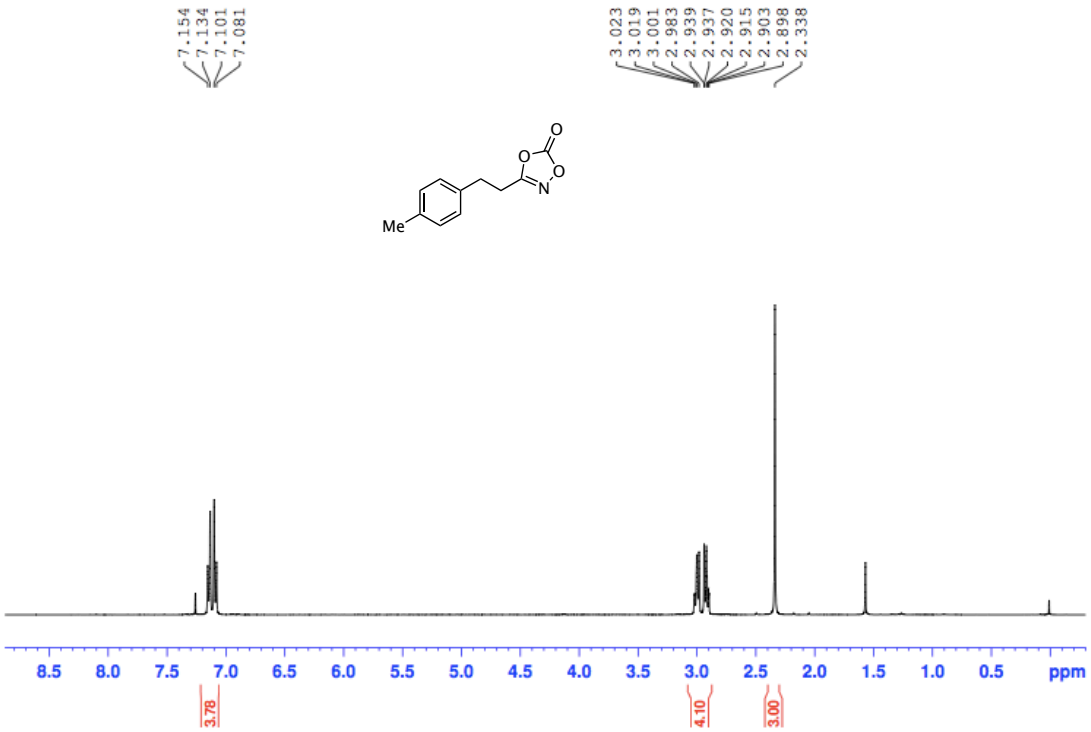

Figure S3.18 ^{13}C NMR Spectrum of 3-(4-methylphenethyl)-1,4,2-dioxazol-5-one (***1i***)

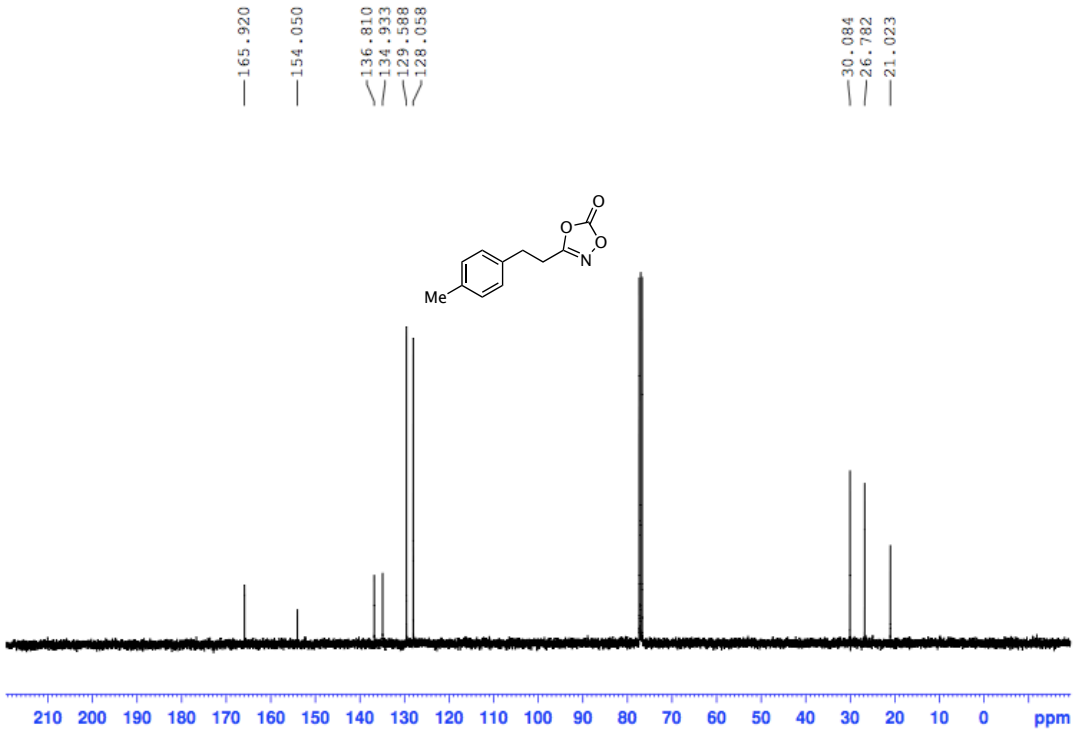

Figure S3.19 ^{1}H NMR Spectrum of 3-(4-methoxyphenethyl)-1,4,2-dioxazol-5-one (***1j***)

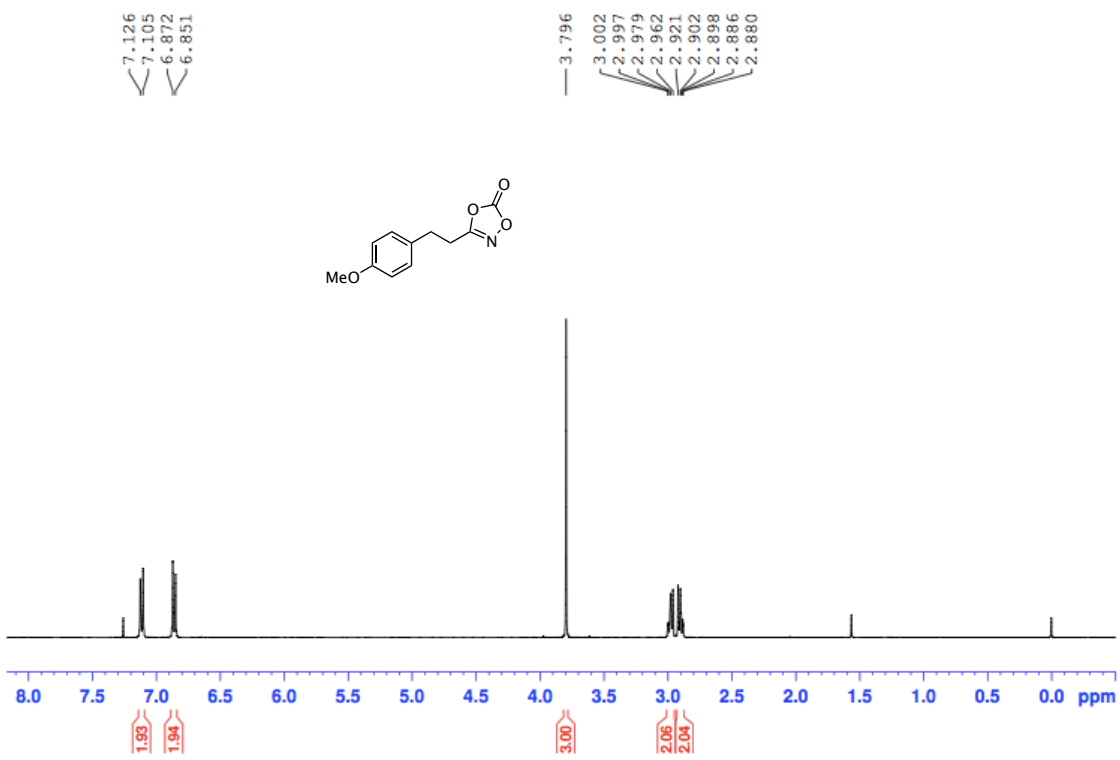

Figure S3.20 ^{13}C NMR Spectrum of 3-(4-methoxyphenethyl)-1,4,2-dioxazol-5-one (***1j***)

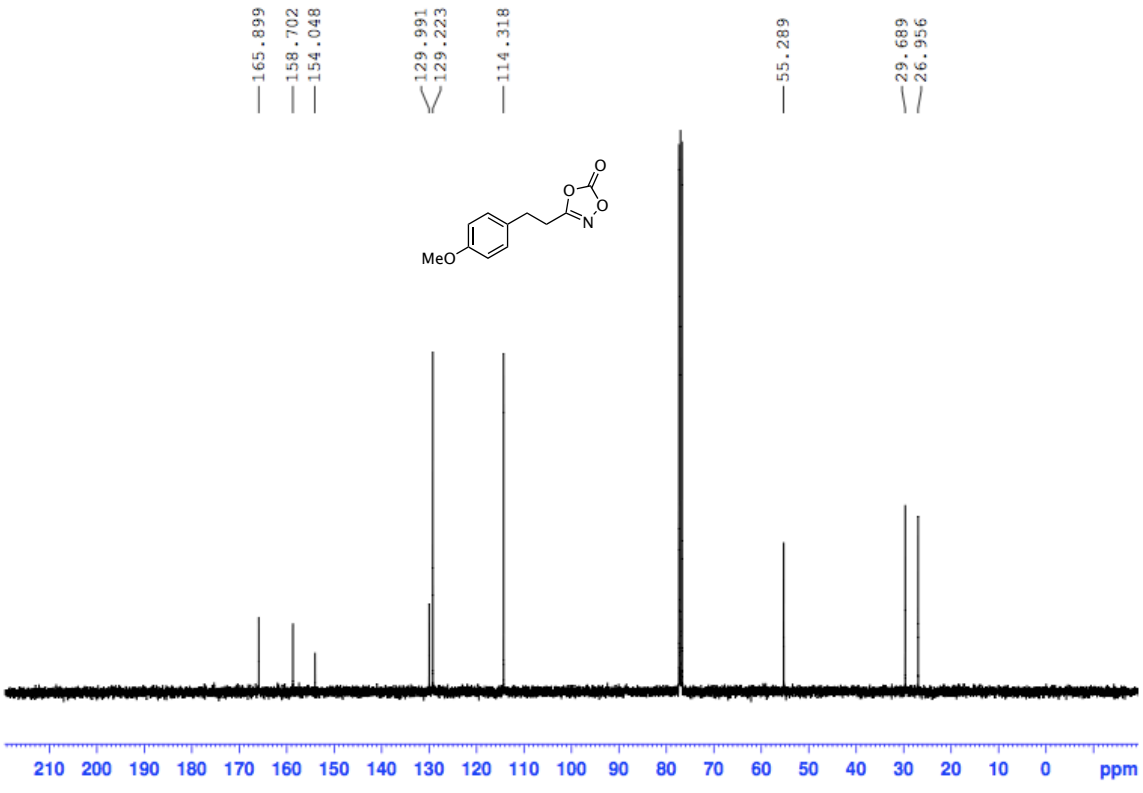

Figure S3.21 ^{1}H NMR Spectrum of 3-(4-bromophenethyl)-1,4,2-dioxazol-5-one (***1k***)

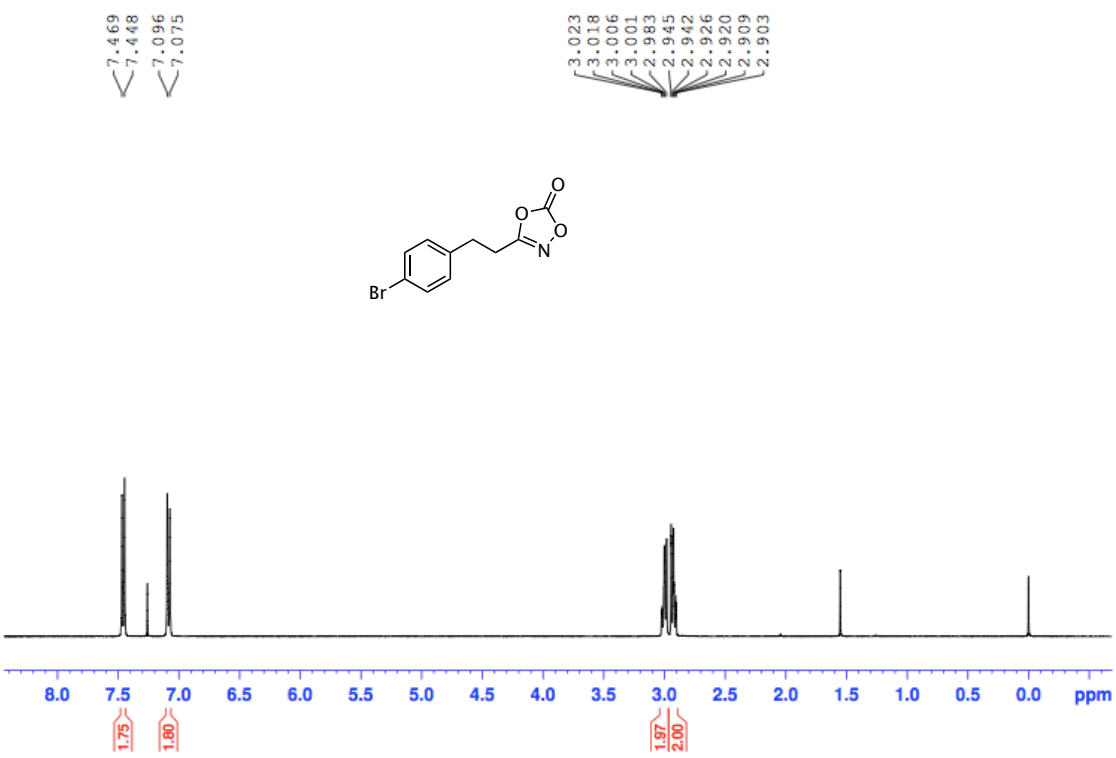

Figure S3.22 ^{13}C NMR Spectrum of 3-(4-bromophenethyl)-1,4,2-dioxazol-5-one (***1k***)

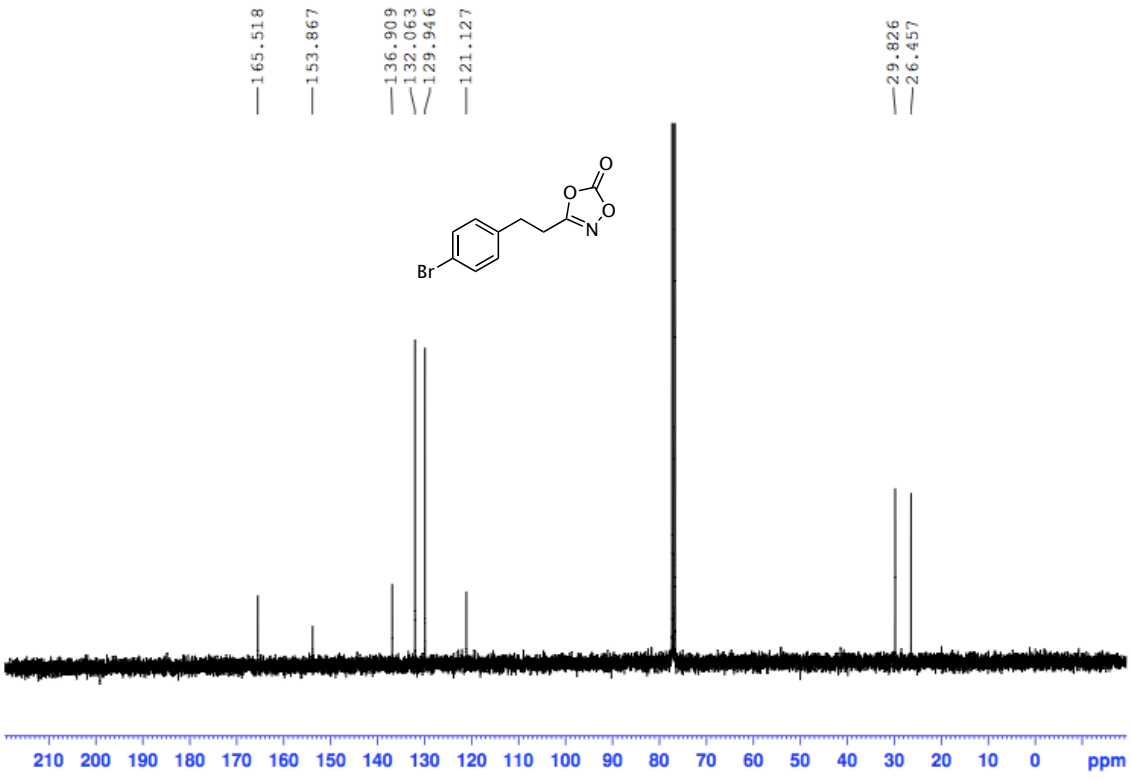

Figure S3.23 ^{1}H NMR Spectrum of 3-(2-methylphenethyl)-1,4,2-dioxazol-5-one (***1l***)

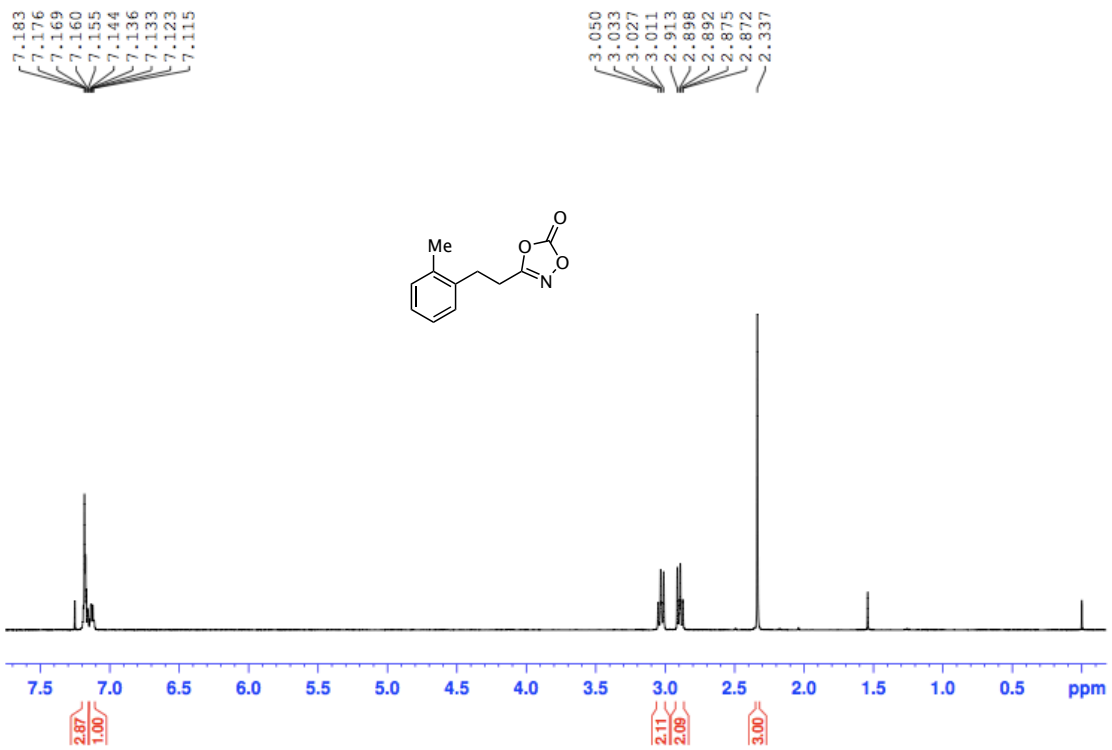

Figure S3.24 ^{13}C NMR Spectrum of 3-(2-methylphenethyl)-1,4,2-dioxazol-5-one (***1l***)

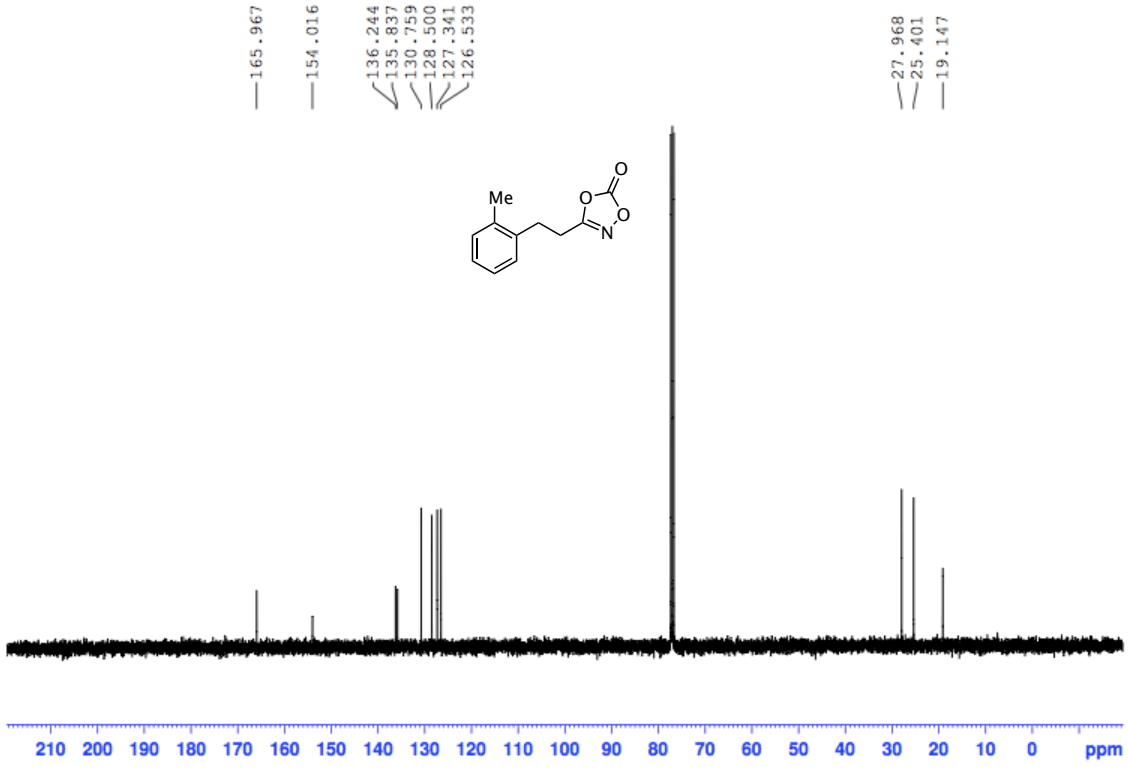

Figure S3.25 ^{1}H NMR Spectrum of 3-(2-methoxyphenethyl)-1,4,2-dioxazol-5-one (***1m***)

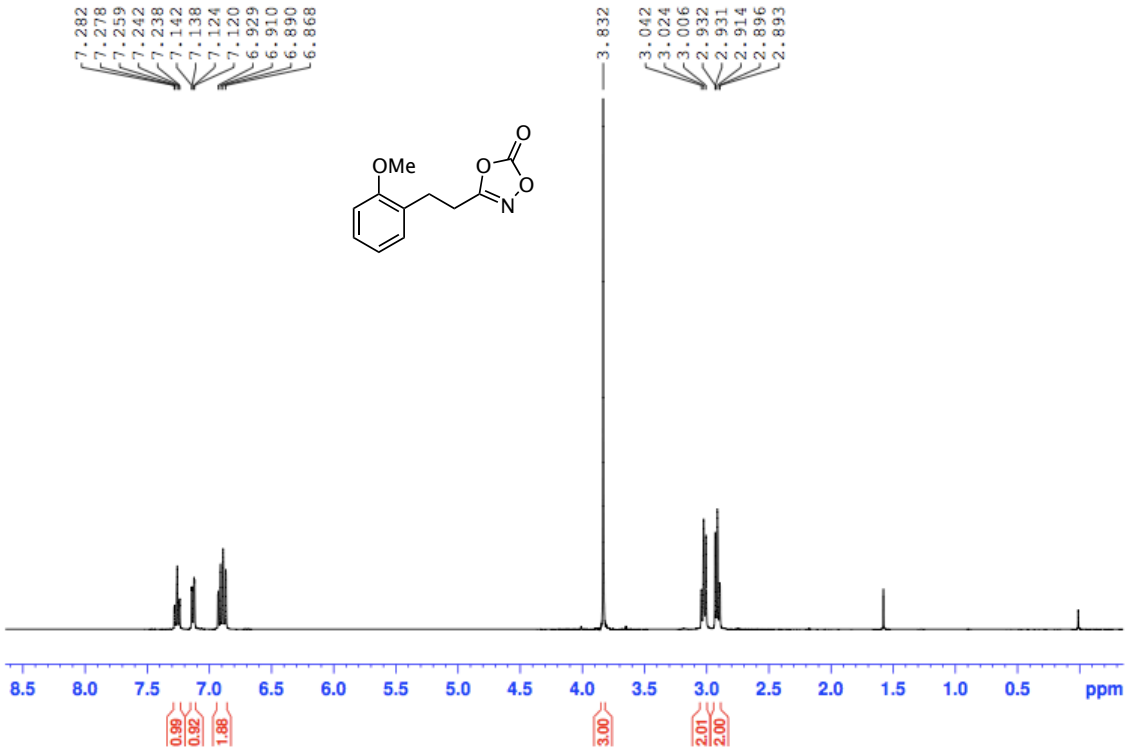

Figure S3.26 ^{13}C NMR Spectrum of 3-(2-methoxyphenethyl)-1,4,2-dioxazol-5-one (***1m***)

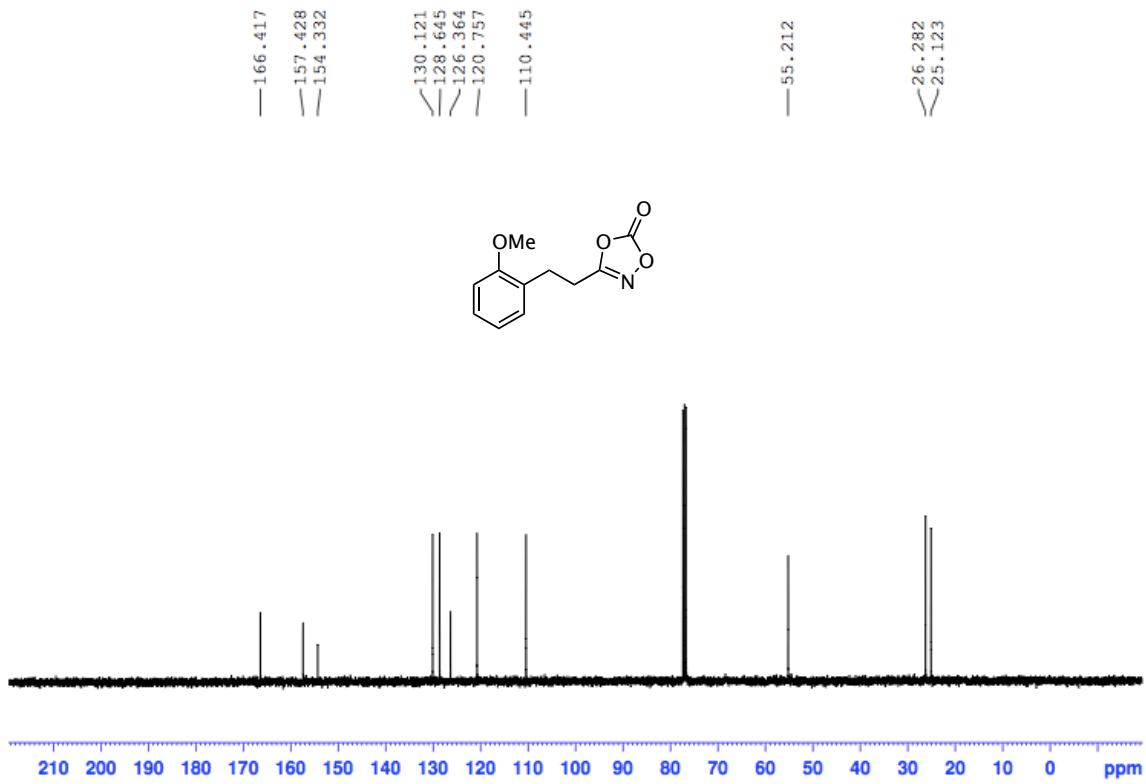

Figure S3.27 ^{1}H NMR Spectrum of 3-(2-bromophenethyl)-1,4,2-dioxazol-5-one (***1n***)

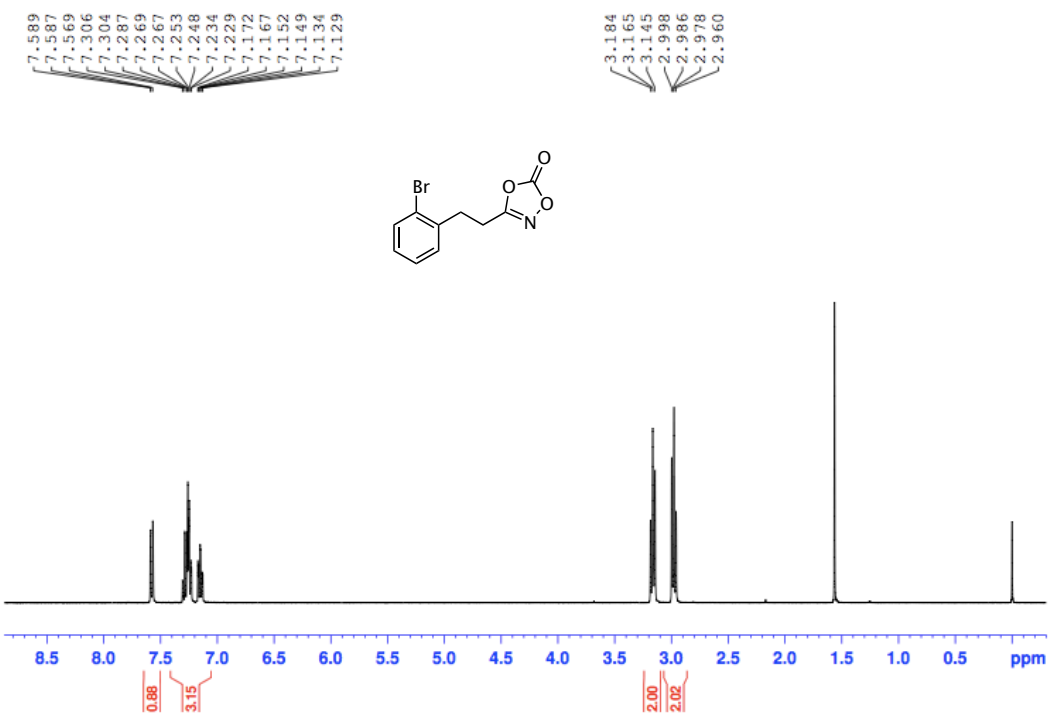

Figure S3.28 ^{13}C NMR Spectrum of 3-(2-bromophenethyl)-1,4,2-dioxazol-5-one (***1n***)

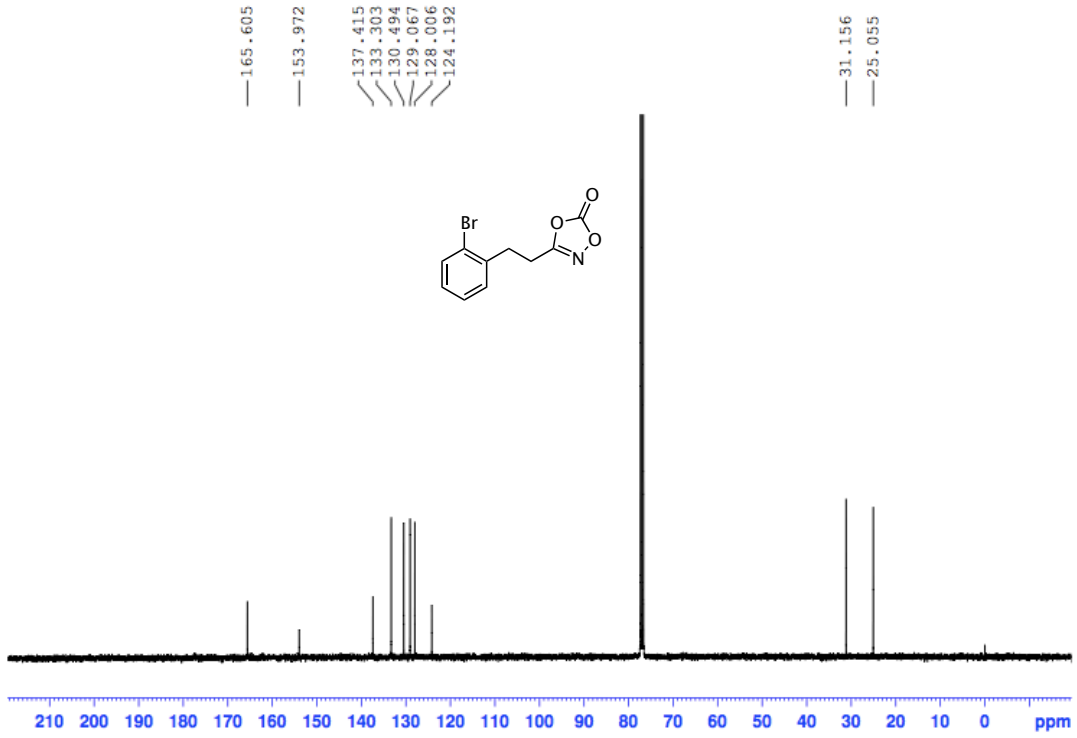

Figure S3.29 ^{1}H NMR Spectrum of 3-(3-methylphenethyl)-1,4,2-dioxazol-5-one (***1o***)

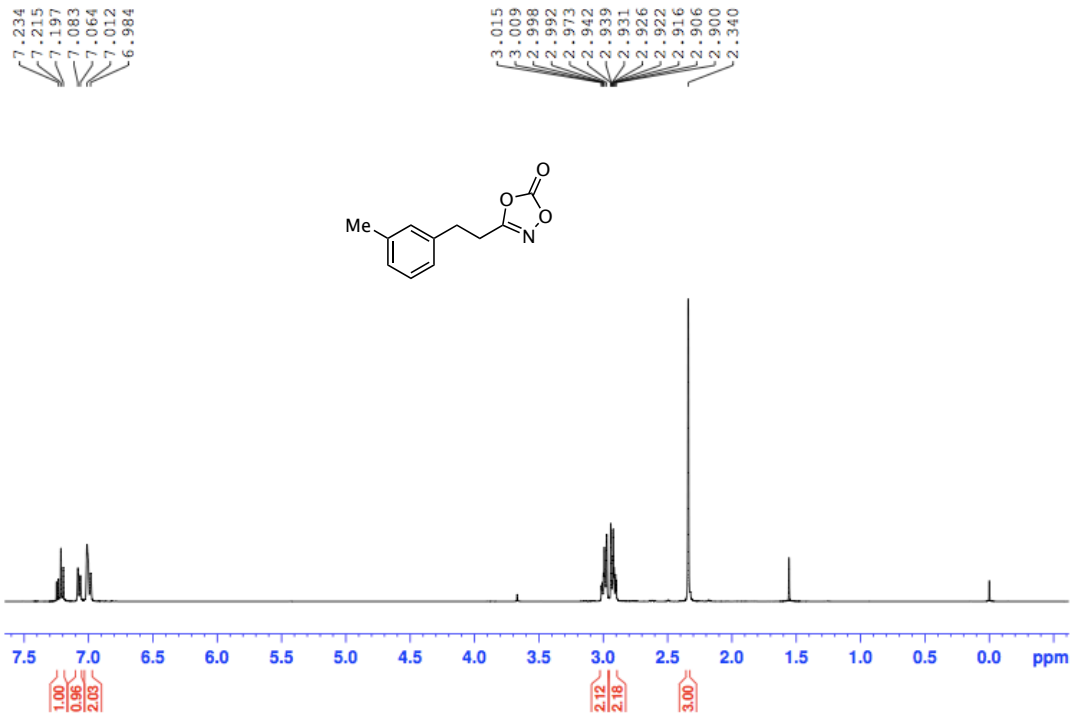

Figure S3.30 ^{13}C NMR Spectrum of 3-(3-methylphenethyl)-1,4,2-dioxazol-5-one (***1o***)

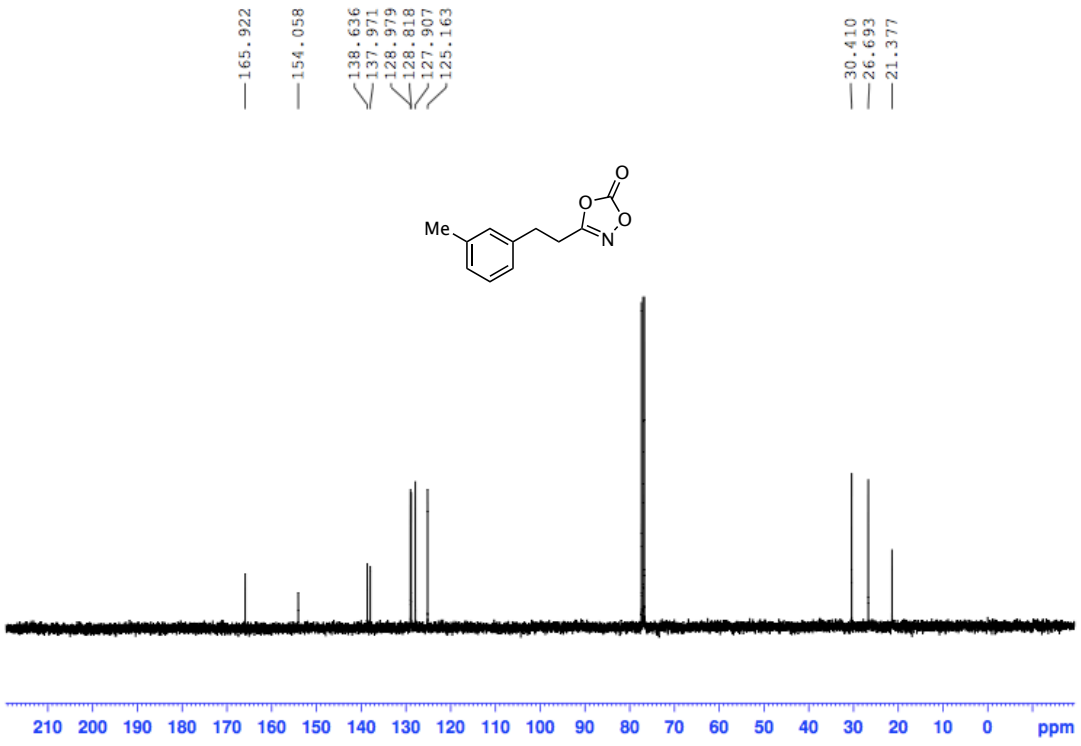

Figure S3.31 ^{1}H NMR Spectrum of 3-(3-methoxyphenethyl)-1,4,2-dioxazol-5-one (***1p***)

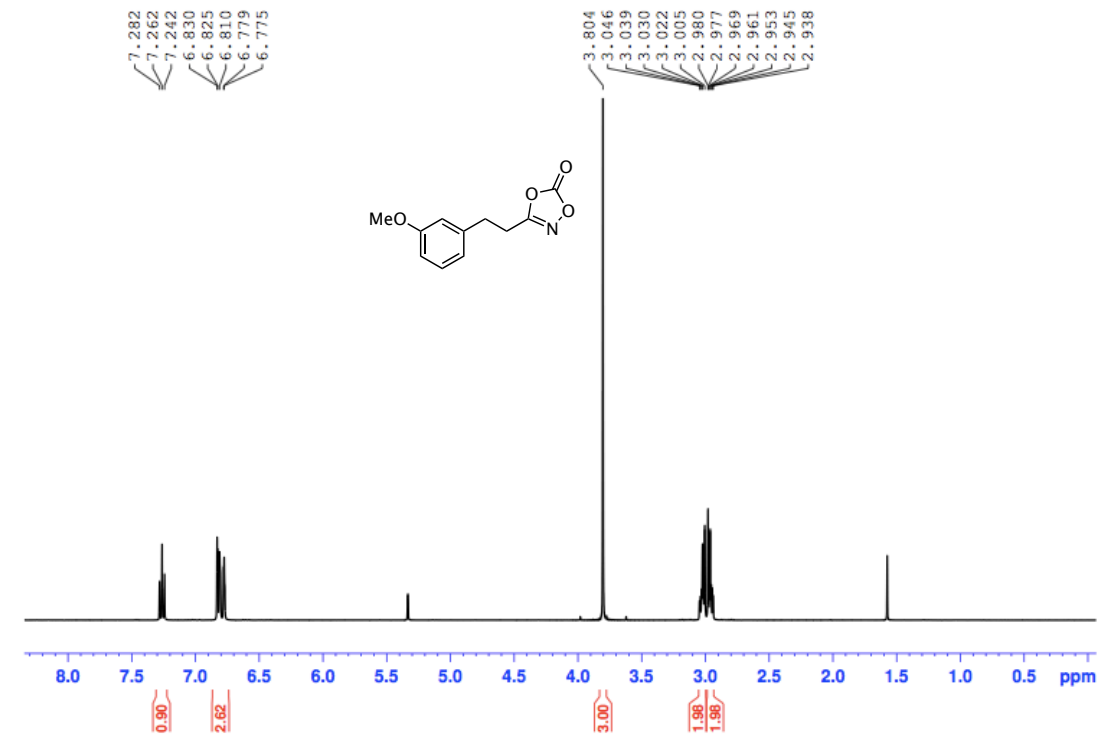

Figure S3.32 ^{13}C NMR Spectrum of 3-(3-methoxyphenethyl)-1,4,2-dioxazol-5-one (***1p***)

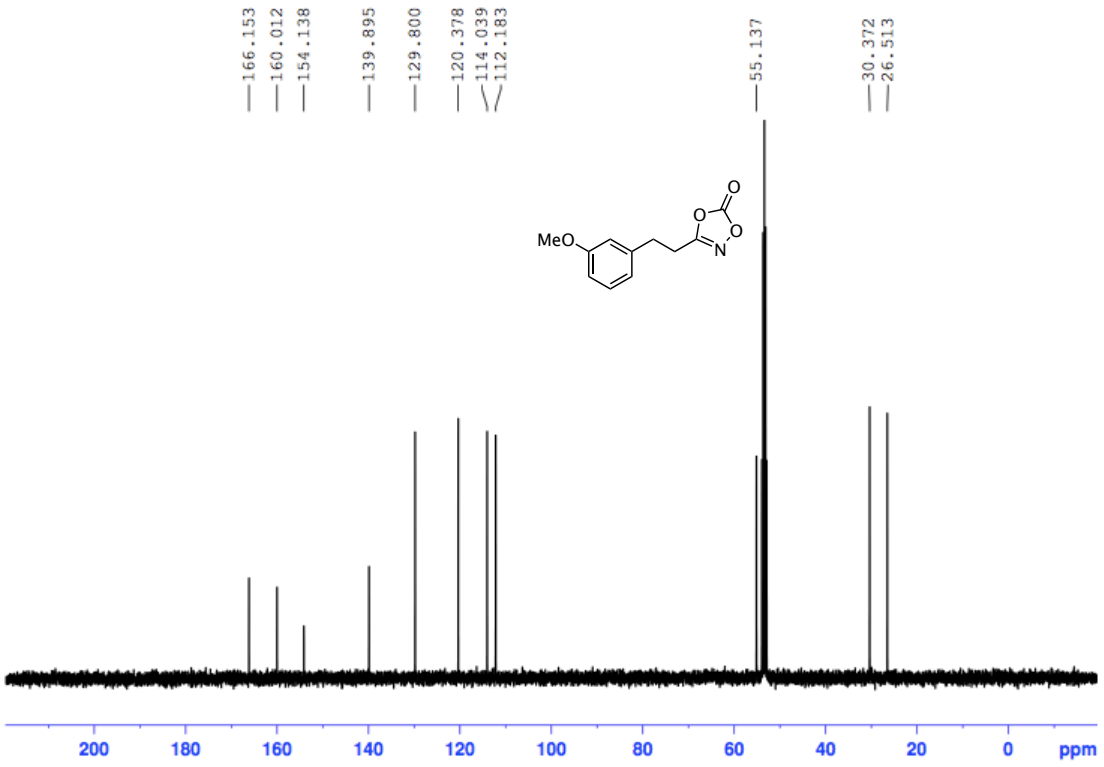

Figure S3.33 ^{1}H NMR Spectrum of 3-(3-bromophenethyl)-1,4,2-dioxazol-5-one (***1q***)

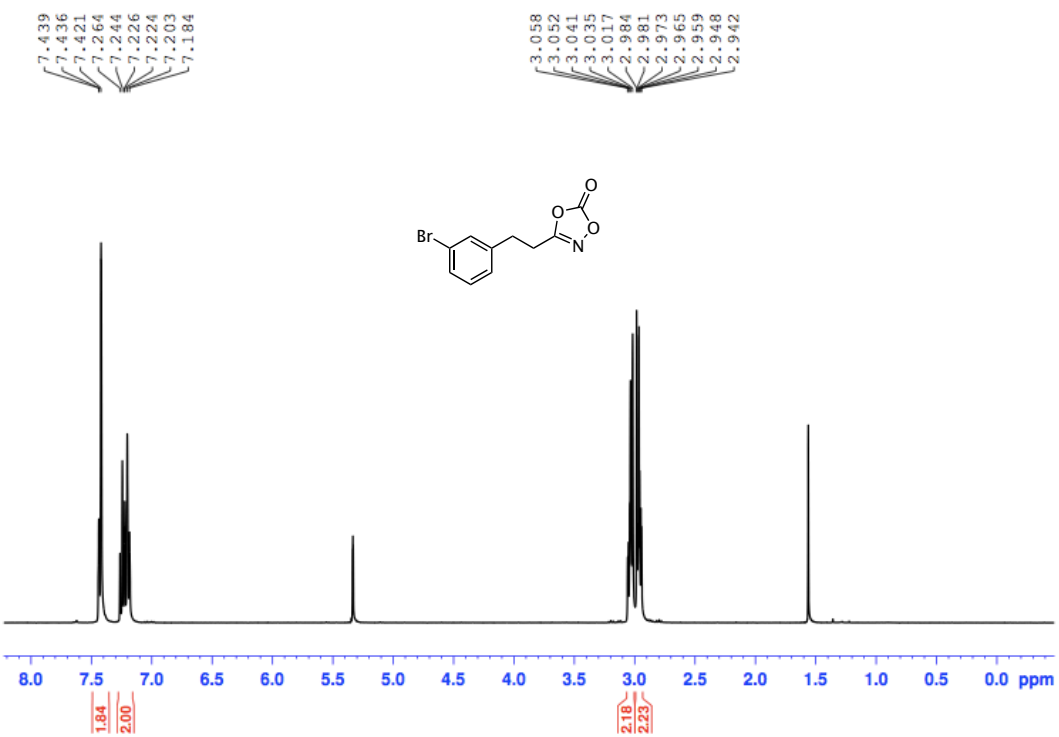

Figure S3.34 ^{13}C NMR Spectrum of 3-(3-bromophenethyl)-1,4,2-dioxazol-5-one (***1q***)

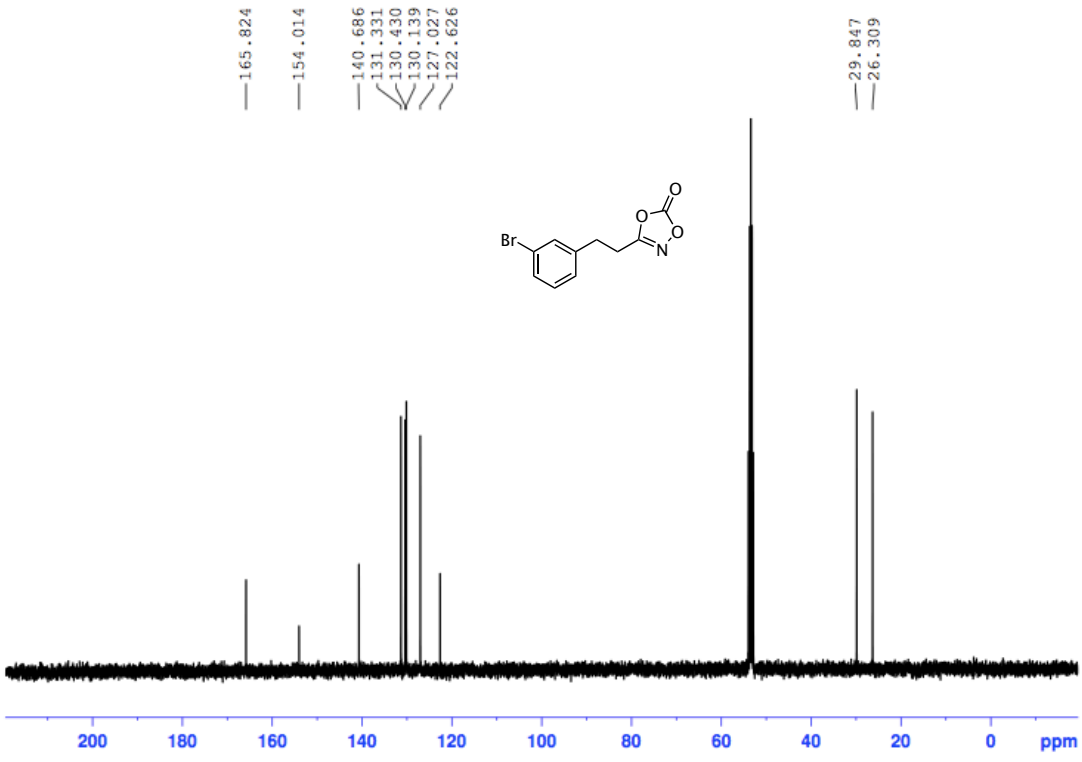

Figure S3.35 ^{1}H NMR Spectrum of 3-(3,4-dimethoxyphenethyl)-1,4,2-dioxazol-5-one (***1r***)

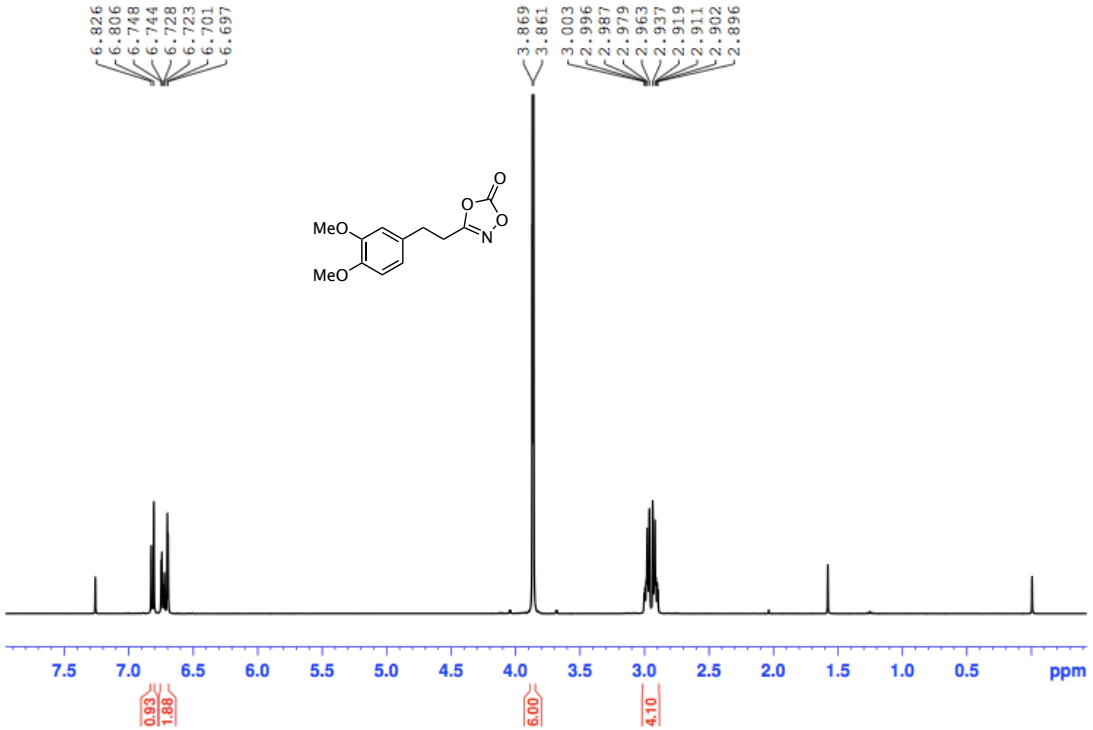

Figure S3.36 ^{13}C NMR Spectrum of 3-(3,4-dimethoxyphenethyl)-1,4,2-dioxazol-5-one (***1r***)

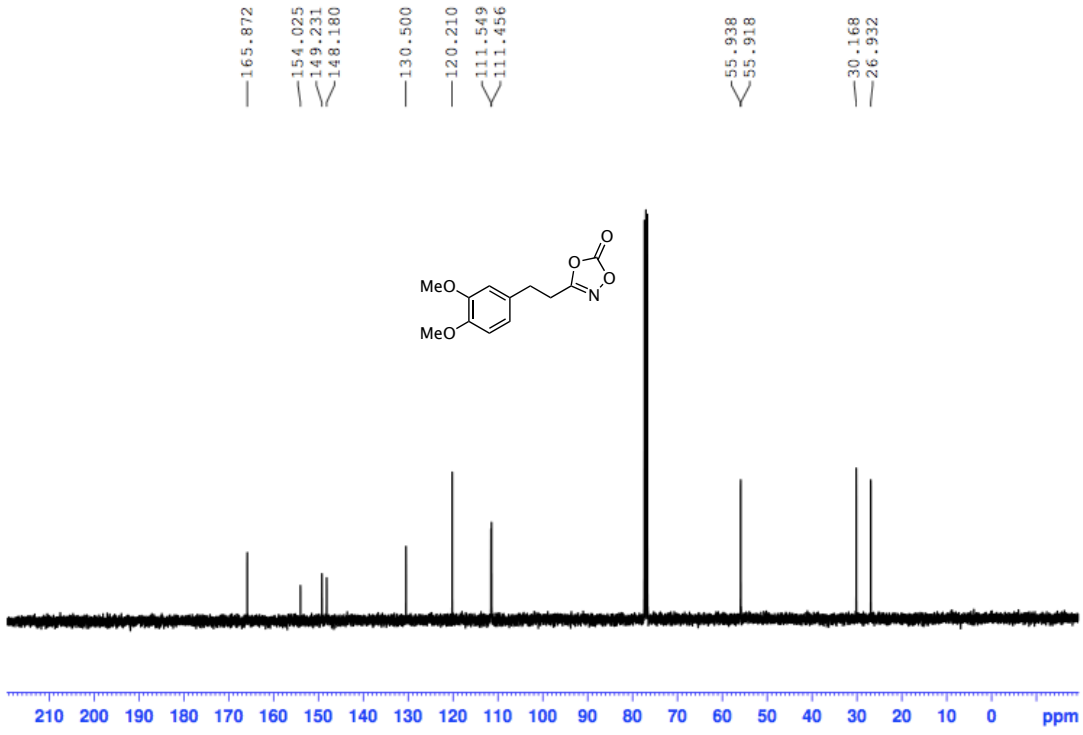

Figure S3.37 ^{1}H NMR Spectrum of 3-(3-methyl-2-phenylbutyl)-1,4,2-dioxazol-5-one (***1u***)

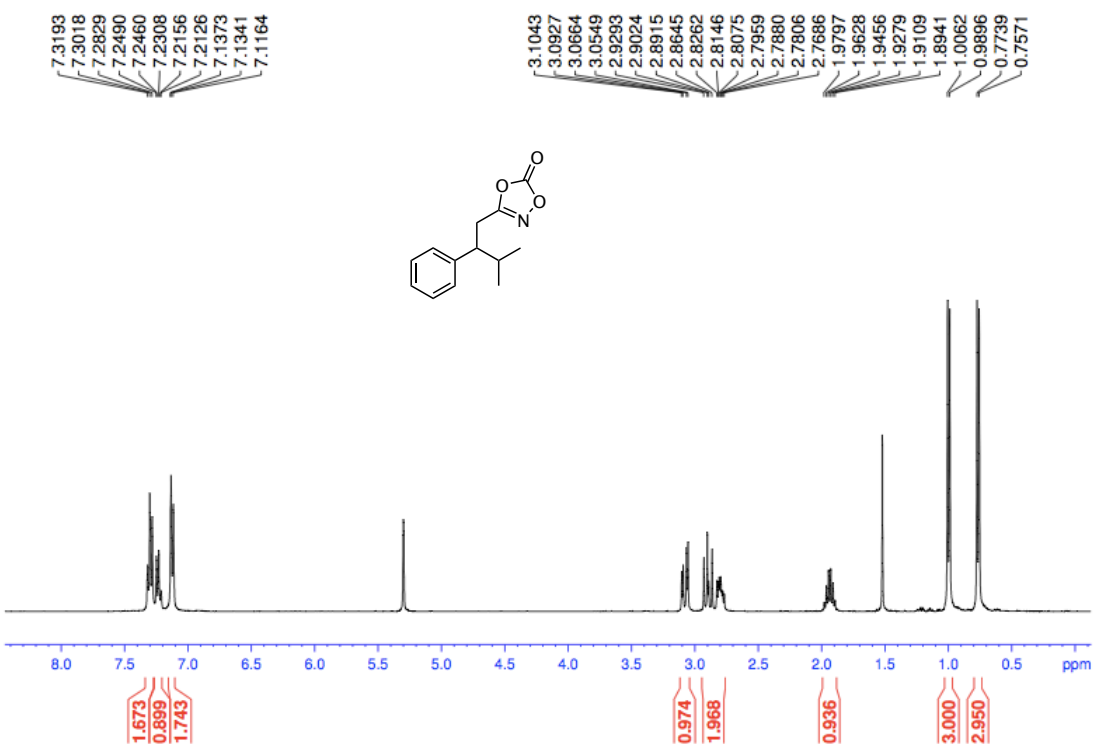

Figure S3.38 ^{13}C NMR Spectrum of 3-(3-methyl-2-phenylbutyl)-1,4,2-dioxazol-5-one (***1u***)

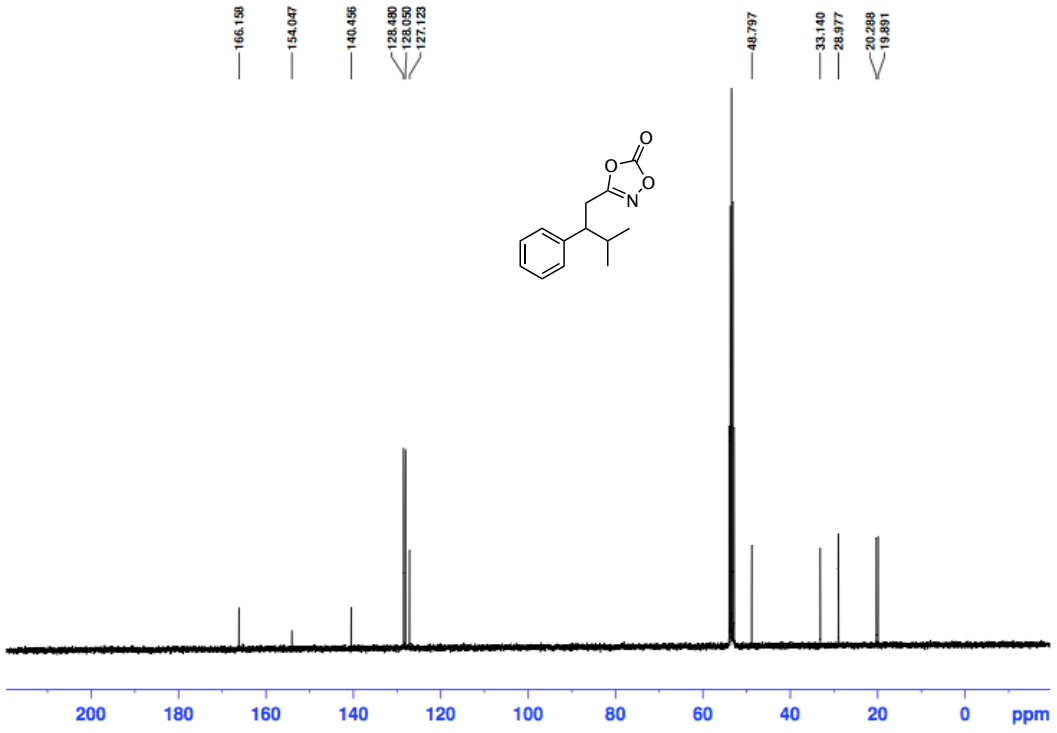

Figure S3.39 ^{1}H NMR Spectrum of 3-(3-methyl-2-(*p*-tolyl)butyl)-1,4,2-dioxazol-5-one (***1v***)

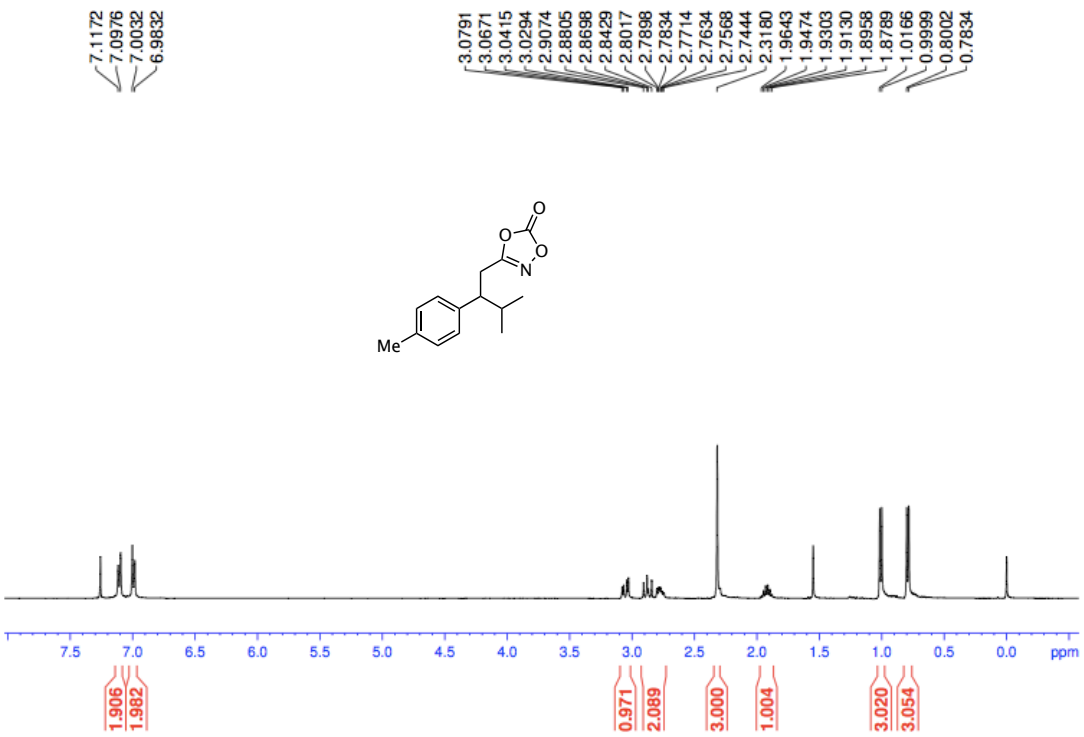

Figure S3.40 ^{13}C NMR Spectrum of 3-(3-methyl-2-(*p*-tolyl)butyl)-1,4,2-dioxazol-5-one (***1v***)

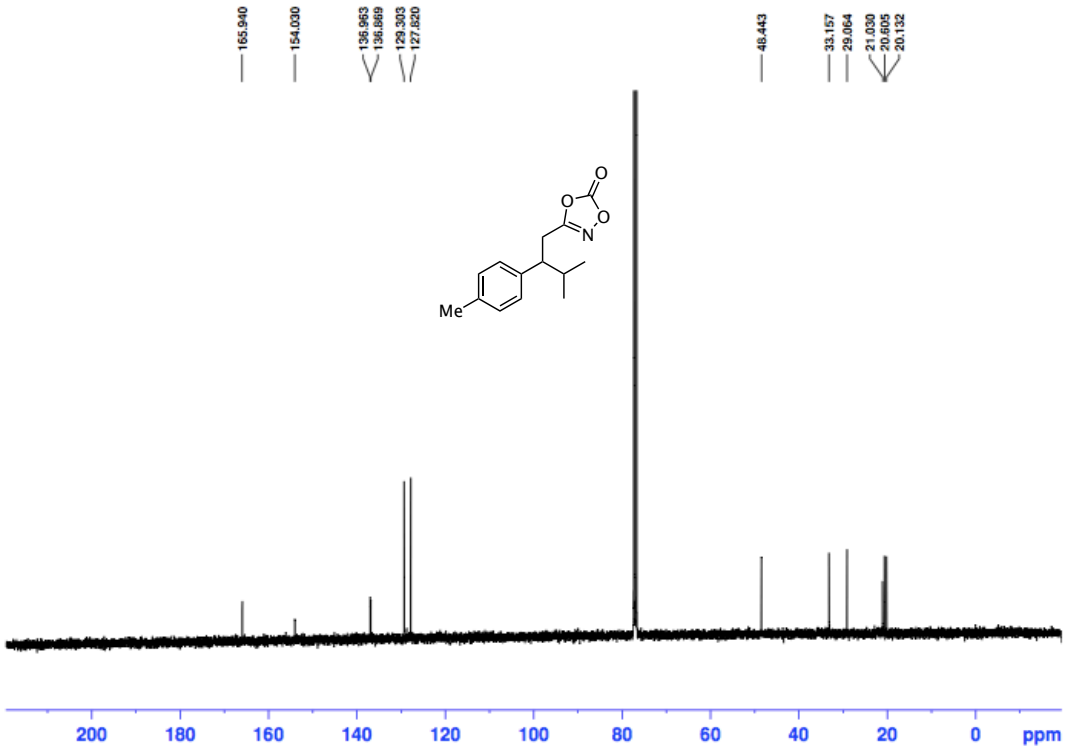

Figure S3.41 ^{1}H NMR Spectrum of 3-(2-(4-methoxyphenyl)-3-methylbutyl)-1,4,2-dioxazol-5-one (***1w***)

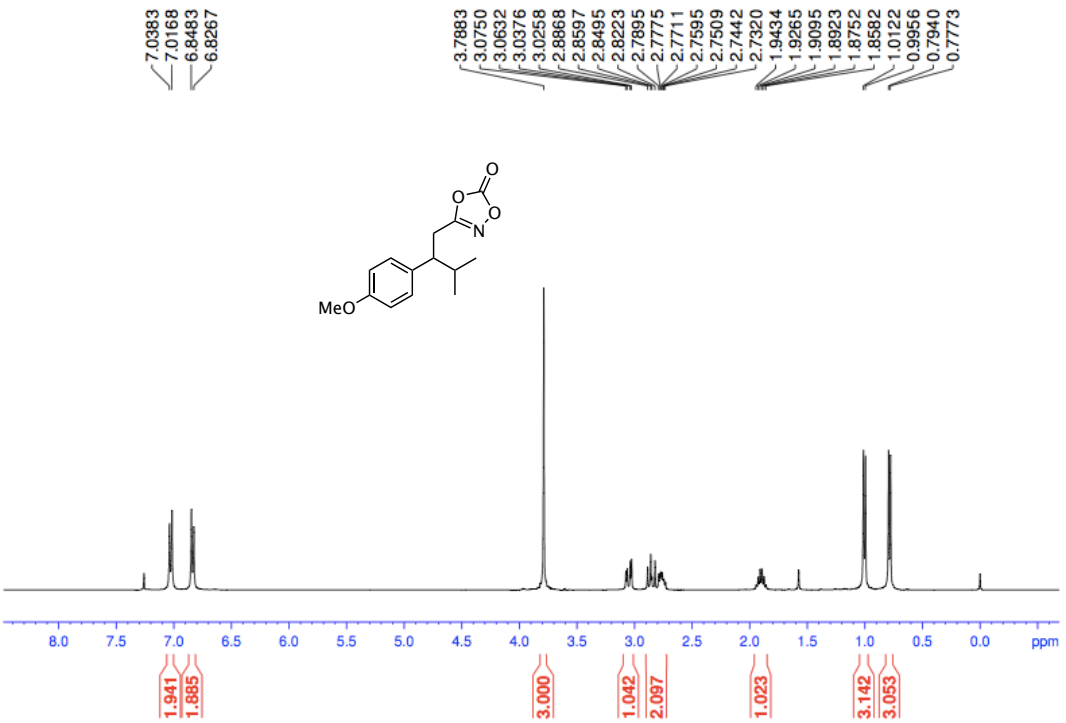

Figure S3.42 ^{13}C NMR Spectrum of 3-(2-(4-methoxyphenyl)-3-methylbutyl)-1,4,2-dioxazol-5-one (***1w***)

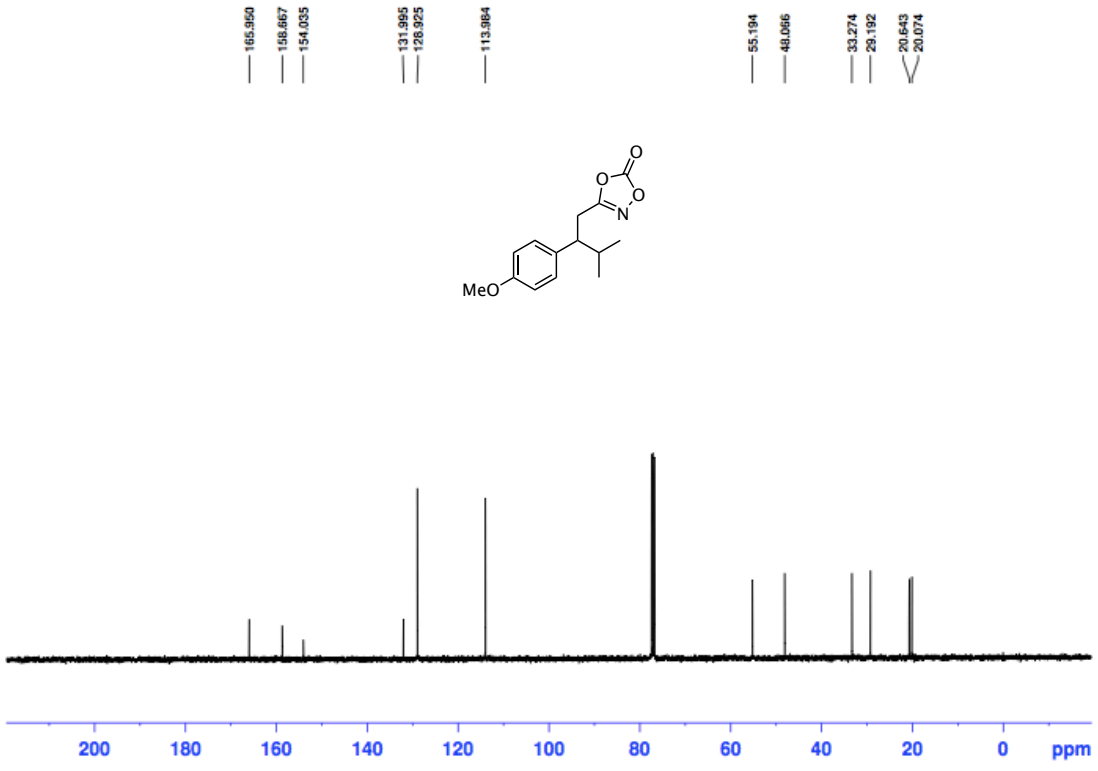

Figure S3.43 ^{1}H NMR Spectrum of 3-(2-(4-fluorophenyl)-3-methylbutyl)-1,4,2-dioxazol-5-one (***1x***)

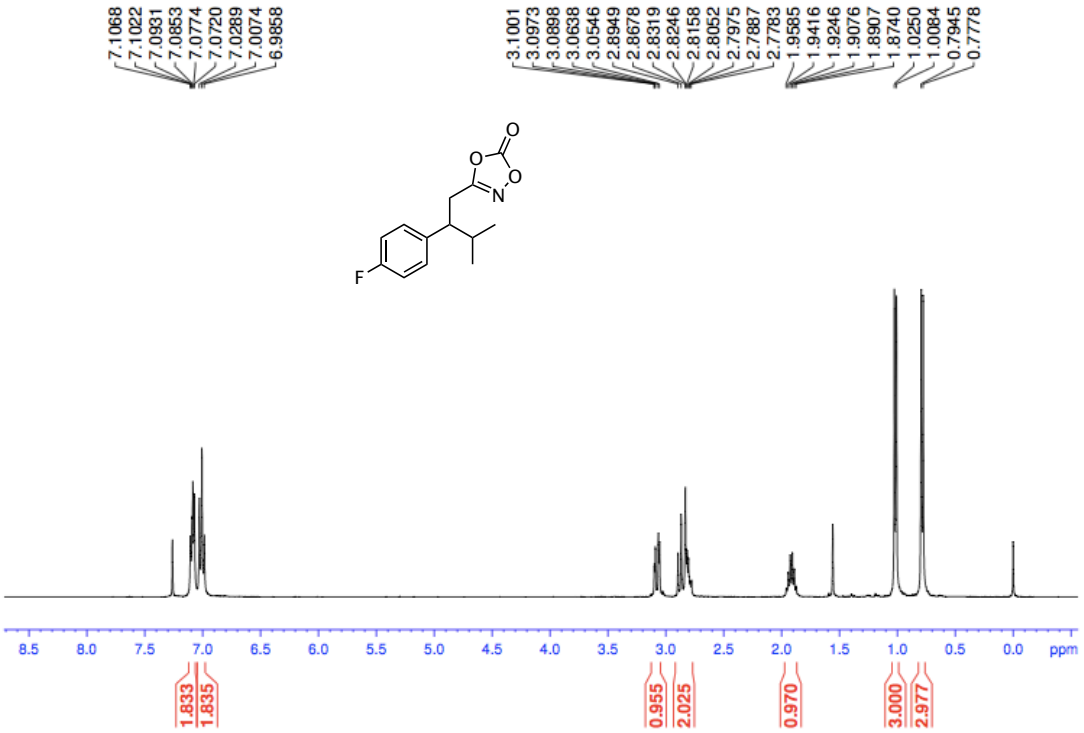

Figure S3.44 ^{13}C NMR Spectrum of 3-(2-(4-fluorophenyl)-3-methylbutyl)-1,4,2-dioxazol-5-one (***1x***)

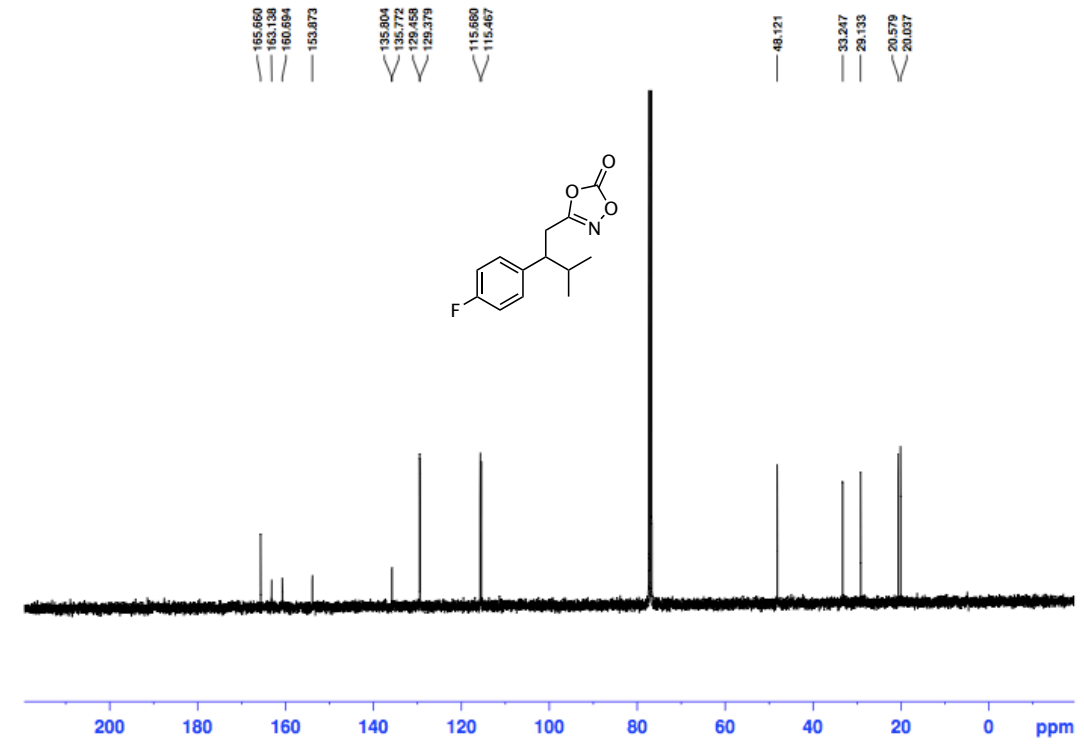

Figure S3.45 ^{1}H NMR Spectrum of 3-(2-(4-chlorophenyl)-3-methylbutyl)-1,4,2-dioxazol-5-one (***1y***)

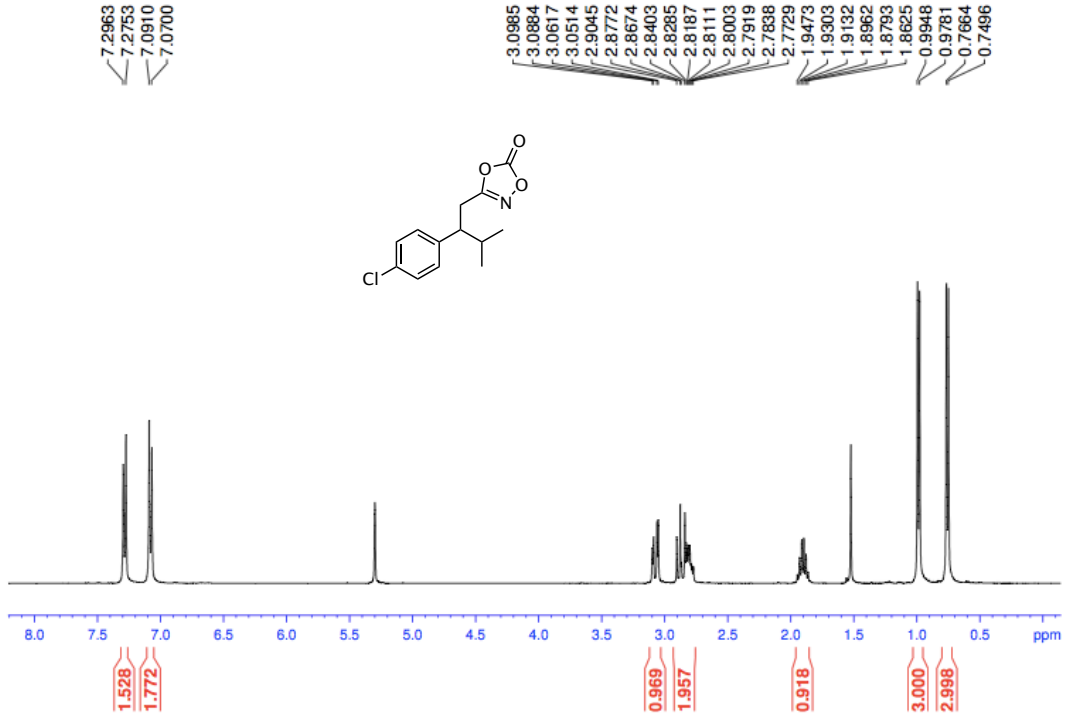

Figure S3.46 ^{13}C NMR Spectrum of 3-(2-(4-chlorophenyl)-3-methylbutyl)-1,4,2-dioxazol-5-one (***1y***)

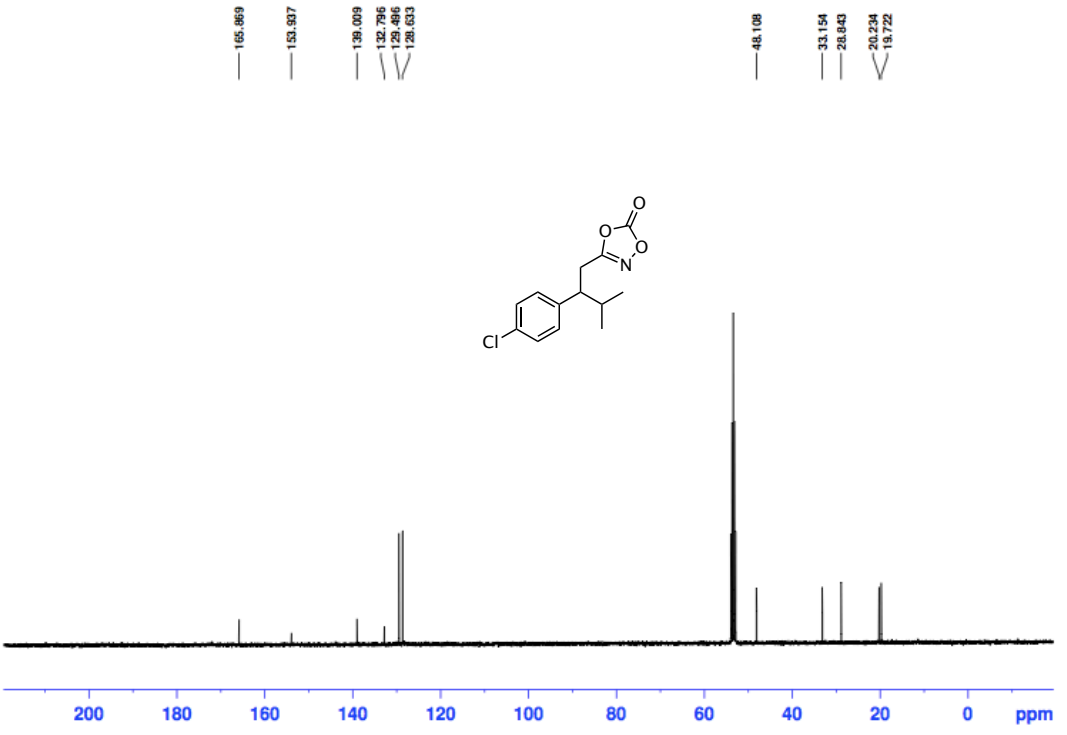

Figure S3.47 ^{1}H NMR Spectrum of 3-(2-(4-bromophenyl)-3-methylbutyl)-1,4,2-dioxazol-5-one (***1z***)

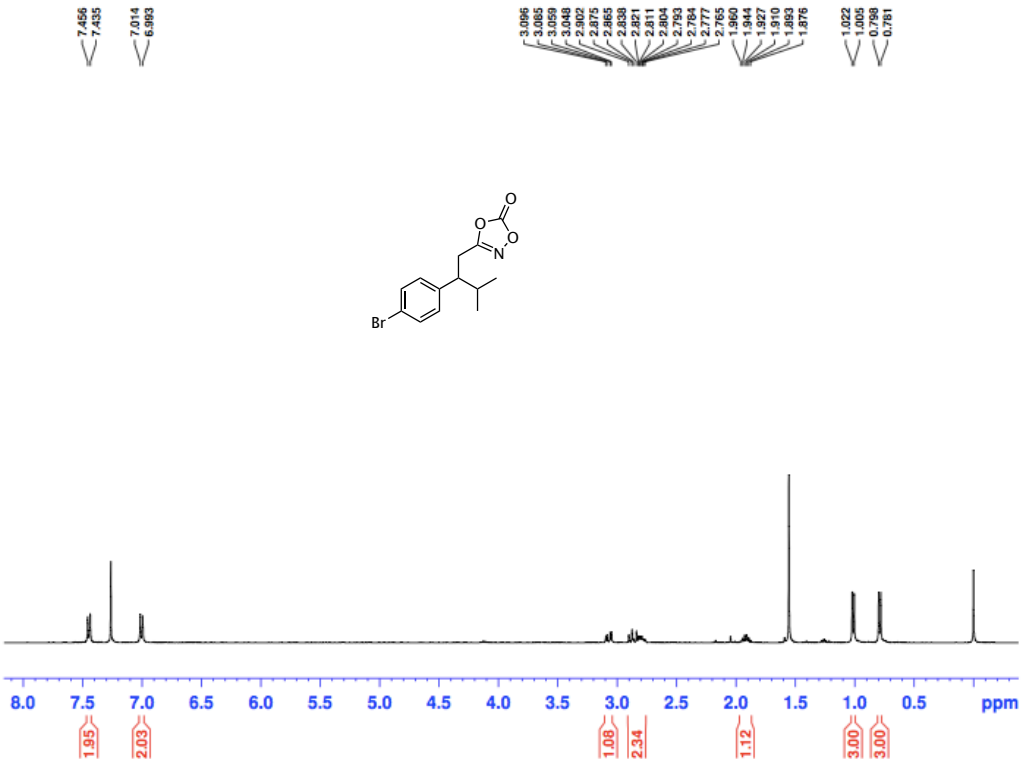

Figure S3.48 ^{13}C NMR Spectrum of 3-(2-(4-bromophenyl)-3-methylbutyl)-1,4,2-dioxazol-5-one (***1z***)

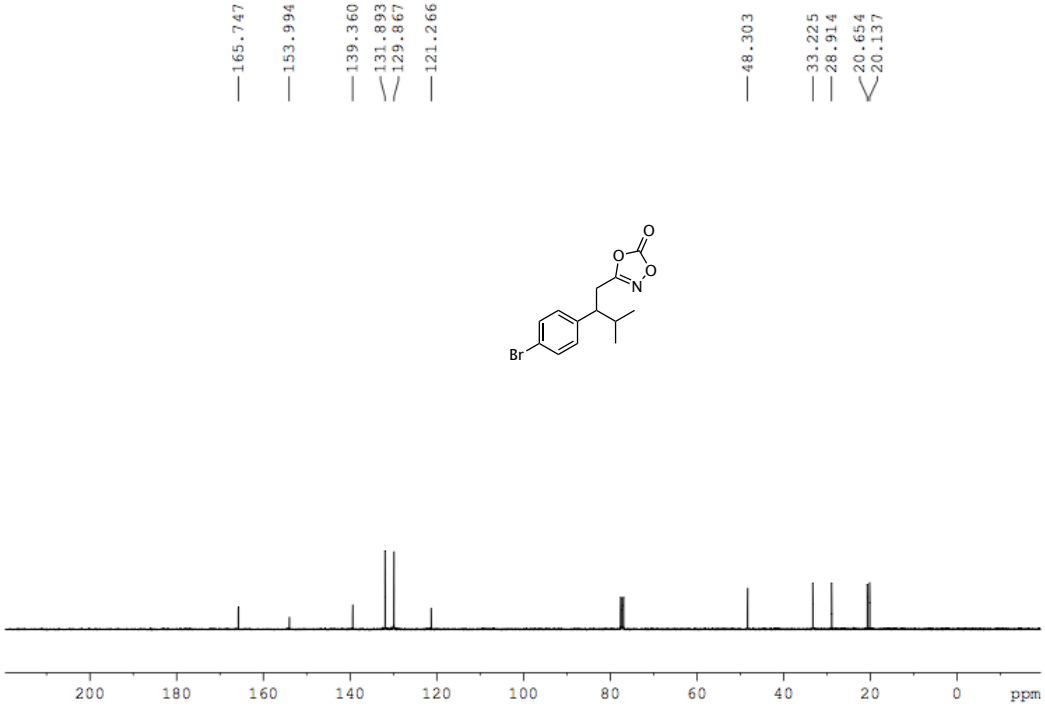

Figure S3.49 ^{1}H NMR Spectrum of 3-(4-hydroxyphenethyl)-1,4,2-dioxazol-5-one (***4a***)

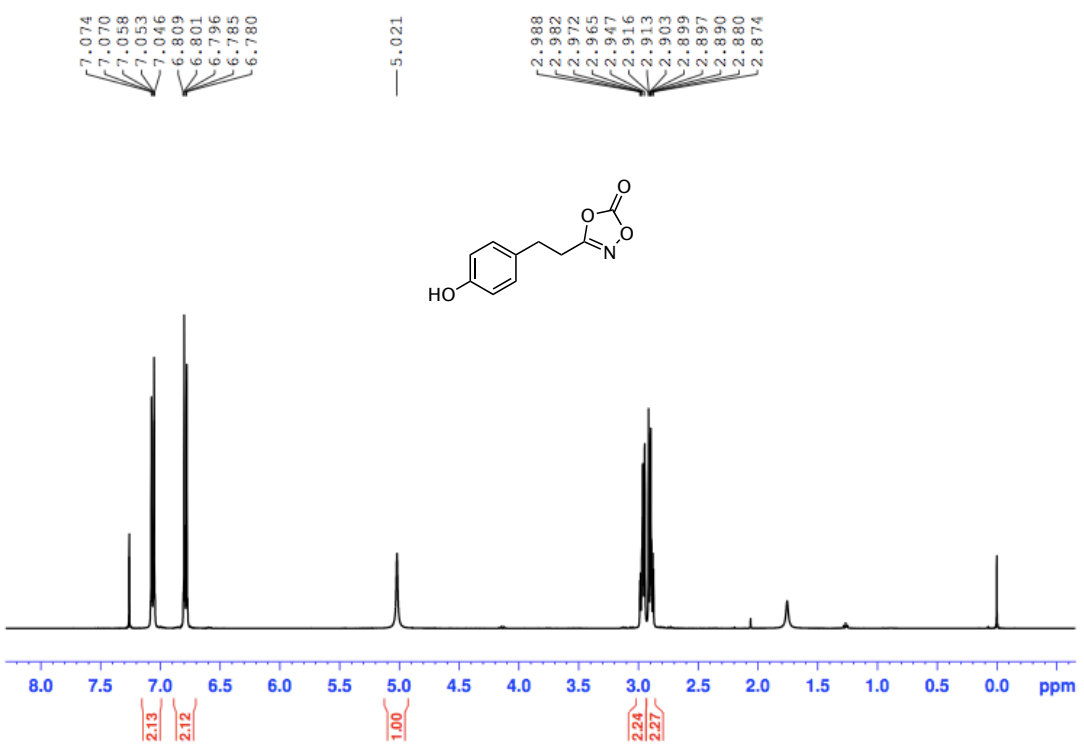

Figure S3.50 ^{13}C NMR Spectrum of 3-(4-hydroxyphenethyl)-1,4,2-dioxazol-5-one (***4a***)

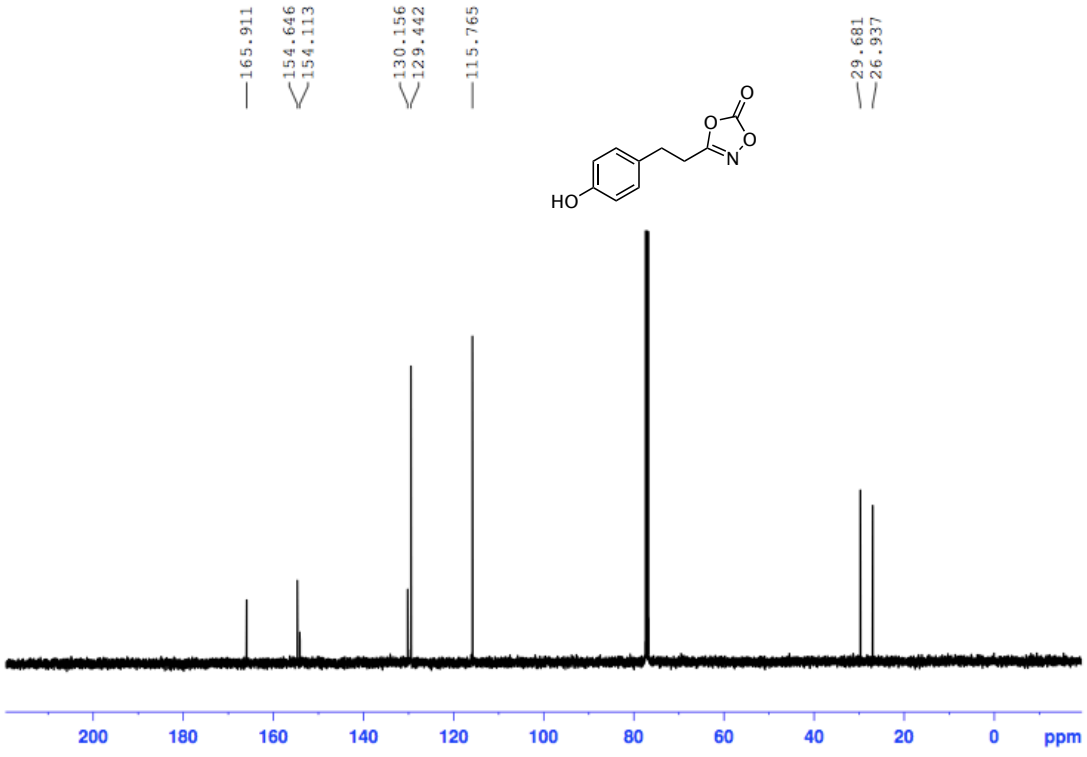

Figure S3.51 ^{1}H NMR Spectrum of 3-(4-hydroxy-3-methoxyphenethyl)-1,4,2-dioxazol-5-one (***4b***)

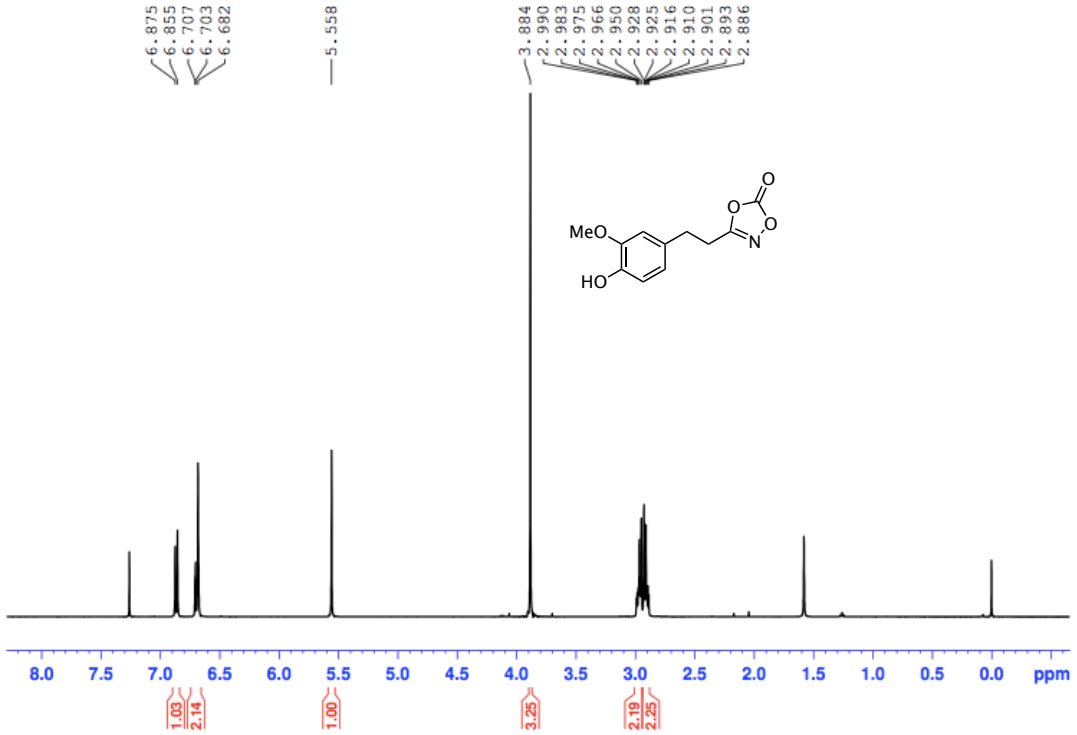

Figure S3.52 ^{13}C NMR Spectrum of 3-(4-hydroxy-3-methoxyphenethyl)-1,4,2-dioxazol-5-one (***4b***)

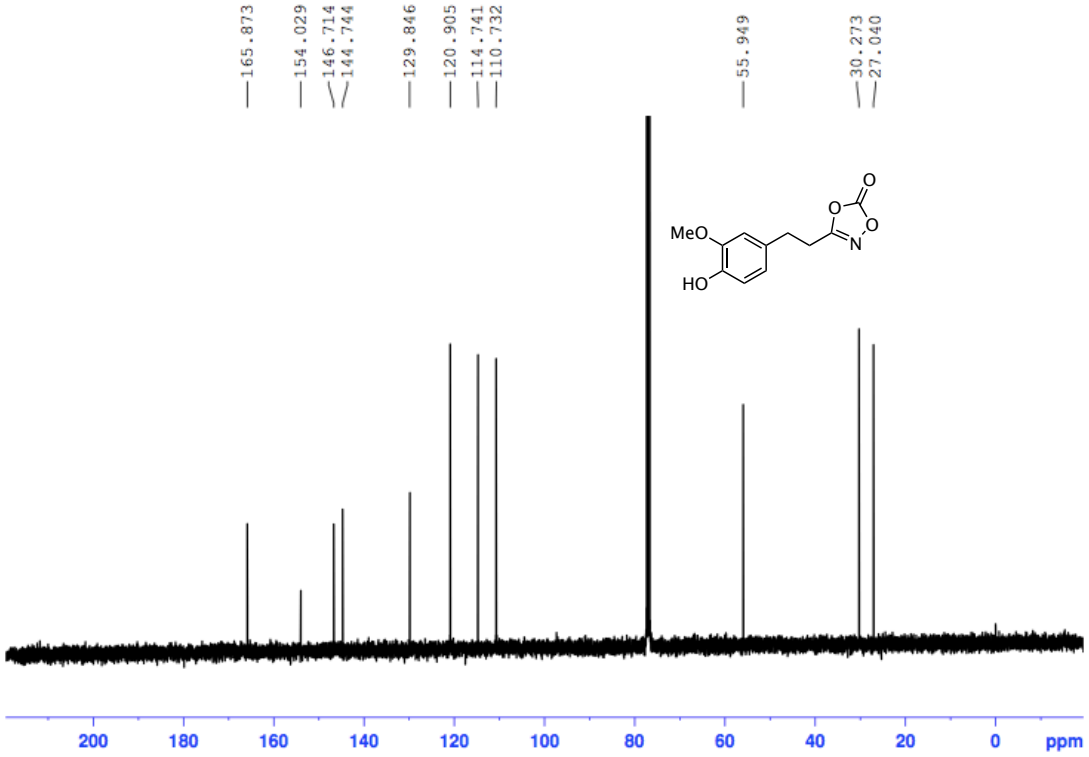

Figure S3.53 ^{1}H NMR Spectrum of 3-(4-hydroxy-2-methoxyphenethyl)-1,4,2-dioxazol-5-one (***4c***)

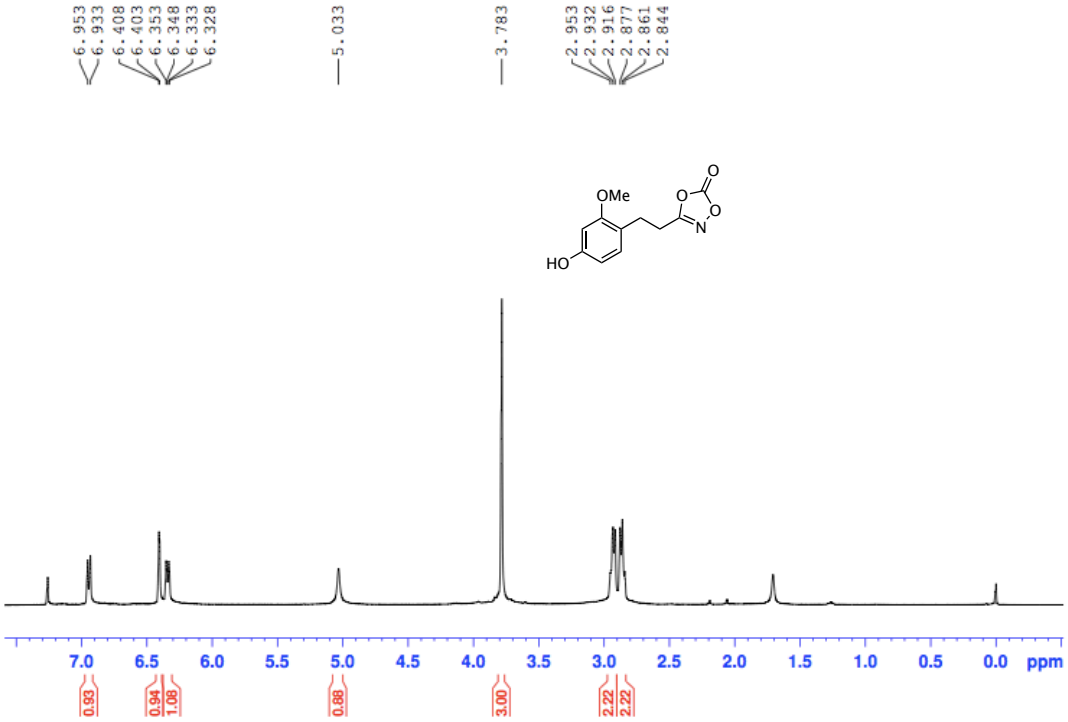

Figure S3.54 ^{13}C NMR Spectrum of 3-(4-hydroxy-2-methoxyphenethyl)-1,4,2-dioxazol-5-one (***4c***)

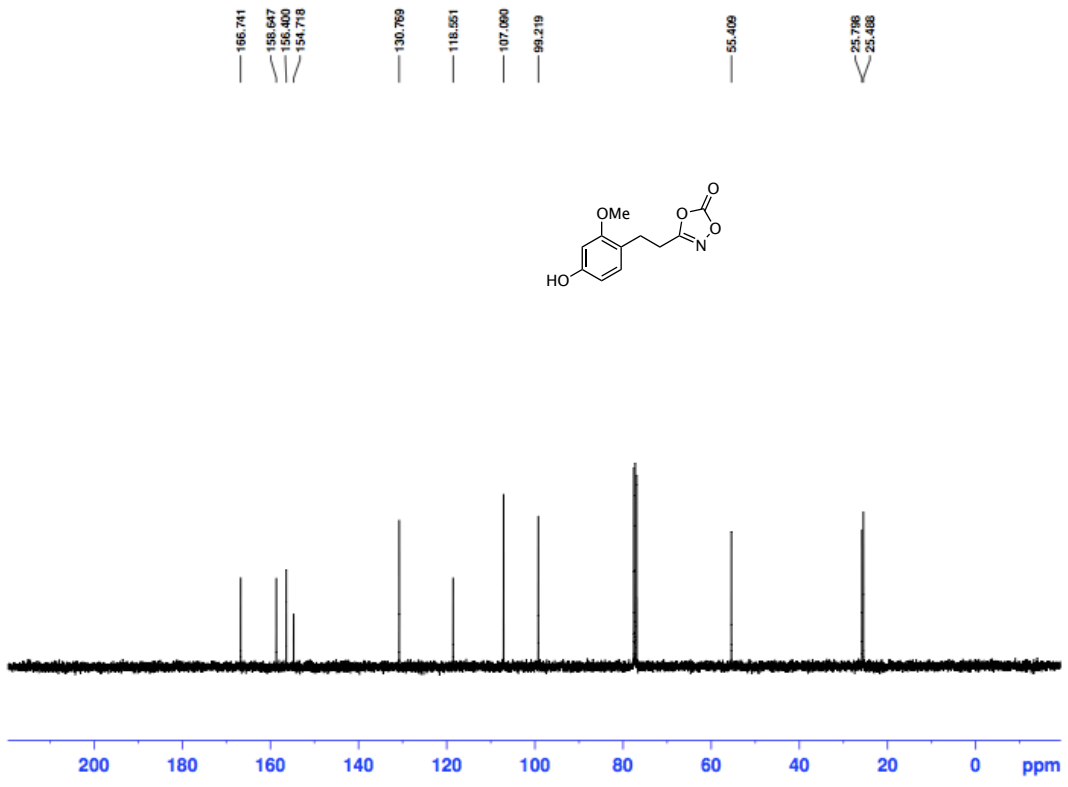

Figure S3.55 ^{1}H NMR Spectrum of 3-(4-hydroxy-3,5-dimethylphenethyl)-1,4,2-dioxazol-5-one (***4d***)

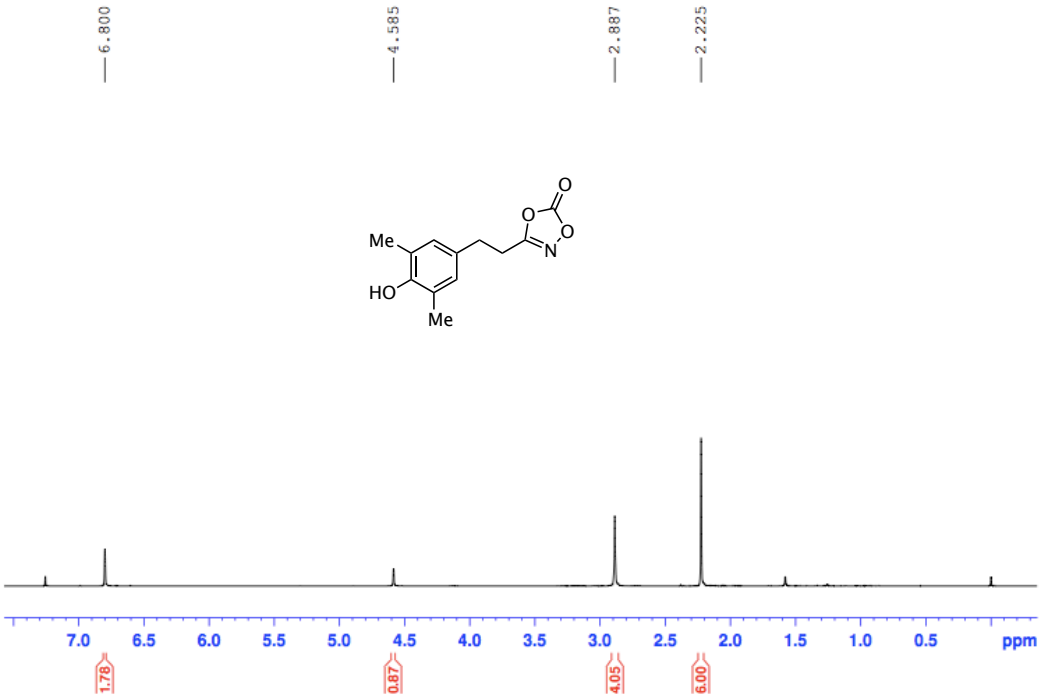

Figure S3.56 ^{13}C NMR Spectrum of 3-(4-hydroxy-3,5-dimethylphenethyl)-1,4,2-dioxazol-5-one (***4d***)

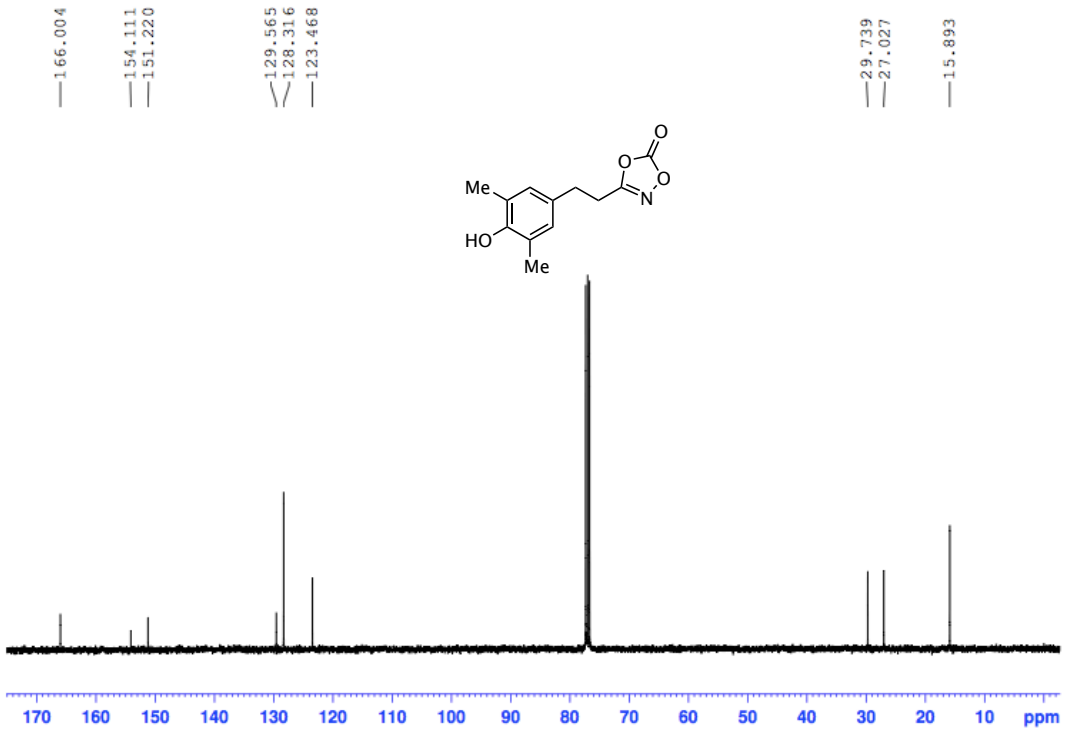

Figure S3.57 ^{1}H NMR Spectrum of 3-(4-hydroxy-2,6-dimethoxyphenethyl)-1,4,2-dioxazol-5-one (***4e***)

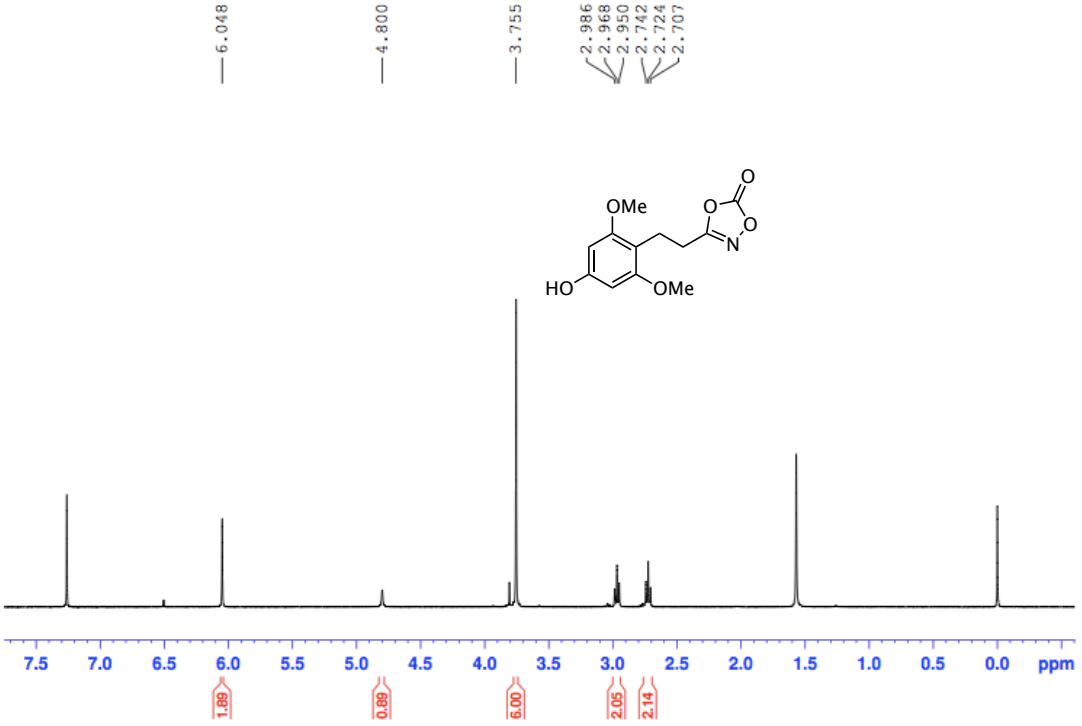

Figure S3.58 ^{13}C NMR Spectrum of 3-(4-hydroxy-2,6-dimethoxyphenethyl)-1,4,2-dioxazol-5-one (***4e***)

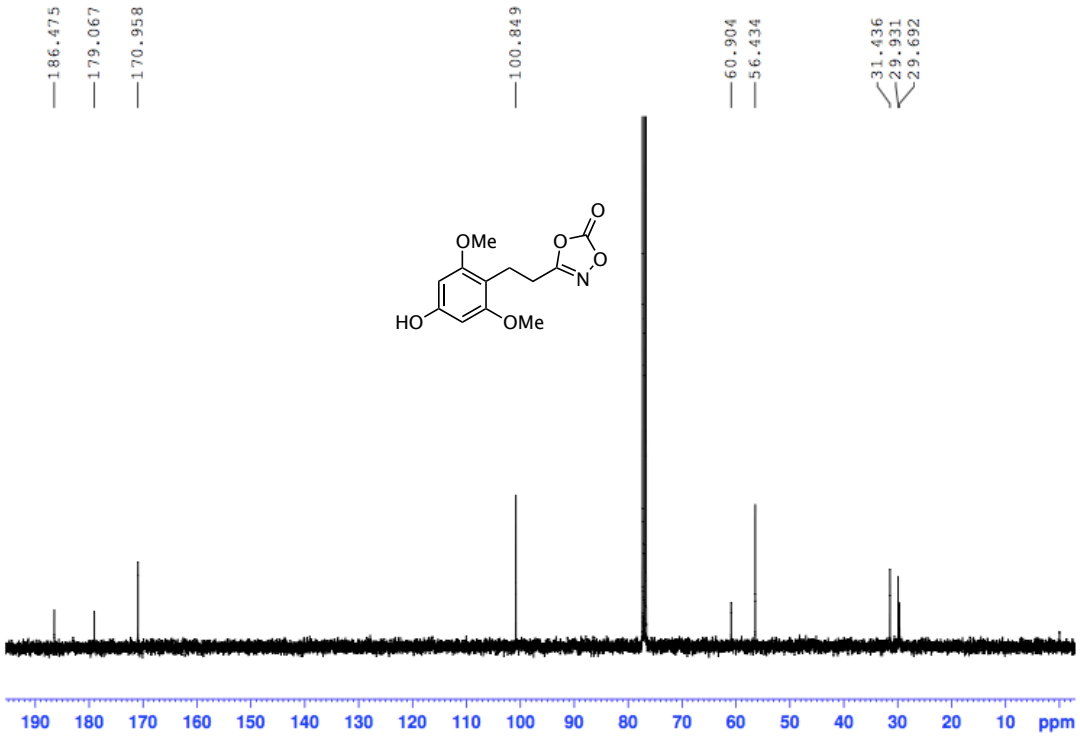

Figure S3.59 ^{1}H NMR Spectrum of 3-(2-hydroxyphenethyl)-1,4,2-dioxazol-5-one (***4f***)

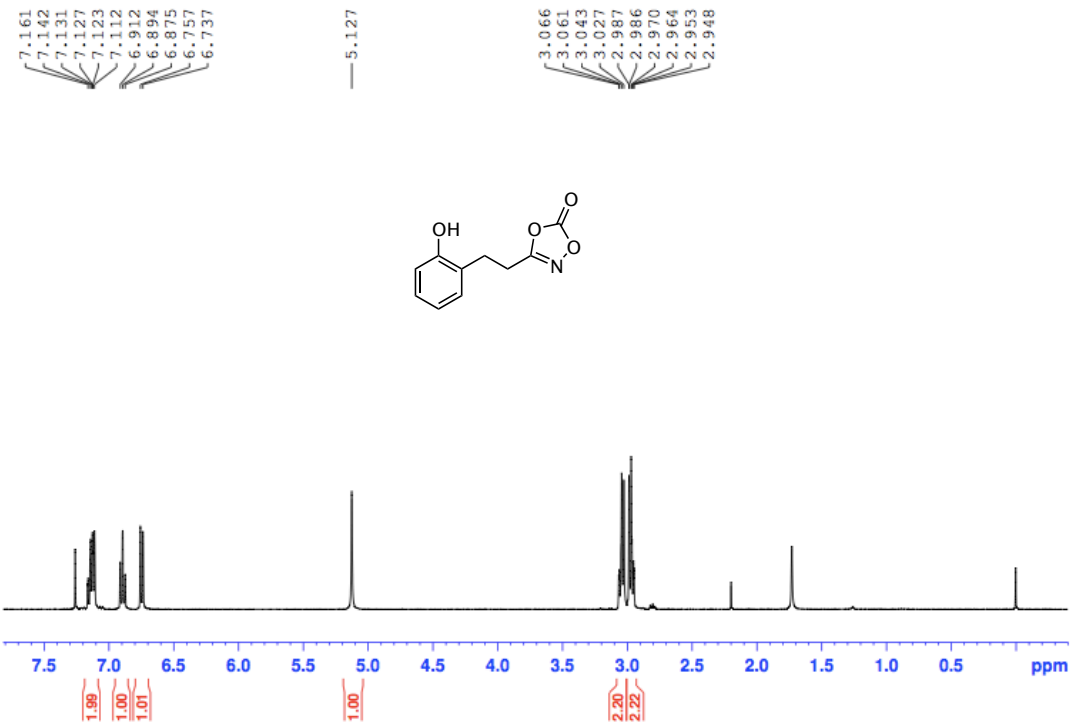

Figure S3.60 ^{13}C NMR Spectrum of 3-(2-hydroxyphenethyl)-1,4,2-dioxazol-5-one (***4f***)

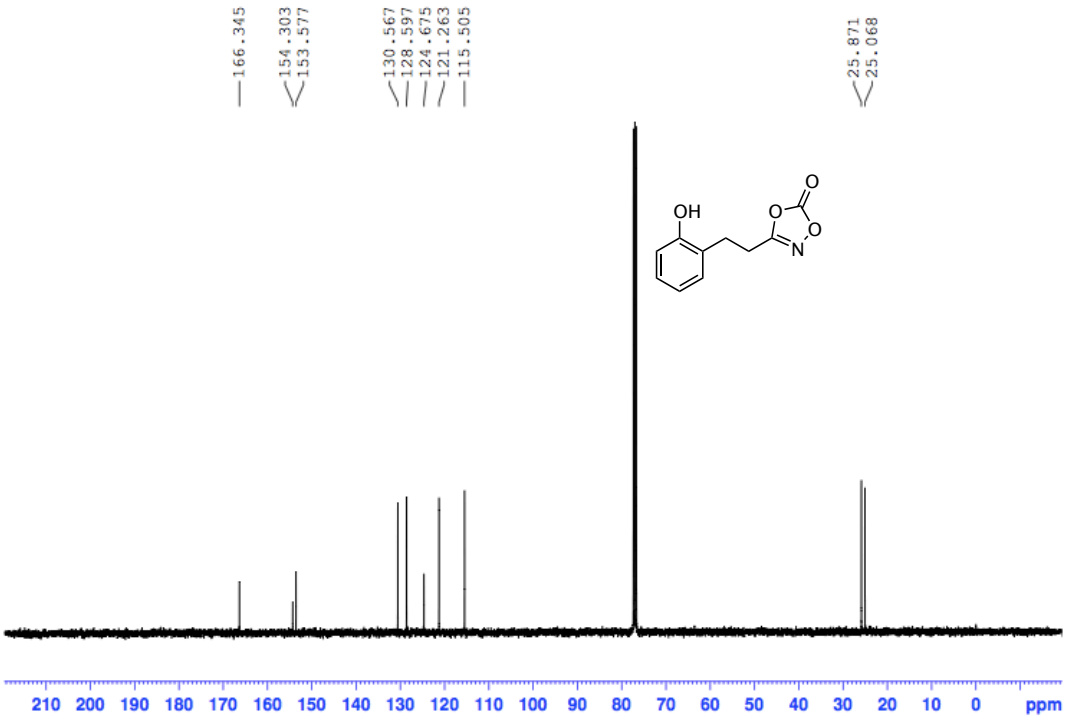

Figure S3.61 ^{1}H NMR Spectrum of 3-(2-hydroxy-4-methoxyphenethyl)-1,4,2-dioxazol-5-one (***4g***)

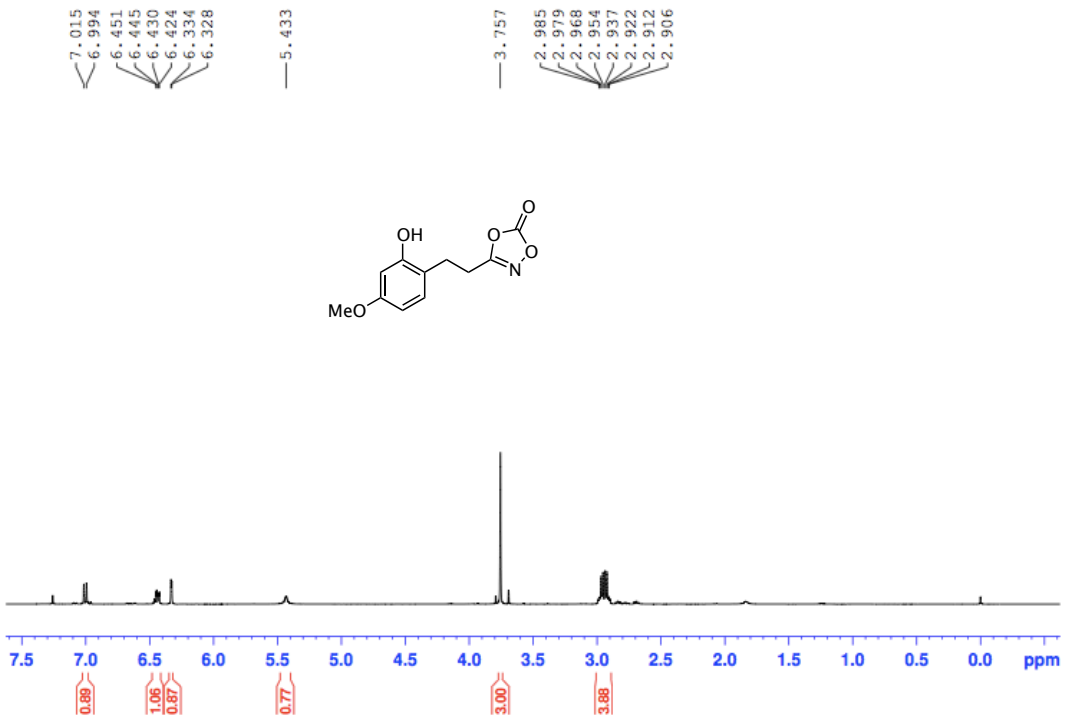

Figure S3.62 ^{13}C NMR Spectrum of 3-(2-hydroxy-4-methoxyphenethyl)-1,4,2-dioxazol-5-one (***4g***)

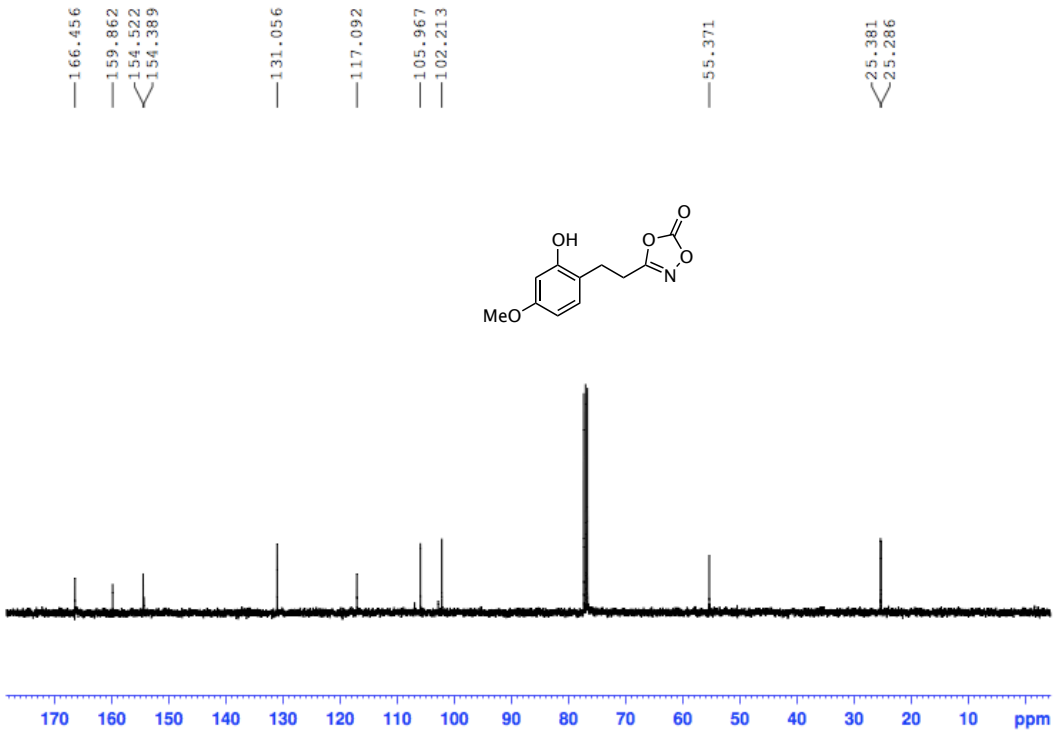

Figure S3.63 ^{1}H NMR Spectrum of ***2a***

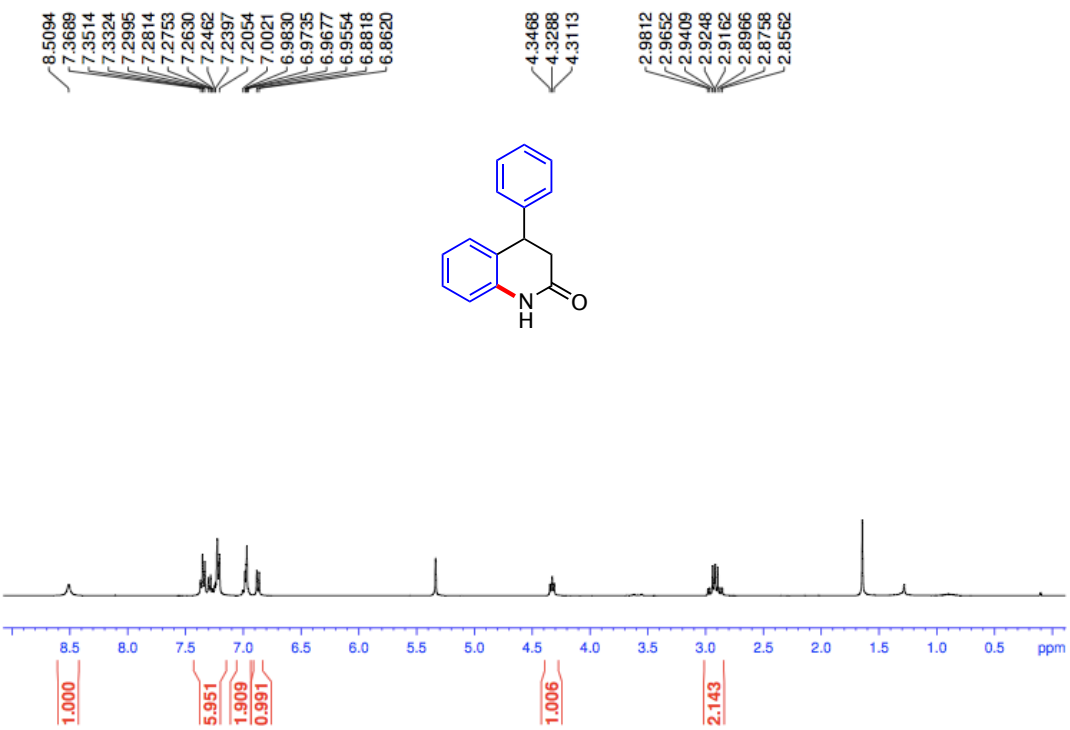

Figure S3.64 ^{13}C NMR Spectrum of ***2a***

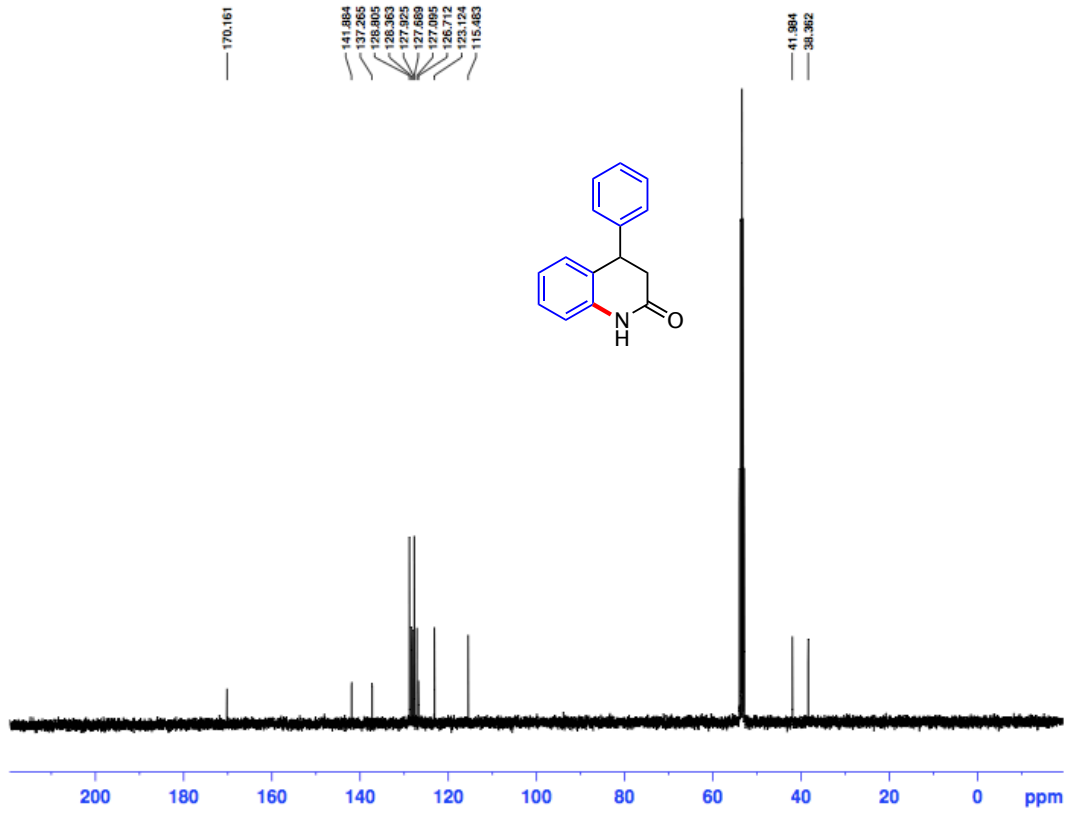

Figure S3.65 ^{1}H NMR Spectrum of ***2b***

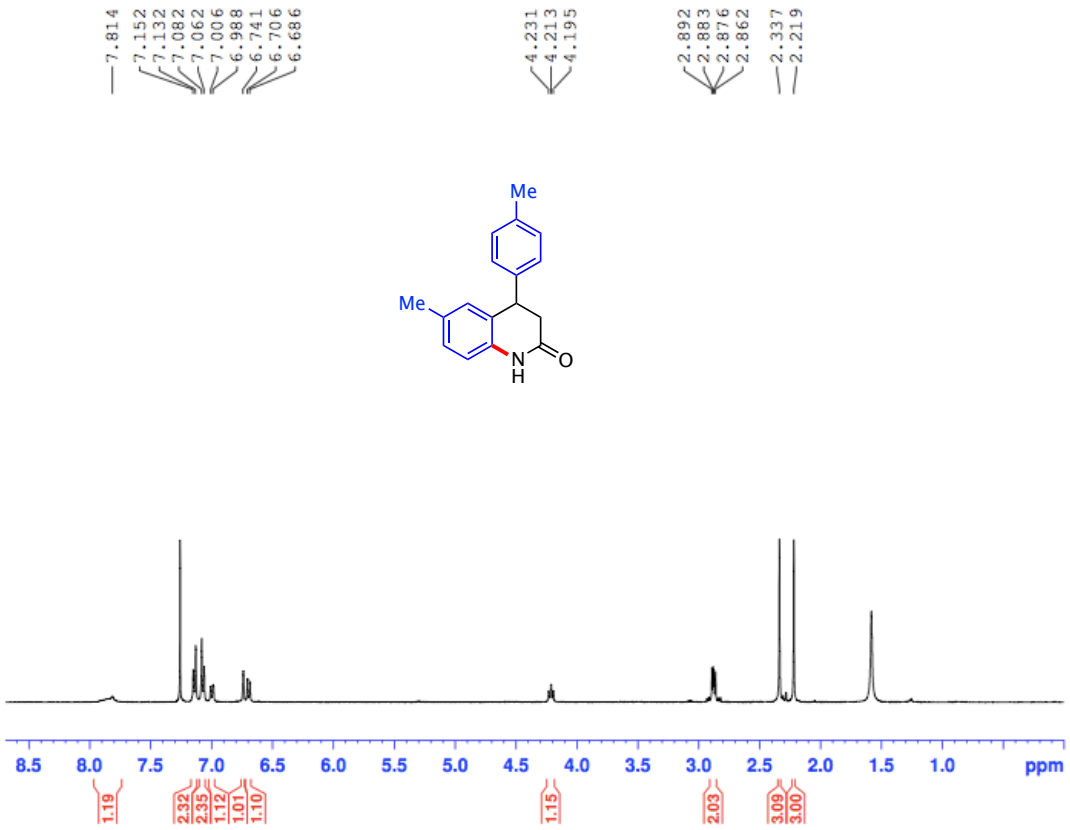

Figure S3.66 ^{13}C NMR Spectrum of ***2b***

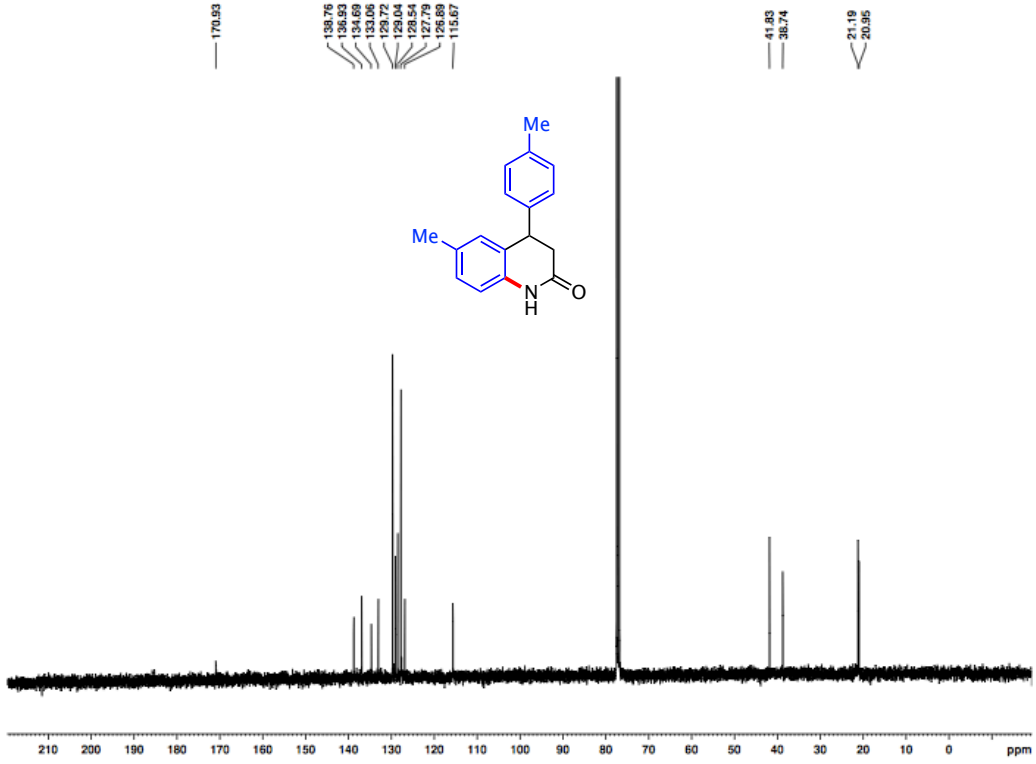

Figure S3.67 ^{1}H NMR Spectrum of ***2c***

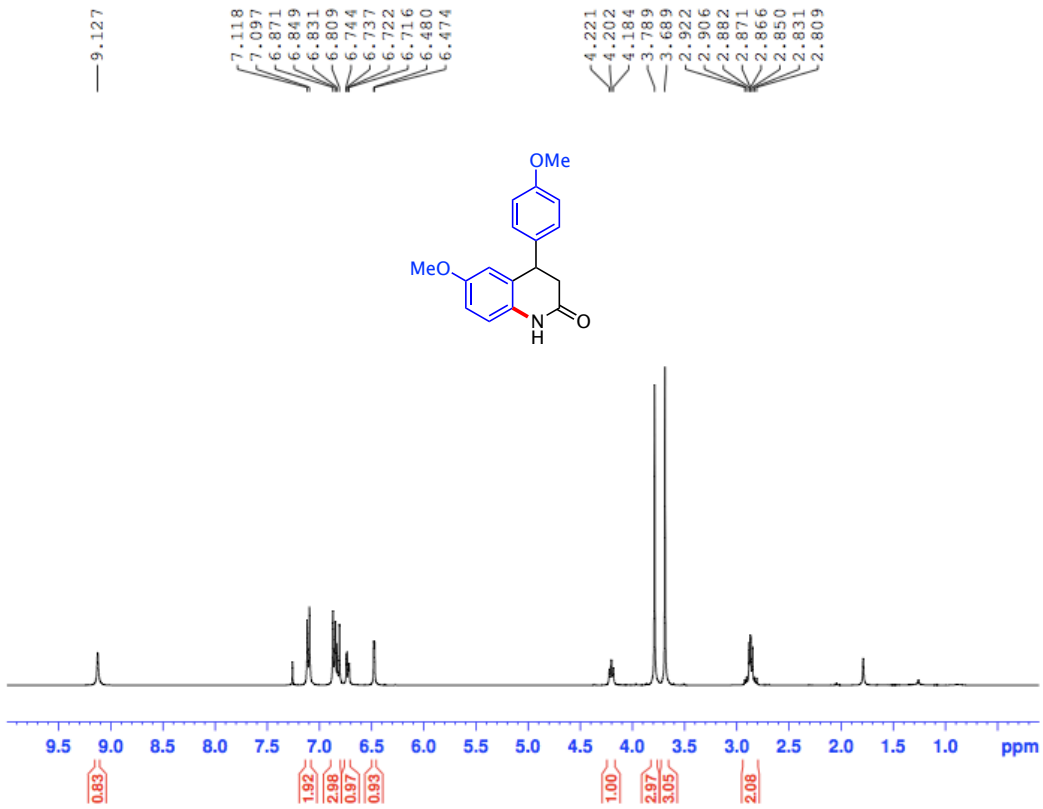

Figure S3.68 ^{13}C NMR Spectrum of ***2c***

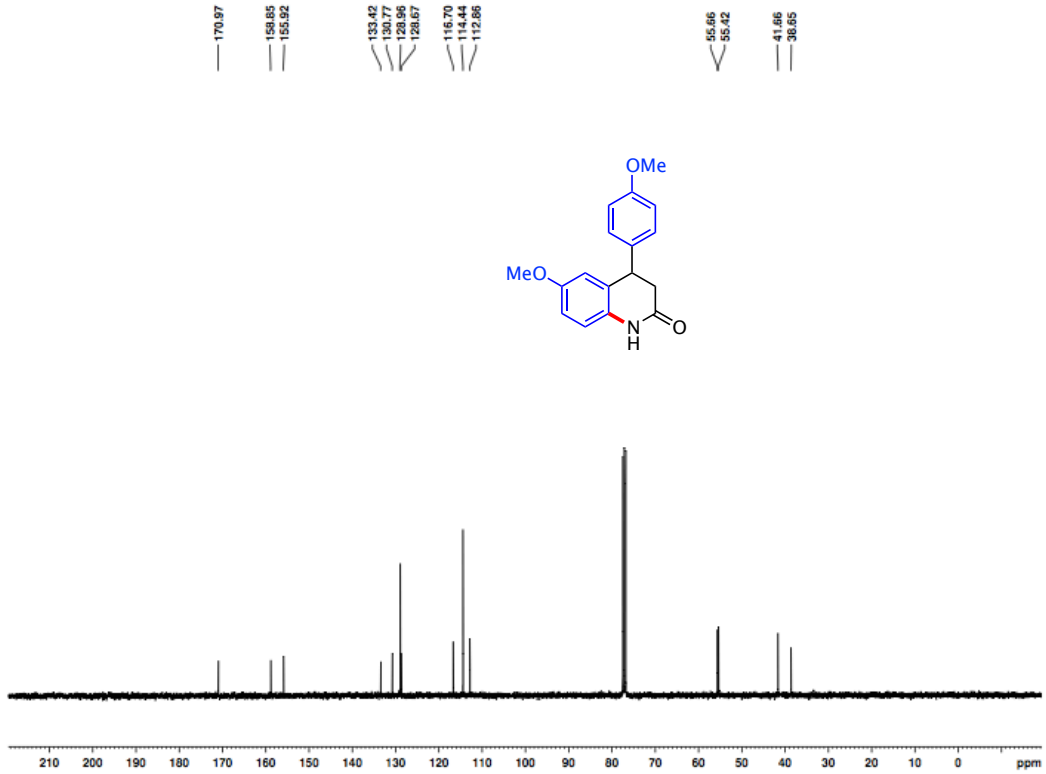

Figure S3.69 ^{1}H NMR Spectrum of ***2d***

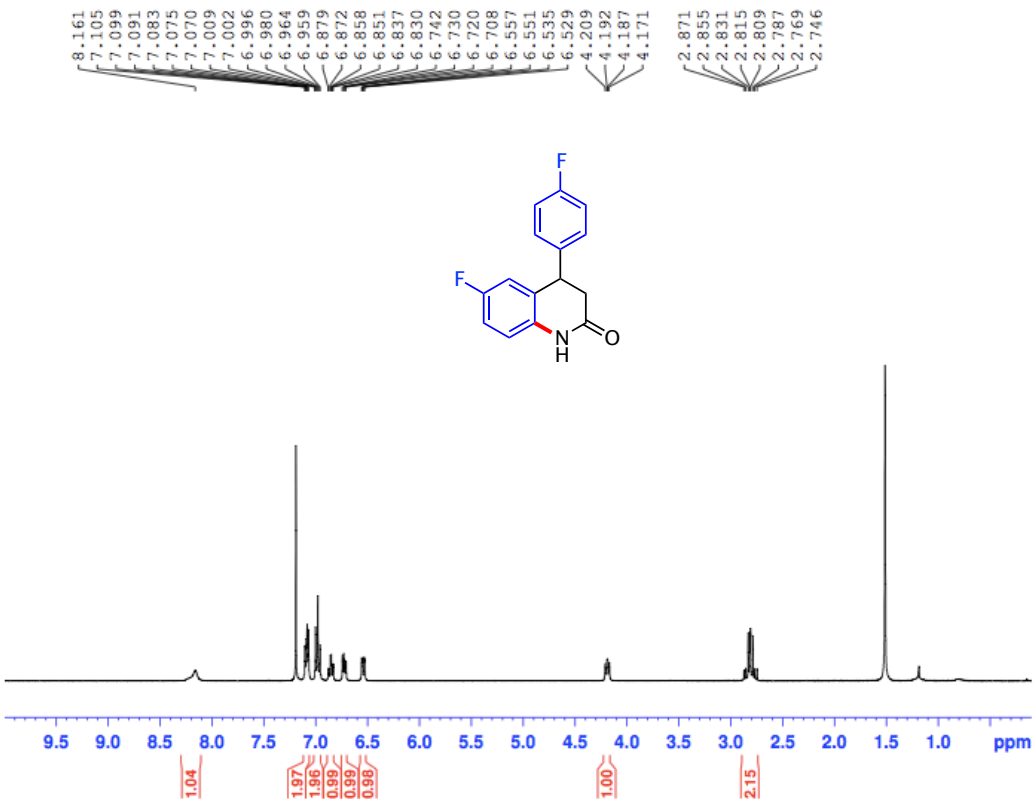

Figure S3.70 ^{13}C NMR Spectrum of ***2d***

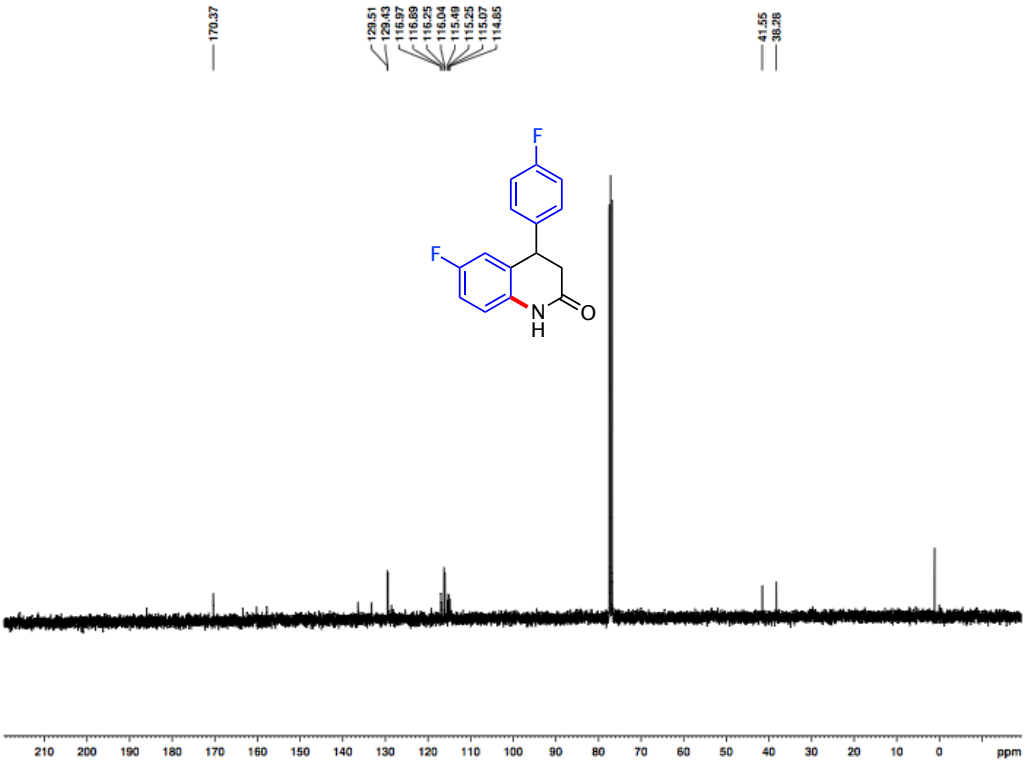

Figure S3.71 ^{1}H NMR Spectrum of ***2e***

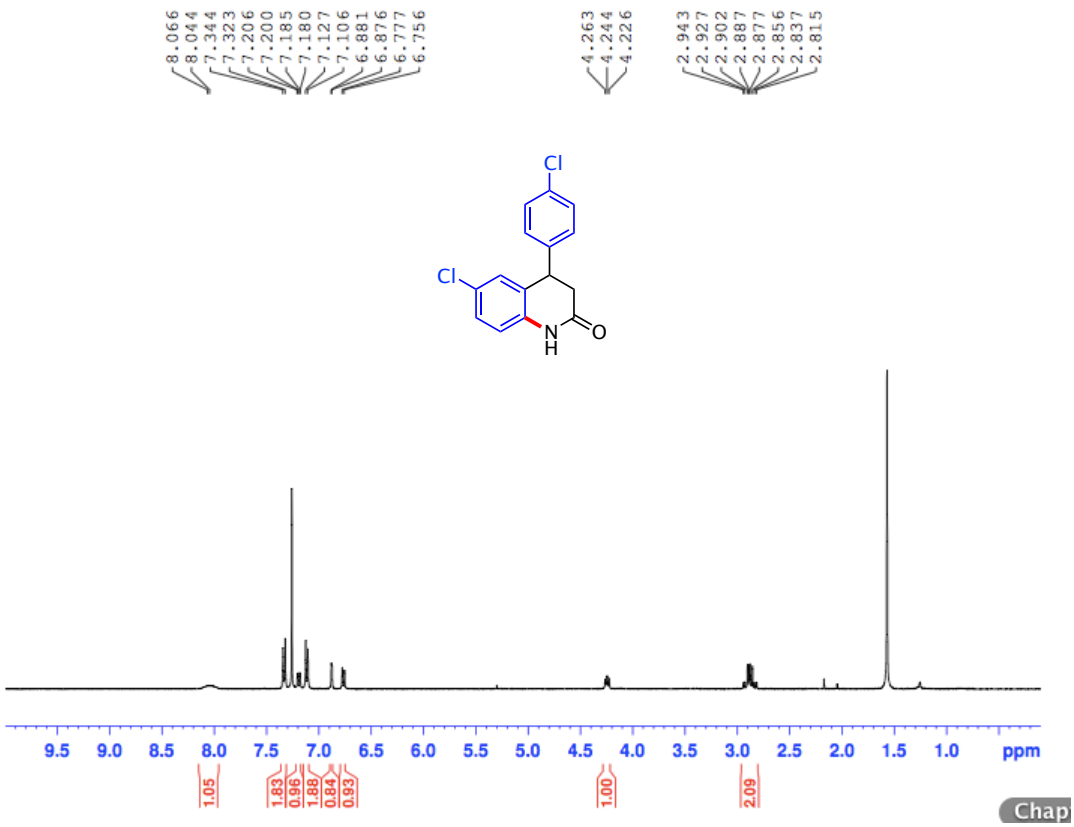

Figure S3.72 ^{13}C NMR Spectrum of ***2e***

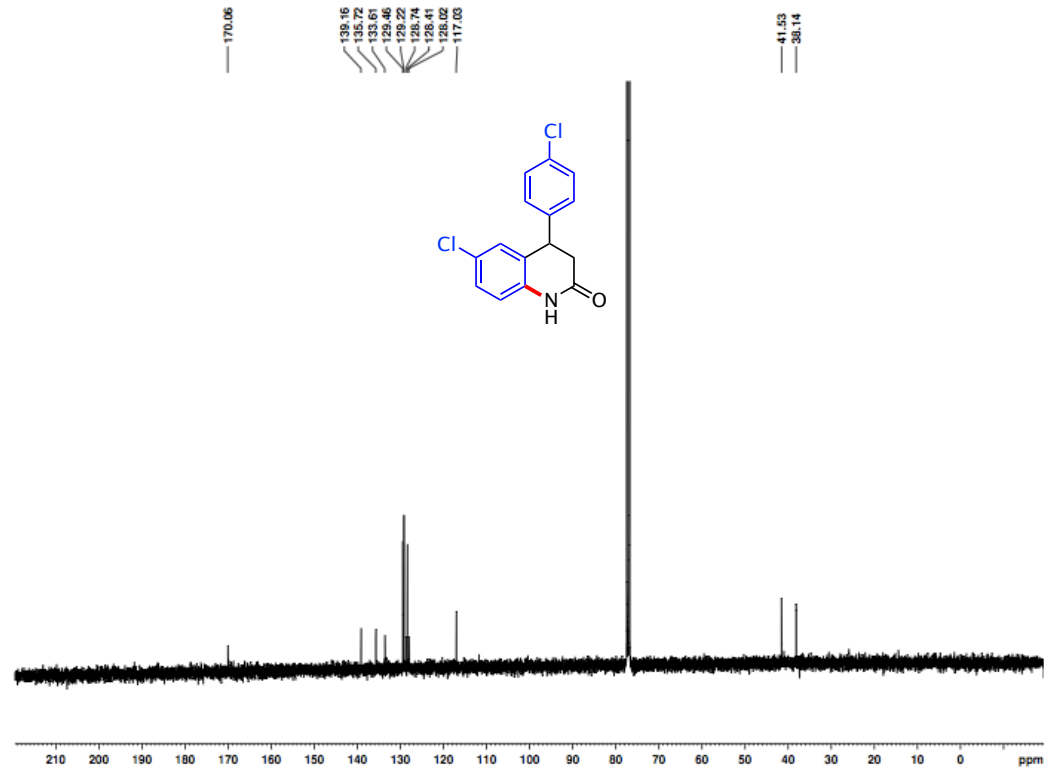

Figure S3.73 ^{1}H NMR Spectrum of ***2f***

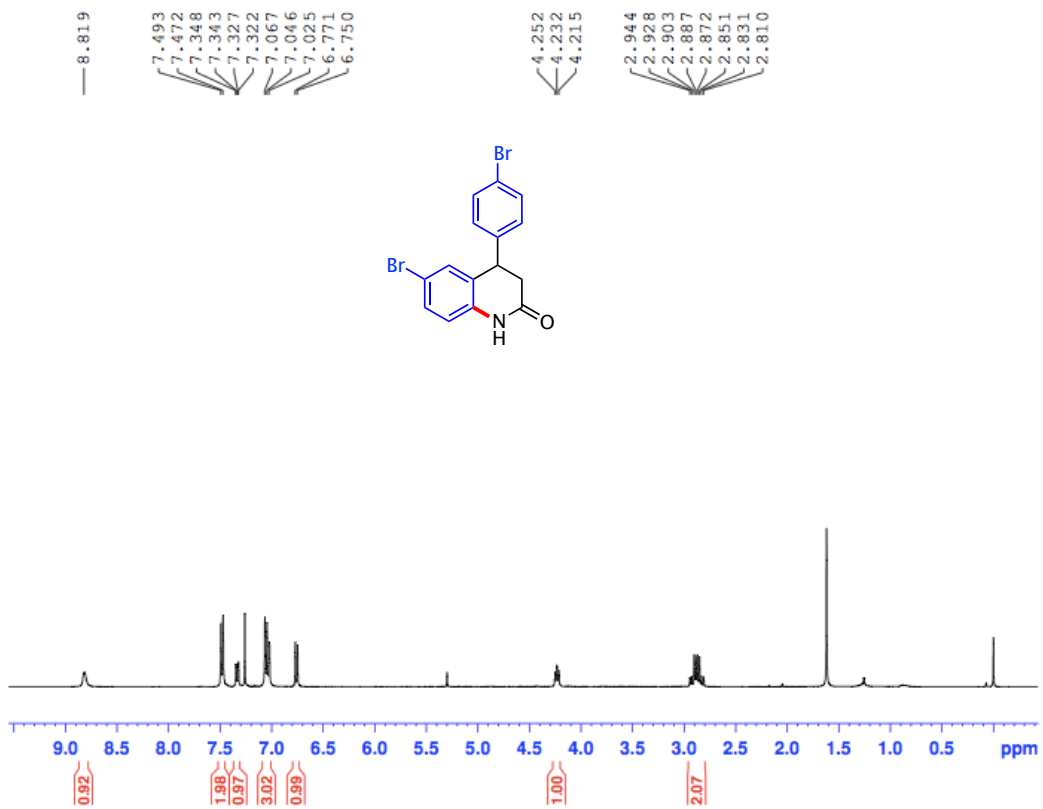

Figure S3.74 ^{13}C NMR Spectrum of ***2f***

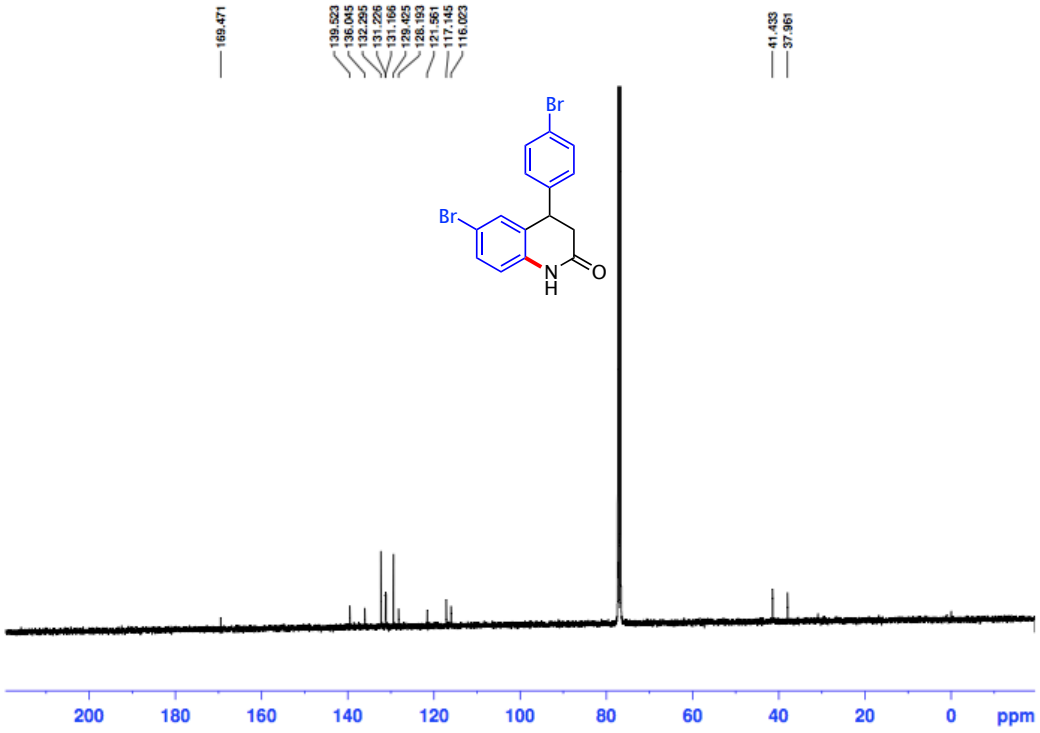

Figure S3.75 ^{1}H NMR Spectrum of ***2h***

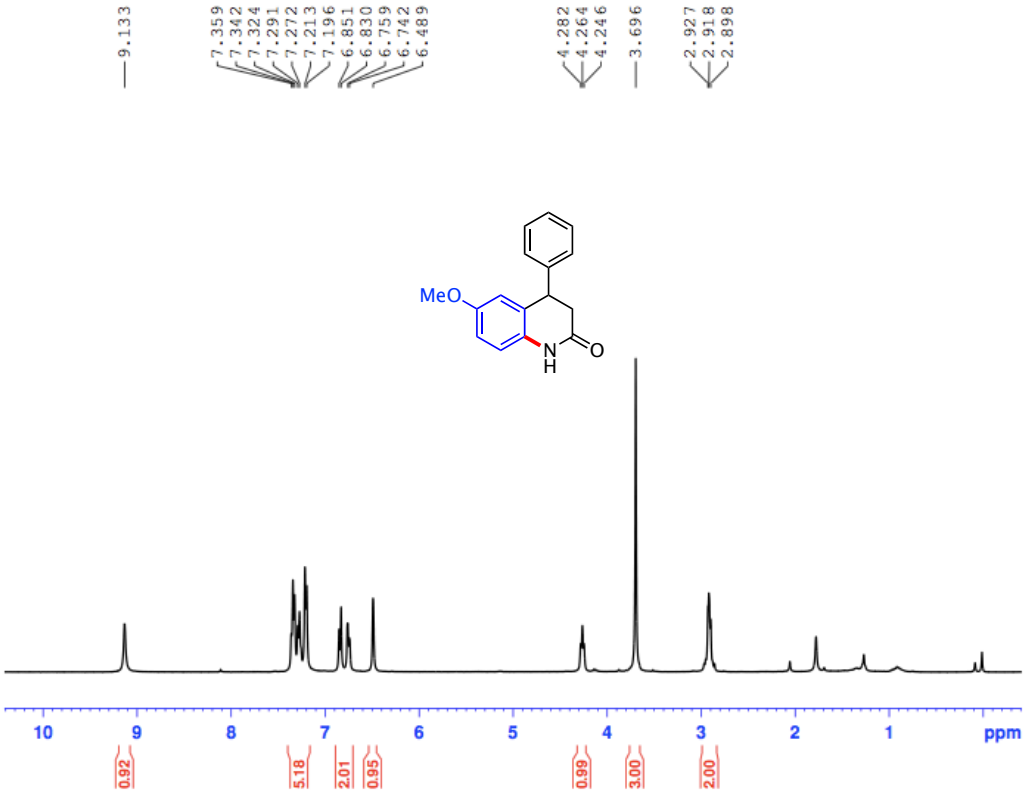

Figure S3.76 ^{13}C NMR Spectrum of ***2h***

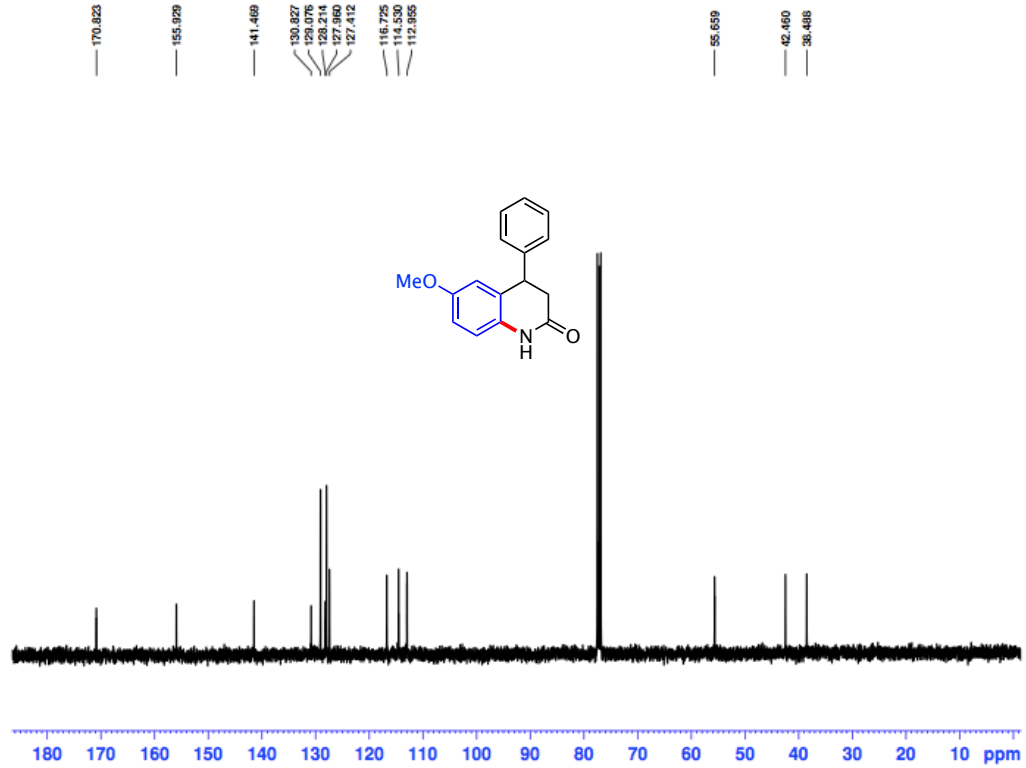

Figure S3.77 ^{1}H NMR Spectrum of ***2i***

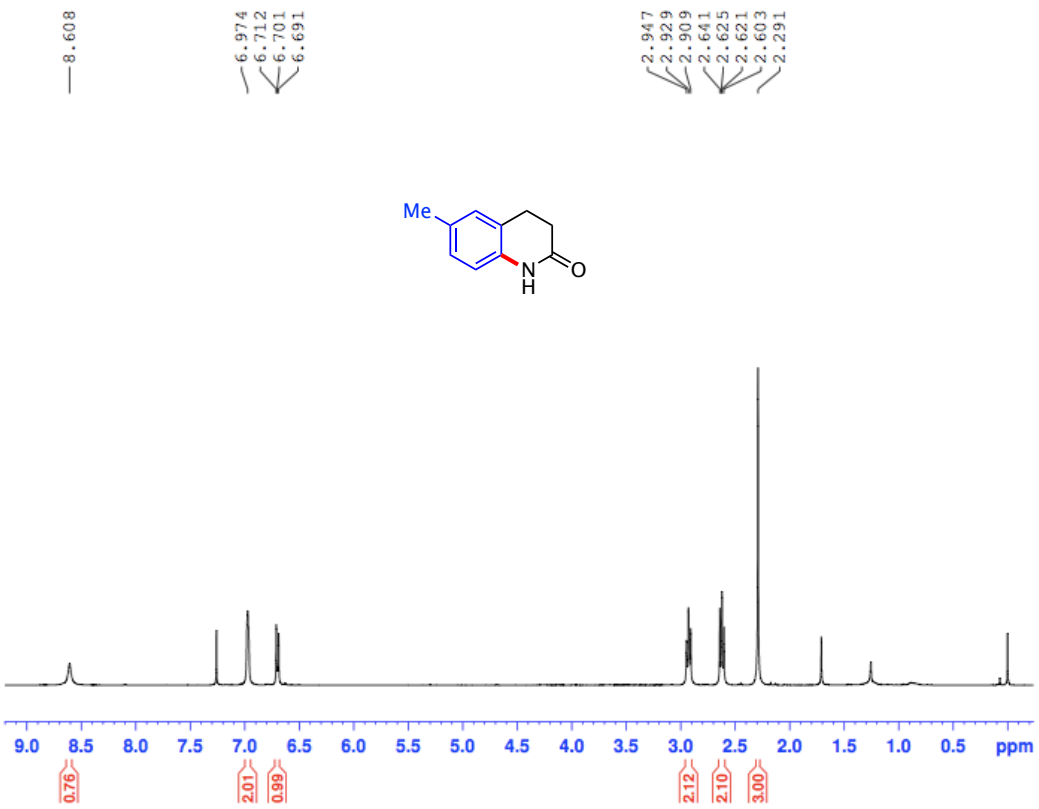

Figure S3.78 ^{13}C NMR Spectrum of ***2i***

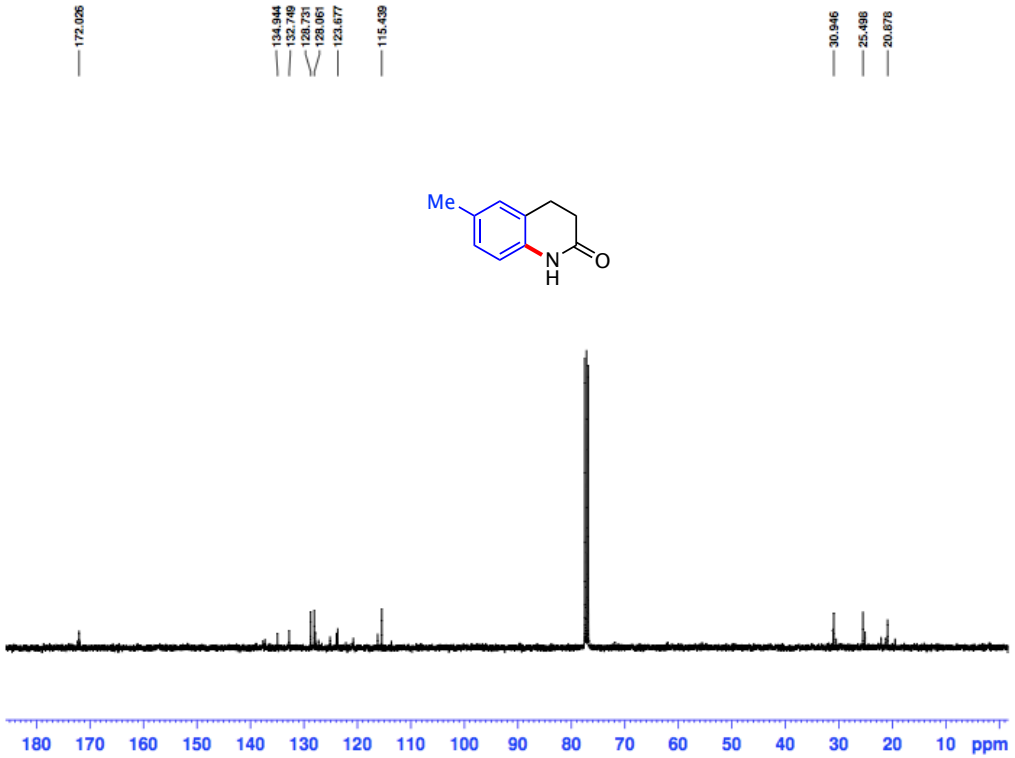

Figure S3.79 ^{1}H NMR Spectrum of ***2j***

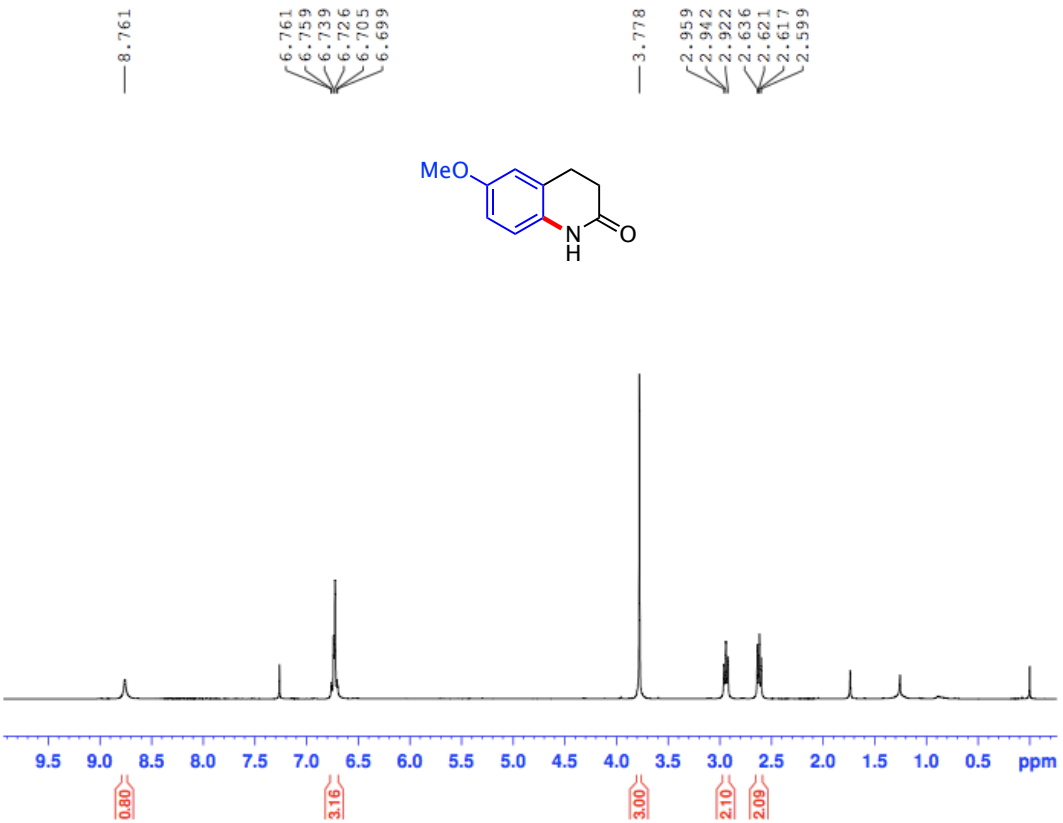

Figure S3.80 ^{13}C NMR Spectrum of ***2j***

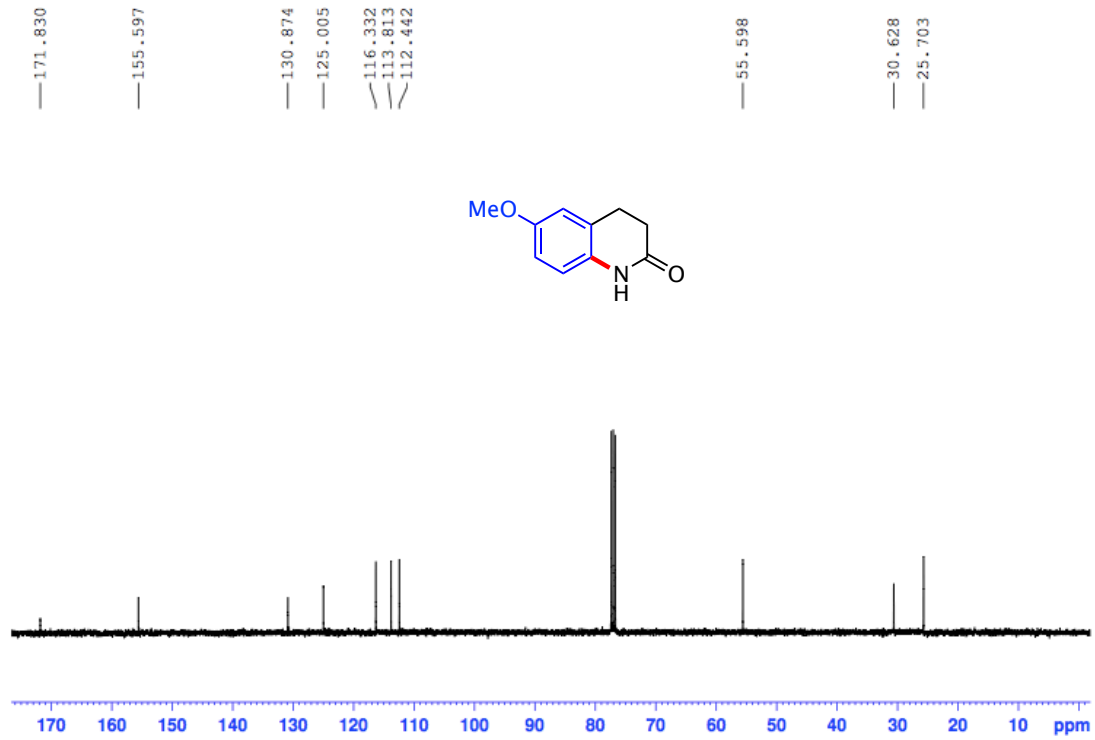

Figure S3.81 ^{1}H NMR Spectrum of ***2k***

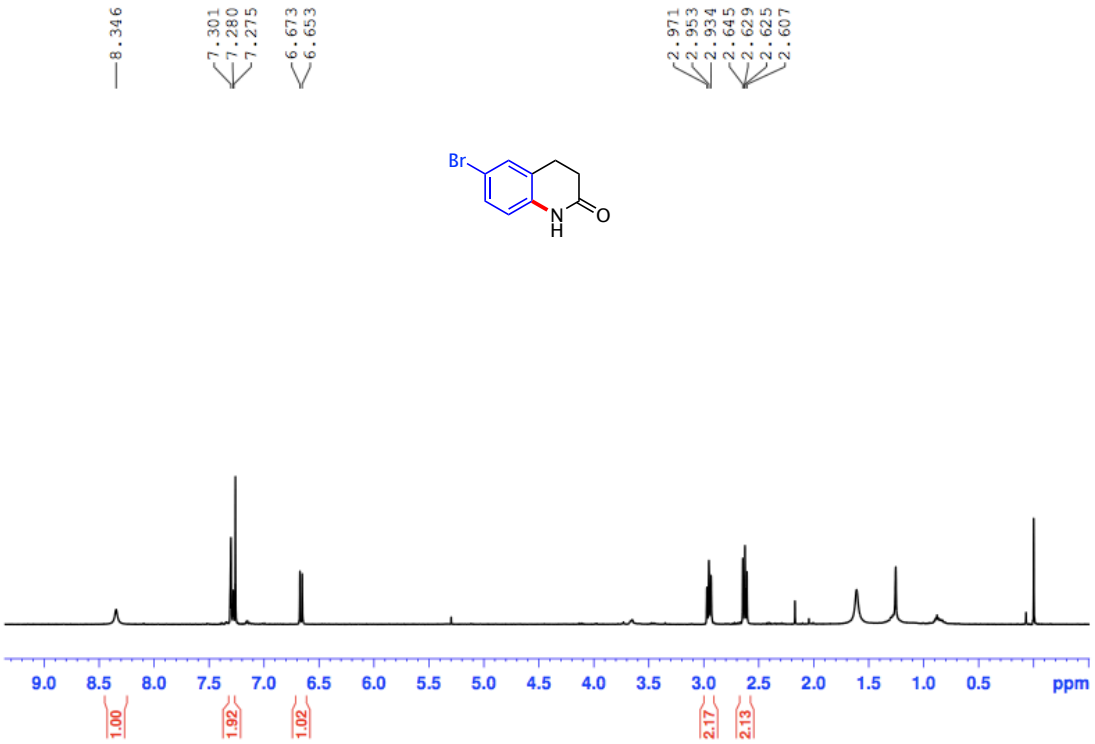

Figure S3.82 ^{13}C NMR Spectrum of ***2k***

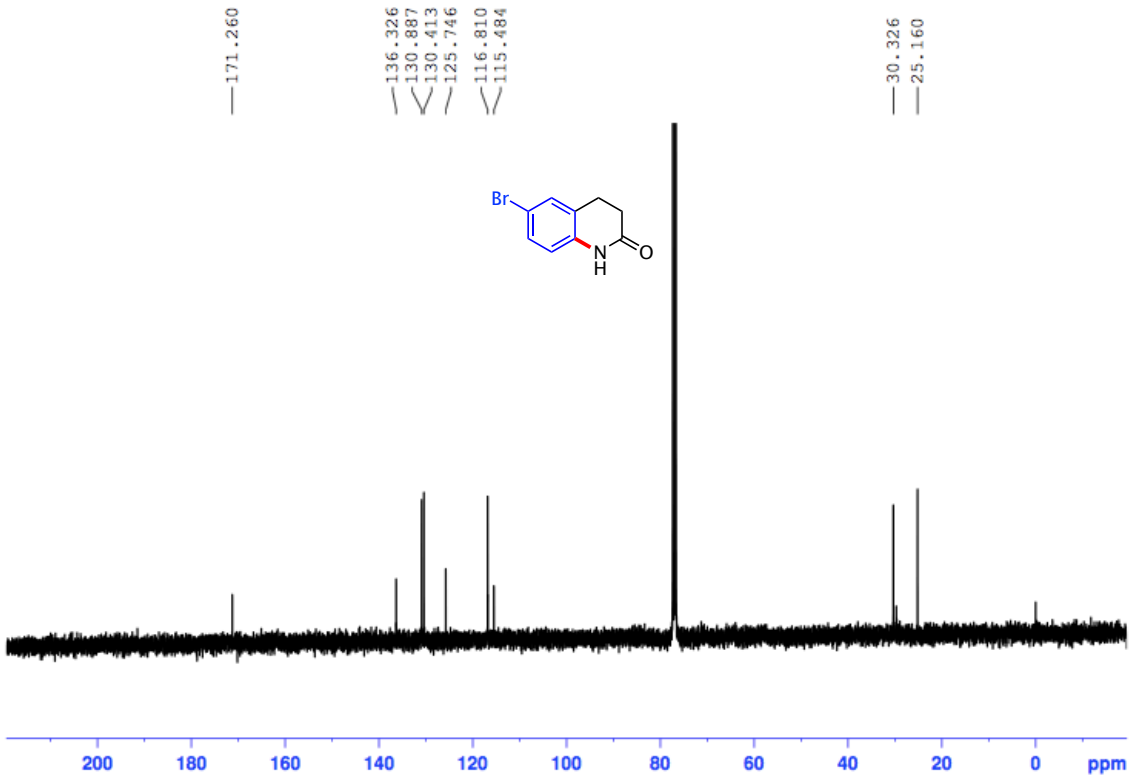

Figure S3.83 ^{1}H NMR Spectrum of ***2l***

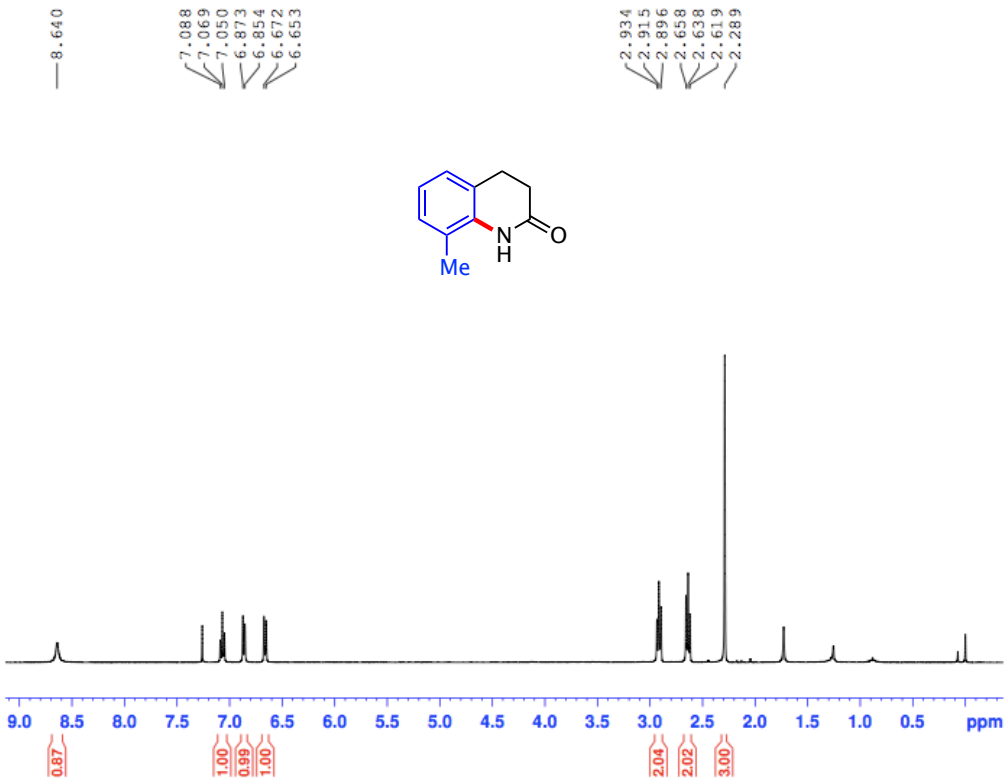

Figure S3.84 ^{13}C NMR Spectrum of ***2l***

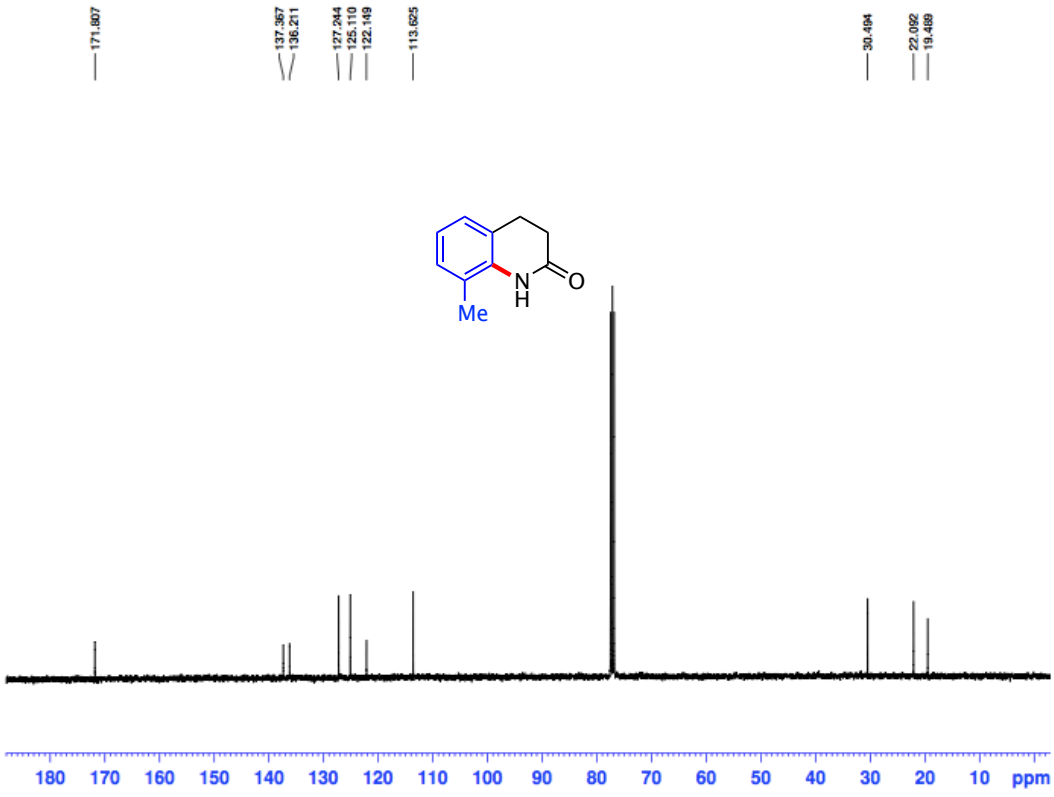

Figure S3.85 ^{1}H NMR Spectrum of ***2n***

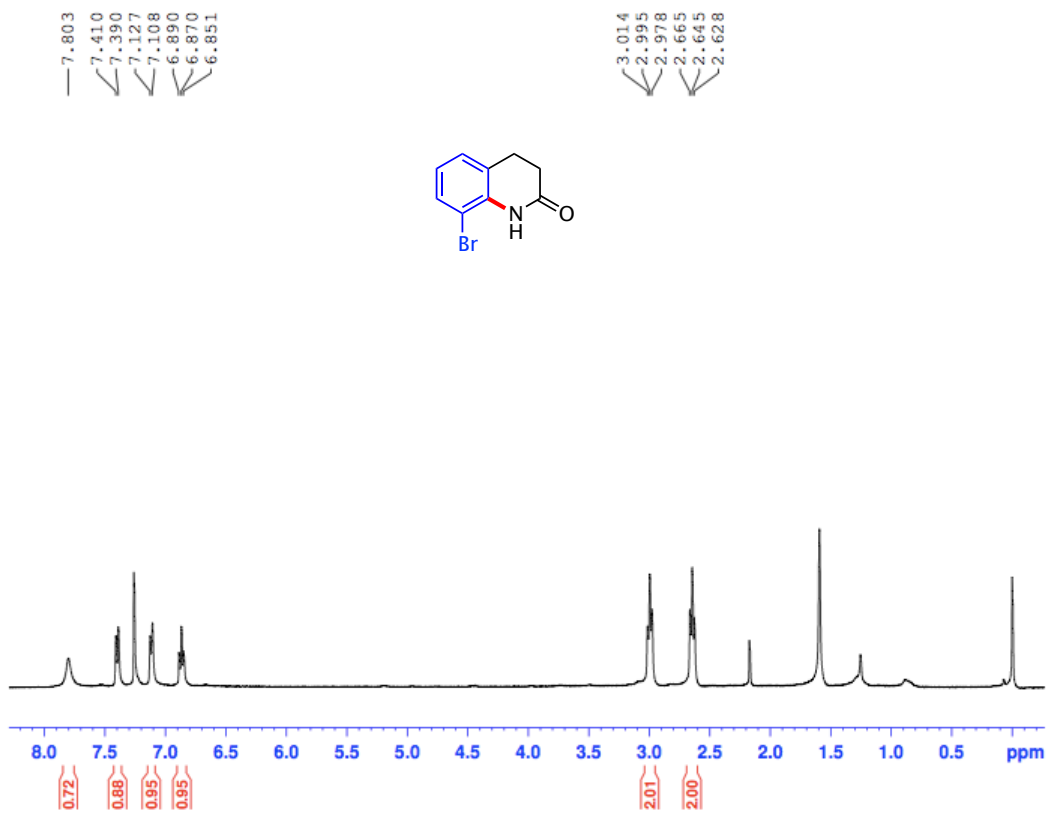

Figure S3.86 ^{13}C NMR Spectrum of ***2n***

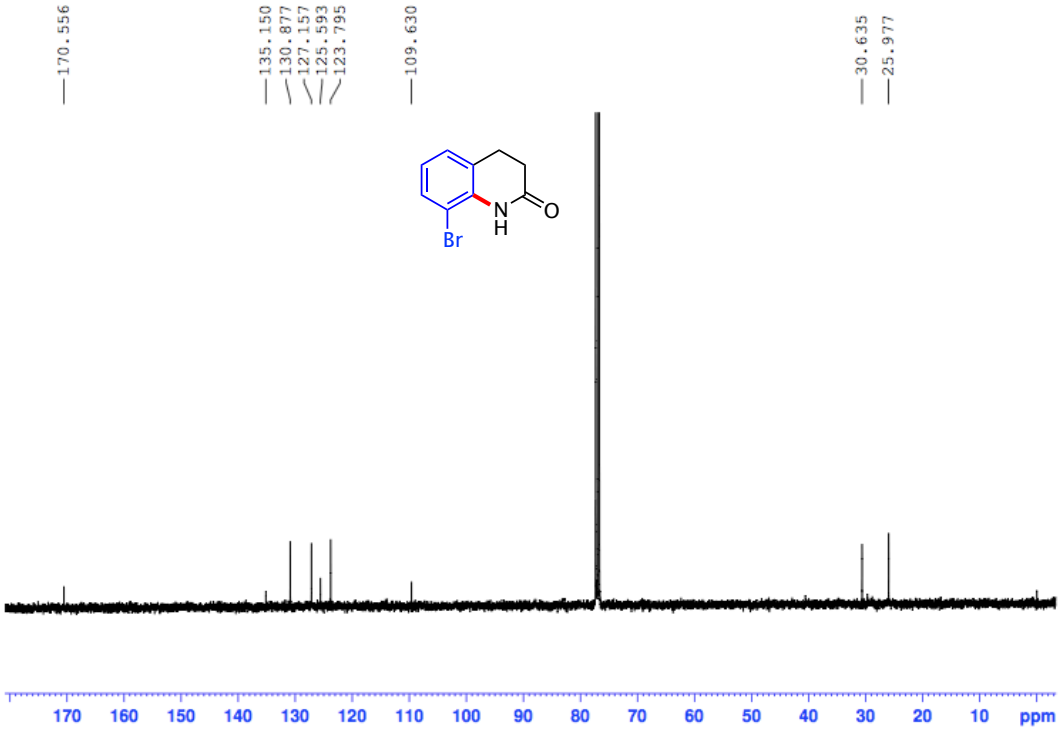

Figure S3.87 ^{1}H NMR Spectrum of ***2r***

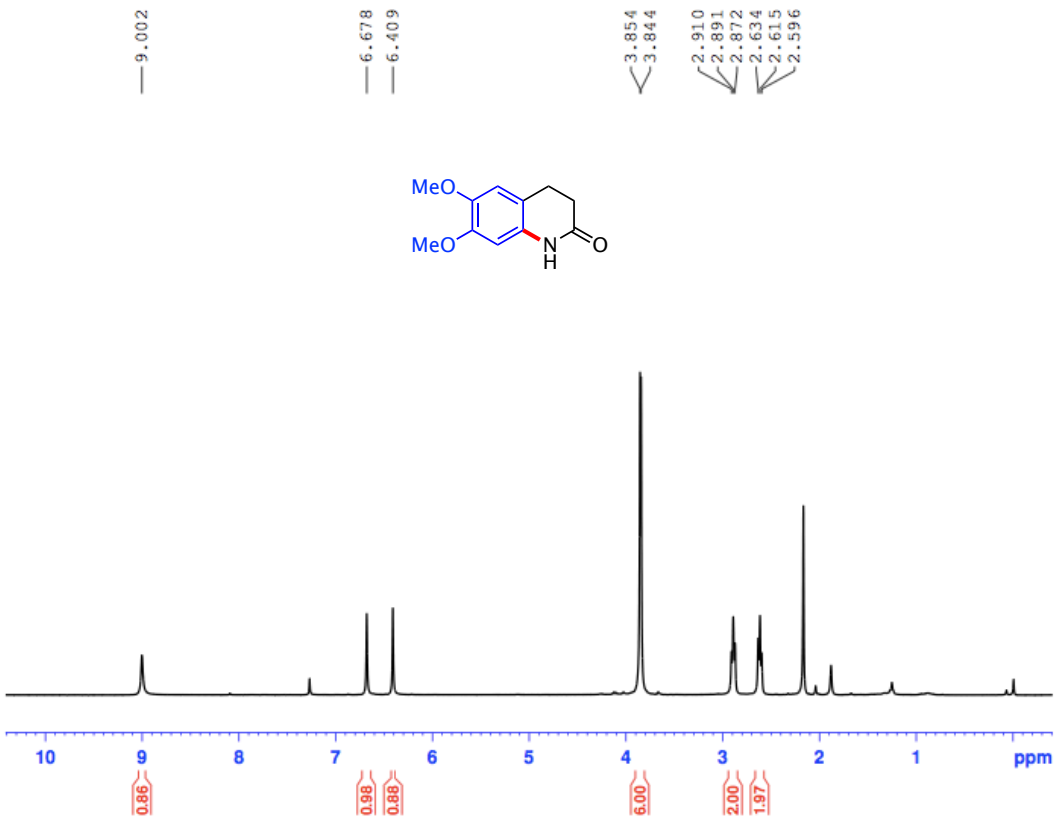

Figure S3.88 ^{13}C NMR Spectrum of ***2r***

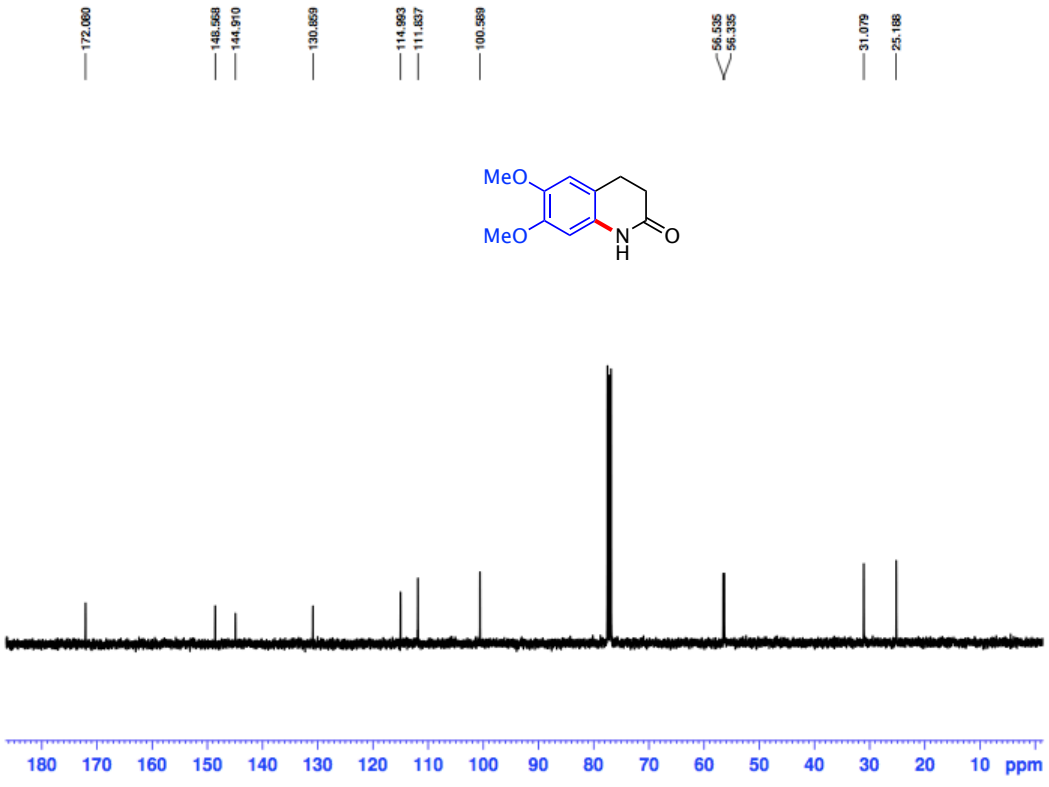

Figure S3.89 ^{1}H NMR Spectrum of ***2s***

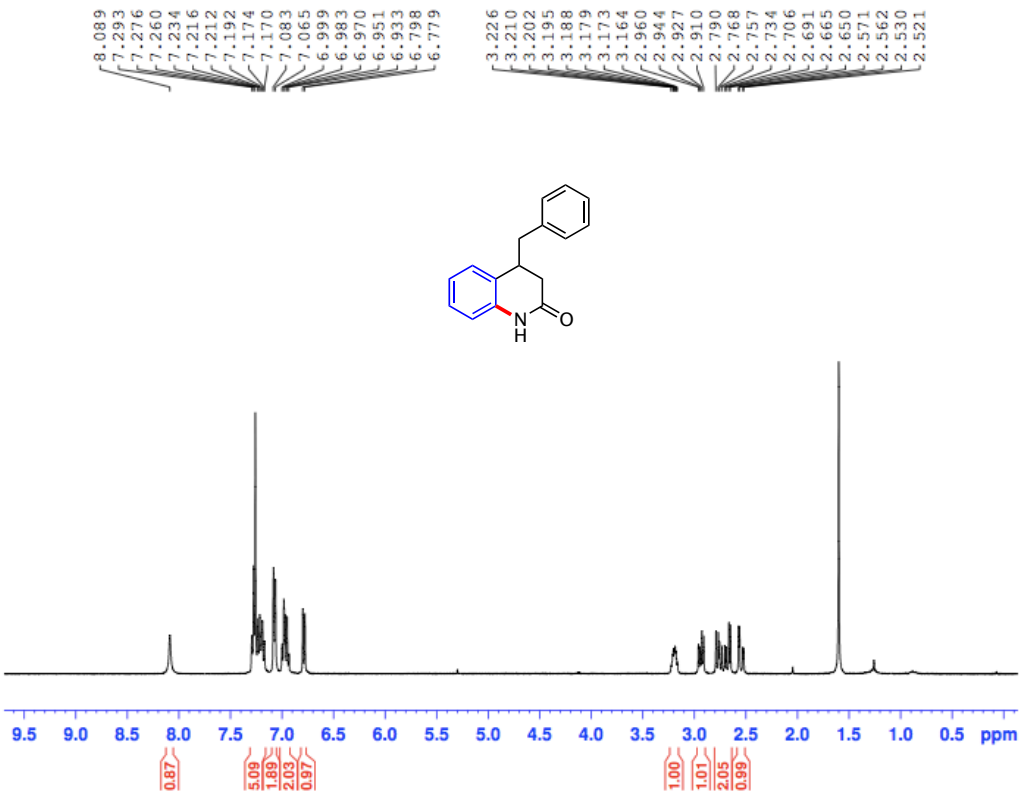

Figure S3.90 ^{13}C NMR Spectrum of ***2s***

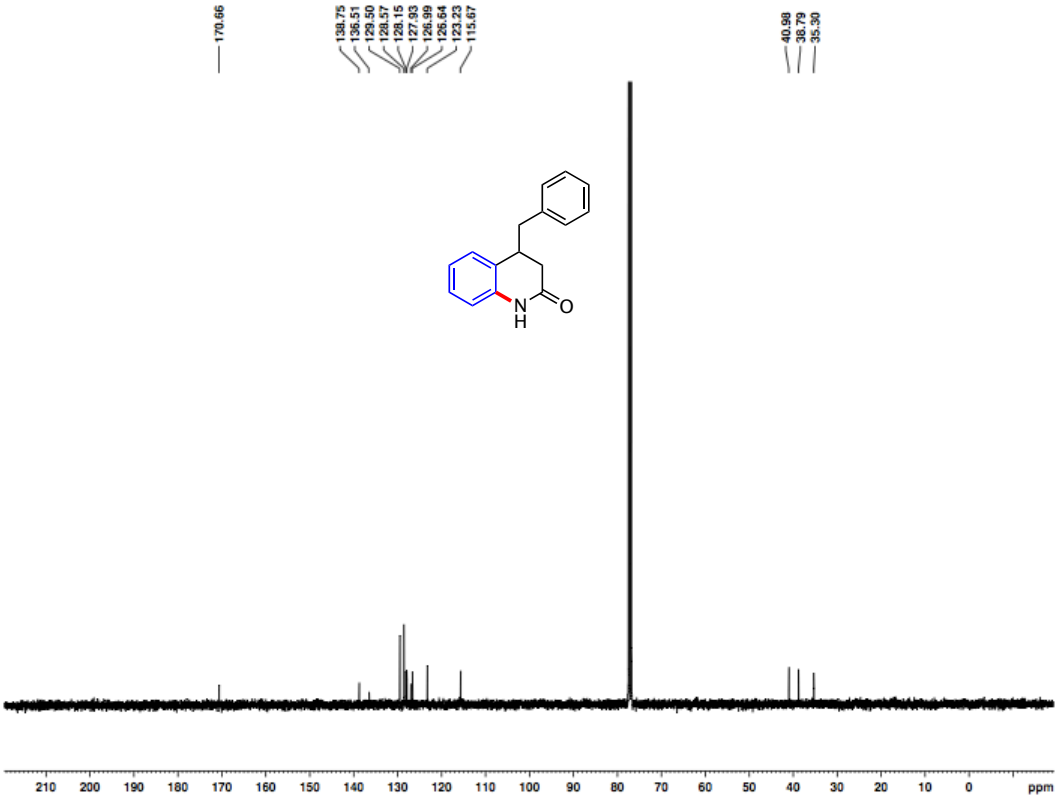

Figure S3.91 ^{1}H NMR Spectrum of ***2t***

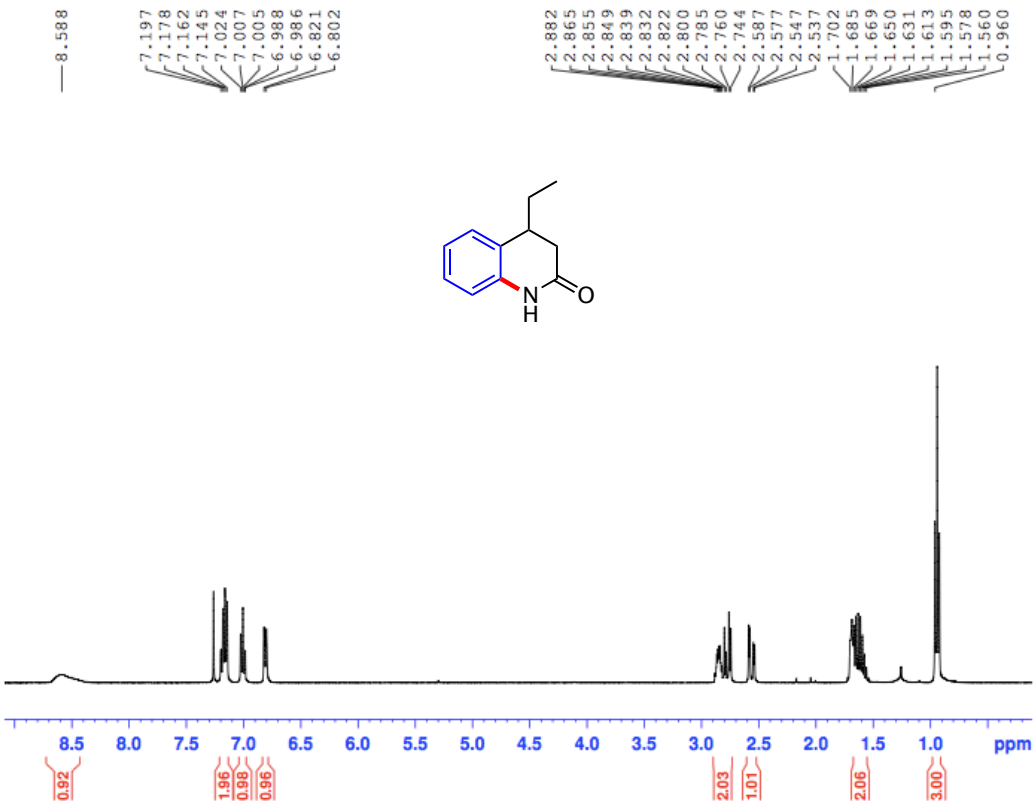

Figure S3.92 ^{13}C NMR Spectrum of ***2t***

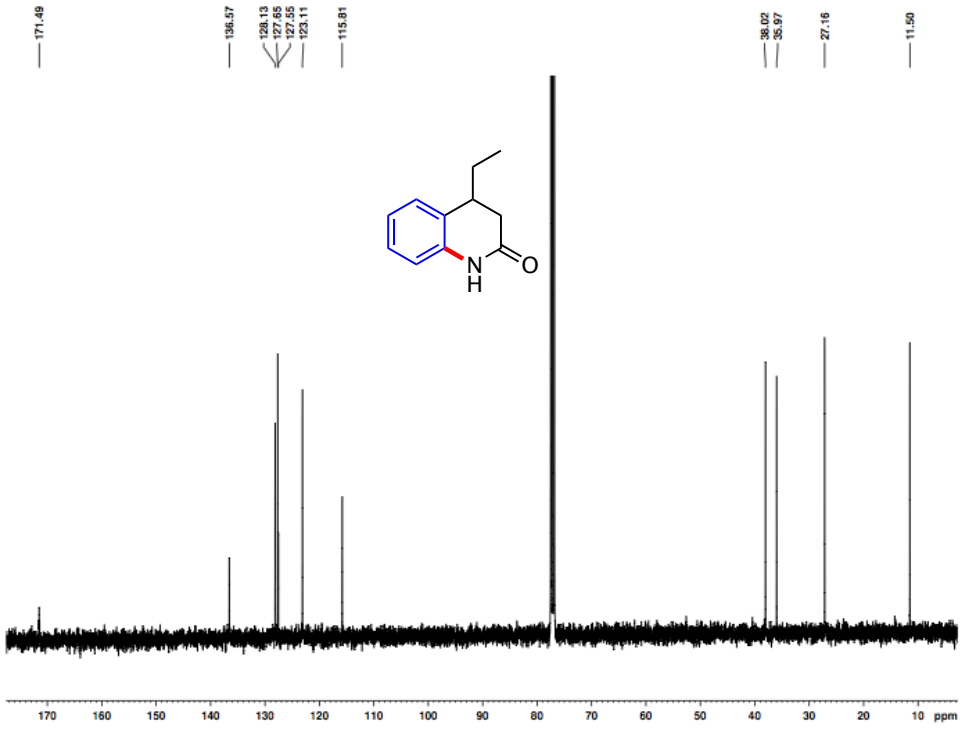

Figure S3.93 ^{1}H NMR Spectrum of ***2u***

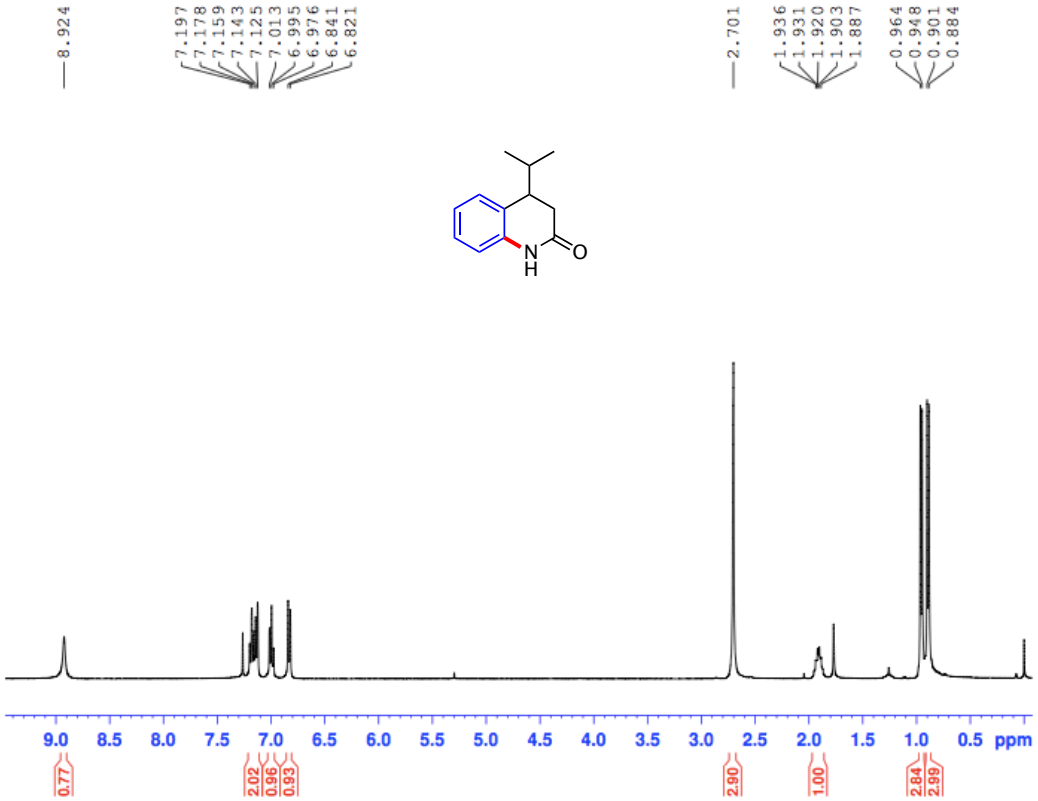

Figure S3.94 ^{13}C NMR Spectrum of ***2u***

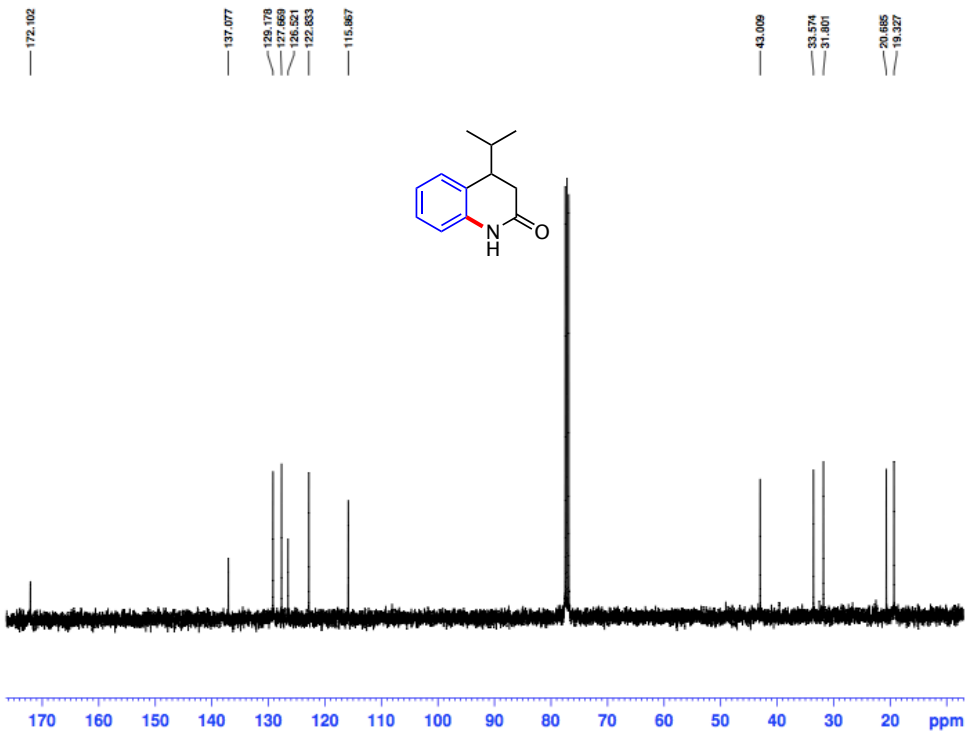

Figure S3.95 ^{1}H NMR Spectrum of ***2v***

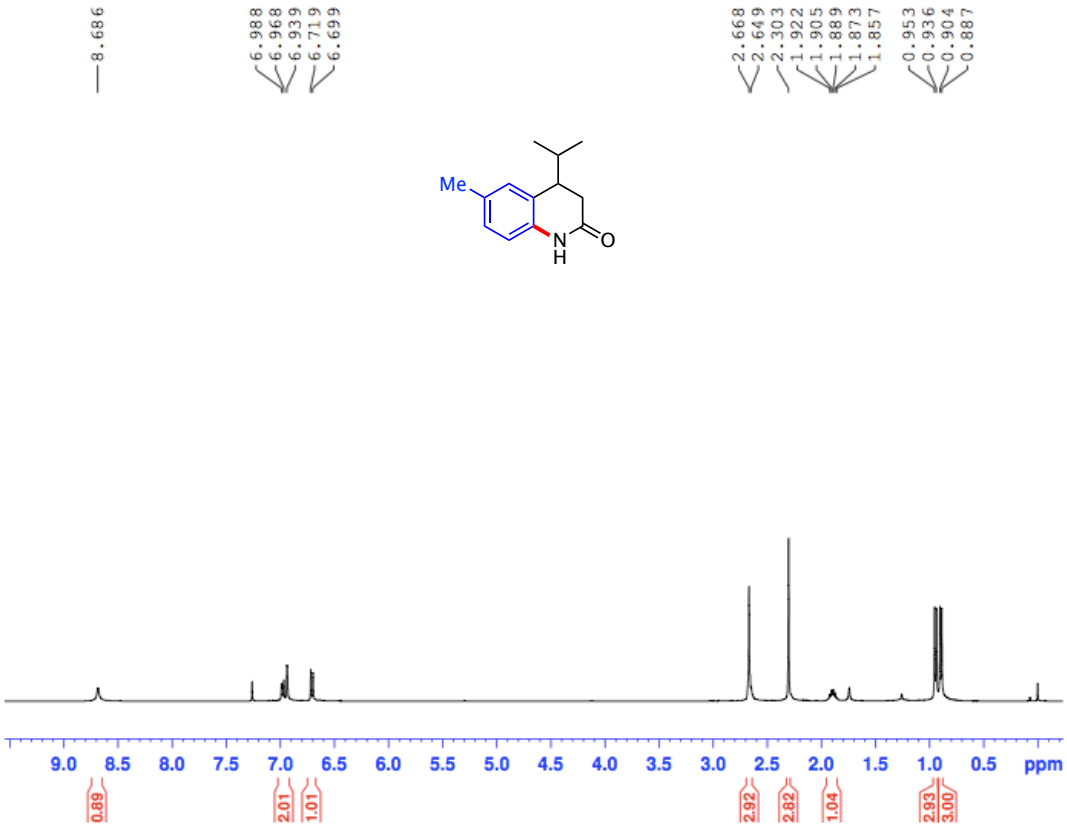

Figure S3.96 ^{13}C NMR Spectrum of ***2v***

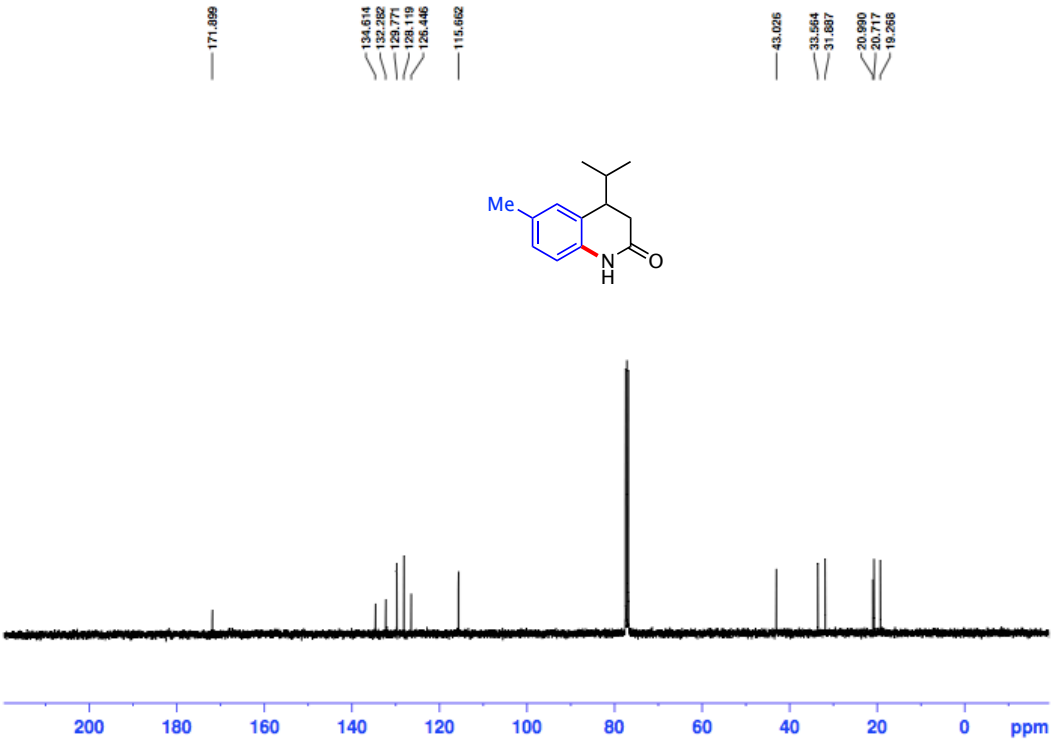

Figure S3.97 ^{1}H NMR Spectrum of ***2w***

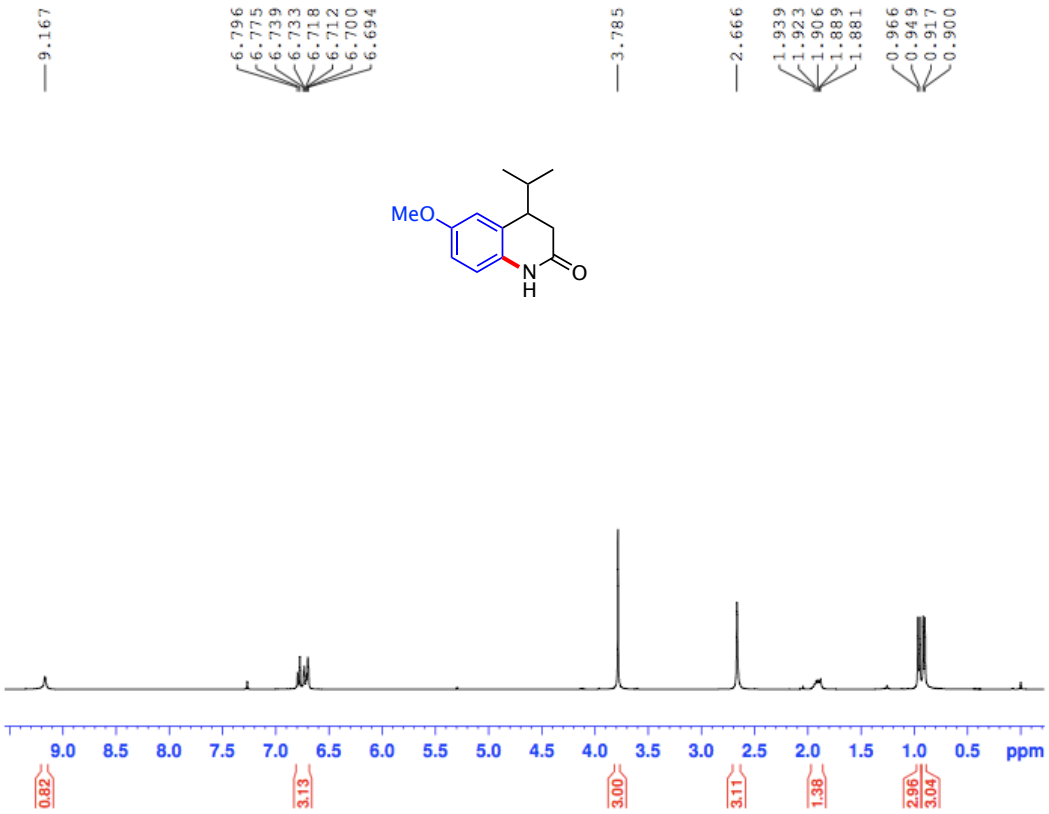

Figure S3.98 ^{13}C NMR Spectrum of ***2w***

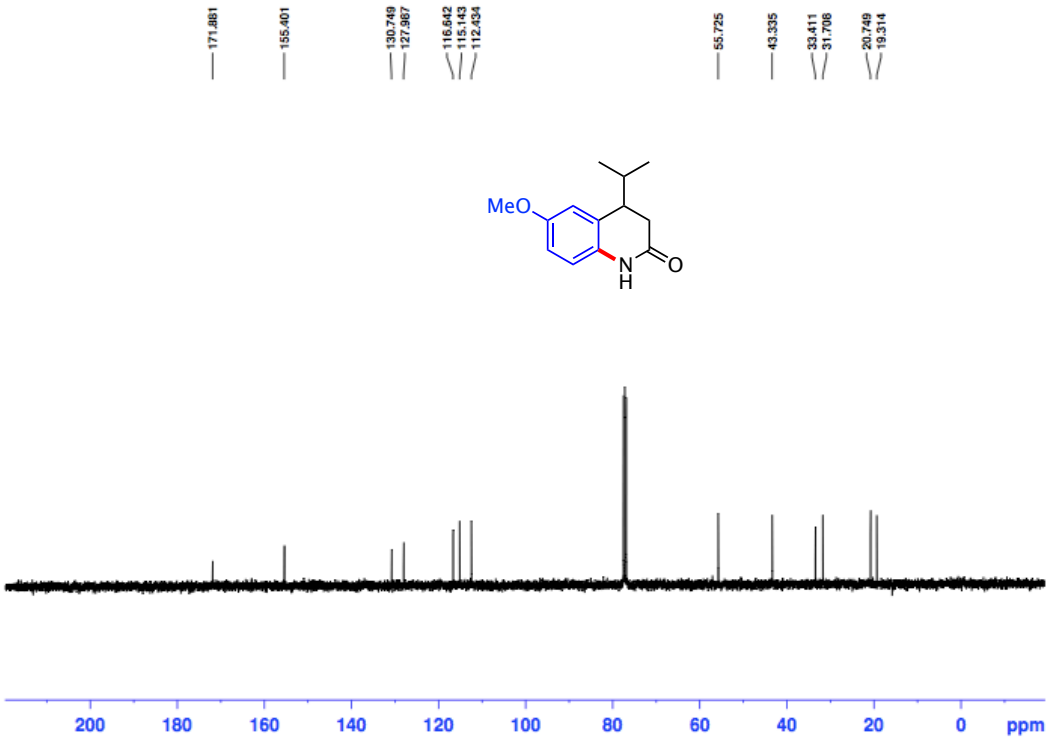

Figure S3.99 ^{1}H NMR Spectrum of ***2x***

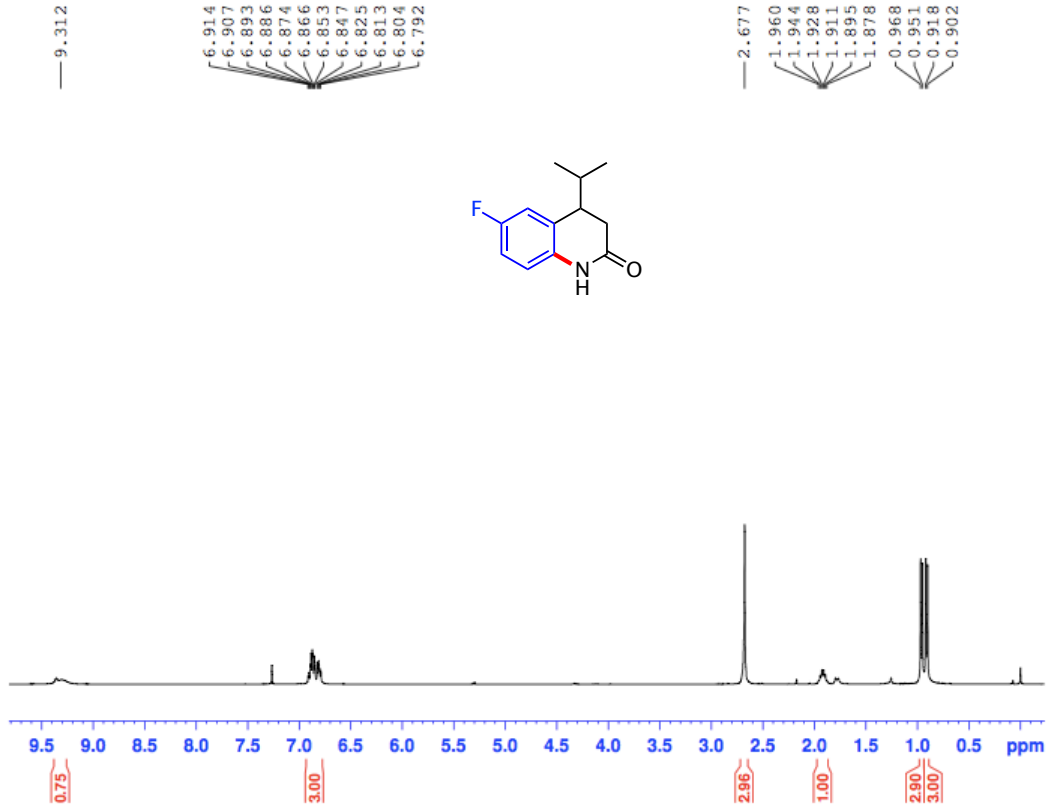

Figure S3.100 ^{13}C NMR Spectrum of ***2x***

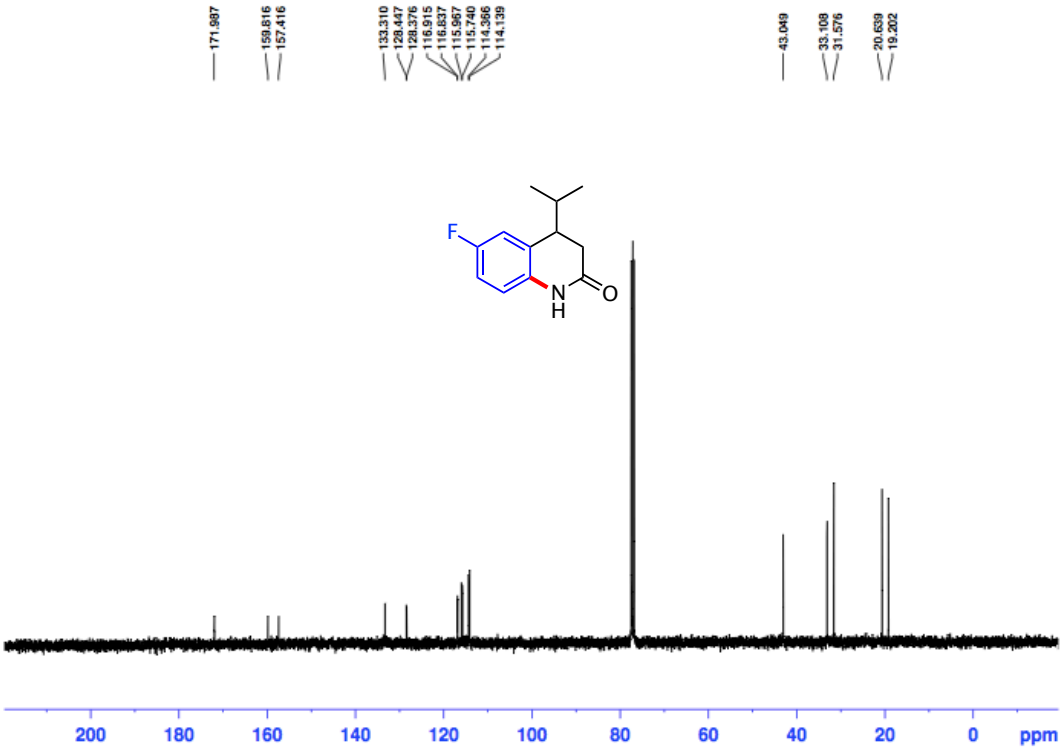

Figure S3.101 ^{1}H NMR Spectrum of ***2y***

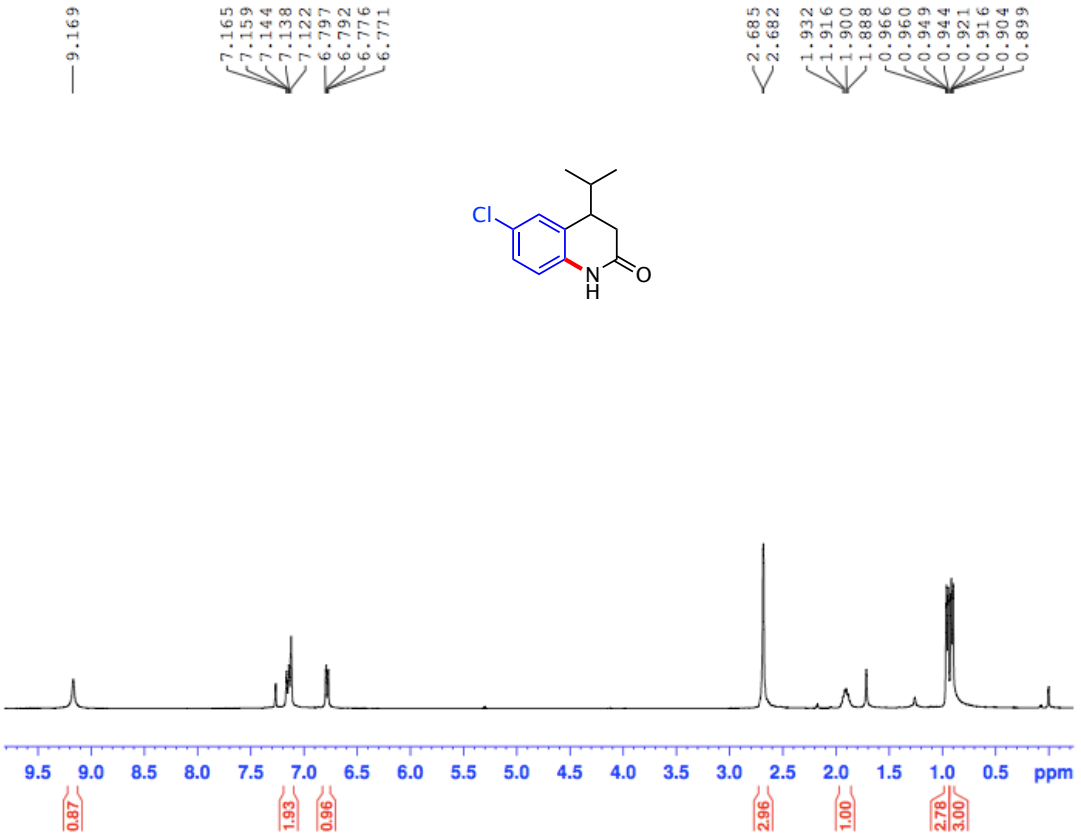

Figure S3.102 ^{13}C NMR Spectrum of ***2y***

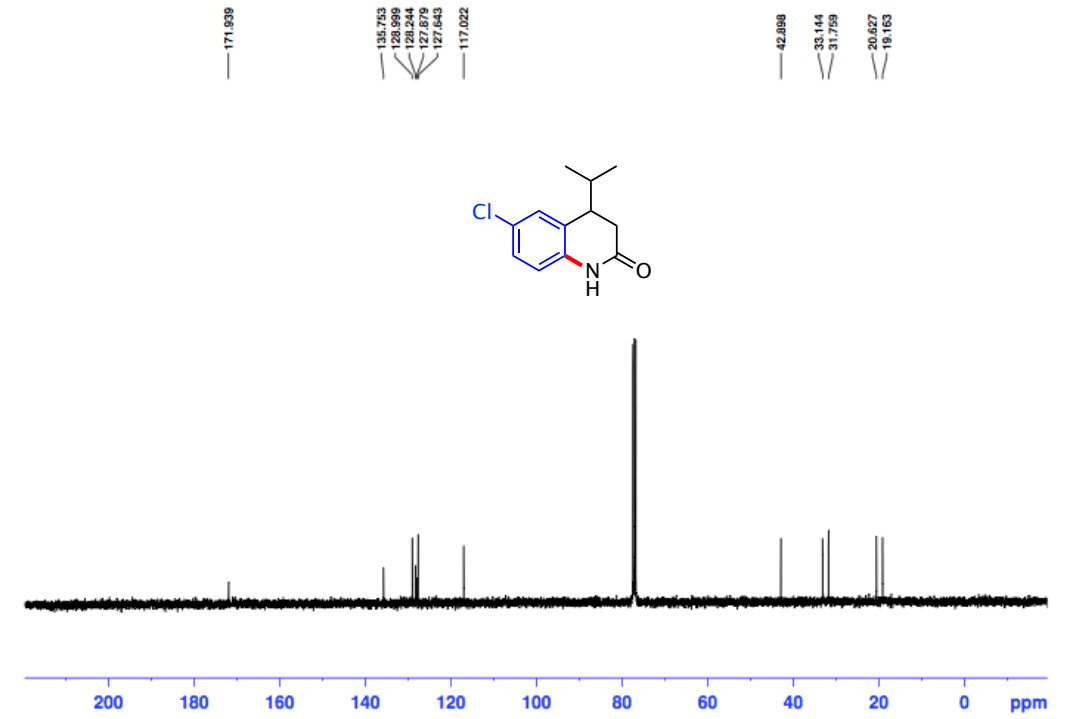

Figure S3.103 ^{1}H NMR Spectrum of ***2z***

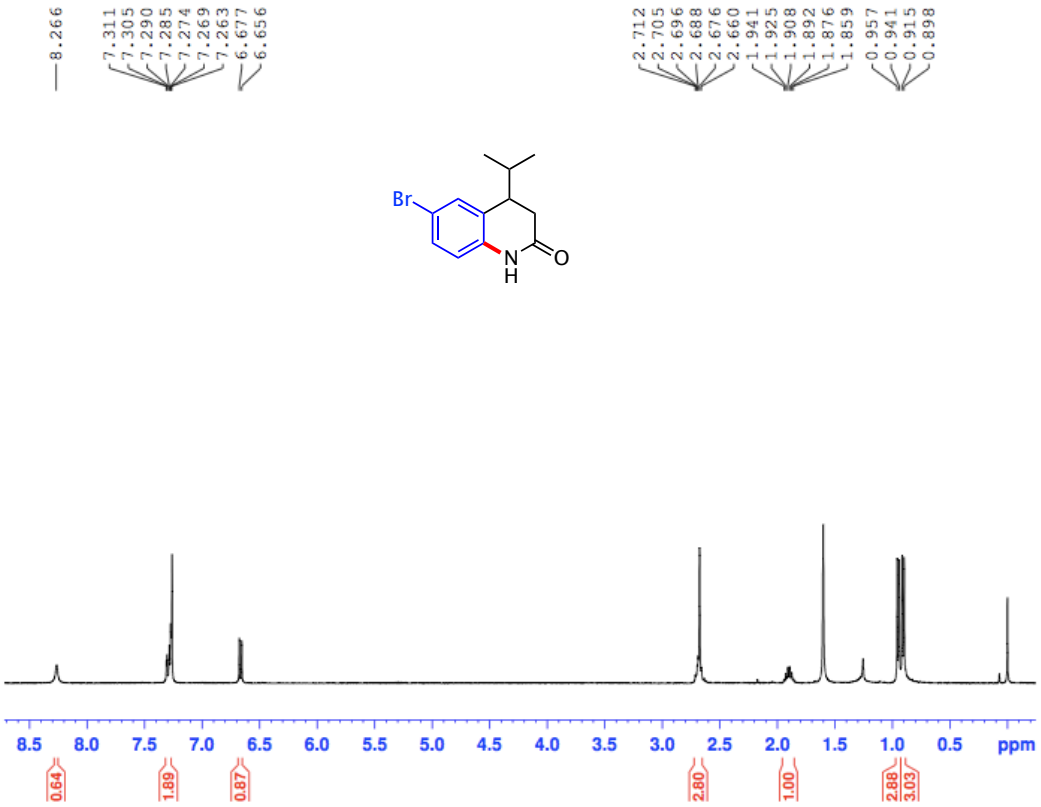

Figure S3.104 ^{13}C NMR Spectrum of ***2z***

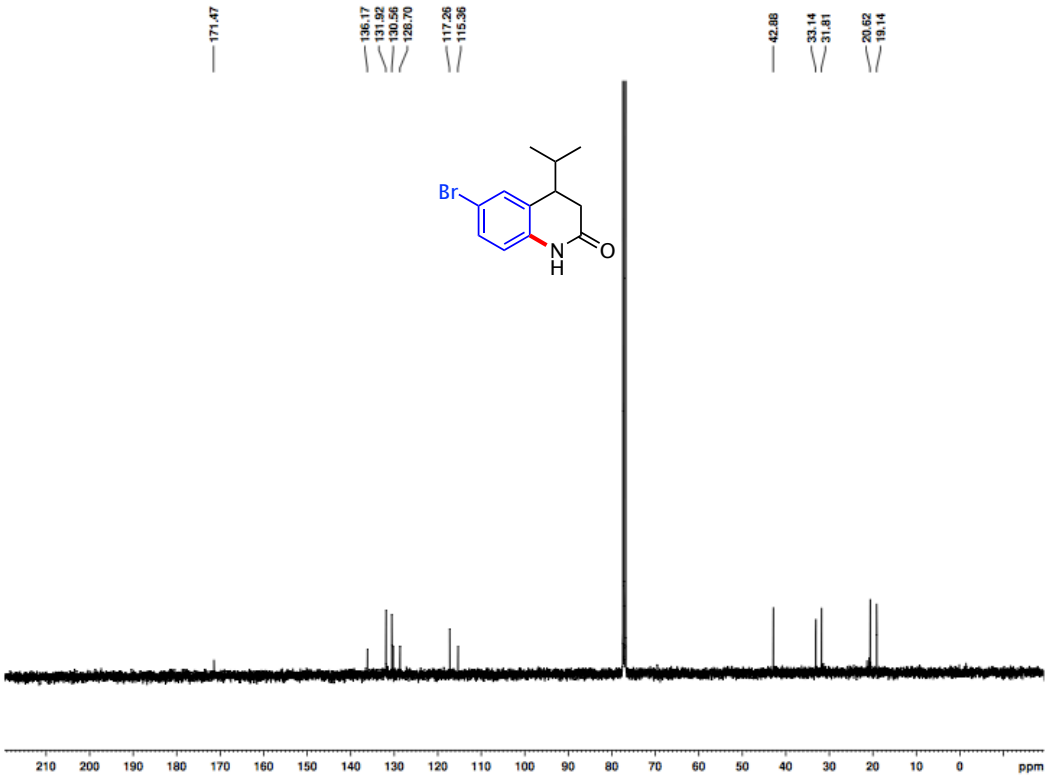

Figure S3.105 ^{1}H NMR Spectrum of ***5a***

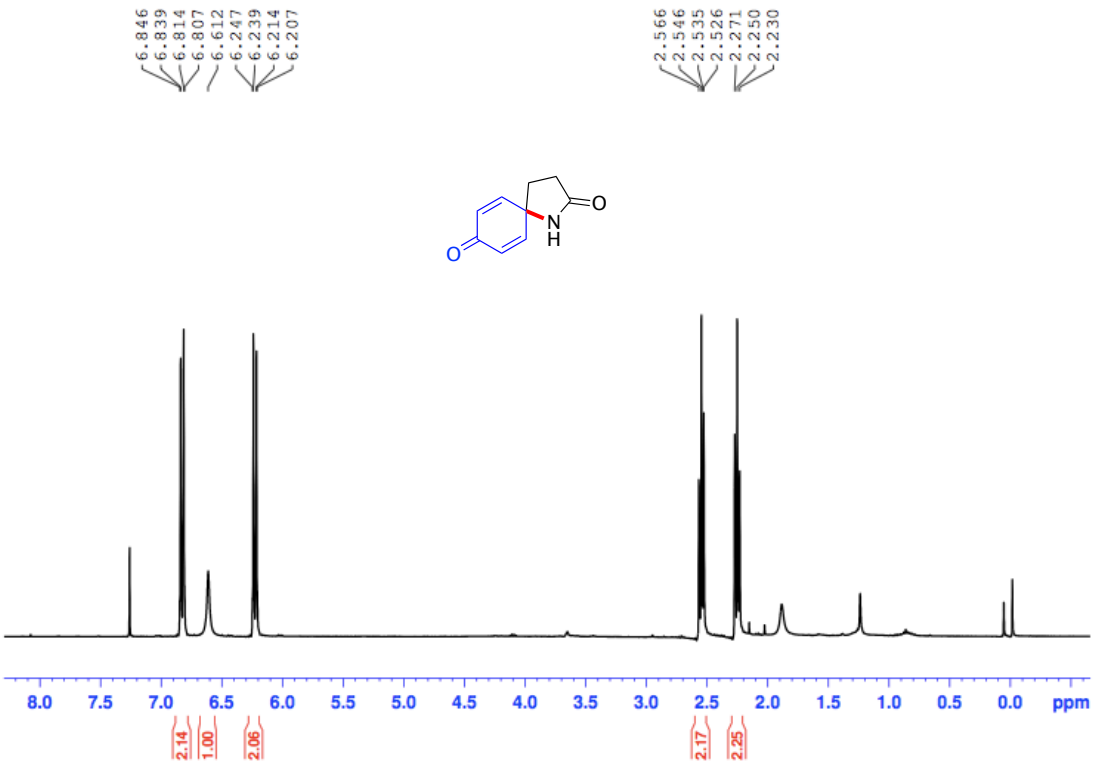

Figure S3.106 ^{13}C NMR Spectrum of ***5a***

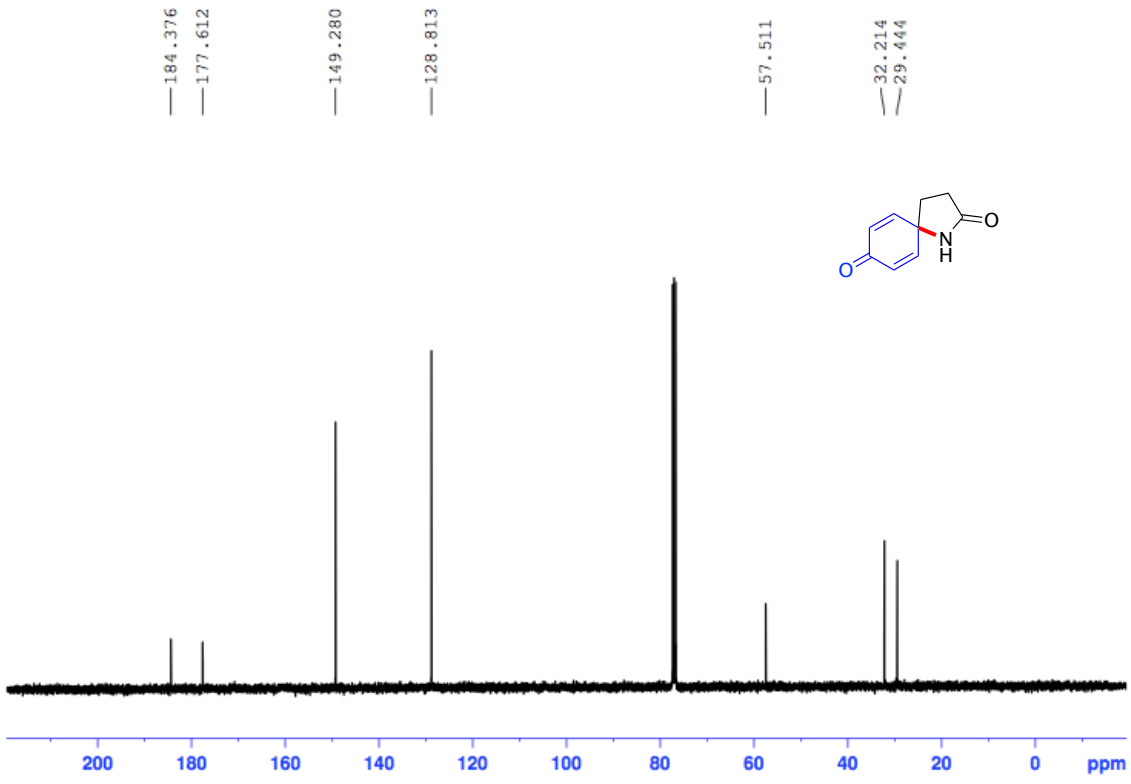

Figure S3.107 ^{1}H NMR Spectrum of ***5b***

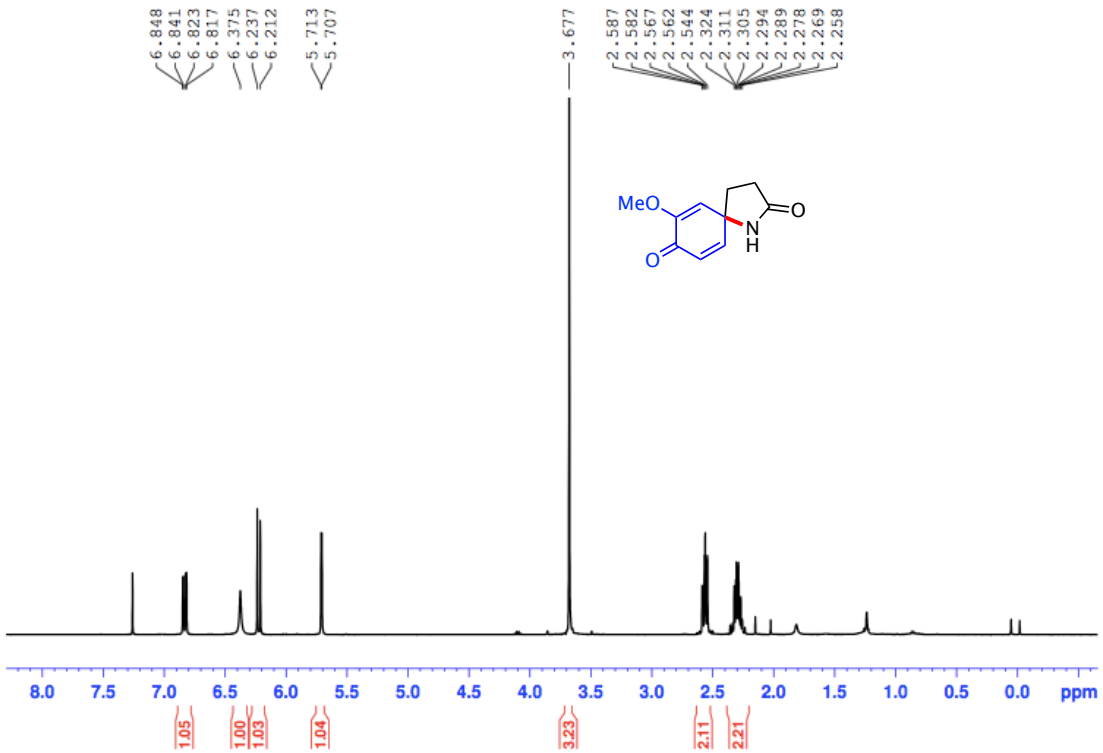

Figure S3.108 ^{13}C NMR Spectrum of ***5b***

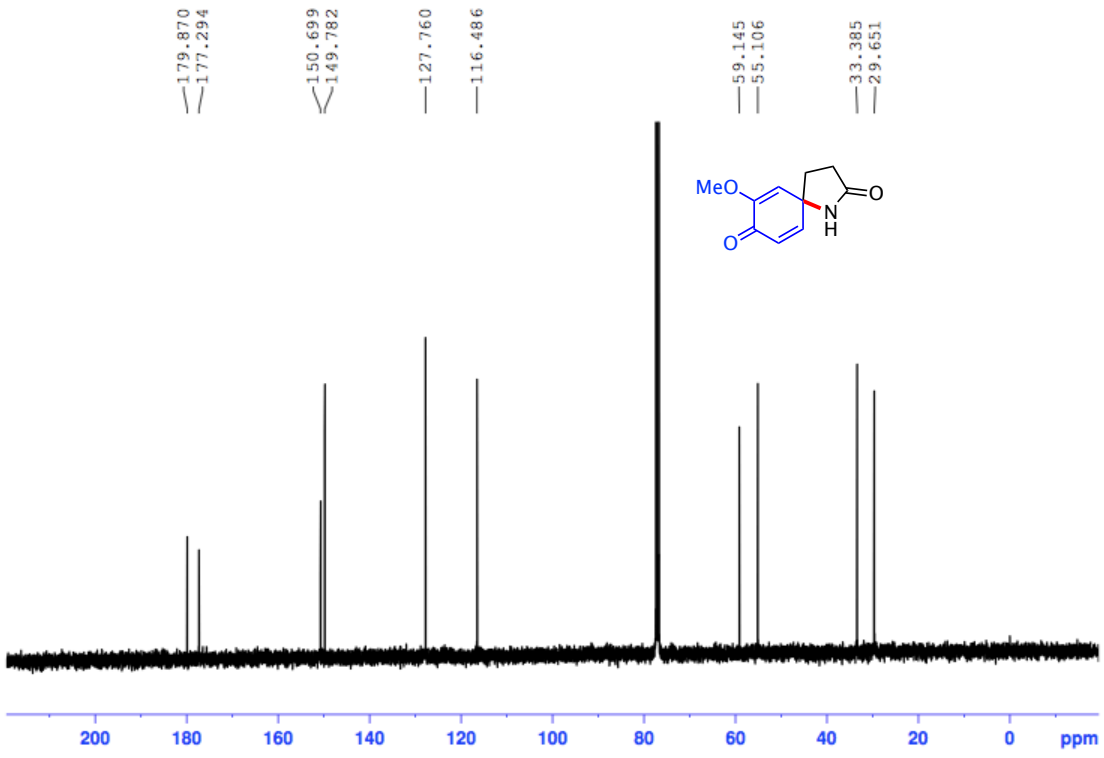

Figure S3.109 ^{1}H NMR Spectrum of ***5c***

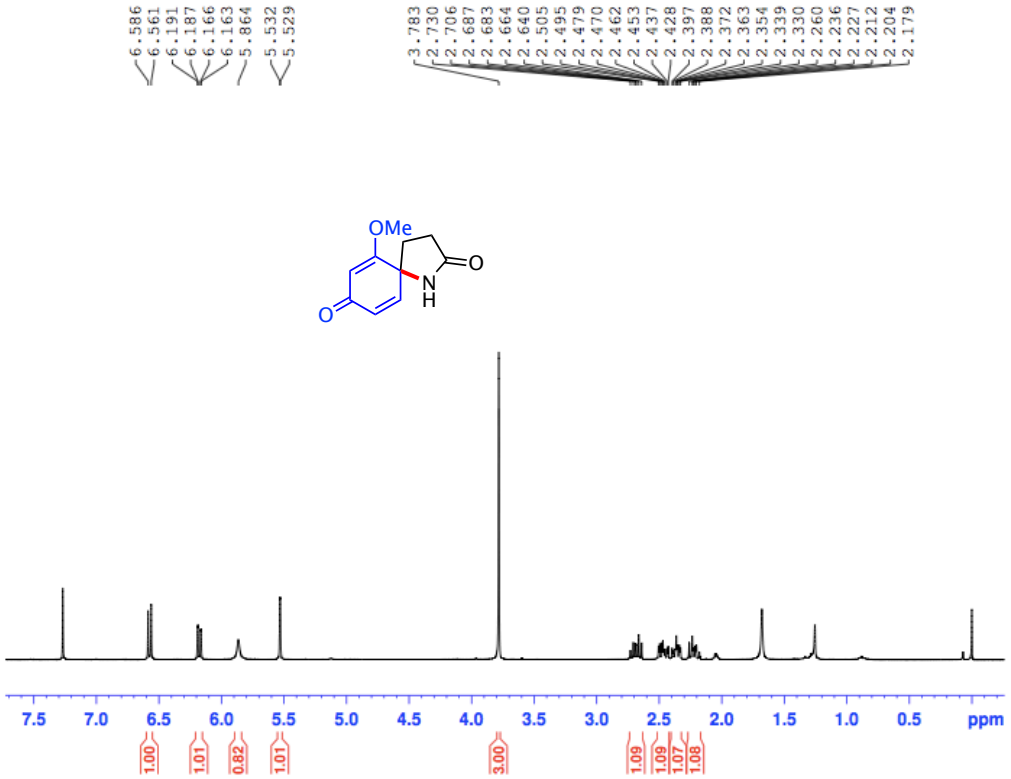

Figure S3.110 ^{13}C NMR Spectrum of ***5c***

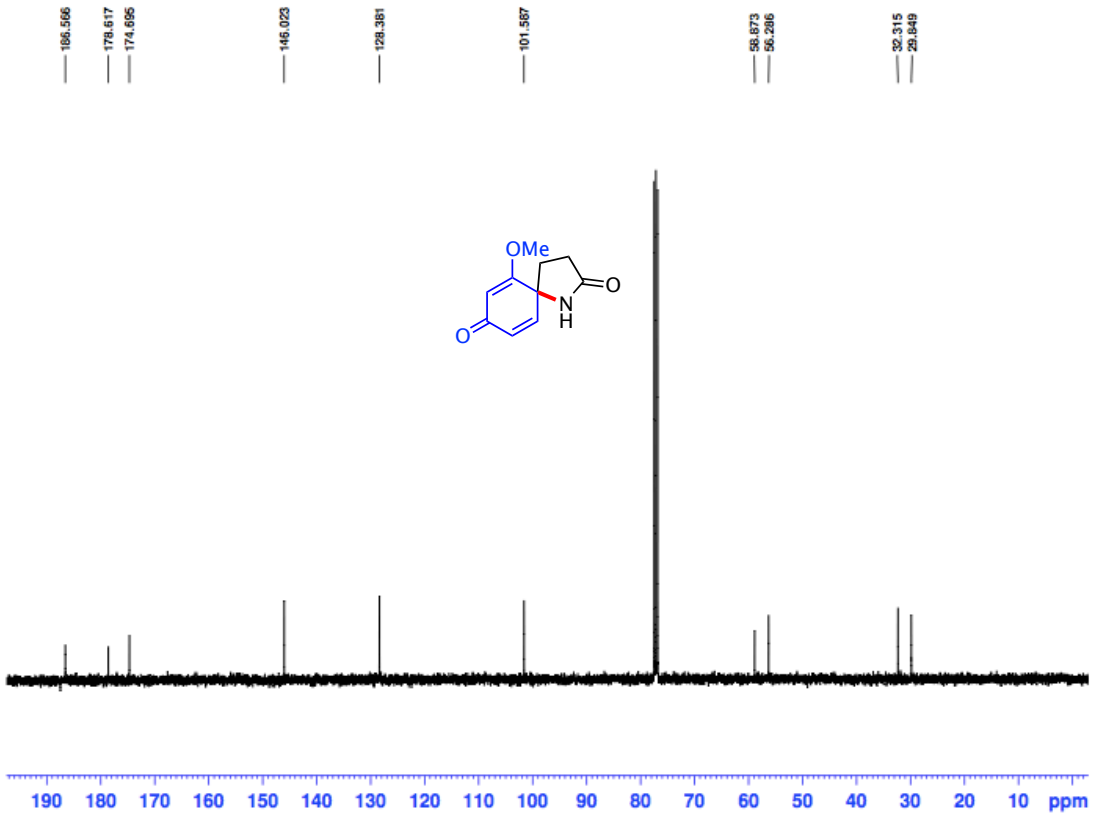

Figure S3.111 ^{1}H NMR Spectrum of ***5d***

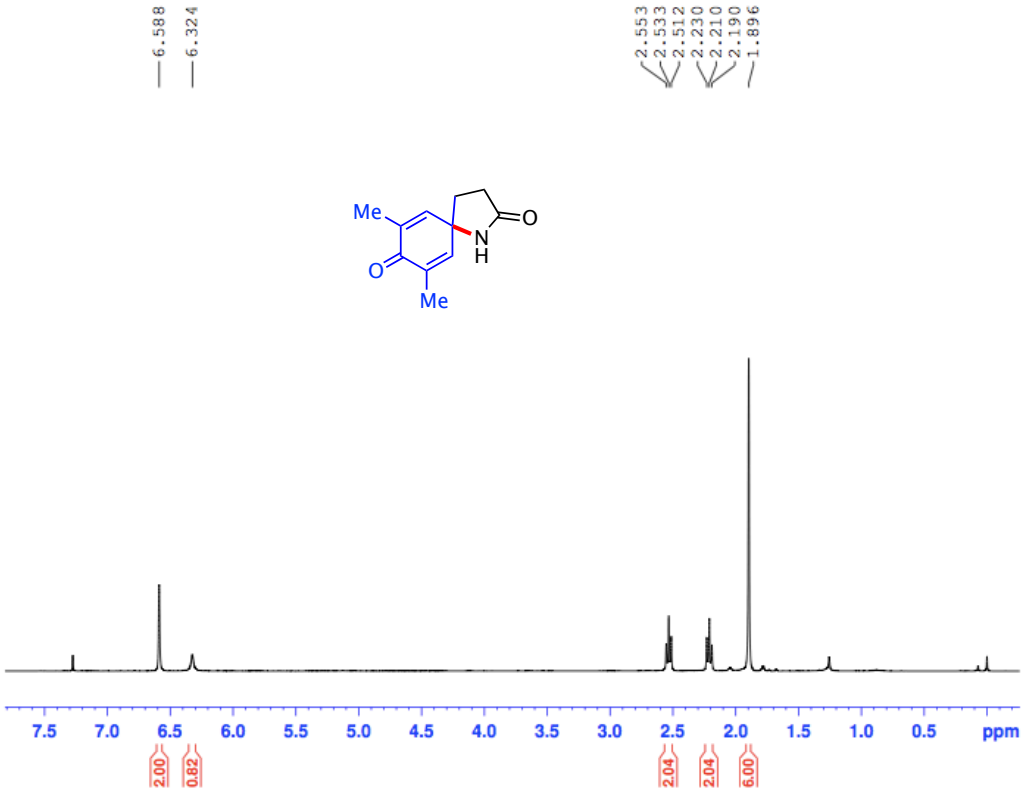

Figure S3.112 ^{13}C NMR Spectrum of ***5d***

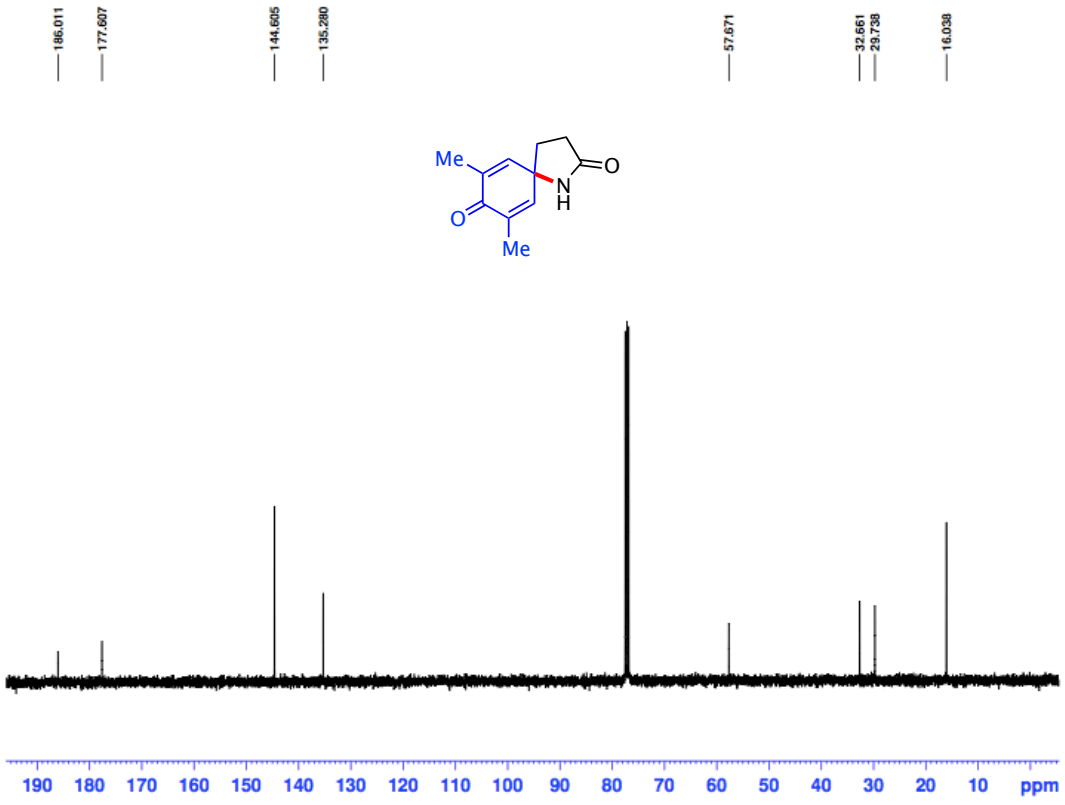

Figure S3.113 ^{1}H NMR Spectrum of ***5e***

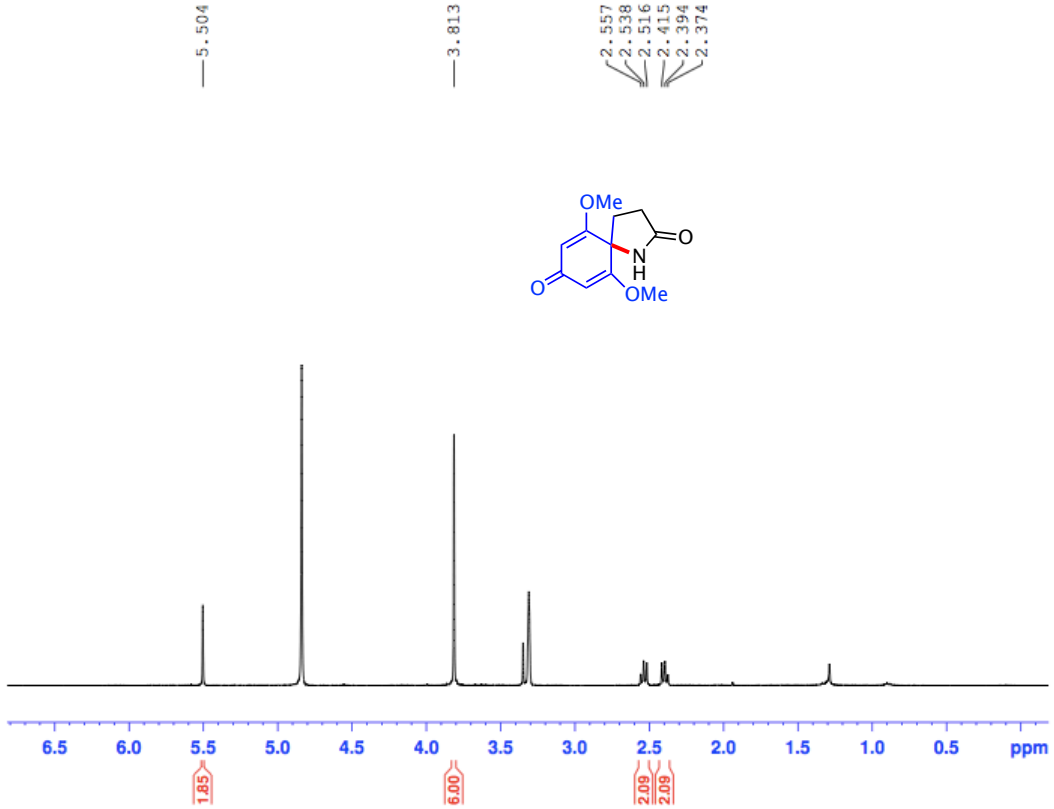

Figure S3.114 ^{13}C NMR Spectrum of ***5e***

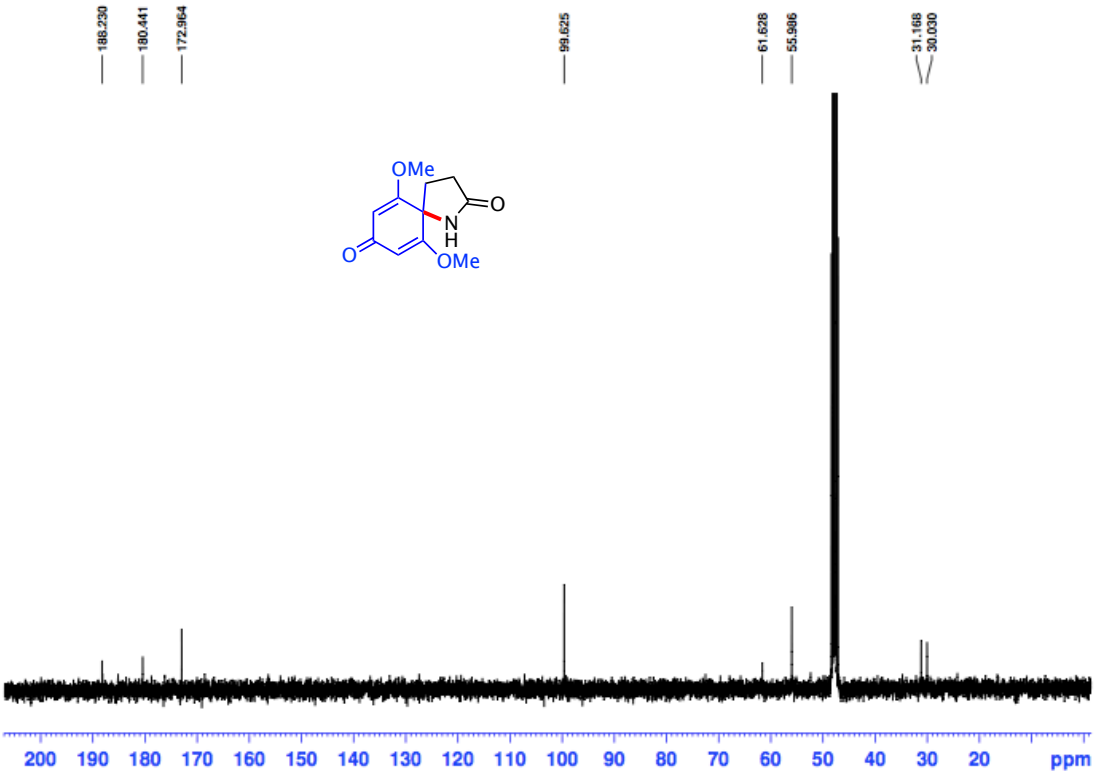

Figure S3.115 ^{1}H NMR Spectrum of ***6g***

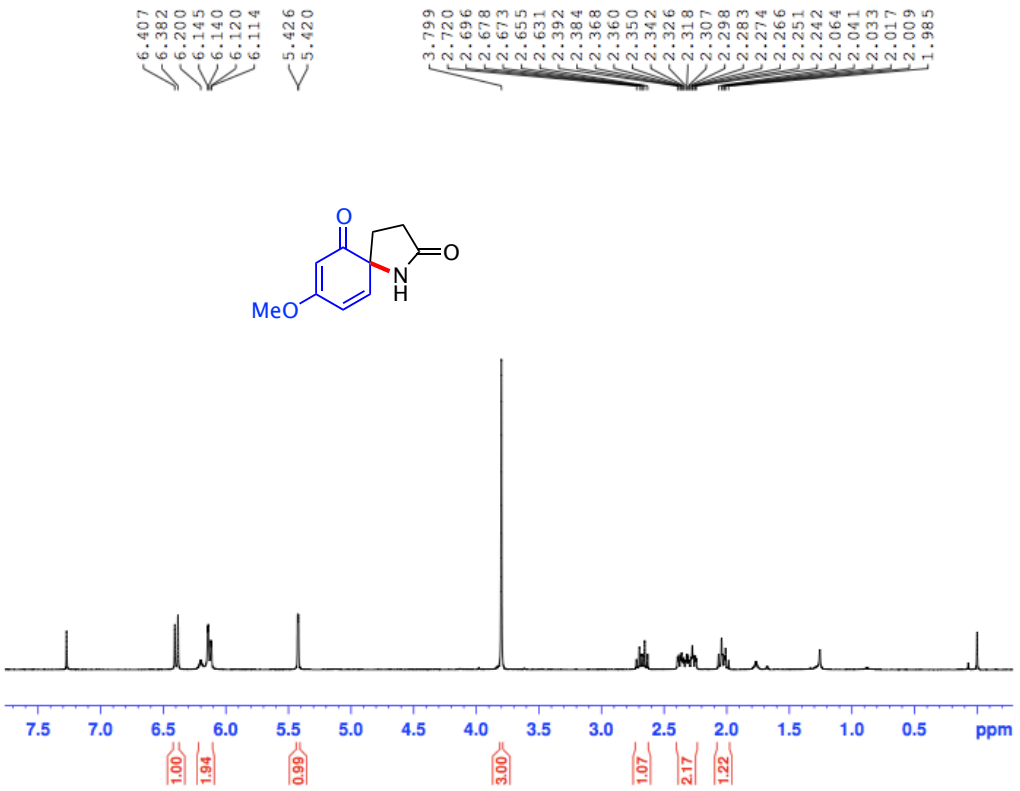

Figure S3.116 ^{13}C NMR Spectrum of ***6g***

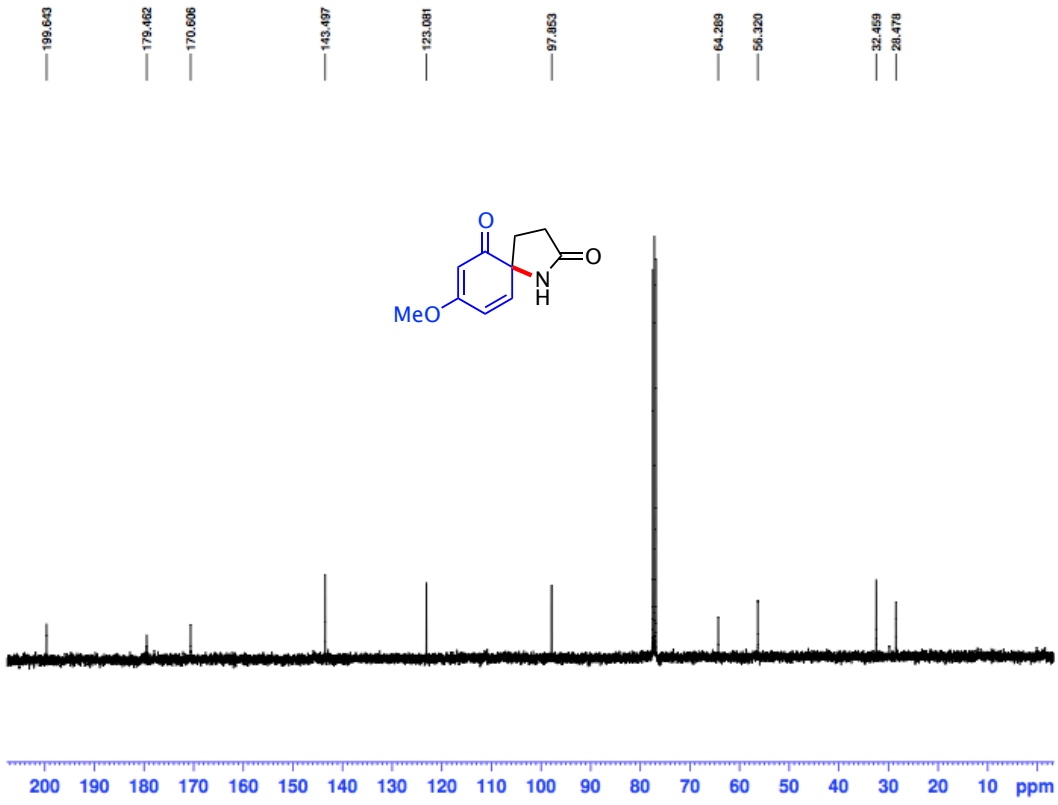

Figure S3.117 ^{1}H NMR Spectrum of **[Ru2]**

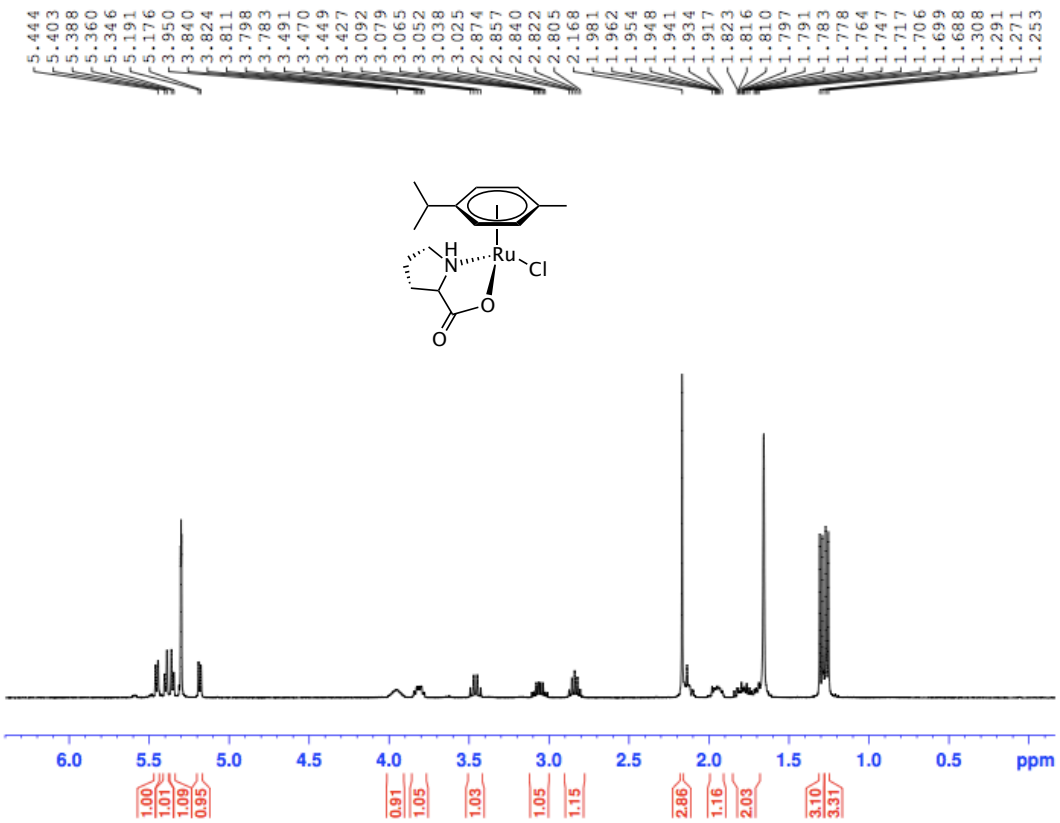

Figure S3.118 ^{13}C NMR Spectrum of **[Ru2]**

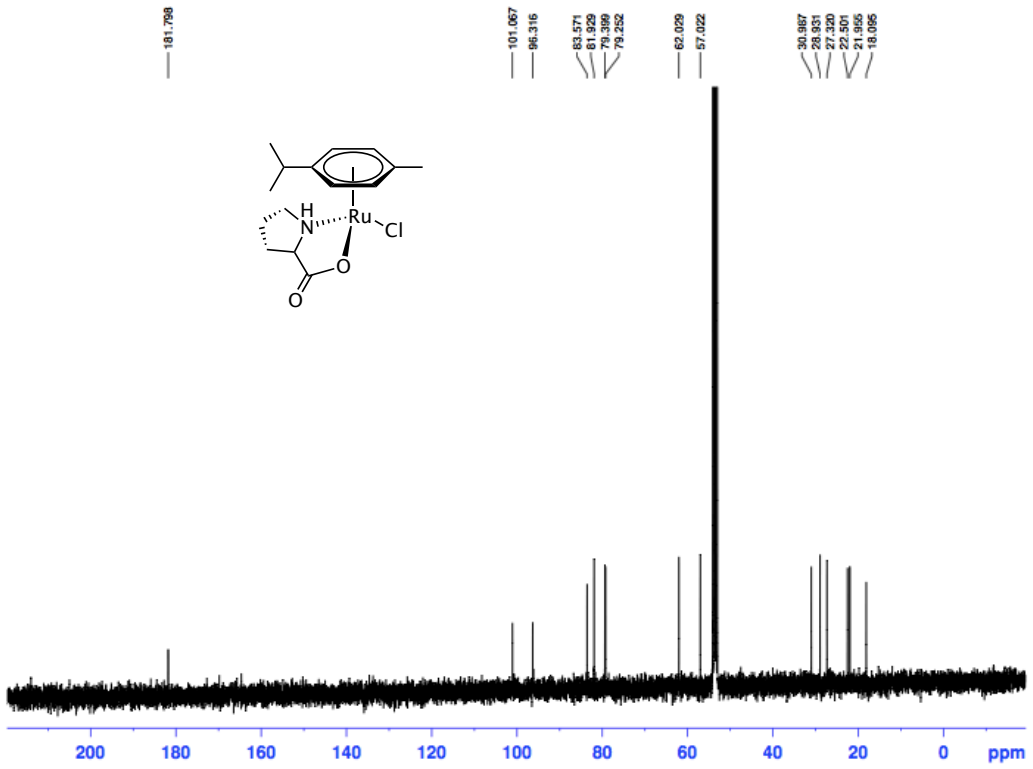

Chapter 4

Enantioselective Ru(II)-Catalyzed Intermolecular Allylic C(sp^3)-H Bond Amidation Reaction of Terminal Alkenes

4.1 Introduction

Allylamines are very important synthetic intermediates for of natural products and pharmaceutical compounds such as (-)-angustureine and (-)-capnellene.[43] Recently, Pd(II)-catalyzed aminations of terminal alkenes are shown to be effective methodology for allylamines synthesis (Scheme 4.1). White and co-workers demonstrated the nucleophilic amination of π-allylpalladium(II) complexes, which are generated by treating a terminal alkenes with a catalytic amount of $Pd(OAc)_2$ and 1,2-bis(phenylsulfinyl)ethane as a ligand. With (+)-(*S,S*)-Cr(salen)Cl (salen = *N,N'*-bis(3,5-di-*tert*-butylsalicylidene)-1,2-cyclohexanediamino) as co-catalyst, the desired allylamines were obtained in moderate to good yields.[44] Liu's group later reported that the analogus Pd(II)-catalyzed allylic C-H amination would give better results is when the terminal alkenes were used in excess. Moreover, a combination of melanic anhydride (40 mol %) in oxygen atmosphere (6 atm) gave the desired allylamines in good yields (53 – 81 %). In both cases, linear allylic amines are found to be the major isomers (> 20:1 L:B), indicating that the regioselectivity is preferred to the nucleophilic attack on at less hindered site of the allyl-Pd(II) intermediate.

Scheme 4.1. Pd-Catalyzed Linear-Selective Allylic Aminations of Terminal Alkenes

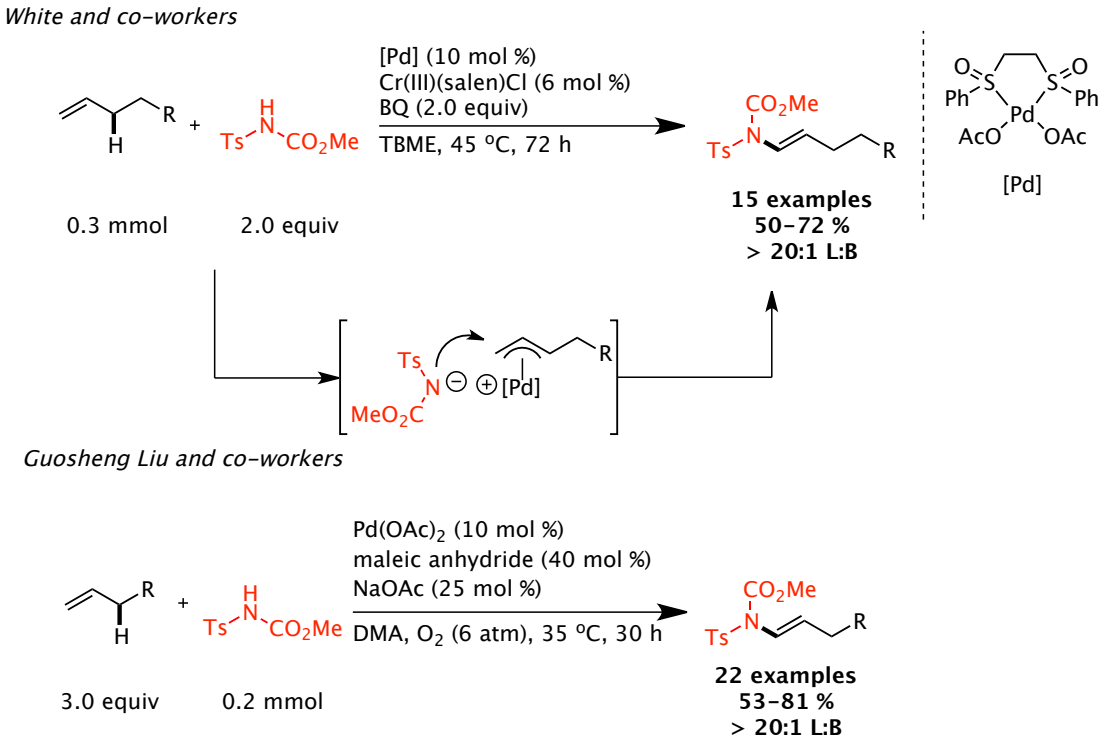

For the branched-selective allylic C-H amidations, Rovis's group[46] and Glorius's group[47] demonstrated the Cp*Ir(III)-catalyzed branched-selective intermolecular allylic C-H amidation reaction of terminal alkenes (Scheme 4.2). Treatment of terminal alkenes (0.1 mmol) and 3-methyl-1,4,2-dioxazol-5-one with $[Cp^*IrCl_2]_2$ as a catalyst, $AgNTf_2$ (15 mol %) and LiOAc or AgOAc (20 mol %) in DCE at 35 °C gave moderate to good yield of allylamines formation. The reaction is highly branched-selective (> 20:1 B:L). The key intermediate was proposed to be the π-allyl-Ir(III)-amido complex, and the selective nitreniod inserted to the C3 of terminal alkenes afforeded the branched allylamides.

Scheme 4.2. Ir(III)-Catalyzed Branched-Selective Amidation of Terminal Alkenes

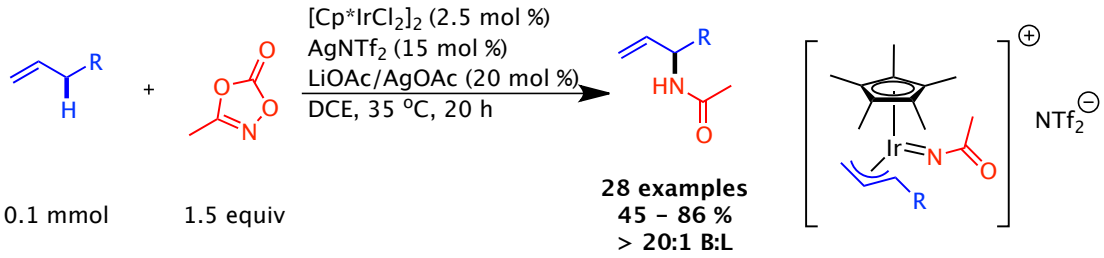

4.2 Results and Discussion

4.2.1 Preliminary Results

To begin, we treated 1-decene (0.1 mmol) and 3-methyl-1,4,2-dioxazol-5-one (1.5 equiv) with a catalytic amount of [Ru(*p*-cymene)Cl_2]$_2$ (2.5 mol %), $AgNTf_2$ (15 mol %) and LiOAc (20 mol %) in DCE (0.5 mL) at 35 °C for 16 h, the desired allylic amide ***3aa*** product was isolated in 10 % (Scheme 4.3).

Scheme 4.3. Preliminary Results

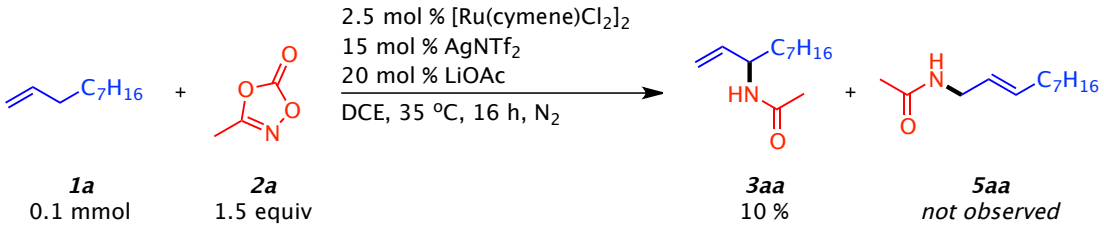

The ^{1}H NMR spectrum was employed to differentiate the branched (***3aa***) and the linear allylamide product (***5aa***). As shown in Figure 4.1, a multiplet at 5.796 – 5.713 ppm corresponds to the allylic proton H_a. For the linear allylamide product, the allylic proton H_a is assigned to doublet of doublets (dd) at δ_H 5.40 ppm.[44] As revealed by the ^{1}H NMR spectrum, the characteristic doublet of doublets signal at 5.40 ppm was

not detected while the multiplet signal at 5.70 ppm was detected so that the product was characterized as branched allylamide product (***3aa***).

Figure 4.1. ^{1}H NMR Spectrum of Allylic Amide Product (***3aa***)

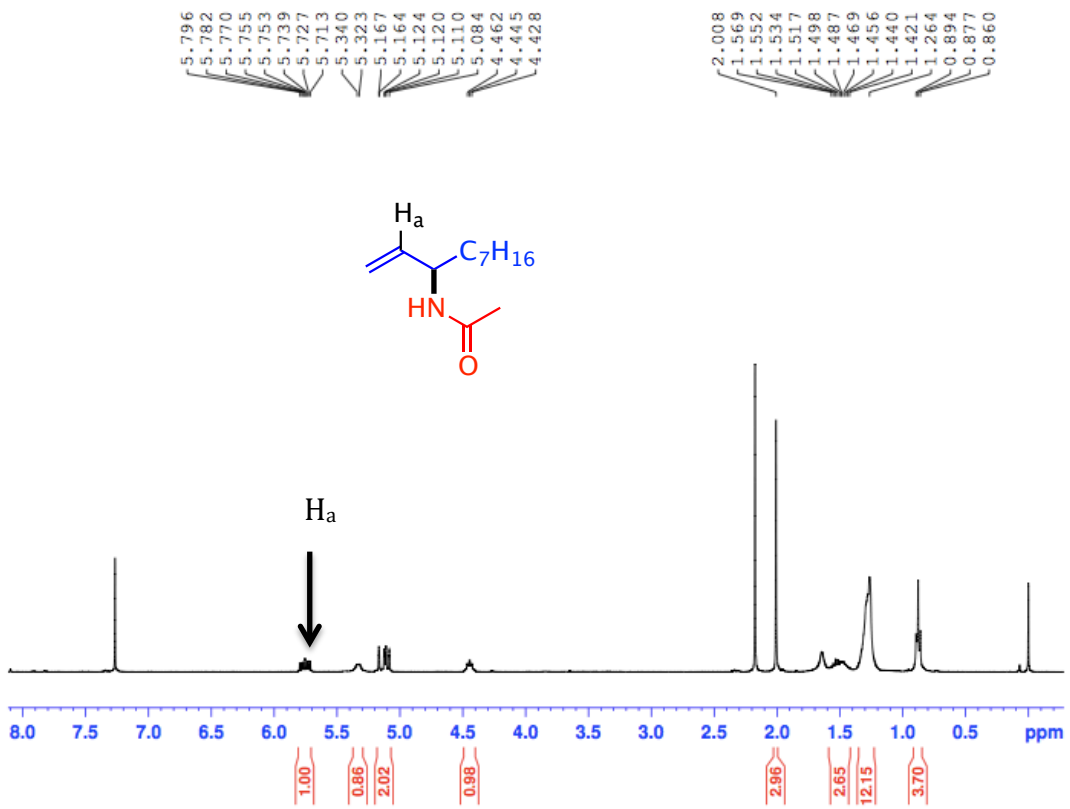

4.2.2 Optimization Results

Silver salts are presumably used to remove the chloride ligands from [Ru(*p*-cymene)Cl_2]$_2$ to generate the coordinatively unsaturated Ru(II) complexes. The optimization study was first initiated by examining the effects of silver salts. As shown in Table 4.1, employing $AgSbF_6$ (entry 2) resulted in improving ***3aa*** formation up to 35 % yield. No product formation was registered when AgOAc, AgTFA and AgOTf were used (entries 3 – 6). Probably, the larger counter anion such as SbF_6^- is to necessary for sustaining the vacant site availability during the C-H activation step

and Ru-nitrenoid formation. A control experiment (entry 7) showed that the allylamide product was not formed in the absence of any silver salts. This finding suggests that the removal of the chlorides is to generate the active Ru(II) complexes.

Table 4.1. Effects of Silver Salts

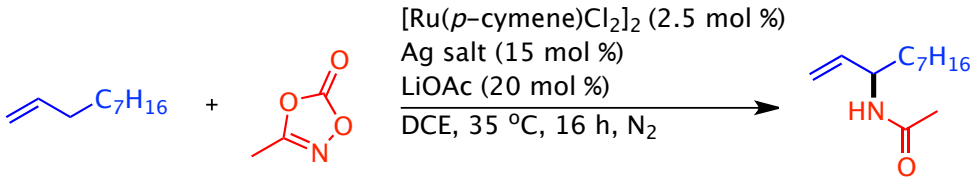

1a 0.1 mmol + ***2a*** 1.5 equiv → ***3aa***

entry	Ag salt	yield (%)[a]
1	$AgNTf_2$	10(10)
2	$AgSbF_6$	35
3	AgOAc	n.r.
4[b]	AgOAc	n.r.
5	AgTFA	n.r.
6	AgOTf	n.r.
7	--	n.r.

[a]Reaction conditions: ***1a*** (0.1 mmol), ***2a*** (1.5 equiv), [Ru(*p*–cymene)Cl_2]$_2$ (2.5 mol %), Ag salt (15 mol %) and LiOAc (20 mol %) in DCE (0.5 mL) at 35 °C for 16 h under N_2 protection. ^{1}H NMR yield using dibromomethane as an internal standard; isolated yield shown in the parathesis. [b]No LiOAc was added.

Next, we investigated the solvent effects on the amidation. Table 4.2 depicts the results for solvent screening. All polar protic solvents such as HFIP, TFE, MeOH and EtOH (entries 1 – 4) failed to give any desired allylamide products. We observed that the 3-methyl-1,4,2-dioxazol-5-one (***2a***) was hydrolyzed by the polar protic solvents. Likewise, employing THF, MeCN, EtOAc, acetone and dioxane (entries 5 – 9) have met with unsuccessful outcome. In this work, only DCE apparently produced the best results.

Table 4.2. Solvent Effects

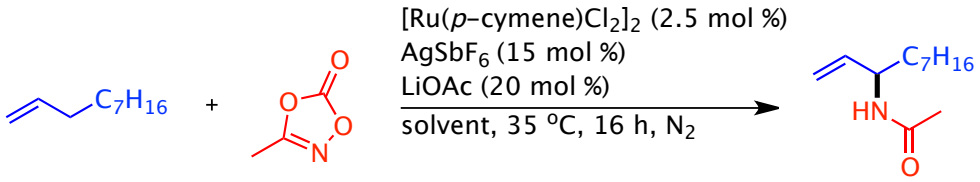

1a 0.1 mmol | ***2a*** 1.5 equiv | ***3aa***

entry	solvent	yield (%)[a]
1	HFIP	6
2	TFE	n.r.
3	MeOH	n.r.
4	EtOH	n.r.
5	THF	n.r.
6	MeCN	n.r.
7	Ethyl Acetate	n.r.
8	Acetone	n.r.
9	Dioxane	n.r.

[a]Reaction conditions: ***1a*** (0.1 mmol), ***2a*** (1.5 equiv), [Ru(*p*–cymene)Cl_2]$_2$ (2.5 mol %), $AgSbF_6$ (15 mol %) and LiOAc (20 mol %) in solvent (0.5 mL) at 35 °C for 16 h under N_2 protection. ^{1}H NMR yield using dibromomethane as an internal standard; isolated yield shown in the parathesis. .

The effect of temperature on the amidation was studied (Table 4.3). The reaction temperature at 60 °C showed no improvement in amidation (entry 1). However, when performing the reaction at temperature higher than 60 °C, the yield of allylamide product formation dropped (entries 2 – 3). Interestingly, the 3-methyl-1,4,2-dioxazol-5-one was employed in a limiting quantity (0.1 mmol) with 1.5 equiv of 1-decene being used, the allylamides were formed in 44 % (entry 4).

Table 4.3. Effects of Temperature on the Amidation

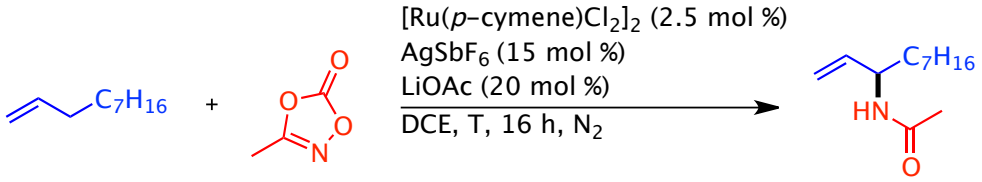

1a 0.1 mmol + ***2a*** 1.5 equiv → ***3aa***

entry	T (°C)	yield (%)[a]
1	60	35
2	80	22
3	100	19
4[b]	35	44

[a]Reaction conditions: ***1a*** (0.1 mmol), ***2a*** (1.5 equiv), [Ru(*p*–cymene)Cl_2]$_2$ (2.5 mol %), $AgSbF_6$ (15 mol %) and LiOAc (20 mol %) in DCE (0.5 mL) at T °C for 16 h under N_2 protection. ^{1}H NMR yield using dibromomethane as an internal standard; isolated yield shown in the parathesis. [b]***2a*** (0.1 mmol) and ***1a*** (2.0 equiv) were used instead.

Regarding to the additive effects, Table 4.4 showed that employing 1.0 equiv of either acetic acid or pivalic acid would result in a good product yields (entry 1 – 2). The trifluoroacetic acid and benzenesulfonic acid gave relatively poor product yields in allylamides formation (entries 3 – 4), persumbly the strong acids hydrolyzed the 3-methyl-1,4,2-dioxazol-5-one (***2a***) into acetamide prior to their reaction with the Ru catalyst. The weak acids such as benzoic acid (entry 5), and inorganic acid such as H_3PO_4 (entry 6) failed to affored better resutls. Addition of water as additives (entry 7) did not result in significant different in product yield. To alleviate the problem of hydrolysis of 3-methyl-1,4,2-dioxazol-5-one (***2a***), ***2a*** was first dissolved in 300 µL of DCE. The solution was then added into reaction mixture in six separate portions (50 µL per 15 mins). With the modified procedure, the prodtuct yields of amidation product increased from 53 % to 68 % based on ^{1}H NMR analysis (entry 10). Employgin less quantity (0.3 and 0.5 equiv) of acetic acid slowed down the rate of

reaction, and yet no further improvement in product yields by employing more actic acid (2.0 equiv) as additives (entries 8 – 11).

Table 4.4. Effects of Additives on Amidation Reaction

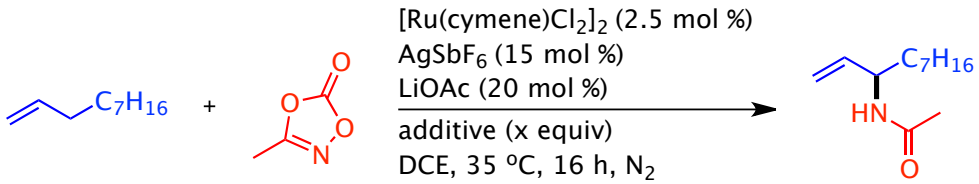

1a 2.0 equiv | ***2a*** 0.1 mmol | ***3aa***

entry	x (equiv)	additive	yield (%)[a]
1	1.0	AcOH	53
2	1.0	pivalic acid	46
3	1.0	TFA	35
4	1.0	benzenesulfonic acid	< 2
5	1.0	benzoic acid	7
6	1.0	H_3PO_4	21
7	1.0	H_2O	33
8[b]	0.3	AcOH	35
9[b]	0.5	AcOH	53
10[b]	1.0	AcOH	68(60)
11[b]	2.0	AcOH	63

[a]Reaction conditions: ***1a*** (2.0 equiv), ***2a*** (0.1 mmol), [Ru(*p*-cymene)Cl_2]$_2$ (2.5 mol %), $AgSbF_6$ (15 mol %), LiOAc (20 mol %) and additive (x equiv) in DCE (0.5 mL) at 35 °C for 16 h under N_2 protection. ^{1}H NMR yield using dibromomethane as an internal standard; isolated yield shown in parathesis.[b]***2a*** was added in bench-wise with 0.3 mL DCE (0.05 mL per 15 mins).

Table 4.5 showed the effects of bases on the amidation. Employing acetate bearing larger size cations (e.g. Na^+, K^+, Cs^+ and Ag^+) than proton gave the desired allylamides in poor to moderate yields (entries 1-5). More basic anions were found to inhibit the amidation reaction (entries 10 – 14). Noted that CF_3COO^- and TfO^- are good leaving groups for C-H activation step.[48] When AgTFA and AgOTf were used instead of LiTFA and LiOTf (entry 15-16), the product yield did not improved. Moreover, an excess amount of LiOAc used would inhibit the amidation reaction (entry 7 – 9). Yet, the product yields dropped from 68 % to 33 % in the absence of LiOAc (entry 6).

Table 4.5. Effects of Bases on Amidation Reaction

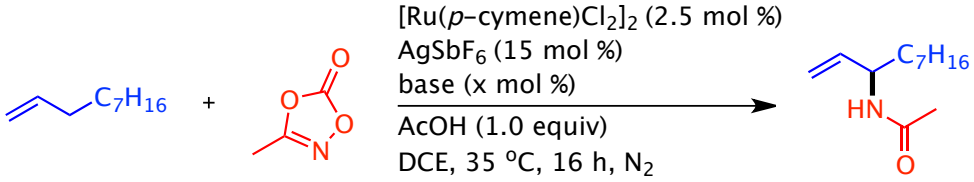

1a 2.0 equiv | ***2a*** 0.1 mmol | ***3aa***

entry	x (mol %)	base	yield (%)[a]
1	20	LiOAc	68
2	20	NaOAc	26
3	20	KOAc	n.r.
4	20	CsOAc	19
5	20	AgOAc	58
6	0	LiOAc	33
7	50	LiOAc	35
8	100	LiOAc	16
9	200	LiOAc	5
10	20	Li_2CO_3	26
11	20	Li*t*OBu	28
12	20	LiTFA	20
13	20	LiOTf	14
14	20	LiOOCPh	31
15	20	AgTFA	14
16	20	AgOTf	22

[a]Reaction conditions: ***1a*** (2.0 equiv), ***2a*** (0.1 mmol), [Ru(*p*-cymene)Cl_2]$_2$ (2.5 mol %), $AgSbF_6$ (15 mol %), AcOH (1.0 equiv) and base (x mol %) in DCE (0.5 mL) at 35 °C for 16 h under N_2 protection. Dioxazolone was added in beach-wise with 0.3 mL DCE (0.05 mL per 15 mins). ^{1}H NMR yield using dibromomethane as an internal standard.

4.2.3 Substrate Scope Studies

The results of substrate scope studies are shown in Table 4.6. The terminal alkenes with linear chain structure (***3aa***, ***3ga*** and ***3ha***) gave the desired branched allylamides in 40 – 60 % isolated yield. For alkenes bearing aryl substituents (***3ca***, ***3da*** and ***3ea***) as substrates, the allylamides were formed in 18 – 35 % isolated yields. Interestingly, the analogus reactions of the alkene with benzyl group (***3fa***) and cyclohexyl group (***3ba***) afforded the corresponding allylamides in 55 % isolated yields. The results

show that the steric repulsion of the terminal alkenes has significant effect on the amidation reaction.

Table 4.6. Substrate Scope Studies of Terminal Alkenes

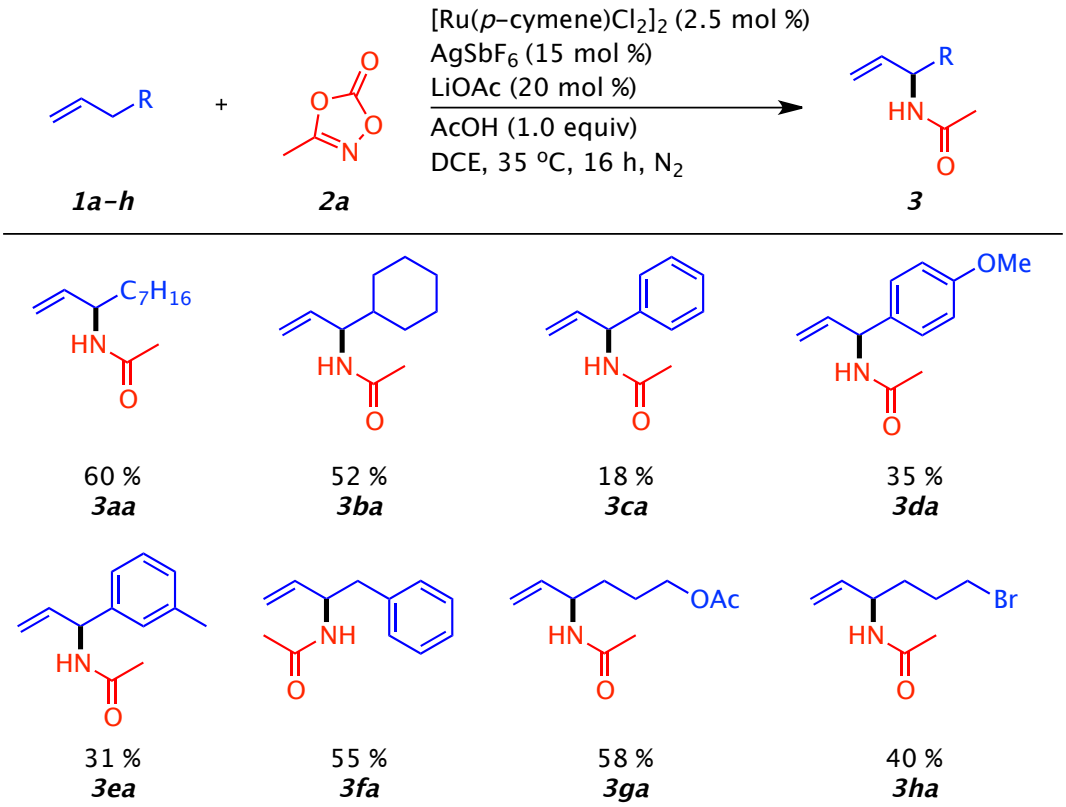

Reaction conditions: alkenes (2.0 equiv), ***2a*** (0.1 mmol), [Ru(*p*-cymene)Cl_2]$_2$ (2.5 mol %), $AgSbF_6$ (15 mol %), LiOAc (20 mol %) and HOAc (1.0 equiv) in DCE (0.5 mL) at 35 °C for 16 h under N_2 protection. ***2a*** was added in bench-wise with 0.3 mL DCE (0.05 mL per 15 mins).

Moreover, the steric properties of the dioxazolones exerted a significant influence on the amidation reaction (Table 4.7). With 1-decene as a substrate, reaction with the dioxazolone with linear chain substituent (***4aa***) afforded the branched allylamides in 61 % isolated yield. However, the analogus reaction of some dioxazolones bearing with a branched substituents (***4ba***) and ring substituents (***4ca***), the yield of the corresponding products was up to 35 %. When the distance between the phenyl group and amide group in the dioxazolone increases (***4ad***, ***4ae*** and ***4af***), the isolated yield of the corresponding product increases. The electron properties of

the phenyl groups did not affect the performance of the amidation reaction (***4ag*** and ***4ah***); the size of the phenyl group appear to enhance the steric repulsion offered by dioxazolone (***4ai***).

Table 4.7. Substrate Scope Studies of Dioxazolones

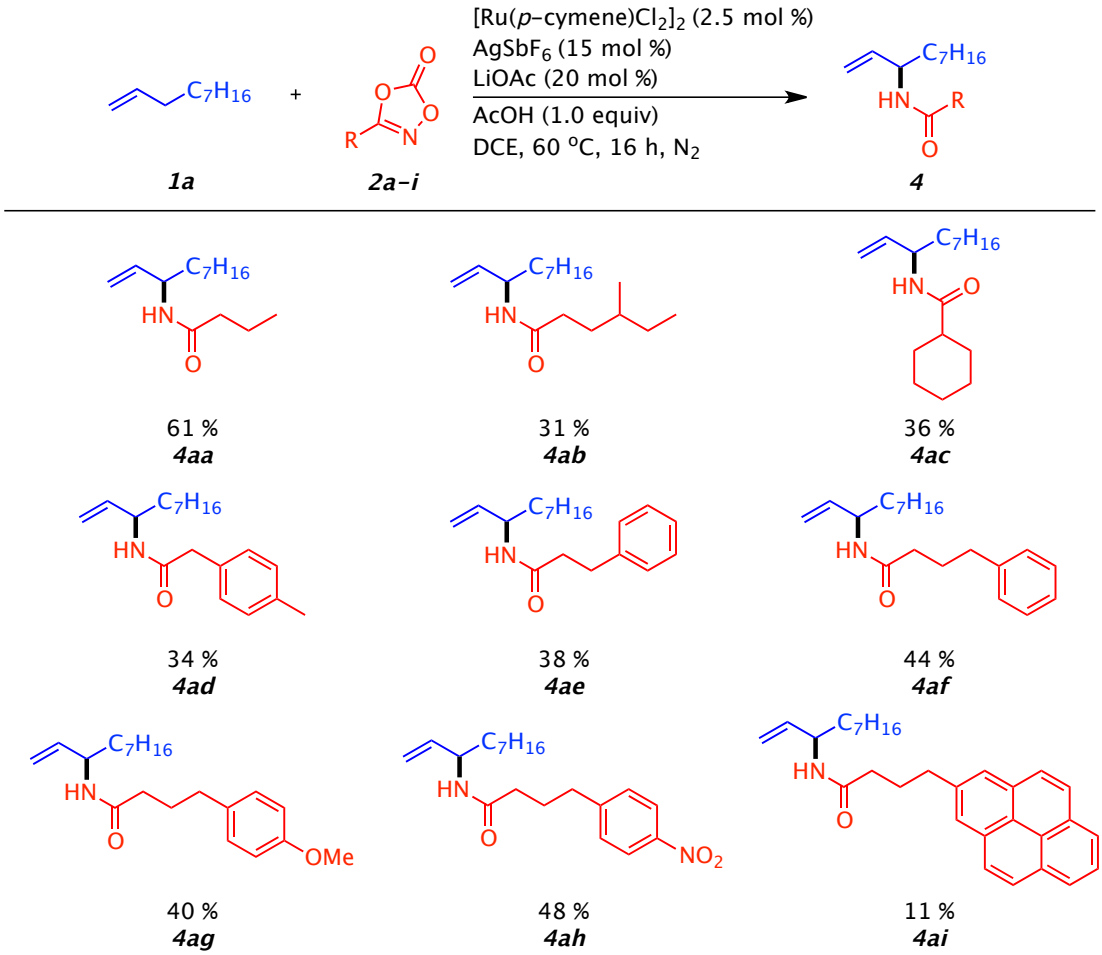

Reaction conditions: ***1a*** (2.0 equiv), dioxazolones (0.1 mmol), $[Ru(cymene)Cl_2]_2$ (2.5 mol %), $AgSbF_6$ (15 mol %), LiOAc (20 mol %) and HOAc (1.0 equiv) in DCE (0.5 mL) at 60 °C for 16 h under N_2 protection.

The mechanism of the amidation reaction was postulated (Scheme 4.4). (1) Removal of chloride ions by $AgSbF_6$ and LiOAc from $[Ru(cymene)Cl_2]_2$ to form the active $[Ru(cymene)(OAc)]^+$ species. (2) Activation of allylic C-H bond of 1-decene. (3) Formation of Ru-nitrenoid intermediate. (4) Nitrenoid insertion onto Ru-C bond to form a new C-N bond. (5) Protonation of the amidation product and turnover to resting state.

Scheme 4.4. Postulated Catalytic Cycle

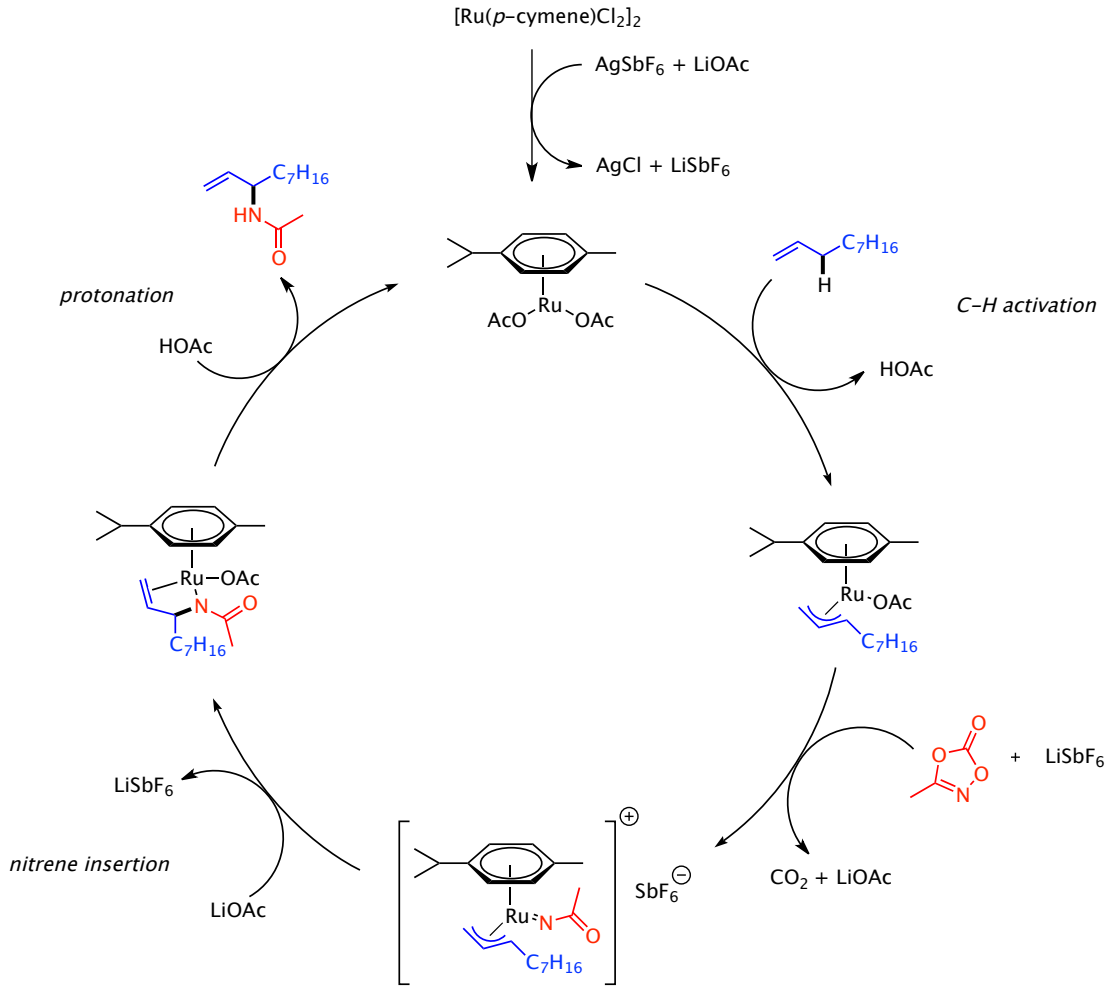

Cramer and co-workers reported the chiral Cp ligand achieves high enantioselective cross coupling reactions in Ir(III), Rh(III), Ru(II) and Co(III)-catalyzed reactions.[50] In their design of the chiral Cp ligand, the bulky substituent of the Cp ligand offers substantial steric repulsion on the coupling partner for enantiodifferentiation. As a result, the more stable enantiomer is dominant in cross coupling reactions. In this work, we also observed similar steric influence in the amidation reaction. The chiral cymene ligand was designed to explore possible development of enantioselective amidation reaction. Scheme 4.5 depicts the synthetic routes of the chiral cymene ligand. The chiral binaphthalene diamine was substituted by bulky sulfonyl chloride to form disulfonylamides followed by the nucleophilic substitution reaction with 1,2-

bis(bromomethyl)-4,5-dimethylcyclohexa-1,4-diene to form the chiral diene ligand in 69 % isolated yield.

Scheme 4.5. Synthetic Routes of Chiral Diene Ligand

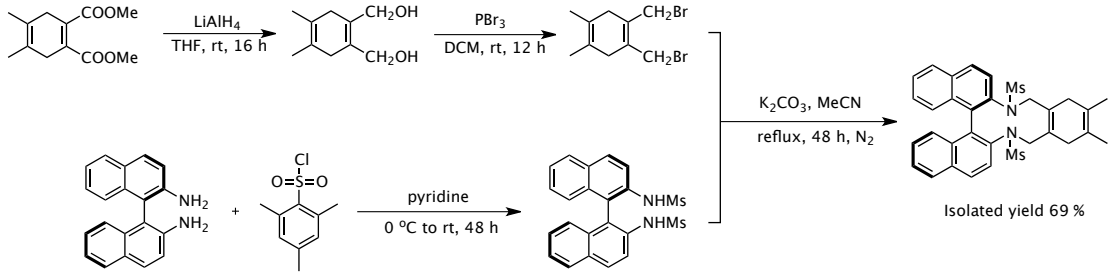

The chiral diene ligand undergoes reductive coordination with $RuCl_3$ in mixture of chloroform and EtOH (1:3) at 80 ^{o}C for 3 days to form chiral **[Ru2]** (2,3-dimethyl-6,19-bis(methylsulfonyl)-5,6,19,20-tetrahydrobenzo[*h*]dinaphtho[2,1-*b*:1',2'-*d*][1,6]diazecine ruthenium(II) dichloride dimer complex) in 64 % isolated yield (Scheme 4.6).

Scheme 4.6. Synthesis of Chiral **[Ru2]**

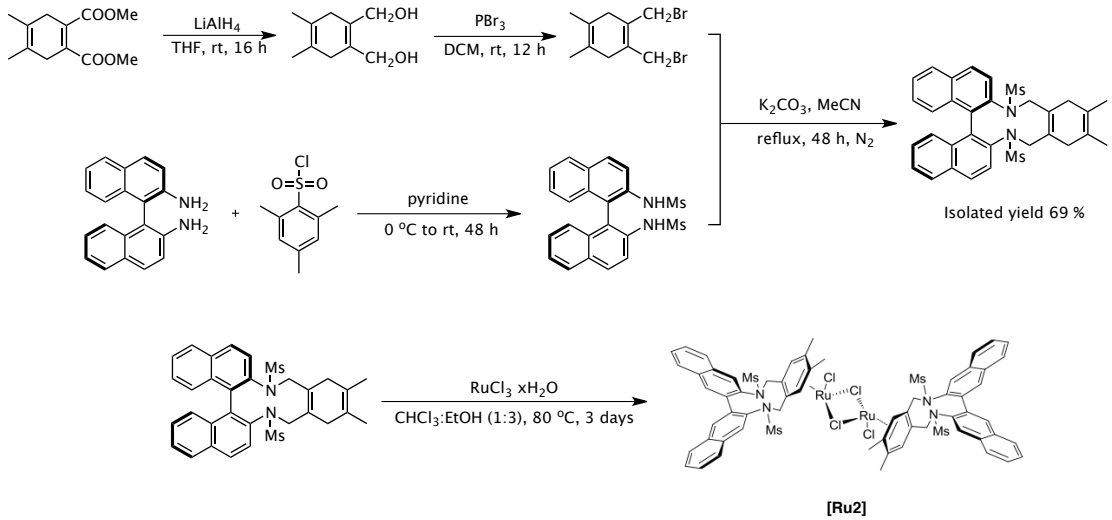

[Ru2]

The chiral **[Ru2]** was used as a catalyst in the reaction between 1-decene (2.0 equiv) and 3-propyl-1,4,2-dioxazol-5-one (0.1 mmol) with $AgSbF_6$ (15 mol %) and LiOAc (20 mol %) in DCE (0.5 mL) at 60 ^{o}C for 16 h (Scheme 4.7). The isolated yield of the amidation product is 60 % and the enantiomeric excess of the product is 10 %. The

enantiomeric excess of the product is not high as the structure of the chiral cymene is 10-membered ring structure. The bulky substituents of the chiral cymene ligand are too far away from the metal center so that the steric repulsion offered by the ligand on the amidating reagent is too low. To improve the enantioselectivity of the reaction, the chiral cymene ligand should be modified in to 8-membered ring structure so the distance between the bulky substituents and amidating reagent can be reduced. The further modification of the ligand in investigation of the reaction will be continued.

Scheme 4.7. Reaction Scheme of Enantioselective Amidation of 1-Decene

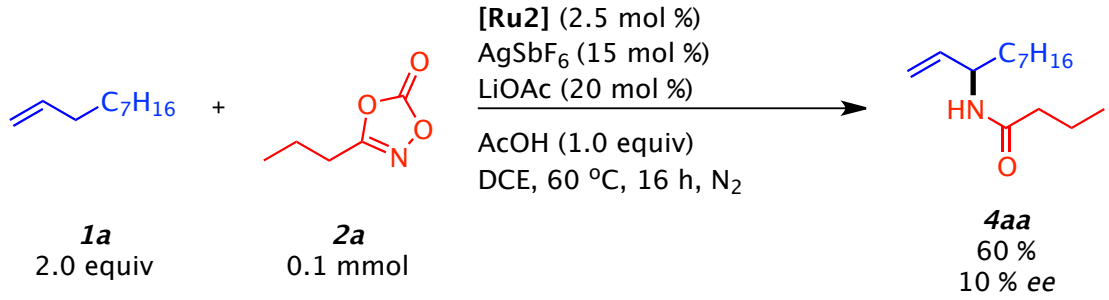

1a
2.0 equiv

2a
0.1 mmol

4aa
60 %
10 % *ee*

4.3 Conclusion

In conclusion, Ru(II)-catalyzed intermolecular amidation reaction of terminal alkenes was developed. The reaction is branch-selective allylic amidation reaction and the performance of the reaction gives moderate to good yield. It was found that the steric factor is very obvious in amidation reaction. Thus, the enantioselectivity of the reaction can be controlled due to the steric factor of the system. The chiral Ru(II) complex **[Ru2]** gives 10 % *ee* in amidation reaction. The chiral cymene ligand is 10-membered ring structure, which did not provide significant steric repulsion between cymene and nitrenoid species. The chiral cymene ligand can be modified to 8-

membered ring structure to enhance the steric repulsion between the cymene ligand and nitrenoid species in the future.

4.4 Experimental Section

Methods

Thin layer chromatography was performed on silica gel plates. Flash column chromatography was performed on a silica gel (Merck, 230-400 mesh) column. ^{1}H and ^{13}C NMR spectra were recorded on a Brüker DPX-400 MHz spectrometer. The chemical shift (δ) values given in ppm and are referenced to residual solvent peaks; carbon multiplicities were determined by DEPT-135 experiments. Coupling constants (J) were reported in hertz (Hz).

Experimental Procedures and Physical Characterizations

Procedures for the Ru(II)-Catalyzed Intermolecular Amidation Reaction of Terminal Alkenes

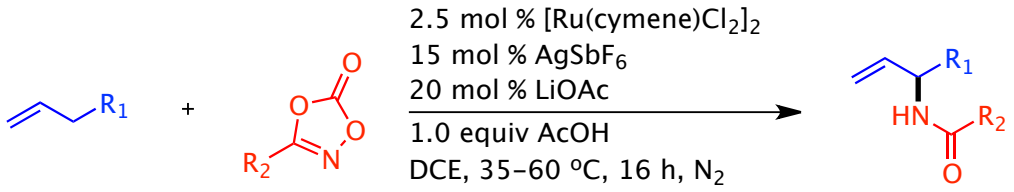

1a–h ***2a–i***

$[Ru(p\text{-cymene})Cl_2]_2$ (0.0025 mmol, 1.5 mg), $AgSbF_6$ (0.015 mmol, 5.2 mg) and LiOAc (0.02 mmol, 1.3 mg), were added to a 8 mL reaction vial, and the vial was evacuated and back-filled with N_2 for three times. Terminal alkenes (0.2 mmol) and HOAc (0.1 mmol, 5,72 µL) were added into 4 mL reaction vial A, and the vial A was evacuated and back-filled with N_2 for the three times. 0.2 mL dry DCE was added into 4 mL vial A through syringe and then the reaction mixture in 4 mL vial was transferred into 8 mL vial. The reaction mixture was stirred at room temperature for 5 min. The dioxazolone (0.1 mmol) was added into another 4 mL reaction vial B, and the vial B

was evacuated and back-filled with N_2 for the three times. 0.3 mL dry DCE was added into 4 mL vial B through syringe. The solution from vial B was added into 8 mL vial in beach-wise (50 µL per 15 min) at 35 – 60 ^{o}C oil baths. After the addition of dioxazolones, the reaction was allowed to react at 35-60 ^{o}C oil baths for 16 h. After 16 h, the reaction crude mixture was filtered by celite and eluted by DCM (~5 – 10 mL). The solvent was removed by vaccum and the amidation products were purified by flash chromatography with n-hexane/EtOAc as an eluent. The characterizations of amidation products are consistence to the literature reports.[46]

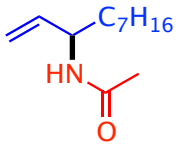

N-(Hept-1-en-3-yl)acetamide (***3aa***)[46]

Reaction Temperature: 35 ^{o}C

Yield: 60 %, white solid

R_f = 0.4 (n-hexane/EtOAc = 1:1)

^{1}H NMR (400 MHz, $CDCl_3$) δ 5.80-5.71 (m, 1H), 5.33 (d, *J* = 6.8 Hz, 1H), 5.17-5.08 (m, 2H), 4.46-4.43 (m, 1H), 2.01 (s, 3H), 1.57-1.42 (m, 2H), 1.27 (m, 12H), 0.88 (t, *J* = 6.8 Hz, 3H).

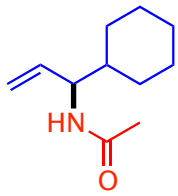

4-Cyclohexylhex-5-en2-one (***3ba***)[46]

Reaction Temperature: 35 ^{o}C

Yield: 52 %, white solid

R_f = 0.3 (n-hexane/EtOAc = 1:1)

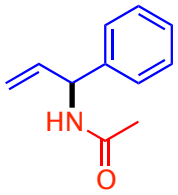

N-(1-Phenylallyl)acetamide (***3ca***)[46]

Reaction Temperature: 35 °C

Yield: 18 %, white solid

R_f = 0.3 (n-hexane/EtOAc = 1:1)

^{1}H NMR (400 MHz, $CDCl_3$) δ 7.37-7.26 (m, 5H), 6.06-5.97 (m, 1H), 5.73-5.63 (m, 2H), 5.25 (m, 2H), 2.04 (s, 3H).

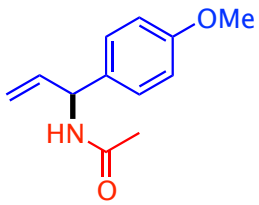

N-(1-(4-Methoxyphenyl)allyl)acetamide (***3da***)[46]

Reaction Temperature: 35 °C

Yield: 35 %, white solid

R_f = 0.25 (n-hexane/EtOAc = 1:1)

^{1}H NMR (400 MHz, $CDCl_3$) δ 7.22 (d, *J* = 8.8, 2H), 6.89-6.87 (m, 2H), 6.04-5.96 (m, 1H), 5.70 (bs, 1H), 5.61-5.57 (m, 2H), 3.80 (s, 3H), 2.02 (s, 3H).

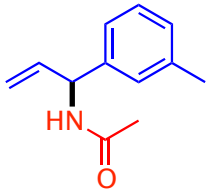

N-(1-(3-Methylphenyl)allyl)acetamide (***3ea***)

Reaction Temperature: 35 °C

Yield: 31 %, white solid

R_f = 0.3 (n-hexane/EtOAc = 1:1)

^{1}H NMR (400 MHz, $CDCl_3$) δ 7.23 (d, *J* = 8.0 Hz, 2H), 7.09 (d, *J* = 8.0 Hz, 2H), 6.04-5.96 (m, 1H), 5.72 (bs, 1H), 5.62-5.59 (m, 1H), 5.26-5.20 (m, 2H), 2.35 (s, 3H), 2.03 (s, 3H).

^{13}C NMR (100 MHz, $CDCl_3$) δ 169.1, 159.3, 137.6, 132.8, 128.7, 115.6, 114.3, 55.5, 54.7, 23.6.

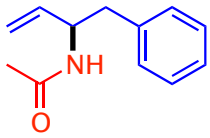

N-(1-Phenylbut-3-en-2-yl)acetamide (***3fa***)[46]

Reaction Temperature: 35 °C

Yield: 55 %, white solid

R_f = 0.25 (n-hexane/EtOAc = 1:1)

^{1}H NMR (400 MHz, $CDCl_3$) δ 7.31-7.17 (m, 5H), 5.85-5.77 (m, 1H), 5.38 (bs, 1H), 5.12-5.08 (m, 2H), 4.82-4.76 (m, 1H), 2.87 (d, *J* = 6.8 Hz, 2H), 1.95 (s, 3H).

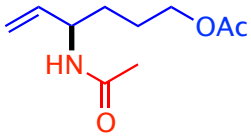

4-Acetamdiohex-5-en-1-yl acetate (***3ga***)[46]

Reaction Temperature: 35 °C

Yield: 58 %, colorless oil

R_f = 0.1 (n-hexane/EtOAc = 1:1)

^{1}H NMR (400 MHz, $CDCl_3$) δ 5.80-5.72 (m, 1H), 5.44 (bs, 1H), 5.15-5.12 (m, 2H), 4.53-4.46 (m, 1H), 4.08 (t, *J* = 6.4 Hz, 2H), 2.05 (s, 3H), 2.01 (s, 3H), 1.70-1.52 (m, 5H).

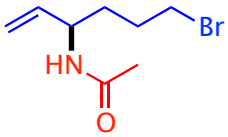

N-(6-Bromohex-1-en-3-yl)acetamide (***3ha***)[46]

Reaction Temperature: 35 °C

Yield: 40 %, colorless oil

R_f = 0.25 (n-hexane/EtOAc = 1:1)

^{1}H NMR (400 MHz, $CDCl_3$) δ 5.81-5.72 (m, 1H), 5.37 (bs, 1H), 5.21-5.13 (m, 2H), 4.53-4.46 (m, 1H), 3.44 (t, *J* = 6.8 Hz, 2H), 2.01 (s, 3H), 1.95-1.79 (m, 2H), 1.77-1.59 (m, 3H).

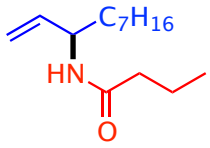

N-(Dec-1-en-3-yl)butyramide (***4aa***)[46]

Reaction Temperature: 60 °C

Yield: 61 %, white solid

R_f = 0.3 (n-hexane/EtOAc = 8:2)

^{1}H NMR (400 MHz, $CDCl_3$) δ 5.78-5.70 (m, 1H), 5.42 (bs, 1H), 5.14-5.05 (m, 2H), 4.46-4.43 (m, 1H), 1.69-1.63 (m, 3H), 1.24 (m, 12H), 0.94 (t, *J* = 7.6 Hz, 4H), 0.85 (t, *J* = 6.4 Hz, 3H).

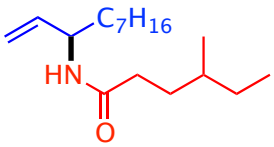

N-(Dec-1-en-3-yl)-4-methylhexanamide (***4ab***)

Reaction Temperature: 60 °C

Yield: 31 %, white solid

R_f = 0.5 (n-hexane/EtOAc = 8:2)

^{1}H NMR (400 MHz, $CDCl_3$) δ 5.76-5.71 (m, 1H), 5.27 (bs 1H), 5.16-5.07 (m, 2H), 4.48-4.44 (m, 1H), 2.23-2.15 (m, 2H), 1.68-1.54 (m, 1H), 1.52-1.50 (m, 1H), 1.49-1.48 (m, 2H), 1.48-1.15 (m, 14H), 0.89-0.86 (m, 9H).

^{13}C NMR (100 MHz, $CDCl_3$) δ 172.7, 138.8, 114.7, 51.2, 35.1, 34.9, 34.3, 32.6, 31.9, 29.5, 29.3, 25.9, 22.8, 19.0, 14.2, 11.4.

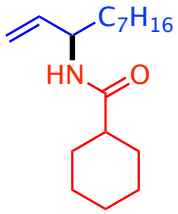

N-(dec-1-en-3-yl)cyclohexanecarboxamide (***4ac***)

Reaction Temperature: 60 °C

Yield: 36 %, white solid

R_f = 0.5 (n-hexane/EtOAc = 8:2)

^{1}H NMR (400 MHz, $CDCl_3$) δ 5.80-5.72 (m, 1H), 5.28 (bs, 1H), 5.14-5.06 (m, 2H), 4.49-4.42 (m, 1H), 2.13-2.05 (m, 1H), 1.89-1.79 (m, 4H), 1.86-1.78 (m, 1H), 1.69-1.66 (m, 4H), 1.64-1.41 (m, 12H), 0.89-0.86 (m, 3H).

^{13}C NMR (100 MHz, $CDCl_3$) δ 175.4, 139.0, 114.5, 50.8, 45.9, 35.1, 31.9, 30.0, 29.9, 29.5, 29.3, 25.9, 25.8, 22.8, 14.2.

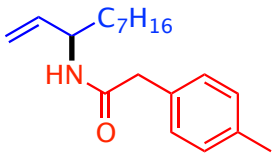

N-(Dec-1-en-3-yl)-2-(*p*-tolyl)acetamide (***4ad***)

Reaction Temperature: 60 °C

Yield: 34 %, white solid

R_f = 0.4 (n-hexane/EtOAc = 8:2)

^{1}H NMR (400 MHz, $CDCl_3$) δ 7.18-7.13 (m, 4H), 5.71-5.63 (m, 1H), 5.20 (bs, 1H), 5.03-4.97 (m, 2H), 4.47-4.42 (m, 1H), 3.56 (s, 2H), 2.35 (s, 3H), 1.48-1.43 (m, 1H), 1.34-1.22 (m, 12H), 0.88 (t, *J* = 6.8 Hz, 3H).

^{13}C NMR (100 MHz, $CDCl_3$) δ 170.6, 138.6, 137.2, 132.0, 129.9, 129.5, 114.5, 51.3, 43.8, 34.9, 31.9, 29.4, 29.3, 25.7, 22.8, 21.2, 14.2.

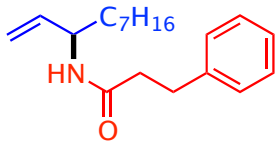

N-(dec-1-en-3-yl)-3-phenylpropanamide (***4ae***)

Reaction Temperature: 60 °C

Yield: 38 %, white solid

R_f = 0.4 (n-hexane/EtOAc = 8:2)

^{1}H NMR (400 MHz, $CDCl_3$) δ 7.30-7.26 (m, 2H), 7.21-7.18 (m, 3H), 5.72-5.64 (m, 1H), 5.20 (bs, 1H), 5.04-4.99 (m, 2H), 4.46-4.39 (m, 1H), 2.98 (t, *J* = 7.6 Hz, 2H), 2.50 (t, *J* = 7.6 Hz, 2H), 1.51-1.39 (m, 2H), 1.37-1.24 (m, 12H), 0.88 (t, *J* = 6.4 Hz, 3H).

^{13}C NMR (100 MHz, $CDCl_3$) δ 171.4, 141.0, 138.6, 128.7, 128.5, 126.4, 114.7, 51.3, 38.8, 35.0, 31.9, 31.9, 29.5, 29.3, 25.7, 22.8, 14.2.

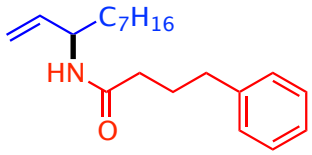

N-(Dec-1-en-3-yl)-4-phenylbutanamide (***4af***)

Reaction Temperature: 60 °C

Yield: 44 %, white solid

R_f = 0.4 (n-hexane/EtOAc = 8:2)

^{1}H NMR (400 MHz, $CDCl_3$) δ 7.30-7.26 (m, 2H), 7.21-7.17 (m, 3H), 5.79-5.70 (m, 1H), 5.26 (bs, 1H), 5.15-5.07 (m, 2H), 4.49-4.42 (m, 1H), 2.66 (t, *J* = 7.6 Hz, 2H), 2.19 (t, *J* = 7.6 Hz, 2H), 2.02-1.95 (m, 2H), 1.56-1.40 (m, 2H), 1.28-1.26 (m, 12H), 0.89-0.86 (m, 3H).

^{13}C NMR (100 MHz, $CDCl_3$) δ 172.0, 141.7, 138.8, 128.7, 128.5, 126.1, 114.8, 51.3, 36.2, 35.3, 35.1, 31.9, 29.5, 29.3, 27.4, 25.9, 22.8, 14.2.

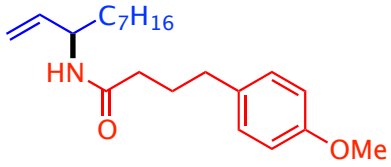

N-(Dec-1-en-3-yl)-4-(4-methoxyphenyl)butanamide (***4ag***)

Reaction Temperature: 60 °C

Yield: 40 %, white solid

R_f = 0.3 (n-hexane/EtOAc = 8:2)

^{1}H NMR (400 MHz, $CDCl_3$) δ 7.09 (d, *J* = 8.4 Hz, 2H), 6.83 (d, *J* = 8.8 Hz, 2H), 5.79-5.70 (m, 1H), 5.23 (bs, 1H), 5.15-5.07 (m, 2H), 4.49-4.42 (m, 1H), 3.79 (s, 3H), 2.60 (t, *J* = 7.6 Hz, 2H), 2.18 (t, *J* = 7.6 Hz, 2H), 1.98-1.91 (m, 2H), 1.60-1.40 (m, 4H), 1.28-1.26 (m, 12H), 0.89-0.86 (m, 3H).

^{13}C NMR (100 MHz, $CDCl_3$) δ 172.1, 158.0, 138.8, 133.7, 129.5, 114.8, 114.0, 55.4, 51.3, 36.2, 35.1, 34.4, 31.9, 29.5, 29.3, 27.6, 25.9, 22.8, 14.2.

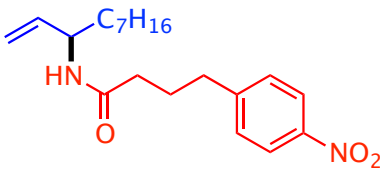

N-(dec-1-en-3-yl)-4-(4-nitrophenyl)butanamide (***4ah***)

Reaction Temperature: 60 °C

Yield: 48 %, white solid

R_f = 0.2 (n-hexane/EtOAc = 8:2)

^{1}H NMR (400 MHz, $CDCl_3$) δ 8.14 (d, *J* = 8.4 Hz, 2H), 7.35 (d, *J* = 8.4 Hz, 2H), 5.79-5.71 (m, 1H), 5.32 (bs, 1H), 5.16-5.09 (m, 2H), 4.49-4.43 (m, 1H), 2.78 (t, *J* = 7.6 Hz, 2H), 2.20 (t, *J* = 7.2 Hz, 2H), 2.04-1.98 (m, 2H), 1.57-1.47 (m, 2H), 1.29-1.26 (m, 12H), 0.89-0.86 (m, 3H).

^{13}C NMR (100 MHz, $CDCl_3$) δ 171.4, 149.7, 146.6, 138.6, 129.4, 123.8, 114.9, 51.5, 35.8, 35.2, 35.0, 31.9, 29.5, 29.3, 26.7, 25.9, 22.7, 14.2.

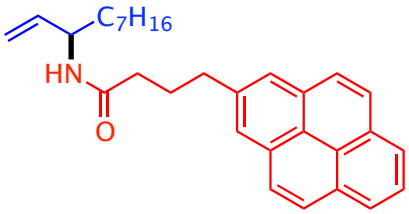

N-(dec-1-en-3-yl)-4-(pyren-2-yl)butanamide (***4ai***)

Reaction Temperature: 60 °C

Yield: 11 %, white solid

Rf = 0.4 (n-hexane/EtOAc = 8:2)

^{1}H NMR (400 MHz, $CDCl_3$) δ 8.29-7.86 (m, 9H), 5.78-5.69 (m, 1H), 5.22 (bs, 1H), 5.16-5.07 (m, 2H), 4.50-4.47 (m, 1H), 3.41 (t, *J* = 7.2 Hz, 2H), 2.32-2.21 (m, 4H), 1.56-1.41 (m, 4H), 1.25-1.24 (m, 12H), 0.89-0.86 (m, 3H).

^{13}C NMR (100 MHz, $CDCl_3$) δ 171.9, 138.7, 136.0, 131.6, 130.1, 128.9, 127.6, 127.5, 126.9, 125.9, 124.9, 123.5, 121.7, 117.5, 114.9, 51.4, 36.4, 35.1, 32.9, 31.9, 29.5, 29.3, 27.6, 25.9, 22.7, 14.2.

Preparation of Chiral **[Ru2]**

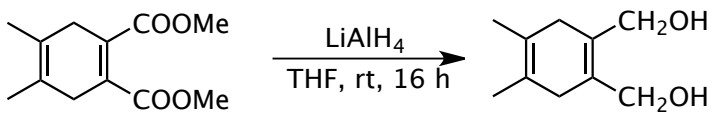

To a solution of dimethyl 4,5-dimethylcyclohexa-1,4-diene-1,2-dicarboxylate (0.5 mmol, 112.1 mg) in dry THF (1 mL) was added $LiAlH_4$ (1 mmol, 38 mg) in dry THF (2 mL) at 0 ^{o}C. The mixture was stirred at room temperature for 16 h. After completion of the reaction, EtOAc (3 mL) was added into mixture and stirred at room temperature for further 30 mins. After 30 mins, water (3 mL) was added into mixture slowly. The precipitate was filtered off and the organic phase was separated. The aqueous layer was extracted with EtOAc (~3 mL) three times and dried with $MgSO_4$. The solvent was evaporated under vaccum to obtain (4,5-dimethylcyclohexa-1,4-diene-1,2-diyl)dimethanol in quantitative yield.

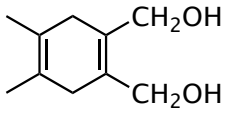

^{1}H NMR (400 MHz, MeOD) δ 4.12 (s, 4H), 2.73 (s, 4H), 1.66 (s, 6H).

^{13}C NMR (100 MHz, MeOD) δ 131.1, 122.4, 60.1, 35.6, 16.8.

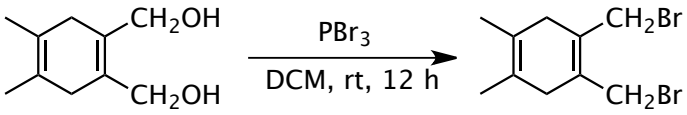

To a solution of (4,5-dimethylcyclohexa-1,4-diene-1,2-diyl)dimethanol (2 mmol, 339 mg) in DCM (22 mL) was added PBr_3 (2 mL) under N_2. The resultant mixture was stirred at room temperature overnight. The reaction crude mixture was diluted with

DCM (45 mL) and washed subsequently with water, saturated $NaHCO_3$ solution and brine. After dried with $MgSO_4$, the solvent was evaporated under vaccum to give 1,2-bis(bromomethyl)-4,5-dimethylcyclohexa-1,4-diene as a pale red liquid and can be used in next step without further purification.

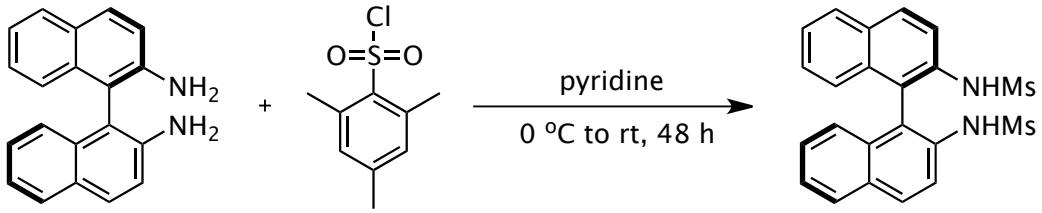

Mesitiyl chloride (5.6 mmol, 0.44 mL) in DCM (10 mL) was slowly added into a stirred solution of pyridine (5 mL) and diamines (2.6 mmol, 740 mg) in DCM (20 mL) at 0 °C. The reaction mixture was stirred at room temperature for 48 h, after which the second portion of mesitiyl chloride (5.6 mmol, 0.44 mL) was added. After 48 h, the reaction mixture was washed subsequently with saturated $NaHCO_3$ solution and brine. After dried with $MgSO_4$, the solvent was evaporated under vaccum and purified by flash column chromatography to give corresponding product as white solid in 84 % yield.

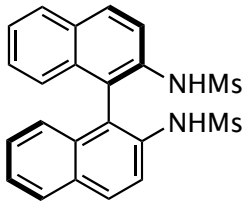

^{1}H NMR (400 MHz, $CDCl_3$) δ 8.11 (d, 2H), 8.04 (d, 2H), 7.97 (s, 2H), 7.49 (t, 2H), 7.33 (t, 2H), 6.99 (d, 2H), 6.07 (s, 2H), 2.98 (s, 6H).

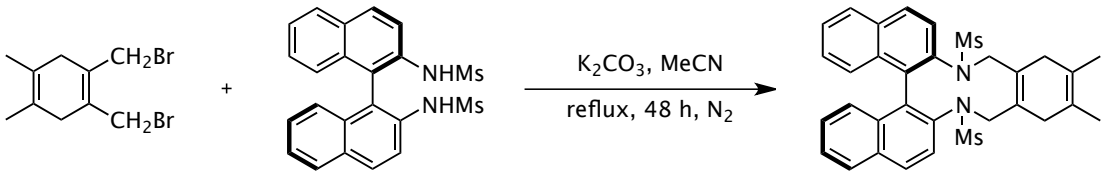

Isolated yield 69 %

To a degassed solution of *N*,*N*'-([1,1'-binaphthalene]-2,2'-diyl)dimethanesulfonamide (1 mmol, 440 mg) in dry MeCN (2 mL) were added K_2CO_3 (5 mmol, 690 mg) and 1,2-bis(bromomethyl)-4,5-dimethylcyclohexa-1,4-diene (1 mmol, 294 mg) under N_2. The reaction mixture was reacted under reflux for 48 h. After cooling to room temperature, the solvent was removed under vaccum. The crude mixture was re-dissolved in DCM and then washed with brine. After dried with $MgSO_4$, the solvent was evaporated under vaccum and purified by flash column chromatography (n-hexane/EtOAc = 3:1) to give corresponding product as a white solid in 69 % yield.

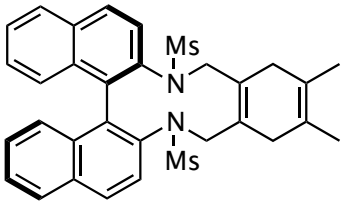

^{1}H NMR (400 MHz, $CDCl_3$) δ 7.95 (m, 4H), 7.65-7.45 (m, 4H), 7.29 (m, 4H), 4.12 (s, 4H), 2.85 (d, 2H), 2.59 (d, 2H), 1.88 (s, 6H), 1.61 (s, 6H).

^{13}C NMR (100 MHz, $CDCl_3$) δ 137.8, 134.5, 133.4, 132.5, 131.4, 129.8, 129.3, 127.9, 127.8, 127.1, 126.9, 122.6, 52.3, 41.0, 37.9, 18.1.

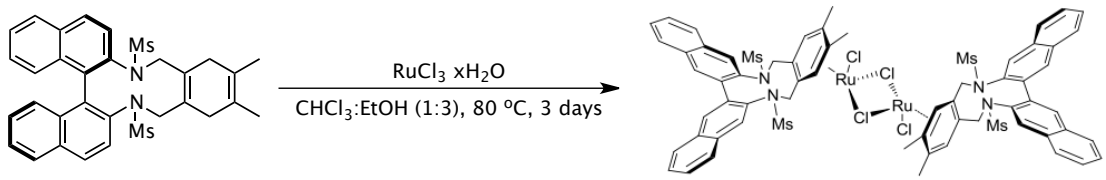

[Ru2]

Hydrated ruthenium trichloride (0.1 mmol, 26.1 mg) and diene amide (0.11 mmol, 63 mg) werer dissolved in the mixture of ethanol and chloroform ($CHCl_3$/EtOH = 1:3) in 100 mL Schlenk Tube. The mixture was stirred at 80 ^{o}C for 3 days. After cooling to room temperature, the red precipitate was filtered off, washed with methanol and dried in air (64 % yield). The complex was recrystallized by dissolving in DCM with diffusion of diethyl ether. The crystal obtained was analyzed in X-Ray Crystalline Spectrometer.

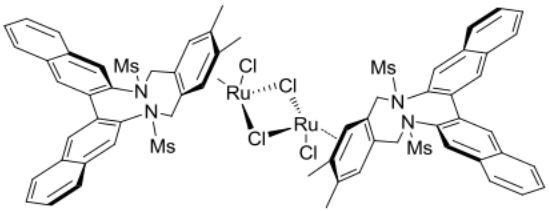

^{1}H NMR (400 MHz, acetone-d_6) δ 8.31 (d, 2H), 8.13 (d, 2H), 8.09-7.90 (m, 2H), 7.88-7.78 (m, 4H), 7.62, (t, 2H), 7.52-7.43 (m, 2H), 7.42-7.37 (m, 2H), 7.36-7.24 (m, 4H), 7.17 (d, 4H), 5.61 (s, 1H), 5.47 (s, 1H), 5.32-5.08 (m, 4H), 4.74 (m, 4H), 4.46 (m, 2H), 2.79 (m, 12H), 2.14-2.09 (m, 12H).

Figure S4.1 ^{1}H NMR Spectrum of *N*-(Hept-1-en-3-yl)acetamide (***3aa***)

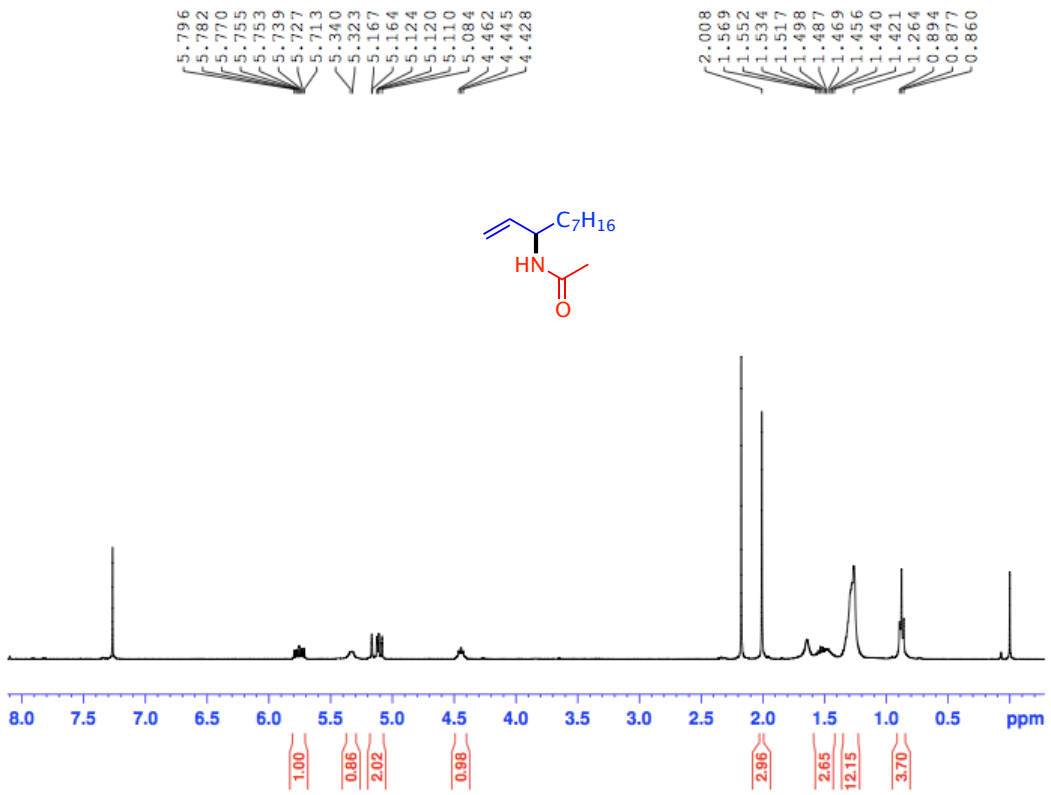

Figure S4.2 ^{1}H NMR Spectrum of *N*-(1-Phenylallyl)acetamide (***3ca***)

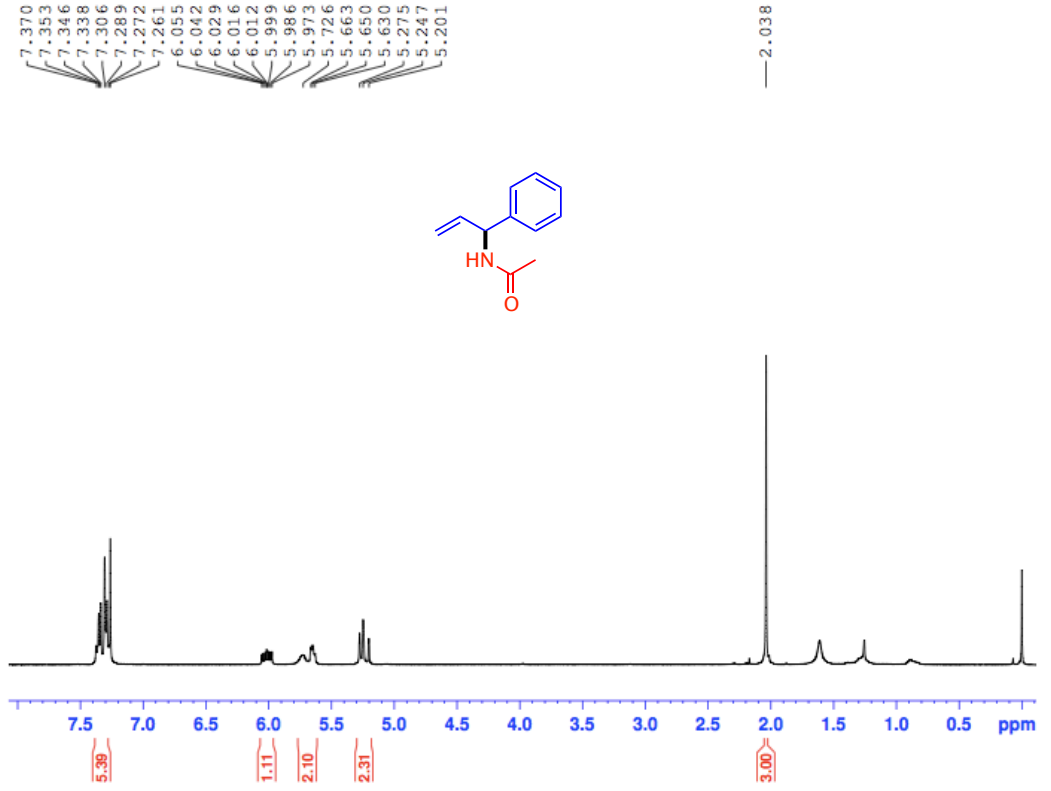

Figure S4.3 ^{1}H NMR Spectrum of *N*-(1-(4-Methoxyphenyl)allyl)acetamide (***3da***)

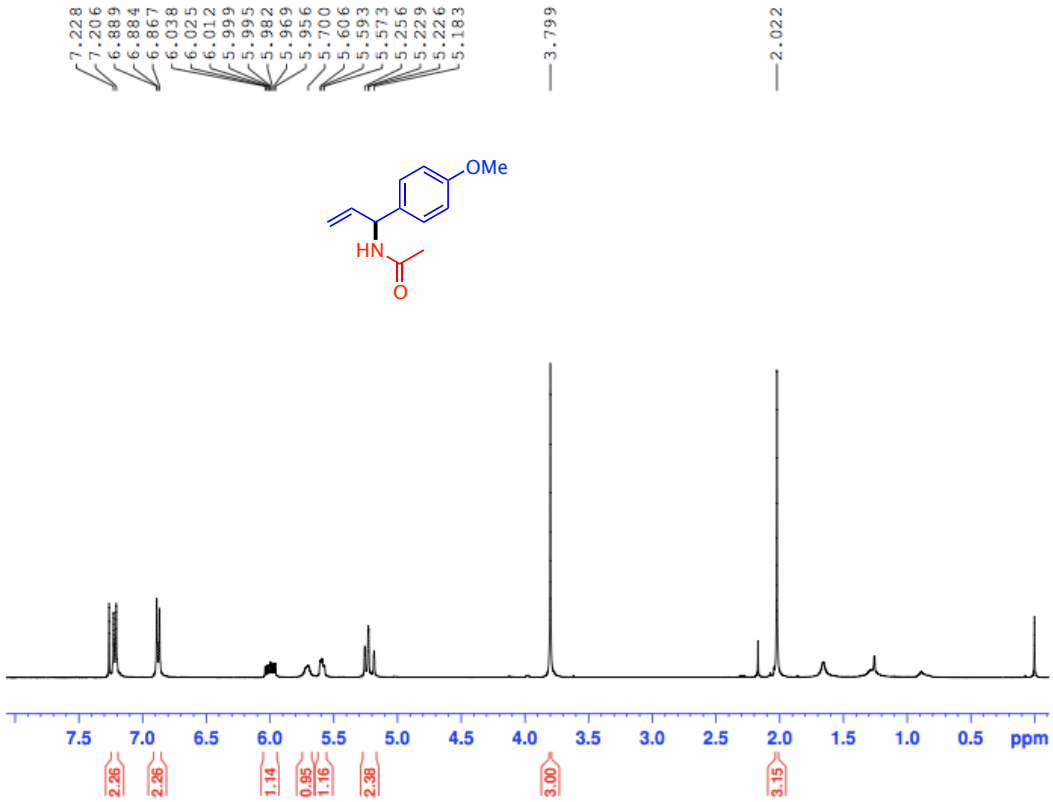

Figure S4.4 ^{1}H NMR Spectrum of *N*-(1-(3-Methylphenyl)allyl)acetamide (***3ea***)

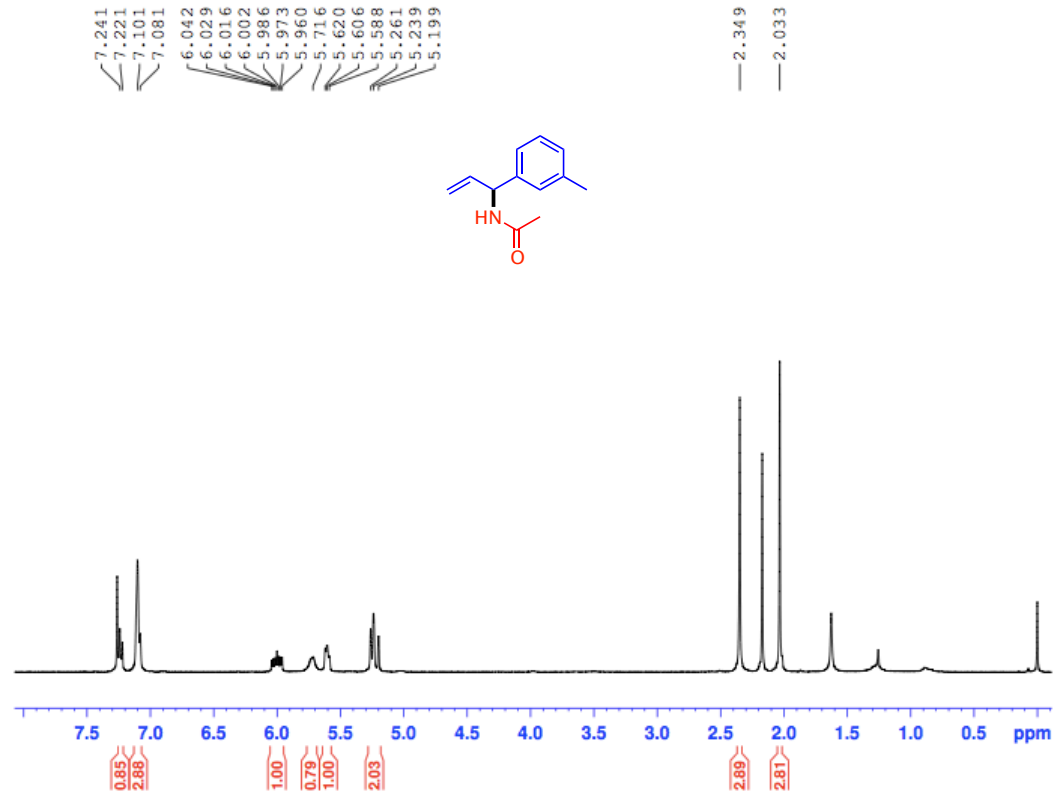

Figure S4.5 ^{13}C NMR Spectrum of *N*-(1-(3-Methylphenyl)allyl)acetamide (***3ea***)

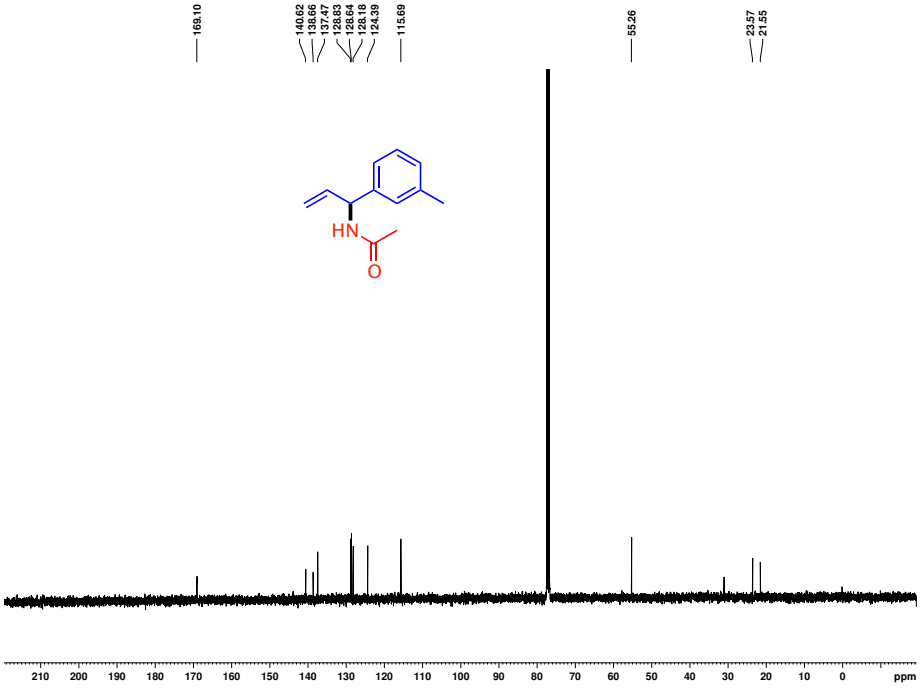

Figure S4.6 ^{1}H NMR Spectrum of *N*-(1-Phenylbut-3-en-2-yl)acetamide (***3fa***)

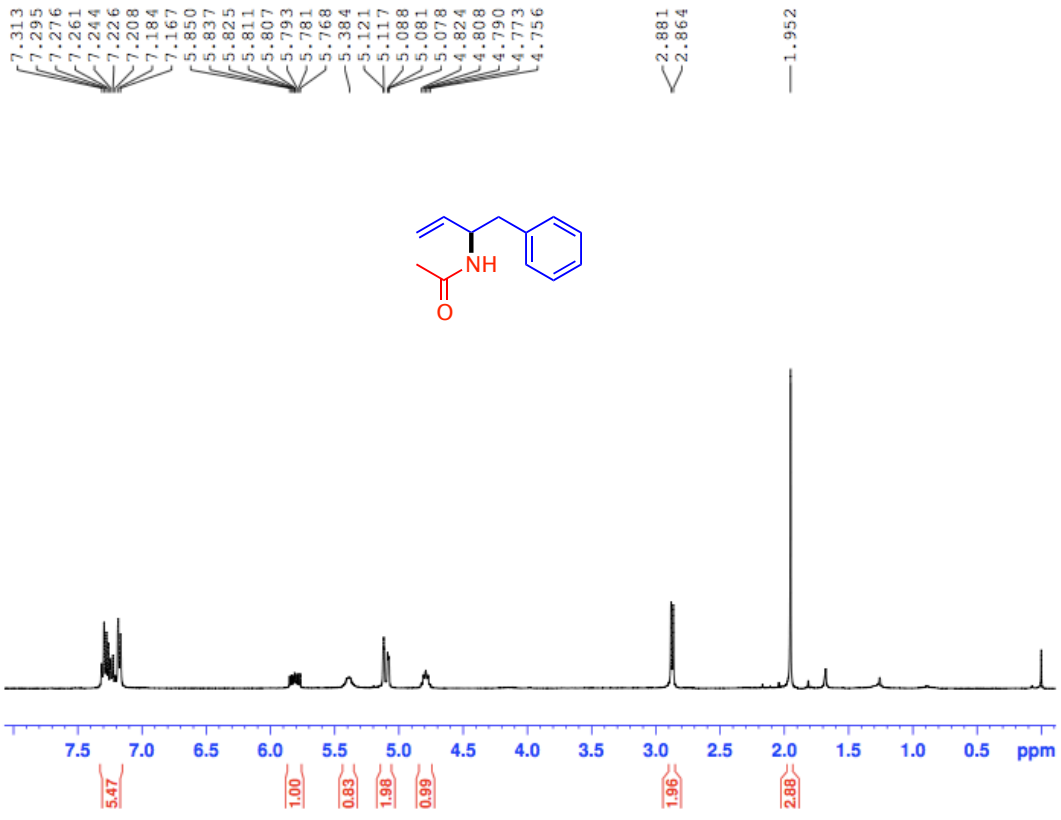

Figure S4.7 ^{1}H NMR Spectrum of 4-Acetamdiohex-5-en-1-yl acetate (***3ga***)

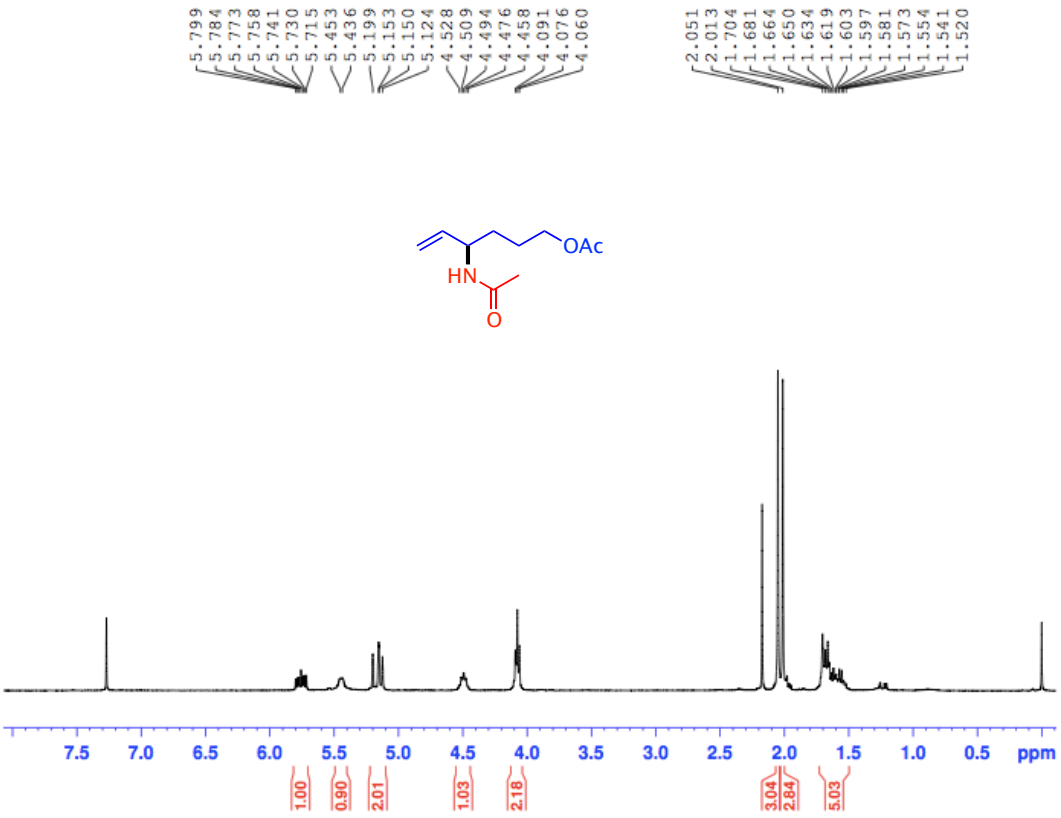

Figure S4.8 ^{1}H NMR Spectrum of *N*-(6-Bromohex-1-en-3-yl)acetamide (***3ha***)

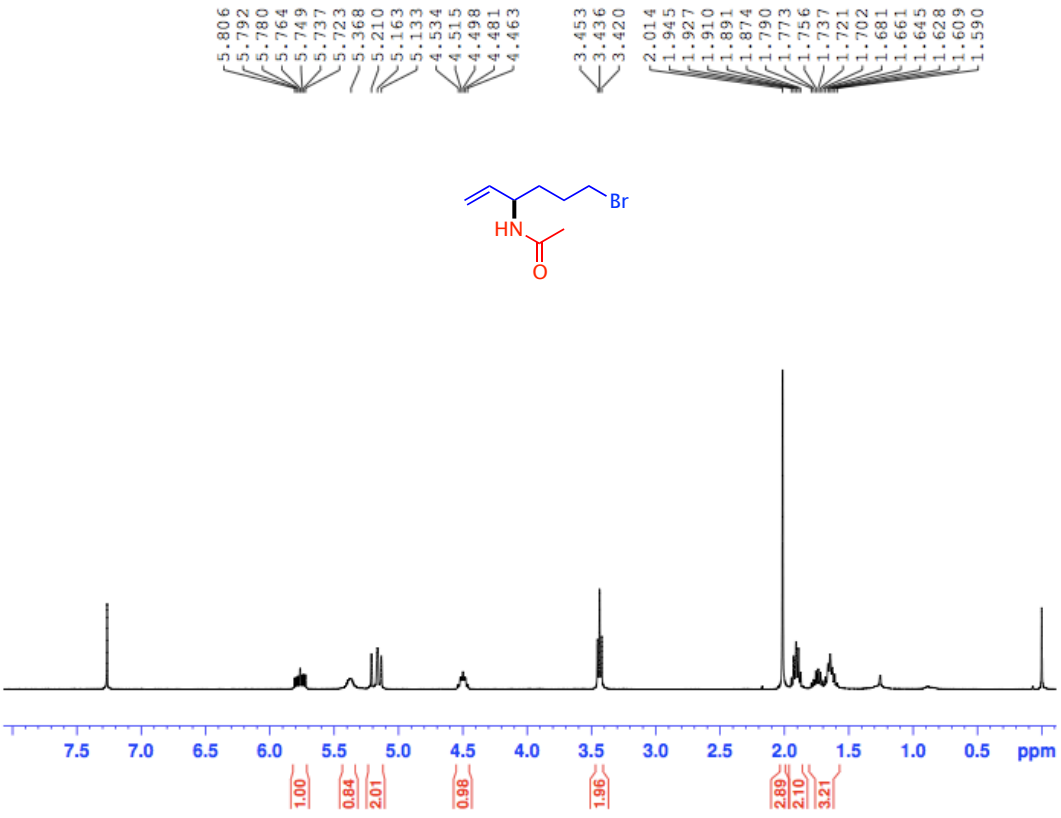

Figure S4.9 ^{1}H NMR Spectrum of *N*-(Dec-1-en-3-yl)butyramide (***4aa***)

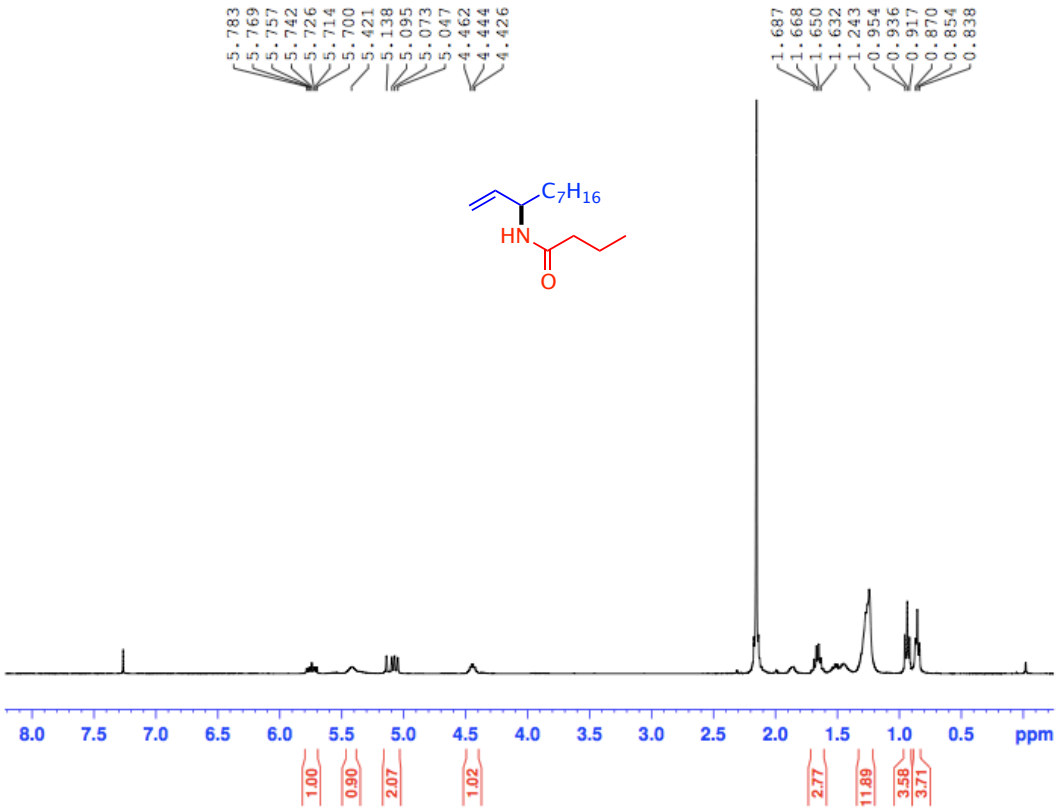

Figure S4.10 ^{1}H NMR Spectrum of *N*-(Dec-1-en-3-yl)-4-methylhexanamide (***4ab***)

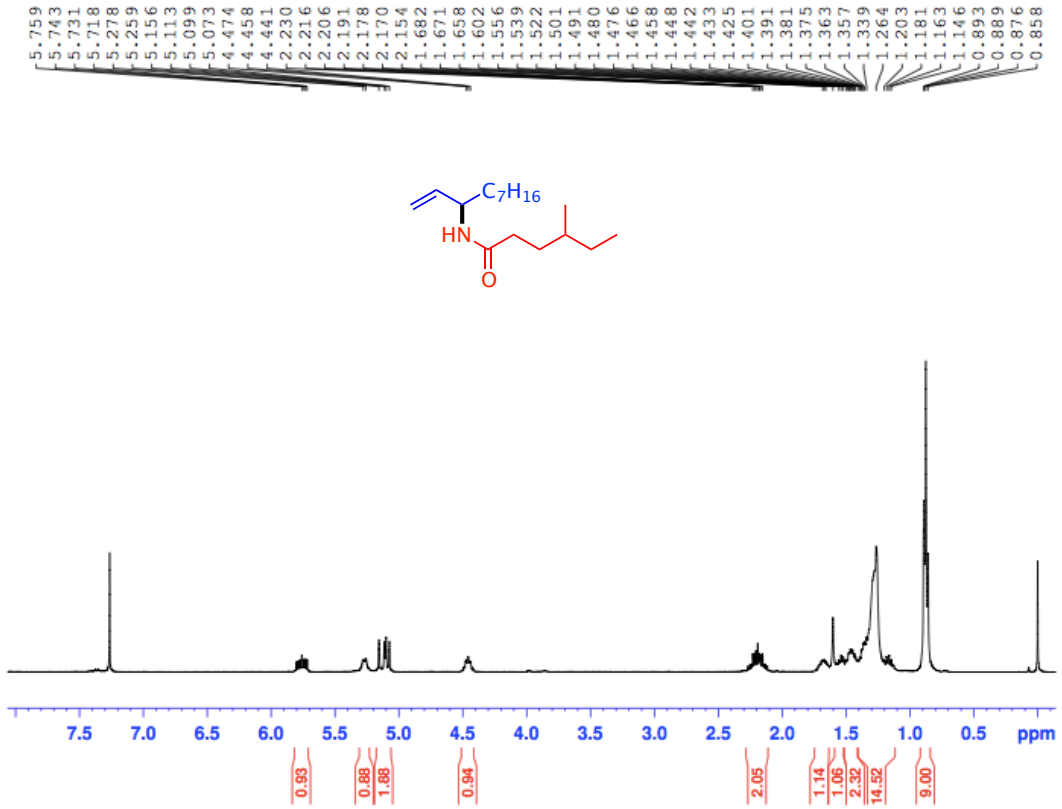

Figure S4.11 ^{13}C NMR Spectrum of *N*-(Dec-1-en-3-yl)-4-methylhexanamide (***4ab***)

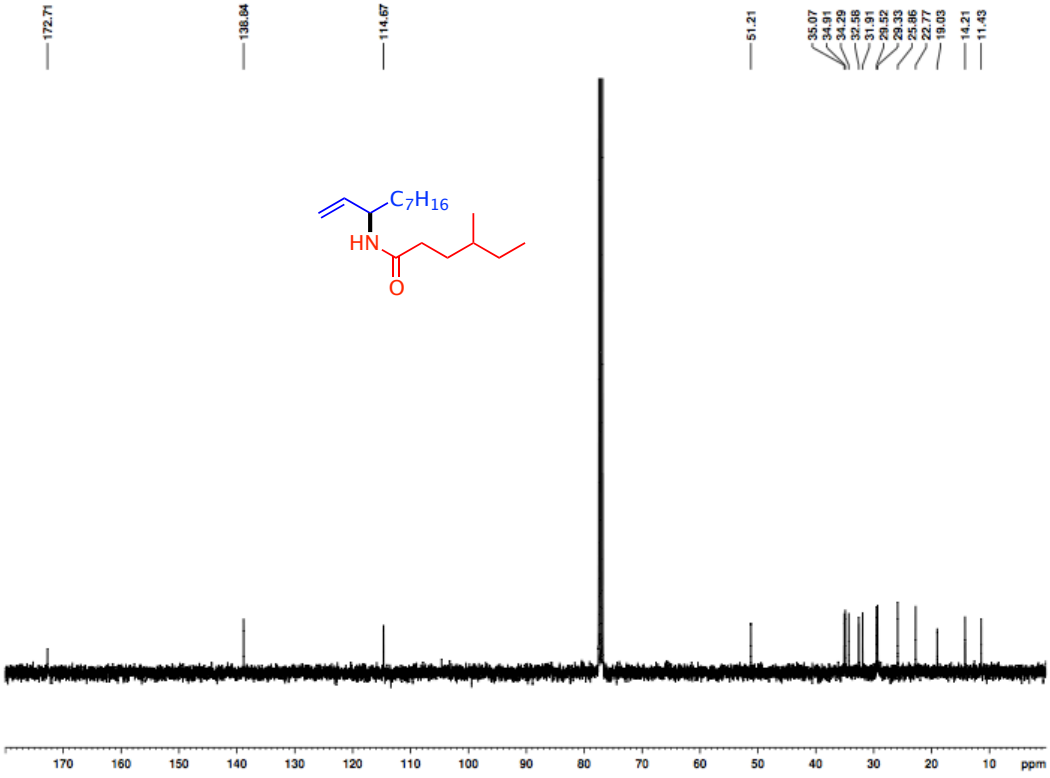

Figure S4.12 ^{1}H NMR Spectrum of *N*-(dec-1-en-3-yl)cyclohexanecarboxamide (***4ac***)

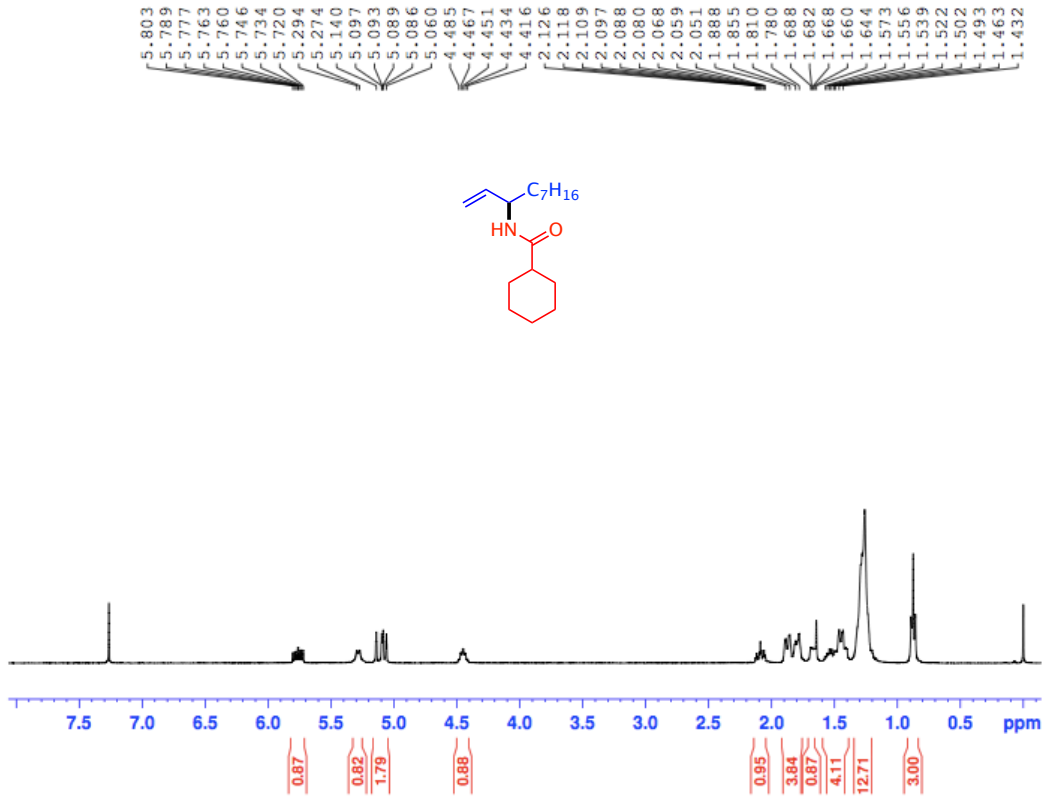

Figure S4.13 ^{13}C NMR Spectrum of *N*-(dec-1-en-3-yl)cyclohexanecarboxamide (***4ac***)

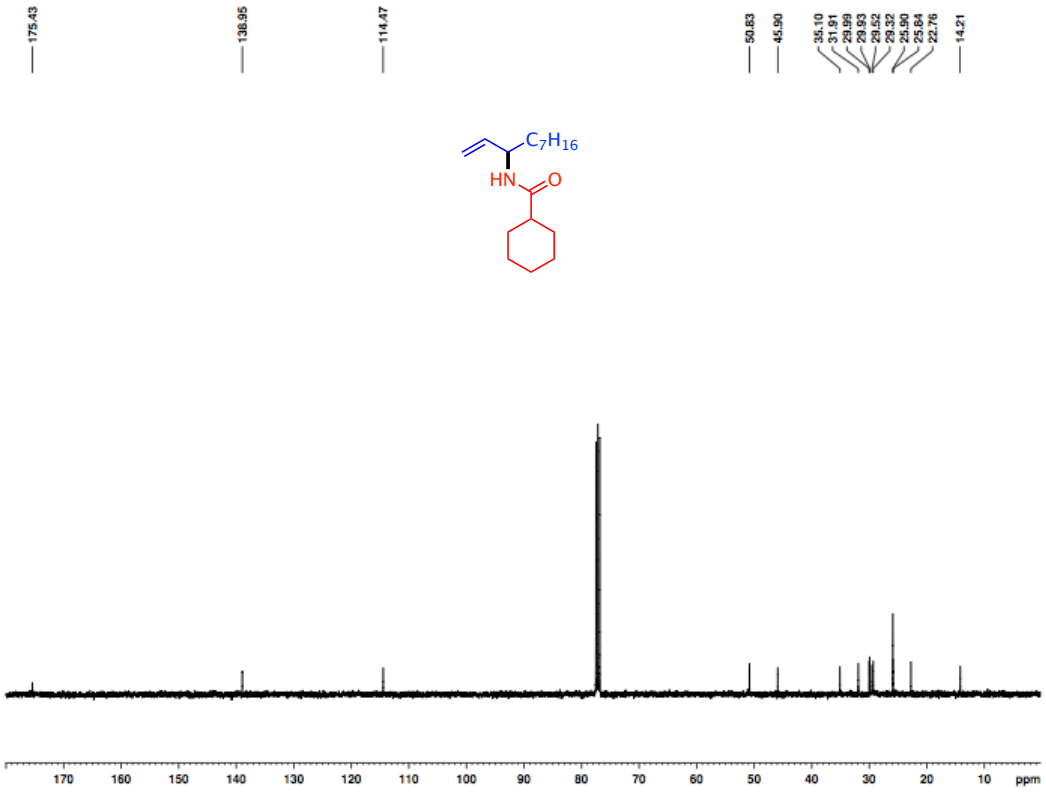

Figure S4.14 ^{1}H NMR Spectrum of *N*-(Dec-1-en-3-yl)-2-(*p*-tolyl)acetamide (***4ad***)

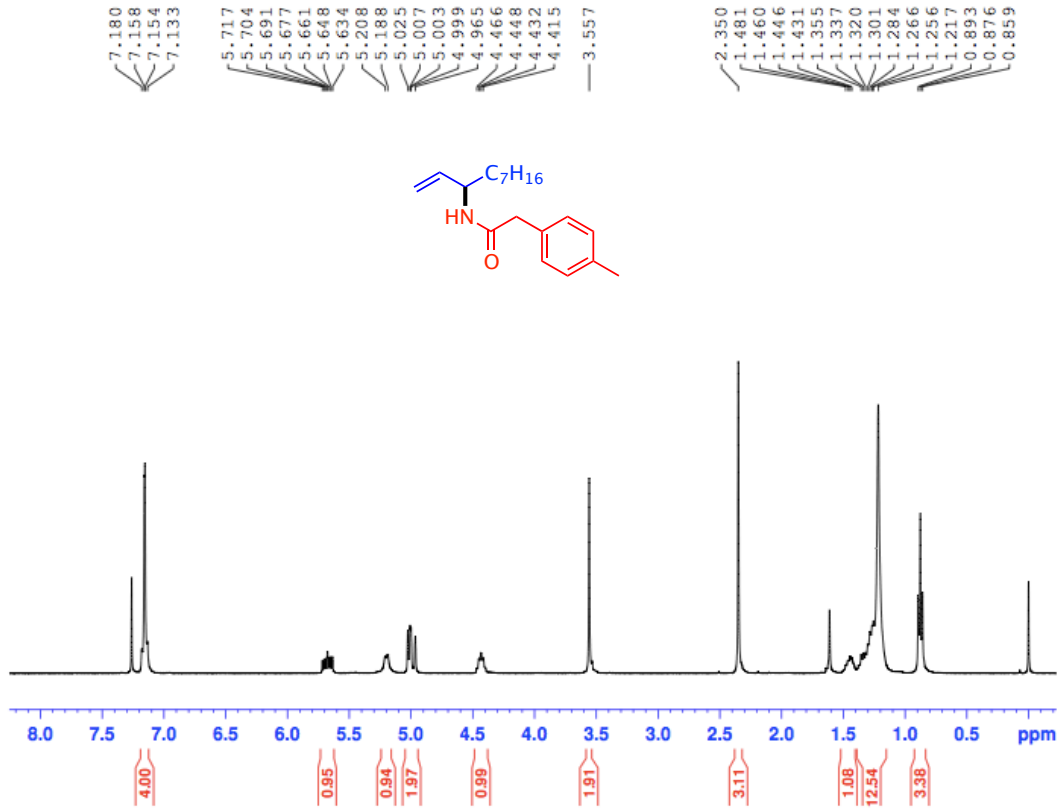

Figure S4.15 ^{13}C NMR Spectrum of *N*-(Dec-1-en-3-yl)-2-(*p*-tolyl)acetamide (***4ad***)

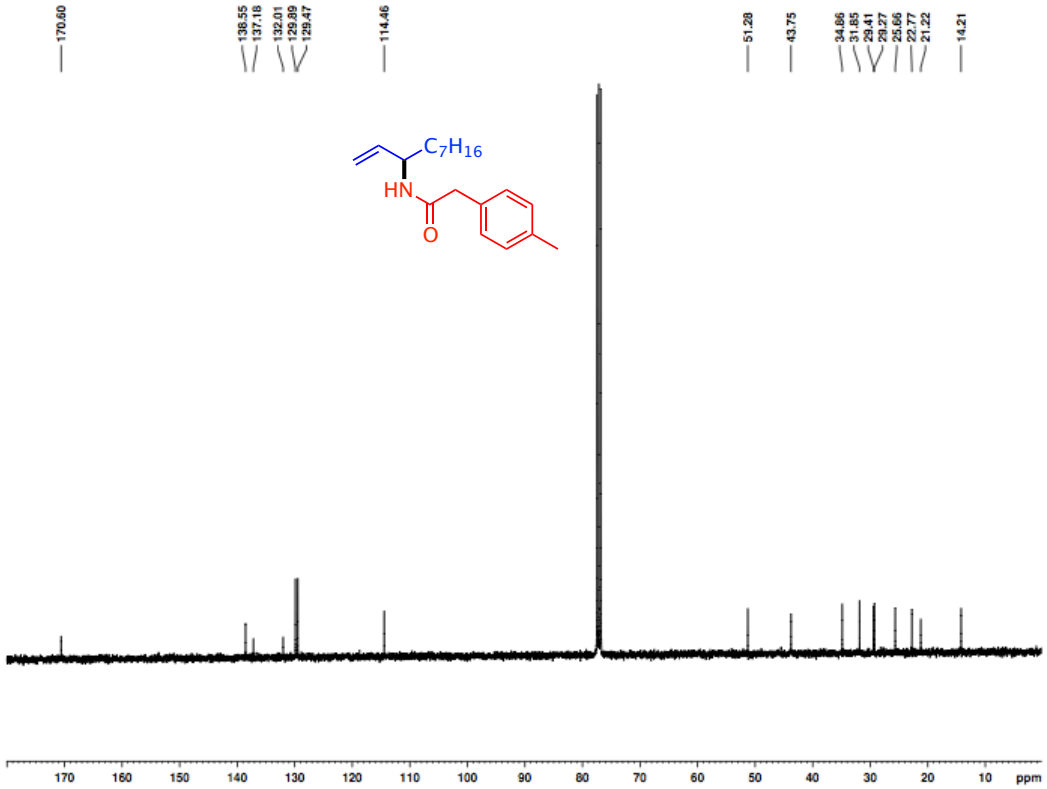

Figure S4.16 ^{1}H NMR Spectrum of *N*-(dec-1-en-3-yl)-3-phenylpropanamide (***4ae***)

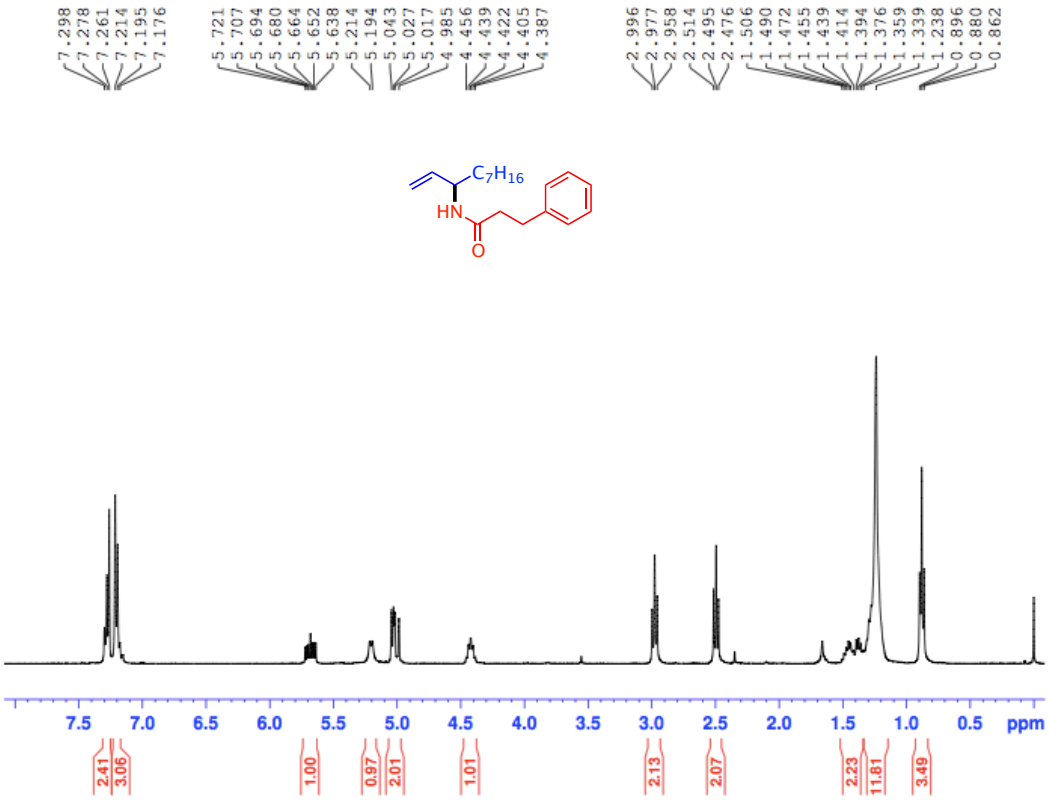

Figure S4.17 ^{13}C NMR Spectrum of *N*-(dec-1-en-3-yl)-3-phenylpropanamide (***4ae***)

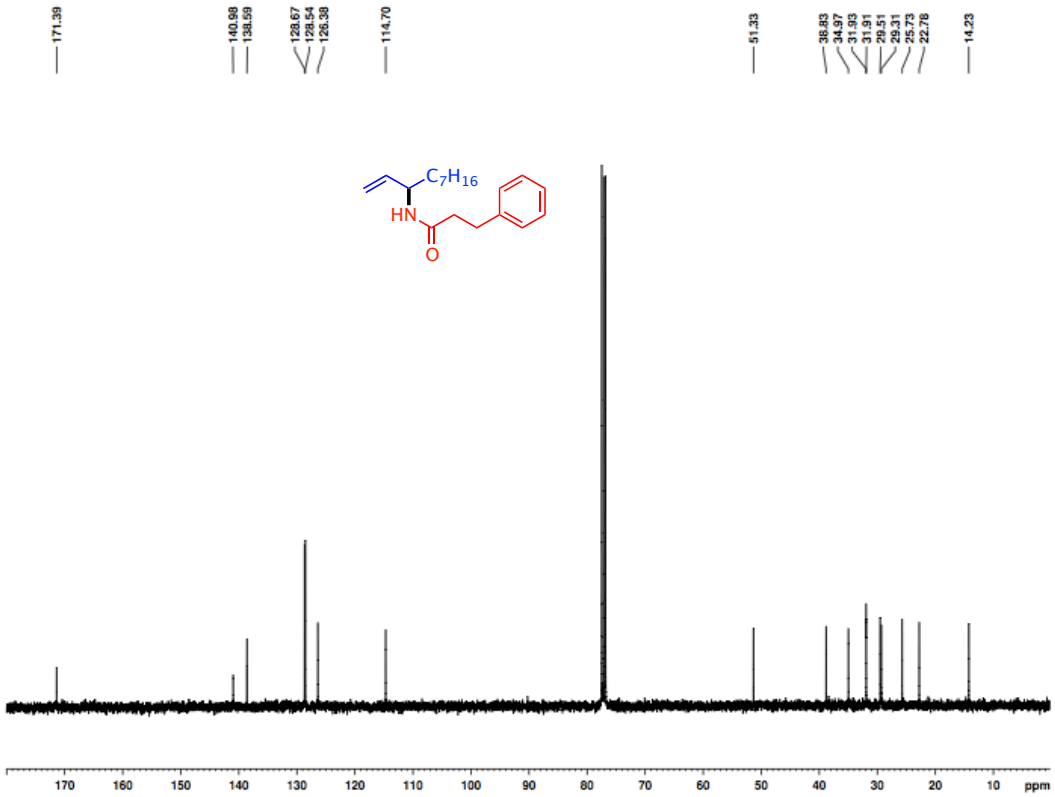

Figure S4.18 ^{1}H NMR Spectrum of *N*-(Dec-1-en-3-yl)-4-phenylbutanamide (***4af***)

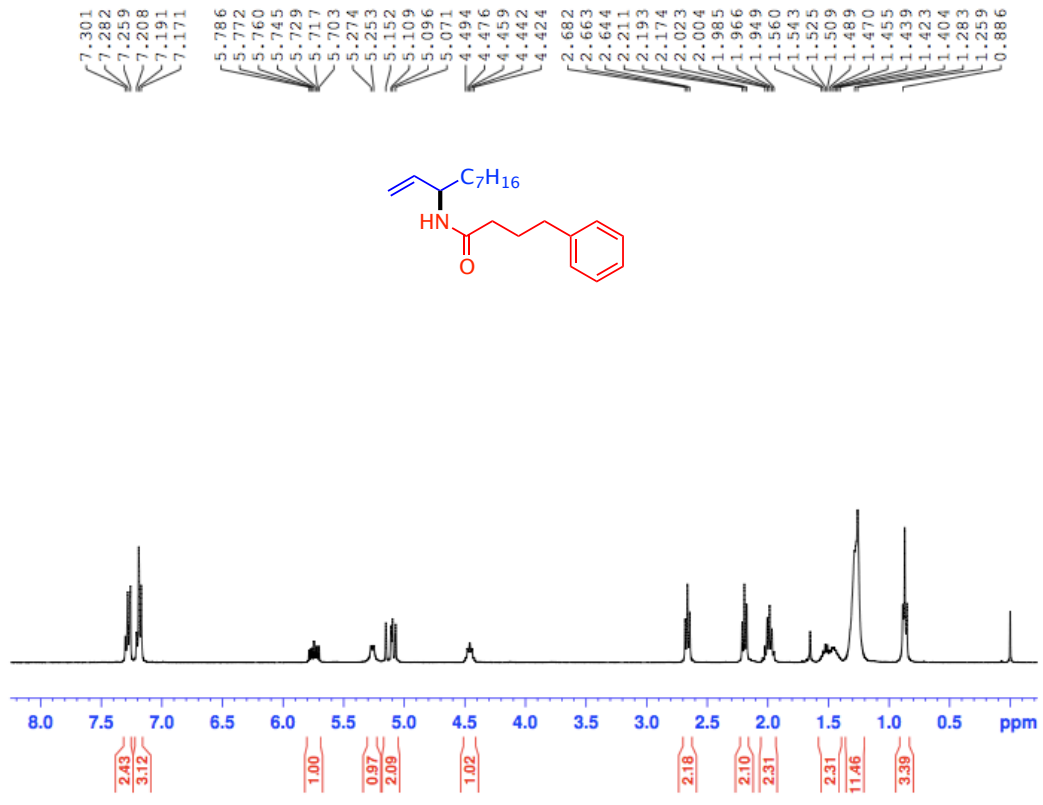

Figure S4.19 ^{13}C NMR of *N*-(Dec-1-en-3-yl)-4-phenylbutanamide (***4af***)

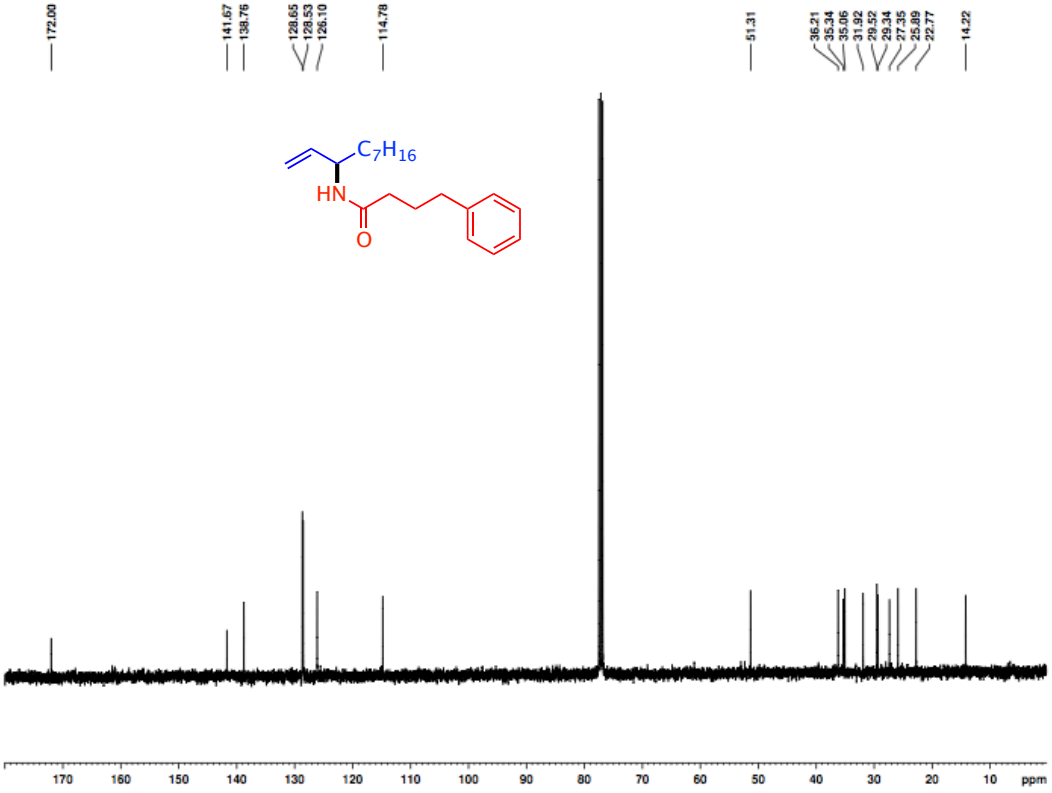

Figure S4.20 ^{1}H NMR Spectrum of *N*-(Dec-1-en-3-yl)-4-(4-methoxyphenyl)butanamide (***4ag***)

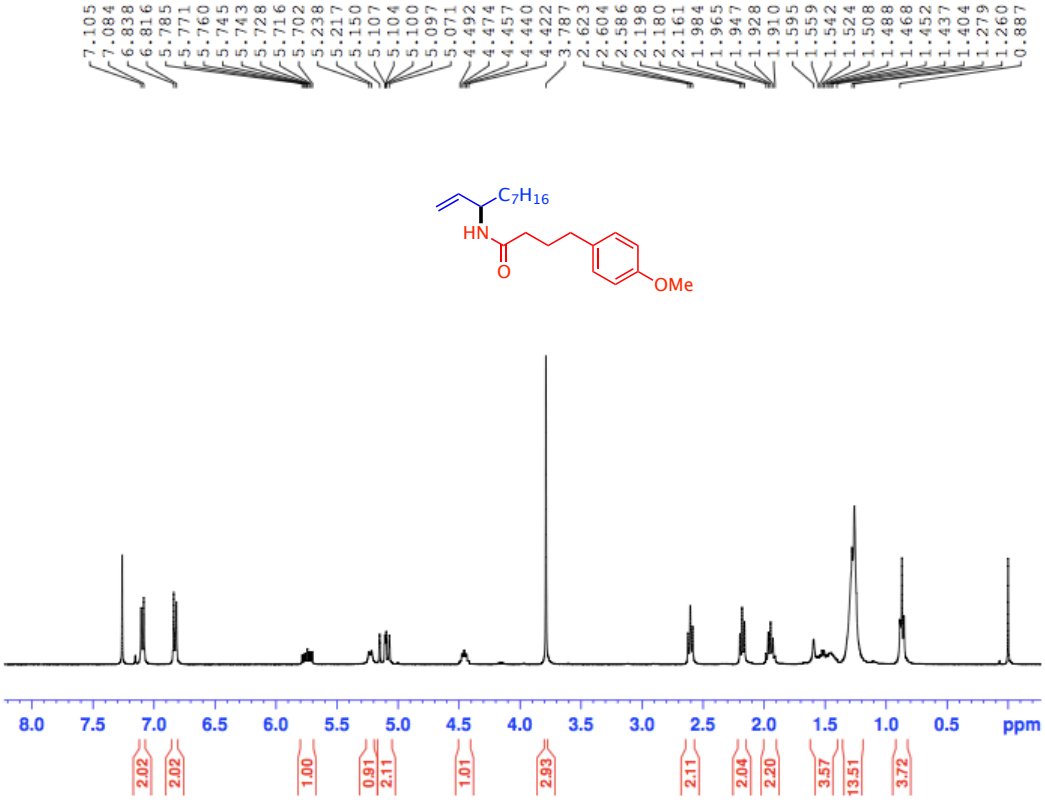

Figure S4.21 ^{13}C NMR Spectrum of *N*-(Dec-1-en-3-yl)-4-(4-methoxyphenyl)butanamide (***4ag***)

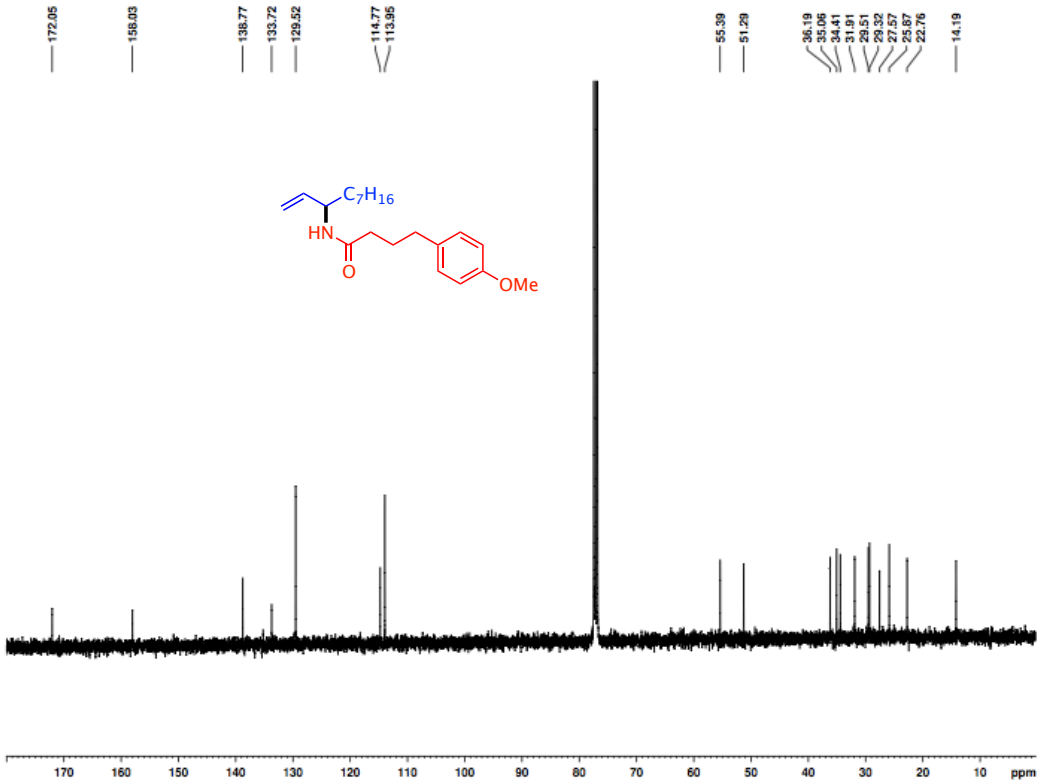

Figure S4.22 ^{1}H NMR Spectrum of *N*-(dec-1-en-3-yl)-4-(4-nitrophenyl)butanamide (***4ah***)

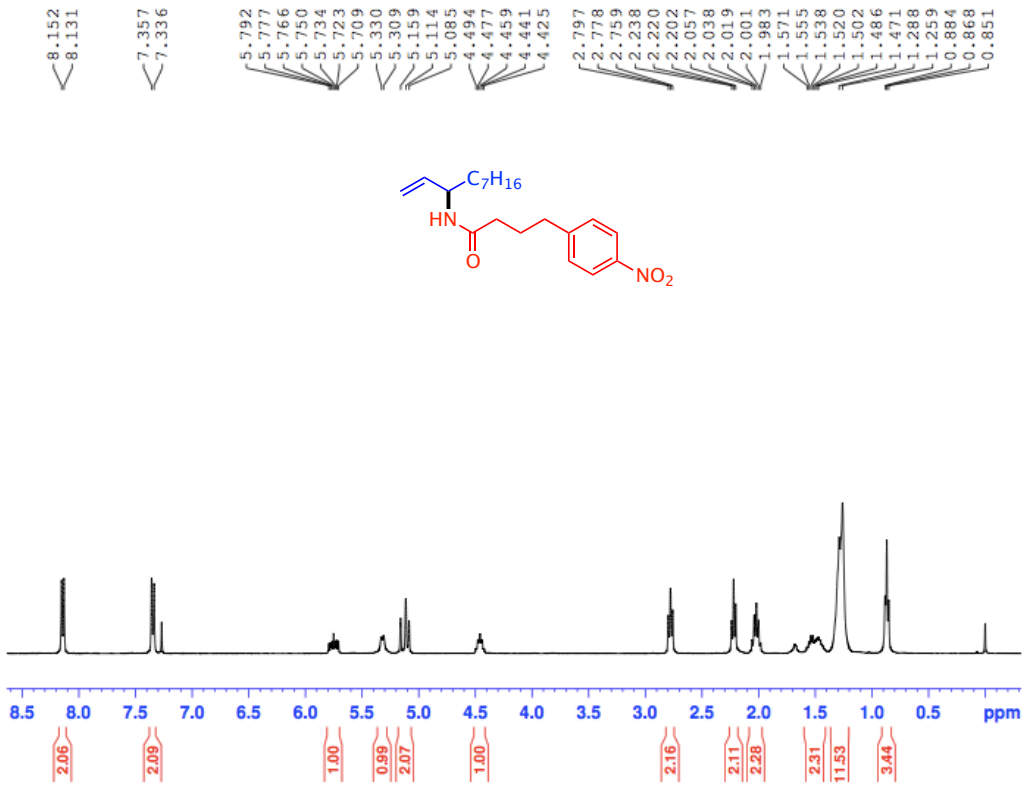

Figure S4.23 ^{13}C NMR Spectrum of *N*-(dec-1-en-3-yl)-4-(4-nitrophenyl)butanamide (***4ah***)

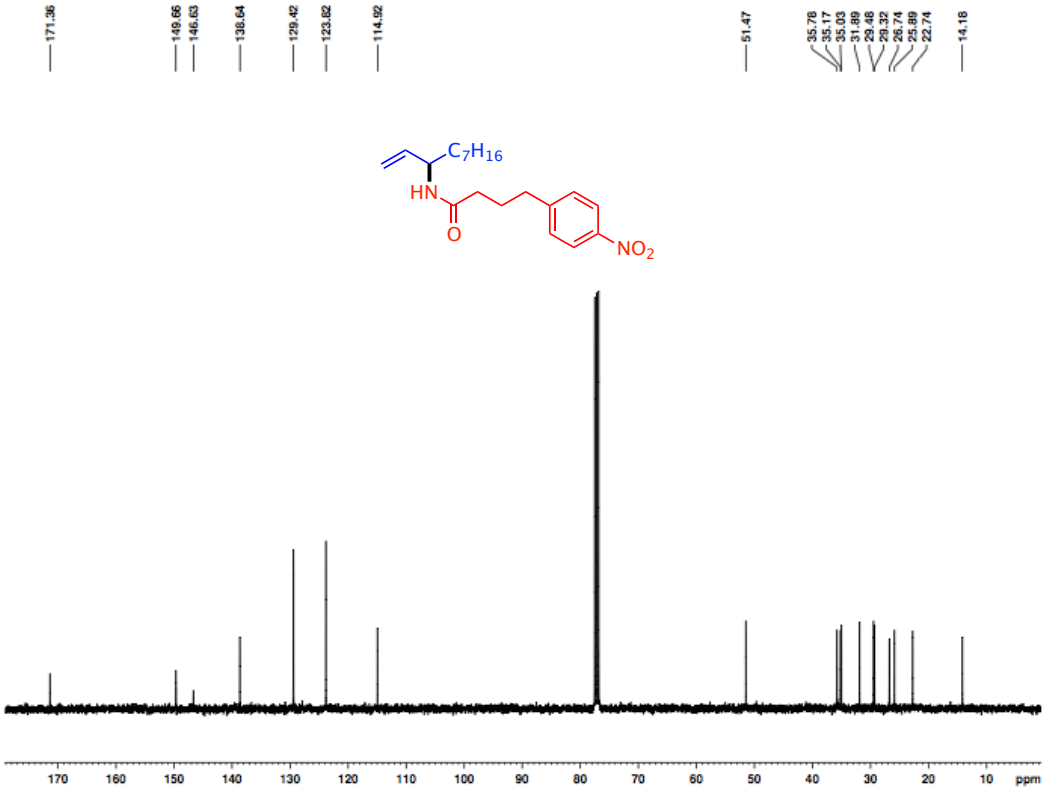

Figure S4.24 ^{1}H NMR Spectrum of *N*-(dec-1-en-3-yl)-4-(pyren-2-yl)butanamide (***4ai***)

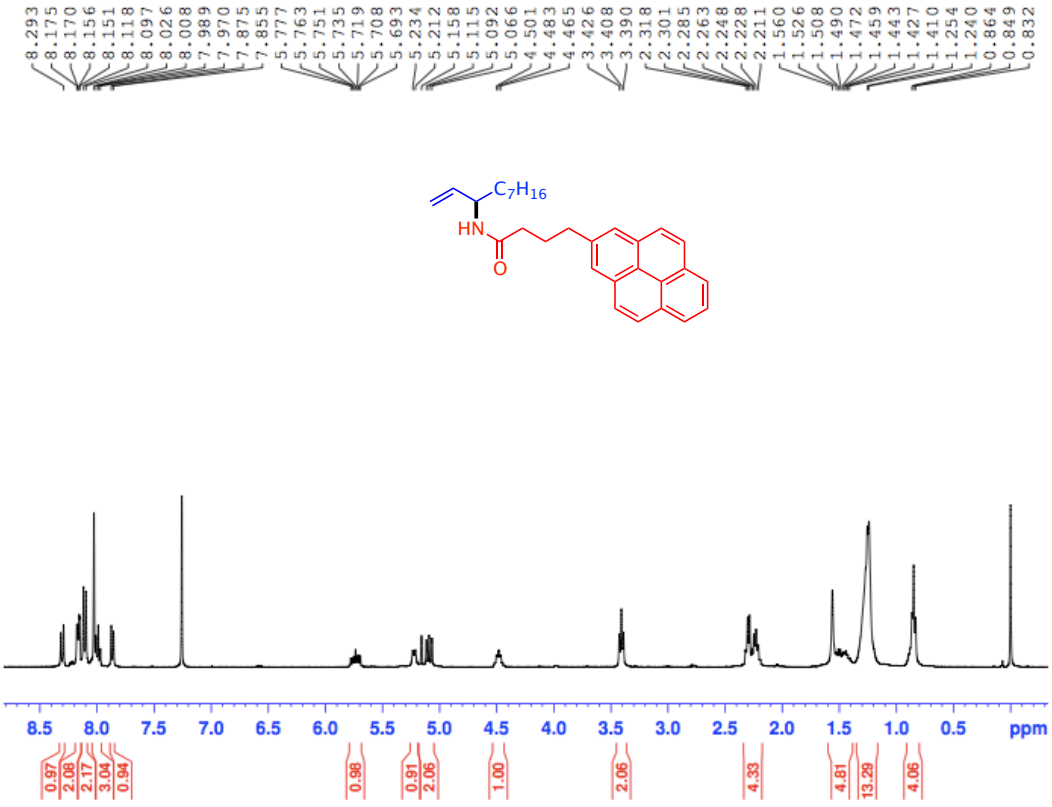

Figure S4.25 ^{13}C NMR Spectrum of *N*-(dec-1-en-3-yl)-4-(pyren-2-yl)butanamide (***4ai***)

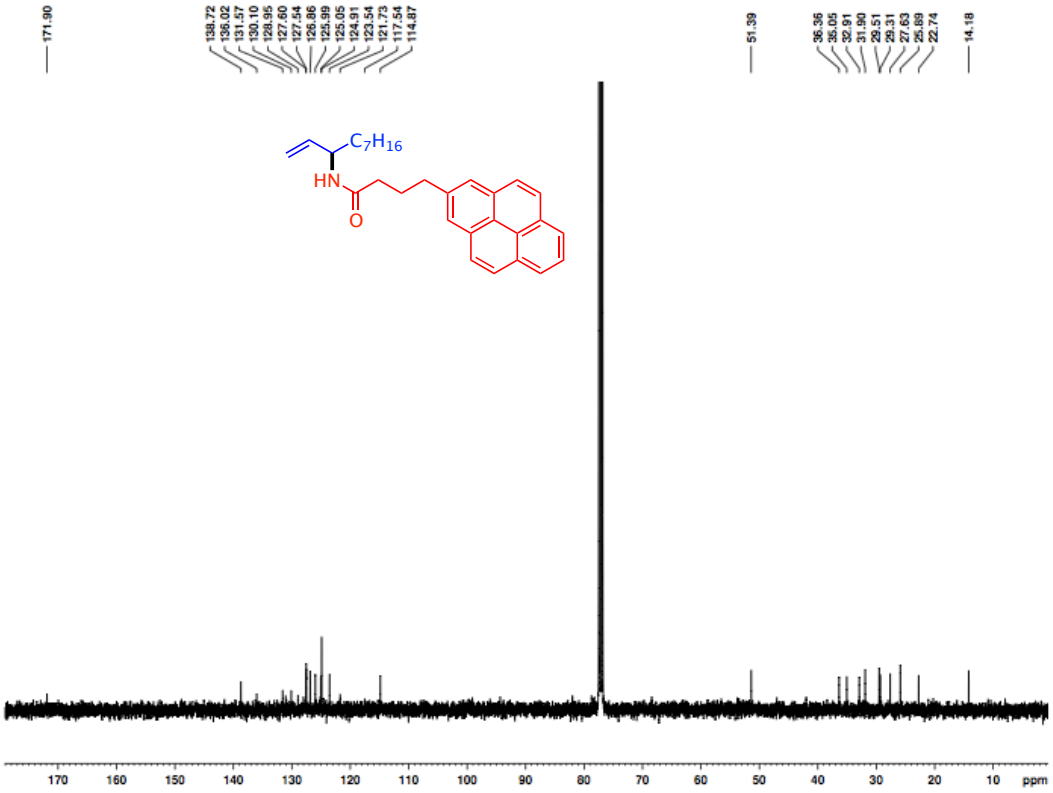

Figure S4.26 ^{1}H NMR Spectrum of (4,5-dimethylcyclohexa-1,4-diene-1,2-diyl)dimethanol

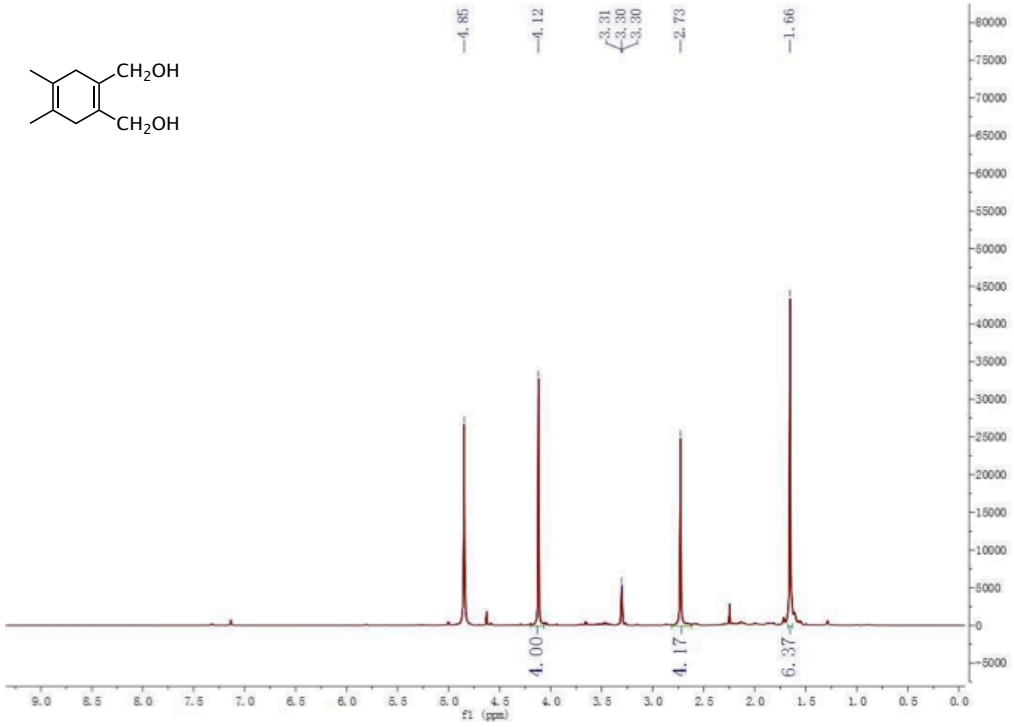

Figure S4.27 ^{13}C NMR Spectrum of (4,5-dimethylcyclohexa-1,4-diene-1,2-diyl)dimethanol

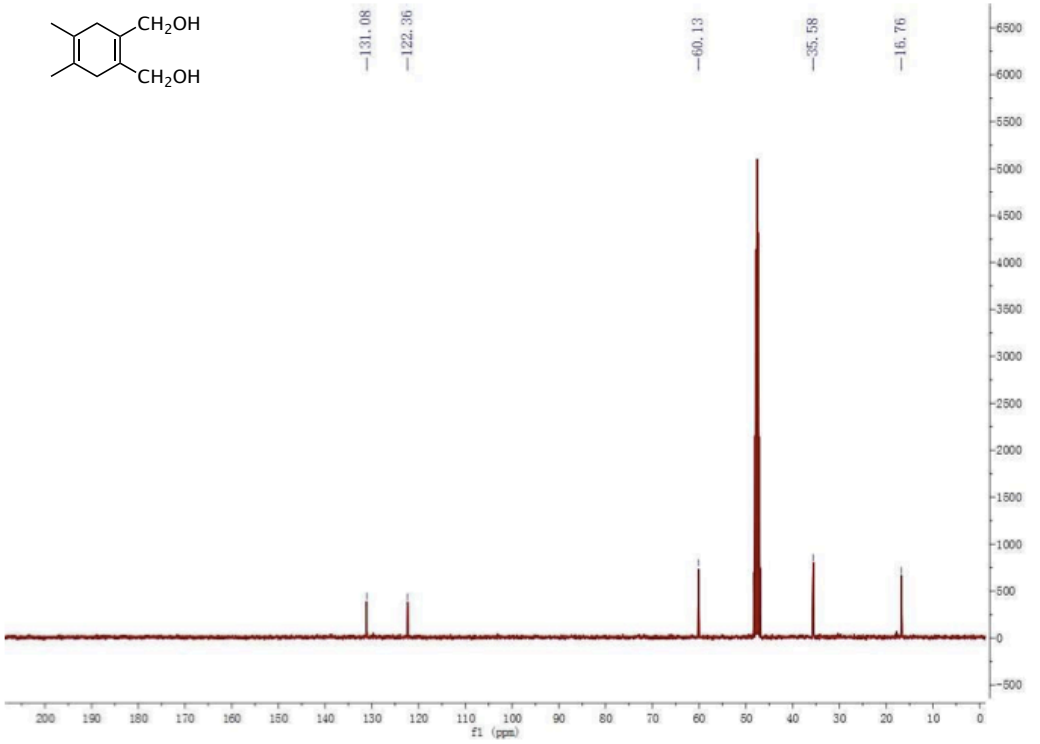

Figure S4.28 ^{1}H NMR Spectrum of *N*,*N*'-([1,1'-binaphthalene]-2,2'-diyl)bis(2,4,6-trimethylbenzenesulfonamide)

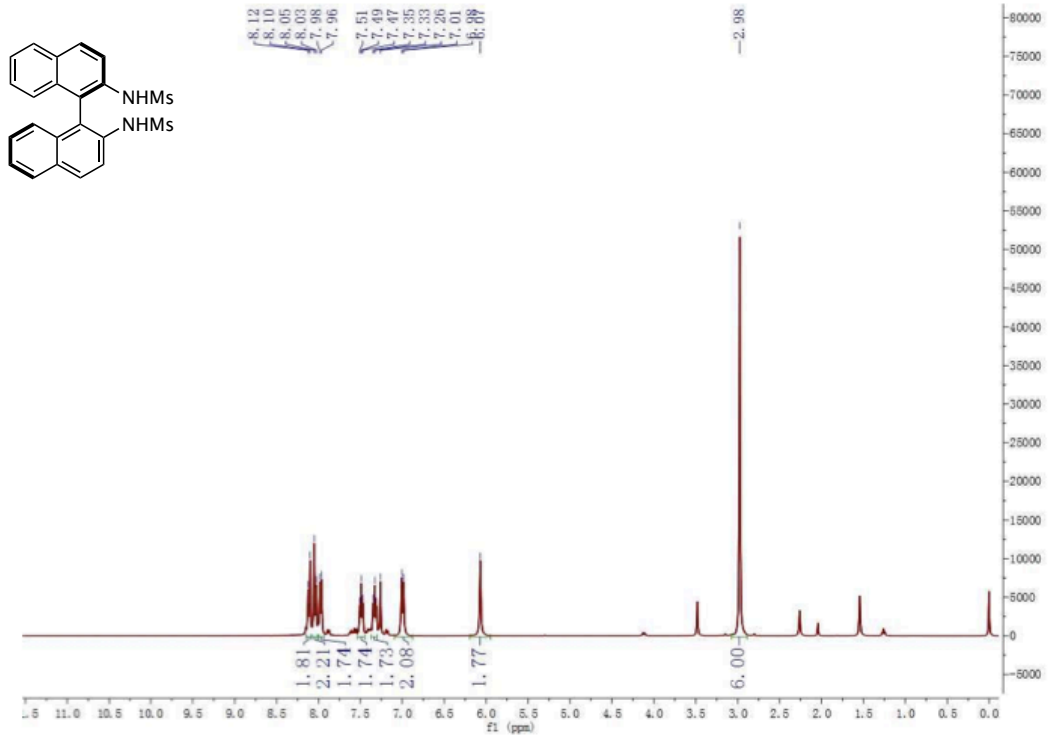

Figure S4.29 ^{1}H NMR Spectrum of 6,19-bis(mesitylsulfonyl)-2,3-dimethyl-1,4,5,6,19,20-hexahydrobenzo[*h*]dinaphtho[2,1-*b*:1',2'-*d*][1,6]diazecine

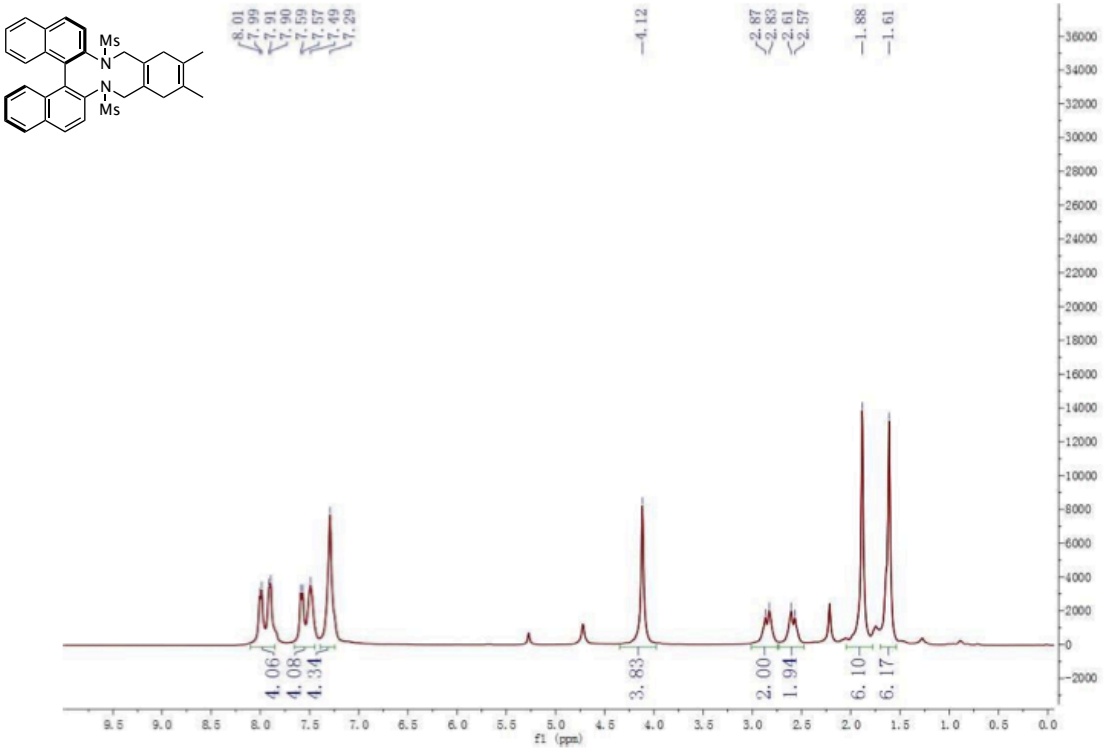

Figure S4.30 ^{13}C NMR Spectrum of 6,19-bis(mesitylsulfonyl)-2,3-dimethyl-1,4,5,6,19,20-hexahydrobenzo[*h*]dinaphtho[2,1-*b*:1',2'-*d*][1,6]diazecine

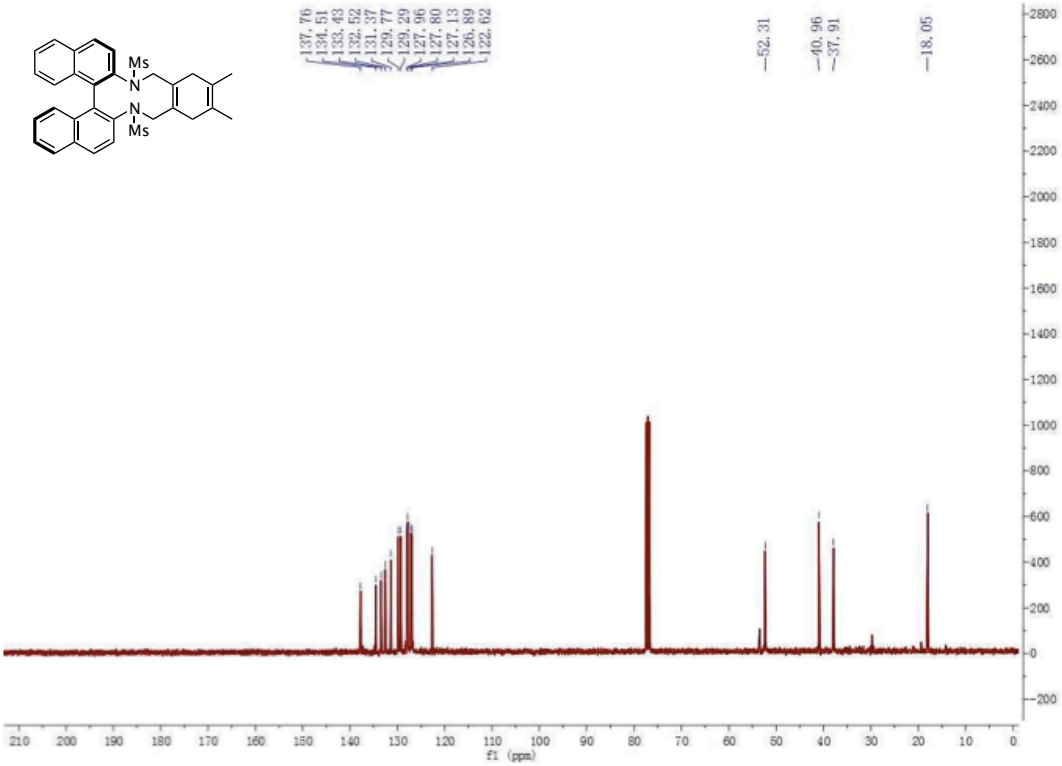

Figure S4.31 ^{1}H NMR Spectrum of **[Ru2]**

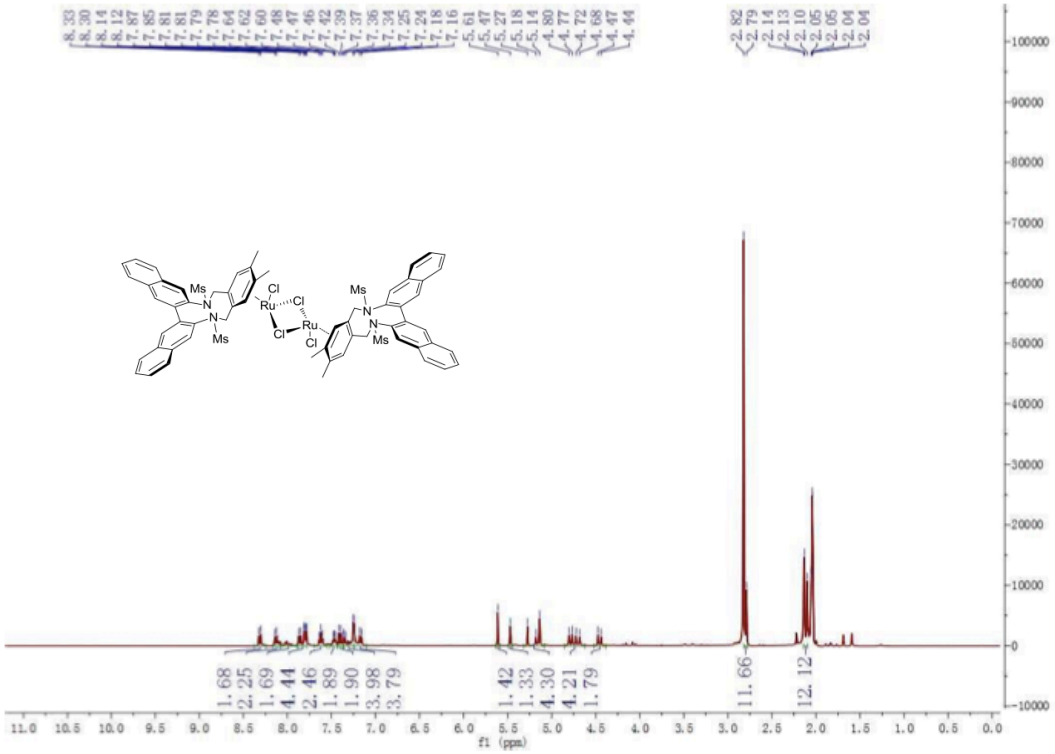

Chapter 5 Conclusion

Regioselective amidation reactions have been explored. Our studies demonstrated Pd(II) and Ru(II) catalysts achieve high regioselective sp^2 C-H amidations coupled with nucleophilic and electrophilic amidating reagents respectively.

In chapter 2, the regioselective non-chelation assisted amidation of simple arenes can be controlled by bulky ligand. By employing [(IPr)Pd$(OAc)_2(H_2O)$] catalyst (IPr = 1,3-bis(2,6-diisopropylphenyl)-2,3-dihydro-1*H*-imidazole), monosubtituted, disubstituted and trisubstituted arenes coupled with phthalimide with $PhI(OAc)_2$ as an oxidant forming *N*-arylphthalimide products up to 67 % yield. The *meta*-isomer is dominant for electron-deficient arenes while the *para*-isomer is dominant for electron-rich arenes. The bulky IPr ligand disfavored the C-N bond formation at *ortho*-position due to steric repulsion between ligand and substituents of arenes. In the mechanistic studies, the rate-determining step of the reaction is C-H bond activation step (k_H/k_D = 3.32) and the rate equation of amidation is rate = $k[PhI(OAc)_2][Pd][Phthalimide]^{0.3}$. That means the oxidation occurred before the C-H bond activation and the resting state of the reaction is Pd(IV) intermediate. Probably, the amidation reaction may go through the Pd(IV) C-H bond activation rather than Pd(II) C-H bond activation. In ESI-MS analysis, the [(IPr)Pd(IV)(Phthalimide)$(OAc)_2(H_2O)$] (m/z = 777) and [(IPr)Pd(IV)(Phthalimide)$(OAc)(H_2O)$(pyridine)] (m/z = 795) were detected in reaction crude mixture. The result showed that the Pd(IV) intermediate is the resting state of the amidation reaction.

In electrophilic amidation, we demonstrated the Ru(II)-catalyzed intramolecular sp^2 C-H amidation rather sp^3 C-H amidation. In chapter 3, the regioselectivity between sp^2 C-H amidation and sp^3 C-H amidation depends on solvent effect and ligand effect. We have prepared the 3-(2,3-diphenylpropyl)-1,4,2-dioxazol-5-one as a model to investigate the effects on regioselectivity. Treatment of 3-(2,3-diphenylpropyl)-1,4,2-dioxazol-5-one with five different Ru(II) complexes (**L1** = *R,R*-DPEN, **L2** = 8-hydroxyquinoline, **L3** = *t*-butyl quinolin-8-ylcarbamate, **L4** = L-proline and **L5** = (*E*)-2-((phenylimino)methyl)phenol) in DCE and TFE. Based on the results, *N,O*-donor ligands (**L2** and **L4**) showed the excellent regioselectivity on sp^2 amidation in TFE solvent (yield of sp^2 = 78 %, yield fo sp^3 = <2 %). In DCE, the performance of both sp^2 and sp^3 amidations were poor in all Ru(II) complexes. By comparing with four different sp^3 C-H bonds (i.e. benzylic C-H, 3^0 C-H, 2^0 C-H and allylic C-H), the [Ru(*p*-cymene)(L-proline)Cl] selectively performed sp^2 C-H amidation up to 81 % yield. In addition, [Ru(*p*-cymene)(L-proline)Cl] is a chiral complex. The enantiomeric excess of amidation was up to 45 % *ee*. Interestingly, the enantiomeric excess of amidation is better in polar aprotic solvents (e.g. DCE and acetone). In polar protic solvents (e.g. TFE and HFIP), the enantioselectivity was inhibited. The reason behind is polar protic solvent molecules formed hydrogen bonding with amino group of L-proline causing the detachment of ligand from Ru(II) center. The chirality of Ru(II) complex was lost leading the low enantiomeric excess of amidation. Designing chiral cymene is the alternative strategy to improve the enantioselectivity amidation because chiral cymene will not be detached from Ru(II) center so that the chirality of the complex can be substained.

In chapter 4, we also demonatrated the Ru(II)-catalyzed intermolecular sp^3 C-H amidation of terminal alkenes with preliminary result in enantiomeric excess. Employing terminal alkenes with dioxazolones, [Ru(*p*-cymene)Cl_2]$_2$ as a catalyst, $AgSbF_6$, LiOAc and HOAc as additives in DCE gave up to 61 % desired products formation. The chiral [Ru(cymene)'Cl_2]$_2$ was prepared and characterized by X-ray crystalline chromatography giving 10 % *ee* in amidation. The results showed that it had kinetic resolution on enatio-determining step of the reaction. Since the chiral cymene ligand is 10-membered ring structure which bulky substituents of ligand is far away from the Ru(II) center. Modifying the ligand into 8-membered ring structure will get bulky substituents closer to Ru(II) center. With the aid of steric factor, the enantioselectivity of amidation can be improved.

References

(1) (a) Paul, F.; Patt, J.; Hartwig, J. F. *J. Am. Chem. Soc.* **1994**, *116*, 5969. (b) Guram, A. S.; Buchwald, S. L. *J. Am. Chem. Soc.* **1994**, *116*, 7901. (c) Louie, J.; Hartwig, J. F. *Tetrahedron Letters* **1995**, *36*, 3609. (d) Guram, A. S.; Rennels, R. A.; Buchwald, S. L. *Angew. Chem. Int. Ed.* **1995**, *34*, 1348.

(2) (a) Fanta, P. E. *Synthesis* **1974**, 9. (b) Ullmann, F.; Bielecki, J. *Chemische Berichte* **1901**, *34*, 2174.

(3) Recent reviews on Pd-Catalyzed Intermolecular C(sp^2)-H Aminations and Amidations, see: (a) Jiao, J.; Murakami, K.; Itami, K. *ACS Catal.* **2016**, *6*, 610. (b) Park, Y.; Kim, Y.; Chang, S. *Chem. Rev.* **2017**, *117*, 9247. (c) Timsina, Y. N.; Gupton, B. F.; Ellis, K. C. *ACS Catal.* **2018**, *8*, 5732.

(4) Recent examples on *ortho* C-H Bond Aminations of Arenes, see: (a) Tsang, S. C. P.; Munday, R. H.; Brasche, G.; Zheng, N.; Buchwald, S. L. *J. Org. Chem.* **2008**, *73*, 7306. (b) Brasche, G.; Buchwald, S. L. *Angew. Chem. Int. Ed.* **2008**, *47*, 1932. (c) Wasa, M.; Yu, J.-Q. *J. Am. Chem. Soc.* **2008**, *130*, 14058. (d) Jordan-Hore, J. A.; Johansson, C. C. C.; Gulias, M.; Beck, E. M.; Gaunt, M. J. *J. Am. Chem. Soc.* **2008**, *130*, 16184. (e) Haffemayer, B.; Gulias, M.; Gaunt, M. J. *Chem. Sci.* **2011**, *2*, 312. (f) Xiao, B.; Gong, T.-J.; Liu, Z.-J.; Liu, L. *J. Am. Chem. Soc.* **2011**, *133*, 1466. (g) Grohmann, C.; Wang, H.; Glorius, F. *Org. Lett.* **2012**, *14*, 656. (h) Neufeldt, S. R.; Sanford, M. S. *Acc. Chem. Res.* **2012**, *45*, 936. (i) Mei, T.-S.; Leow, D.; Xiao, H.; Laforteza, B. N.; Yu, J.-Q. *Org. Lett.* **2013**, *15*, 3058. (j) Shang, M.; Zeng, S.-H.; Sun, S.-Z.; Dai, H.-X.; Yu, J.-Q. *Org. Lett.* **2013**, *15*, 5286. (k) Tran, L. D.; Roane, J.; Daugulis, O. *Angew. Chem. Int. Ed.* **2013**, *52*, 6043. (l) Yu, D.-G.; Suri, M.; Glorius, F. *J. Am. Chem. Soc.* **2013**, *135*, 8802. (m)

Grohmann, C.; Wang, H.; Glorius, F. *Org. Lett.* **2013**, *15*, 3014. (n) Allen, L. J.; Cabrera, P. J.; Lee, M.; Sanford, M. S. *J. Am. Chem. Soc.* **2014**, *136*, 5607. (o) Patel, P.; Chang, S. *ACS Catal.* **2015**, *5*, 853. (p) Kim, H.; Chang, S. *ACS Catal.* **2015**, *5*, 6665. (q) Zhu, D.; Yang, G.; He, J.; Chu, L.; Gong, W.; Chen, K.; Eastgate, M. D.; Yu, J.-Q. *Angew. Chem. Int. Ed.* **2015**, *54*, 2497. (r) Kim, H.; Park, G.; Park, J.; Chang, S. *ACS Catal.* **2016**, *6*, 5922. (s) Kim, Y.; Park, J.; Chang, S. *Org. Lett.* **2016**, *18*, 1892. (t) Ng, K.-H.; Chan, A. S. C.; Yu, W.-Y. *J. Am. Chem. Soc.* **2010**, *132*, 12862. (u) Ng, K.-H.; Ng, F.-N.; Yu, W.-Y. *Chem. Commun.* **2012**, *48*, 11680. (v) Ng, K.-H.; Zhou, Z.; Yu, W.-Y. *Org. Lett.* **2012**, *14*, 272. (w) Ng, K.-H.; Zhou, Z.; Yu, W.-Y. *Chem. Commun.* **2013**, *49*, 7031.

(5) Thu, H.-Y.; Yu, W.-Y.; Che, C.-M. *J. Am. Chem. Soc.* **2006**, *128*, 9048.

(6) (a) Leow, D.; Li, G.; Mei, T.-S.; Yu, J.-Q. *Nature* **2012**, *486*, 518. (b) Wan, L.; Dastbaravardeh, D.; Li, G.; Yu, J.-Q. *J. Am. Chem. Soc.* **2013**, *135*, 18056. (c) Yang, Y.-F.; Cheng, G.-J.; Liu, P.; Leow, D.; Sun, T.-Y.; Chen, P.; Zhang, X.; Yu, J.-Q.; Wu, Y.-D.; Houk, K. N. *J. Am. Chem. Soc.* **2014**, *136*, 344. (d) Deng, Y.; Yu, J.-Q. *Angew. Chem. Int. Ed.* **2015**, *54*, 888. (e) Chu, L.; Shang, M.; Tanaka, K.; Chen, Q.; Pissarnitski, N.; Streckfuss, E.; Yu, J.-Q. *ACS Cent. Sci.* **2015**, *1*, 394.

(7) For a review on Directing Group-Assisted *meta*-C-H Bond Functionalization of Arenes: (a) Dey, A.; Agasti, S.; Maiti, D. *Org. Biomol. Chem.* **2016**, *14*, 5440. (b) Dey, A.; Sinha, S. K.; Achar, T. K.; Maiti, D. *Angew. Chem. Int. Ed.* **2019**, *58*, 10820. Recent examples on non *ortho*-Selective C-H Bond Functionalization: (c) Bag, S.; Patra, T.; Modak, A.; Deb, A.; Maity, S.; Dutta, U.; Dey, A.; Kancheria, R.; Maji, A.; Hazra, A.; Bera, M.; Maiti, D. *J. Am. Chem. Soc.* **2015**, *137*, 11888. (d) Modak, A.; Mondal, A.; Watile, R.; Mukherjee, S.; Maiti, D. *Chem. Commun.* **2016**, *52*, 13916. (e) Mera, M.; Sahoo, S. K.; Maiti, D. *ACS Catal.* **2016**, *6*, 3575. (f) Dey, A.; Agasti, S.; Maiti, D. *Org.*

Biomol. Chem. **2016**, *14*, 5440. (g) Maity, S.; Hoque, E.; Dhawa, U.; Maiti, D. *Chem. Commum.* **2016**, *52*, 14003. (h) Patra, T.; Bag, S.; Kancheria, R.; Mondal, A,; Dey, A.; Pimparkar, S.; Agasti, S.; Modak, A.; Maiti, D. *Angew. Chem. Int. Ed.* **2016**, *55*, 7751. (i) Bag, S.; Jayarajan, R.; Mondal, R.; Maiti, D.; *Angew. Chem. Int. Ed.* **2017**, *56*, 3182. (j) Modak, A.; Patra, T.; Chowdhury, R.; Raul, S.; Maiti, D. *Organometallics* **2017**, *36*, 2418. (k) Dutta, U.; Modak, A.; Bhaskararao, B.; Bera, M.; Bag, S.; Mondal, A.; Lupton, D. W.; Sunoj, R. B.; Maiti, D. *ACS Catal.* **2017**, *7*, 3162. (l) Maji, A.; Dahiya, A.; Lu, G.; Bhattacharya, T.; Brochetta, M.; Zanoni, G.; Liu, P.; Maiti, D. *Nature Commun.* **2018**, *9*, 1.

(8) Shrestha, R.; Mukherjee, P.; Tan, Y.; Litman, Z. C.; Hartwig, J. F. *J. Am. Chem. Soc.* **2013**, *135*, 8480.

(9) Marchetti, L.; Kantak, A.; Davis, R.; DeBoef, B. *Org. Lett.* **2015**, *17*, 358.

(10) (a) Boursalian, G. B.; Ngai, M.-Y.; Hojczyk, K. N.; Ritter, T. *J. Am. Chem. Soc.* **2013**, *135*, 13278. (b) Boursalian, G. B.; Ham, W. S.; Mazzotti, A. R.; Ritter, T. *Nature Chem.* **2016**, *8*, 810. (c) D'Amato, E. M.; Borgel, J.; Ritter, T. *Chem. Sci.* **2019**, *10*, 2424.

(11) Bandara, H. M. D.; Jin, D.; Mantell, M. A.; Field, K. D.; Wang, A.; Narayanan, R. P.; Deskins, N. A.; Emmert, M. H. *Catal. Sci. Technol.* **2016**, *6*, 5304.

(12) (a) Kawakami, T.; Murakami, K.; Itami, K. *J. Am. Chem. Soc.* **2015**, *137*, 2460. (b) Sun, K.; Wang, X.; Liu, L.; Sun, J.; Liu, X.; Li, Z.; Zhang, Z.; Zhang, G. *ACS Catal.* **2015**, *5*, 7194. (c) Xie, W.; Yoon, J. H.; Chang, S. *J. Am. Chem. Soc.* **2016**, *138*, 12605.

(13) Kim, H. J.; Kim, J.; Cho, S. H.; Chang, S. *J. Am. Chem. Soc.* **2011**, *133*, 16382.

(14) Kantak, A. A.; Potavathri, S.; Barham, R. A.; Romano, K. M.; DeBoef, B. *J. Am. Chem. Soc.* **2011**, *133*, 19960.

(15) (a) Samanta, R.; Bauer, J. O.; Strohmann, C.; Antonchick, A. P. *Org. Lett.* **2012**, *14*, 5518. (b) Manna, S.; Serebrennikova, P. O.; Utepova, I. A.; Antonchick, A. P.; Chupakhin, O. N. *Org. Lett.* **2015**, *17*, 4588.

(16) (a) Chu, L.; Wang, X.-C.; Moore, C. E.; Rheingold, A. L.; Yu, J.-Q. *J. Am. Chem. Soc.* **2013**, *135*, 16344. (b) Chu, L.; Xiao, K.-J.; Yu, J.-Q. *Science* **2014**, *346*, 451.

(17) For reviews on Enantioselective Chiral Cp Metals-Catalyzed Functionalization: (a) Newton, C. G.; Kossler, D.; Cramer, N. *J. Am. Chem. Soc.* **2016**, *138*, 3915. (b) Smits, G.; Audic, B.; Wodrich, M. D.; Corminboeuf, C.; Cramer, N. *Chem. Sci.* **2017**, *8*, 7174. (c) Newton, C. G.; Wang, S.-G.; Oliveria, C. C.; Cramer, N. *Chem. Rev.* **2017**, *117*, 8908. For examples of Enantioselective Chiral CpRh(III)-Catalyzed Functionalization: (d) Ye, B.; Cramer, N. *Science* **2012**, *338*, 504. (e) Ye, B.; Cramer, N. *Angew. Chem. Int. Ed.* **2014**, *53*, 7896. (f) Wodrich, M. D.; Ye, B.; Gonthier, J. F.; Corminboeuf, C.; Cramer, N. *Chem. Eur. J.* **2014**, *20*, 15409. (g) Ye, B.; Cramer, N. *Acc. Chem. Res.* **2015**, *48*, 1308. (h) Ye, B.; Cramer, N. *Synlett* **2015**, *26*, 1490. (i) Duchemin, C.; Cramer, N. *Chem. Sci.* **2019**, *10*, 2773.

(18) (a) Hong, S. Y.; Park, Y.; Hwang, Y.; Kim, Y. B.; Baik, M.-H.; Chang, S. *Science* **2018**, *359*, 1016. (b) Huh, S.; Hong, S. Y.; Chang, S. *Org. Lett.* **2019**, *21*, 2808. (c) Hong, S. Y.; Chang, S. *J. Am. Chem. Soc.* **2019**, *141*, 10399. (d) Wang, H.; Park, Y.; Bai, Z.; Chang, S. *J. Am. Chem. Soc.* **2019**, *141*, 7194.

(19) Xing, Q.; Chan, C.-M.; Yeung, Y.-W.; Yu, W.-Y. *J. Am. Chem. Soc.* **2019**, *141*, 3849.

(20) Sánchez, C.; Méndez, C.; Salas, J. A. *Nat. Prod. Rep.* **2006**, *23*, 1007.

(21) Horton, D. A.; Bourne, G. T.; Smythe, M. L. *Chem. Rev.* **2003**, *103*, 893.

(22) Zhang, Y.-H.; Shi, B.-F.; Yu, J.-Q. *J. Am. Chem. Soc.* **2009**, *131*, 5072.

(23) Recent reviews on the use of *N*-heterocyclic carbene ligands for Pd-catalyzed cross coupling reactions, see: (a) Kantchev, E. A. B.; O'Brien, C. J.; Organ, M. G. *Angew. Chem. Int. Ed.* **2007**, *46*, 2768. (b) Marion, N.; Nolan, S. P. *Acc. Chem. Res.* **2008**, *41*, 1440. (c) Díez-González, S.; Marion, N.; Nolan, S. P. *Chem. Rev.* **2009**, *109*, 3612. Examples such as Heck Reactions, see: (d) Yang, C.; Nolan, S. P.; *Synlett.* **2001**, *10*, 1539. For Suzuki-Miyaura Coupling Reactions, see: (e) Grasa, G. A.; Viciu, M. S.; Huang, J.; Nolan, S. P. *J. Org. Chem.* **2001**, *66*, 7729. (f) Grasa, G. A.; Viciu, M. S.; Huang, J.; Zhang, C.; Trudell, M. L.; Nolan, S. P. *Organometallics* **2002**, *21*, 2866. For Buchwald-Hartwig Aminations, see: (g) O'Brien, C. J.; Kantchev, E. A. B.; Chass, G. A.; Hadei, N.; Hopkinson, A. C.; Organ, M. G.; Setiadi, D. H.; Tang, T.-H.; Fang, D.-C. *Tetrahedron* **2005**, *61*, 9723.

(24) Martínez, C.; Muñiz, K. *Chem. Eur. J.* **2016**, *22*, 7367.

(25) (a) Whitfield, S. L.; Sanford, M. S. *J. Am. Chem. Soc.* **2007**, *129*, 15142. (b) Whitfield, S. R.; Sanford, M. S. *J. Am. Chem. Soc*. **2008**, *27*, 1683. (c) Arnold, P. L.; Sanford, M. S.; Pearson, S. M. *J. Am. Chem. Soc*. **2009**, *131*, 13912. (d) Racowski, J. M.; Ball, N. D.; Sanford, M. S. *J. Am. Chem. Soc.* **2011**, *133*, 18022. (e) Powers, D. C.; Lee, E.; Ariafard, A.; Sanford, M. S.; Yates, B. F.; Canty, A. J.; Ritter, T. *J. Am. Chem. Soc*. **2012**, *134*, 12002. (f) Topczewski, J. J.; Sanford, M. S. *Chem. Sci.* **2015**, *6*, 70. (g) Cook, A. K.; Sanford, M. S. *J. Am. Chem. Soc.* **2015**, *137*, 3109.

(26) For nucleophilicity of arenes, see: (a) M. Patz, H. Mayr, *Angew. Chem. Int. Ed.*, 1994, **33**, 938-957. (b) M. F. Gotta, H. Mayr, *J. Org. Chem.*, 1998, **63**, 9769-9775. (c) A. J. Hickman, M. S. Sanford, *ACS Catal.*, 2011, **1**, 170-174.

(27) (a) Larsen, T. O.; Smedsgaard, J.; Frisvad, J. C.; Anthoni, U.; Christophersen, C. *Biochem. Syst. Ecol.* **1999**, *27*, 329. (b) Uchida, R.; Imasato, R.; Tomoda, H.; Omura, S.

J. Antibiot. **2006**, *59*, 652. (c) An, C.-Y.; Li, X.-M.; Luo, H.; Li, C.-S.; Wang, M.-H.; Xu, G.-M.; Wang, B.-G. *J. Nat. Prod.* **2013**, *76*, 1896. (d) Chen, M.; Shao, C.-L.; She, Z.-G.; Wang, C.-Y. *J. Nat. Prod.* **2014**, *77*, 2720.

(28) (a) Mieriņa, I.; Jure, M.; Stikute, A. *Chem. Heterocycl. Compd.* **2016**, *52*, 509. (b) Koltunov, K. Y.; Walspurger, S.; Sommer, J. *Chem. Commun.* **2004**, 1754. (c) Lee, E.; Han, S.; Jin, G. H.; Lee, H. J.; Kim, W.-Y.; Ryu, J.-H.; Jeon, R. *Bioorg. Med. Chem. Lett.* **2013**, *23*, 3976.

(29) Guan, L.-P.; Jin, Q.-H.; Tian, G.-R.; Chai, K.-Y.; Quan, Z.-S. *J. Pharm. Pharmaceut. Sci.* **2007**, *10*, 254.

(30) Ye, F.; Alper, H. *Adv. Synth. Catal.* **2006**, *348*, 1855.

(31) Park, J. O.; Youn, S. W. *Org. Lett.* **2010**, *12*, 2258.

(32) Li, B.; Park, Y.; Chang, S. *J. Am. Chem. Soc.* **2014**, *136*, 1125.

(33) For selected reviews on the C-H amination, see: (a) Armstrong, A.; Collins, J. C. *Angew. Chem. Int. Ed.* **2010**, *49*, 2282. (b) Roizen, J. L.; Harvey, M. E.; Du Bois, J. *Acc. Chem. Res.* **2012**, *45*, 911. (c) Dequirez, G.; Pons, V.; Dauban, P. *Angew. Chem. Int. Ed.* **2012**, *51*, 7384. (d) Louillat, M.-L.; Patureau, F. W. *Chem. Soc. Rev.* **2014**, *43*, 901. (e) Jiao, J.; Murakami, K.; Itami, K. *ACS Catal.* **2016**, *6*, 610. (f) Park, Y.; Kim, Y.; Chang, S. *Chem. Rev.* **2017**, *117*, 9247. (g) Sauermann, N.; Meyer, T. H.; Qiu, Y.; Ackermann, L. *ACS Catal.* **2018**, *8*, 7086.

(34) (a) Stokes, B. J.; Dong, H.; Leslie, B. E.; Pumphrey, A. L.; Driver, T. G. *J. Am. Chem. Soc.* **2007**, *129*, 7500. (b) Shen, M.; Leslie, B. E.; Driver, T.G. *Angew. Chem. Int. Ed.* **2008**, *47*, 5056. (c) Nguyen, Q.; Sun, K.; Driver, T. G. *J. Am. Chem. Soc.* **2012**, *134*, 7262. (d) Hennessy, E. T.; Betley, T. A. *Science* **2013**, *340*, 591. (e) Prier, C. K.; Zhang, R. K.; Buller, A. R.; Brinkmann-Chen, S.; Arnold, F. H. *Nat. Chem.* **2017**, *9*, 629.

(35) (a) John, A.; Byun, J.; Nicholas, K. M. *Chem. Commun.* **2013**, *49*, 10965. (b) Paudyal, M. P.; Adebesin, A. M.; Burt, S. R.; Ess, D. H.; Ma, Z.; Kürti, L.; Falck, J. R. *Science* **2016**, *353*, 1144.

(36) (a) Park, J.; Lee, J.; Chang, S. *Angew. Chem. Int. Ed.* **2017**, *56*, 4256. (b) Hwang, Y.; Park, Y.; Chang, S. *Chem. Eur. J.* **2017**, *23*, 11147. (c) Park, J.; Chang, S. *Angew. Chem. Int. Ed.* **2015**, *137*, 4534. (d) Park, Y.; Park, K. T.; Kim, J. G.; Chang, S. *J. Am. Chem. Soc.* **2015**, *137*, 4534. (e) Park, Y.; Jee, S.; Kim, J. G.; Chang, S. *Org. Process Res. Dev.* **2015**, *19*, 1024.

(37) (a) Scriven, E. F. V.; Turnbull, K. *Chem. Rev.* **1988**, *88*, 297. (b) Bräse, S.; Gil, C.; Knepper, K.; Zimmermann, V. *Angew. Chem. Int. Ed.* **2005**, *44*, 5188. (c) Li, D.; Wu, T.; Liang, K.; Xia, C. *Org. Lett.* **2016**, *18*, 2228.

(38) (a) Hwang, Y.; Park, Y.; Kim, Y. B.; Kim, D.; Chang, S. *Angew. Chem. Int. Ed.* 2018, *57*, 13565. (b) Hwang, Y.; Jung, H.; Lee, E.; Kim, D.; Chang, S. *J. Am. Chem. Soc.* **2020**, 142, 8880.

(39) Jung, H.; Schrader, M.; Kim, D.; Baik, M.-H.; Park, Y.; Chang, S. *J. Am. Chem. Soc.* **2019**, *141*, 15356.

(40) Biancalana, L.; Abdalghani, I.; Chiellini, F.; Zacchini, S.; Pampaloni, G.; Crucianelli, M.; Marchetti, F. *Eur. J. Inorg. Chem.* **2018**, *26*, 3041.

(41) (a) Wu, Q.-F.; Wang, X.-B.; Shen, P.-X.; Yu, J.-Q. *ACS Catal*. **2018**, *8*, 2577. (b) Shao, Q.; Wu, Q.-F.; He, J.; Yu, J.-Q. *J. Am. Chem. Soc.* **2018**, *140*, 5322. (c) Wu, Q.-F.; Shen, P.-X.; He, J.; Wang, X.-B.; Zhang, F.; Shao, Q.; Zhu, R.-Y.; Mapelli, C.; Qiao, J. X.; Poss, M. A.; Yu, J.-Q. *Science* **2017**, *355*, 499. (d) Shao, Q.; He, J.; Wu, Q.-F.; Yu, J.-Q. *ACS Catal.* **2017**, *11*, 7777.

(42) Liu, R.; Yang, Z.; Ni, Y.; Song, K.; Shen, K.; Lin, S.; Pan, Q. *J. Org. Chem.* 2017, *82*,

8023.

(43) Li, G.; Huo, X.; Jiang, X.; Zhang, W. *Chem. Soc. Rev.* **2020**, *49*, 2060.

(44) (a) Pattillo, C. C.; Strambeanu, I. I.; Calleja, P.; Vermeulen, N. A.; Mizuno, T.; White, M. C. *J. Am. Chem. Soc.* **2016**, *138*, 1265. (b) Osberger, T. J.; White, M. C. *J. Am. Chem. Soc.* **2014**, *136*, 11176. (c) Strambeanu, I. I.; White, M. C. *J. Am. Chem. Soc.* **2013**, *135*, 12032. (d) Stang, E. M.; White, M. C. *J. Am. Chem. Soc.* **2011**, *133*, 14892. (e) Gormisky, P. E.; White, M. C. *J. Am. Chem. Soc.* **2011**, *133*, 12584. (f) Reed, S. A.; Mazzotti, A. R.; White, M. C. *J. Am. Chem. Soc.* **2009**, *131*, 11701. (g) Rice, G. T.; White, M. C. *J. Am. Chem. Soc.* **2009**, *131*, 11707. (h) Reed, S. A.; White, M. C. *J. Am. Chem. Soc.* **2008**, *130*, 3316. (i) Young, A. J.; White, M. C. *J. Am. Chem. Soc.* **2008**, *130*, 14090.

(45) Liu, G.; Yin, G.; Wu, L. *Angew. Chem. Int. Ed.* **2008**, *47*, 4733.

(46) Lei, H.; Rovis, T. *J. Am. Chem. Soc.* **2019**, *141*, 2268.

(47) Knecht, T.; Mondal, S.; Ye, J.-H.; Das, M.; Glorius, F. *Angew. Chem. Int. Ed.* **2019**, *58*, 7117.

(48) (a) Yang, F.; Ackermann, L. *J. Org. Chem.* **2014**, *79*, 12070. (b) Bechtoldt, A.; Ackermann, L. *Chem. Cat. Chem.* **2019**, *11*, 435. (c) Rogge, T.; Ackermann, L. *Angew. Chem. Int. Ed.* **2019**, *58*, 15640.

(49) Lo, V. K.-Y.; Guo, Z.; Choi, M. K.-W.; Yu, W.-Y.; Huang, J.-S.; Che, C.-M. *J. Am. Chem. Soc.* **2012**, *134*, 7588.

(50) For reviews on Enantioselective Chiral Cp Metals-Catalyzed Functionalization: (a) Newton, C. G.; Kossler, D.; Cramer, N. *J. Am. Chem. Soc.* **2016**, *138*, 3915. (b) Smits, G.; Audic, B.; Wodrich, M. D.; Corminboeuf, C.; Cramer, N. *Chem. Sci.* **2017**, *8*, 7174. (c) Newton, C. G.; Wang, S.-G.; Oliveria, C. C.; Cramer, N. *Chem. Rev.* **2017**, *117*, 8908.

For examples of Enantioselective Chiral CpRu(II)-Catalyzed Functionalization: (d) Kossler, D.; Cramer, N. *J. Am. Chem. Soc.* **2015**, *137*, 12478. (e) Kossler, D.; Perrin, F. G.; Suleymanov, A. A.; Kiefer, G.; Scopelliti, R.; Severin, K.; Cramer, N. *Angew. Chem. Int. Ed.* **2017**, *56*, 11490. (f) Kossler, D.; Cramer, N. *Chem. Sci.* **2017**, *8*, 1862. (g) Kossler, D.; Cramer, N. *Chimia* **2017**, *71*, 186. (h) Park, S. H.; Wang, S.-G.; Cramer, N. *ACS Catal.* **2019**, *9*, 10226.

(51) For synthesis of (*R*)-***2i***, see: (a) Kim, Y.; Shin, E.-K.; Beak, P.; Park, Y. S. *Synthesis* **2006**, *22*, 3805. (b) Paquin, J.-F.; Stephenson, C. R. J.; Defieber, C.; Carreira, E. M. *Org. Lett.* **2005**, *7*, 3821. For synthesis of (*S*)-***2i***, see: (c) Zhang, L.; Qureshi, Z.; Sonaglia, L.; Lautens, M. *Angew. Chem. Int. Ed.* **2014**, *53*, 13850.

(52) (a) Britschgi, A. *et al*. Dihydroquinolinones as Anticancer Agents and Their Preparation. *PCT Int. Appl.*, 2019043208, 07 May 2019. (b) Arista, L. *et al*. Preparation of Pyridinone Derivatives and Their Use as Selective Alk-2 Inhibitors. *PCT Int. Appl.*, 2019102256, 31 May 2019.

(53) Wu, L.; Hao, Y.; Liu, Y.; Wang, Q. *Org. Biomol. Chem.* **2019**, *17*, 6762.

(54) (a) Occhiato, E. G.; Ferrali, A.; Menchi, G.; Guarna, A.; Danza, G.; Comerci, A.; Mancina, R.; Serio, M.; Garotta, G.; Cavalli, A.; De Vivo, M.; Recanatini, M. *J. Med. Chem.* **2004**, *47*, 3546. (b) Lucas, S.; Heim, R.; Ries, C.; Schewe, K. E.; Birk, B.; Hartmann, R. W. *J. Med. Chem.* **2008**, *51*, 8077. (c) Karaki, F.; Ohgane, K.; Fukuda, H.; Nakamura, M.; Dodo, K.; Hashimoto, Y. *Bioorg. Med. Chem.* **2014**, *22*, 3587.

(55) (a) Akira, I.; Masahiko, U.; Kouji, K.; Yukihiko, H.; Hiroshi, K.; Hiromu, H. *Chem. Pharm. Bull.* **2001**, *49*, 822. (b) Mendelovici, M. *et al.* Processes for Preparing 6-Hydroxy-3,4-dihydroquinolinone and *N*-(4-methoxyphenyl)-3-chloropropionamide.

PCT Int. Appl. 2001070697, 27 Sep 2011. (c) Gieshoff, T.; Kehl, A.; Schollmeyer, D.; Moeller, K. D.; Waldvogel, S. R. *J. Am. Chem. Soc.* **2017**, *139*, 12317.